CHEMICAL AND PHYSICAL DYNAMICS OF MARINE POCKMARKS WITH INSIGHTS INTO THE ORGANIC CARBON CYCLING ON THE MALIN SHELF AND IN THE DUNMANUS BAY, IRELAND

BY

Michal Szpak, M.Sc.

Thesis submitted for the Degree of Doctor of Philosophy

Supervisor: Dr Brian Kelleher

Dublin City University

School of Chemical Sciences

March, 2012

Declaration

I hereby certify that this material, which I now submit for assessment on the programme of study leading to the award of Doctor of Philosophy is entirely my own work, that I have exercised reasonable care to ensure that the work is original, and does not to the best of my knowledge breach any law of copyright, and has not been taken from the work of others save and to the extent that such work has been cited and acknowledged within the text of my work.

Signed: _____

(Candidate) ID No.: _____

Date: _____

Abstract

Pockmarks are specific type of marine geological setting resembling craters or pits. They are considered surface expression of fluid flow in the marine subsurface. Pockmarks are widespread in the aquatic environment but the understanding of their formation mechanisms, relationship with marine macro- and micro-biota and their geochemistry remains limited. Despite numerous findings of these features in Irish waters they received little attention and remain poorly studied. In this work extensive geophysical data sets collected by the Irish National Seabed Survey and its successor the INFOMAR project as well in situ sediment samples were utilized to provide baseline information on the nature of some of these features, the processes they are fuelled by and their geochemical characteristics. Pockmarks from open shelf (Malin Shelf) and bay, fjord like environment (Dunmanus Bay) are compared and theories of their formation are formulated. Sediment from these features was extensively studied utilizing advanced geotechnical and geochemical tools to describe and quantify processes taking place in the subsurface. Organic matter was characterized on a molecular level by combined biomarker and advanced Nuclear Magnetic Resonance approach.

Acknowledgements

The research of which fruits are presented in this thesis was a wonderful journey, full of exploration of scientific ideas, acquiring knowledge and learning about inner strengths and weaknesses. This journey would not be possible if not the support and dedication of many people. I would like give my thanks to all of them and express gratitude for their support in all of the good and bad moments that I have encountered while working on this project.

I would like to dedicate this thesis to my wife Justyna. Your unflinching support, love and patience were the biggest source of strength and motivation I needed to complete this work. To my parents Janusz and Teresa as well as my brother Łukasz, I thank You for the instilled values that led me to pursue a degree in science: curiosity of the world, ambition and perseverance.

Special thanks go to my mentor Brian Kelleher for giving me continuous support, advice, for his great resourcefulness and encouragement and for being a good friend. I thank my collaborators and partners in the Geological Survey of Ireland, Xavier Monteys and Koen Verbruggen for sharing their time and knowledge and for making my off shore experience possible. I also would like to thank the crew and the captains of the RV Celtic Explorer and RV Celtic Voyager as well as all staff from Irish Marine Institute for their expertise and help given during the preparation and execution of all research cruises I had the privilege to participate in. Special thanks to Andrew Simpson, his research group and technical staff for the invaluable help in acquiring NMR spectra and for their advice and insight during their interpretation. I also would like to thank to my colleagues Kris Hart, Shane O'Reilly, Sean Jordan, Vasileios Kouloumpos, Leon Barron, Adrian Spence, Margaret McCaul, Brian Murphy, Brian Moran, Carla Meledandri for all the hours of productive and purely fun coffee breaks we have spent together breaking the often so tedious laboratory routine. Finally I would like to give my thanks to all academic and technical staff of the School of Chemical Sciences, Dublin City University for Your support and advice during this project.

Declaration

Bathymetry, backscatter and sub bottom data was collected in 2003, 2006 and 2007 as part of the INSS (Irish National Seabed Survey) program and its successor, the INFOMAR (Integrated Mapping for the Sustainable Development of Ireland's Marine Resources) program (Dorschel et al., 2010). The data was accessed through collaboration with the Geological Survey of Ireland (GSI) and Irish Marine Institute (MI) and in accordance with the open and free access policy announced by The Minister for Communications, Marine and Natural Resources, Mr. Noel Dempsey T.D. in 2007.

Towed electromagnetic (EM) data were acquired during a geo-hazard and hydrocarbon reconnaissance survey of the Malin Shelf in 2009 (GSI/PIP – IS05/16 project, Monteys et al., 2009 and Gracia et al., 2009). The data was accessed through collaboration with the Dr Xavier Monteys, Dr Koen Verbruggen (GSI), Dr Xavier Garcia (Dublin Institute for Advanced Studies, Ireland) and Dr Rob Evans (Woods Hole Oceanographic Institution, USA). The result of this collaboration was published as Szpak et al., 2011.

The author acknowledges that ownership and credit for the acquisition and processing of the above mentioned data is that of the above mentioned institutions and individuals. The authors own work involved manipulation and interpretation of the data in a novel way not pursued by any of the data owners.

The NMR experiments were performed by Prof Andre Simpson (Environmental NMR Center, University of Toronto, Canada). All sample preparation and interpretation of the results was conducted by the author. Foraminifer counting was performed by Dr Soledad Garcia-Gil (Dpto Geociencias Marinas, University of Vigo, Spain). Sample pre-concentration and results interpretation was conducted by the author. Pore water sulphate and chloride analysis of the Dunmanus Bay core was performed by Dr Carlos Rocha (Trinity College Dublin, Ireland). Benthic survey along with data processing and preliminary interpretation was conducted as contract analysis by AQUAFAC International Services Ltd., Ireland during research cruise CE09_023 organized and led by the author.

Table of Contents

CHAPTER 1 – INTRODUCTION

1.1 Pockmarks as seabed structures

1.1.1 What are pockmarks?

Pockmarks are a specific type of geological setting resembling craters or pits (Figure 1). These recently discovered geological facies are hard to observe because they are predominantly found in inaccessible aquatic environments on Earth (Judd and Howland, 2007). Pockmarked seafloor is often compared to the lunar surface and according to Schumm (1970) some lunar surface features could have been formed in the same way as terrestrial pockmarks. Similarly, high resolution data obtained from the Mars Global Surveyor satellite revealed pockmark-like features on Mars (Komatsu et al. 2000). Generally, terrestrial pockmarks can be described as shallow depressions usually formed in the soft, fine-grained seafloor surface (Hovland and Judd, 1988).

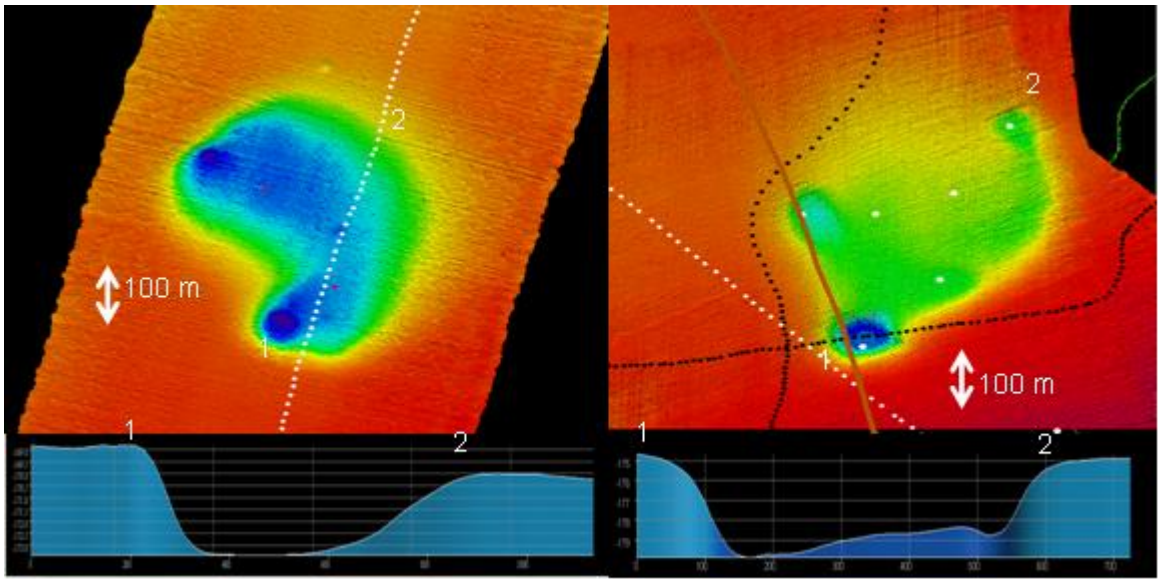

Figure 1. Shaded relief bathymetry image and depth profiles of pockmark features of the Malin Sea. Dotted lines depict electromagnetic (EM) survey transect lines of the vessel, red and white dots depict sampling sites (Monteys et al. 2008a).

Pockmarks are usually sub-circular but can be elongated by currents and resemble ellipsoidal craters (Josenhans et al. 1978; Boe et al. 1998) or composite when two or more pockmarks merge (Stoker, 1981). Asymmetric, elongated and trough-like pockmarks have also been reported (Hovland and Judd, 1988). Pockmarks are widespread and have been reported in a variety of aquatic environments such as lakes or deltas as well as in oceans, seas and estuaries (MacDonald et al. 1994; Dando et al. 1991; Taylor, 1992; Berkson and Clay, 1973; Hovland et al. 1997). At present, no differences have been identified between freshwater, seawater and estuarine pockmarks. They can be found isolated, occurring in groups referred to as "pockmark fields" (which may exceed 1000 km^2) (Fader, 1991, Kelley et al. 1994) or as large chains of craters known as "pockmark trains" (Pilcher and Argent, 2007). With diameters of up to 2000 m and depths reaching 45 m pockmarks comprise an interesting and important component of the seabed's morphology.

1.1.2 Historical background

Elusive to the scientific community which regarded them as geological curiosities, pockmarks were finally uncovered thanks to the development of the side-scan sonar and towed photographic cameras in the mid-1960s. This new technology made detailed seafloor mapping possible and revealed the abundance of previously unknown seafloor morphological features such as mud volcanoes and hydrothermal vents. Shortly after the first pockmark had been explored by a manned submersible dive offshore Nova Scotia (1969), the first scientific paper related to pockmarks by King and MacLean (1970) was published. In the next decade marine scientists reported pockmarks in numerous locations in different parts of the world. With the use of modern high quality 2D and 3D seismic technology, scientists have been able to confirm that pockmarks are not necessarily recent features but rather a result of natural processes taking place on geological time scales. Cole et al. (2000) reported large pockmarks of Palaeogene age in the North Sea, hidden under the contemporary seabed. These erosive features were located beneath the pockmarked Witch Ground Basin which strongly suggests historical continuity of pockmark formation processes. Solheim and Elverhoi, (1993) also reported relict features in the Barents Sea created at the end of the last glacial period when retreating ice sheets triggered rapid methane hydrate dissociation resulting in an explosive pockmark formation. Based on combined acoustic and geochemical evidence Solheim and Elverhoi, (1993) concluded that deep, thermogenic gas source is responsible for formation of these features.

There is also evidence of fluid flow in historical records, some dating as far as 2000 years ago. Petroleum products from areas where hydrocarbon seeps frequently occurred were often

utilized by local communities. Native Americans impregnated their boats with tar, which was also used to fuel torches and lamps, insulate huts and baskets as well as improving hunting weapons. (Judd and Howland, 2007). Natural hydrocarbon deposits were also an inspiration to myths, legends and even religions. In Pitch Lake at La Brea, in southwest Trinidad, the largest natural asphalt deposit was for local tribes a manifestation of God's power and has been included in Arawak tribal mythology. Natural eternal flames of gas seeps were crucial in ancient Persian beliefs and are central to the Zoroastrian faith. Furthermore, a number of gas vents were reported in ancient times in the Olympos valley on the south coast of Turkey. The area known as the Yanartaş area or 'Flaming Rock' and its spontaneously ignited gas was used as a reference point by sailors and fire cults and led to the erection of a temple devoted to Hephaestus, divine protector of fire. Olympus flaming rocks are also a source to the first ever Olympic fire (Hosgörmez, 2006). These examples show the fluid flow is a global, widespread process and not limited to marine environments.

Submarine groundwater discharges, observed in ancient times, have been reported by Taniguchi et al. (2002). These non-petroleum seepages have been reported as far as 2000 years ago: a submarine spring offshore from Latakia, Syria in the Mediterranean which was used as a source of freshwater for the city; discharging groundwater in the Black Sea coast and coastal springs used by the Etruscans for "hot baths" are mentioned (Judd and Howland, 2007).

1.1.3 Formation of pockmarks

Since their discovery, numerous theories for the formation of pockmarks have been proposed. It has been suggested that terrestrial pockmarks may be sub-glacial or permafrost features, meteorite impact craters, World War II bomb craters, wrecks sites or even the nests of bottom-dwelling creatures including dinosaurs (Judd, 1981; Hovland et al. 1984; Judd and Hovland, 2007). In more recent years these theories have been revised in favour of the fluid migration theory proposed by King and MacLean (1970) in their pioneering work. Although not conclusive for all pockmarks, this theory is still the most robust and has been supported by a large volume of evidence provided by various authors (McQuillin and Fannin, 1979; Josenhans et al. 1978; Judd, 1981; Hovland, 1981a; 1981b; 1982; 2003). It suggests that two types of fluid are involved in the formation process of the majority of pockmarks: 1. groundwater springs or submarine groundwater discharges; 2. hydrocarbon gas, both biogenic and thermogenic in origin. Although fluids are commonly considered a synonym of liquids, the physical definition of fluid encompasses both liquids and gases. This is due to their shared physical properties that distinguish them from solids. Fluids contrary to solids cannot resist deformation caused by continuously applied shear stress.

Under such conditions fluids will '*flow*' and change shape as long as the force is applied. However liquids and gases respond differently to pressure. Liquids are considered incompressible as they resist change of volume with increasing pressure. Gases on the other hand are easily compressible. These properties are exploited in every day products such as pressured deodorants, where compressed gas is a carrier for cosmetic formulation. Similarly many scientific instruments require compressed carrier gas such as helium or hydrogen in gas chromatography systems. Pressure casings utilized in marine research are often in filled with incompressible oils to protect the content from great external pressures encountered underwater. Finally pockmark formation is only possible due to the ability of liquids and gases to '*flow*' through the pores and voids of the seabed. These buoyant fluids migrate from the source rocks through faults, cracks and discontinuities according to pressure gradients and exploiting every permeable formation to find their way to escape through the seabed. The migration pathways are not exclusively vertical and depend on the seabed structure and energy of the fluid. Fluid migration might be interrupted by impermeable barriers such as trap structures, salt deposits, compacted fine grained sediment formations, permafrost, gas hydrates or even ice. Fluid can be either trapped by the formation, resulting in accumulation to a point of seal failure, or redirected through more permeable bodies such as sand lenses or gravel patches. Judd and Hovland, 1988 (and recently Judd and Hovland, 2007) introduced a conceptual model of initial pockmark formation through a virgin seabed (Figure 2). In this model increased pore fluid pressure creates dome-like deformation of the sediment surface (A). This process is accompanied by multiple fractures and cracks in the seabed structure caused by fluid induced stress on the seabed. Eventually a hydraulic connection is established between the over pressurized fluid and the water column. In such a system the high pressure gradient becomes the main driving force of a violent release of the over pressurized fluid (B). These escaping fluids entrain bottom sediment and lift the fine grained material into the water column. Suspended sediment might be carried away by currents or redeposited depending on the grain size distribution. Generally fine grains remain suspended longer and strong bottom currents will transport them away from the pockmark while coarser grains are likely to settle within or close to the pockmark (C). As fluid migration intensity drops due to reservoir depletion the side walls of pockmarks collapse because fine sediments typical of pockmark areas can support only a very gentle slope marking the birth of a new crater. In this the model initial fluid escape through undisturbed seabed is violent and results in displacement of a large volume of surface sediment and disturbance of the sediment on the path of the escaping fluid. Due to the destructive character of the formation of a new pockmark the old main migration pathway might be altered or sealed shut. In such case subsequent venting events might be as violent as the initial formation event. However the extent of sediment disturbance depends on the pressure gradient, sediment structure and the volume of migrating fluid. In extreme scenarios fluidisation

and liquefaction of the sediment might take place resulting in formation of mud and sand volcanoes, clastic dykes and sometimes pockmarks. In cases of milder events, established hydraulic connections are likely to be utilized by the migrating fluids in the future producing less violent venting events. However the simple model discussed above is based on the most commonly encountered fluid accumulation and subsequent migration scenario. Comparing this model with detailed settings studies we discover that in many cases sediment structure is not uniform and permits other fluid migration mechanisms. Woolsey et al. 1975 and Nichols et al. 1994 reported that sediment structure, particularly grain size differences between layers and fluid migration intensity might result in different escape features. Coarser material, such as gravel, presents no sufficient resistance and does not allow accumulation of fluids in the subsurface. Freely escaping fluid does not have sufficient energy to entrain the grains thus no seabed escape feature is formed. However, decreasing grain size of the seabed sediments causes more and more of fluid to be accumulated, over pressured and subsequently released with greater force. Both authors concluded that pockmarks are most likely to be formed with seabed seals composed of silts and clays.

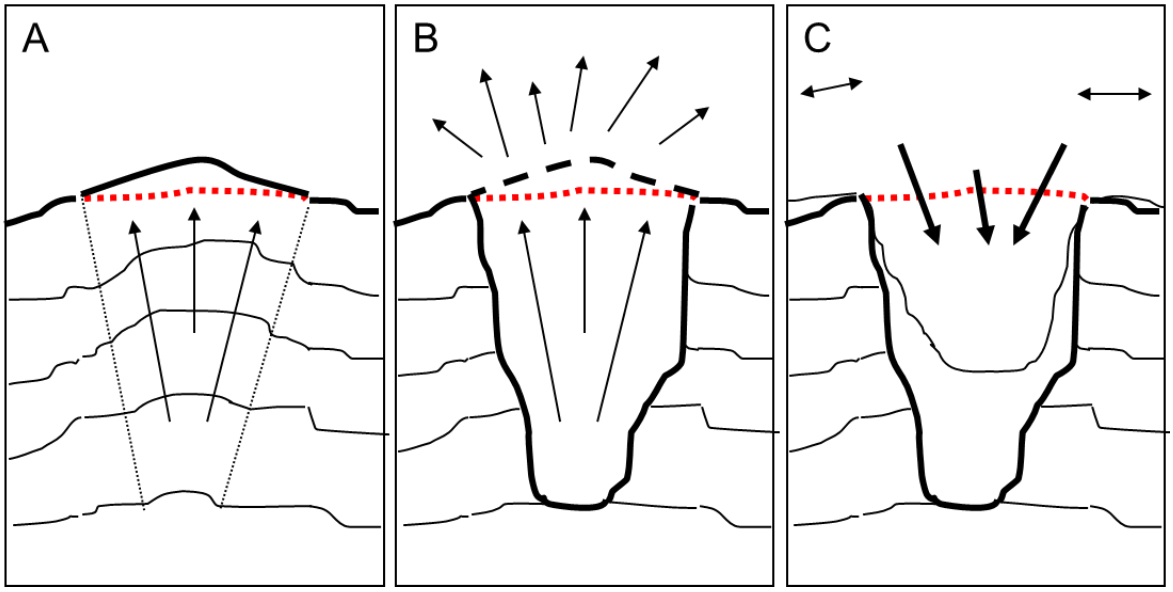

Figure 2. Suspected pockmark formation mechanism. A - seabed doming caused by increasing fluid pressure; B - blow-out of the gas charged sediment and creation of the sediment plume in the water column; C - sedimentation of the coarse material and the fine grains, joint with side walls slumping. Red dotted curve depicts initial seabed profile. Concept after Hovland and Judd, 1988.

These sediment classes offer enough resistance to over pressure fluids and cause doming of the sediment as described by Judd and Hovland, 1988 and 2007. Hydraulic connection between over pressured fluid and the water column might be established as a direct effect of fluid capillary movement creating doming, cracks and fissures. However this process can be also influenced by

external forces often referred to as the '*triggering events*'. In the context of pockmark formation three types of triggering effects are often mentioned: earthquakes, human activity and natural processes affecting the hydro- and lithostatic pressure on the fluid facies in the sediment such as wave and tidal activity, sediment loading and unloading and long term changes in the sea level (Judd and Hovland, 2007).

Since evidence of active fluid venting, even in thoroughly studied settings, is scarce other formation theories have been also been proposed. Paull et al. 2002 suggested a *"freshwater ice rafting"* mechanism, where periodically freezing freshwater can bind and eventually float the sediment away resulting in shallow pockmark formation. Permafrost can reduce sediment permeability and therefore create favourable conditions for gas entrapment. The accumulated gas can be released violently when the ice seal melts and the permeability of the sediment is restored (Bondarev et al. 2002 and Kvenvolden et al. 1993). Boulton et al. 1993 reported cases of ice sheet induced groundwater discharges which could be linked to pockmark formation. In such a system stress imposed by ice sheets increases pore water pressure which escapes through the sediment, collapsing the seabed.

1.1.4 Detection of pockmarks, shallow gas and other fluids in the water column and the sub surface

Terrestrial pockmarks are predominantly located in inaccessible aquatic environments. Early hydrographic surveys were able to detect depressions in the seabed but imperfect equipment could not provide any answers about the origins of these features. The development of side-scan sonar technology and towed photographic cameras in the late 1960s revealed that some of the depressions are something more than bathymetric anomalies. The most obvious proof of fluid presence in the seabed is visually observed seepage. However, active seepage is rare, often periodic and difficult to observe in deeper waters (Judd and Howland, 2007). The formation fluids: liquids (groundwater) and gases (C_1-C_4 hydrocarbons) have different properties that allow the detection of their seepage. Groundwater expulsions can be detected by means of tracking the salinity changes in the water column surrounding the studied area. This analysis can be performed *in situ* with use of commonly employed conductivity, temperature and depth sensors (CTDs). The CTD is often mounted on a rosette frame that additionally allows collection of discrete water samples from selected depths for further analysis. However, this instrument is incapable of reaching the seabed. For practical and safety reasons it must be maintained a few meters above the seabed. In settings where gentle groundwater seepage is expected and strong bottom currents are present the salinity changes might not be recorded accurately. Alternatively, similar low-powered CTD sensors can be

mounted on autonomous instruments such as remote operating vehicles (ROV), autonomous underwater vehicles (AUV) and manned submersible vehicles (MSV) for more detailed examination (e.g. Christodoulou et al. 2003). Similarly the detection of dissolved methane or hydrogen sulphide can be recorded by commercially available underwater sensors such as METS sensor (Franatech GmbH, Germany; e.g. Garcia and Masson, 2004; Newman et al. 2008; Christodoulou et al. 2003). However, modern seismic and acoustic instrumentation can detect gas presence without employment of expensive ROVs, AUVs, MSVs or towed underwater video systems (Underwater TV) which are most commonly used for visual inspection of the seabed. The most commonly employed remote systems for gas detection are: single and multibeam echo sounders (SBES and MBES), side scan sonars (SSS), high frequency sub-bottom profilers (SBP) and high powered 2D and 3D seismic systems. Both seismic profilers and hydro acoustic systems utilize sound waves to gather information about the sediments and the water column. The different acoustic impedances of water, gas and sediment layers made it possible to distinguish between gas affected sediments and virgin seabed. Moreover they provide valuable information about seabed geology and basin evolution through time. However the properties of gas in the subsurface are among others a function of the type of the sedimentary body in which they are dispersed. The acoustic properties of gas bubbles in the sediment and water column change with their size and with the wavelength of the applied acoustic beam. When an acoustic wave passes through a gaseous body the speed of sound is reduced, sonic energy becomes scattered and sound attenuation increases (Hampton and Anderson, 1974; Wilson et al. 2008). The change of these parameters is closely related to the bubble radius which affects the bubble resonance frequency, the so called Minnaert resonance (Devaud, et al. 2008). When the acoustic frequency of the emitter matches the acoustic frequency of the bubble it causes the bubble to behave as a harmonic oscillator which results in the acoustic signal attenuation rising to its maximum. The acoustic frequency is inversely proportional to wavelength of the acoustic pulse. Therefore we can also say that the maximum attenuation is observed when the wavelength of the acoustic signal of the emitter is optimal to cause harmonic oscillation of the bubble (Judd et al. 1997). In cases where bubble radius is considerably smaller than the wavelength of the acoustic signal the sound velocity decreases substantially with moderate increase of signal attenuation. If bubble radius is larger than that of the wavelength the signal is effectively scattered (Judd and Hovland, 2007). However in a reality the bubbles exist in a range of sizes limited only by porosity of the sediment. Also the modern acoustic and seismic instrumentation emits a broad range of frequencies causing all of the above mentioned acoustic responses to be found simultaneously. This approach is not without limitation as sound wave propagation through the water column and sediment is limited by the absorption of the acoustic signal which is linked to the signal frequency. Low frequency systems can penetrate deep into the

seabed at a cost of decreased resolution. They are invaluable in deep gas prospecting. High frequency systems on the other are more versatile and can be used to study the water column (e.g. sonars), topography of the seabed (e.g. SBES, MBES and SSS) as well as the first ten of meters of seabed (e.g. SBP).

The acoustic properties of the gas bubbles in the sediment (Wilkens and Richardson, 1998) and in the water column (Jackson et al. 1998) make interpretation of acoustic data challenging. The acoustic response of gas results in complex and often subtle signals that can be accurately ascribed only with thorough understanding of the setting and applied methods. In practise the interpretation of acoustic profiles and seismograms comes down to isolation of characteristic anomalies that are not present in the unaffected seabed and show acoustic characteristics of fluid presence or presence of fluid altered (disturbed) sediment. According to Schubel, 1974 as little as approximately 0.1% (v/v) of gas present in the sediment can reduce the speed of sound penetrating a sedimentary body by a third. This change is reflected in the seismograms as characteristic visible patterns (e.g. Kim et al. 2008). There are several types of signals that over the years have been ascribed to fluid presence and fluid reworked sediments (reviewed by Schubel, 1974 and recently by Judd and Hovland, 1992 and Judd and Hovland, 2007):

- Acoustic turbidity (AT). This signal can be described as chaotic reflectors created by absorbed and scattered acoustic signals. On sub bottom profiles they can be spotted as dark smears creating discontinuities or masking of sediment layering. Often indicative of so called “gas front” which is the upper boundary of the shallow gas accumulation. Because of the acoustic signal absorption this signature is frequently encountered with another type of signal so called acoustic blanking. Many authors do not distinguish between those two signals and use them interchangeably.
- Acoustic blanking (AB). This signal has a form of weakened or absent reflectors. The exact meaning of the AB is poorly understood and widely debated. This signal is likely to be indicative of active fluid migration or fluid related sediment structure alteration, particularly when other evidence of fluid presence is recorded. However acoustic signal effects such as signal starvation cannot be ruled out (Judd and Hovland, 2007). As mentioned above AB is often linked with AT and can be result of signal absorption by overlaying gas bearing sediments. AB often has vertical orientation. AB in the sub bottom profiles can be described as white patches encountered within the acoustic penetration range.
- Enhanced reflectors (ER). This signature has the form of strong lateral reflectors caused by back scattering of acoustic signal. It can be observed isolated or extending from areas of AT. According to Judd and Hovland, 1992 ER are associated with minor gas accumulations

formed in permeable facies of sediments such as silts rich in sands. Change in the size of pore voids in such facies permits formation of larger gas bubbles that scatter acoustic signal more effectively.

- Columnar disturbances (CD). Often referred to as '*gas chimneys*', CDs are vertical signatures in the form of disturbed reflectors or acoustic transparent areas similar to those typical of AB. They reflect vertical fluid migration and migration induced sediment disturbance. They often coincide with sediment doming.
- Sediment doming (SD). This signature has the form of low profile crescent-shaped relief observed on top of the seabed often associated with CD. This signature visualizes swelling of the seabed caused by over pressured fluid in the sub surface. SD occurs mainly in seabed with fine grained sediments overlaying more permeable formations.
- Gas plumes (P). This signature is observed in the water column in the form of acoustic reflectors caused by scattering and acoustic resonance of gas bubbles. Plumes are usually vertical, columnar signatures though they can have hyperbolic shape (so called '*comet marks'*) caused by different ascension speeds of bubbles of different sizes. In practise plumes are difficult to distinguish from fish shoals since air in swim bladders produce a similar signature to that of seeped gas. A good indicator distinguishing between the two is the direction of migration of the acoustic target. Fish shoals will most likely move on a horizontal plane while escaping gas will migrate strictly upward with some offset caused by currents. Moreover Judd et al. 1997 concluded after analysis of fish shoals behaviour and acoustic signatures typical of fish that "*seepage bubble streams are likely to be vertically-extended, whereas shoals of fish are more likely to be diffuse and horizontally-extended*".

There also other commonly reported signatures typical for deep seismic data such as: bright spots (equivalent to ER in sub bottom profiles), signal pulldowns (effect of decreased sound velocity in the form of a hyperbolic reflector), flat spots (reflector caused by acoustic impedance difference at the boundary of gas accumulation), pagoda structures (trapezoidal areas of AT) and bottom-simulating reflectors (BSRs; strong backscatter reflectors similar to those typical of hard ground). However in this work seismic data is not presented therefore these signals will not be discussed in detail. Although geophysical instruments can provide valuable information about physical properties of the seabed they cannot provide information on the geochemistry of the sediments. To understand the nature of the accumulated or vented fluid ground-truthing activities must be conducted.

1.1.5 The distribution of pockmarks around the world

Pockmarks have been reported in numerous locations in different types of aquatic environments. However, the global distribution of these features suggests that there are types of oceanographic settings where pockmarks occur more frequently than others. These settings usually have relatively high sedimentation rates, contain fine-grained sediments and are rich in organic matter. Coastal settings such as lagoons, raises (flooded), fjords and deltas or plains are believed, among others, to be pockmark prone (Judd and Howland, 2007). In these settings a constant flux of sediment and organic rich debris carried by rivers creates favourable conditions for pockmark formation. Similarly in quiet bays and coves sheltered from strong currents and atmospheric influence microbial activity drives shallow anoxia in sediments and creates optimal conditions for microbial methanogenesis. In these settings, biologically driven gas production saturates the sediment with methane which may result in pockmark formation or aid the process (Nelson et al. 1979; Pimenov et al. 2008). On the continental shelves, especially in sedimentary basins, organic matter accumulates and is diagenetically transformed by biotic and abiotic processes (Newman et al. 2008). These early and late diagenetic transformations fuel processes that have the capability to alter the seabed morphology. Also parts of the continental slope are frequently marked with pockmarks especially where less active sediment transport from the shelf creates accumulations of sedimentary matter similar to shelf basins (Paull et al. 2002; Casas et al. 2002). On the continental rise, seepages are likely to occur in the characteristic sediment accumulations in the vicinity of major rivers. These so called deep-sea fans are created during submarine landslides also called turbidites (Gontharet et al. 2007; Pierre and Fouquet, 2007). Turbidites happen periodically when the sedimentary material accumulated on the continental slope over the years reaches critical mass and slumps down the slope onto the continental rise. Deep-sea fans resemble alluvial fans found on land. There are only a few examples of pockmarks in the abyssal plains (4000-6000 m). Blake Ridge (east off shore Florida, South Carolina; USA) methane hydrate related pockmarks are a good example (Flood, 1981). Nevertheless there are a number of features such as troughs, craters and considerably thick (up to 1 km) deposits of sediments called *contourites* created by deep water currents that may be affiliated with seabed fluid flow (Judd and Howland, 2007). Pockmarks may also be found near plate tectonic settings, especially in locations with thick sedimentary layers (Orange et al. 1999; Lorenson et al. 2002). However in most of these settings the energy and volume of expelled fluids promotes other morphological features such as mud volcanoes, hydrothermal systems and others (Jamtveit et al. 2004; Suess and Massoth, 1984; Davis et al. 1987).

1.1.6 The distribution of pockmarks around Great Britain and Ireland

Shallow gas accumulations and pockmark features are widespread around the Great Britain and Ireland (Figure 3). The discovery of petroleum and gas fields in the North Sea over 150 years ago triggered intensive prospecting and mapping efforts led by national survey agencies which greatly improved the knowledge of the seabed morphology in this part of the World. On the United Kingdom Continental Shelf (UKCS), Irish Sea and the North Sea mapping efforts were led by British Geological Survey (BGS), British Petroleum (BP) and Statoil. On the Irish Continental Shelf seabed mapping was conducted through national seabed survey programs: the Irish National Seabed Survey (INSS) and its successor the Integrated Mapping for the Sustainable Development of Ireland's Marine Resources programme (INFOMAR) coordinated by Geological Survey of Ireland (GSI) and Irish Marine Institute (MI). Moreover at least several multidisciplinary projects targeted seeps, seep related structures and fauna in these waters: Mapping of the European Seabed Habitats (MESH), Chemosynthetic Ecosystem Science programme (ChEss) part of the Census of Marine Life (CoML), Atlantic Coral Ecosystem Study (ACES), Environmental Control on Mound Formation Along the European Margin (ECOMOUND) and sister GEOMOUND programme, Hotspot Ecosystem Research on the Margins of European Seas programme (HERMES) and notably UNESCO Training Through Research programme. However, despite extensive surveying the number of confirmed and reported active seeps is very small in contrast to the widespread presence of shallow gas in this area (Judd and Hovland, 2007). Detecting and confirming the presence of an active seepage requires use of several tools, which are not routinely used during mapping cruises, such us underwater video equipment, ROVs and manned submersibles. Moreover understanding the nature of the fluid requires a targeted approach with ground-truthing of both sediment and the water column.

Because of cost and equipment availability acoustic evidence of gas presence in the water column is often accepted as sufficient particularly when there is other indirect evidence of gas presence in the studied area such us a gas accumulation in the sub surface or presence of methane derived authigenic carbonates (MDACs). Using this approach Judd et al. 1997 utilized archive shallow seismic profiles and included acoustic properties of gas bubbles in the water column to estimate that on the UKCS alone, excluding North Sea there are approximately 173 000 seeps (Figure). Regrettably there are no published estimates of seep occurrences and their density in the Irish Exclusive Economic Zone (IEEZ). In the North Sea pockmarks are mainly present in the Witch Ground Basin (Dando et al. 2007) and the Norwegian Trench (Hovland, 1981). These pockmarks were predominantly created in the postglacial muddy sediment formations.

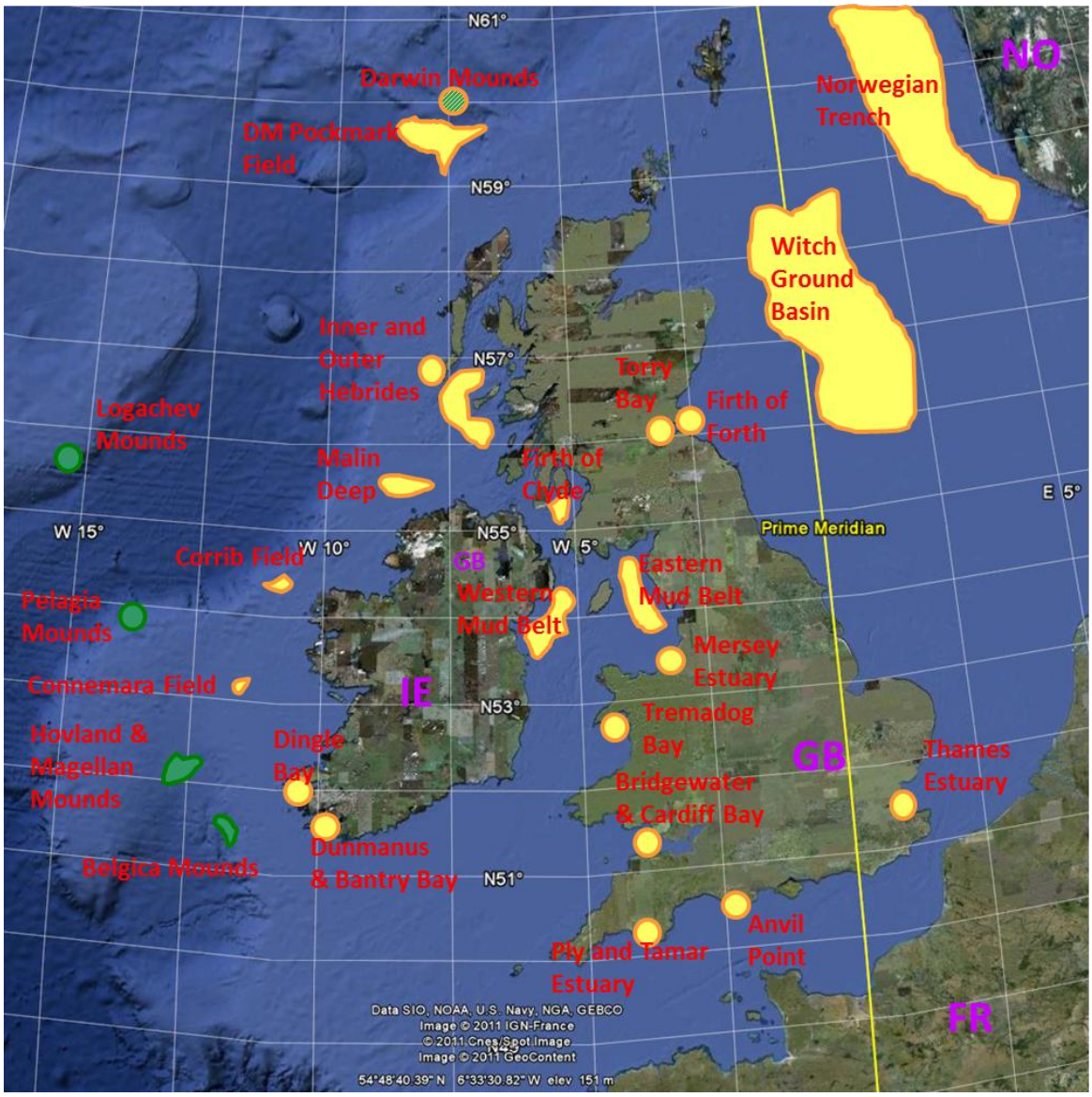

Figure 3. Locations of seeps and seep related structures around the Great Britain and Ireland. Yellow areas denote locations and approximate surface area of shallow gas accumulations and pockmarked seabed. Green areas denote location of areas with accumulations of biologically derived structures. Darwin Mounds are seep derived, however the cold water corals have adopted the MDACs as support for their colony (see text). Image created with Google Earth. For references see text.

However the gas in this area is mainly thermogenic in origin from Carboniferous and Jurassic sedimentary formations (Cornford, 1998). Accumulations of similar origin are also present in the Torry Bay, Firth of Forth, in waters of near to Anvil Point (Judd et al. 2002; Selley, 1992) and in Codling Fault where abundant MDACs mounds were reported (Judd et al. 2007; Croker et al. 2005). Organic rich Tertiary and Quaternary deposits as well as buried peats and lignites are also a common source of microbial gas around Great Britain and Ireland (Judd and Hovland, 2007). In the

North Sea (Block UK 15/25) giant pockmarks (named Scanner, Scotia and Challenger) were reported with gas originating from ancient peat (Hovland and Sommerville, 1985; Judd and Hovland, 2007). In the sediments of the Thames estuary (Judd and Hovland, 2007) and in the Inner Hebrides (Farrow, 1978) shallow gas accumulations are possibly related Quaternary and Tertiary formations. In a review by Taylor, 1992 other near shore gas occurrences are reported in major estuaries, bays and fjords such as Mersey, Tees, Ply, Tamar, Bridgewater, Cardiff and Tremadog. Similarly in the Inner Hebrides Taylor, 1992 suggest microbial sources. In the Irish Sea shallow gas and pockmarks are found predominantly in the areas of Western and Eastern Mud Belts as well as in the Firth of Clyde (Yuan, et al. 1992; Judd et al. 2007). Pockmarks and seeps were also reported in the Outer Hebrides and Rockall Trough which was targeted by the petroleum industry (Hitchen and Stoker, 1993 and Waddams and Cordingley, 1999). There are extensive pockmark fields and shallow gas occurrences in the Malin Deep area on the Malin Shelf (Monteys et al. 2009). This area received very little scientific attention in comparison to other areas on the Atlantic Margin. Further west, across the Rockall Trough and south, on the Porcupine Bank and the Porcupine Seabight, abundant carbonate mound structures were reported (Wheeler, et al. 2007). To date no association of these features with gas seeps have been found. Kenyon et al. 2003 suggested that these structures have been derived from cold-water corals (*Lopheria pertusa* and *Madrepora oculata*) rather than MDACs. However similar features in the northern part of the Rockall Trough are found in the vicinity of pockmarks and detailed studies revealed that they are a product of non-biological fluid related processes (Masson, et al. 2003). Pockmarks have been found on the seabed above the majority of Irish hydrocarbon fields in both western and eastern waters (Games, 2001 and Bentham, et al. 2008). Finally pockmarks have also been reported in some of the western Irish bays such as Dingle Bay, Bantry Bay (Monteys, 2009 personal communication) and recently discovered pockmarks of Dunmanus Bay (Szpak et al. 2009).

It is clear that shallow gas and its various seabed surface expressions are abundant in the waters around Great Britain and Ireland. There are areas however that received very little attention and are unknown to the wider scientific community. Almost no scientific publications discuss the extensive shallow gas and pockmarks form the Malin Shelf area. Despite interesting geology, reviewed by Dobson, 1974 and excellent, publically available data sets collected by the INSS and INFOMAR programmes. Similarly occurrences of pockmarks in Dunmanus Bay, Co Cork have not been reported to the scientific community.

1.1.7 Importance of pockmarks and pockmark related fluid flow occurrences

1.1.7.1 Contribution to carbon cycle

Studies on the impact of pockmarks on the environment and their significance for man have provided a vast amount of evidence to suggest that these are interesting and important geological features. From a global point of view, as pockmarks comprise one of the geomorphological indications of fluid flow, and gas flow in particular, they may be considered as contributors to the global methane and carbon cycles. So far however, no attempt has been made to estimate their isolated input (Judd and Hovland, 2007). Furthermore, poor knowledge about other oceanic methane sinks and sources makes it very difficult to speculate about the overall oceanic contribution to the global methane cycle (Lambert and Schmidt, 1993). Generally accepted estimates of oceanic methane emission range from 1.3 x 10^{12} g CH_4 / year to 16.6 x 10^{12} g CH_4 / year (Ehhalt and Schmidt, 1978). These estimates suggest that oceans are a minor source of methane emissions to the atmosphere but Judd and Howland, 2007 argue that this conclusion is premature. They suggest that these and subsequent approximations were based on very small data sets of limited flux measurements. An interesting study performed by Owens et al. 1991 for example suggests that an area representing 0.43% of total ocean's surface "*can contribute between 1.3 to 133% of the total oceanic flux of methane*". Based on this and other studies they conclude that this discrepancy clearly suggests that global methane fluxes need to be revised. Methane input to the atmosphere estimated by Kvenvolden et al. 2001 is based not only on flux sizes but also the availability of geological methane to the seabed. This estimation suggests that geological sources such as seeps, mud volcanoes and gas hydrates provide 30 x 10^{12} g CH_4 / year to the seabed. The loss to the water column (due to dissolution, oxidation and methanotrophic activity) reduces this flux to around 20 x 10^{12} g CH_4 / year (10 to 30 x 10^{12} g CH_4 / year). These first estimates are clearly conservative approximations especially when taking into account the limitation of the data sets they were based on as well as the geological and geographical context. Studies such as this by Owens et al. 1991 show that understanding of sinks and fluxes of methane in contemporary oceans is still poor and that estimates of methane emission from the oceans must be studied further. Recent reviews by Judd, 2003 and 2004 outline the importance of the seabed methane contribution. Judd and Howland, 2007 suggest that an additional 11 to 18 x 10^{12} g CH_4 / year should be included in the seabed budget (based on the findings of Bange et al. 1994). Therefore, the proposed contribution increases to 21 -

48 x 10^{12} g CH_4 / year (4 to 9% of global budget). However to understand the importance of these estimates they need to put in the right context.

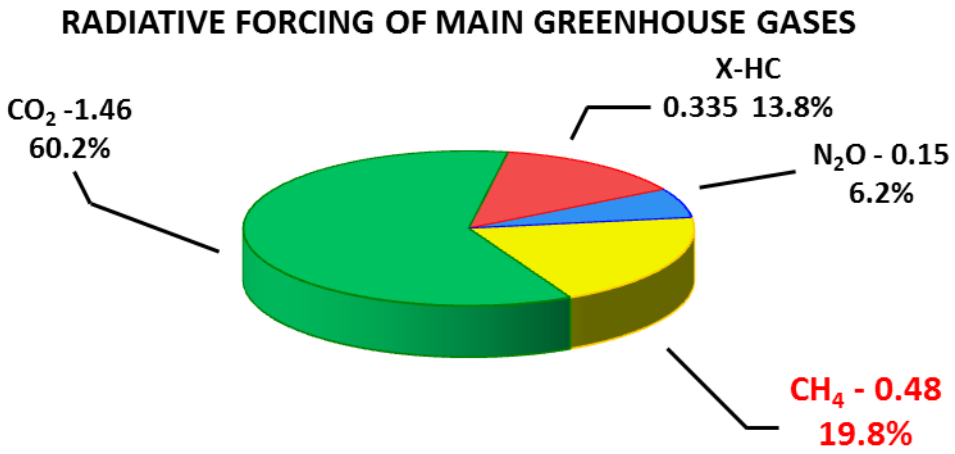

Figure 4. Radiative forcing of main greenhouse gases including the anthropogenic halogenated species (X-HC). All values in W/m^{-2}, values below denotes percentage of total forcing. Data after Climate Change 2001: The scientific basis by IPCC.

The best way to achieve that is to look in more detail into the seepage associated methane cycle and its individual fluxes, processes that govern them and the impact on global cycles. In general carbon cycling can be described as a suite of major environmental processes that exchange carbon between its major reservoirs. Although the oceans are an important component of the carbon cycle, oceanic carbon is mainly in a form of carbon dioxide and carbon dioxide derived species. When considering methane (CH_4) as a carbon source, oceans are believed to be a minor contributor (Raven and Falkowski, 1999) with an emission to the atmosphere ranging from 1.3 x 10^{12} g CH_4 / year to 16.6 x 10^{12} g CH_4 / year (Lambert and Schmidt, 1993). Current knowledge about methane's oceanic sinks is still poor (Judd and Howland, 2007) and these estimates are subject to intensive research worldwide (Ehhalt et al. 2001). Methane is the most common fluid involved in the pockmark formation process and a potent greenhouse gas (Judd and Howland, 2007). Although methane's concentration in the atmosphere is considerably lower than carbon dioxide (363 ppmv of CO_2 and 1745 ppbv of CH_4 in 1998), methane is approx. 25 times more effective in trapping heat and is responsible for about 20% (0.48 W/m^{-2}) of the total radiative forcing of the so called long-lived greenhouse gases (Figure 4). Radiative forcing describes the change of irradiance of the tropopause,

the lowest of atmospheric layers due to external factor change (sun activity, greenhouse gas concentration). Radiative forcing values are often reported as relative to those from year 1750 (IPCC) which marked the beginning of anthropogenic influence on atmospheric composition (Highwood et al. 1999).

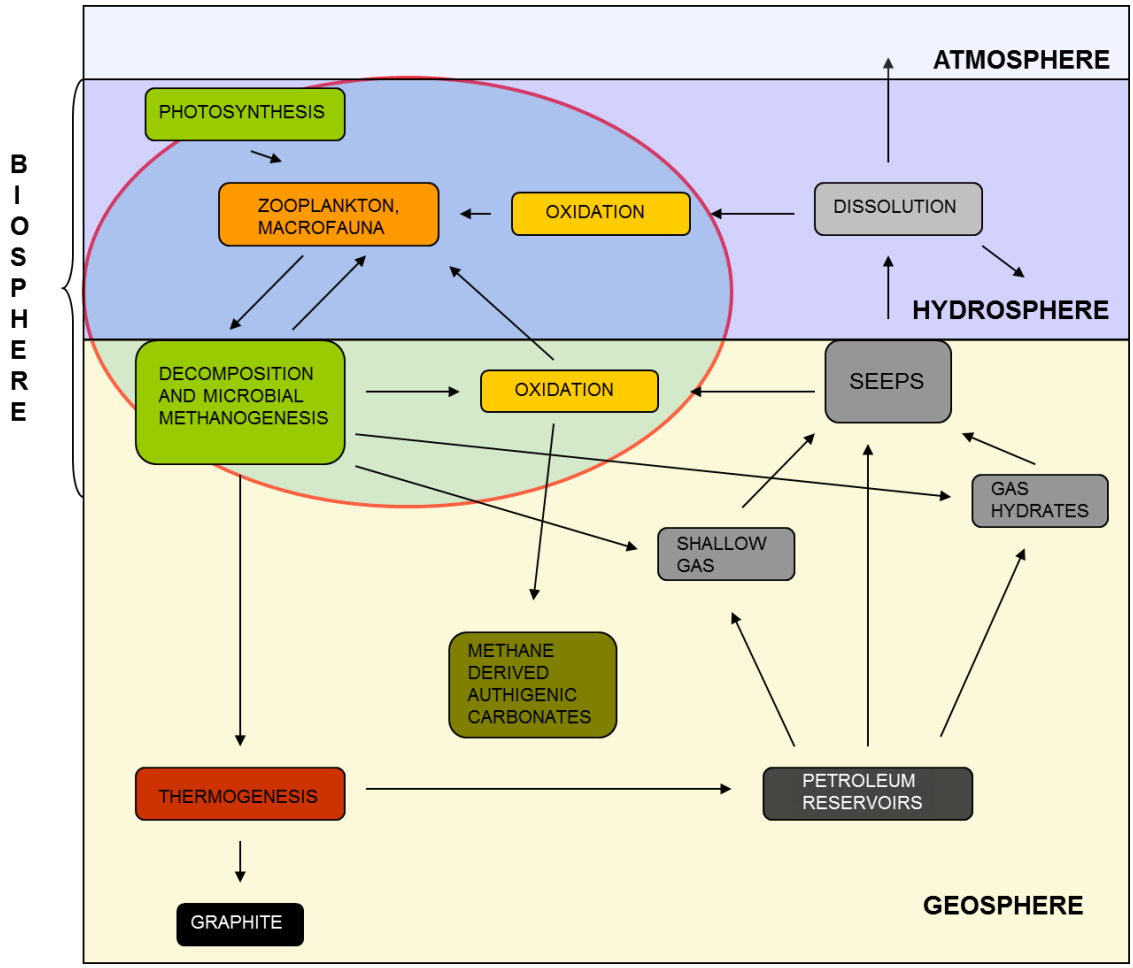

Figure 5. Diagram illustrating fate of marine methane in relation to the global carbon cycle. Redrawn from Judd and Howland, 2007.

Since 1750's methane concentration in the atmosphere has risen threefold (from 650 ppbv to approximately 1800 ppbv in 1998) and is still rising. Seabed methane emissions have not yet been widely recognized by the scientific community and are rarely included in the global carbon cycling budgets. This is a result of vast gap of knowledge about fluxes of methane in the subsurface. Judd and Hovland, 2007 point out that currently researchers (e.g. IPCC) and textbooks do not recognise the seabed as a methane source in the carbon cycle estimates. Methane seems to be mentioned mainly in the context of petroleum and its exploration: "*Indeed, it seems to be generally accepted that the only natural flux of carbon across the seabed interface is the burial of organic matter,*

which becomes incorporated in petroleum, gas hydrates, and limestone reservoirs. Commonly, the only recognized marine return pathway is extraction of petroleum by the oil and gas industry". Methane is a relatively labile carbon form and can undergo rapid transformations that are challenging to study. Moreover as mentioned in the previous paragraphs seeps are spontaneous and unpredictable phenomenon, which makes direct studies difficult to organise and conduct. Widely used acoustic methods are also imperfect and do not allow estimation of reservoirs and shallow gas accumulations. These are some of the reasons behind the lack of understanding of seep associated methane fluxes and sinks. Based on their review of various fluid flow settings Judd and Howland, 2007 propose the following fluxes and reservoirs as revised seabed methane cycle components (Figure 5):

- the migration of methane to the seabed;
- incorporation of methane into gas hydrate reservoirs;
- methane transformation at the seabed and associated fluxes to the biosphere (biomass) and the methane derived authigenic carbonate (MDAC) reservoir;
- the migration of methane into the water column;
- microbial oxidation in the hydrosphere (biomass);
- emission to atmosphere.

Although these fluxes are based on known and understood processes, due to insufficient research they are not easily quantifiable. Methane cycling in the water column on the other hand involves much better studied and understood groups of processes. Methane concentration in the oceans varies with depth (Figure 6). The major flux of methane in oceans comes from the microbial methanogenesis process in the photic zone (F_5) and transportation from rivers and estuaries (F_1). Although approximately 90% of the methane in rivers and estuaries does not reach the ocean (Upstilll-Goddard et al. 2000) and is either emitted to the atmosphere (94%) or oxidized (6%) it is still a major source. Despite these losses the overall methane concentration in rivers (Upstilll-Goddard et al. 2000) and estuaries (Sansone et al. 1999) is higher than shelves (Kelley, 2003) and open oceans (Holmes et al. 2000) and creates a positive concentration gradient. Further distribution of methane is affected by perturbation due to water mixing during weather events (F_3), air and sea exchange (F_2) and upwelling processes (F_4). Fluxes F_3 and F_2 are of particular importance because of the supersaturation of the surface oceanic water with methane (Lambert and Schmidt, 1993). Methane concentration in the water column reflects the water stratification due to temperature, salinity and density differences (Figure 6,red curve). Surficial water (ZONE I) hosts intensive microbial activity especially in the photic zone with the methane production peak located in the so

called pycnocline (zone of rapid density change due to salinity and temperature fluctuation). Methanogenesis in this zone occurs in microenvironments of particles falling from the photic zone (F_5). In deeper waters (ZONE II) methane is a carbon source for methane oxidizing microorganisms and its concentration is low.

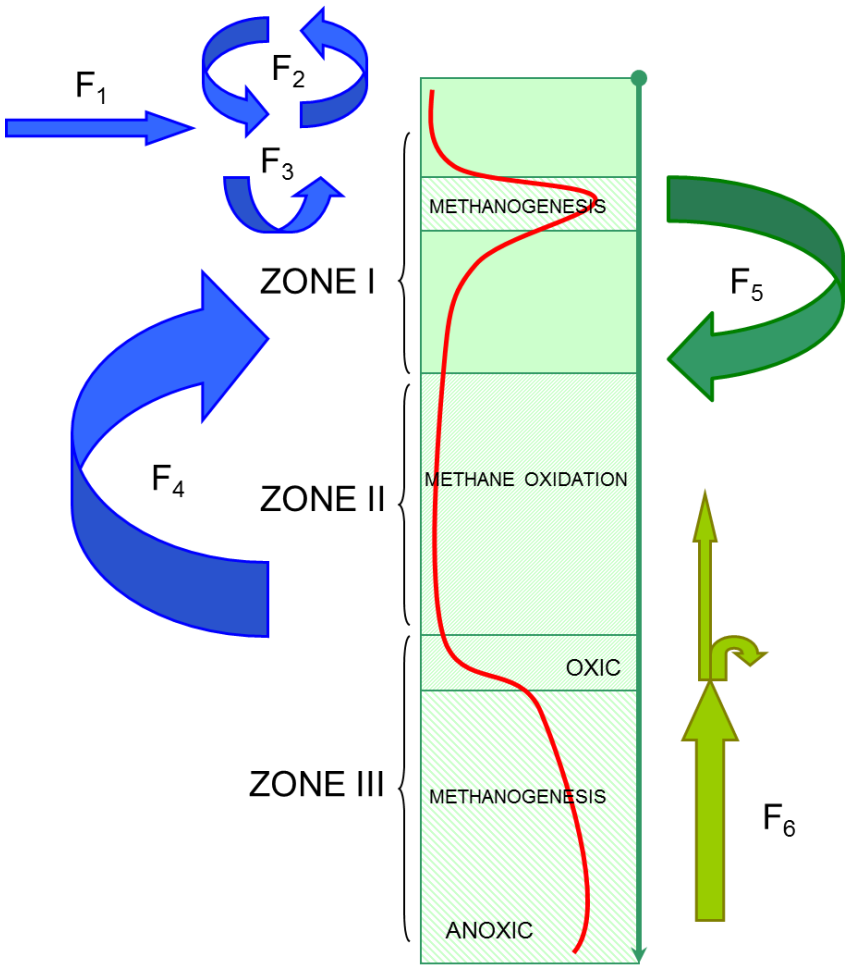

Figure 6. Methane cycle in the oceans, modified after Judd and Howland, 2007. Arrows are not proportional to the flux size, red curve depicts methane concentration change with the water depth.

In the sediments (ZONE III) methanogenesis can occur only under anoxic conditions because methanogenic *Archaea* (the only so far identified methanogenic microorganisms) are strict anaerobes. Exceptions such as *Methanosarcina barkeri* have been reported (Peters and Conrad, 1995) which shows that some methanogens can withstand prolonged oxygen stress (Kato et al. 1993; Estrada-Vasquez et al. 2003). Methane produced in the deeper sediments can be oxidized in the surface oxic sediment or in the water column and provided the flow is strong enough it can reach the upper parts of the water column (F_6). Oxygen penetration in sediment is believed to be very limited (excluding very sandy sediments), therefore depletion of methane in surface sediments must be driven by a different mechanism. In normal coastal sediments the oxic zone is usually a few

mm thick (Cai and Sayles, 1996) and microbial methane conversion into CO_2 has been suggested (Devol and Ahmed, 1981). This theory has been supported by a large body of evidence from methane profile measurements (Martens and Berner, 1977), radiotracer experiments (Iversen and Jorgensen, 1985) and stable isotope studies (Alperin et al. 1988) but until recently such organisms have not been identified (Boetius et al. 2000). Discovery of a microbial consortium of anaerobic methane oxidizers and sulphate reducing bacteria (AOM/SRB) revealed the mystery of methane disappearing in the upper parts of sediment (DeLong, 2000). The anaerobic methane oxidation (AMO) competes with reverse methanogenesis (RM) in the upper sedimentary layer often referred to as the sulphate-methane interface (SMI) or sulphate-methane transition zone (SMTZ). The biochemical mechanism is unknown but *Archaea* are suspected to reverse their normal metabolic pathway and oxidize methane instead of producing it (Equation 1). This metabolic pathway is energy efficient only if the hydrogen end product is quickly removed from the system and its concentration does not exceed a certain point (Hoehler et al. 1994).

$$CH_4 + 2H_2O \Rightarrow CO_2 + 4H_2$$

Equation 1. Reverse methanogenesis of *Archaea* in AOM/SRB consortia.

In the anoxic marine sediment SRB utilize excess H_2 produced by Archaea, to gain energy by converting sulphate into sulphide (Equation 2, see also Figure 8).

$$H^+ + 4H_2 + SO_4^{2-} \Rightarrow HS^- + 4H_2O$$
$$CH_4 + SO_4^{2-} \Rightarrow HCO_3^- + HS^- + H_2O$$

Equation 2. Hydrogen oxidation by SRB in AOM/SRB consortia and net AOM/SRB process equation.

Also methane from deeper abiotic sources that reaches the SMTZ through upward migration can be oxidized by AMO (F_6).

1.1.7.2 Pockmarks and gas and oil exploration

Pockmarks and seeps in general are valuable and effective tools for determining if a sedimentary basin has petroleum potential. Presence of seepage may indicate that source rocks are present and by the nature of fluid expelled, valuable conclusions on their maturity and origin may be drawn (Judd and Hovland, 2007). The distinction between microbial and thermogenic gas for instance, can made based on molecular composition of the gas or its isotopic signature. In the first

case so called *"wetness"* of gas (C_{2+}) is determined which is methane (C_1) to higher hydrocarbon (ethane C_2, propane C_3, butane C_4 and pentane C_5) ratio (Equation 3):

$$C_{2+} = \left[1 - \left(\frac{C_1}{\sum C_{1-5}}\right)\right] \times 100$$

Because microbial methanogenesis yields with exclusively methane while thermogenic processes produce also higher hydrocarbons assessing the relative contribution of higher components helps elucidate the source of methane. It is generally accepted that three classes of gas are distinguished by this method (Faber and Stahl, 1984; Floodgate and Judd, 1992). For $C_{2+} < 0.05\%$ the gas is considered microbial in origin, for $C_{2+} < 5\%$ the gas is considered dry and thermogenic and finally for $C_{2+} > 5\%$ we consider the gas wet and thermogenic. In case of petroleum fluids more classes are distinguished: the condensate ($C_{6\text{-}15}$), crude oil (C_{15+}), naphthenes (cycloalkanes) and aromatic hydrocarbons (Judd and Hovland, 2007). This classification can be supported by evaluation of the isotopic signatures of methane, so called carbon and hydrogen stable isotopic ratios ($\delta^{13}C$ and δD respectively reported in δ notation; Equation 4):

$$\delta_x = \left[\frac{(R_a)sample}{(R_a)standard} - 1\right] \times 1000$$

Where R_a is the ^{13}C / ^{12}C ratio or ^{2}H / ^{1}H ratio relative to Vienna PeeDee Belemnite (VPDP, $\delta^{13}C$ = 0‰, with ^{13}C / ^{12}C = 0.0112372 absolute ratio) and Vienna Standard Mean Oceanic Water (VSMOW, δD = 0‰, with ^{2}H / ^{1}H = 0.00015575 absolute ratio) standards. Isotopic signatures are widely accepted as useful indicators of shallow gas origin (Whiticar, 1999). However their interpretation must be conducted with great dose of scientific scrutiny as commonly reported cut off points for microbial ($\delta^{13}C$ between -60 and -80‰) and thermogenic ($\delta^{13}C$ between -60 and -20‰) sources vary and reported isotope ratio ranges overlap (Judd and Hovland, 2007). Cross correlation plots of both signatures are particularly useful as they can provide additional information on the nature of process involved and not only discriminate between biotic and abiotic sources (Figure 7). Similarly in case of petroleum, isotopic signatures can be applied to describe kerogen type. However, more commonly H / C and O / C ratios are used for that purpose. It is important to notice that most of the world's major petroleum reservoirs and many of largest known gas and oil fields have been discovered by drilling near or on seepage sites as pointed out by Hedberg, 1980. In the Santa Barbara Channel (California, USA), rich aquatic seepages have already been exploited. Between 1982 and 1987, 600 barrels (1bbl ≈ 160 litres) of oil have been produced, and gas production rates varied from 3×10^5 to 9×10^5 m^3 / month (Judd and Howland, 2007).

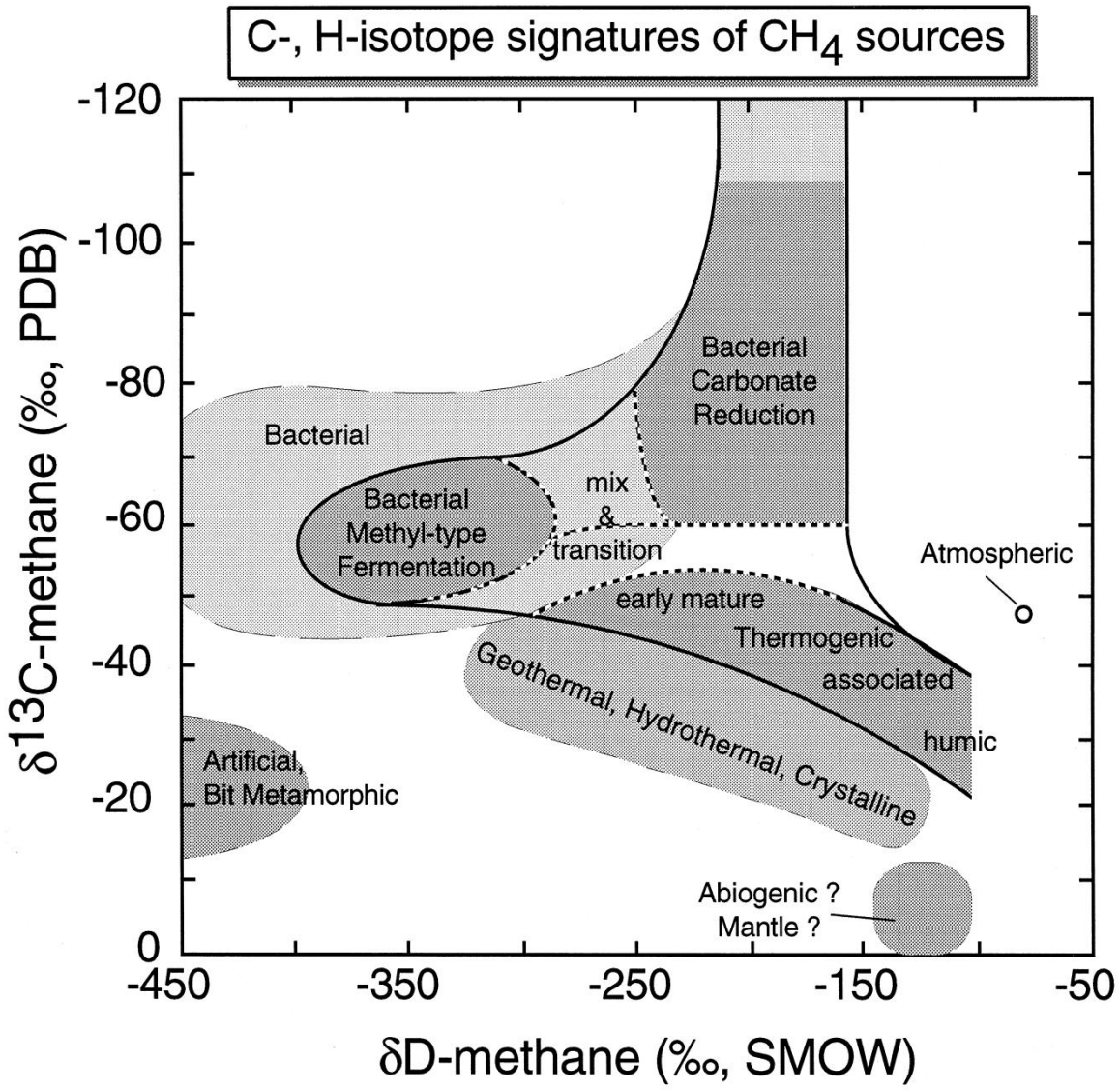

Figure 7. Carbon Deuterium (CD) diagram describing sources of methane and possible formation processes involved. Figure from Whiticar, 1999.

Natural liquid hydrocarbon emissions to the hydrosphere have been estimated to range from 0.2 to 2.0 x 10^{12} g / year with a best estimate of 0.6 x 10^{12} g / year (Kvenvolden and Cooper, 2003). They also note that *"Recent global estimates of crude-oil seepage rates suggest that about 47% of crude oil currently entering the marine environment is from natural seeps, whereas 53% results from leaks and spills during the extraction, transportation, refining, storage, and utilization of petroleum. (..) Thus, natural oil seeps may be the single most important source of oil that enters the ocean, exceeding each of the various sources of crude oil that enters the ocean through its exploitation by humankind."* These figures provide evidence of existing potential in natural seepage exploitation.

1.1.7.3 Pockmarks and gas hydrates

Gas hydrates can be indirectly affiliated with pockmarks. Presence of these features can indicate "hydrate-prone" seafloor and suggest that active venting is necessary for hydrate formation and growth (Zhou et al. 1999; Torres et al. 1999; Bouriak et al. 2000). Gas hydrates are ice like crystalline compounds composed of gas entrapped in a hydrogen-bonded lattice of water molecules. Gas hydrates or clathrates are a very potent natural resource. One volume of hydrate can release up to 172 volumes of methane gas (Sloan, 1998). The global reservoir of methane hydrates was initially overestimated but after more detailed analysis and understanding of hydrate formation mechanisms it is currently estimated to be 1 to 5 x 10^{15} m^3. Methane clathrates are difficult to exploit because they are stable only at narrow conditions of pressure and temperature. Consequentially they also pose a serious threat to offshore activities. Moreover, hydrates are believed to play an important role in past major climatic shifts (Benton and Twitchett, 2003; Ryskin, 2003). The "Clathrate Gun" hypothesis suggests that increasing ocean temperature and/or falls in sea level may trigger widespread hydrate dissolution and start a chain reaction of methane induced global warming. As mentioned above, specific conditions of pressure and temperature as well as a sufficient flux of gas are required for gas hydrates to form. In marine environments these conditions are met only at water depths greater than 500 m, where the temperature is generally lower than 10^{o}C and the overlying water column is source of the required pressure. Because of these specific conditions only pockmarks reported in deeper environments may be linked with marine hydrates (Judd and Hovland, 2007).

1.1.8 Do pockmarks contribute to the food web?

Although there is a division in the scientific community, many suggest that seepages affiliated with pockmarks may contribute to the food chain and support and promote local biological activity. The evidence published to date shows that in settings where intensity of fluid expulsion is high a genuine relationship can be observed between local communities and vented fluids, however the evidence is not conclusive from sites where only moderate to low venting takes place. Abundance differences of micro-, meio- and macrofauna on or near to pockmarks and background seabed suggests that there is a genuine relationship between seepage sites and these communities (Straugham, 1982). Densities of fish otoliths (fish ear bones) inside giant pockmarks in the UK block 15/25 (North Sea) reached 42,188 per m^2 compared to less than 82 per m^2 in the sediments outside and imply that fish may be attracted to these features (Dando, 2001). Also Levin et al. 2000 reported that from among 201 organisms found at three sites in northern Californian

Shelf, 55 were found only near seeps, and 59 were not present at seepage areas at all. In previous work by Dando, et al. 1991 from the same site differences in epifauna and infauna distributions were reported. They have concluded that at least some of the organisms (*Thyasira sarsi* and *Astonomena southwardorum*) utilize vented fluids in their metabolism, and that pockmarked sediment had lower abundance and species density than the unaffected seabed. However the overall conclusion of Dando, et al. 1991 based on combined biological survey and isotopic studies was that *"(...) the biology of a North Sea pockmark with an active methane seep suggest that the methane carbon is not contributing to the carbon of the surrounding infauna on a significant scale."* and that *"There is little evidence that isotopically light methane carbon is making a significant contribution to the tissue carbon of the benthic invertebrates around the pockmark."* Jensen et al.1992 also reported that isotopic signatures ($\delta^{13}C$) of tissue samples of local invertebrates were not significantly isotopically depleted ($\delta^{13}C$ ranged from -17 to -24 ‰) to be derived from isotopically light methane ($\delta^{13}C$ = -63.5‰) and hence inferred that seeped carbon makes little direct contribution to their nutrition. However the isotopic signature of "*Beggiatoa-like*" bacteria scraped from sandstone was on the other hand depleted ($\delta^{13}C$ = -43.4‰) indicating a link between light methane and these communities. Although reports linking higher fauna and venting fluids are rare and almost exclusively come from settings with intensive fluid expulsion there are examples of similar higher organisms dependence on venting fluids in less energetic environments. MacDonald et al. 1990 reported methanotrophic mussels (*Tamu childressi*) in brine-filled pockmark in the Gulf of Mexico. Boetius et al. 2000 reported large populations of bivalves (*Calyptogena* sp.) and bacterial mats in the pockmarked seabed of the Hydrate Ridge. A number of symbiotic organisms were discovered in active seep sites i.e. Vacelet et al. 1995, 1996 reported a carnivorous methanotrophic sponge (*Cladorhiza*). Several species of worms (Southward et al. 1981), bivalves (Childress et al. 1986; Barry and Kochevar, 1998, Taylor and Glover, 2010), gastropods (Sasaki et al. 2010) and other species (Kiel et al, 2010) associated with seepages were also reported. These examples suggest that pockmarks may be special ecosystems. If not supporting the communities through venting at least by providing a unique dwelling environment and shelter. After reviewing publications relating to fluid flow related biological activity Judd and Hovland, 2007 reiterated the question they formulated nearly twenty years ago (Judd and Hovland, 1989): *"were we so blinded by the light of photosynthesis that the contribution of chemosynthesis has been overlooked?"*. Precipitation of carbonate minerals in close vicinity of seepages is a relatively common phenomenon but until recently not well understood. The discovery of unique 'microbial consortiums' of anaerobic methane oxidizers (AOMs) and sulphate reducing bacteria (SRB) (Figure 8) allowed understanding of the biochemical mechanism of carbonate precipitation (Boetius et al. 2000).

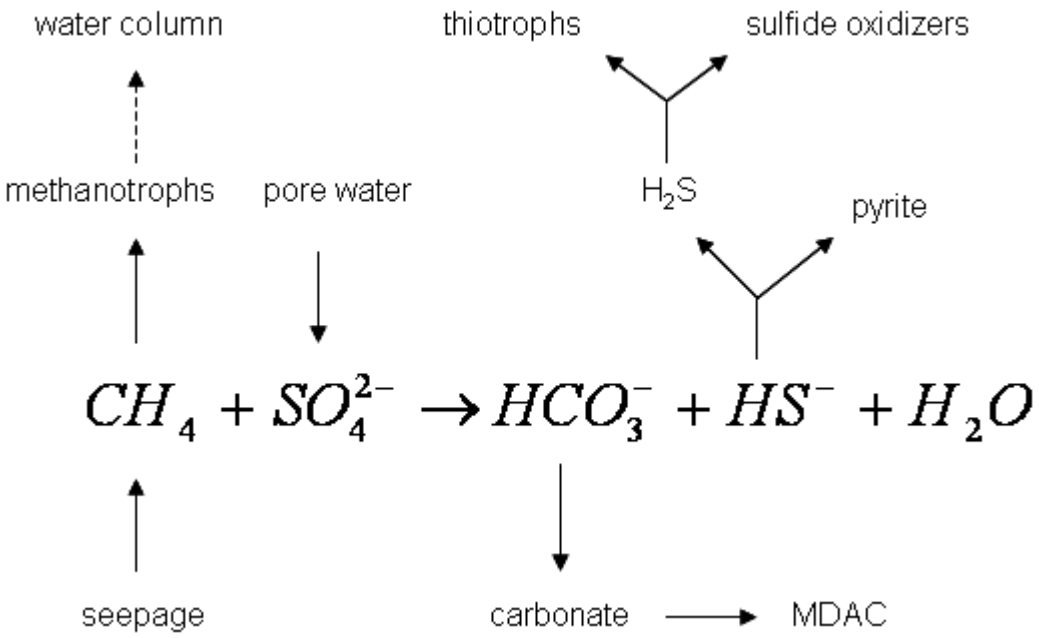

Figure 8. Proposed novel anaerobic methane oxidation mechanism (simplified) with sulphate as oxidant.

Precipitating carbonate minerals often form reefs and mounds (also referred to as "chemoherms" or more widely "bioherms"). These features are commonly linked to high biological activity (e.g. Hydrate Ridge Teichert et al. 2005; Darwin Mounds, Masson et al. 2003). Bacterial mats are an interesting example of the close relationship of microbes with the fluids expelled from the seabed. These conglomerates of thiotrophs (organisms oxidizing sulphide and/or sulphur as a main part of their metabolism) use seeping gases as carbon and sulphur sources and their presence is often a clear indication of active seepage. Most notably genus *Beggiatoa*, but also *Thiothrix* and *Thioploca* spp. are commonly encountered at active seepage sites (Judd and Howland, 2007). Finally, benthic organism variations within and outside pockmarks have been proposed as a tool for seep detection (Jones, 1993). In his work Jones, 1993 noticed statistically significant differences in the foraminifer assemblages within and outside of the pockmark. Among others pockmark sediment had a lower abundance and diversity and higher dominance of species than the control site. It is also worth noting that some theories on the origin of life on Earth suggest that methanogenic and methane consuming microbes such as *Archaea* played a crucial role in changing the ancient environment into a more hospitable place for new forms of life (Zimmer, 2001). Gold, 1999 suggested that life migrated to the surface from the deep, and that microbial communities inhabiting seafloor seepages represent the pioneer organisms that emerged from the primary biosphere (so called 'deep hot biosphere'). Successors of these organisms evolved and extended into new habitats such as the hydrosphere, upper lithosphere and atmosphere. Results from a number of studies seem to confirm

that estimates of the subsurface microbial biomass and the extent of the *"deep hot biosphere"* may have been undervalued (Judd and Howland, 2007; Wellsbury et al. 2000; Parkes, 1999).

1.1.9 Potential and dangers associated with pockmarks

The implications of seabed pockmarks and fluid flow for human offshore activity can be both beneficial and hazardous. Gas escaping through the seabed can either erode the seabed or accumulate underneath creating shallow gas pockets. Pockmarks are considered an obstacle for seabed installations, mainly because they can form in a spontaneous and unpredictable manner (Ellis and McGuinness, 1986) but also because their profile makes it much more difficult to install flat constructions such as pipelines (Judd and Howland, 2007). Gas pockets together with gas hydrate layers pose a serious threat to drilling activities. Drill puncture may trigger dangerous blowouts caused by liberation of over-pressurised gas or cause hydrate dissociation. Fluid displacement caused by over-pressured migrating gas causes surface sediment density to decrease and loose its strength. This in effect makes the seabed completely unsuitable for any installations and a threat to existing ones. Shallow gas is responsible for approximately one third of all drilling blowouts (Prince, 1990) and the loss of many lives and valuable equipment (Judd and Howland, 2007). However puncture induced blowouts have rather limited range while gas accumulations can be responsible for much more significant events. Submarine slope failure risk increases in areas with thermogenic gas, rich presence of organic matter, gas prone sediments and gas hydrate deposits (Hampton et al. 1996; Prior and Hooper, 1999; Locat, 2001; Leroueil et al. 2003). In the event of seafloor slope failure massive volumes of sedimentary matter are involved. In the largest recorded seabed slide "The Storegga Slide", on the Norwegian Margin, 3500 km^3 of sediment was moved when part of the shelf edge slumped (Bondevik et al. 2003). Despite evidence of gas seepage on the surface of Storrega Slide (including pockmarks and the presence of a large gas field), this slide was probably caused by earthquake and gas may have played its part in weakening the sedimentary structure of the slope. There are at least two geological records of seabed slide induced tsunamis: the Sissano tsunami caused by a slump of 5-10 km^3 of sediments struck the north shore of Papua New Guinea in 1998 (Tappin et al. 2001) and The Storegga tsunami caused by the above mentioned Storrega Slide in 8200 BP whose effect can be observed in sedimentary records on the Norwegian and UK coasts (Bondevik et al. 1997; 2006). Rapid gas release can also significantly reduce buoyancy and stability of surface vessels. Escaping gas bubbles dilute the water and reduce its density creating a patch of frothy water and any vessel entering this zone may lose its buoyancy and possibly sink (McIver, 1982). If gas release is not vigorous enough to sink the ship it may still seriously damage crucial electronic systems (Bondarev et al. 2002). Gas release events such as these

are believed to be linked to the infamous "Bermuda Triangle" disappearances of vessels and aircrafts. Although scientists are sceptical and many suggest that there is nothing unusual in the area or in the number of losses there, the Blake Ridge gas hydrates rich sediments which partially overlays with the Bermuda Triangle boundaries have made this hypothesis plausible. Massive gas release can also be devastating for local marine ecology. In 1994 in offshore Namibia, an anoxic event caused by a massive release of hydrogen sulphide rich gas killed fish and other fauna in vast numbers (Bruchert et al. 2004). The Cape Hake (*Merluccius capensis*) population in the area was reduced to less than 30% of its normal level with serious economic implications for Namibia (Weeks et al. 2004; Judd and Hovland, 2007).

Despite the hazards, seafloor fluid flow has potential that can be very beneficial to humanity. Some of these benefits may be directly linked with pockmarks. Seeps of freshwater were utilized for centuries (Taniguchi et al. 2002) and with novel approaches and knowledge of modern hydrology their potential as a source of water can be effectively exploited at present. Groundwater discharges can also enrich the seabed in minerals. Commeau et al. 1987 reported groundwater seeps on the Florida Escarpment where hypersaline and sulphidic water was saturated enough to cause pyrite precipitation. Studies revealed that sediment from this area contained 30% pyrite and 4% barium-strontium sulphates. With fluid temperatures reaching between 350 and 404^{o}C (Chevaldonne, 1997) geothermal and hydrothermal fluids can be an effective source of thermal energy. There is a significant potential for marine hydrothermal systems. The permeability of rocks and the seabed in the vicinity of the hydrothermal venting sites is considerably lower than typical seabed and suggest constant water mass exchange which carries vast amounts of thermal energy (Judd and Hovland, 2007). According to Fyfe, 1994 full exchange of the oceanic water (1.4 x 10^{21} kg H_2O) through the seabed would take approximately 10 million years. This suggests that every second 4.45 million kg of H_2O is being exchanged through the seabed in a process of venting. At present engineering constraints such as corrosiveness of the fluids and energy transportation hinder exploitation of marine hydrothermal energy. Nevertheless in countries such as Iceland, New Zealand, Canada and many others, land equivalents of hydrothermal and geothermal vents have been efficiently supplying heat.

Hydrothermal vents are also a potential source of metallic-ore minerals. Widespread ferromanganese nodules containing high concentrations of iron and manganese (9-27% and 8-40% respectively) but also nickel, copper and cobalt (Pryor, 1995) can be linked to hydrothermally induced precipitation processes. As mentioned, commercial exploitation of gas and liquid hydrocarbon seepages are still rare and available technology makes it possible only in areas where source rocks are covered by a thin layer of sediment, but seepages can be a very potent natural

resource for the future. Similar technological challenges still preclude gas hydrate exploitation. It is agreed that gas hydrates represent the greatest reservoir of methane carbon on the planet (Kvenvolden, 1983; Max, 2003) and that their energy content exceeds all other fossil fuel resources (coal, oil and conventional gas) (Showstack, 2000). More detailed estimations indicate that from 2 x 10^{14} m^3 (Hovland et al. 1999; Soloviev, 2002) to 21 x 10^{15} m^3 (Kvenvolden, 1999) of hydrocarbon gases are entrapped in hydrate cages. Although many deposits have already been identified and hydrate presence was confirmed by groudtruthing and coring surveys, continuous reports of new sites makes it difficult to map their global distribution. Seabed with the potential for gas hydrate growth needs a sedimentary layer of at least 2 km thickness and this criterion is met by 35.7 x 10^6 km^2 or approximately 10% of the area of the world's oceans (Soloviev, 2001). These figures highlight the major significance and potential of hydrates to the global energy industry. Seepage areas could be linked to unusual biological activity, although further research is necessary to discover if there is a genuine connection on all trophic levels. There are a number of examples when seeps and seepage derived structures such as methane-derived authigenic carbonates (MDACs) are coincidentally connected to high biological productivity. Masson et al. 2003 reported seep derived mounds adapted by cold water corals in the North Sea. Reports from local fishermen of increased fishing yields, near or on the seepage areas and seepage derived structures are not uncommon (Levy and Lee, 1988; Orange et al. 2002). Biotechnology has also recognized seepage potential: microbes inhabiting vents have been employed to utilize sulphide waste (Van Dover, 2000) and in production of pristine bioproteins (Hovland and Mortensen, 1999). Because chemosynthetic microbial communities possess unique attributes they may become a valuable source of useful genetic material as well as novel bioactive compounds for industrial, agricultural, environmental, pharmaceutical and medical users (Querellou, 2003).

1.2 Carbon cycling

1.2.1 The global carbon cycle

The global carbon cycle is a constant process of exchanging different forms of carbon between Earth's main systems: atmosphere, geosphere, hydrosphere and biosphere. It is a balanced process of a continuous accumulation and release from so called sinks through natural geological, biological, hydrological and anthropogenic processes. The importance of investigations into the carbon cycling has been widely recognized by the scientific community as well as by authorities and by public opinion (Climate Change 2001: The scientific basis by the Intergovernmental Panel on Climate Change – IPCC i.e.). Carbon is the main building block in biomass; energy production

in the modern world as well as important branches of industry are based on carbon and the atmospheric forms of carbon, carbon dioxide (CO_2) and methane (CH_4) have a profound effect on Earth's climate. Despite intensive research on the fate of carbon in the modern environment, its fluxes and transformation mechanisms are still not fully understood. Phenomena like missing carbon sinks and response of the cycle to growing anthropogenic influences are still poorly understood. Natural carbon cycling has been influenced by anthropogenic activities for centuries but until recently these influences were considered minor (Figure 9). The beginning of the industrial revolution (1750s) resulted in anthropogenic influences becoming significant. The carbon cycle is believed to respond to change by altering flux sizes and storing additional carbon emissions in environmental sinks. The human perturbation of this cycle is considered small but important because of the net effect on the existing environment. The main anthropogenic sources of additional carbon in the system are from fossil fuel (coal, oil and natural gases) combustion and changes in land use (deforestation, soil cultivation and food production). Fluxes of CO_2 emissions due to fossil fuel combustion (F_{A4}) and cement production (F_{A3}) reached values of 5.4 Pg C / year in the 1980s (5.3 and 0.1 Pg C / year respectively) but the revised figure for the 1990s was higher and reached 6.4 Pg C / year. The balance between land uptake (F_{A2}) and changes in land use (F_{A1}) indicates that assimilation of CO_2 is greater than emission (1.7 Pg C / year and 1.9 Pg C / year respectively). The negative flux of 0.2 Pg C / year into the land reservoir is partially sequestering the excess of CO_2 emitted to the atmosphere by fossil fuel burning. Another part of excessive anthropogenic CO_2 is being removed from the atmosphere by ocean sequestration (F_{A5} - 1.9 Pg C / year). These fluxes represent the anthropogenic caused imbalance of natural carbon exchange between atmosphere, land and ocean. The oceans are the largest active carbon sink on Earth (38000 Pg C). The oceanic carbon sink alone is approximately 50 times greater than the atmospheric and 20 times greater than the terrestrial pool. It is also an important regulator of atmospheric CO_2 concentration. Up to 1.9 Pg C / year (F_{A5}) as CO_2 is being sequestered from the atmosphere by the oceans. This negative flux is attributed to the carbon cycle's natural response to increased anthropogenic emissions. Since the industrial revolution oceanic CO_2 uptake has increased by up to 30%. The driving forces of CO_2 exchange between atmosphere and oceans differ dependent on the time scale. And so physico-chemical processes, altering CO_2 solubilisation, are the main driving force over short time scales (years to decades). Biological activity is the most important driving factor in the longer time frame (centuries to millennia). Finally on the geological time scale (millions of years) very small changes in both inorganic and biological processes regulate the CO_2 fluxes (Raven and Falkowski, 1999). The processes mentioned above are often referred to as the "solubility pump" and the "biological pump". The solubility pump is a process driven by seawater temperature, alkalinity and thermohaline water circulation.

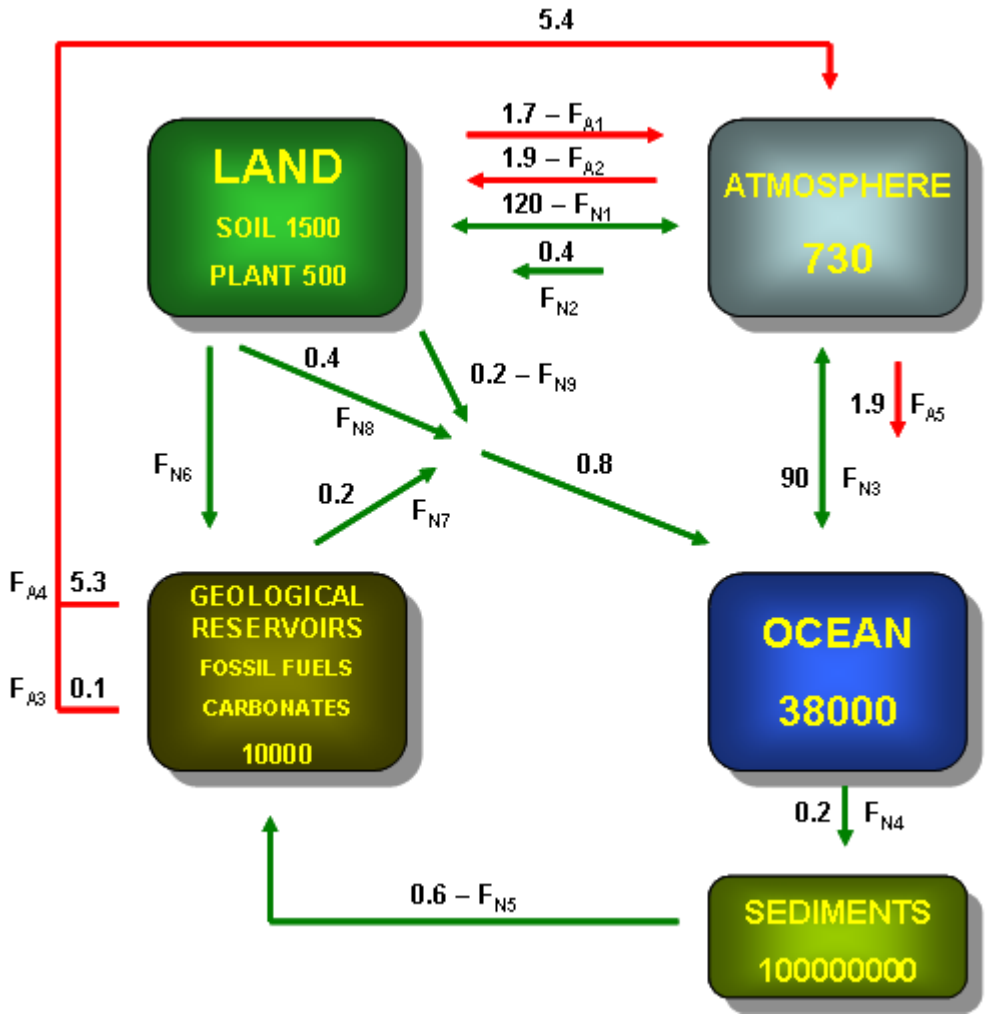

Figure 9. Diagram of natural carbon cycle with main anthropogenic perturbations. Red arrows depict anthropogenic carbon fluxes, green arrows depict natural carbon fluxes. Flux units are Pg – 10^{15}g C / year, storage units are Pg. Flux sizes after Climate Change 2001: The scientific basis by IPCC.

This process regulates the balance between dissolved inorganic carbon species (Equation 5).

$$CO_{2(aq)} + H_2O \Leftrightarrow H_2CO_3 \Leftrightarrow HCO_3^- + H^+ \Leftrightarrow CO_3^{2-} + 2H^+$$

Equation 5. Forms of carbon dioxide present in the oceans.

In the ocean free dissolved carbon dioxide is approximately 1%, bicarbonates 91% and carbonates 8% of total dissolved inorganic carbon (DIC). These proportions are a result of an equilibration process between negative (CO_3^{2-}, Cl^-, HCO_3^-, SO_4^{2-}) and positive ions (Na^+, K^+, Ca^{2+}, Mg^{2+}) which regulates the pH of oceanic water. Biological pump processes take place in the photic (euphotic) zone of the ocean and are related to the primary productivity by autotrophic organisms such as

algae, phytoplankton and plants. These organisms produce biomass which is consumed by zooplankton or sinks down to the deeper waters and is further processed by heterotrophs or deposited on the seabed. Calcified skeletons or bodies of calcifying organisms are referred to as the "*hard tissue pump*" while the remaining organic detritus is known as the "*soft tissue pump*". Ocean stratification due to water warming and acidification may strongly influence the biological pump in the future if environmental conditions become more severe. For example, it has been suggested that stratification can decrease nutrient supply to the photic zone and therefore reduce primary production (Behrenfeld et al. 2006). Decreasing pH will alter the ability of calcifying organisms to precipitate $CaCO_3$ and incorporate it into their bodies (Orr et al. 2005). Carbonate bodies or their fragments act as ballast in the transportation of carbon detritus to the seabed (Armstrong et al. 2002), therefore the whole mechanism may be disturbed. Even though only 0.4% of the autotrophic organic carbon reaches the seabed (F_{N4} of 0.2 Pg C / year) it provides an important link between fast cycling carbon pools (atmosphere, hydrosphere, biosphere and land surface) and slow pools that cycle in the geological time scale (sediments) (Middelburg and Meysman, 2007). Furthermore organic matter buried in the sediments is a carbon source for the deep biosphere which according to last estimates accounts for approx. 30% of living biomass (Gold, 1992; Whitman et al. 1998). This buried sedimentary organic carbon is transformed into fossil organic carbon on a geological time scale with a rate of 0.6 Pg / year (F_{N5}). Fast cycling carbon sinks exchange carbon through enormous fluxes of primary production and respiration. The exchange between land's biosphere and the atmosphere (F_{N1}) reaches 120 Pg C / year. Hydrosphere and atmosphere exchange through physical air-sea processes (F_{N3}) reaches 90 Pg C / year. F_{N2} of 0.4 Pg C / year represents CO_2 fixation by plants and transportation to the soil carbon pool. This is partially balanced by alluvial export of dissolved organic carbon into the oceanic pool (F_{N9} of 0.2 Pg C / year). The process of weathering and land erosion is responsible for a combined flux of 0.4 Pg C / year (F_{N8} and F_{N7}). The first part of the process is described by the "*Urey reactions*" (Equation 6). They describe the decomposition of crust rocks, which is caused by carbonic acid formed by atmospheric CO_2 and followed by silicate precipitation (F_{N8}) (Urey, 1952).

$$CO_2 + H_2O \Leftrightarrow H_2CO_3$$
$$2CO_2 + H_2O + CaSiO_3 \Leftrightarrow Ca(HCO_3)_2 + SiO_2$$
$$2CO_2 + H_2O + MgSiO_3 \Leftrightarrow Mg(HCO_3)_2 + SiO_2$$

Equation 6. Urey reactions describing the terrestrial weathering processes and rock metamorphism (reverse).

Dissolved bicarbonate species as well as silica (as $Si(OH)_4$) enrich the groundwater in inorganic carbon and finally reach the oceans through fluvial transport. In oceans carbonate precipitation

occurs (Equation 7). This is the only environment where carbonates are precipitated in the form of CO_3^{2-} salts.

$$Ca(HCO_3)_2 \Leftrightarrow CaCO_3 + CO_2 + H_2O$$
$$Mg(HCO_3)_2 \Leftrightarrow MgCO_3 + CO_2 + H_2O$$

Equation 7. Marine precipitation of bicarbonate species.

The second flux (F_{N7}) represents sequestration of atmospheric CO_2 on land by dissolution of exposed carbonates by a weak acid H_2CO_3 formed during rainfall. These carbonates are exposed marine deposits which were not transformed back into silicates in the metamorphic process (Equation 8).

$$CaCO_3 + CO_2 + H_2O \Leftrightarrow Ca(HCO_3)_2$$
$$MgCO_3 + CO_2 + H_2O \Leftrightarrow Mg(HCO_3)_2$$

Equation 8. Dissolution of exposed marine deposits.

Transformation of land stored carbon into fossil carbon is represented by the flux F_{N6}, which still needs to be quantified. Moreover volcanic activity provides an additional carbon flux in to the atmosphere (not shown on the diagram). This flux is rather small compared to others included in the diagram; it is estimated at 0.02 – 0.05 Pg C / year.

1.2.2 Coastal carbon cycle

As mentioned in the previous paragraph the oceans are one of the largest carbon reservoirs in the global carbon cycle. Both the water column and sedimentary matter contain different types of organic and inorganic carbon that cycle continuously within these reservoirs. Carbon in the oceans has many molecularly diverse forms which represent inputs from other reservoirs at different stages of its transformation. Among all carbon forms organic matter in marine sediments is one of the most complex and diverse. It is also an important component of global sulphur, nitrogen and oxygen cycles. In coastal zones, as defined by Ver et al. 1999 as all areas up to 200 meters water depth including bays, lagoons, estuaries and near shore banks, carbon cycling is affected by two major carbon reservoirs: open ocean and land. A conceptual model of the carbon cycle in coastal zones has been proposed by Mackenzie et al. 1998. It is modified here to depict flux sizes that illustrate the main cycling of inorganic and organic carbon in shallow waters (Figure 10). Ver et al.

1999 studied the last 300 years of carbon cycling, starting from the industrial age until 1995 by employing the thirteen-reservoir, process-driven carbon cycle model called TOTEM.

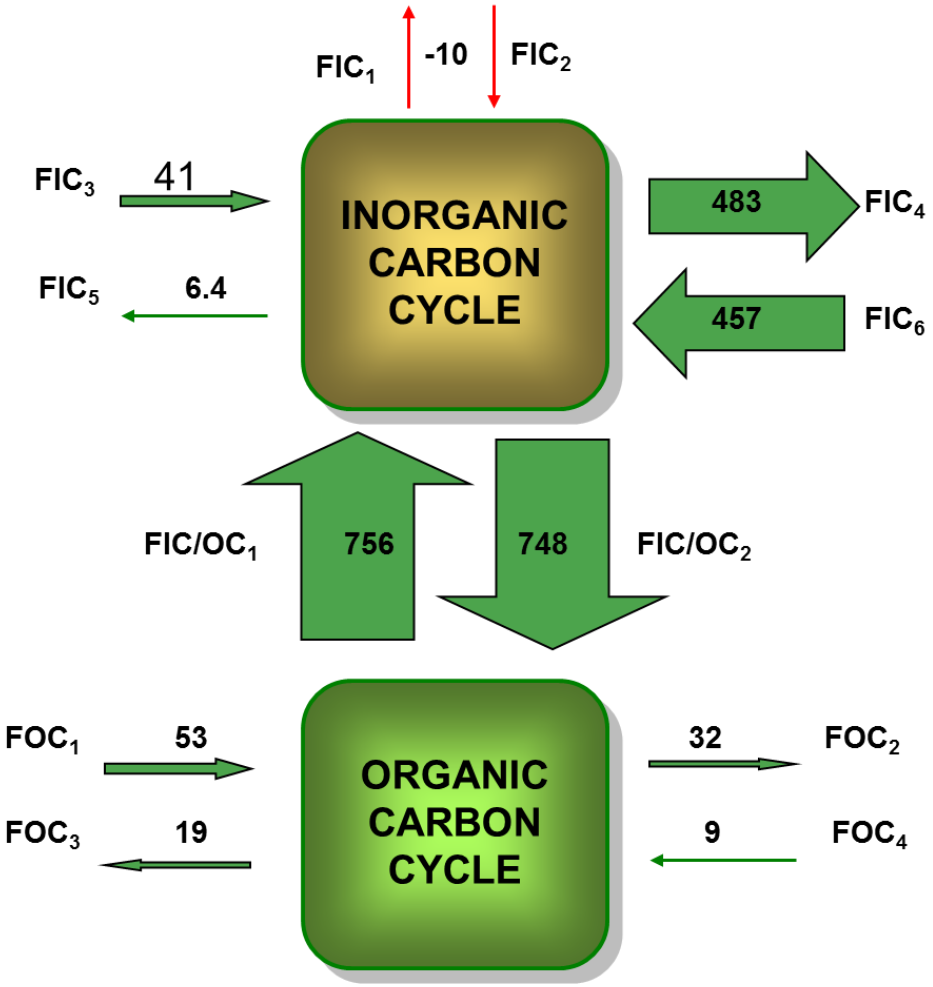

Figure 10. Coastal zones carbon cycle. Flux units are 10^{12} mol C / year. Arrow width is proportional to the flux size. Red arrow indicate negative flux, green arrows indicate positive flux. FIC – inorganic carbon flux; FOC – organic carbon flux. Flux values after Ver et al. 1999, concept after Mackenzie et al. 1998.

The model includes coupled C-N-P-S biogeochemical cycles in estimating of the effect of the four major environmental perturbations on the carbon cycle: (1) C,N, and S emission from fossil fuel burning; (2) gaseous C emissions as a result of changes in land-use activities, increase of dissolved and particulate matter fluxes, organic matter transport and effects on biological production; (3) extensive use of nitrogen and phosphorus containing fertilizers and (4) discharges of sewage containing reactive C,N, and P. According to this model, presently, CO_2 is being exchanged between the atmosphere and the inorganic carbon reservoir (FIC_1, FIC_2). Negative net values for FIC_1 and FIC_2 indicate that in the coastal zone CO_2 is being emitted to the atmosphere with a rate of

-10 x 10^{12} mol C / year thus coastal zones are net heterotrophic. This value is an indicator of the net ecosystem productivity (NEP) and describes the balance between the gross primary production (GPP) and the total respiration and decay in the coastal ecosystems. According to the NEP theory the system is net heterotrophic when the total amount of carbon produced in the process of respiration and decay is greater than the total amount of carbon produced in the process of photosynthesis (NEP<0). The system is autotrophic when the amount of carbon sequestered by photosynthetic processes is greater than the amount produced in the process of respiration and decay (NEP>0). The inorganic cycle receives inputs of land derived carbon such as dissolved inorganic carbon (DIC) river fluxes, surface runoff and groundwater flow (FIC_3). These combined fluxes have a rate of 41 x 10^{12} mole C / year and are rather moderate sources of inorganic carbon. According to the chemical equilibrium in the oceans, CO_2 is released during $CaCO_3$ precipitation (Equations 7&9), transported from deeper ocean (FIC_6 – 457 x 10^{12} mol C / year) and brought up in the process of respiration, decay and organic matter diagenesis (FIC/OC_1 – 756 x 10^{12} mol C / year). These are major sources of inorganic carbon in this cycle.

$$Ca/Mg^{2+} + 2HCO_3^- \Leftrightarrow Ca/MgCO_3 + CO_2 + H_2O$$

Equation 9. Liberation of CO_2 in the process of precipitation of carbonates.

$CaCO_3$ deposition in the sediments, accumulation in biota (FIC_5 – 6.4 x 10^{12} mol C / year), CO_2 uptake in the process of photosynthesis (FIC/OC_2 – 748 x 10^{12} mol C / year) and exchange with open ocean (FIC_4 – 483 x 10^{12} mol C / year) are the outflows from the coastal inorganic carbon cycle. Organic and inorganic carbon cycles are linked through large fluxes of respiration, decay and photosynthetic activity. These fluxes are biologically driven and include the processes of reduction and oxidation of organic matter and biological pump processes which sequester the CO_2 from the atmosphere through the ocean's photic zone. As mentioned above, the main influx of carbon in the organic carbon cycle is related to the photosynthetic activity of the phytoplankton in the photic zone (FIC/OC_2). Apart from this process, inflow of fluvial and land derived dissolved (DOC) and particulate (POC) organic carbon is an important source of organic material and can account for up to 53 x 10^{12} mol C / year. Transport of dissolved organic material from the deeper ocean (FOC_4) through water mass mixing, tied to oceanic current activity, can reach a rate of 9 x 10^{12} mol C / year. Apart from organic matter diagenesis (FIC/OC_1), organic carbon is removed from the coastal zone through accumulation of organic matter in the sediments (FOC_3 – 19 x 10^{12} mol C / year) and exchange with the open ocean (FOC_2 – 32 x 10^{12} mol C / year).

1.2.3 The organic carbon cycle

The discussed above the organic carbon cycle can be divided into fast cycling biological and slow cycling geological sub cycles (Figure 11). The biological cycle has a half-life extending from days to tens of years while in the geological cycle carbon is transformed over a timescale of millions of years. These sub cycles differ also with respect to the size of their reservoirs. The biological cycle reservoir is estimated to hold 2.7-3.0 x 10^{12} tons of organic C, while the geological cycle is over three orders of magnitude larger and is estimated to hold approximately 6.4 x 10^{15} tons of organic C. Both of these cycles are connected through a small leakage through which deposited organic matter is incorporated into the geological reservoir via natural process of oxidation. The turnover of this leakage is estimated between 0.01% and 0.1% of total organic carbon (Tissot and Welte, 1984). The biological cycle starts with photosynthetic activity of various organisms resulting with transformation of gaseous CO_2 into living biomass. The organic carbon bound in this biomass travels through several trophic levels and ultimately with the death of the organism is deposited in soil and sediment. A portion of the organic carbon is completely reduced by microbial activities into carbon dioxide and re-enters the biological cycle while the remaining more recalcitrant organic matter is incorporated into the fossil sediments. It is estimated that from a total of 2.0 x 10^9 tons of organic carbon deposited on the seabed mainly in the form dissolved and particulate organic matter (DOC/POC) 1.7 x 10^9 tons is reduced to CO_2 in reactive sediments and re-enters the biological cycle in the form of dissolved inorganic carbon (DIC). Moreover Middelburg and Meysman, 2007 suggest that only 0.4% of the carbon fixed by phytoplankton is incorporated in fossilized form: kerogen, oil and gas. These estimates however are only accurate from global cycle point of view. Coastal systems, particularly systems with large riverine input experience high fluxes of terrigenous organic matter. This terrigenous organic carbon, despite being nitrogen depleted and hence less attractive for microorganisms, is also mainly (~70%) oxidized before it reaches the seabed (Hedges et al. 1995). The exact mechanism of this transformation still remains elusive, however case studies from several systems suggest that overall burial rates in such settings can be higher than the global estimates (e.g. Masiello, 2007; Galy et al. 2007). Similarly burial rates of organic matter derived from primary productivity differ in the open ocean and the coastal systems. According to Berger et al. 1989 i.e. in the open oceans 0.3 g OC m^{-2} per year derived from primary productivity reaches the seabed and only 0.01 g OC m^{-2} per year is buried. In the coastal settings these values are higher and reach 8 g OC m^{-2} per year and 1 g OC m^{-2} per year, respectively. Collectively all processes, both biotic (mainly microbially mediated transformations) and abiotic (mainly mineral catalysed transformations), of alteration of organic carbon prior to deposition and in the early stages of burial are referred to as '*diagenesis*' (Killops and Killops, 2005).

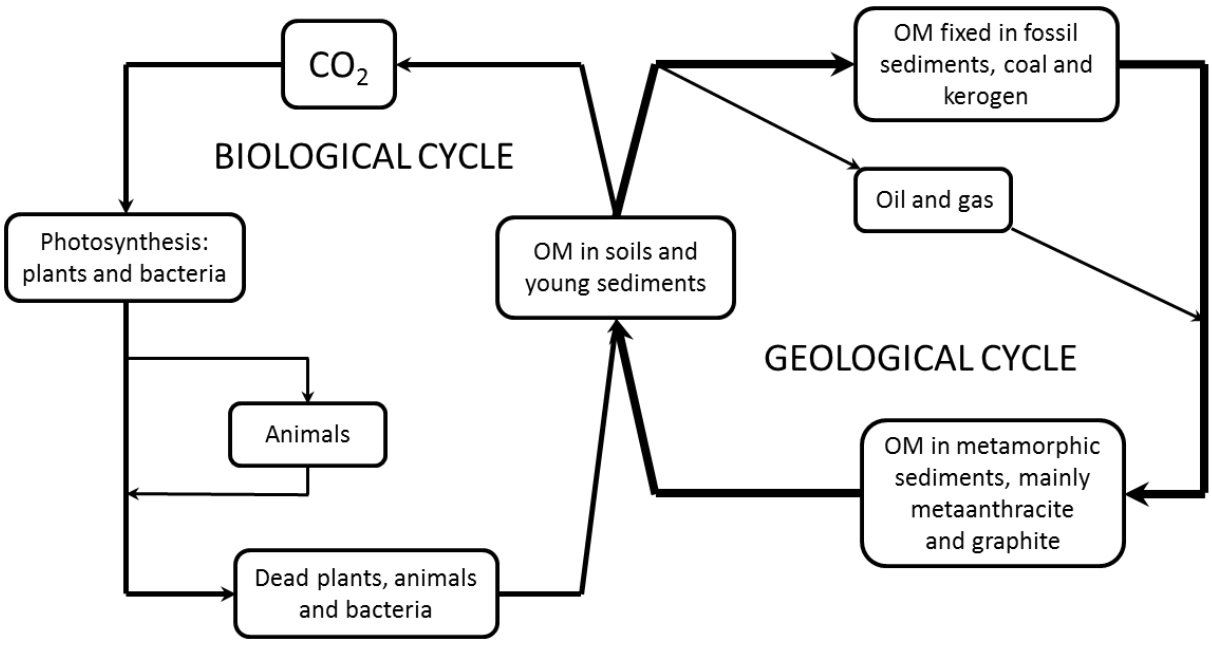

Figure 11.The organic carbon cycle. Modified after Tissot and Welte, 1984.

The buried organic carbon, initially altered by diagenetic processes, is subjected to increasing temperature and pressure which restricts biological activity but on the other hand allows abiotic, transformations to intensify. These thermal processes of alteration of organic carbon are referred to as '*catagenesis*'. Depending on depositional, thermal, pressure conditions as well as source of organic matter this process results with kerogen and oil of different maturity, gases of different wetness and coals of different coalification stage. The boundary between diagenesis and catagenesis is not sharp. Thermally driven changes occur during diagenesis at temperatures as low as 60^{o}C and there are also thermophilic microbes that thrive even in temperatures exceeding 100^{o}C (Wharton, 2002). However, the rates of these processes and therefore their impact on the organic matter become more and more limited during this transition. The last stage of carbon transformation occurs deep in the crust where temperature and pressure conditions allow high-grade metamorphic processes (Schulz and Zabel, 2005). The final form of carbon is highly defunctionalized and has a high degree of aromaticity such as graphite and metaanthracite. The processes leading to these forms of carbon are called '*metagenesis*'. On the Malin Shelf however, the sediments studied are considered young and therefore the pathway of transformation of the organic matter is largely limited to diagenetic processes. The transformations of individual constituents of OM and their importance for generation of kerogen have been widely debated in the scientific community over the years. According to the classical approach kerogen is formed from highly organized plant biopolymers and macromolecules that survive the enzymatic degradation and escape the microbial mineralization during early diagenesis.

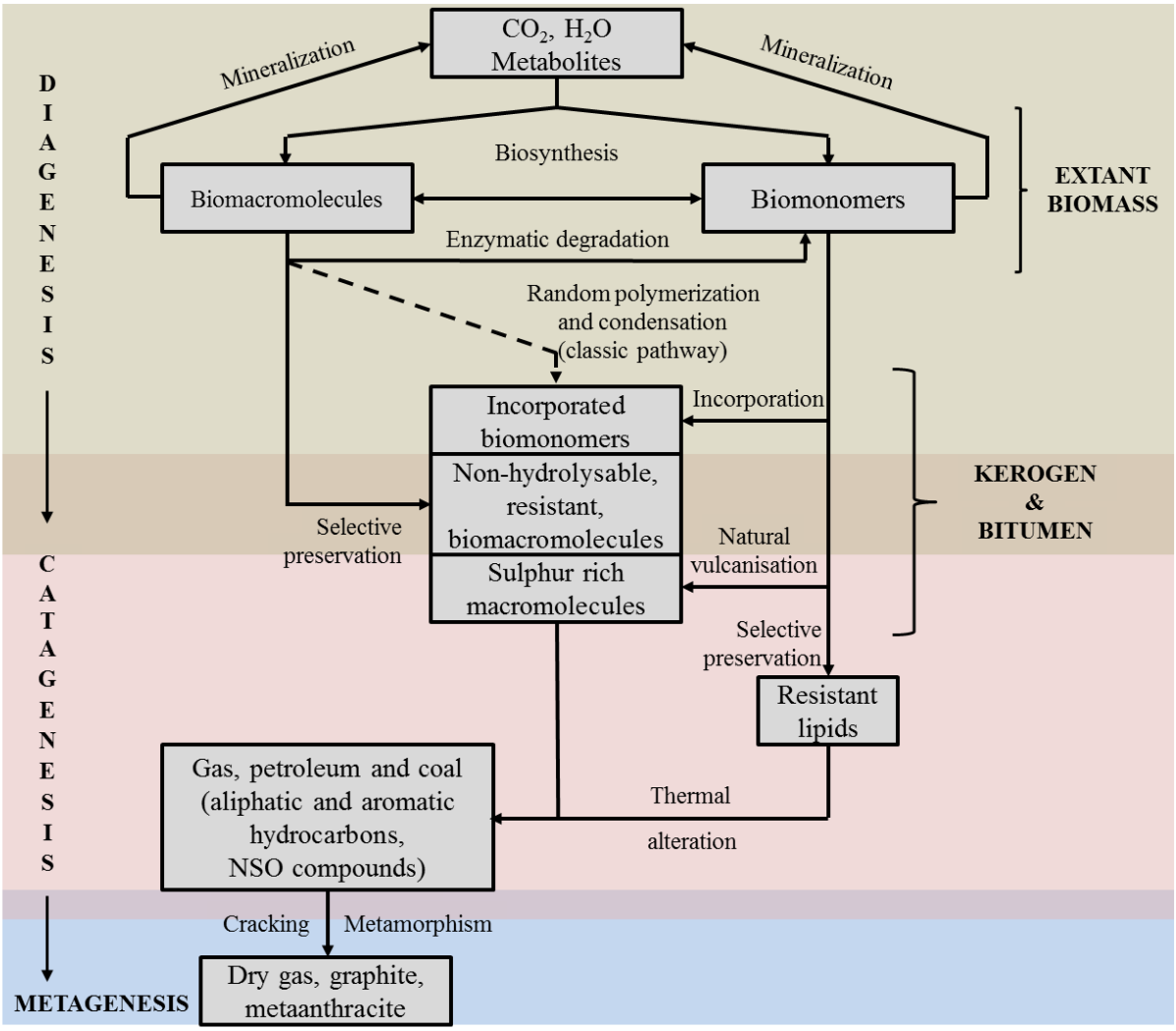

Figure 12. Major pathways of kerogen formation and transformation of organic matter. Modified after Schulz and Zabel, 2005 and Tegelaar et al. 1989.

Buried and degraded organic remains through process of random polymerization and condensation form new geomacromolecules considered kerogen precursors: humin, humic acids and fulvic acids (Tissot and Welte, 1984). Over time with the progressing diagenesis these heterogeneous geopolymers lose superficial hydrophilic groups through processes such us elimination of water (from hydroxyl groups i.e.), carbon dioxide (from carbonyl groups i.e.) ammonia (from aminosugars ie.), hydrogen sulphide (from thiols i.e.) and undergo further combination reactions resulting with complete insolubilization. During that process sulphur enriched compounds and monomeric recalcitrant diagenetic breakdown products are also incorporated into the geopolymer structure. Further defunctionalisation and condensation finally leads to kerogen. However the discovery of highly aliphatic, non-hydrolysable biompolymers such as algaenans (Philip and Cavlin, 1976), cutans (Nip et al. 1986) and suberans (Tagelaar et al. 1995) in extant plants and

fossil material has shown that selective preservation of biopolymers appears to be an important contributing mechanism (Tegelaar et al. 1989) (Figure 12). Although these biopolymers are found in living organisms in very low amounts they are likely to be concentrated once the more labile material is mineralized. Moreover it has been suggested that cutan and sporopollenin are in fact a diagenetic polymerization product of cuticular lipids as they are infrequently found in plant matter (Stankiewicz et al. 2000). The discussion on that matter continues and so far the extent of humic like materials contribution to kerogen formation remains uncertain (Killops and Killops, 2005).

1.3 Aspects of methodology

1.3.1 Physical properties of sediments

1.3.1.1 Particle size distribution

Particle size is a basic but very important physical property of all geological samples including soils and sediments. It correlates strongly with many natural micro and macro processes and can be employed in evaluating anthropogenic influence on the environment. Particle size is used to determine sedimentation rates and sedimentation type (Sperazza et al. 2004), develop sedimentation models (Agrawal and Pottsimth, 2000) and to unravel the historical fluctuations of sedimentary matter (Zuhlsdorff et al. 2007). Particle size analysis (PSA) can be a valuable tool in environmental monitoring. Vandecasteel et al. 2002 used combined chemical and granulometric analysis of alluvial surface soils to identify places affected by disposal of dredged sedimentary material. Conclusions about deep and intermediate currents strength in Northern Atlantic waters in the last 25 k years derived from particle size measurements by McCave et al. 1995 show that this simple parameter can be used to study macro processes in the environment. McCave et al. 1995 demonstrated that sorting effects of currents, directly related to their strength is accurately reflected in the seabed grain size distributions while other proxies such us nutrient distribution proved to be influenced by processes not related to ocean circulation. Moreover, the recently reported correlation between the grain size and chemical properties of nanominerals and their possible influence on all of the main Earth's systems including biosphere and its productivity (Hochella Jr et al. 2008), demonstrates the breadth of applications for particle size data from natural samples. The complexity of natural matrices is present at many levels including chemical, mineralogical, biological and physical properties. This high variability can be exploited as a specific fingerprint of natural material. One of the commonly studied parameters in such forensic investigation is particle size

analysis of soils and sediments (Pye et al. 2004). Separation of grains into size classes and their subsequent multi technique (i.e. elemental composition by ICP-AES or ICP-MS and organic nitrogen and carbon stable isotope composition by IR-MS) analysis can be used to find fractions that demonstrate the smallest variability between subsamples and can be used in forensic comparison studies (Pye at al. 2005; 2006). The composition of organic matter has also been linked to specific particle size fractions. In the work by Gonzales et al. 1985 where a deltaic environment was studied, enrichment of plant debris-derived lipids was reported in the coarse fraction, as well as a depletion of lipid material and signs of microbial activity in the clay fraction. Adams and Bustin, 2001 discussed in detail variations in parameters such as total organic carbon (TOC), carbon nitrogen ratios (C/N) and surface area (SA) in relation to particle size distribution in the petroleum source rocks formation context.

Although particle size distribution is a simple parameter its accurate determination can be problematic when analysing natural samples. Geological material is highly heterogeneous, contains different amounts of debris (i.e. plant roots and branches, biogenic carbonates) and particles of different shapes. Furthermore, mineral density can vary significantly (Clifton et al. 1999) while different samples can contain organic material of different origin and at varying concentrations. These properties make accurate particle size determination challenging. There are several methods for sizing geological samples and all are based on different principles with their own benefits and drawbacks. It is very important to acknowledge that different sizing methods estimate different diameters for the same particle based on the property that particular method measures. For instance dry or wet sieving will sort sizes of particles according to sieve aperture, hydrometers will sort particles according to their settling velocity, laser systems will sort particles according to their volume and mass and all of them may result in different equivalent particle diameters. Traditional methods of sizing include methods based on sieving and sedimentation methodologies such as pipette and hydrometer techniques (Beuselinck et al. 1998, Weber et al. 2003). These techniques are time consuming, involve the separation of different fractions, require large amounts of material and suffer from inaccuracy and low resolution (Eshel et al. 2004). Also techniques based on electrical sensing (Milligan and Kranck, 1991) and X-ray absorption (Campbell, 1998) has been proposed. Although these methods are still time consuming they are much more precise and less error prone than the classic sizing techniques (Sperazza et al., 2004). Among all sizing techniques diffraction based methods seem to be the best compromise between the amounts of sample and labour required and the resulting precision and accuracy.

Laser diffraction was introduced for the sizing of materials with well-known and defined optical properties such as fuel spray droplets (Ballester and Dopazo, 1996), pharmaceutical solids

(Kippax and Morton, 2008; Stevens et al. 2007) and paints (Rawle, 1996). In laser diffraction based systems a beam of monochromatic light is scattered by the suspended particles with the varying angle being proportional to particle size. Light scattered at the same angle is focused by Fourier lenses and directed into one of the detectors to form a stable diffraction pattern. Laser diffraction systems are volume-sensitive because the mathematical model (based on so called '*Fraunhofer-Mie theory'*) assumes that the diffraction pattern of a particle equals that of a sphere with a volume equal to that of the measured particle (Jonasz, 1987). For nonspherical particles this assumption is not valid and in the case of natural geological samples where nonsphericity is common phenomenon laser diffraction can only provide an approximate estimation of particle size distribution. Nevertheless in comparison with previously mentioned sizing methods, laser granulometry offers several advantages: it requires less sample per measurement, it is much faster and requires less sample pre-treatment, it can present results continuously in real time, measurements are independent of particle density (contrary to sedimentation based techniques), the system does not require calibration and can provide high repeatability and resolution. Ironically, small sample sizes increase the risk of errors from subsampling of highly heterogeneous natural material. Nonetheless with all the advantages of laser diffraction sizing it is becoming more and more popular.

Fraunhofer theory predicts a diffraction pattern created by a solid, opaque disc which passes through the laser beam. This theory assumes that: particles are spherical, non-porous, opaque and that all particles diffract the light with the same efficiency. Natural samples rarely meet the assumptions made in the Fraunhofer model. This model is not precise enough in describing the light scattering and can only be successfully applied to measure particles that are considerably larger than the wavelength of light from the laser. To extend the application of laser diffraction systems to smaller particles and particles that do not meet the Fraunhofer model assumptions the Mie theory was introduced. The Mie theory describes light scattering more accurately and takes into account the diffusion and absorption of light by the measured particles. Although Mie theory likewise assumes sphericity of particles it allows extension of the measurment range of laser diffraction systems to the finest minerals, such as clays, commonly present in geological samples (de Boer et al. 1987). The assumption about the sphericity of the particle is a necessary simplification because it allows use of a one dimensional descriptor of the particle: its apparent diameter. Nonspericity of particles in laser sizing systems and their effect on the measurement has been discussed in detail by Jonasz, 1991. The author concludes that a particle's projected area averaged over all possible orientations is greater than the projected area of a sphere with equal volume to that of a measured particle. In other words "*nonsphericity of marine particles causes underestimation of their projected areas calculated from equivalent spherical volumes determined with volume-sensitive*

particle counters" (Jonasz, 1987). Therefore a shift towards larger apparent diameters is observed when analyzing nonspherical particles. The significance of this effect increases with the size of particle and is negligible for particles smaller than 0.1μm. The main disadvantage of the Mie theory is that it requires the refractive index value of the measured material in order to calculate particle size distribution accurately. Complex refractive index (**ñ**) is a measure of how much the light speed changes when passing through a particle (the real part - $\mathbf{n_r}$) and how much light is absorbed by the particle; in other words how transparent the measured particle is (the imaginary part - **i**). The distribution is less sensitive to the imaginary part of the refractive index than the real part which can significantly change the frequency curve in the clay-size range (Eshel et al. 2004). Given that geological samples are complex mixtures of numerous minerals, each of which has a different refractive index varying from n_r – 1.48 for calcite to as much as n_r – 3.19 (Munoz et al. 2006) for hematite, good estimation of this parameter is necessary for accurate particle sizing.

1.3.1.2 Density of the sediment

Density is important physical property of marine sediments. It describes or it is at least related to seafloor parameters such as vertical stress, porosity and mineralogy (Burdige, 2006). Density is an essential component of many sediment accumulation models (e.g. Dadey et al. 1992) as it is directly related to hydraulic sorting of particles. Moreover it can also be correlated with other parameters such as: $CaCO_3$ (Snoecks and Rea, 1994), organic carbon content (Avnimelech et al. 2001) and biogenic silica content (Tribble et al. 1992). Bulk density (ρ_{bulk}) is the most common method of defining sediment density. It refers to the whole sediment mass (m_{matrix}) including mineral matrix and pore fluid (m_{fluid}) and its volume (v) (Equation 10).

$$\rho_{bulk} = \frac{m_{matrix} + m_{fluid}}{v}$$
$$m_{fluid} = m_{liquid} + m_{gas}$$

Equation 10. Formula describing bulk density of the sediment.

It is also referred to as "wet" bulk density to distinguish from "dry" bulk density which refers to the density of a dried sample. The relation between density and porosity (φ) can be expressed by the following formulae (Breitzke, 2000a):

$$\rho_{bulk} = \varphi\rho_{liquid} + (1-\varphi)\rho_{matrix}$$

$$\varphi = \frac{\frac{m_{H_2O}}{\rho_{H_2O}}}{\frac{m_{H_2O}}{\rho_{H_2O}} + \frac{\left(m_{solids} - \left(Sm_{H_2O}\right)\right)}{\rho_{solids}}}$$

Equation 11. Relationship between density and porosity. Porosity expressed as function of dry bulk density.

Knowing the water content (m_{H2O}) and the solid's density (dry bulk density; ρ_{bulk}) and fractional salinity (S) we can calculate the porosity (Equation 11) and verify remote electromagnetic measurements. The porosity of sediment in normal conditions, contrary to density, decreases with depth. This phenomenon is known as sediments compaction and sediment compacted this way are referred to as "normally consolidated". The sediment surface is under stress from hydrostatic pressure (Equation 12).

$$P_{hydro} = \left(\rho_{H_2O} h_{H_2O} g\right) + P_{atm}$$

Equation 12. Formula describing hydrostatic pressure. Symbols denote: water column density - ρ_{H2O}, height of the water column - h_{H2O}, gravitational constant - g.

Beneath the surface, sediment is under so called vertical stress (Equation 13), which is the pressure of overlaying sediment (h_{sed}) transmitted by grains themselves:

$$\sigma_{vertical} = \rho_{bulk} h_{sed} g$$

Equation 13. Vertical stress as a function of bulk density.

This is usually the dominant stress but in some circumstances horizontal components are as important (Judd and Hovland, 2007).The pore fluids counteract the increasing grain pressure and reduce vertical stress. When pressure becomes too high, fluids are squeezed out from the contracting pore space. This leads to further compaction and finally cementation when precipitation occurs and pore space is filled with crystallized salts. The less fluid that is present in pores the more shear stress can be withstood by sediment; the sediment is more rock-like. In some of the cases mentioned above stress induced fluid migration is not possible or occurs too slowly. Consequently, fluid becomes over-pressurised in the sedimentary body. The cause of over-pressurised pore fluid and decreases in sediment density is usually tectonic compression or when low permeability sediments accumulate very quickly (Judd and Howland, 2007). Over-pressurized pore fluids are one

of the two major fluid flow driving forces, the other being sediment buoyancy related to either existence of low density mineral layers or fluid retention. Presence of a negative density gradient can result in an upward migration to restore a positive density gradient by pushing through overlaying high density sediments or by fluidization of the sediments. Naturally occurring features such as faults may and often do trigger fluid migration. The second mechanism is usually affiliated with gas pockmark formation.

Table 1. Dry bulk densities of selected minerals and marine sediments. Expanded after Burdige, 2006.

Pure Mineral	ρ_{solids} **[gcm^{-3}]**
Quartz	2.65
Calcite	2.71
Aragonite	2.95
Felspar	2.54-2.76
Chlorite	2.70
Kaolinite	2.60
Montmorillonite	2-2.7
Illite	2.6-2.9
Magnetite	5.1-5.2
Pyrite	5-5.02
Zircon	4.6-4.7
Garnet	3.1-4.3
Tourmaline	2.82-3.32
Mixed sediments	
Terrigenous sediments (continental slope and shelf)	
Fine sand (92% sand; 4% silt; 3.4% clay)	2.71
Sandy mud (32% sand; 41% silt; 27% clay)	2.65
Mud (5% sand; 41% silt; 54% clay)	2.70
Deep-sea red clay (0.1-3.9% sand; 19-59% silt; 37-81% clay)	2.74
Deep-sea diatomaceous ooze (3-8% sand; 37-76% silt; 17-60% clay)	2.46
Deep-sea calcareous ooze (3-27% sand; 40-76% silt; 8-56% clay)	2.66

In the past, dry bulk density was often derived from mineralogical information rather than by direct measurement (Burdige, 2006). This route can be used in reverse and dry bulk density with support of particle size data can aid mineralogical studies. Different sediment mineral components

have different density values (Table 1). In natural environments sediment density is controlled by the mass fractions of different minerals. The resultant density is an average of multimineral contributions. Clusters of heavy minerals can be spotted easily as they will alter density significantly when present in sufficient concentrations. Density of sediment can be measured using of several techniques. Classic techniques such as the wet sediment volume measurement, liquid dispersion or density bottle methods are often bias prone (Hilton et al. 1986) while modern techniques require sophisticated equipment but are rapid and non-destructive (Gerland and Villinger, 1995; Rothwell and Rack, 2006).

In this study we employ helium pycnometry. This technique has been successfully applied in some studies (Dadey et al. 1992) and is commonly employed in material science to describe the density of materials similar to fine grained "consolidated" sediments. Helium pycnometry is a gas displacement method based on Boyle's law (Equation 12) that determines the volume of the studied specimen via the Archimedes fluid displacement principle (an object immersed in a fluid will displace an amount of fluid equal to the object's volume). In this technique He (helium) gas is commonly used because it is an inert gas and its atomic dimensions allow penetration of pores up to 0.25 nm. In some cases N_2 (nitrogen) and SF_6 (sulphur hexafluoride) can be used. The specimen is inserted into a cell of known volume and the He is introduced until pressure in the cell reaches a predefined level. When this occurs gas is expelled into a second cell and its volume is determined by use of Boyle's law. This step is repeated until five consecutive readings fall within the predefined precision. Constant temperature is provided by an internal heating system and cell insulation.

$$p_1 V_1 = p_2 V_2$$
$$T, n = const$$

Equation 12. Boyles Law. In a closed and isothermal system pressure (p) and volume (v) are inversely proportional. T - temperature in K, n - number of moles.

1.3.1.3 Foraminifera and ^{14}C dating

To discuss the origin of a seabed and seabed features it is necessary to accurately determine the age of the sediment. Dating of the sediment also provides essential information for calculating sedimentation rates, which in turn indicate the rates of material transportation from land and marine sources (Davies et al. 1977). This data can be subsequently used in models reconstructing paleoenvironmental conditions (Zuhlsdorff et al. 2007). Moreover dating allows all the records of

the events preserved in the deposited sediment to be placed in time. Over time different dating techniques have been proposed to determine the accurate age of marine materials. Most often used is the phenomenon of radioactive isotope decay (Equation 13). Knowing the proportion of radioactive nuclei to stable nuclei in a sample as well as the characteristic half life time of these species allows us to accurately determine the age of the studied material. Isotopes of different elements have been used for dating purposes. Although ^{14}C is the most established method it allows the dating of material of only up to 62,000 years old (Plastino et alo. 2001) ($t_{1/2}$ = 5730 years).

$$N(t) = N_0 e^{-\lambda t} = N_0 e^{-t/\tau}$$
$$t_{1/2} = \frac{\ln 2}{\lambda} = \tau \ln 2$$

Equation 13. Equations describing the relation of the radioactive decay and half time. N_0 – number of atoms at t_0; λ - decay constant; $t_{0.5}$ – half life; τ - mean lifetime

Therefore radiocarbon dating is applicable for relatively young material. Dating on geological timescales requires more stable materials. For that purpose other isotopes are employed. Uranium ^{234}U and ^{238}U (Chebykin et al. 2005), lead ^{210}Pb (Aycik et al. 2004), as well as thorium ^{230}Th and helium ^{3}He (Boyce et al. 2005), cesium ^{137}Cs (Aycik et al. 2004), rubidium ^{87}Rb and strontium ^{87}Sr (Barton Jr. et al. 2004), potassium ^{40}K and argon ^{40}Ar (Sandler et al. 2004) are commonly used. The accuracy and applicability of some of these techniques is still debated (Clauer et al. 2005; Smith, 2001). An interesting approach to recreate the geochronology of sediments is by using racemization of amino acids (Harada et al. 1997; Goodfriend and Stanley, 1996). In this technique the natural process of equalization of the concentration of D/L amino acids is used. With death of an organism the biochemical mechanisms that control amino acid chemistry cease to exist and a slow racemization process begins. Knowing the racemization rate constant, the age of the material can be determined. Unfortunately this method's applicability to sediments is rather poor, since it requires closed systems with sufficient biogenic material present in the whole record, which would be unusual in marine sediments (Millard, 2006). Optical luminescence techniques are another alternative to isotope-based dating techniques (Prescott and Robertson, 1997). It utilizes a "bleaching" effect that certain types of minerals (quartz etc.) are prone to when exposed to sunlight. Recent studies have demonstrated that results obtained with that technique correlate with carbon dating and can be successfully applied to marine sediments (e.g. Olley et al. 2004). Despite the variety of alternative techniques, radiocarbon (^{14}C) dating is still the most popular and the most reliable way of age determination for recent sediments but it requires a source of carbon in the whole sediment record. This carbon is provided by small organisms called planktonic and benthic

foraminifera also referred to as "forams". The applicability of forams for carbon dating purposes has been well established with a large supporting body of evidence (see reviews: Crofield, 2003; Keeling, 2007; Colman, 2007). Foraminifera are very diverse (around 270,000 species) shell bearing (*testate*), single celled organisms (*protozoa*) with thread-like pseudopodia (*granulorecticulosa*). Their shells are mainly built from $CaCO_3$ but also can consist of incorporated grains of different materials (see review by Lipps, 1973). Foraminifera have a geological range from early Cambrian (542 mya) to present which makes them very useful in broad timescale dating (Boyle, 1988; Zachos et al. 2001). Beside dating, foraminifera are used as microfossil indicators of oil presence (Stankiewicz et al. 1997), as oil pollution biomarkers (Morvan et al. 2004) and in paleobathymetry (Aharon and Gupta, 1994), paleoclimatology (Hamilton, 1957; Schwarzschild, 2001), reconstruction of oceanic current variability (Lund et al. 2006), heavy metals and radioactive contamination bioindicators as well as other oceanic pollution studies (Jayaraju et al. 2008), monitoring of ocean acidification (Kuffner et al. 2008), and coral reef assessment (Hallock et al. 2003). Analysis of foraminifera is not a complicated process, though it is very laborious. The fine fraction of a sediment (usually <0.125 mm by wet sieving) must be removed and the individual shells are hand-picked under the microscope. The analyst must distinguish between species and morphotypes (sinistral or dextral) of hundreds of specimens. Selected groups of forams (planktonic usually) are separated and afterwards counting is used for carbon ^{14}C dating.

1.3.1.4 Natural radioactivity

Low levels of radioactive nuclei are naturally present in the marine environment. The weathering and recycling of terrestrial minerals and rocks is the main source of natural radioisotopes. The most abundant natural radioactive species are isotopes of potassium ^{40}K, rubidium ^{87}Rb, thorium ^{232}Th, uranium ^{235}U and ^{238}U and natural decay (thorium and uranium series) process products: polonium Po, radium Rd, radonium Rn and lead Pb (IAEA, 1988).

$$
\begin{aligned}
&{}^{A}_{Z}X \xrightarrow{\alpha} {}^{A-4}_{Z-2}Y + {}^{4}_{2}He \\
&{}^{A}_{Z}X \xrightarrow{\beta+} {}^{A}_{Z+1}Y + e^{-} + \upsilon_e^{-} \\
&{}^{A}_{Z}X \xrightarrow{\beta-} {}^{A}_{Z-1}Y + e^{+} + \upsilon_e \\
&{}^{A}_{Z}X \xrightarrow{\beta+} {}^{A}_{Z+1}Y^{*} + e^{-} + \upsilon_e^{-} \xrightarrow{\gamma} {}^{A}_{Z+1}Y + \gamma
\end{aligned}
$$

Equation 14. General equations of an alpha and beta (±) radioactive decay and gamma emission.

Marine sediments are good radioactivity receptacles (or sinks) compared with other marine materials (Noureddine et al. 1998). The physical properties of sediment (in particular particle size)

and the radionuclides chemical and physical properties determine the uptake of radioactivity by the seabed (NAS, 1971; Lukac et al. 1999). Radioactivity measurements have been proposed as a tool for the prediction of physical properties of the seabed (Ligero et al. 2000) because of their good correlation with organic carbon concentration, and physical properties such as particle size distribution and bulk density. Natural isotopic decay can be linked to geothermal processes. This allows the use of radioactive species as tracers of such processes and can also be employed to evaluate their intensity. As an example radon ^{222}Rn concentration ($t_{1/2}$ = 3.8 days) has been successfully used as a tracer of groundwater fluid expulsion (Judd and Hovland, 2007). The most abundant anthropogenic nuclides are plutonium ^{238}Pu, americium ^{241}Am, cesium ^{137}Cs and strontium ^{90}Sr but this may increase as research in this area grows (Moon et al. 2003; WOMARS, 2005). The sources of anthropogenic radioactive material input into the environments are diverse. According to IAEA (WOMARS, 2005; MARDOS, 1995) three main sources exist: atmospheric nuclear weapon testing; the Chernobyl accident (UNSCEAR, 2000; McKenna and Longworth, 1995) and discharges from nuclear reprocessing plants, in particular Sellafield, UK and Cap de la Hague, France (OSPAR III, 2000; Keogh et al. 2007). Other named sources are sea dumping of nuclear waste; discharges from nuclear power plants; sunken nuclear submarines, satellites and weaponry. Commercial and scientific radioisotopes usage is believed to be far less significant (WOMARS, 2005). Both natural and artificial radioactivity has an effect on aquatic organisms. The natural sources can be a significant contributor since the concentrations of the radioactive nuclides vary considerably with the type of minerals as well as with the geological conditions (Brown et al. 2004). Nevertheless natural processes in the seabed and water column create favourable conditions for radioactivity accumulation (UNSCEAR, 2000; Mihai et al. 1999 etc.) and therefore they should be monitored. Depending on emitter type, chemical character of the radionuclide and its form in the environment different techniques are employed to extract a species from a matrix and quantitatively enrich and analyse it (see review by Myasoedov and Pavlotskaya, 1989). Extraction of radionuclides can be performed by classic methods such as selective extraction chromatography (Michel et al. 2008), ion chromatography and ion exchange methods (Mobius et al. 1995), precipitation and co-precipitation (Mobius et al. 1995) sublimation (Zhuikov, 2005) and electrophoresis (Erk et al. 1998). Also novel approaches have been proposed such as targeted sequential extraction (Lucey et al. 2007) and magnetic extraction (McCubbin et al. 2004) as well as improvements of existing protocols (Emerson and Young, 1995). Comparitive studies confirm that methods are well established and demonstrate consistent performance (Vianna et al. 1995; Tauhata et al. 2006). After radionuclides are isolated, samples are usually analysed by liquid scintillation counting techniques which have proven reliable and fast in the case of both α- and β- emitters (Equation 14) (Schonhofer, 1995). Alternatively, for dry samples, proportional flow 2π or 4π counters are used (Myasoedov and

Pavlotskaya, 1989). Except the total emission count, also the strength (amplitude) of α- and β-pulses can be differentiated and used to identify and quantitatively characterize radioisotopes. As a matter of fact, most radioisotopes emit gamma rays of specific energy and intensity (Uosif, 2007). The strength of the emission can be determined by gamma spectrometry. Regarding novel approaches, techniques such as chelation IC (Shaw et al. 2000), isotope dilution sector field ICPMS (Hinrichs and Schnetger, 1999), laser fluorometry (Premadas and Srivastava, 1999) and popular isotope dilution thermal ionization mass spectrometry, ID-TIMS (Parrish and Noble, 2003) can be mentioned (see review by Clement et al. 2001).

1.3.1.5 Core logging

Core logging is a generic term describing high resolution, mostly non-destructive, physical properties measurements conducted on line during core sample collecting or shortly after the core retrieval. This sediment core sample analysis technique was historically developed and implemented by the petroleum industry in 1940s in the form of so-called '*wireline logging*' of exploratory boreholes and oil wells (Pointecorvo, 1941) and was later adapted to soil core measurement (Bernhard and Chasek, 1955). The first core logger designs limited their use to boreholes and they were able to measured only density of the sediment by means of gamma ray attenuation. However in the 1960s the first automated system for whole core measurements, called GRAPE, was presented (Evans, 1965). Development of this system allowed high resolution bulk density of intact seabed cores to be recorded and it was popularized greatly by the Ocean Drilling Program (ODP). The great potential of this technique was further enhanced by addition of other sensors, such as compressional sound wave velocity (P-wave, Schultheiss and McPhail, 1989). This allowed construction of synthetic seismograms, more precise structural and seismic correlations, quality assessment of unopened cores and even acoustic sediment classification (e.g. Breitzke, 1997; 2000b). Robinson, 1993 introduced a loop-based magnetic susceptibility (MS) sensor. The degree of '*magnetisability*' of sediments is frequently used in provenance and correlation studies as well as diagenetic and speciation studies of Fe-bearing minerals (e.g. Somayajulu et al. 1978; Kasten et al. 1998: Heider et al. 1996). Further development of automated track core logging systems brought in even more useful add-ons such as: non-contact electrical resistivity and digital colour imaging systems, gamma spectroscopy, grey reflectance and diffusive spectral reflectance sensors (e.g. Merrill and Beck, 1995; Broecker et al. 1990; Weaver and Schultheiss, 1990). With such capabilities the application of logging data was expanded to the fields of paleoceanography and paleoclimatology (e.g measurements of productivity variations during glacial-interglacial cycles derived from grey reflectance data, Bond et al. 1992), mineralogy (e.g. sediment colour analysis

used to determine geochemical proxies, Nederbragt et al. 2006), chronostratigraphy (e.g. correlation of colour logs with isotopic proxies of marine sediment cores, Rogerson et al. 2006), environmental protection (e.g. characterization of sediment cores contaminated with petroleum fluids with use electrical resistivity logging, Atekwana et al. 2004) and many others. Commercially available core loggers are now widely used by industry and academic users. By June 2005 the number of the multi-sensor core logger (MSCL, GEOTEK) reached 84 and made this system the most popular logging instrument (Rothwell and Rack, 2006). This system operates in vertical (half cores) and horizontal (whole cores) configuration and is capable of measuring all above mentioned physical properties with 1 mm resolution with 12 m of core per hour throughput.

1.3.2 Geochemical properties of sediments

1.3.2.1 Estimation of organic and inorganic carbon content

Inorganic and organic carbon are important components of marine sediments. Concentrations of both of these components can vary greatly depending on oceanographic regime and depositional conditions. Relative enrichment in either of the components is often used to determine the origin of the sediment and is a useful indicator of the biological activity in the water column and the sediment itself despite all of the organic carbon and nearly all of the inorganic carbon as well (in the form of carbonate) in marine environment being of biogenic, including anthropogenic, origin (Schulz and Zabel, 2006). In general sediments closer to landmass are referred as '*terrigenous'* and are characterized by moderate to high organic carbon contents and high lithic components (quartz, feldsprar, mica) derived from land erosional processes. Inorganic carbon in these sediments can be present in substantial amounts or even completely dominate the sediment composition, particularly in high energy environment. The biogenic or calcareous component is derived mainly from phytoplankton detritus as well as skeletons of benthic organisms. Open ocean or '*deep sea'* sediments (pelagic and hemipelagic) usually have low lithic component, with the exception of red clays, and are dominated by calcareous and siliceous material derived from $CaCO_3$ bearing organisms and biogenic opal (SiO_2), respectively. The organic carbon content in marine sediments can vary by orders of magnitude. The concentration is influenced by the supply of organic matter, its form or availability (labile or recalcitrant), the rate of preservation, oxygen avaiability and the activity of benthic organisms. In general only a fraction of organic carbon is buried in the deep sediments, the majority is mineralized in the first meters. Henrichs and Reeburgh, 1987 estimated that between 20 and 90% of organic carbon of shelf and estuarine sediments is mineralized in these processes which collectively are referred to as the '*early diagenesis*'. The

spectrum of typical organic carbon contents in shelf sediments varies greatly as these settings are considered the most dynamic oceanic environments (Schulz and Zabel, 2006). In areas of low productivity and lower sedimentation rates organic carbon contents can be similar to those typical of hemipelagic and outer shelf environments and vary between 0.3 and 1%. On the other hand areas within oxygen minimum zones (lowest oxygen saturation in the water column) and that experiencing intensified sedimentation and upwelling can exhibit surface sediment organic carbon contents exceeding 10% (Schulz and Zabel, 2006). Moreover specific sedimentary layers created during anoxic events so called '*sapropels*' i.e., have been reported to exceed 30% organic carbon by weight (Emeis et al. 1996; Thomson, et al. 2006). From the first order geochemical information derived from these analyses they also provide very important practical information to guide further sample processing. Many analytical procedures require the organic and/or inorganic carbon to be removed as it interferes or complicates further analysis (such as particle size analysis or DNA extraction).

1.3.2.2 Major and trace elements

Major and trace elements occur naturally in marine sediments, mainly as structural components of minerals. Anthropogenic activity can result in certain metals accumulate in marine setting to a point when they become toxic and have impact on aquatic ecosystems. Cycling of major elements (Fe, Mn, S, Si, and Ca) and trace elements (Co, Cd, Cu, Ni, Zn and Mo) also plays an important role in mineral and organic matter diagenesis (Burdige, 2006). Inorganic material in marine sediments can be divided into four classes: authigenic, biogenic, detrital and anthropogenic. Authigenic material is created *in situ* in the sediment, on its surface as well as in the water column. The formation mechanisms are related to direct precipitation from the water column or through chemical reactions in the sediments. The most important authigenic minerals are nonbiogenic carbonates such as dolomite - $CaMg(CO_3)_2$ (Moore et al. 2004) and rhodochrosite – $MnCO_3$ (Burke and Kemp, 2002); manganese and iron oxides (MgO, FeO) often enriched with nickel, copper and cobalt (Burdige, 2006); phosphate minerals, carbonate, fluoroapatite (Ruttenberg et al. 1993); sulfide minerals: mackinawite (FeS), greigite (Fe_3S_4), pyrite (FeS_2) (Morse, 1999) and different types of phyllosilicates (clays). In the context of fluid flow it is worth mentioning that hydrothermal fluids expelled through the seabed are often enriched in metal ions (Elderfield and Schultz, 1996; Alt, 2003). The biogenic material is dominated by biogenic carbonates: calcite and aragonite – $CaCO_3$ (Jahnke and Jahnke, 2004) and amorphous hydrated silica – SiO_2 x nH_2O (Vrieling et al. 2002) which are produced by algae, zooplankton and diatoms. Nevertheless phosphate, iron and manganese minerals can also be important biogenic component (Burdige, 2006). The detrital

component is mainly a result of land weathering and erosion and to a smaller extent, volcanic activity. These processes are most significant in coastal and continental margin zones due to their proximity to land masses. Dissolution of salt (NaCl, KCl) deposits, limestone ($CaCO_3$) and silicate rocks as well as red-ox processes (e.g. pyrite oxidations) are the most common detritus formation mechanisms (Burdige, 2006). Finally, anthropogenic input has been widely discussed in the recent years. Heavy metal contamination is usually observed in industrialized and urbanized areas and harbours (Wilhelmy and Flegal, 1991; Rudneva, 2003; Caplat et al. 2005). As reported by some researchers, this input can spread into adjacent shelf and continental margin zones (Birch, 2000; Ponce-Velez et al. 2006).

Determination of metal contents in marine sediments is not a trivial task. The worldwide inter-comparison analytical exercise performed by the International Atomic Energy Agency (IAEA) in 1990-1997 revealed a significantly poor performance of the participating commercial laboratories in determining trace metals in marine sediments and biological samples (Coquery et al. 1999). In relation to trace metals in marine sediments, 19% of the participants decreased in their performance (reported not accurate values) and as much as 36% were reported to be consistently poor. The complexity of these analyses is reflected in scientific literature where numerous comparison studies, new methodologies and method optimization protocols are published (Trim et al. 1998; D'Amore et al. 2005, Lo and Sakamoto, 2005; Chen and Ma, 2001). A variety of extraction and instrumental methodologies have been proposed but accurate and reliable analysis is still challenging. Among the most popular methods are: gas chromatography –GC (Sillanpaa and Ramo, 2001), high performance liquid chromatography – HPLC (Nowack et al. 1996), ion chromatography – IC (Cardellicchio et al. 1999), inductively coupled plasma spectrometry – ICP (Gasparics et al. 1997), atomic absorption spectrometry – AAS (Macias-Zamora et al. 1999), capillary electrophoresis - CE (Ali and Aboul-Enein, 2002), voltametric methods, i.e. polarography (Kowalska et al. 2002) and recently proposed X-ray fluorescence (Giancoli Barreto et al. 2004) [for other less popular methods see detailed review by D'Amore et al. 2005]. Most of these techniques are destructive and involve extraction of analytes in harsh conditions of concentrated acids at elevated temperature and pressure. Milder protocols such as weak acid extraction or complexation with EDTA extract only chelate-available or CH_3COOH-available species, thus are not useful for total metal analyses.

1.3.2.3 High resolution major and trace analysis by X-ray fluorescence scanning

Recent developments of X-ray fluorescence (XRF) scanners enable non-destructive, very high resolution (30 μm) major and trace element profiling of sediment cores. In general XRF scanners operate on the principle of emission of secondary X-rays emitted by material components

that have been excited by bombardment of high energy X-rays. In other words atoms exposed to high energy X-rays lose one or more electrons from inner atomic shells which are subsequently filled with electrons from the other shells with the emission of the energy in form of an X-ray pulse. The emission energy and wavelength varies between different atoms making the element fingerprinting and abundance estimation possible (Rothwell and Rack, 2006). The first XRF scanner (CORTEX) was developed 1988 in Holland and offered resolution of 1 mm and initially logged only K and Sr profiles. It was later modified to log Al, Si and elements heavier than Sr (Jansen et al. 1998). This instrument was successfully used at sea even in difficult weather conditions. The second generation scanner (AVATECH) become available in 2002 and offered greater sensitivity and element mass range from Al to U (Richter et al. 2006). Other popular XRF scanners are Eagle μProbe (Roentgenanalytic Messtechnik GmbH, Haschke, 2006) and ITRAX (Cox Analytical Systems, Croudace et al. 2006), the scanner used in this study. The XRF technique despite advantages such as: high resolution, fast and non-destructive analysis, has significant limitations. XRF scanners analyse only the surface of the sediment and excitation volume is very small hence they are best suited to homogenous samples. Mineralogy and grain size changes can influence the result and must be taken into account when analyzing data. Also sensitivity of the XRF method favours heavier elements with Al and Si being the least reliable. Moreover the collected data can be affected by pore fluids that tend to collect on the surface, and the surface roughness can lead to artifacts and false signals. Despite these limitations however XRF element profiles are very useful in tracking sedimentological, environmental and diagenetic changes as well as correlation studies (Croudace et al. 2006).

1.3.2.4 Molecular and bulk characterization of organic matter

The characterization of organic matter because of its complexity requires target specific, sequential approaches and very often sophisticated techniques and instrumentation. In many cases the first step of the organic matter analysis is the analysis of so called '*bulk parameters*' often referred to as '*first order analyses*' such as total organic/inorganic carbon, nitrogen and sulphur (TOC/TIC; TN, TS) analysis of stable isotope ratios of these elements and others like hydrogen i.e. ($^{13}C/^{12}C$; $^{15}N/^{14}N$; $^{34}S/^{32}S$; $^{2}H/^{1}H$) and Rock-Eval pyrolysis. The analysis of these first order proxies can be very informative and answer questions about the origin of the organic matter, changes in depositional regime, paleoenvironmental conditions and give first insight into its composition (Schulz and Zabel, 2005). The interpretation of these parameters often requires additional information from other parameters such as sedimentation rates or grain size distribution i.e. Berner and Raiswell, 1983 demonstrated that pyrite sulphur is positively correlated with remnant organic

carbon (S/OC ratio) and can be indicative depositional environment (oxic vs. anoxic).Veto et al. 1994 have shown that it is possible to estimate pre-diagenetic content of organic carbon from the stoichiometric relationship of OC oxidation via sulphate reduction corrected for diffusive loss of volatile H_2S in non-bioturbated sediments. Also C/N ratios were extensively used by geochemists as a marine/terrigenous organic matter proxy. Because of higher TN contents in typical marine organic matter low C/N ratios (C/N: 4-10) were considered indicative of dominant marine character while higher values (C/N: >20) pointed into more terrigenous material. However many authors report that this ratio is not as reliable as it was previously thought (see Meyers, 1997 for review). Nitrogen rich marine organic matter is preferentially degraded during early diagenesis thus TN content can be underestimated in areas with sufficient water depth raising the overall C/N ratio. The sorption by clay minerals of inorganic nitrogen released during diagenesis is another mechanism observed in deep water sediments that biases the C/N toward lower values. Moreover the C/N ratio differs in coarse and fine grain size fractions, hence hydraulic sorting of the sediment during transportation can affect it. It is now accepted that this ratio is only useful as a crude marine/terrigenous source indicator and is the least biased in shallow marine sediments (Schulz and Zabel, 2005). Bulk stable carbon and hydrogen isotope ratios ($^{13}C/^{12}C$; $^{2}H/^{1}H$; $^{15}N/^{14}N$) are considered more reliable parameters and apart of discrimination between marine and terrigenous matter allow insight into the type of plant matter deposited and the hydrological conditions of the environment supporting these parent plants (Schulz and Zabel, 2005) (Table 2). These ratios (reported in δ notation) reflect the stable isotope composition of the source as well as processes of fractionation between isotopes (Table 2) during photosynthesis ($\delta^{13}C$), the hydrological cycle (δD) and other processes. In a general physical sense the isotopic fractionation is a process of discrimination between light and heavy isotope of the nuclei. In most cases isotopic fractionation is caused by reduction of vibrational energy of a system that is in a chemical equilibrium when smaller (lighter) molecule is introduced instead of larger (heavier) molecule. On physicochemical level isotopic composition of nuclei influences its properties such as diffusivity, atomic velocity or strength of chemical bonds (Urey, 1947). A good example of this type of fractionation is slightly faster evaporation of isotopically 'light water' ($H_2{}^{16}O$) compared to isotopically 'heavy water' ($H_2{}^{18}O$) or calcite-water oxygen isotope fractionation during calcite precipitation (e.g. Demeny et al. 2010). Mass-independent fractionation is rare however it was reported for oxygen and sulphur isotopes in geological samples (Clayton et al. 1973 and Halevy et al. 2010 respectively). In a biological sense isotopic fractionation is the preferential use of the light isotope over the heavier isotope by organism's cellular organelles in the natural biological processes such as photosynthesis or biosynthesis of lipids (Hayes et al. 1993; Sessions et al. 1999).

Table 2. Typical isotopic composition of carbon sources, autotrophic and heterotrophic biomass, bulk types of OM as well as examples of isotopic fractionation processes. Data after Killops and Killops, 2005; Schulz and Zabel, 2005 and the references therein.

Isotopic composition of the C source	**$\delta^{13}C$ (‰)**
Atmosphere CO_2	-7
Dissolved CO_2	-6
Bicarbonate HCO_3^-	+1.5
Isotopic composition of the organism biomass	**$\delta^{13}C$ (‰)**
C3 plant	-23 to -34
C4 plant	-6 to -23
CAM plant	-11 to -33
Algae	-8 to -35
Cyanobacteria	-3 to -27
Green bacteria	-9 to -21
Red bacteria	-26 to -36
Purple bacteria	-19 to -28
Methanogenic bacteria	+6 to -41
Terrigenous OM	-29
Marine OM	-19
Soil under C3 vegetation	-27
Soil under C4 vegetation	-14
River mouth POM	-27
Shallow fan deposit	-25
Slope fan deposit	-22
Deep fan deposit	-21

Isotopic fractionation (ε_c)	**$\delta^{13}C$ (‰)**
Equilibrium between atmospheric and dissolved CO_2	0.7
Equilibrium between dissolved CO_2 and bicarbonate	9
Equilibrium between bicarbonate and calcite	2
CO_2 assimilation by terrigenous C3	22
CO_2 assimilation by C4	4
CO_2 assimilation by CAM	15
CO_2 assimilation by marine C3	25
Bicarbonate assimilation by phytoplankton	12
CO_2 assimilation by marine chemotrophes	25
CO_2 incorporation into methanogen biomass	40
CH_4 production during freshwater microbial methanogenesis	40
CH_4 production during marine microbial methanogenesis	70
CH_4 incorporation into methanotroph biomass	20
CO_2 production by methanotrophy	25
Isotopic fractionation (ε_D)	**δD (‰)**
Precipitation in the tropics	0
Precipitation in high latitude mountainous areas	< -150
Precipitation in arid areas	100
Biosynthesis of *n*-alkyl lipids	100 to 250
Biosynthesis of polyisoprenoidal lipids	150 to 350
Biosynthesis of algal sterols	201

Bulk $\delta^{15}N$ has been used to differentiate between algal and land derived matter. Peterson and Howarth, 1987 have shown that isotopic differences in nitrogen sources are preserved in the organic matter of the organisms. The isotopic signature of the marine nitrate ($\delta^{15}N$ from 7 to 10‰) assimilated by algae and atmospheric nitrogen utilized by C3 plants ($\delta^{15}N$ = 0‰) is preserved in their respective biomass ($\delta^{15}N$ of 0.4±0.9 for algae and $\delta^{15}N$ of 8.6±1.0 for the C3 plants). However Meyers, 1997 points out that environmental change and isotope discriminating processes such as

denitrification of dissolved nitrate in oxygen depleted waters (isotopic modification of available nitrogen by selective release of $^{14}N_2$) or incorporation of dissolved nitrogen by nitrogen fixing algae may shift the bulk isotopic ratio towards anomalous values. Cross correlation of these bulk parameters allow greater insight into the nature of the dominant process shaping the isotopic composition of the OM. This approach is particularly helpful in studies of source rocks as it allows correlation of oil source bitumen with petroleum regardless of biodegradation and associated isotopic composition changes (Tissot and Welte, 1984). Similarly Rock-Eval pyrolysis and other pyrolytic techniques (Curie-point pyrolysis; off-line pyrolysis i.e.) permit the assessment of hydrocarbon potential and identification of the type and maturity of OM present in the sediment or source rock. Rock-Eval pyrolysis allows measurement of the amount of free hydrocarbons and hydrocarbon-type compounds present (by gradual thermal volatilization), the amount of hydrocarbons generated through thermal cracking (by kerogen pyrolysis at temperatures from 300 to 550^{o}C), the amount of oxygen in the OM (estimated from the amount of CO_2 produced during pyrolysis) and the maturity of the OM (estimated from temperature of maximum pyrolysis yield). The data is usually presented in the form of van-Krevelen cross correlation plots of Hydrogen and Oxygen Indices (HI and OI) correlated to atomic ratios of H/C and O/C respectively allowing ascription of one of the kerogen types and the state of the OM alteration. Gas chromatography assisted pyrolytic techniques (particularly Py-GC-MS and Py-FIMS) allow further identification of pyrolysis products on a molecular level (Rullkotter and Michaelis, 1990). These pyrolysis products can often be used as specific source structural indicators i.e. lignin (e.g. Schulten and Gleixner, 1999).

More specific characterization of sedimentary OM requires in most cases separation of the whole OM or the fraction of interest from the solid matrix and/or removal of chemical species interfering with the analysis. This not a trivial task as the OM in sediments and soils is part of a highly heterogeneous system where it interacts with metal ions, mineral colloids and clays (Hatakka, 2001). Naturally this chemical and molecular complexity of the OM requires target specific approaches in both isolation and analysis. Complete isolation of organic matter from mineral matrix is yet to be achieved however extraction of individual chemical groups of OM constituents is possible by exploiting their chemical properties. As described by Stevenson, 1994 optimal extraction should: isolate unaltered material, be free of inorganic contaminants, yield with fractions representing parent material across entire mass range and be universally applicable to all types of sediments and soils. Such method is yet to be discovered for marine organic matter however over the years different approaches have been tested and current refined extraction techniques are more efficient and less destructive. Reported OM extraction methods have generally

been adopted from petrologic and petroleum studies, and modified accordingly to facilitate extraction from marine sediment matrix. The most efficient OM extraction technique reported involves sequential use of aqueous 0.1 M sodium hydroxide (NaOH) solution. This technique allows extraction yields of up to 80%. Other approaches involve the use of both organic and inorganic media such as sodium carbonate (Na_2CO_3, η=30%), sodium pyrophosphate ($Na_4P_2O_7$, η=30%), ethylenodiaminotetracetic acid (EDTA, η=16%), ethylene diamine (EDA, η=63%), dimethyl sulfoxide (DMSO, η=23%), formic acid (HCOOH, η=55%) and many others (review Hayes et al., 1985). The sodium hydroxide extraction yield increases with the concentration of the base and time of extraction however in such conditions undesirable oxidation of OM is known to occur. This can be minimized with the use of extractant solution sparged with inert gas (e.g. nitrogen or argon) as well as performing the extraction in protective atmosphere of such gases (Hatakka, 2001). Other known undesirable effects associated with this technique are hydrolytic breakdown of macromolecules, amino-carbonyl condensation, and contamination with dissolved silica (Senesi and Loffredo, 2005). The extraction efficiency can also be improved by pretreatment with hydrofluoric and hydrochloric acids (HF-HCl) to remove the Ca and other polyvalent cations. Moreover this pretreatment originally used for de-ashing of coals and kerogens (Saxby, 1970; Robl and Davis, 1993) is the method of choice for removal of paramagnetic material interfering with the solid state NMR analyses (Skjemstad et al. 1994). Paramagnetic ions lead to significant signal broadening and very poor quality of the NMR spectra (Baldock, et al. 1992). Other methods of their removal that involve particle size and density fractionation, and even hand picking of organic fractions (Oades et al. 1987) are not applicable to fine grained material, which might contain high ash content, and can result with misrepresentation of the whole OM in both soil and sediment. Moreover in recent sediments a significant part of the OM can be labile matter that is protected by associations with the sedimentary matrix (e.g. Meyer, 1994, Keil et al. 1994). Because HF-HCl pretreatment dissolves the inorganic matrix the liberated OM can be released to the aqueous HF-HCl solution and lost in the pretreatment process. Durand and Nicaise, 1980 have shown this procedure can result with losses of up to 50% of the organic carbon in recent marine sediments and in some soils 92% of the carbon is solubilized and lost (Rumpel et al. 2002). Not all NMR experiments require HF-HCl pretreatment. Solution NMR experiments also termed '*liquid NMR*' experiments are performed on the directly extracted OM and usually offer greater resolution than solid state NMR experiments however the latter are considered better suited for the OM studies. In the solution NMR experiments effects such as: low solubility of the OM in suitable NMR solvents, solubility related formation of colloidal suspensions and sample fractionation, pH effects on the chemical shifts and signal obscuration by solvent peaks complicate the analysis and the interpretation of the results (Sannigrahi, 2005). Additional to potential carbon loss sediment de-

ashing can result in alteration of the organic matter. However Rumpel et al. 2006 have shown that these alterations can be identified only with the use of more sensitive techniques such as Py-GC-MS. They found changes in quantity and composition of saccharides and lignin fractions of the OM after HF treatment however these changes were not observed in both ^{13}C CP/MAS NMR and FTIR experiments due to lower sensitivity of these methods. To minimize carbon loss in the de-ashing procedure Gelinas et al. 2001b proposed a protocol for recovery of solubilized organic carbon by removal of Ca and residual HF, paramagnetic metals and dissolved salts from the solute by selective precipitation and ion retardation chromatography.

The OM is often partitioned into an organic solvent soluble fraction so called the '*bitumen*' and an insoluble fraction referred to as the '*kerogen*'. This division however does not include the geomacromolecules that survived the early stages of microbial diagenesis and are considered one of the precursors for kerogen. Humin, humic acids and fulvic acids are generally partitioned based on their solubility in bases and acids while kerogen is neither soluble in non-oxidizing acids, bases and organic solvents (Breger, 1961). Other methods involve molecular size partitioning (e.g. gel permeation chromatography or ultrafiltration), charge characteristics partitioning (e.g. polyacryloamide gel electrophoresis), adsorption partitioning (e.g. adsorption on alumina or methylmethacrylate resins such as XAD-8). Kerogen is a highly defunctionalized geomacromolecule finely dispersed in the sedimentary matrix. Because it is a polymeric substance it is challenging to determine its molecular building blocks and extract it effectively without alteration. The most popular methods of studying kerogen composition are based on destructive oxidation and pyrolysis products analysis. Non-destructive approaches include solid-state Fourier Transformation-Infrared Spectroscopy (FT-IR) and, more popular recently, solid state ^{13}C NMR and other spectral methods (e.g. fluorescence and electron spin resonance spectroscopies). Bitumen on the other hand consists of low molecular weight substances mainly lipids and corresponding sulphur bearing compounds (Schulz and Zabel, 2005). Bitumen components can be further partitioned based on their solubility differences in polar and apolar solvents. Effective analysis of low molecular weight molecules can be performed with chromatographic methods such as High Pressure Liquid Chromatography (HPLC) or Gas Chromatography (GC). These methods are particularly powerful coupled with mass selective detectors (MS) and in case of GC the isotope ratio mass selective detectors (ir-MS) as identification based only on retention time is very limited. These are the principle techniques in the OM compound specific molecular analysis often termed '*molecular marker*' approach, as they can identify source specific groups of molecules or individual compounds often referred to as '*biomarkers*'. The concept of molecular markers came from early work by Alfred Treibs who studied petroporphyrins in shales, bitumens and oils. Treibs, 1936

discovered structural similarities between petroporphyrins and plant chlorophylls and proposed that the latter are the diagenetically modified precursors of the petroporphyrins. The degradation pathway proposed by Treibs, 1936 was the first molecular evidence for biogenic origin of petroleum linking biological precursor with its diagenetic product (Eganhouse, 1997). With the development of modern analytical instrumentation more and more biological markers were discovered and implemented to describe diagenetic processes in the sediment, origin of the OM, contamination, structure and activity of microbial communities and others. However, although biomarker analysis is a very potent technique it is not without limitation. Ideal biomarkers must be source specific and have a conservative behaviour in the environment. In practise these prerequisites are met only to a varying degree. Biomarkers introduced to the environment are subject to various physical and chemical processes discussed in the previous paragraphs which determine among others their spatial distribution and degree of alteration. Some of them are a product of a unique process and can be ascribed to specific organisms and/or specific environmental conditions others however are less specific and must interpreted in a wider context. For example long chain alkenones $C_{37:2}$ (heptatriaconta-15E,22E-dien-2-one) and $C_{37:3}$ (heptatriaconta-8E,15E,22E-trien-2-one) exclusively produced by marine algae (*Haptophyceae*) are used as palaeo-seawater temperature indicators. These compounds are produced only in specific temperature conditions (5-28^{o}C) and their sedimentary record can be used to reconstruct past seawater temperature (Brassell et al. 1986). Similarly temperature dependent (0-35^{o}C) structural modification of core lipid structures by marine archaea *Crenarchaeota* was used to develop a biomarker based paleothermometer (Schouten et al. 2002).

1.4 Aims and objectives

The first aim of this research is to (1) provide insight in to the nature of the sediments on the Malin shelf (Chapter 2) and in the Dunmanus Bay (Chapter 4) and provide necessary data for the validation of the acoustic seabed classification models of both areas. The Malin area is a commercially important fishery grounds where large landings of pelagic (e.g. herring) and demersal fish (e.g. cod, haddock). Shellfish are not commercially exploited however they and other invertebrates are part of the food web. Dunmanus Bay on the other hand is an important spawning and nursery site actively used in mariculture for farming of salmon and was classified as part of the Biologically Sensitive Area by INFOMAR project. Despite the economic and conservational importance of these areas they received very little attention and there is virtually no knowledge of geochemical and physical properties of the seabed in the scientific literature concerning these areas.

Both sites show surface expression of fluid expulsion is present in the form of pockmark features. Behaviour of fluids in the subsurface sediments is still poorly understood phenomena. Active fluid systems can have serious implications for off shore activities but also promote special ecosystems that might require protection. Second aim of this research is to (2) provide insight into the fluid system present in the subsurface, investigate the nature of the fluids and their interaction with the seabed and the water column, estimate the activity of the pockmark features and potential influence on biota (Chapter 2 and 4). The third objective is to (3) provide insight in to the nature and molecular composition of organic matter on the Malin Shelf, discuss the sources and potential transportation routes of organic matter and provide baseline biomarker inventory in this area (Chapter 3).

CHAPTER 2 – GEOCHEMICAL AND PHYSICAL CHARACTERIZATION OF THE MALIN SHELF SEDIMENTS COUPLED WITH INSIGHTS INTO THE FLUID FLOW PROCESS IN A LARGE COMPOSITE POCKMARK

2.1 Introduction

2.1.1 Geology of the bedrock and the sediments of the Malin Shelf

The Malin Sea is an extensive area of ca. 23000 km^2 located off Malin Head on the northern Irish coast. Geographically, the area lies between longitudes 10^o and 6^o W, and between latitudes 55^o and $56^o30'$ N and is of complex geology. The area comprises sediment filled elongated depressions (also called graben) separated by rare outcrops and uplifted bedrock formations. These depressions were formed as a result of a land mass being downthrown and are usually accompanied by parallel or semi parallel faults. Estimated formation time of these facies ranges from the Late Carboniferous (312 – 304 Ma) to post Hercynian (Late Paleozoic). The geological structure of the Malin Sea has been proposed by Dobson and Evans, 1974 and consists of several components: the Coll-Tirre-Skerrvore-Stanton Banks Outer Hebrides Platform basement blocks lie the north, while part of the Inner Hebrides Trough falls into the Blackstone and Colonsay Basins southwest. The Malin Basin and Main Donegal Basin are found further west while the South Donegal Basin is central with the Isle-Donegal Platform being located in the south. Since 1974 several researchers have studied the Malin Sea and boundaries areas but the first review by Dobson and Whittington, 1992, containing the synopsis of this work, was published much later.

The thickness of the sedimentary layer above the bedrock varies from 30 to more than 200 meters. These sediments contain material from the Upper Carboniferous (312 - 304 million years old [Ma]), Permo-Triassic (304 – 204 Ma), Lower Jurassic (204 – 183 Ma), Middle Jurassic (183 – 165 Ma), a thick section of Cretaceous (151 – 71 Ma) and Lower Tertiary (71 – 28 Ma) periods. In the Mesozoic, periods of uplift and erosion limited sedimentation. The same processes in the Tertiary were accompanied by extensive igneous activity, therefore igneous dykes and other intrusions can be frequently observed underneath and sometimes above the seabed. The latest thick

Quaternary sediments (2.6 Ma until present) are dominated by glaciomarine material and contain the record of three of the five glacial cycles that took place in the Pleistocene over this area. Evidence of glacial shelf signatures (e.g. furrows, marginal moraines) marking the extent of the British Irish Ice Sheet were found in the INSS and INFORAR data sets and reported by Dunlop et al. 2010. The stratigraphic description of the Quaternary sediments include several formations: the most recent sediments, the so called Lorne Formation, followed by post glacial, thick, fine grained shelf deposit from the Jura Formation; silty clays with dropstones from the Barra Formation (26 kya); till remnants from the Hebrides Formation, silt and clays with dropstones from the Stanton Formation (118-50 kya); not identified sediment type from the Cana Formation; diamicton of clays with boulders from the Malin Formation and the oldest stiff micaceous clays with dropstones from the Skerryvore Formation (Figures 13 and 14).

2.1.2 Structural geology of the Malin Shelf

The studied area of circa 260 km^2 is located in the centre of the Malin Sea between $7^o40'$ and $8^o30'$ W longitude and between $56^o00'$ and $55^o50'$ of N latitude. The northern boundary is determined by a Stanton Banks Fault and lies just 1' south from the feature itself. On the south it rests on the Malin Terrace. On the west the area opens towards the Main Donegal Basin and South Donegal Basin, with few minor faults and folds. On the east the study area falls into Skerryvore Trough and Skerryvore Fault which crosses throughout the basin (Figure 14). Studies have shown that gas leakage may be related to the presence of major faults underneath the seabed Kutas et al. 2004. In this context it is worth noting that underneath the studied basin there are three important faults. The Skerryvore Fault passes throughout the whole basin, while two minor faults are at the western boundary that may be involved in the gas upward migration. In the studied area, some of the detected pockmarks occur in lines tens of km long following the main geological structures (NE-SW Skerryvore Fault, NW-SE Stanton Banks Fault). Above the seabed surface, the Malin Sea is an area open to high wave energy from a swell dominated Northern Atlantic (McDowell et al. 2005). The closest landmass is Malin Head and Lough Swilly south of the study area. Hydrocarbons have been encountered in several of the northwest offshore basins, particularly associated with thicker permotriassic sequences. Hydrocarbon prospects rely on the existence of Carboniferous source rocks, however, Jurassic to Cretaceous source rocks have also been documented in the region. Palaeogene reactivation of fractures may have allowed the leakage of reservoired hydrocarbons to the upper subsurface (Parnell,1992).

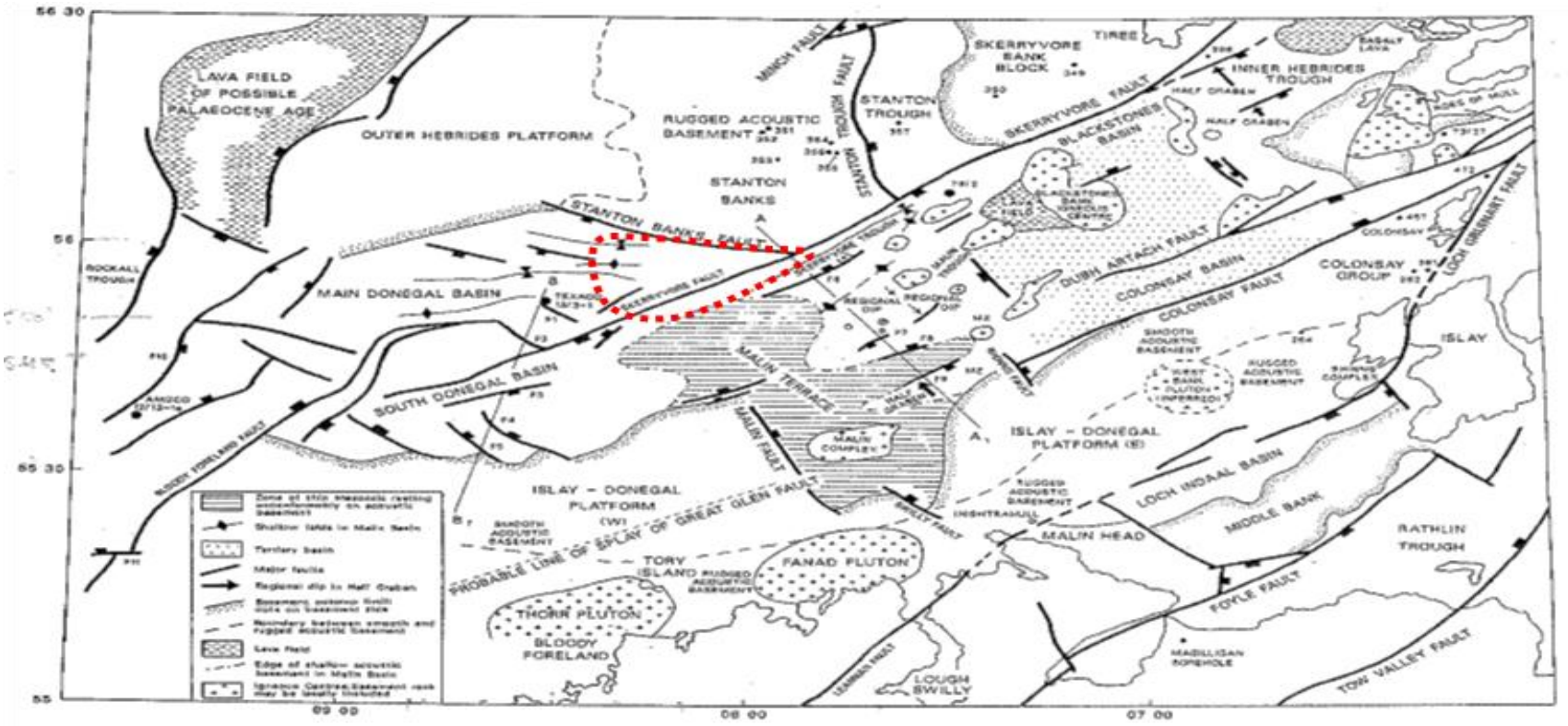

Figure 13. Geological map of the Malin Sea area with study area described with red dashed lines. Image reproduced from Dobson et al. 1974.

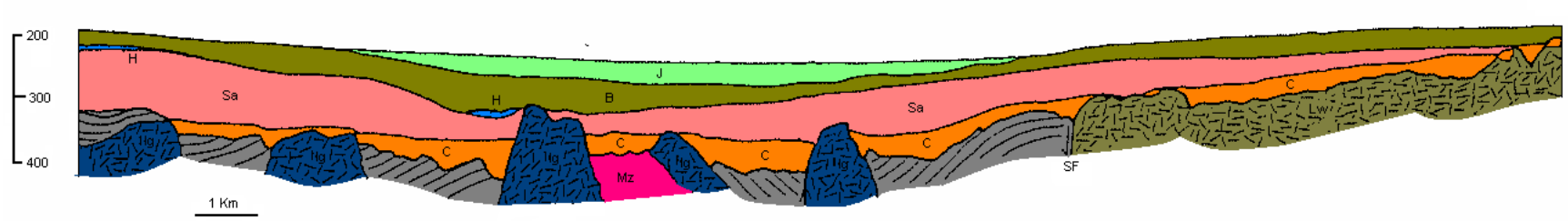

Figure 14. Shallow seismic profiles interpreted by Dobson et al. 1974 showing the Quaternary stratigraphy. Line is crossing the study area from N to S at 7°50'W. Abbreviations refer to sedimentary formations. J – Jura; B – Barra; Sa – Stanton; C – Cana; H – Hebrides; Mz – Mesozoic; Ig – Igneous; Lw – Lewisian; SF – Skerryvore Fault.

2.1.3 Oceanography of the Malin Shelf

The Malin Shelf area is under the influence of the Irish Coastal Current (ICC) which originates in the Goban Spur (south-western part of the Irish Shelf) and migrates northward through the Porcupine area, the western coast of Ireland, the Rockall Trough and the western boundary of the Malin Sea area on the Malin Shelf and Hebrides Shelf and further north (Fernand et al. 2006). The ICC strength is seasonal and has been found to be more intensive and variable in the winter than in the warm seasons. This current carries nutrients, sedimentary and other particulate material as well as heat and is an important migration path for juvenile fish and larvae.

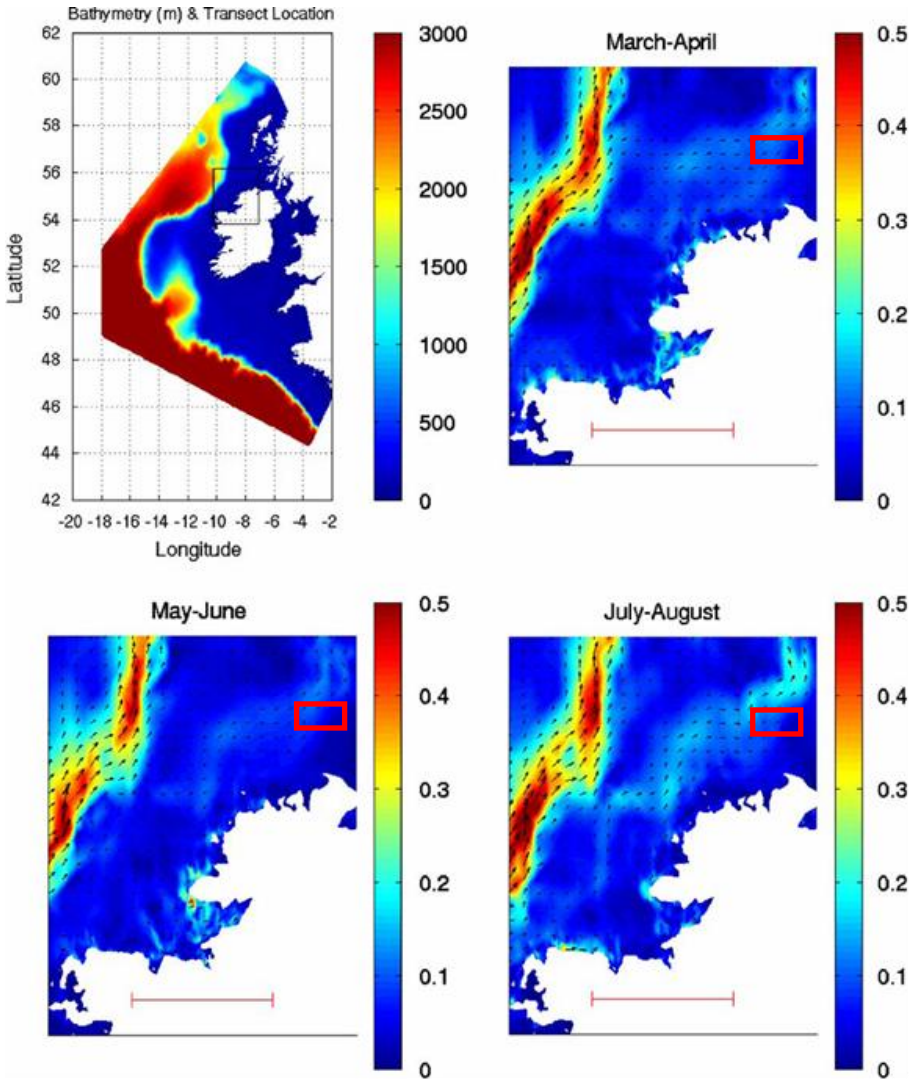

Figure 4. Seasonal variability of the surface shelf edge current with speed (ms^{-1}) and velocity averaged for the top 30m. Red rectangle is the studied area. Image adopted from Lynch et al. 2004

Concentrations of nutrients (nitrate, phosphate and silicate) on the Malin Shelf have been reported to be lower than in open ocean waters (Hydes et al. 2004). Moreover, the shelf edge current is nutrient depleted when compared with oceanic waters but N, P and Si are enriched compared with open shelf waters. However this current show seasonal recruitment (Lynch et al. 2004) and can affect the oceanographic parameters of the Malin Shelf waters as well as deliver suspended material from the Irish Shelf (Figure 15). Hydes et al. 2004 also suggest that waters east of 8.7^{o} W do not mix with the oceanic waters, which confirms the observations of Fernand et al. 2006. The water mixing mechanism in the Malin Sea is bound to tidal activity by vertical mixing and is both diffusive and physical (Fernand et al. 2006). Seasonal stratification due to thermal, haline and density gradients was observed in the Malin Sea waters. This stratification in the studied area is mainly caused by temperature differences, while in the areas of freshwater inputs (Lough Swilly i.e.) it is caused by salinity differences. Stratification has been linked to the distribution of a certain species of zooplankton (Williams et al. 1994) but is not the growth limiting factor.

2.1.4 Hydrobiology of the Malin Shelf

The results of a hydrobiological survey from August 1996 published by Gowen et al. 1998 provide interesting information about plankton distribution among others in the Malin Shelf, including the studied area of the Malin Sea. The following description is based on their work. The distribution of plankton in the water column is seasonal it should not be used as a reference for a broader time scale, because of variability of the growth limiting environmental conditions. Nevertheless it still provides valuable information about the ecosystems in the past and its plankton derived organic matter inputs. Five sampling stations of that survey were positioned on the boundaries of the study area; stations 35 and 37 on the northern boundary, stations 12 and 13 on the southern boundary and station 33 on the western boundary. Water column analysis data from these stations provides insights into the hydrological conditions in the studied area. Salinity values of 35.2 in the shallower section and 35.4 in the northern section are very close to the maximum salinity recorded on the shelf edge. Thermal stratification of the water column is clearly described by a series of isoclines in both areas, while salinity differences are more profound in the deeper section. Density values follow the trend of the thermocline at 50 m with values spanning from 1026.4 to1027.1 kgm^{-3}. Further to the east (Islay Island) horizontal water stratification is disturbed due to water inflow from the North Channel. It is described as vertical haline and thermal fronts. Detailed nitrate measurements confirm the finding of Hydes et al. 2004 that ICC carries water enriched in nutrients compared to shelf waters. Nitrate values spanned from 1.0 mmol m^{-3} in the western part of the shelf, or 1.0 to 1.5 mmol m^{-3} in the eastern part, south of Islay Island at the mouth of the Northern Channel to 0.2 to 0.5 mmol m^{-3} in the study area. Chlorophyll, despite the fact that it is an indicator of primary

productivity does not follow this trend. In the study area chlorophyll concentrations ranged from 0.5 to 1.0 mg m^{-3} with similar values at the shelf break (western boundary) and high values of 7.0 to 10.0 mg m^{-3} at the entrance to the Northern Channel. Phytoplankton was dominated by dinoflagellates, and five species were identified as present in substantial concentrations (>50%) throughout the southern Malin Shelf: diatom *Proboscia alata* (79%) and dinoflagellates: *Ceratium furca* (68%); *C. fusus* (75%); *C. tripos* (75%); *Protoperidinium depressum* (54%). The spatial distribution of phytoplankton in surficial water in the area of study varied significantly between 1 cell ml^{-1} and 150 cells ml^{-1}. The physical water regime (thermal and haline conditions) was distinct enough from surrounding waters to result in specific phytoplankton and zooplankton distributions. Two species were identified to have partial geographical preference to this area: *Halosphaera minor* (Ochrophyta), also detected to the south, west and east but not in the Northern Channel; and *Limacina retroversa* (Mollusca) also occurring south west. Furthermore *Paralia sulcata* (Ochrophyta); *Rhizosolenia setigera* (Ochrophyta); *Amphidoma caudate* (Myzozoa); *Dinophysis rotundatum* (Dinoflagellata) and *Gymnodinium* spp. (Dinoflagellata)were detected in the waters of the same physical regime, but not all in the studied area. Among zooplankton, four species of copepod (Arthropoda) were dominant in the entire Malin Shelf area: *Pseudocalanus elongate*; *Temora longicornis*; *Acartia clausi* and *Calanus* spp which reached $8.7 – 9.1x10^3$ individuals m^{-2}; $1.3\text{-}2.7x10^3$ ind. m^{-2}; $1.0\text{-}2.9x10^3$ ind. m^{-2} and $10.6\text{-}32.0x10^3$ ind. m^{-2} respectively. Also, typical oceanic species and warm/sub-tropical species could be observed, typically throughout the warm seasons. The diversity of plankton in the Malin Shelf, as by comparison with similar waters in the south coast of Ireland, is much lower and the waters are considered impoverished.

2.1.5 Pockmark distribution in the Malin Shelf

Up to 214 depressions deeper than 0.5 m were detected in the area of nearly 1000 km^2. Water depth in the area ranged from 140 to 180 m, with an average depth of 164 m. Apart from two locations where depressions were clustered, pockmarks are sub-circular and comprise one unit. The unit size ranges from 40 to 850 m, and depth ranged from 0.5 to 8.5 m, with an average maximum diameter of 124 m and average crater depth of 1.02 m (Table 3). The pockmark sidewall slopes are relatively steep reaching values up to 8^o. Overall the Malin Shelf seabed has a very gentle slope with an average gradient of 0.2^o (maximum - 0.6^o) towards the south and a gentle inside slope towards the centre of the area (Malin Deep, 8.23 W; 55.92 N). The studied field can be divided into five clusters based on their affiliation with the structural and morphological components of the basin (Figure 17). Pockmarks on the north-western edge of the basin follow the minor faults and folds (III) entering the basin from the west (Figure 11) and occur mainly in elongated, semi linear clusters. The northern group (V) follow one of two

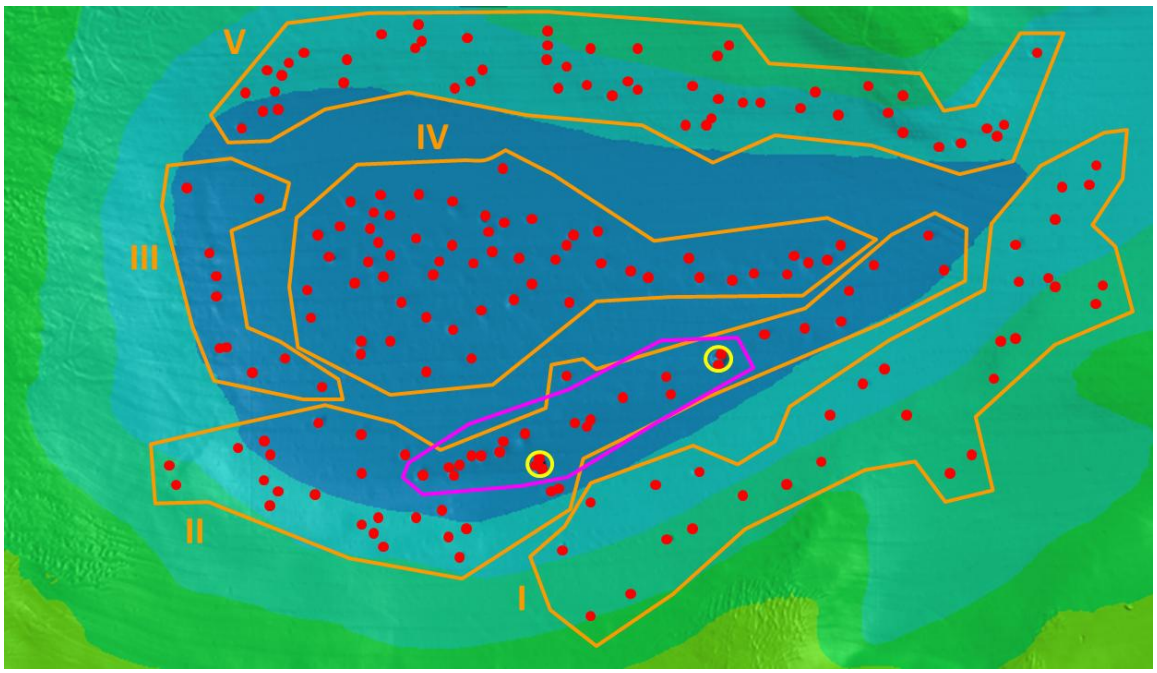

Figure 17. Shaded relief bathymetry of the Malin Shelf with pockmark features arranged into groups (Roman numerals) related to morphology and structural features of the basin. Red dots denote unit pockmark, two composite pockmarks are marked with yellow circles, Malin Deep micro-basin is marked with pink line.

main faults in this area – the Stanton Bank Fault. However pockmarks here are not equally distributed with prominent clusters in western and central parts of the area. The central part of the basin the Malin Deep (IV) has the highest number of units but they appear to be scattered without any pattern. South of the Malin Deep (II) pockmarks are clearly aligned with the major fault crossing the Malin Shelf area, the Skerryvore fault. In this area pockmarks occur in "*train*" like formations (Pilcher and Argent, 2007).

Table 3. Malin Shelf pockmarks distribution characteristics.

Pockmark group	No of units	Estimated total area [km^2]	Estimated pockmark density [units/km^2]	Dimensions [m]			Depth [m]	
				Max	Min	Average	Max	Min
I	30	82.1	0.36	180	80	135	2.1	0.5
II	49	86.3	0.57	850	65	254	8.5	0.5
III	10	8.7	1.15	210	55	90	2.0	0.5
IV	75	98.3	0.76	780	110	195	6.0	0.5
V	50	71.1	0.70	220	50	100	2.0	0.5

Moreover the only two composite pockmarks are present in this area, indicating intensified subsurface activity. Some of the largest pockmarks in the Malin Shelf are clustered in the

micro-basin located in the central part of this area. The last pockmark group (I) is associated with the Malin Terrace which is southern boundary of the Malin Shelf. This pockmark group is also parallel to the Skerryvore fault, however pockmark density is considerably lower and all pockmarks occur as isolated units without discrete linear patterns. The pockmarks located in the Malin Shelf micro-basin show the strongest correlation with geological structural components, suggesting a genuine link between faults and surficial fluid expulsion occurrences. Moreover a strong positive correlation (R^2 – 0.8) between maximum diameter and depression depth is observed in this area, as well as medium positive correlation (R^2 – 0.31) to water depth.

2.1.6 Objectives

The first objective was to validate the acoustic seabed classification model derived from backscatter, single beam and multi beam datasets by the Geological Survey of Ireland as well as provide basic information on geochemistry of the seabed. This is achieved by the analysis of physical and geochemical properties and reported in section 2.3.1. The second objective was to understand the nature and the magnitude of fluid flow in the subsurface sediments underneath the largest composite pockmark in the Malin Shelf. To discuss the interaction of the fluids with the seabed, evaluate the activity of the pockmark and construct a conceptual model of fluid flow. This is achieved by correlation of acoustic and electromagnetic data with physical and geochemical properties of the sediments. The results are reported in sections from 2.3.2 to 2.3.5.

2.2 Materials and Methods

2.2.1 Sediment samples

Sediment samples were collected during the 2008 RV Celtic Explorer (CE08). Samples were collected with use of grab samplers (Day and Shipek Grabs), gravity corers (1 and 3 m barrel length) and Vibracorer (6 m barrel length). Sample locations, types, full name and sampling water depth are shown in Table 4. Cores were cut on deck into 1-1.5 m sections immediately after retrieval. Sections end caps were wax-sealed for additional protection. The vibracores were refrigerated for the duration of the cruise and afterwards scanned for physical properties on a Multi-Sensor Core Logger (MSCL; Geotek, United Kingdom) sub-sampled and frozen. Grab samples and gravity cores were stored refrigerated for the duration of the cruise, sub sampled off shore and stored frozen.

Table 4. Sediment samples collected from the Malin Shelf.

Sample	Depth	Latitude	Longitude	Length	Type	PSA	Metals
BS07	179	55.85750	-8.13560	-	Grab Sample	+	+
BS09	178	55.85880	-8.13530	-	Grab Sample	+	+
BS11	180	55.85850	-8.13681	-	Grab Sample	+	+
BS12	175	55.85520	-8.13340	1.0	Gravity Core	+	
BS16	168	55.89012	-8.00120	1.0	Gravity Core	+	
BS17	164	55.89082	-7.96610	1.9	Gravity Core	+	
BS20	177	55.91485	-8.26503	-	Grab Sample	+	+
BS21	174	55.91563	-8.27460	2.4	Gravity Core	+	+
BS22	171	55.91904	-8.29981	2.4	Gravity Core	+	
BS23	169	55.91952	-8.31577	-	Grab Sample	+	+
BS24	172	55.91322	-8.31452	-	Grab Sample	+	+
BS25	164	55.92173	-8.34671	-	Grab Sample	+	
BS26	175	55.86251	-8.15265	-	Grab Sample	+	+
BS27	176	55.86150	-8.15026	-	Grab Sample	+	+
VC_044	175	55.85980	-8.14500	5.8	Vibracore	+	
VC_045	180	55.85680	-8.13720	5.9	Vibracore	+	

2.2.2 Geophysical characterization of the seabed and the subsurface

2.2.2.1 Bathymetry

Bathymetric data was acquired in 2003 and 2006 as part of the INSS (Irish National Seabed Survey) and its successor, the INFOMAR (Integrated Mapping for the Sustainable Development of Ireland's Marine Resources) program (Dorschel et al. 2010). Data were acquired on board the R.V. Celtic Explorer and R.V. Celtic Voyager using a Kongsberg-Simrad EM1002 multibeam echo sounder, with an operational frequency of 93-98 kHz and pulse length of 0.7 ms and a very low survey speed (2-3 knots). Resulting bathymetric terrain models were gridded at 5x5 m. High resolution bathymetry was crucial in identifying smaller gas escape features (Monteys et al. 2008a).

2.2.2.2 Backscatter data

Backscatter data was acquired in 2003 and 2006 as part of the INSS (Irish National Seabed Survey) and its successor, the INFOMAR (Integrated Mapping for the Sustainable Development of Ireland's Marine Resources) program (Dorschel et al. 2010). Backscatter data was collected using two independent and complementary methodologies: Multi Beam Echo Sounder (MBES) and Single Beam Echo Sounder (SBES) time series backscatter measurements. The MBES backscatter data was acquired along bathymetry data as described

above and processed with EM1002 MBES software. The SBES backscatter was acquired using the Simrad EA 400 single beam system is a dual frequency hydrographic echo sounder, the vessels system used two transducers at 38 kHz and 200 kHz. Backscatter values for all frequencies were logged in Simrad datagram files.

2.2.2.3 Sub bottom profiler

Sub-bottom profiler data was acquired in 2003 and 2006 as part of the INSS (Irish National Seabed Survey) and its successor, the INFOMAR (Integrated Mapping for the Sustainable Development of Ireland's Marine Resources) program (Dorschel et al. 2010). The data was acquired using a heave-corrected SES Probe 5000 3.5 kHz transceiver in conjunction with a hull-mounted 4°x4° transducer array. Acquisition parameters, data logging and interpretation were carried out using the CODA Geokit suite. Both Raw Navigation string and Heave Compensation string are fed into the Coda DA200 system (from the Seapath 200). An average estimated acoustic velocity of 1650 m/s was used to calculate the thickness of the sedimentary units. Acoustic penetration in some areas was in the order of 60 m below seabed with approximately 0.4 m vertical resolution.

2.2.2.4 Towed electromagnetic data

Towed electromagnetic (EM) data were acquired during a geo-hazard and hydrocarbon reconnaissance survey of the Malin Shelf in 2009 (GSI/PIP – IS05/16 project, Monteys et al. 2009 and Gracia et al. 2007). The towed-electromagnetic system discussed in this work consists of a ~40 m-long array, which is towed in contact with the seafloor at speeds of 1-2 knots. The EM transmitter, a horizontal magnetic dipole, generates harmonic magnetic fields over a range of frequencies (~200 Hz – 200 kHz), and the three receivers, tuned to measure these magnetic fields, are towed at fixed distances behind (4 m, 12.6 m and 40 m) and provide average conductivities over seafloor depths roughly one-half the source-receiver offset (i.e. ~2 m, 6 m and 20 m below seafloor respectively). At a given frequency the strength of magnetic fields decays away from the transmitter as a function of the conductivity of the seafloor (i.e., according to the skin depth), decaying more rapidly in more conductive media. Measurements are made roughly every 10 m along the tow-line, so sensitivity to lateral variations in structure is high. Each receiver measures data at 3 distinct frequencies (Evans, 2007) and in general the information from the 6 pieces of information (3 amplitudes and 3 phases) on each receiver are combined into a single apparent resistivity measurement -the resistivity of the uniform seafloor that best matches the observations. The frequencies are chosen based on skin-depths between the transmitter and receiver for a range of likely seafloor conductivities. That is, the highest frequency is appropriate for a highly resistive seafloor while the lowest frequency is appropriate in the case where the seafloor is quite conductive -the higher frequency fields in this case having been more attenuated. It is therefore possible, and sometimes desirable, to examine single

frequency data, using the most appropriate frequency based on the observed conductivities. The sensitivity of the magnetic dipole-dipole system, along with the physics of the propagation of the fields through the seafloor was presented in Cheesman, 1989. Further details of the system are given in Evans, 2007. The system has been used previously across an area of gas discharge in the Gulf of Mexico (Ellis et al. 2008). In this instance, extremely high conductivities within the subsurface were seen, resulting from the advection of warm briny fluids from depth towards the seafloor. This response was the opposite expected for a gas rich sub seafloor, for which conductivity should decrease.

2.2.3 Physical properties of the sediment

2.2.3.1 Particle size analysis

Method development

Particle size distribution measurements were carried out in compliance with International Standard ISO-13320-1:1999 to meet the highest standards of analysis and provide repeatable and accurate results. Samples were subjected to thermo-gravimetric analysis to estimate the amount of moisture, organic and inorganic carbon. These are important parameters that help to choose the best dispersion method and avoid distribution variations due to nonsphericity of inorganic debris. Details of organic and inorganic carbon estimation protocols are presented the Chapter 1, par 1.3.2.1. The standard dry sieving analysis was chosen as a preliminary sizing technique to sieve out and evaluate the percentage of coarse material in the sediments. All coarse, sandy samples were air dried while fine, muddy samples were freeze dried to avoid solidification of the sediment. In the vast majority of samples the percentage of coarse material did not exceed 5% and sieved out material was mainly identified as biogenic carbonate debris (fragments of shells, tubes, skeletons and fish bones) with a few drop stones only. Therefore, dry sieving results were mainly used to evaluate the amount of biogenic fraction in the studied samples. Organic carbon content varied from <0.2% to 0.5% (CHN analysis) and from 0.7% to 1.9% (TG analysis). Based on these results a chemical disagglomeration agent was chosen to partially remove organic matter and to level the agglomeration of particles. Additionally, the effect of ultrasonic energy was studied on selected samples to evaluate its potential as an aid to chemical disagglomeration and study its effect on the breaking up of biogenic carbonates in situ within the sedimentary matrix.

The application of ultrasonic energy is easy and fast and is therefore a popular way of disagglomerating soil and sediment samples (Chappell, 1998). Re-aggregation and/or grain shattering are common drawbacks of this method especially if recommended exposure times are exceeded (ISO-13320-1:1999). The optimal ultrasonication time was suggested to be less than 6 minutes; further ultrasonication would result in breaking the grain particles (Chappell, 1998) but

also may create favourable conditions for flocculation of the clays (Konert and Vandenberghe, 1997) and result in an underestimation of this fine fraction. Although the overall impact of excessive ultrasonic action has been suggested to be low (Sperazza et al. 2004) the research conducted in this field was mainly based on the analysis of soils and alluvial and lacustrine sediments. To investigate the effect of ultrasound and stirring on marine sediment disagglomeration selected samples were analysed at different ultrasound exposure times. One of the symptoms of grain shattering is increasing beam obscuration. In this case the newly formed particles feed the population of grains circulating in the presentation unit of the laser sizing system and reduce the suspensions permeability which is measured by obscuration percentage. Therefore, a constant increase of obscuration may indicate constant formation of new particles (Chappell, 1998). A sample was ultrasonicated for a period of 30 min and particle size distribution was measured every 5 min to verify the effect of ultrasonic energy on marine sediment. Obscuration increased gradually during the experiment suggesting new grains (shards) formation. Standard percentile {D(v, x) describe the size values corresponding to cumulative distribution at 10%, 50% and 90%; D[4,3] is a de Brouckere mean diameter and describes a diameter of a sphere that has the same volume ratio as particle of interest} values also decreased gradually with time confirming previously reported observations for different types of sediments. Also, the frequency curve showed gradual building up of fine grains (<10 μm) with simultaneous shift of the bigger particles towards the smaller diameters. Observed decrease in concentration of large grains was not linear. In the first phase (0-15 min) the concentration was rising or shifting and suggests that initially disagglomeration was the preferable process or larger particles were being formed. In the second phase (20-30 min), the overall concentration started to drop gradually which is most likely caused by breaking of the bigger particles. Variation in the fines zone reached 18.8% (as coefficient of variation - CV) with other percentiles values below 5%. Similar results were obtained for different samples (BS-24, BS-20). The disagglomerating effect of the ultrasounds exposure is rapid. In the first minutes aggregates are broken down and elongated exposure results in grain shattering. Ultrasonication has been effective in disagglomeration of chemically pre-treated samples and the optimal time was identified as 300 seconds.

Pump and stirring speed can have an effect on particle size distribution because of their capability to compensate density and sample reservoir volume (Sperazza et al. 2004). To investigate these effects a sample was ultrasonicated for 15 min and the particle size distribution was measured for another 55 min in 5 min increments. A shift towards smaller grain size was detected just as in the previous experiment. Surprisingly after 55 min of stirring without any additional stimulation the fine grain concentration increased, with a concomitant simultaneous decrease of larger grain concentration. A gradual decrease in values of the statistical descriptors (standard percentiles) observed during constant ultrasonication was not recorded when the sample was not ultrasonicated after initial dispersion. This observation is in agreement with

findings reported by Sperazza et al. 2004 where pump speed and stirring impact on the median particle size has been estimated as low. Variation (as coefficient of variation) of the standard percentiles in the plateau phase was very low, with values not greater than 2.7% (Table 5). The values of the statistical descriptors remained steady indicating minor changes in the particle size distribution. Nevertheless gentle trends are visible and are probably caused by in-solution collisions (in solution) between the grains and the moving parts of stirring and pumping mechanisms. It suggests that this mechanism can alter the distribution only in long term studies. Considering the results above the optimal time for ultrasonic dispersion was set to 5 min. Visual inspection of the grains was not possible at this time and therefore visual assessment of grain shattering and confirmation of this mechanisms was not possible. Subsequent analysis of different samples (BS-24, BS-27, BS-20 and BS-21) suggested that the impact of ultrasonication may vary from one sample to another (e.g. BS-20 and BS-21) and it is possibly directly related to sample mineral composition and resistance to ultrasonic stress.

Table 5. Values of standard percentiles during the plateau phase. For terms definition see text.

time [min]	D(v, 0.1) [μm]	D(v, 0.5) [μm]	D(v, 0.9) [μm]	D[4,3] [μm]	obscuration [%]
15	2.35	47.91	106.15	51.42	16.5
20	2.38	47.43	106.55	51.34	16.5
25	2.34	46.59	105.75	50.67	16.4
30	2.3	46.23	106.42	50.67	16.2
35	2.29	45.77	106.59	50.49	16.3
40	2.31	45.39	107.03	50.43	16.3
45	2.32	45.28	107.94	50.63	16.3
60	2.39	44.54	107.13	50.09	16.4
70	2.35	44.15	106.72	49.74	16.4
SD	0.03	1.25	0.63	0.53	
AV	2.34	45.92	106.70	50.61	
CV	**1.48**	**2.73**	**0.59**	**1.05**	

Influence of the biogenic fraction on the particle size distribution

Accurate determination of particle size distribution (PSD) in marine sediments is often complicated by the presence of nonminerals, frequently derived from living organisms. Physical separation of these particles from the sedimentary matrix by dry sieving is not always possible. The presence of these particles can significantly alter the PSD of the sediments. Because it is not uncommon for marine sediments to be enriched and sometimes dominated by biogenic carbonates (Morse and Mackenzie, 1990 i.e.) it is important to evaluate their influence on PSD. Furthermore, nonsphericity of all sediment particles and biogenic carbonates especially (because of their size) appears to be an important factor in the determination of PSD when applying volume-sensitive techniques such as laser granulometry (Jonasz, 1987). To demonstrate how carbonate debris influences particle size distribution, carbonate free, natural marine sediment samples (CFS) with addition of known amounts and size ranges of biogenic

carbonates were analysed by the laser diffraction system. Additionally, the effect of ultrasonic energy on mixed samples was studied to evaluate its potential as a countermeasure for altering particle size distribution carbonate material presence.

To assess the level of sphericity (or nonsphericity), all fractions including the CFS were studied by Scanning Electron Microscope (SEM) (Hitachi S-3000N VP system). The recorded images were obtained with 5kV of electron energy. Images revealed that by comparison to the sedimentary matrix (CFS), the nonsphericity of the carbonate fractions is apparent, while the CFS has obviously more spherical morphology (Figure 18). Most of the fractions have shown low level of roundness and could be described as elongated thin plates. This observation is in agreement with the morphological features of the material that the carbonate debris derives from. Shells, as protective outer layers, should be rigid and durable but also as thin as possible This helps to minimize energy consumption during their formation and "exploitation" i.e. transportation. This feature is related to thickness of carbonate debris particles. Although natural shells exist in a variety of shapes and sizes the artificially crushed debris is usually a mixture of relatively uniform shapes and sizes with very few outstanding particles.

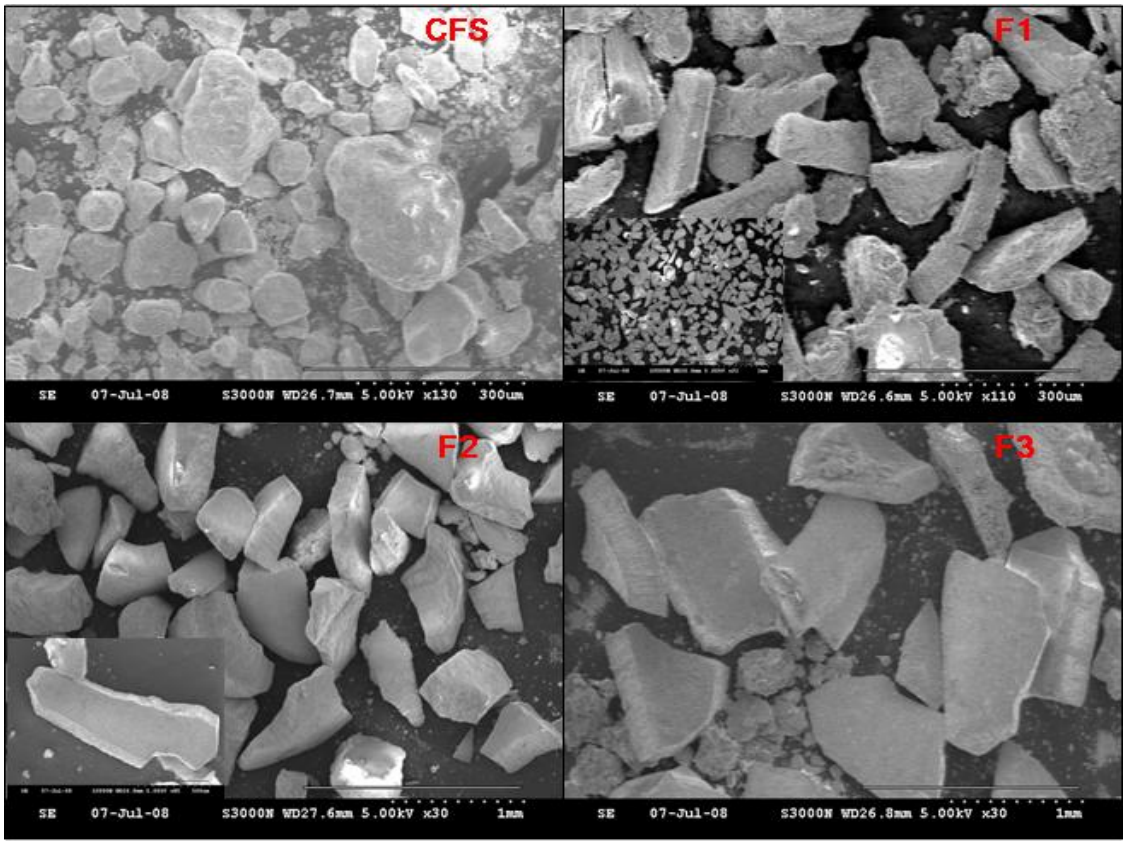

Figure 18. Compilation of SEM photographs depicting biogenic carbonate fractions (F1, F2, F3) and sedimentary matrix (CFS).

Biogenic carbonates rejected in dry sieving analysis of marine sediment cores were used as precursor to fractions used in this study. Specimens larger than 850 μm were ground and sieved

in certified test sieves to obtain three fractions: 850-500 μm (F3), 500-212 μm (F2) and 212-106 μm (F1). Natural marine sediment was treated with a 10% (v/v) hydrochloric acid solution to remove any natural carbonate material present. Samples were subsequently washed with several volumes of water and oven dried at 70^{o}C.

Dry sediment was homogenized with mortar and pestle and spiked with known amounts of carbonate fractions. A Malvern Mastersizer S laser diffraction based granulometer with a wet presentation unit was used to determine PSD. The system was set to polydisperse analysis model and 30HD presentation (standard-wet) was employed with 0.05-880 μm measuring range (300RF lens). Obscuration of the beam was maintained between 10% and 30%. Stirring and pump speed was set to maximum, background scan was taken before every analysis, dispersant was degassed by ultrasonication prior measurement. Samples were analysed four times and the result was averaged. Standard percentiles were calculated by a Malvern software package and the mean was calculated according to arithmetic method of moments. GRADISTAT software was used to verify calculations (Blott and Pye, 2001). The influence of sub-sampling on the distribution was tested by four consecutive analyses of carbonate free sediment. Highest variability was observed for D[v,10] standard percentile (16.4%), while other standard percentiles and means show acceptable variability (<4%). Addition of 10% (w/w) particulate carbonate fractions into the CFS matrix had a minor effect on the distribution (Table 6). The observed effect results from the fact that very small amounts of particles were needed to obtain a 10% (w/w) carbonate enrichment in the sample; these particles were not abundant enough to alter the distribution. A concentration increase to 20% (w/w) yielded some significant changes. Mean and D(v, 0.9) increase (63% and 110% respectively) is a result of the introduction of particles of greater sizes than observed in the matrix (CFS) distribution.

Table 6. The effect of individual carbonate fractions concentration on the statistical PSD descriptors after 5 min of ultrasonic treatment

5 min US	D(v, 0.1) [μm]	% change	D(v, 0.5) [μm]	% change	D(v, 0.9) [μm]	% change	mean [μm]	% change
CFS	7.39	-	88.79	-	189.45	-	112	-
F1, 10%	6.71	-9.2	93.69	5.5	207.19	9.4	119.7	6.8
F2, 10%	6.92	-6.4	91.32	2.8	224.82	18.7	127.6	13.9
F3, 10%	7.34	-0.7	93.58	5.4	223.87	18.2	130	16.0
F1, 20%	5.52	-25.3	98.48	10.9	220.46	16.4	125.7	12.2
F2, 20%	7.88	6.6	110.73	24.7	398.25	110.2	182.7	63.1
F3, 20%	6.85	-7.3	100.32	13.0	288.97	52.5	152.2	35.9
CV		11.8		3.7		2.9		3.9

Surprisingly, the coarsest fraction (F3) did not have the strongest effect on the studied parameters probably due to insufficient grain concentration and relatively short measurement time (5000 sweeps, 8 seconds). Additionally, grains exceeding the lens range were not included

in distribution. In natural sediments a broader range of biogenic carbonates might also be expected. The addition of two and three fractions (F1-2 and F1-3, respectively) was performed to study their cumulative effect on PSD. Time of analysis was elongated (20000 sweeps, 40 seconds) to ensure better reflection of grain concentration in distributions (Table 7. Just as in the previous experiment 10% (w/w) concentrations of both F1-2 and F1-3 carbonate mixtures did not significantly alter studied parameters. More concentrated samples again substantially affected PSD. Median and mean changes ranged from 23 to 37% and from 30% to 63% respectively. The most significant effect was again observed for the F1-2 mixture at 30% (w/w) concentration. F1-3 contains the coarsest grains and had a major effect on D(v, 0.9) and significantly altered the mean values even at the medium concentration. As expected, a major effect on PSD can be observed when the size of particles exceeds the sedimentary matrix distribution.

Table 7. The effect of combined carbonate fractions concentration on the statistical PSD descriptors, after 5 min of ultrasonic treatment.

5 min US	D(v, 0.1) [μm]	% change	D(v, 0.5) [μm]	% change	D(v, 0.9) [μm]	% change	mean [μm]	% change
CFS	7.39	-	88.79	-	189.45	-	112.03	-
F1-2, 10%	8.46	14.5	96.01	8.1	224.61	18.6	129.55	15.6
F1-3, 10%	9.21	24.6	98.39	10.8	228.69	20.7	134.07	19.7
F1-2, 20%	7.24	-2.0	101.1	13.9	265.61	40.2	146.15	30.5
F1-3, 20%	10.05	36.0	109.13	22.9	379.58	100.4	176.94	57.9
F1-2, 30%	7.4	0.1	121.58	36.9	358.22	89.1	183.19	63.5
F1-3, 30%	7.54	2.0	109.83	23.7	367.13	93.8	173.83	55.2
CV		11.8		3.7		2.9		3.9

The effect of elongated exposure to ultrasonic energy was studied on all sample types. Calculated values were approximately 10 to 20% higher than those recorded without ultrasonication (Table 8).

Table 8. The effect of individual carbonate fractions concentration on the statistical PSD descriptors after 15 min of ultrasonic treatment.

15 min US	D(v, 0.1) [μm]	% change	D(v, 0.5) [μm]	% change	D(v, 0.9) [μm]	% change	mean [μm]	% change
CFS	5.74	-	83.15	-	176.63	-	103.3	-
F1, 10%	4.94	-13.9	87.6	5.4	197.85	12.0	111.4	7.9
F1, 20%	4.24	-26.1	92.72	11.5	214.5	21.4	118.9	15.1
F2, 10%	5.7	-0.7	89.27	7.4	219.46	24.2	122.2	18.3
F2, 20%	6.26	9.1	109.1	31.2	388.07	119.7	178.5	72.8
F3, 10%	5.53	-3.7	88.28	6.2	204.76	15.9	116.6	12.9
F3, 20%	5.65	-1.6	98.29	18.2	290.19	64.3	150.02	45.3
CV		16.4		5.3		3.9		5.2

The slight increase observed was most likely caused by grains fracturing and shattering, which could explain the positive correlation of laser obscuration and the time of ultrasonication. There was no distinguishable difference between fracturing of the biogenic carbonate particles and mineral matrix components. The observed decrease in concentration of larger grains within the 50-400 μm range and gradual increase in concentration of smaller particles within the 0.3-30 μm range is typical for ultrasound induced particle breakage (Chappell, 1998; Sperazza et al. 2004). The ultrasonic action was ineffective in negating the carbonate debris effect on PSD and its statistical descriptors because of the simultaneous disintegration of CFS and carbonate fractions.

Method overview

Air and freeze dried samples were sieved through a set of certified standard test sieves with mesh sizes 5.6, 4.0, 2.8, 2.0, 1.4, 1.0 and 0.85 mm. Material retained on each sieve was weighed to estimate coarse grain distribution. Sample preparation included grinding with a mortar and pestle and chemical disagglomeration with a 4.4% sodium pyrophosphate ($Na_4P_2O_7$ – tetrasodium pyrophosphate, MW 260.9 $gmol^{-1}$) solution. An aliquot of sample was placed in a polypropylene (PP) tube and a dispersant aid was added with a 5:1 (v/v) ratio in relation to sediment volume. Samples were incubated in a water bath for 3-4 hours at 95^{o}C and vortexed every hour. After incubation samples were cooled down under running water, left to settle for 6 hours and the excess of dispersant was pipetted out and replaced with deionized water. Fractions below 850 μm mesh size were analysed with a long bench type Mastersizer S laser granulometer (Malvern Instruments Ltd., UK). The system was fitted with 2 mW He-Ne laser (633 nm wavelength) with 18 mm beam diameter. The optical system was fitted with a 300RF (reverse Fourier) lens with 0.05 - 880 μm size range and the detector set comprised an array of 42 solid state detectors, 1 centre detector and 2 backscatter detectors. A wet sample presentation unit with built-in ultrasonic horn was used to disperse samples. A standard - wet 30HD presentation was applied during the measurement and the main sample dispersant was degassed tap water. Water degassing was achieved by ultrasonication for 5 minutes prior to measurement. Electronic and dispersant background was scanned prior to every analysis. The suspension of sediment was placed directly into the presentation unit of the laser sizing system. Stirring and pump speed values were set to maximum and the sample was circulated in the presentation unit for two minutes before measurement. After this time the sample was ultrasonicated for another 5 minutes and analysed. The Instrument performed 4 scans, each scan included 5000 sweeps and results were averaged.

2.2.3.2 Density

Method development

The density of environmental samples is not an intrinsic property and depends on the form in which the material is analysed. When investigating the structural properties of sedimentary layers samples should be undisturbed for "wet" bulk density measurements or undisturbed and dried for "dry" bulk density (Dadey et al. 1992). When investigating grain densities to aid mineralogical studies samples should be powdered and tapped to obtain so called "tapped" grain density (Al-Jaroudi et al. 2007). In this study both properties were determined. As with every complex sample, repeatable subsampling is an important factor for good precision of the measurements. Therefore reproducibility was tested on one of the samples (BS-24) and yielded a precision of 0.2% in the worst case.

Method overview

Sediment for dry bulk density measurement was sampled from a wet core with a polypropylene (PP) coring tube and dried for a period of 48 hours at 70^{o}C. For grain density measurements of sediments samples were air or freeze dried and pulverized with a mortar and pestle prior to measurement. In addition to tapped grain density and bulk dry density the effect of thermal carbonate material removal and thermal mineral transformation on density was studied. Samples were incinerated at 800^{o}C for 24 hours to remove carbonate material and stored in a desiccator prior to measurement. Samples were incubated at 1000^{o}C for 24 hours for mineral pyrolysis. This study was conducted as a test for the instrument rather than an investigation of physical properties.

2.2.3.3 Foraminifera and ^{14}C dating

Foraminifera analysis

Samples were wet sieved through a certified standard test 0.125 mm sieve to remove fine grains and particulates and to obtain a fraction often referred to as the total assemblage (Schiebel et al. 1997). Concentrated wet coarse fractions were refrigerated (4^{o}C) until analysis. Prior to the foraminifera counting samples were oven dried (50^{o}C). If the assemblages contained excessive interfering material (dirt, organic matter i.e.) they were soaked in diluted sodium hexametaphosphate [$(NaPO_3)_6$] - (Calgon, SHMP) prior to drying. Selected fractions of planktonic forams were used for radiocarbon dating and foraminifer counting was conducted by Dr. Soledad Garcia-Gil (Dpto Geociencias Marinas, University of Vigo, Spain) as a collaborative effort. The method was based on a protocol published by Murray, 2006.

^{14}C dating analysis

Selected fractions were hydrolysed with phosphoric acid (H_3PO_4) at 60°C to release all of the carbon in the sample in the form of carbon dioxide. The CO_2 was cryogenically (-80°C) purified and partitioned into ^{14}C and ^{13}C fractions which are subsequently catalytically (Fe/H_2 or Co/H_2 at 625°C) converted to graphite and analysed by Accelerated Mass Spectrometry (AMS). Oxalic acid I and II (Olsson, 1970) were used as standards (NIST-SRM-4990 and NIST-SRM-4990c respectively). Carrara marble (Różański et al. 1992) was used as a blank (IAEA-C1). Carbon dating was performed according to a protocol disclosed by the Woods Hole Oceanographic Institution (National Ocean Sciences Accelerated Mass Spectrometry, NOSAMS, www.whoi.edu/nosams) as a contract analysis.

2.2.3.4 Natural radioactivity

Total Tritium analysis

Samples for radiometric analysis were oven dried and sieved through 1.0 mm sieve. Total tritium analysis ($^1H^3HO$ and OB^3H – organically bound tritium) was conducted by pyrolysis. Samples were combusted in a two stage pyrolyser where $^1H^3TO$ is initially oxidized at 850°C on an alumina/Pt catalyst and the remaining carbon and organic material (OBT) is oxidized with a further temperature increase. The gaseous pyrolysis products were collected in water bubblers and an aliquot of the aqueous solution was made alkaline. Subsequently, sodium thiosulphate ($Na_2S_2O_3$) was added and the solution was distilled to remove both radioactive and non-radioactive interferences. A liquid scintillation counter was used to determine the tritium content. Counting efficiency was determined with tritiated water of known activity.

Gross α/β counts analysis

For gross α/β measurements samples were evaporated to dryness in the presence of suphuric acid (H_2SO_4). The material was than ashed in a furnace to produce a sulphated residue. An aliquot of the residue was evenly distributed on a stainless steel planchet to produce a "thick source" and was analysed in a Berthold LB 770 α/β counter. The instrument was calibrated with ^{241}Am for α- and ^{40}K for β- determination.

High resolution γ spectrometry

High resolution gamma spectrometry was performed with high purity germanium Ge detectors and computerized multi-channel analyser. An aliquot of powdered sediment is placed into a standard geometry container which is subsequently placed on the detector and analysed. The system was calibrated with a mixed gamma reference material in the range of 60 keV –

1836 keV. The signal analysis was performed with peak search and peak shape software, identification of a radionuclide was performed based on a validated isotope library match.

2.2.3.5 Physical properties logging

Instrument calibration

Sediment cores were logged on MSCL-S system (GEOTEK, UK) in the British Ocean Sediment Core Research Facility (BOSCORF, UK) according to standard GEOTEK protocols. Each sensor was calibrated independently using the same liner as that used during the cruise. Once the calibration process was complete the core logging procedure with MSCL-S system was automated. The core was presented on to the feeding rack and secured with ball screw pushing element connected to the stepper motor. In each core a small hole was drilled in the liner, 5 cm from the top of the core. A thermocouple was inserted through this hole to ensure a constant measurement of sediment temperature throughout the measurement. Sealing wax was removed from the end caps and the entire liner surface was cleaned and dried to ensure perfect adhesion of the ultrasonic transducers and eliminate the possibility of contamination of their epoxy surface that slides on the liner.

Core diameter

Core diameter is very basic property of a logged core. Accurate determination is of upmost importance as it influences all other measured parameters and is used in processing of raw data. Core diameter was measured by laser micrometers (0.02 mm resolution) mounted on displacement transducers. These are spring loaded transducers designed to push against the surfaces of bars of standard liner diameter. Calibration of this system was achieved by series of measurement of calibration bars of standardized dimensions to establish the relationship between computed displacement and true value of the tested standard.

P-wave

P-waves are primary, high velocity seismic waves that, during propagation through a solid matrix, cause alternating compression and dilation movements in the direction of propagation. P-wave velocity is related to the density and moduli of rigidity and incompressibility of the material (Equation 15). Typical P-wave velocity values are: 330 m/s in the air, 1480 m/s in seawater, 5-8 km/s in an earthquake.

$$V_p = \sqrt{\frac{\kappa + {}^4/_3\ \mu}{\rho}} = \frac{d}{t}$$

Equation 15. Definition of P-wave velocity (V_p) where κ – modulus of incompressibility, μ – modulus of rigidity, ρ – density, d – distance travelled, t – time required to travel distance d.

P-wave velocity is sensitive to temperature fluctuations therefore all cores were equilibrated to room temperature prior to measurement (approximately 6 hours). Core quality strongly affects the ability to acquire P-wave velocity data (Blum, 1997). Acoustic coupling of the ultrasonic transducers and the liner can be disturbed by liner damage created during sampling and by incomplete liner fill with the sediment particularly at the ends of the core. Cracks and voids in the sediment will of course form naturally during core decompression if the sediment is not sufficiently lithified. Moreover free gas, often present in the young sediments, will expand considerably upon extraction from the seabed surface causing micro fractures that make P-wave measurements impossible.

The GEOTEK, MSCL-S system consists of two piezoelectric ultrasonic transducers mounted on an epoxy resin surface and is rinsed with water during analysis to create a better acoustic coupling. Transducers are mounted serially and consist of a transmitter and a receiver. Two linear variable-displacement transformers (LVDT) measure the core diameter and are able to compensate for liner unevenness created during sampling. P-wave is generated as a 230 kHz pulse (or 500 kHz in case of PWT 500 transducer), with 1 kHz amplitude.

Calibration of this system requires several steps ensuring appropriate operation across the entire range of P- wave signal levels. In the first step the so called '*P-wave travel time offset – PTO*' is established by measuring P-wave travel time through a liner filled with distilled water according to the following relationship:

$$PTO = t_{tot} - \frac{(d_{tran} - d_{lin})}{V_t}$$

Equation 16. P-wave travel time offset, where t_{tot} – total travel time recorded, d_{tran} – distance between transducers, d_{lin} – total liner thickness, V_t – P-wave velocity in distilled water at temperature t.

This experiment is repeated at different set of temperatures and salinities to bracket for naturally occurring conditions. Recorded PTOs are input to the processing panel resulting in a calibration plot. In the next step transducer displacement is measured on a series of acrylic blocks with known dimensions to establish correct output voltage to mm relationship. This is to ensure that the thickness of the core is measured accurately.

$$t'_{tot} = t_0 - t_{ele} - 2\frac{d_{lin}}{v_{lin}}$$

Equation 17. Total time traveled between transducers corrected for thickness of the liner and hardware delay, where t_0 – raw total travel time, t_{ele} – hardware delay, d_{lin} – average liner thickness, v_{lin} – liner acoustic velocity.

Finally the total travel time (t_{tot}) between transducers is affected by three types of delay. Two of these are related to electronic systems of the instrument and are not going to be discussed here. The third delay is caused by the travel time through the liner walls. The correction for this time is included by measuring the average thickness of the liner and the sonic velocity of the liner material and including these parameters in the total core travel time delay (Equation 17) and core sonic velocity calculations.

Wet Bulk Density by γ ray attenuation

In this method medium energy gamma rays (0.1-1 MeV) are passed radially through the sediment core and interact with minerals mainly through the so-called '*Compton scattering*' process (Evans, 1965; Ellis and Singer, 2007). Other effects such as: photoelectric effect and electron-positron pair generation are negligible. Compton scattering occurs when a high energy gamma photon collides with sediment mineral components which absorbs part of its energy and release it in the form of loosely bound electrons from the outer shells. The intensity of attenuated gamma rays is related to the density of the material they pass through (Equation 18).

$$I = I_0 e^{-\mu\rho d} \qquad \rho = \frac{1}{\mu d} ln \frac{I_0}{I}$$

$$\mu = \Phi \frac{\rho_{fluid}\mu_{fluid}}{\rho} + (1 - \Phi)\frac{\rho_{solid}\mu_{solid}}{\rho}$$

Equation 18 Gamma ray attenuation intensity (I) in the Compton scattering process is related to source intensity (I_0), sediment wet bulk density (ρ), distance travelled by gamma rays (d) and material Compton mass attenuation coefficient (μ). Since sediment core is heterogeneous material consisting of fluids (pore water, gases) and solids (sediment grains) their individual coefficients must be factored into the equation.

It is obvious from the above relationships that to accurately determine coefficient μ we need to know the porosity (Φ), a property derived from density which we try to measure. This problem is overcome by use of so called '*processing porosity*' as a starting value further refined in a series of iterations (Weber et al. 1997) using μ from a known range of 0.0774 cm^2/g for dry sediment and 0.0850 cm^2/g for sea water. Usually less than five iterations are required to calculate true porosity (Whitmarsh, 1971; Weber et al. 1997). Drastic changes in lithology can affect measured density as the system assumes that coefficient μ is constant throughout the entire core. This can easily be corrected once the core is opened.

The GEOTEK system is equipped with a ^{137}Cs source (660 keV) and a scintillation detector that counts transmitted gamma rays for a user determined time. This system was set to 1 cm resolution with 4 s count time (0.5% precision). The system was calibrated against a standard composed of telescopic aluminium rod of varied thickness (six intervals) inserted into the liner and filled with deionized water. Aluminium was chosen because it has a similar μ

coefficient to minerals commonly occurring in marine sediments. The prepared standard was logged as normal core starting with pure water (100% porosity) followed by increasing aluminium diameter to only aluminium (0% porosity). The liner used for calibration was identical to that used during sampling hence no corrections for liner material differences were necessary.

Magnetic Susceptibility

Magnetic susceptibility (κ) is the degree of magnetization of a studied material when placed in a magnetic field. It is a dimensionless property (commonly reported in $*10^{-6}$ SI) determining whether material is paramagnetic (magnetization is not retained without external magnetic field; κ from 10^{-3} to 10^{-5}), ferromagnetic (magnetization is permanent even without external magnetic field; $\kappa > 10^{-2}$) or diamagnetic (opposed magnetic field is created to the applied external magnetic field, non-magnetic materials; $\kappa < 0$). Magnetic susceptibility is related to density (Equation 19).

$$\chi = \frac{M/H}{\rho}$$

$$\kappa = M/H$$

Equation 19. Magnetic mass susceptibility (χ) is proportional to magnetization per unit volume (M) and applied magnetic field (H) and inversely proportional to density of the material (ρ). Magnetic susceptibility expressed per unit volume (κ) is dimensionless quantity.

Magnetic properties of sedimentary minerals can vary greatly. Non-iron bearing minerals such as quartz, feldspar, magnesite, halite, gypsum have diamagnetic properties. Clays such as illite and montmorillonite containing metal ions in their crystal lattice (e.g. Ni, Fe) are paramagnetic while kaolinite devoided of these presents diamagnetic properties. Other important paramagnetic minerals are pyrite, olivine and biotite. Strong magnetic properties can indicate the presence of ironoxohydroxides, haematite, magnetite, greigite and goethite.

Magnetic susceptibility in MSCL-S can be measured using two different sensors. The Bartington loop sensor which is used for unopened whole round cores and the Bartington point sensor which requires contact with the sediment and was used for analysis of split core sections. The point sensor is less sensitive and more susceptible to temperature variations, also it only measures MS of an area of Φ = 1cm. Because of these limitations the loop sensor was used. The sensor generates low intensity (approx. 80 A/m), alternating magnetic field (H-field; 0.565 kHz). Magnetic effect is recorded as oscillation frequency change and converted to κ values. The loop sensor is calibrated absolutely by the manufacturer and requires only periodic checks with a stable iron oxide standard. The measured value must fall within the manufacturer's

specified limits otherwise it is indicative of deterioration of electronic components. Drift correction and correction for loop and liner geometry (Bartington correction) are included in the software algorithm and automatically applied. The effects of liner and conveyor belt were studied by analysis of distilled water filled core liner and core liner filled with standard of known κ. For standard material liners this correction was be applied with values derived from single experiment and did not have to be repeated every run.

Electrical resistivity

Electrical resistivity describes the how strongly a material resists the flow of electric current. Electrical resistivity is opposite to electrical conductivity which is a measure how easily material conducts the electric current. Traditionally electrical resistivity was used for reservoir characterization as it is directly related to porosity and the nature of the interstitial fluids. The ratio of solid and fluid resistivity is also known as the formation factor (Archie, 1942) and is commonly used to describe changes in sediment lithology and its composition (Equation 20). This relationship is known as the '*Archie's law*':

$$F = \frac{R_{solids}}{R_{fluids}} = a\Phi^{-m}$$

$$R_{solid} = \frac{a\mathrm{R}_{fluid}}{\Phi^{m}S^{n}}$$

Equation 20. Archie's law and expanded relationship of porosity (Φ) and resistivity of solid (R_{solid}) and fluid (R_{fluid}) components of the sediment, where F is the formation factor, S describes saturation, m is the cementation exponent and n is the saturation exponent and a is the tortuosity factor.

Traditionally electrical resistivity was measured by so called '*galvanic method*' with use of electrodes inserted into the sediment. This approach suffers from many limitations and currently a non-contact inductive method is preferred (Jackson et al. 2006). In this method current flowing through a coil generates a high frequency magnetic field in the sediment which induces electrical current flow. This flow generates a weak magnetic field that is measured by a receiver coil. This method is also often referred to as the '*EM method*' short for electromagnetic.

MSCL-S uses a double paired NCR sensor mounted underneath the feeding rack. Since resistivity is variable with temperature, control of this parameter is necessary during measurements. The sensor requires 1 hour warm-up period to minimize drift. The system was calibrated against a series of saline solutions of known concentrations (35, 17, 8.75, 3.5, 1.75 and 0.35 g/dm^3 of NaCl) filled into prefabricated core liner.

High resolution imaging

After splitting, the core was imaged with a GeoScan CCD camera (3 CCD panels each 2048 pixels resolution). The camera was fitted with a Nikon lens and high frequency fluorescent lamps illuminating the core from two sides and minimizing reflection and topography effects.

2.2.4 Geochemical properties of the sediment

2.2.4.1 Estimation of organic and inorganic carbon content

Method development

Selected samples were combusted in a muffle furnace at a range of temperatures to estimate moisture, organic and inorganic carbon content. Two independent methods were chosen: the loss-on-ignition and classic CHN analysis. Recommended combustion temperatures in the loss-on-ignition method vary depending on material and application of this method. Boyle, 2004 reported that organic carbon removal from alluvial sediments is only complete at temperatures reaching 550^{o}C and thermal oxidation below that temperature can result in an underestimation of organic carbon. Thermally stable humic material is most likely responsible for incomplete organic carbon oxidation. Nevertheless, exceeding 500^{o}C may result in severe dehydroxylation of clays in particular (Byers et al. 1978) and introduce a dewatering effect into the loss on ignition measurements which on clay rich, carbonate free sediments may be up to 5% of sample weight as reported by Dean Jr, 1974. Obtaining a temperature compromise in thermo-gravimetric studies is not possible because of the chemical complexity of sediment components (Leong and Tanner, 1999). Leong and Tanner, 1999 also reported that the organic carbon content in marine sediment samples, when determined by the loss-on-ignition method, tends to be overestimated as high as by a factor of 3 when compared to CHN analysis. In this study organic carbon content determined by the loss-on-ignition method was also higher than for CHN analysis by a factor ranging from 2.2 to 5.4. Given the above loss-on-ignition method was not further used in favour of CHN analysis. However the detection limit of the CHN analysis was limited by the precision of the analytical balance used and could be further improved with a more precise balance.

Method overview

Loss on ignition

All experiments were carried out in ceramic crucibles. Prior to analysis crucibles were washed with deionized water and fired in a furnace at 1000^{o}C for 24 hours to remove any organic and inorganic material present on the surface and weighed. Clean crucibles were handled with care to avoid contamination and stored in a desiccator above thermally activated silica gel beads. Between different stages of the experiment samples were also stored in a

desiccator. Samples were baked at 100°C for a period of 24 hours to estimate the moisture content. Subsequently samples were baked at 500°C for 24 hours to evaluate organic carbon (OC) content. Experiments were performed in duplicate.

CHN analysis

Prior to analysis, aliquots of sediments were placed in polypropylene (PP) centrifuge tubes and a 1 N hydrochloric acid solution was added to remove inorganic sample constituents. Acid was added in small aliquots to control frothing. Samples were centrifuged at 6000 rpm for 5 minutes and the supernatant was discarded. Sediment residue was then re-suspended in deionized water and centrifuged. Aqueous supernatant was decanted and discarded. Samples were oven dried and grounded with a mortar and pestle. Carbonate free sediment aliquots were sealed in tin foil capsules and combusted at ~960°C. Conversion of carbonates to chlorides as well as hydration can cause weight increase which has to be negated by a correction factor (Van Iperen and Helder, 1984). Samples were run in duplicate.

2.2.4.2 Major and trace elements analysis

Method development

Mild extraction and complexation methods for total metal analysis of sediments are considered not suitable because of incomplete and often selective extraction of analytes therefore strong acids digestion was chosen. Microwave assisted extraction was an attractive alternative due to significantly reduce extraction times and reagent volumes (Lamble and Hill, 1998) but special PTFE digestion vessels are costly and their relatively short life time ruled this technique out as cost inefficient. Taking into account the on-going debate about applicability of different acid mixtures for complete release of the analytes from the sedimentary matrix (Scancar et al. 2000; Trimm et al. 1998; Gungor and Elik, 2006) the USEPA method 3050B was chosen as the most reliable and applicable (US EPA, 1996). Although hydrofluoric acid (HF) is generally recommended to ensure the complete release of metals some studies have demonstrated that the use of other reagents does not significantly affect the analytes recovery rate (Trimm et al. 1998). Moreover HF acid requires special digestion vessels that are expensive and were not available at the time of the study.

Method overview

The chosen method involves a concentrated nitric acid (~34% HNO_3) digestion in near boiling conditions (~95°C) until no brown fumes (nitrogen oxides - N_xOy) are observed. The sample was concentrated to approximately half-volume and cooled to room temperature. Subsequently, concentrated hydrogen peroxide (30% H_2O_2) was added in small aliquots and the sample was heated (~95°C) to trigger peroxide reaction. When effervescence was not observed despite the addition of new aliquots of H_2O_2, the sample was concentrated and cooled down.

1:2 concentrated hydrochloric acid (~12% HCl) was then added and the mixture refluxed (~95^{o}C) for 15 min. The final stage involved filtration through acid-washed glass fibre filters (Whatman 41) and subsequent transferral of the extract into acid-washed volumetric flasks. Samples were then analysed by Inductively Coupled Plasma – Atomic Emission Spectrometer (ICP-AES). Quantitative analysis was performed against a range of multi-element standard solutions (1.0; 2.0; 3.0; 4.0; 5.0; 7.5; 10.0 ppm).

Table 9. Replicate analysis of 0.5 ppm standard metal mix spiked in to ARM.

0.5 ppm replicate	Al	Ca	Cd	Co	Cr	Cu	Fe	Mg	Mn	Ni	Pb	Zn
1	18738	21369	12534	5898	10800	6028	35252	1630	85707	5787	1078	21264
2	18976	20941	12077	5871	10801	6066	34048	1668	83974	5636	1027	20855
3	18720	20828	12049	6842	10841	6088	34103	1646	83770	5721	1037	20701
AV	18811	21046	12220	6204	10814	6061	34468	1648	84484	5715	1047	20940
SD	143	285	272	553	23	30	680	19	1064	76	27	291
CV [%]	**0.76**	**1.36**	**2.23**	**8.91**	**0.22**	**0.50**	**1.97**	**1.16**	**1.26**	**1.32**	**2.58**	**1.39**

Quality control involved the use of method blanks and artificial reference material blanks (ARM) and spiked (0.5 ppm) artificial reference material blanks (SARM). The ARM used was a mixture of chromatographically clean sand and clay (95:5 w/w). Standards were run in triplicate to assess coefficient variation between analyses (Table 9). Recovery of individual elements varied between 96.6 and 106.5%.

2.2.4.3 High resolution major and trace elements profiling by X-ray fluorescence scanning

Instrument and calibration

Prior to analysis cores were split open and the sediment surface was carefully smoothed with a spatula to minimize surface roughness. If possible all voids or gaps were covered with sediment to eliminate pore fluid accumulation during the run. Sediment was covered with X-ray transparent clean film to protect the surface of the sediment during analysis and minimize sediment drying. If surface imperfections could not be smoothed without removing large portions of the sediment the path of the X-ray beam was adjusted to avoid collecting data in these areas. The instrument was fitted with a 3kW Mo X-ray tube operating in the 30 kV, 30 mA mode which is suitable for a broad element range (Croudace et al. 2006). Radiograph was

operating in the 55 kV, 50 mA mode. The instrument was fitted with a laser triangulation system to ensure equal distance between the X-ray emitted and the sample, which minimizes the surface roughness effects. The system was operated with a Si-drift detector (SDD; Lechner et al. 2001). Sensitivity of the system and efficacy of the Mo source was tested against marine sediment MAG-1 standard (USGS) prior to measurements. Count time was set to 35 s per increment. Scanning resolution was chosen individually between 500, 1500 or 2000 μm increments depending on core length and estimated analysis time. Instrument calibration was achieved through control software and Q-Spec program which allows real time analysis of a single core and peak-fitting to obtain best spectrum quality expressed by on line calculated error analysis. This procedure was repeated prior a new core analysis.

Artefact considerations

XRF major and trace element profiles, despite many advantages, must be interpreted with great care and understanding of the limitations of XRF scanners. These instruments are a relatively new development and many researchers point out insufficient discussion of their analytical performance and consider artefacts and false signals a valid concern for use of these instruments. During this study we have observed two types of artefacts that can commonly be encountered by other researchers during analysis. First were false positive signals from pore fluids accumulating on the surface of the cores. Young sediments usually contain large volumes of fluids that tend to accumulate on the surface as the core sits on the instrument rack. It is not always possible to smooth the surface enough to minimize formation of small pore fluid pockets that interfere with the analysis. The effect of one such fluid pocket was increased As and S counts indicating pyrite presence in the very top oxic/suboxic section of the core. As pyrite formation occurs in anoxic conditions (e.g. Furukawa and Barnes, 1995; Wang and Morse, 1994) these signals were considered false positives. The second type of artefact observed was signal change due to oxidation of the surface of the core. It is a known phenomenon that oxidation of sulphides to sulphate occurs in a manner of hours after the core has been exposed to air. Since Itrax analysis can take up several hours and penetration of X-ray is minimal chemical changes on the surface of the core can affect entire profiles. To investigate the effect of this process on element profiles fresh, non-oxidized sediment was exposed at the edges of the core at the beginning of the Itrax run and the core was scanned normally (Figure 19). The XRF profiles have shown that fresh surface profile has considerably higher counts of S and affects profiles of other elements and element ratios. It is an important artefact to consider when working with anoxic sediments, and to date there is no solution that could eliminate the oxidation of the oxygen sensitive minerals. These effects as well as the ones mentioned before where considered when interpreting the XRF element profiles. Interpretation was conducted with the help of high resolution core photographs to ensure elimination of topography related false positive signals.

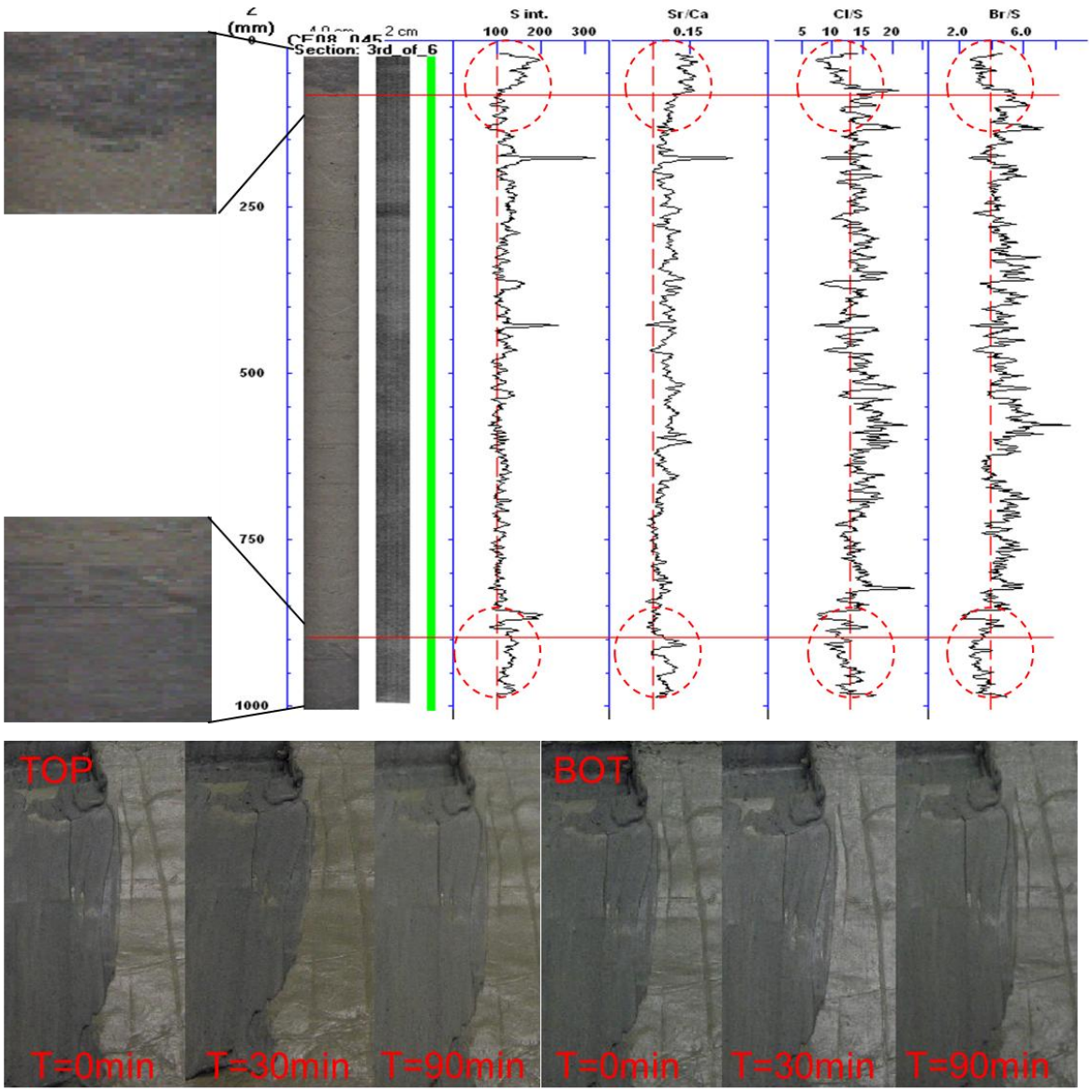

Figure 19. The effect of oxidation of sulphides during Itrax XRF scanner run on selected element ratios.

2.2.4.4 Pore water sulphate and chloride

Method overview

Sediment blocks (ca. 35 g) were extracted from the core with syringes with cut off tips and transferred into 50 ml Teflon centrifuge tubes. The tubes were spun for 15 min at 6000 rpm and supernatant was collected with a syringe and a needle and stored in refrigerator until analysis. Concentrations of sulphate and chloride in the pore water were determined with suppressed ion chromatography on a DX-120 Dionex Ion Chromatograph with an eluent generator (K_2CO_3) module and a conductivity detector. Separation was achieved on a chromatographic system composed of an anion exchange column and a guard column. The mobile phase was Nanopure grade water (18MΩ) which was automatically amended with hydroxide ions to a preset concentration (15 mM of OH^-). The mobile phase flow was set to 1.0 ml/min and suppressor current was set to 25 mA. The instrument was calibrated with a five

point calibration curve of standard anion mix and blanks. IAPSO sea water standard was unavailable at the time of the analysis. Precision was evaluated by quadruple analysis of random samples and was 1.4%. Samples were diluted 1:200 with Nanopure prior analysis grade water (18MΩ) and injected manually in duplicate. All samples were analysed in one batch with standards being analysed every 6 samples. Peaks were integrated manually in the Chromelion software package.

2.3 Results and discussion

2.3.1 Characterization of the Malin Shelf sediments

2.3.1.1 Physical properties of the surface sediments

Sediment sample analysed for physical and geochemical properties are shown in Figure 20. Acoustic characterization is the first step in determining what type sediment dominates the seabed. This approach focuses on remote techniques such as multi and single beam echo sounding (MBES, SBES) to collect data on acoustic response of the seabed when exposed to acoustic pulses over a range of signal frequencies.

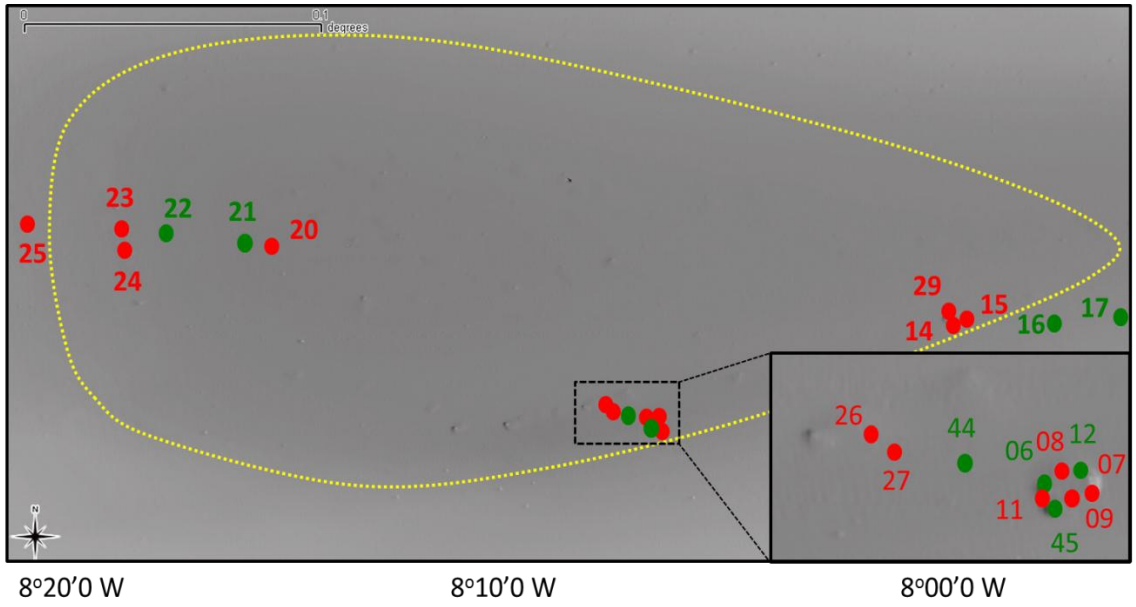

Figure 20. Shaded relief bathymetry of the Malin Shelf with the locations of grab (red) and core (green) samples analysed for physical and geochemical properties. Yellow delineation depicts the Malin Deep, central part of the Malin Shelf. Insert shows magnification of the pockmark P1 area.

The date is then analysed and used to construct a so-called '*Acoustic Sediment Classification*' model (ASC) that separates seabed types based on their acoustic properties. Such a model for the Malin Shelf was created by Geological Survey of Ireland and reported by Monteys, et al.

2009 and Monteys, et al. 2008a (Figure 21). ASC models are an important deliverable of acoustic seabed surveying efforts as they are crucial for habitat mapping and further planning of biological surveys as well as targeting specific seabed areas and morphological structures (e.g. McGonigle et al. 2010; Rein et al. 2011). This model however must be validated by ground-truthing activities to correlate specific acoustic groups with intrinsic properties of the sediment such as sediment particle size and grain density.

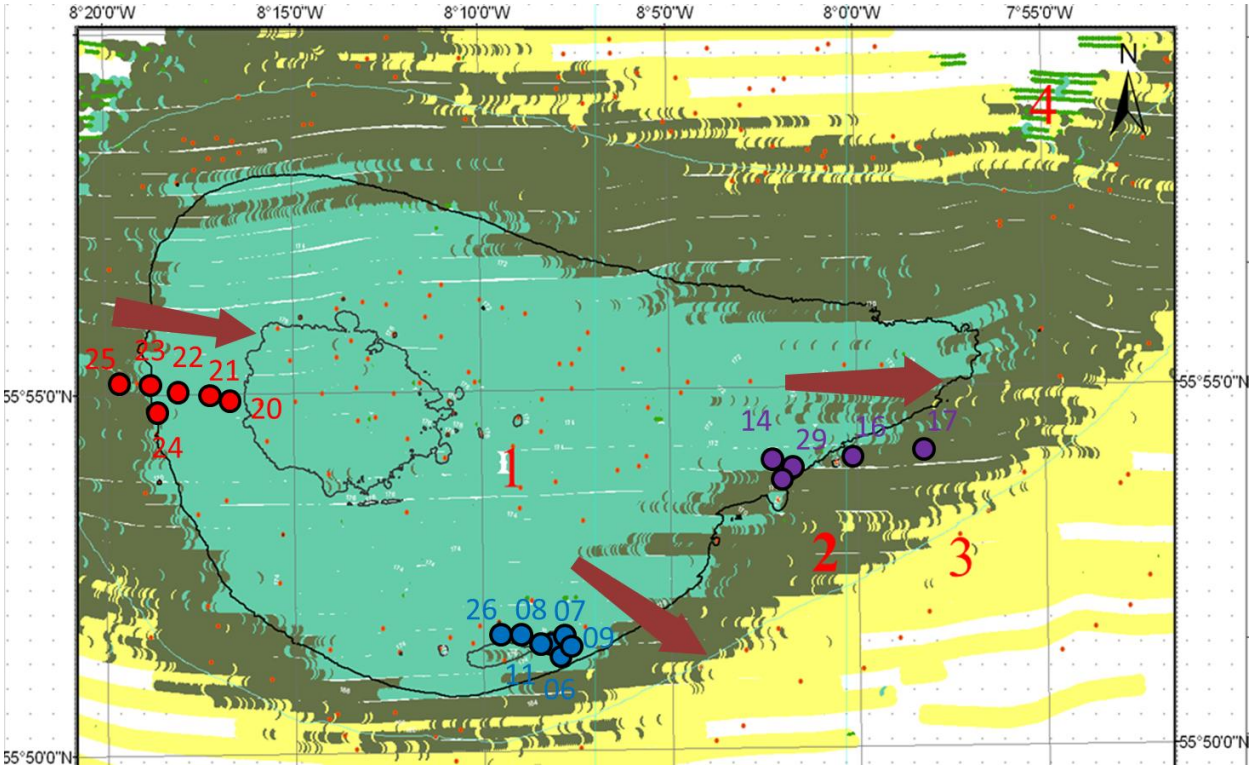

Figure 21. Acoustic seabed classification model of the Malin Shelf after Monteys et al. 2008a. Backscatter derived acoustic classes are depicted with different colors and numbers 1 to 4. Large circles denote sampling locations for particle size analysis, colors denote sampling groups, small red dots represent pockmarks deeper than 0.5m. Arrows symbolize decreasing or increasing trend in mean grain size.

According to the ASC model (Monteys, et al. 2009 and Monteys, et al. 2008a) sediments in the Malin Shelf can be divided into four acoustic classes based on backscatter intensity (Table 10). Three of these classes (1 to 3) present very similar acoustic properties with the last class being considerably different (4). Acoustic backscatter strength is defined as mean echo amplitude collected by the receiver in decibel (dB) (Wilmut, et al. 2009). The first three classes can be described as soft sediments as they easily absorb and scatter a large portion of the acoustic pulse energy while the backscattering is low (from -30 to -40 dB). Hard ground such as rock outcrops and consolidated sediments on the other hand, backscatter the majority of the acoustic pulse (from 0 to -20 dB) mainly because it is not able to penetrate the hard surface. According to this model on the Malin Shelf the majority of the surface sediment is young and

unconsolidated material of similar acoustic properties. This is a typical acoustic characterization of glacio-marine seabed expected in this area (Dobson et al. 1974), a conclusion further supported by the pockmark distribution across the acoustic classes. Pockmarks representing seabed collapse structures are known to be formed predominantly in soft sediment. In the Malin Shelf they are roughly equally distributed across all low-backscatter acoustic classes suggesting similar, soft type of the seabed.

Table 10. Backscatter intensity [dB] in the Malin Shelf, σ denotes standard deviation.

Acoustic classes	Backscatter intensity			% of pockmarks in the acoustic area
		[dB]	σ	
1	Low	-32.0	1.8	45
2	Low	-32.0	1.7	18
3	Low	-31.5	2.2	30
4	High	-18.5	5.1	0

Nevertheless pockmarks can also be associated with hard ground in areas where intensified fluid flow results in precipitation of authigenic carbonate slabs and solidification of the surface sediment with MDAC cement (see Chapter 1 for details). Such outcrops interwoven with pockmark features would increase backscatter signals. This is not the case in the Malin Shelf as there are no pockmark features present associated with high backscatter areas. Because of similar acoustic properties discrete sample analysis was essential to discuss textural characterization of these sediments. Core and grab samples were collected in three sampling groups (Figure 20&21) covering the western, eastern boundary of the Malin Deep and the Malin micro basin. Particle size distribution (PSA) of the sediment indicates that acoustic classes 1 and 2 differ in grain composition.

In general, surface sediments are characterized by higher mean grain size decreasing towards the centre of the Malin Deep with decrease in concentration of the coarse grain component. Sediments in the acoustic class 2 generally fall under Muddy Sand textural group while group 1 can described as Sandy Mud (Table 11). This is particularly evident in the western boundary with average mean grains of 103.7 μm and the sand content decrease from 64.1 % (BS25) to 38.1 % (BS20) within the Malin Deep area is paired with a constant increase in mud content (35.9 and 61.9 %, respectively). Transition from Muddy Sand to Sandy Mud is clearly visible. As expected this transition does not reflect sorting of the sediments as the relative proportion of coarse and fine fractions varies only slightly from unity (from 0.56 to 1.62 in BS25 and BS20 respectively).

Table 11. Particle size distribution of surface sediments in the Malin Shelf.

Sample	Mean [μm]	Sorting [σ]	Composition					Textural group
			% clay	% silt	% mud	% sand	% shell	
BS25	134.9	2.378	6.3	29.6	35.9	64.1	0.0	Muddy Sand
BS23	114.1	2.230	6.0	33.8	39.7	60.3	0.0	Muddy Sand
BS24	95.0	2.268	6.9	40.8	47.7	52.3	0.0	Muddy Sand
BS22	81.4	1.921	5.2	47.7	52.9	46.4	0.0	Muddy Sand
BS21	130.9	2.097	4.6	31.8	36.4	63.1	0.5	Muddy Sand
BS20	66.1	2.236	8.8	53.1	61.9	38.1	0.0	Sandy Mud
BS26	69.4	2.131	7.4	52.2	59.6	40.4	0.0	Muddy Sand
BS08	57.7	2.114	8.5	61.7	70.2	29.8	0.0	Sandy Mud
BS07	58.5	2.139	8.4	59.0	67.5	32.5	0.0	Sandy Mud
BS09	58.3	2.157	8.5	59.2	67.8	32.2	0.0	Sandy Mud
BS11	62.8	2.119	8.0	55.7	63.6	36.4	0.0	Sandy Mud
BS06	48.3	2.229	10.4	67.3	77.7	22.3	0.0	Sandy Mud
BS14	65.7	2.353	10.0	56.4	66.4	32.9	0.7	Sandy Mud
BS29	60.1	1.952	6.6	61.5	68.1	31.9	0.0	Sandy Mud
BS16	48.0	2.226	10.4	64.7	75.1	21.9	2.9	Sandy Mud
BS17	71.2	2.140	7.3	50.8	58.1	40.4	1.5	Muddy Sand

The transition is not entirely smooth, as expected in such dynamic environment, with areas rich in sand being still present within the Malin Deep (e.g. BS21). In the western boundary average mean grain size is considerably lower (61.2 μm) however the transition from Sandy Mud into Muddy Sand is still distinguishable. Samples on the edge of the acoustic group 1 (BS29 and BS14) have high mud contents (68.1 % and 66.4 %, respectively) and relatively low sand content (31.9 % and 32.9 %, respectively) similar to that of inner Malin Deep samples from across the boundary (BS20). The outer sample shows a decrease in the fine grained component and increase in mean grain size (71.2 μm). Similarly the transition is not sharp which is reflected in lateral patches of acoustic class 2 entering the Malin Deep area (Figure). The third sampling group has an average mean grain size of 60.2 μm and relatively low sand content varying from 22.3 % to 40.4 % (BS06 and BS26, respectively). In this part of the basin pockmarks are frequent and the sediment surface is not homogeneous with craters acting as sinks for the finest grains (BS06 and BS08) and the outer seabed being enriched in coarser grains (e.g. BS26). This process of natural hydraulic sorting disturbs the trend visible in the other two locations however samples falling under acoustic class 2 (BS26) show enrichment in

coarse grains as described by the ASC model. There are however visible differences in PSD between individual sampling groups. The differences arise most likely from changes in the sedimentological regime. The western sampling group has by far the highest mean grain size but is also the most exposed to the high energy environment of the western seaboard. It is also the area furthest from the land mass and closest to the shelf break. According to Lynch et al. 2004 this area could be experiencing effects of the coastal currents. The sandy layer in core BS21 has a depth of half a meter and is locally enriched in shell debris (up to 5.9%). Mean grain size also rises with depth, peaking at 0.3 mbsf with 185 μm and gradually decreasing to 130 μm at 0.55 mbsf and finally rapidly decreasing to 61.2 μm at 0.6 mbsf marking a change in the lithology. Such a layer may also be a remnant of periodic change in the sedimentological regime indicating increase of energy of the depositional system in this area. Interestingly BS21 was the only sediment core that contained such a prominent sandy layer although other cores show enrichment in the biogenic component (up to 7.1 % and 10.6 % in BS17 and BS16, respectively). According to Dunlop et al. 2010 the western boundary of the Malin Shelf was under the influence of the main ice stream flow lines and is frequently scarred by iceberg scours. Frequent sand ribbons west of the Malin Deep could also be a source of this coarse material. The silt and clay enriched lithology (two units) underneath the coarse layer shows mean grain size of 45 μm (from 0.6 to 2.35 mbsf) while the next core toward the center of the Malin Deep (BS22) shows a change from 56 μm in the top unit (from 0.1 to 0.6 mbsf) to 20 μm in the lower unit (from 0.7 to 2.3 mbsf). Similar mean average grain size change can be observed in the western boundary (BS16 and BS17) and the southern cluster excluding pockmark locations (BS15). This suggests that similar processes controlled deposition of these stratigraphically correlated units across the entire Malin Deep. Unfortunately low sample density makes more in depth analysis of the controls of the depositional processes in this area troublesome.

Dry bulk density measurements from grab samples and core BS21 show less variation than expected and their contribution to the ASC model is rather limited. Samples from the western boundary however had higher dry tapped density values than these from southern sampling site (Table 12). These differences quite possibly reflect the changes in silt and clay content relative to sand content which is dominated by quartz (ρ: 2.65 - 2.66 g/cm^3). This relationship is more pronounced in tapped density results from the BS21 core which had the highest sand content of all studied samples, yielding considerably higher density values. Down core tapped density which reflects mineralogical changes (Al-Jaroudi et al., 2007) rather than structural properties which are not preserved in pulverized samples show a gradual increase to values exceeding 2.7 g/cm^3. This trend is in agreement with an increase in clay and silt content. Fine grained minerals, particularly clays have high density values (ρ: 2.6 - 2.9 g/cm^3) and will increase cumulative density of the sediment enriched in these components. Average clay content

in unit 2 of the BS21 core is almost four times higher than in unit 1 and the silt content is two times higher (18.4 % and 60.9 %, respectively). Dry bulk density of the BS21 core on the other hand reflects the structural properties of the sediment (Dadey et al. 1992) similar to wet bulk density which is discussed below. Dry bulk density linearly decreases with depth (slope: 0.0075; R^2 - 0.80) which suggests normal consolidation processes and a compaction effect. Increasing density values are also moderately in agreement with the composition of the sediment: increasing silt (from 31.0 to 54.5%) and clay content (from 4.0 to 17.3%) and decreasing sand content (from 64.7 to 28.2%).

Table 12. Dry bulk density and tapped bulk density values for selected grab BS21 core samples

Sample (tapped)	Density [g/cm^3]	SD	Sample (tapped)	Density [g/cm^3]	SD	Sample (block)	Density [g/cm^3]	SD
BS07	2.6443	0.0004	BS21 0.1	2.6618	0.0002	BS21 0.1	2.6891	0.0001
BS09	2.6473	0.0005	BS21 0.5	2.6759	0.0001	BS21 0.5	2.6977	0.0001
BS23	2.6530	0.0003	BS21 1.0	2.6630	0.0000	BS21 1.0	2.7024	0.0002
BS24	2.6533	0.0009	BS21 1.5	2.6893	0.0001	BS21 1.5	2.7034	0.0000
BS25	2.6581	0.0007	BS21 2.0	2.7140	0.0001	BS21 2.0	2.7046	0.0002

Overall there is a good agreement between PSA data and the ASC model in the studied areas. The ground-truthing suggests that acoustic class 1 comprises fine grained dominated sediments with and average sand content approximately ≤40% and mean grains size ≤70 μm. Sediments from this class fall in the Sandy Mud textural group. Class 1 also shows slight enrichment in clay content reaching around 10 % in samples from pockmark locations. Sediments from acoustic class 3 comprise of silt rich sands with average silt content ≤55% and mean grain size in this class varies from 70 to 140 μm. Sediments from this class fall under Muddy Sand textural group. Dry bulk density values show little variability which is expected in a setting dominated by relatively homogenous sediments. Down core trends can be attributed to increasing silt content and compaction of the sediment. Distinguishing between these two effects is troublesome without information on mineralogy of the sediments. Due to the low variability of density values broader conclusion cannot be drawn at this time however, they can successfully employed in and aid future mineralogical investigations.

2.3.1.2 Major and trace elements screening

Cumulative input of heavy metals such as: lead, copeer, zinc, mercury and cadmium on to the Atlantic Seaboard and the Malin Shelf between 1990 and 1996 reached 82.4 tonnes (OSPAR, 2000). Among major sources the OSPAR Commission named direct and riverine

discharges, mariculture, waste dumping and to lesser extent atmospheric inputs. Selected sediment samples were analysed for major and trace element content to provide baseline information and evaluate potential anthropogenic contribution to the Malin Shelf sediments.

Grab samples

Results from grab samples show great similarities in metal distribution across the Malin Shelf reflecting little variability in sediment composition. There is no significant difference in elemental composition between northern (20, 23, and 24) and southern (07, 09, 11, 26 and 27) sampling clusters. This implies that surface sediments in Malin Shelf originate from the same source. This observation is supported by physical property data discussed above and observations from the acoustic seabed classification model. Although mineralogical studies were beyond the scope of this work, based on major and trace elements distribution it is justified to assume similar mineralogical composition of the surface material on the Malin Shelf.

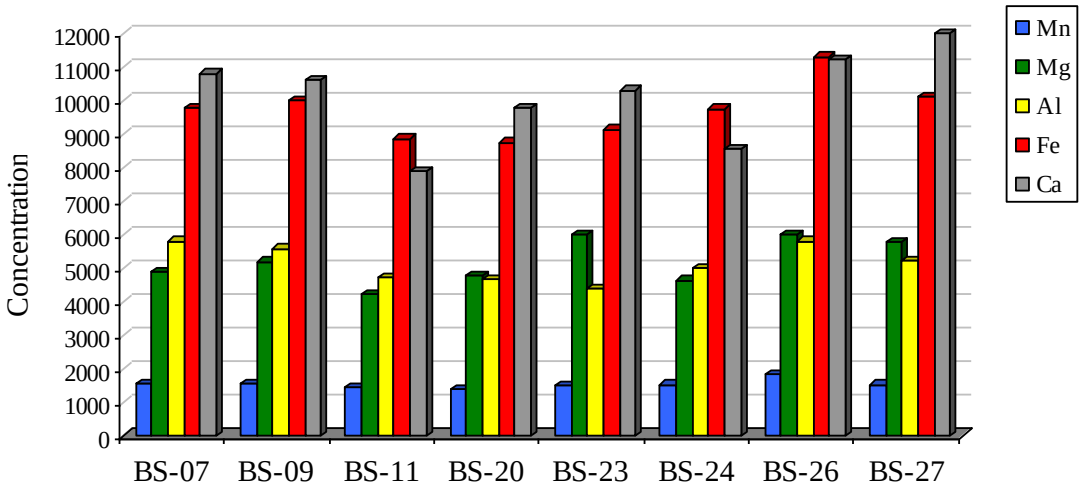

Figure 22. Major elements concentration in Malin Shelf samples. All values in mg/kg except Ca: 10^{1} mg/kg and Mn: 10^{-1} mg/kg for better profile visualization.

The most abundant elements, Fe and Ca (8750-11300 mg/kg; 78900-122000 mg/kg, respectively) show little variation (Figure 22). The consistency of Ca concentration is in agreement with inorganic carbon estimation data, where similar profiles were obtained for the Malin Shelf samples and the remaining major elements all show a consistent profile. Mg and Al concentrations are similar (4210-5980 mg/kg and 4410-5810 mg/kg respectively) in most of the samples. Mn is least concentrated and varies from 138 to 183 mg/kg. Similarly, trace elements occur in a consistent profile (Figure 23). Zn is the most dominant metal (16.4-21.4 mg/kg) but Cr and Ni are abundant as well (12.7-16.3 mg/kg and 8.8-12.0 mg/kg respectively). The remaining elements, Co, Cu and Pb seem to have similar concentrations with mean values of 1.96 mg/kg, CV: 10%; 2.84 mg/kg, CV: 25% and 2.58 mg/kg, CV: 29% respectively. Cadmium

was not detected which is an important finding because of report of elevated cadmium content in some shellfish from this region (Xavier Monteys personal communication).

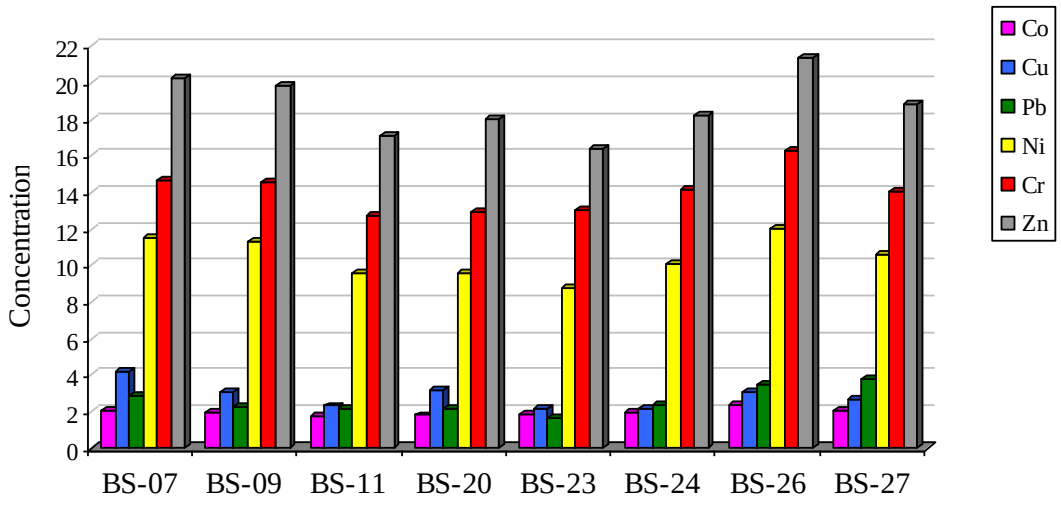

Figure 23. Trace elements concentration in Malin Shelf samples. All values in mg/kg.

BS-21 core

All samples present a similar major element concentration profile (Figure 24). Samples from the bottom of the core (0.8 and 2.1m) are enriched in Al, Mg, Fe and Mn (5000-22100 mg/kg; 4760-13800 mg/kg; 9250-35000 mg/kg and 1560-4310 mg/kg, respectively).

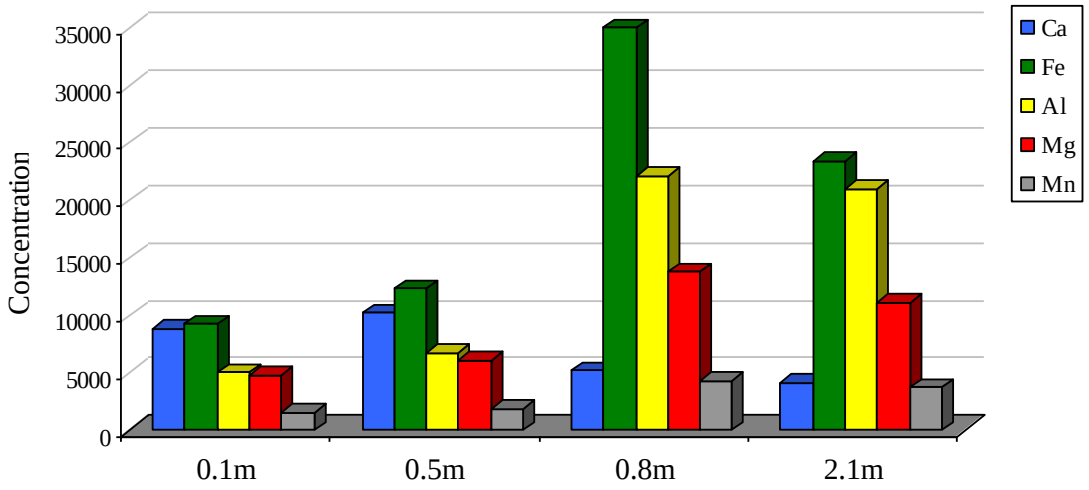

Figure 24. Major elements concentration changes with depth in BS-21 core. All values in mg/kg except Ca: 10^{1} mg/kg and Mn: 10^{-1} mg/kg for better profile visualization.

This trend correlates with mud and clay concentrations and also with Fe (R^2 - 0.97 and 0.91, respectively) Mg (R^2 - 0.99 and 0.98, respectively) and Mn (R^2 - 0.99 for both). The observed pattern suggests a strong mineral influence. Depletion of Ca is similar to the decrease of biogenic carbonate content with depth. A similar element distribution is observed for trace

minerals (Figure 25). Again the highest concentrations were detected in the last two samples (0.8 and 2.1m) excluding the most abundant Zn which peaked in 0.5 m (20.6-73.6 mg/kg). For the remaining elements the highest variability is observed for Ni and Cr (9.8-32.7 mg/kg and 13.9-43.1 mg/kg, respectively) with moderate concentration changes for Pb, Cu and Co (2.5-8.0 mg/kg; 2.6-14.2 mg/kg and 3.8-10.0 mg/kg, respectively).

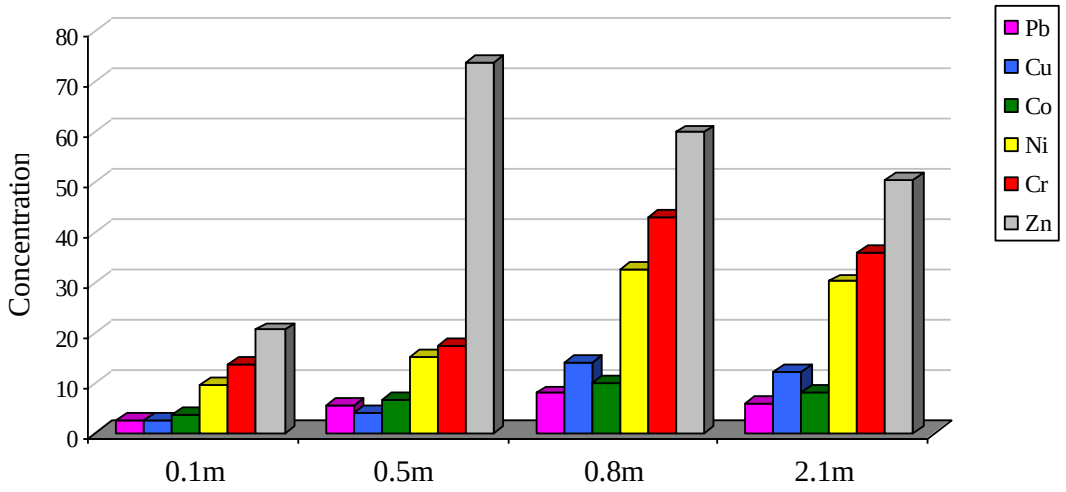

Figure 25. Trace elements concentration in Malin Shelf samples. All values in mg/kg.

BS06 core

The major elements become more concentrated with depth but the most enriched is the 0.5 m layer (Figure 26). Fe, Al and Mg concentrations were highest at this level (13300-31800 mg/kg;

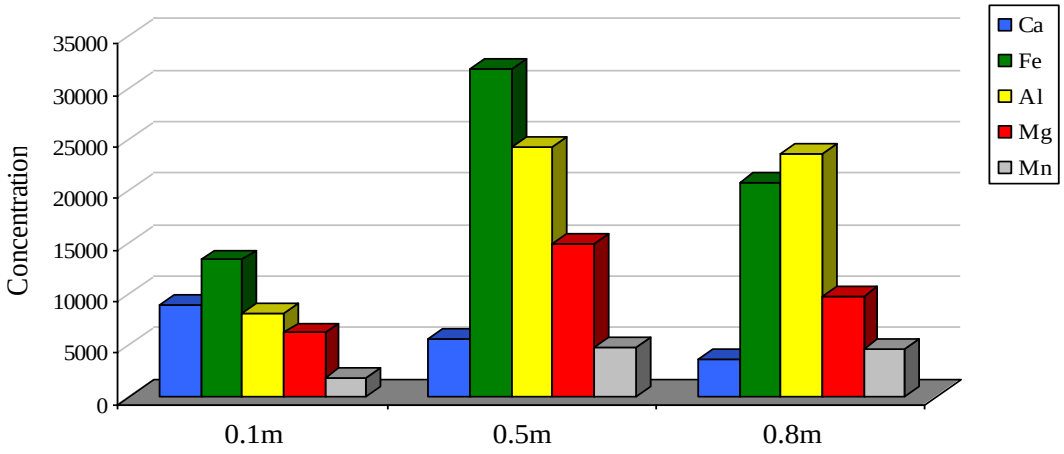

Figure 26. Major elements concentration changes with depth in BS-06 core. All values in mg/kg except Ca: 10^{1} mg/kg and Mn: 10^{-1} mg/kg for better profile visualization.

8060-24300 mg/kg and 6200-14900 mg/kg, respectively). The Mn concentration, after the initial increase, (190-479 mg/kg) was less variable in the bottom section of the core (479-464 mg/kg). Ca concentration dropped with depth (89600-36100 mg/kg) but this change does not

reflect the changes in the biogenic carbonate content. Trace element concentration shows minimal variability in the deepest sections of the core (Figure 27). Mean values in these sections range from 8.0 to 59.8 mg/kg (for Pb and Zn respectively) and the variability ranges from 2.1 to 6.4% (for Co and Ni respectively).

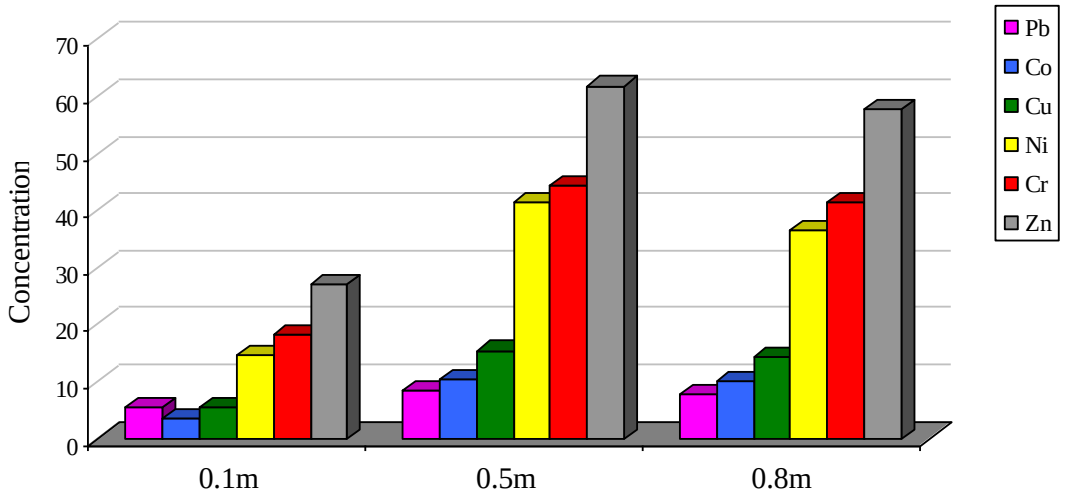

Figure 27. Trace elements concentration changes with depth in BS-06 core. All values in mg/kg.

Comparison of BS06 and BS21 cores

BS-21 contained samples from outside the pockmark features while BS-06 is a core from inside the pockmark. Nevertheless sampling stations were located at different parts (BS-21 at central-western part of the Malin Deep; BS-06 pockmark cluster at southern part of the Malin Deep) of the basin therefore any conclusions drawn are more likely to be related to the geographical location and/or lithology rather than the pockmark feature itself. Major elements show a moderately good correlation (n: 5; R^2 - 0.79) and similar trends (Figure 28) between cores in the surficial sediment (0.1 m). A higher concentration of elements can be observed in the BS-06 core, excluding Fe which is slightly more abundant in BS-21 core. Similar trends can be observed for trace metals (Figure 29) and there is a very good correlation between data (n: 5; R^2 - 0.98). The Co concentration is slightly higher in BS-21 than BS-06. Second layers (0.5 m) are less cohesive, although the main trend is visible. Again both main and trace elements are much more abundant in the BS-06 core. This trend is not preserved for Fe which is more than twice (x2.2) the concentration in BS-21 than BS-06 and Zn (18% more abundant). The smallest variability between cores is observed for Mn, Co and Pb. In the third section significant differences between Ca and Fe are observed. Ca concentration is four times (x4) higher in BS-06 than BS-21 while Fe content is ten times ($x10^{-1}$) lower.

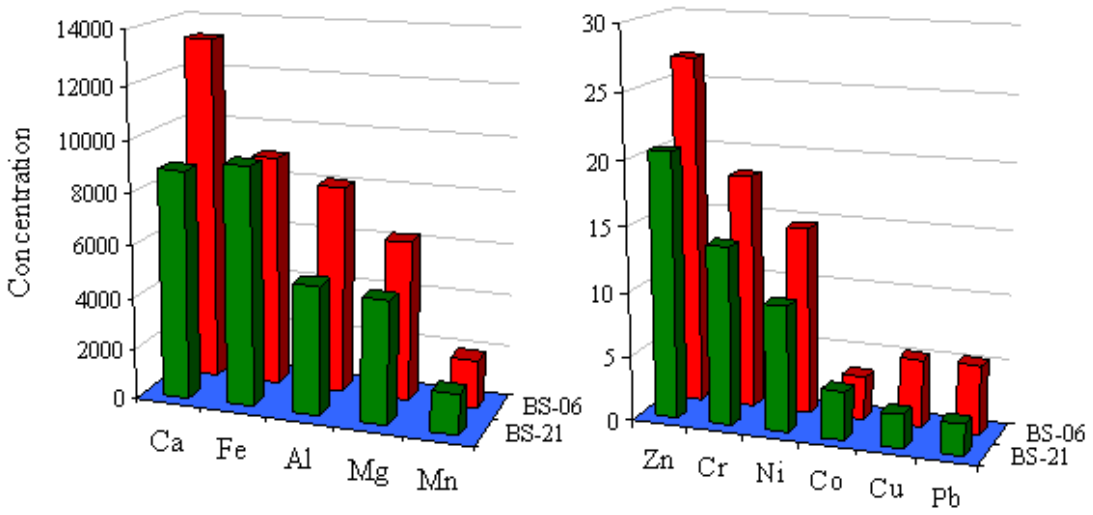

Figure 28. Major and trace metals concentrations in BS-21 and BS-06 at 0.1m depth. All values in mg/kg except Ca: 10^1 mg/kg and Mn: 10^{-1} mg/kg for better profile visualization.

The correlation between cores is poor for the major elements due to outlying Fe and moderately good for the trace metals (n: 5; R^2 - 0.68). The remaining major elements show similar trends (Figure 30). Trace element concentrations in this section are nearly identical, with little variability between Ni and Zn which is reflected in a high correlation coefficient (R^2 - 0.99). Generally there is a better data agreement in trace metal concentrations (cumulative curve n: 18; R^2 - 0.97) than the major metals. Nevertheless individual trends in the cores are preserved which suggests that the mentioned differences are specific to these local environments and reflect small changes in lithology.

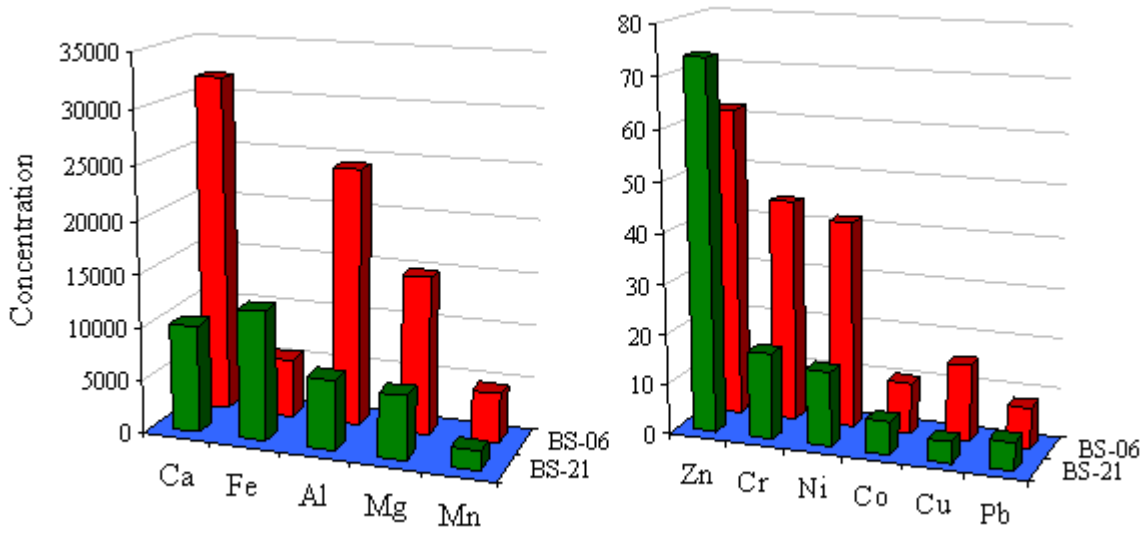

Figure 29. Major and trace metals concentrations in BS-21 and BS-06 at 0.5m depth. All values in mg/kg except Ca: 10^1 mg/kg and Mn: 10^{-1} mg/kg for better profile visualization.

Calcium concentrations, for instance can be easily affected by biogenic components. The results are in general agreement with proposed trace metal diagenesis mechanisms (Burdige, 2006). According to these mechanisms low concentrations in surficial sediments is a result of slow accumulation rates and benthos activity. The mechanism predicts an increase in concentration in the shallow sediments on the redox boundary and decrease below it.

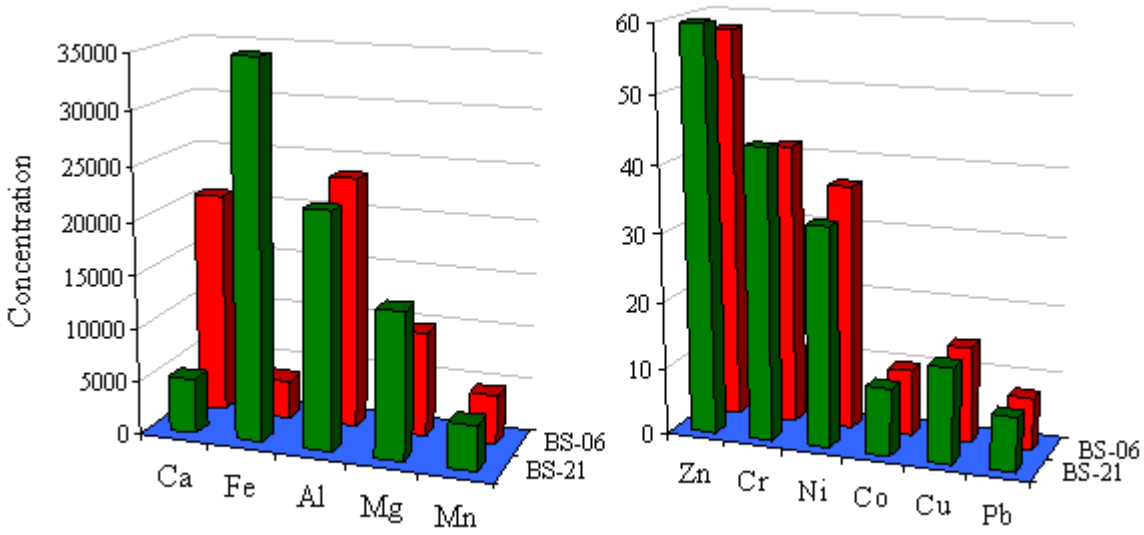

Figure 30. Major and trace metals concentrations in BS-21 and BS-06 at 0.8m depth. All values in mg/kg except Ca: 10^{1} mg/kg and Mn: 10^{-1} mg/kg for better profile visualization.

Of course the above burial mechanism is very simplistic and the diagenesis of specific metals should be investigated individually. Obtained data can be useful for creating a baseline of sediments elemental composition. Unfortunately low spatial density of the reported dataset impairs more in depth discussion of elemental composition and its provenance. Importantly the concentration of analysed major and trace elements were within background values proposed by OSPAR commission and typical for marine sediments in general. Burdige, 2006 compiled typical major and trace element concentration values reported in various marine sediments (Table 13). Malin Shelf sediments can be considered a pristine environment.

Table 13. Metal concentrations in different sediment types; values in mg/kg except for Fe (%). Data after Burdige, 2006 and references within.

	average shale	nearshore mud		Atlantic clay	carbonate ooze
Mn	850	850	850	4000	1000
Fe	4.72	6.5	6.99	8.2	0.9
Co	19	13	13	38	7
Ni	68	35	55	79	30
Cu	45	56	48	130	30
Cr	90	60	100	86	11
Pb	20	22	20	45	9
Zn	95	92	95	130	35

2.3.1.3 Radioactive nuclides screening

Increased levels of radioactive nuclides of anthropogenic origin were reported in the past on the Malin Shelf (OSPAR III, 2000; Keogh et al. 2007; Vintro et al. 2009) were identified as related to Sellafield plant discharges to the Irish Sea which were then transported by currents to the Malin Shelf. The Sellafield plant is a nuclear fuel processing plant and reported accidental and process derived discharges resulted in increased levels of radionuclides (^{137}Cs in particular) in the local waters, shellfish and sediment. Total discharges from the nuclear sector in the years 2005-2009 reported by the OSPAR commission (OSPAR, 2011) were estimated to reach 0.28 TBq with 30% of the load originating in the UK, the Sellafield plant being the major source. For the purpose of screening, sediments from the eastern boundary were analysed for radionuclide activity to assess their accumulation, or lack of it, in the Malin Shelf.

Radiometric analysis revealed low activity in the studied samples. Organic bound and water carried tritium levels were below the detection limits of the method (0.0079 Bq/g). Gross α/β is a measure of total activity of all α- and β-emitters in the sample. Although external eco-toxicity of this kind of ionization energy is low due to a very short mean free path the internal toxicity is very high because of the high energy. Also, the size of the organism is a factor; smaller organisms have more penetrable bodies than the larger ones. In the studied sample both α and β activity was very low (Figure 19).

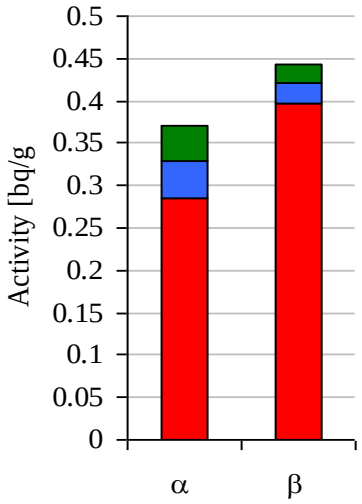

Figure 31. Gross α/β radioactivity for BS-25 sample (western boundary of the Malin Deep). Note that reported value: red + blue bar. Red bar describes the minimal value; blue and green bars represent ± error

Samples were also analysed for 35 γ-emitters and only 10 were present above detection limits (Figure 20). The γ-radioactivity levels in the studied samples were low but in agreement

with the surface water data (OSPAR, 2000). Most of the detected radionuclides (isotopes of Bi, Cs, K, Pb, Ra, U) are associated with natural minerals (Budrige, 2006). In this group ^{40}K and ^{210}Pb were the strongest emitters (0.299 and 0.083 Bq/g respectively). Both Ac and Tl are present at low concentrations and are also likely due to be the part of natural background. Nuclides associated with the Sellafied re-processing plant such as ^{234}Th or ^{131}I were not detected. Importantly, long lived nuclides such as ^{137}Cs where detected only in natural concentrations indicating a lack of anthropogenic input.

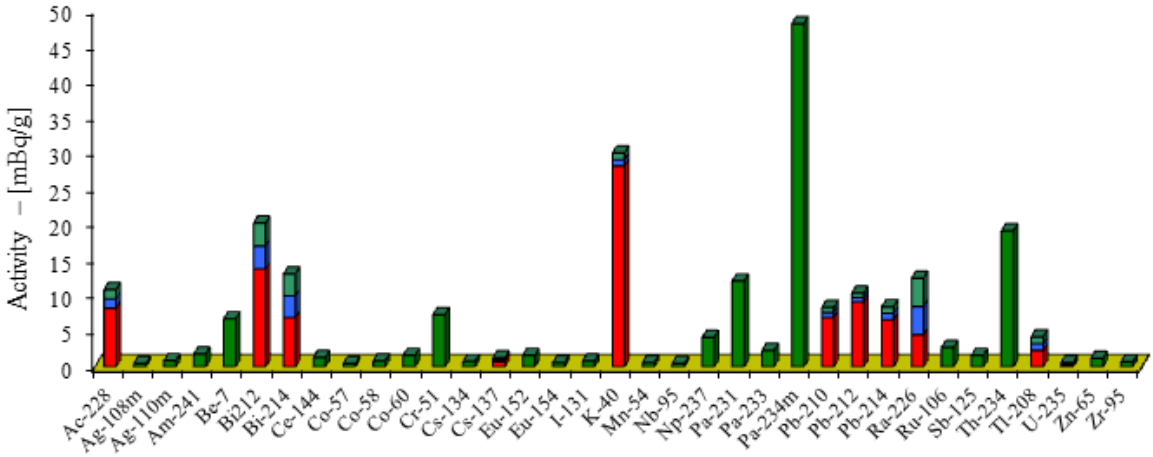

Figure 32. Gamma emitters in the BS-04 sample. Red bars indicate detected value reduced by the measurement negative (-) error (blue bar); light green bars depict positive (+) error. Dark green bars depict detection limits for the remaining radionuclides. All values in mBq/g except for ^{40}K and ^{210}Pb 10 mBq/g.

2.3.1.4 Foraminifera and ^{14}C analysis

Five distinct species of planktonic (planktic) foraminifera were isolated from the core (BS21): *Globigerina bulloides* sinistral and dextral (left and right coiled morphotypes), *G. quinqueloba*, *G. glutinata*, *Neogloboquadrina pachyderma* (both *sinistral* and *dextral*) and *Globorotalia inflata*. Unidentified species contents were below 10.3% and around 5% in the surficial sediments (0.1 and 0.6m). The dominant species in all samples was the *dextral* morphotype of *N. pachyderma* (Figure 33) whose concentration was consistent (n: 7; SD: 4.86; CV: 10.7%) throughout the entire core (mean: 45.4%). The *sinistral* morphotype was far less abundant (2.78-11.9%). Concentrations of *N. pachyderma* morphotypes are moderately well correlated only in the first 1.5m (n: 6; R^2 - 0.66). The second most abundant species is the *sinistral* morphotype of *G. bulloides* (Figure 34), with the *dextral* morphotype approximately twice to four times less abundant (x2.2 and x3.9 respectively). Both morphotypes peak at 1.0 m creating a dome shaped trend. Averaged data shows moderately good correlation between morphotypes (n: 5; R^2 - 0.67). *G. quinqueloba*is is the only species that shows clear negative concentration trend in the BS-21 sediment record (Figure 35).

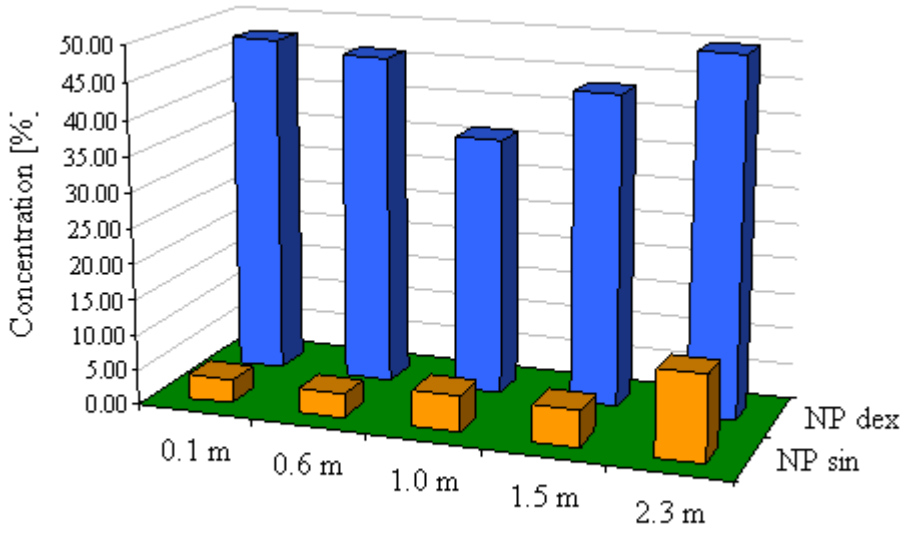

Figure 33. *N. pachyderma* (NP) counts in the BS-21 core. Data for 0.1 and 0.6m are averaged from replicates.

The concentration of this species decreased from 12.4 to 2.4%. *G. glutinata* remains moderately consistent (n: 3; mean: 7.3%) with a slight decrease in concentration at 1.0 and 2.3 m. These drops increase the overall variation coefficient to 26% (mean: 6.17%; SD: 1.62). *G. inflata* was detected only in surficial layers (0.1 and 0.6 m) and reached an average value of 3.1%. The concentration of these forams reveal that over the time represented by the analysed sedimentary record there were no signs of glacial conditions and the species distributions suggest temperate waters.

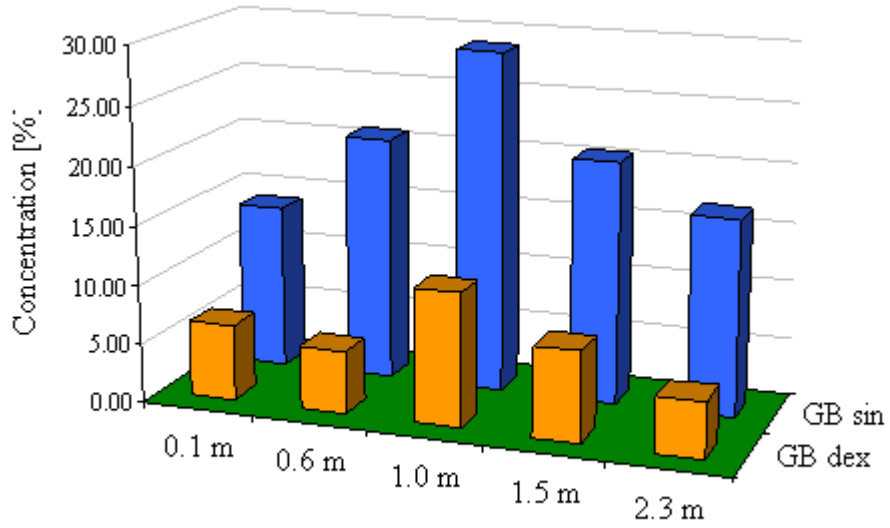

Figure 34. *G. bulloides* (GB) counts in the BS-21 core. Data for 0.1 and 0.6m are averaged from replicates.

The main evidence is provided by the presence of *N. pachyderma* which is a well-recognized tool in paleoclimatology; glacial-interglacial climate reconstructions in particular (Bauch et al. 2003). This species is commonly used due to its broad tolerance to sea surface temperature and preference for low salinity. The *sinistral* morphotype is abundant in cold waters and has been reported to live in ice (Hilbrecht, 1996).

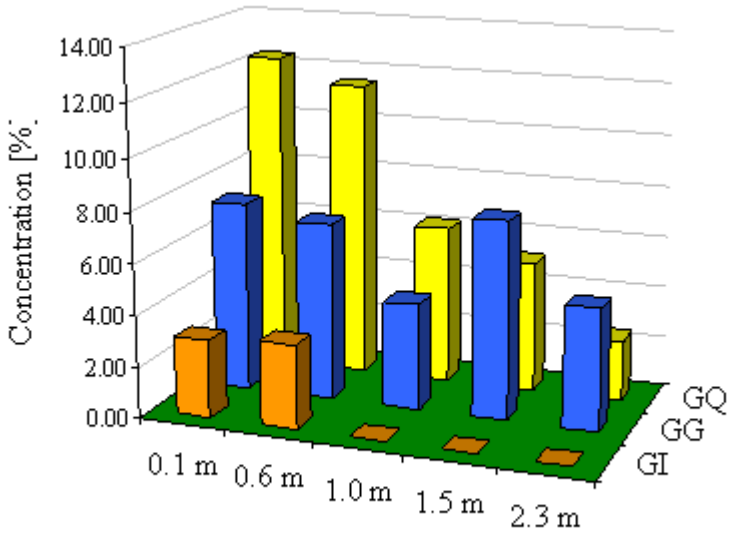

Figure 35. *G. quinqueloba* (GQ), *G. glutinata* (GG) and *G. inflata* (GI) counts in the BS-21 core. Data for 0.1 and 0.6m are averaged from replicates.

In addition to being an indicator of moderate waters the *dextral* morphotype is also a good indicator of surface water density (preferring densities above 25.5 kg/m^3). High concentrations of the *dextral* morphotype are moderately well linearly correlated with depth (n:5 ; R^2 - 0.79) when the % of dextral morphotype relative to total *N. pachyderma* is used. *G. bulloides* and G. *glutinata* are usually coexisting species. They prefer productive waters but have different feeding strategies (algae and diatoms respectively). Commonly an inverted trend between these two species can be observed (Hilbrecht, 1996). This trend is present in BS-21 but because of the low abundance of G. *glutinata* is not very obvious. Higher concentrations of *G. bulloides* compared to G. *glutinata* are typical of high productivity areas and upwelling zones. The opposite relationship is observed for open seas and marginal areas. Because of a broad tolerance for physical conditions (temperature, salinity, density and stratification) these species are not that useful as climate indicators (Asano et al. 1968). It has been suggested that these species are useful (*G. bulloides* especially) in palaeoceanographic investigations, despite a small number of studies (Schiebel et al. 1997). *G. inflata* are usually inhabitants of so called transitional environments thus occur in low abundance in typical marine sediment. A transitional environment usually refers to an environment at or near a transition between land and the sea (lagoons, deltas, etc.). *G. inflata* as a dominant species which occurs mainly between

subtropical and polar water masses and prefers little seasonal temperature variation. It also has a relationship with salinity, density and stratification which was observed in mostly winter seasons (Hilbrecht, 1996).

Radiocarbon dating was performed on assemblages extracted from the same core. Because of low abundance of foraminifera large portions of sediment were consumed to extract them. This limited the radiocarbon sample density as remaining material was required for further analyses. The species of choice for dating was *G. inflata.* However it was not present in sufficient concentration in the entire core, therefore a mixed assemblage was used (Mpf - *G. bulloides*; *G. inflate*; *N. pachyderma*; *G. quinqueloba*) in the last two measurements. This approach allowed dating the entire core however the results were not fully conclusive. Dating indicates that the entire core consists of Holocene record. The sand on the surface of the core (0.1 mbsf) is 2960±35 years old and the entire sandy unit (0.55 mbsf) accumulated over 4560±30 years (0.12 m/kyr). The change of lithology is coupled with drastic changes in sedimentation rates. First 40 cm of sediment accumulated over a period of only 300 years (4850±55 years at 1.0 mbsf). The age of the deepest dated point (2.3 mbsf) was surprisingly 4700±60 years which suggests that certain species in the mixed assemblages used are biasing the dating results toward younger ages. This is most likely a result of different radiocarbon accumulation in each of these species arising from their different feeding strategies. However, high sedimentation rates in this part of the shelf are not uncommon. The dating of BGS borehole 71/9 just west of the Malin Shelf showed sedimentation rates of 0.75 m/ky in the first 6 meters (10 ky) followed by a staggering 3.5 m/ky in the next 30 m (Xavier Monteys, GSI, personal communication). It is therefore safe to assume that first 6 m of the seabed in the Malin Shelf are Holocene record, however further radiocarbon analyses should be conducted to verify this assumption.

2.3.2 Evidence of gas in the sediment

Pockmarks are considered surface expressions of seabed fluid expulsion. Although the exact formation mechanisms remain elusive, three types of formation fluids are thought to be responsible for formation of most pockmarks: groundwater springs, hydrocarbon gas and hydrothermal gas (Judd and Hovland, 2007). The Malin Deep remains separated from aquifer influence by the Malin Terrace bedrock with very low hydraulic conductivity (Dobson, 1992). Sampling locations and main structural features of this area are shown in Figure 36. There is also no evidence of groundwater discharge from historical and more recent oceanographic surveys (Gowen et al. 1998, Monteys et al. 2008a). Detection of past and periodic events however require seabed sampling as only changes in pore water chemistry can show evidence of freshwater influence.

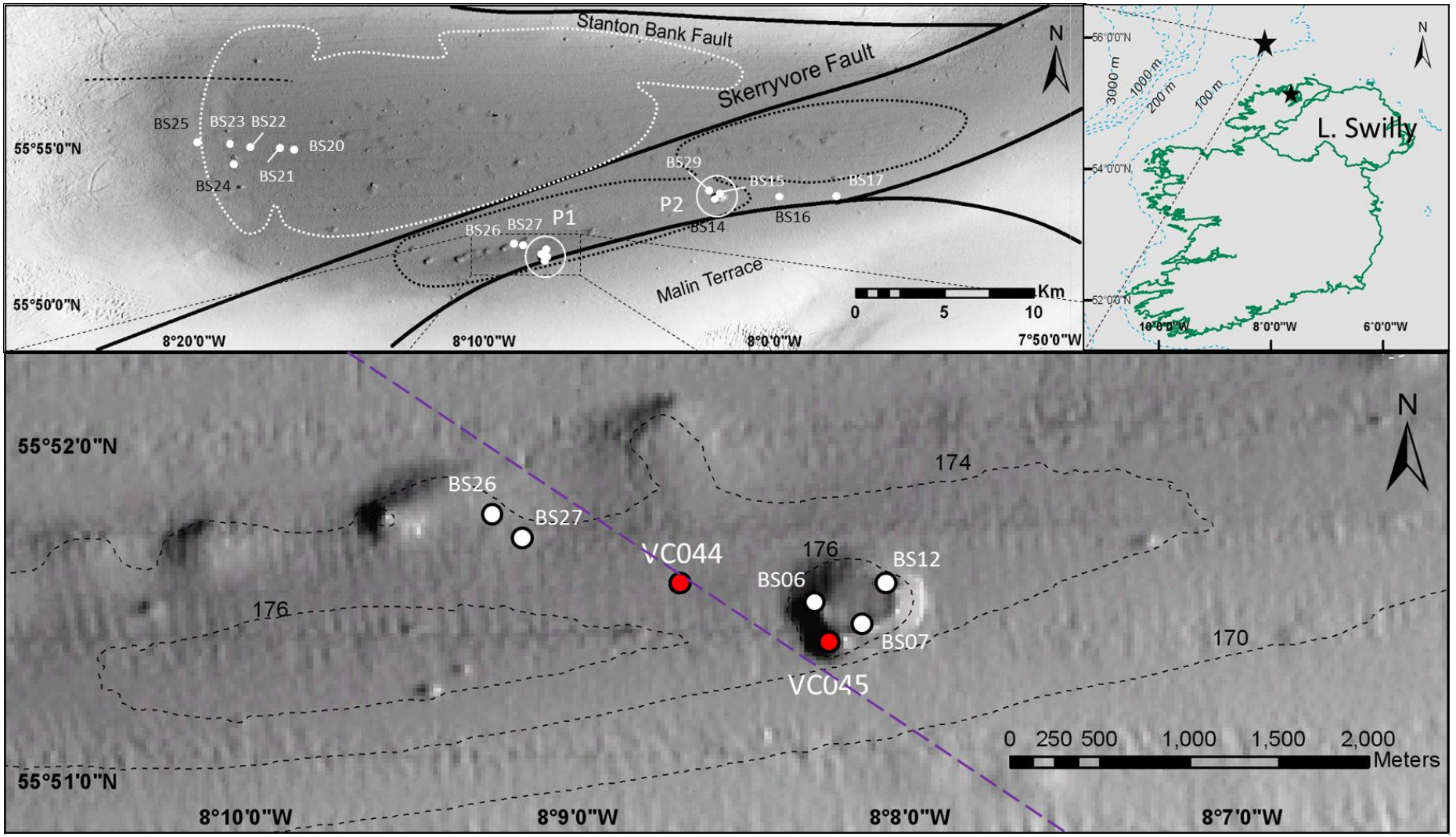

Figure 36. Multibeam shaded relief bathymetry with major structural features: Skerryvore Fault (SKF) and Stanton Bank Fault (SBF) and index map with site location (top panel). Despite the large scale linear pockmark clusters are clearly visible in the Malin Deep micro basin south of SKF, marked with a black dotted line. Several minor unit pockmarks are visible in the Malin Deep area marked with a dotted light grey line. Composite pockmarks are labelled P1 and P2. Detailed sampling site map (bottom panel) shows structural details of targeted composite pockmark, EM track line is shown as violet dashed line.

In the studied setting, chloride concentrations were typical for marine environments and have shown little variability down the cores (Figure 37). There we also no significant differences between pockmark core (VC_045) and reference core (collected outside of the pockmark, VC_044) with chloride concentrations being moderately positively correlated (R^2=0.46). However, hydro-acoustic surveys have revealed the presence of shallow gas throughout the entire Malin Deep area (Garcia et al. 2007).

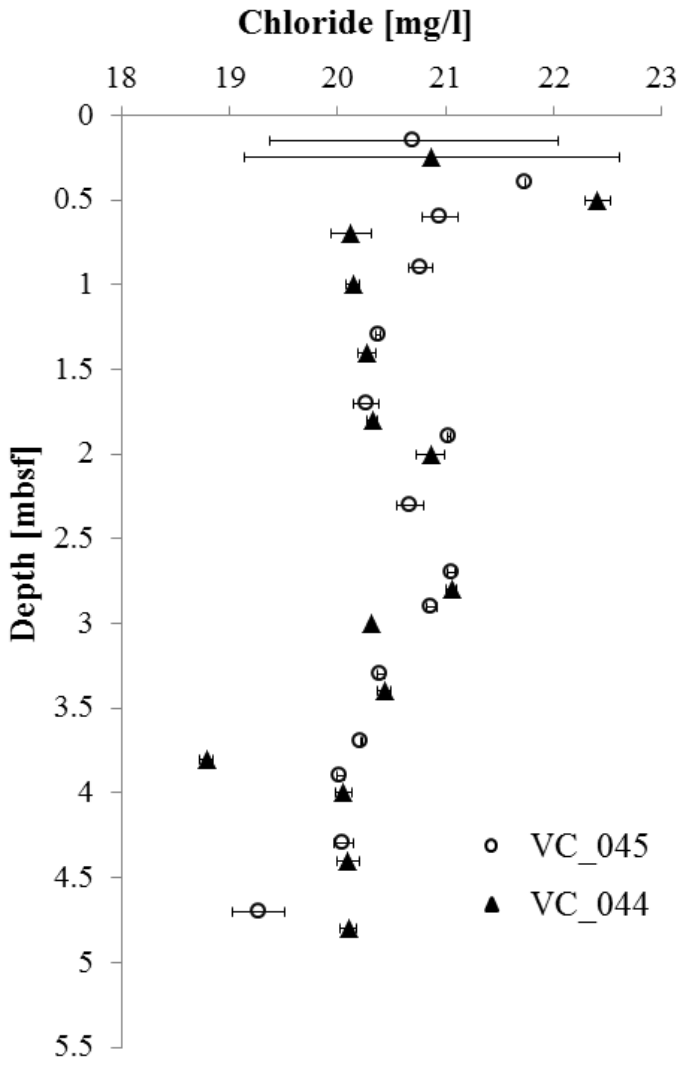

Figure 37. Chloride concentration profile versus depth in the pockmark and reference cores.

Most of the features in the Malin Deep area are sub circular unit pockmarks scattered across the 23000 km^2 of seabed. However in the micro basin on the southern boundary of the Malin Deep (Figure 36) there are several composite features created by repeating venting events. This might indicate that fluids underneath these features reach the seabed water interface more frequently than in other places. Sub-bottom profiler data clearly illustrate a visible gas pocket underneath one of the composite pockmark (P1) (Figure 38). There is no shallow gas accumulation underneath the other composite pockmark (P2) indicating a deeper source.

However gas enhanced reflectors and sediment disturbance were visible (data not shown), therefore P1 was selected as a primary coring target.

Multiple gas enhanced reflectors (ER) are observed above the gas pocket just above the gas front characterized by visible acoustic turbidity (AT) and acoustic blanking (AB) below caused by a decrease in the backscatter of the acoustic signal. These signals mark the impermeable boundary of this shallow gas accumulation. Just above the gas front more discreet ERs are visible, parallel to the strata, possibly indicating gradual upward migration of gas and accumulation in more gas permeable, coarser sediment layers such as sand lenses or gravel patches. Similar signals are present west of the pockmark where particle size and logging data from vibracore 044 confirmed the presence of sandy layers that coincide with the observed lateral ER (Figure 38). Interestingly during the on-deck sample processing vigorous degassing was observed at the reference site but regrettably volatiles sampling was not possible during the cruise. Since initial pockmark formation through a virgin seabed is believed to have a violent, blow-out like characteristic subsequent fluid migration is likely to utilize already established pathways including temporary reservoirs (Judd and Hovland, 2007). However more recent studies (e.g. Hovland et al. 2010) suggest that gentle venting events might occur periodically outside of the main pockmark feature until the reservoir is over pressured enough to force its way through the original seal. Directly underneath the pockmark (P) is featureless, mixed sediment is visible, possibly a remnant of pockmark formation, contrary to clear lamination that is visible in sediments in the vicinity of this feature. Moreover numerous occurrences of vertical acoustic blanking (AB) are present in the surrounding sediments. The exact meaning of vertical AB is still poorly understood and widely debated. These signals are likely to be indicative of active fluid migration or fluid related sediment structure alteration, particularly with other evidence of fluid in the subsurface. However acoustic signal effects such as signal starvation or amplitude blanking cannot be ruled out (Judd and Hovland, 2007). Interestingly though, these signals are clearly more abundant above and in the vicinity of igneous intrusions (Dy) which are commonly associated with fluid migration pathways (Khilyuk et al., 2000). Based on the marine electromagnetic data, there is also a strong correlation between shallow gas, pockmark features and low electrical conductivities (Figure 38). The area of lowered conductivity matches the extent of the gas pocket recorded in the sub bottom profiles and is likely to be the dominant factor responsible for the conductivity minimum in this area indicating migration of gas to the upper 6 m of the seabed from the underlying gas reservoir. We observe an increase in the electrical conductivity on the edges of the unit pockmarks (S1 and S2) and a drop below regional levels within the pockmark as well as an anomalous increase (A) west of the pockmark. Similar signals (conductivity lows and spikes) were observed in other gas bearing sediments in the Malin Deep area. The presence of gas and changes in sediment porosity and/or sediment facies is expected to modify the conductivity of the seafloor.

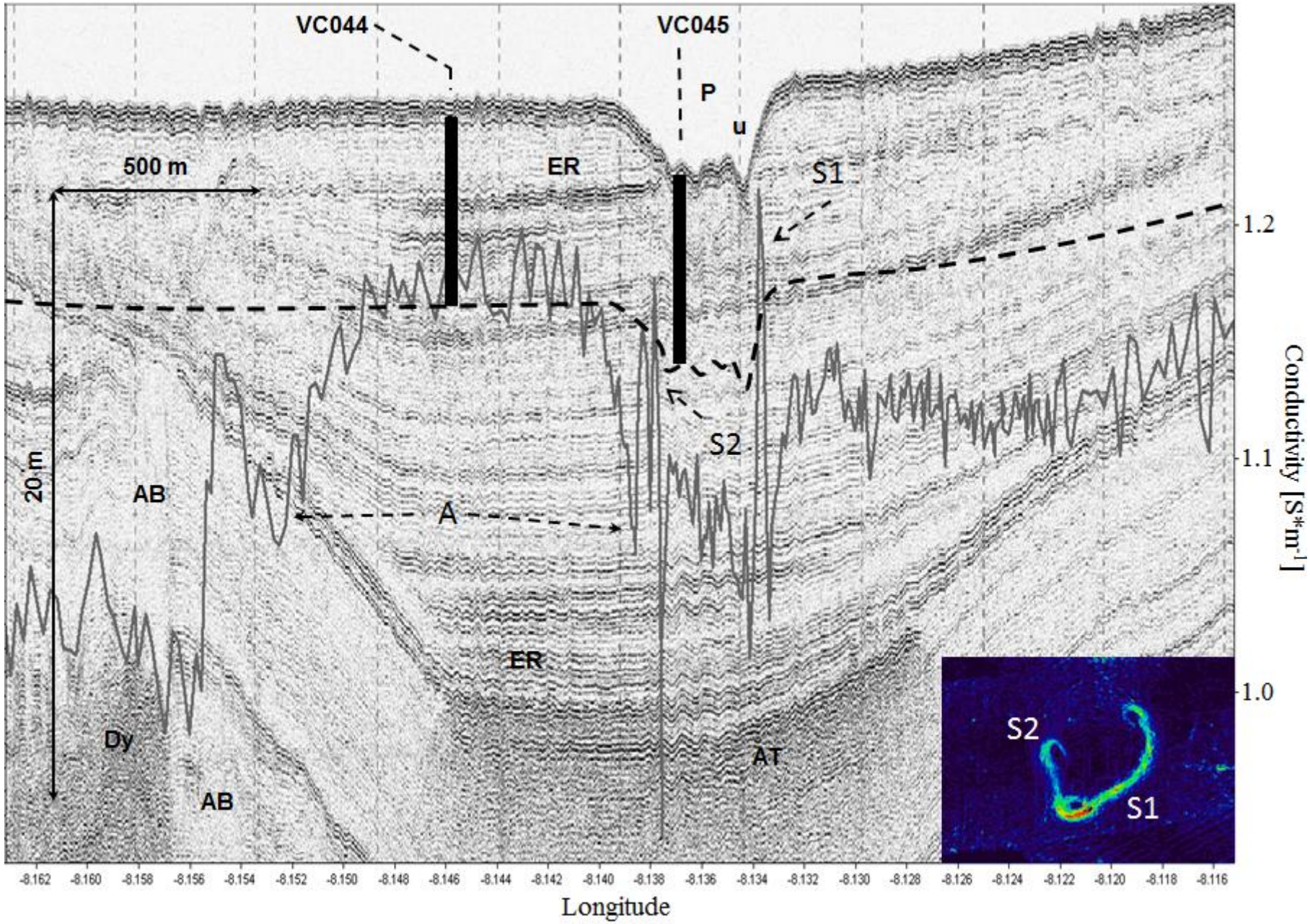
VC044
VC045
P
u
500 m
ER
S1
S2
20 m
AB
A
ER
Dy
AB
AT
1.2
1.1
1.0
Conductivity [S*m-1]
-8.162 -8.160 -8.158 -8.156 -8.154 -8.152 -8.150 -8.148 -8.146 -8.144 -8.142 -8.140 -8.138 -8.136 -8.134 -8.132 -8.130 -8.128 -8.126 -8.124 -8.122 -8.120 -8.118 -8.116
Longitude

Figure 38. Sub-bottom 3.5 kHz profile (pinger) of the composite pockmark (P) in the Malin Deep micro-basin with one of the pockmark units (u) visible. The pockmark is 750 m wide (measured from opposing ends) with three sub-circular units approximately 50 m wide and 8.5 m deep. Overlayed grey line showing conductivity measurements derived from towed EM system. High conductivity values are present in both sides of the pockmark (S1 and S2) and are associated with disturbed sediment on the edges of the unit pockmarks, which exhibits higher porosities due to fluid displacement and increased slope (bottom right insert). The largest conductivity anomaly (A) correlates accurately with the extent of the strong reflector in the sub bottom record associated to gas facies and cannot be explained by changes in sediment structure. Gas enhanced reflectors (ER), acoustic turbidity (AT) and numerous vertical acoustic blanking (AB) signals particularly in the vicinity of igneous body (Dy) are clearly visible. Vertical bold lines depict approximated locations of two 6 m long vibracores collected at the site, length of the lines is to scale. Parallel dashed black line depicts the extent of the seabed that is imaged with the TEM.

Gas within the sediment framework will act as an electrical insulator, potentially decreasing conductivity by several orders of magnitude. However, the degree to which the bulk conductivity will be modified by the gas phase depends on several parameters including the gas concentration and how it is distributed between grains (Evans, 2007). As suggested by Judd and Hovland, 2007 and Cathles et al. 2010 upward gas migration can cause pore fluid displacement and local over-saturation zones and even fluidization of the seabed surface during the initial pockmark formation. The presence of such pore fluid rich areas would certainly result in an increased conductivity signature (such as signatures S1 and S2). Although fluid migration pathways are not clearly defined in the shallow seismic record the lateral, parallel to the strata, gas related signatures indicate that fluid displacement might contribute to the increased conductivities observed at the edges of the pockmark. Evidence of increased methane flux derived from sulphate profiles supports this explanation (see par. 2.3.4). Lower conductivity within the pockmark could be caused by the presence of free gas or by changes in the physical properties of the sediment arising from sediment structure collapse due to escaping gas. This in turn could have caused a redistribution of sediments, resulting in a more heterogeneous physical environment. Carbonate cementation and pore water freshening can also cause a decrease in conductivity. Nevertheless there is no evidence for obvious methane derived authigenic carbonate (MDAC) in the sub bottom profiles (see Figure 38), video lines and core and grab samples. Moreover the geographical location and hydrogeological setting of the Malin Shelf makes pore water freshening an unlikely scenario. However changes in the sediment structure cannot explain the anomalous conductivity increase (A) recorded west of the pockmark feature. The shallow magmatic body occurring around this area at the depth of 18 mbsf (Figure 38) is also too deep to have any effect on the conductivity recorded for the first 6 m of the seafloor. Anomalous conductivity increases were recorded however by the last EM receiver (see

Methods). This anomaly coincides with lateral ER observed in sub bottom profile which suggests a genuine relationship between conductivity and the presence of gas.

Interestingly, Atekwana et al. 2004 and Allen et al. 2007 reported that higher bulk conductivities in sediments are associated with microbial activity stimulated by the presence of petroleum hydrocarbons. They found a higher percentage of hydrocarbon degrading microbial populations in sediment characterized by increased bulk conductivity and showed that the higher conductivity may result from increased fluid conductivity related to microbial degradation. Furthermore Abdel Aal et al. 2010a demonstrated in a controlled environment that exo-polymeric substances produced by micro colonies and adhering to grains increase the conductivity of the system. Abdel Aal et al. 2010b also show that live microbial biomass increased the conductivity of the system while the presence of dead cells resulted with considerably smaller responses. Since migration of light hydrocarbon gas is observed in the Malin Shelf sediments it is therefore possible that changes in microbial population and their activities contribute to higher conductivity signals such as the discrete conductivity spike (A). This observation is supported by the abundant peptidoglycan signatures in NMR data.

2.3.3 Origin of the shallow gas

The origin of shallow gas remains unclear although deep structural features of this setting suggest a deep source. The pockmark spatial distribution is axially correlated with primary (Skerryvore Fault and Stanton Bank Fault) and secondary faults and folds. Fluid accumulation facies are present at the base of the post glacial, fine-grained Jura formation with evidence of possible lateral migration toward the centre of the basin. Sub bottom data suggests that Tertiary igneous intrusions indeed act as natural obstacles for stratified diffusive fluid migration and might contribute to numerous gas accumulations by channelling and focusing fluid into shallow pockets (Monteys et al. 2008b). The Malin Deep is a setting with thick fine-grained (mean: 30 μm, n=50) sediment cover and quite high sedimentation rates ranging from 30 cm/ky to over 130 cm/ky in the last 5 ky (based on planktonic foraminifera radiocarbon analysis).With sufficient flux of organic carbon to the seabed these sedimentological conditions would have favoured shallow anoxia and intensive microbial methanogenesis (Stein, 1990). However the organic carbon content of the surface sediments do not exceed 0.5% (mean 0.35%, n=9) and with only a fraction of that reaching the methanic zone it appears that without a deep, organic rich carbon source rock microbial methanogenesis is likely to be a contributor rather than the dominant source of the Malin Deep gas.

2.3.4 Pockmark activity

Intensive video surveying was carried out to assess the activity and surface topography of the studied pockmark. We did not record any hard ground outcrops (MDACs), bacterial mats, increased macro-fauna accumulation or obvious seepage in any of the video lines despite several crossings of all of the pockmark sub-units. The pockmark's seabed topography did not differ from that of the surrounding seabed. Video data clearly suggest that this pockmark remains dormant and fluid activity is confined to the sub-surface sediments as visualized by the sub-bottom data (see 2.3.2 and Figure 38). Interestingly, pore water sulphate profiles from both cores show a slight concave up curvature (Figure 39).

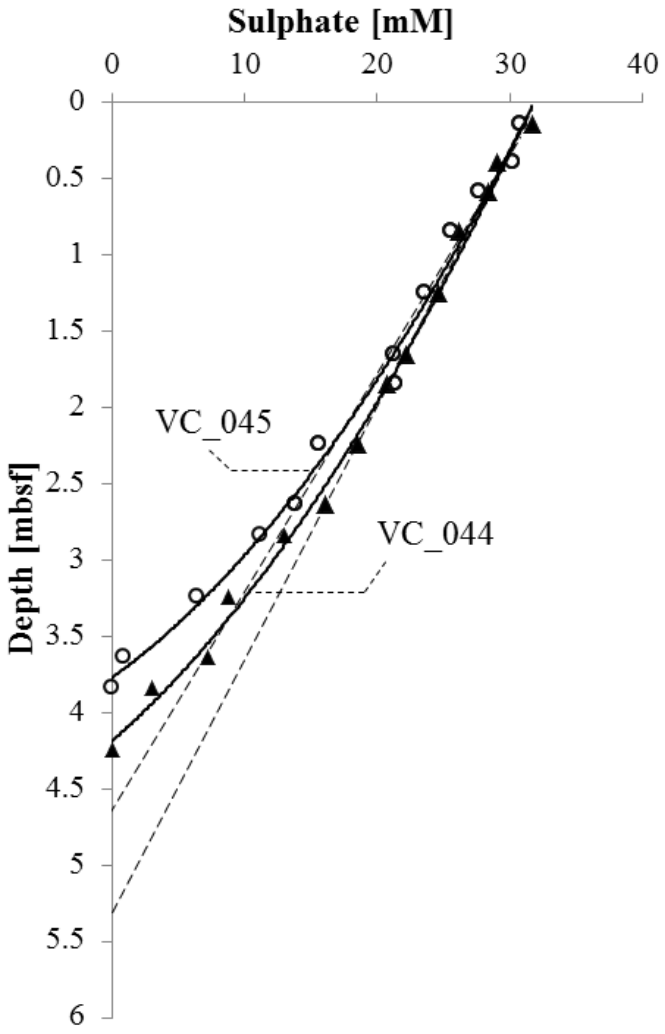

Figure 39. Sulphate concentration versus depth for inside (VC045) and outside (VC044) pockmark cores. Black curves are second order polynomial fit showing non-linear concentration change with depth indicating flux variation.

Both profiles show a clear linear gradient to around 2.7 mbsf with the pockmark core showing a slightly higher rate of sulphate consumption than in the reference core (6.6 mmol/m^3m and 6.0

mmol/m^3m, respectively). From around 3.2 mbsf new shallower gradient was observed in both cores indicating more rapid sulphate removal than expected in a stead state scenario. Similarly, the pockmark core gradient is higher than the one in the reference core (12.0 mmol/m^3m and 9.4 mmol/m^3m, respectively). According to Niewohner et al., 1998 and Borowski et al. 1996 rapid change in depositional conditions and/or upward methane flux, control the shape of the sulphate profiles in settings with a high methane flux derived from intensive methanogenesis as well as deeper sources. In a steady state situation sulphate profiles are straightened out by intensive anaerobic oxidation of methane (AOM) fuelled by methane migrating towards the surface. Although oxidation of organic carbon also plays a role in sulphate reduction the rate of these processes favour more rapid AOM which effectively controls the sulphate profile shape. High sulphate reduction rates and availability of readily degradable organic matter are crucial in low methane flux scenarios as shown by Ferdelman et al. 1999. Hensen, 2003 demonstrated that recent changes in methane flux will affect the sulphate profile curve. In the case of decreased flux a concave down profile is expected, with consumption of sulphate by degradation of organic matter being the controlling process. Increased flux will cause a concave up sulphate profile as was the case with both cores studied here. Kink type profiles can over time be transformed into concave up profiles. The kink profile origin is uncertain and it is possible that they can form in more than one scenario. Zabel and Schulz, 2001 postulated sedimentary slide, Fossing et al. 2000 suggested a non-local transport mechanism such as irrigation of bubble ebullition and Schulz et al. 1994 proposed sulphide re-oxidation via Fe-hydroxides. Hensen et al. 2003 argues that they are short-lived phenomenon and represent a transient state that is smoothed out after the event took place by the dominant controlling processes. In the context of the studied pockmark, Malin Deep changes in sulphate profiles might indicate that methane from the shallow reservoir (Figure 38) was migrating upwards and influencing microbial processes in the first few meters of the seafloor and the sulphate-methane transition zone (SMTZ also termed sulphate depletion zone) in particular. Additionally, the flux intensity varies between the collected cores directly over the shallow gas reservoir (VC_045) and the reference core (VC_044). Both profiles show evidence of an increased upward methane flux but in the reference core the flux is 25% lower (3.2 mmol CH_4 m^{-1} yr^{-1}) than directly above the reservoir (4.3 mmol CH_4 m^{-1} yr^{-1}) and results in a deeper SMTZ (4.2 mbsf and 3.8 mbsf respectively). Sulphate flux was calculated assuming steady-state conditions and according to Fick's first law of diffusion (Equation 21) and corrected for sediment tortuosity (Equation 22) as suggested by Schulz and Zabel, 2006 and assuming stoichiometric balance between downward sulphate flux and upward methane flux $J_{sw,SO_4^{2-}} = J_{sw,CH_4}$ (Borowski et al. 1996). D_{sw} is the sulphate diffusion coefficient in sea-water at 5 ^oC (5.72 x 10-10 m^2 s^{-1}, Boudreau, 1997), D_{sd} is diffusion coefficient in sediment, θ^2 is tortuosity derived from electrical conductivity (Boudreau, 1997; θ^2 is 2.19 and 2.05 for the VC_044 and VC_045 respectively), Φ is sediment porosity (mean

derived from gamma ray attenuation measurements from top of both cores to SDZ; Φ is 0.55 and 0.59 for the VC_044 and VC_045 respectively).

$$J_{sw,SO_4^{2-}} = -\Phi D_{sd} \frac{\partial C}{\partial x} \quad (21)$$

$$D_{sd} = \frac{D_{sw}}{\theta^2} \quad (22)$$

Although there are no columnar disturbances in the sparker data the single beam data (SBES) supports the upward fluid migration scenario. As shown on Figure 38 apart from ER and AB observed in sparker data, additional vertical and lateral signal amplitude changes are observed. These signals are present in the exacts locations of gas related signals in the sparker data, however due to the lower energy of SBES resulting in faster signal starvation they are not as uniform as in the sparker record. Shallow ERs were picked up by the instrument for instance while the deep ones of similar intensity (when compared in sparker data) were not recorded. It is unlikely that these signals are related to sediment lithology as they discontinuous and chaotic in orientation. Frequencies used in SBES allow recording gas bubbles of different sizes that are invisible to the sparker due to their different resonance frequency (see Chapter 1). Single beam data shows clear migration pathways, both vertical and lateral, extending over the entire width of the gas pocket. The strongest signals are visible underneath the pockmark however two other migration fronts can be seen underneath the reference site and above the eastern section of the gas pocket.

Geophysical data and pore water sulphate profiles suggest that gas is migrating towards the surface in multiple locations but never reaches the seabed water column interface. Several video tows did not detect active venting. There is no evidence of gas plumes in the MBES and SBES record. However, ERs and sediment disturbances observed just above the seal suggest that gas is locally released from the shallow gas pocket and migrates upwards. The migrating gas front penetrates strata of different permeability and is frequently laterally distributed in more porous lithologies. This lateral migration possibly acts as a safety valve, distributing pressurized fluids over a larger surface and preventing further upward channelling through the sediment.

2.3.5 Composite pockmark (P1) formation conceptual model

The composite pockmark P1 located in the southern part of the Malin Deep consists of three sub circular units. It is one the largest pockmarks in the Malin Shelf with a maximum width of 750 m, and individual unit width ranging from 80 to 100 m. In the deepest part (u1) it has a depth of 8 m (Figure 40). The surrounding seabed consists of fine sandy mud and is relatively flat with no other distinct morphological features.

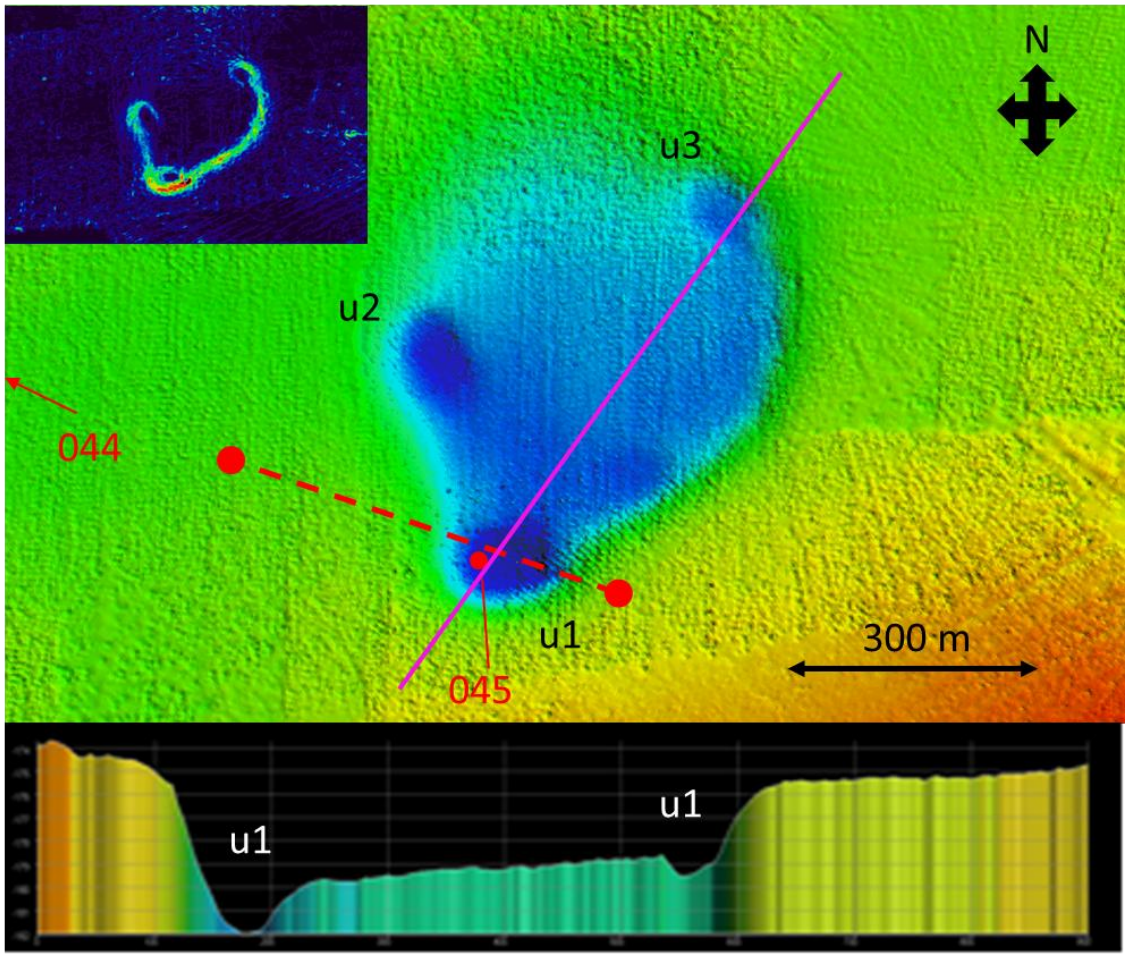

Figure 40. Multi beam shaded relief bathymetric profile of composite pockmark P1 with three sub units visible (u). The extent of shallow pocket gas, defined as the extent of AT at the gas seal interface, derived from sparker data is depicted by red dashed line. Numbers denote vibracore locations. Top insert shows pockmark edge slope changes. Bottom panel shows depth profile of the entire pockmark (pink solid track line).

Water depth in this location varies from 175 m outside and 185 m inside unit 1 of the pockmark. The pockmark edge slopes vary between 1-3^{o} however locally reach up to 10^{o} (Monteys et al. 2009). It is the only documented pockmark in the Malin Shelf with relatively shallow gas accumulation in the sub bottom record and evidence of upward gas migration. Sub surface data (shallow seismic and SBES, see Figures 38&41) clearly indicate active fluid migration. The acoustic data as well as pore water sulphate profiles suggest the fluid to be gas, possibly methane.

To date few researchers considered pockmark formation mechanisms and this process still remains not fully understood. This is mainly because the variability of physical seabed conditions make it troublesome to develop single unifying model. The first conceptual model was that of Hovland and Judd, 1988 derived from the hypothesis of King and MacLean, 1970 of fluid migration as a force responsible for pockmark formation.

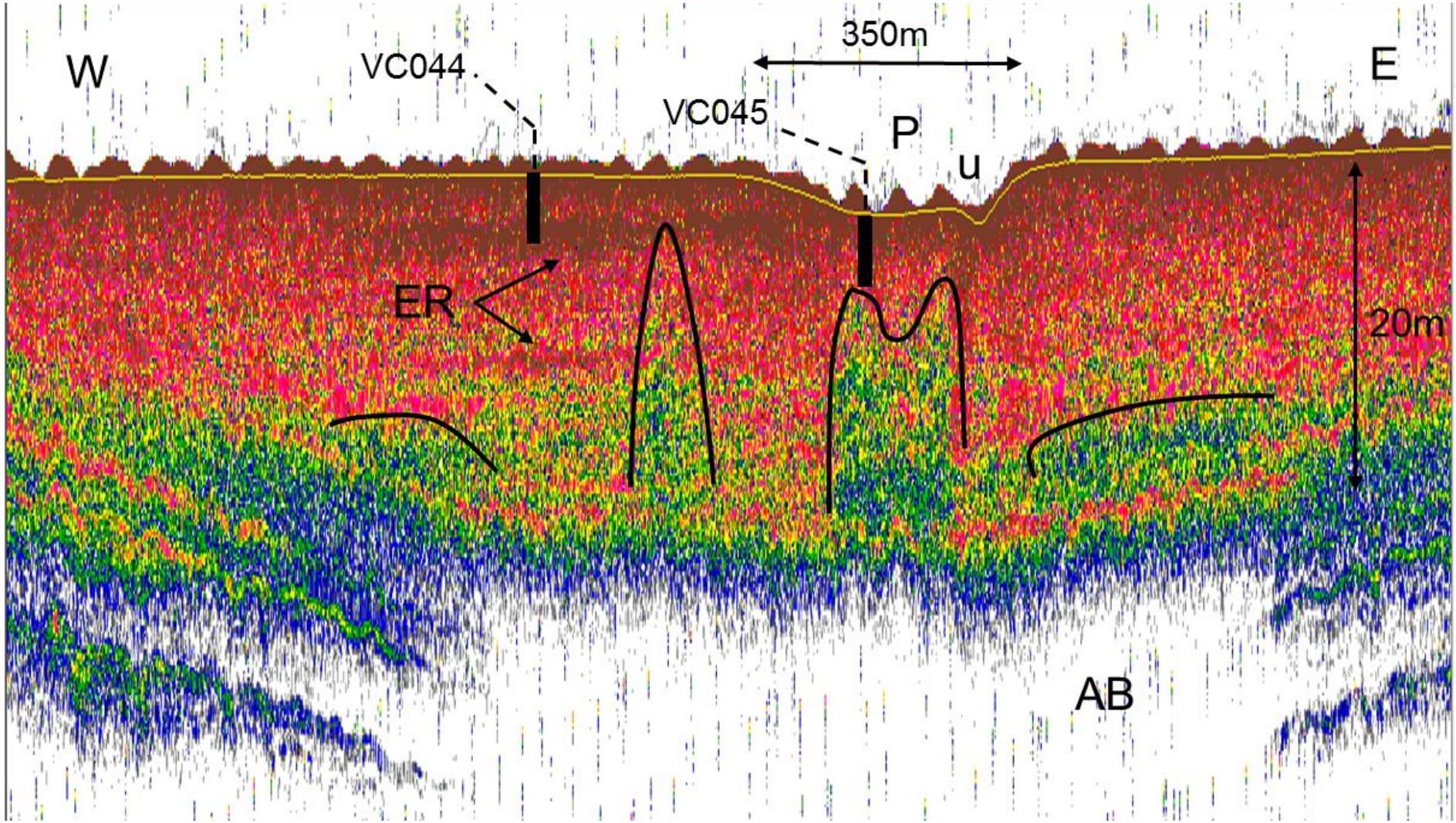

Figure 41. Single beam echo sounder profile of the composite pockmark (P) in the Malin Deep micro-basin. Several gas fronts marked with black lines are visible as well as enhanced reflectors (ER) and acoustic blanking caused by gas accumulation (AB).

This model assumes upward migration of gas through minor reservoirs to a point of accumulation in the shallow sediments to the point of over-pressure of the accumulated gas. The venting event is preceded by establishing of hydraulic connection with the water column. This model is discussed in more detail in Chapter 1. Sub sequent venting events may occur periodically utilizing the same escape pathway once the reservoir is recharged. Alternatively formation of new units can occur in case of original migration channels being shut down by seabed collapse. Judd and Hovland, 2007 suggest however that this process in uncommon and the original migration pathways are major sources of subsequent venting events. Cathles et al. 2010 related to this model and expanded it by considering the physics of a '*gas piston*' model that addresses capillary processes taking place when a gaseous body travels through water saturated sediment. They note that gas migration is impeded by the presence of pore fluids and provided it is sufficiently pressurized gas displaces pore fluids above the gas front (or gas piston) resulting in changes in fluid saturation and sediment strength. They also conclude that the diameter of the gas piston determines the diameter of the formed unit pockmark. Bui et al. 2007 applied the distinct element method (DEM) to simulate interactions between migrating fluids and solid particles of the sediment framework and showed that this model is applicable to explain the formation of pockmarks and mud volcanos alike. Both of these models however focus on vertical migration mechanisms and neglect lateral migration through more permeable bodies. Hovland, et al. 2010 points out that: "*(..) if there are general dips, domes, or other lateral inhomogenities in permeability distribution below the pockmark, the fluid pathways will be modified accordingly. It will always be the path of lowest resistance that is used by migrating pore-waters and gas".* Such lateral permeable bodies are present in the subsurface underneath the P1 pockmark and there is evidence that gas accumulates in these facies. The migration of fluid through a porous medium is described by Darcy's law (Equation 23).

$$Q = \frac{\kappa A}{\mu x}\left(\frac{\partial P}{\partial x}\right)$$

Equation 23. Darcy's law describing fluid flow rate through homogenous rock formation.

This law states that fluid flow rate (Q) depends on permeability of the solid phase (κ), dimensions of the formation the fluid is traveling through (surface area of cross section – A; and the length of the pathway – L), viscosity of the fluid (μ) and the pressure gradient ($\partial P/\partial x$). Formation permeability is the key parameter that is directly linked to porosity of the sediment and grain size distribution as expressed in Kozeny-Carman's equation (Carman, 1956; Schulz and Zabel, 2005). The Kozeny-Carman's equation (Equation 24) does not include information on proportions of grain size fractions which govern the size of pores and offers only approximated permeability values.

$$\kappa = \frac{d_m^2}{72k}\frac{\Phi^3}{(1-\Phi)^2}$$

Equation 24. Permeability as a function of mean grain size (d_m) and porosity (Φ).

Closer estimation of permeability requires either direct measurements or an empirical approach (Lovell, 1985; Fisher et al. 1994). Permeability of different sediment size fractions can vary by orders of magnitude depending on concentrations of fine grained components (Table 14).

Table 14. Typical physical properties of grain size fractions. Schulz and Zabel, 2005 and references within.

Property	Sand	Silt	Clay
Porosity (Φ) [%]	50	60	80
Mean grain size (d_m) [10^{-6} m]	70	30	2
Permeability (κ) [m^2]	$5.4x10^{11}$	$2.3x10^{-12}$	$7.1x10^{-15}$

It is clear from the above that grain size distribution, porosity and permeability are closely related and changes in these properties might affect fluid migration pathways.

The evidence for fluid flow discussed in the previous paragraphs is complemented by evidence from physical properties of the sediment. The sub bottom data shows that core VC_044 collected west of the P1 feature penetrated area of gas enhanced reflectors (Figure 38) between 2 and 4 mbsf. During cutting of the core in sections vigorous degassing was observed joined with sulphide odour. Regrettably it was not possible to analyse the volatiles during the cruise. Particle size data from this core shows that sections in question contain two sandy layers. The average sand content in this core oscillates around 8-10% and increases to nearly 30% in the first unit and to 26% in the second unit (Figure 42). This change in coarse grain content is reflected in mean grain size increase (to 54 μm, with an average of 28 μm excluding sandy layers) and decrease in silt and clay (70 and 1.7 % respectively). This layer is also visible on the high resolution images due to characteristic void like marks on the sediment that are created during core splitting with a cheese wire. These changes in lithology are also reflected in density/porosity logs. Gamma density (wet bulk density) shows an increase in the area of the sandy layer from 1.81 to a peak of 1.98 g/cm^3. Porosity decreases from 62% to a minimum of 45%, these values are in agreement with typical porosities reported by Schulz and Zabel, 2005 (Table 14). Similarly P-wave velocity increases in the sand rich region from 1475 to 1550 m/s as the acoustic wave propagation through sandy bodies is faster than through fine grained sediments. Finally resistivity shows an increase in the discussed layer from 0.5 to 0.7 Ωm. This is also expected as in marine sediments electric current is conducted only through pore fluids while solid sediment frameworks acts as insulators.

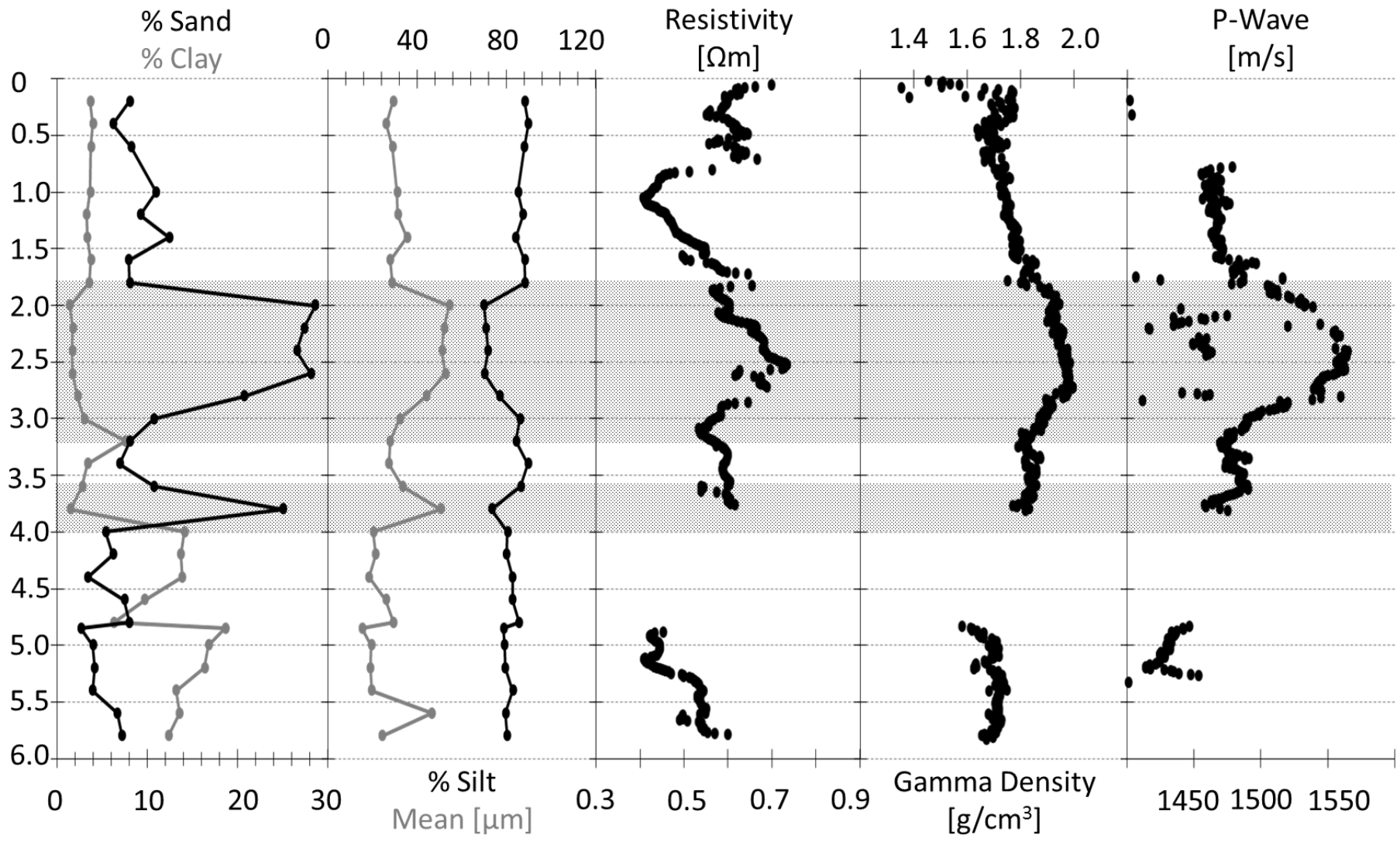

Figure 42. Physical properties of the VC044 core. Shaded are shows the sand rich layers observed on the sparker data.

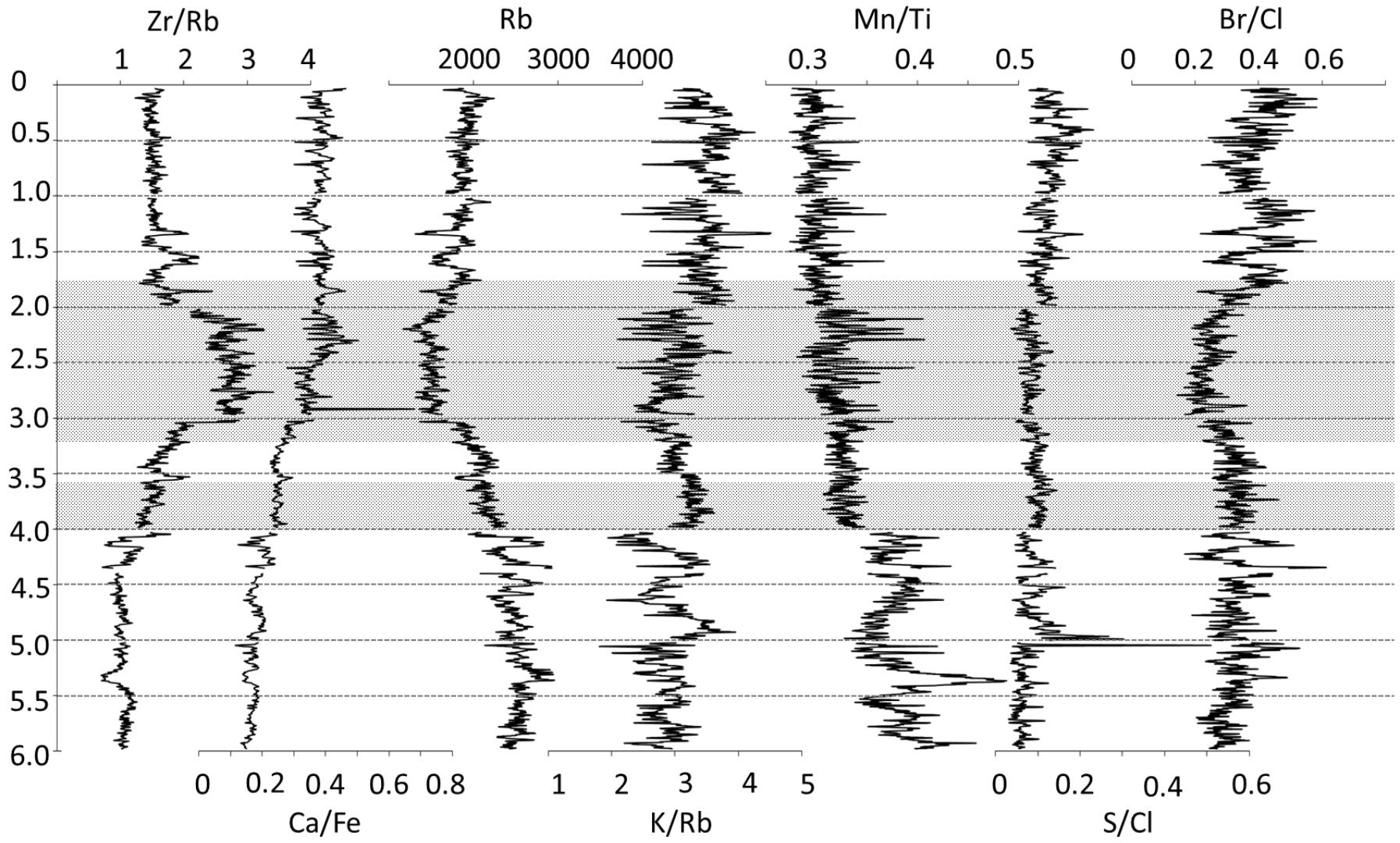

Figure 43. XRF profiles of selected elements and element ratios in the VC044 core.

Lower porosity in this layer leaves less void space for pore fluids than in the fine grained sections with higher porosity. There is also a possibility that residual gas bubbles trapped in the sediment contributed to the increase in resistivity as free gas is a very strong insulator. However the majority if not all of the gas escaped during core retrieval due to pressure change. Free gas in sediments expands rapidly in atmospheric pressure conditions and can be only preserved with use of specialized coring equipment that maintains hydrostatic stress on the sediment core such as HYACINTH coring system (Schultheiss et al. 2006). In situ the resistivity in this area in fact decreases as discussed above. This is contrary to what would be expected in gas charged sediment. The EM derived conductivity profiles show broad increases correlated with the lateral gas ER. This somehow confusing finding must be discussed in the context of operational limitation of the remote EM system. The reported conductivity is an average over 6 m of seabed and does not target a specific layer. Moreover migrating gas will displace conductive pore fluids as reported by Cathles et al. 2010 which will contribute to the signal increase. Finally there is evidence from NMR experiments that conductivity increase might be related to microbial activity. Lithology change is also clearly observed in the XRF element profiles (Figure 43). Zr is a conservative element (similarly to Ti and Al which are resistant to chemical and physical erosion) often showing enrichment in turbidite deposits (Croudace et al. 2006). Rb on the other hand is associated with detrital clays (Rothwell et al. 2006). The Zr/Rb ratio is a good sediment provenance indicator as it is sensitive to both grain size changes and origin of the clays (Chen et al. 2006). This profile is mirrored by the Ca/Fe profile. This ratio can be used to detect carbonate rich layers, however its strong correlation to sediment texture makes very useful for identification of individual lithological units (Rothwell et al. 2006). Both profiles match ideally with the grain size parameters showing increase in the ratios in the sand rich layers unit. Moreover slightly different Zr/Rb ratios atop and below the sand might indicate a change in depositional regime between these two muds. The K/Rb profile is also indicative of detrital clay mineral however due to Cl absorption of potassium X-rays it often reflects changes in the porosity (Rothwell et al. 2006). This appears to be true in this case as porosity decreases steadily to about 3 m after which an inverted trend is observed (porosity profile is derived from gamma ray density measurement and is a mirror reflection of the density profile shown). The gradual increase in clay content is also recorded in the Rb profile. Interestingly the second sand layer appears to have less coarse material than suggested by grain size distribution. The Zr/Rb and Rb profiles show less obvious drops in signal intensity compared to the major sand layer. The Mn/Ti ratio is a good indicator of redox diagenesis (Croudace et al. 2006). Mn oxides are naturally used up by bacteria in succession to oxygen/nitrate and mobilized from the solid phase. In shelf environments however the oxidation cascade progresses rapidly due to availability of electron acceptors (organic matter). The depletion of oxygen and nitrate is

complete in first few centimetres of sediment. Moreover 4 m marks the depletion of sulphate and all Mn oxidation front signals would be expected above that depth as sulphate reduction offers less energy for the microorganisms than reduction of Mn oxides. Therefore observed increase in the Mn/Ti ratio with some interesting secondary trends might be related to past oxidation fronts but more likely is a grain size effect as it is correlated with physical properties. Changes in the S/Cl ratio might indicate organic matter rich layers but is also indicative of pyrite formation. In the last meter of the VC044 core magnetic susceptibility increases (profile not shown), which might indicate formation of ferromagnetic transitional minerals such as pyrrhotite or greigite (Furukawa and Barnes, 1995). Also the Br/Cl ratio is can show organic matter due to higher organic bound Br content. However because both elements naturally occur in the pore fluids porosity effects can be dominant. Decreases in this ratio are correlated with porosity changes in the core visible in the sand rich layer.

Overall there is excellent agreement between element profiles and physical properties showing strong evidence of permeable layers in the VC044 core. We conclude therefore that these sandy layers quite possibly have the potential to act as temporary reservoirs for migrating gas as assumed in the model proposed by Hovland and Judd, 1988. Such a scenario is not considered in the models proposed by Cathles et al. 2010 and Bui et al. 2007. Considering that, according to Cathles et al. 2010 the gas piston must reach height equal to half of its base for the sediment quickening to take place, the gas chimney below pockmark P1 must be lower, as there is no evidence of erosion or sediment disturbance that would suggest otherwise. The presence of many permeable layers can possibly cause significant pressure drop on the front of the gas chimney as the gas can be distributed across a significantly higher surface area. The time of gas residence in these reservoirs and its availability to migrate further is an important factor to consider since it controls the effective pressure drop of the main gas column. In the most extreme scenario such lateral reservoirs might even shut down upward migration as the hydrostatic and lithostatic pressure will be higher than that of over pressured gas. This might further result in regeneration of the capillary seal and cutting of the supply of gas to the gas chimney which will stop formation of new pockmark features. In cases where a lateral reservoir holds the newly accumulated gas and its further migration is negligible, and assuming that initial pressure drop was not high enough to restore the capillary seal, the gas front is likely to migrate further up after gas pressure builds up again and the reservoir will only delay this process but not stop it completely.

The presence of pockmarks with multiple units is the ultimate evidence that the gas found its way to reach the surface and erode the seabed. The sparker data shows discontinuities in the sediment strata underneath the pockmark which can be indicative of highly disturbed sediment. This disturbance could be caused by violently escaping gas (Figure 44). Physical properties of the core collected from inside (VC_045) the pockmark seems to show evidence of

this process (Figure 45). The upper 3.7 m of the core shows no major lithology changes reflected in grain size distribution (unit 1). Around 0.8 m there is a single thin coarse layer (38% sand). The mean grain size varies significantly for the first 2.5 m with two distinct maxima at 0.8 m and 2.3 m (88 μm and 69 μm respectively). Silt and clay content oscillates around 83% and 10% respectively. Contrary to undisturbed seabed, stratification in this core was not preserved despite the evidence of distinct layering in the surrounding seabed from the sub bottom data and properties of the reference core (VC_044, Figure 38 and 42).This is clearly shown by changes in sediment sorting. Average sorting for the reference site was 1.79 while in the pockmark core it was considerably higher and reached average of 2.17.

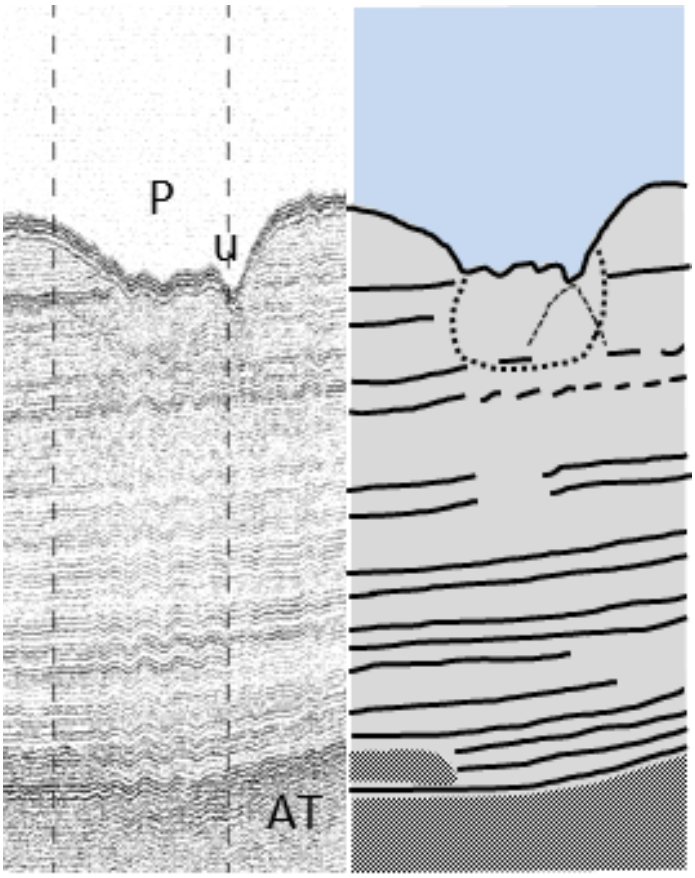

Figure 44. Magnification of sub bottom profile (sparker) of the pockmark P1. Interpretation of the data is shown on the right panel. Solid lines depict individual strata, weak hyperbolic signal underneath the pockmark unit (u) is an acoustic artefact possibly caused by pockmark walls (Judd and Hovland, 2007). The approximated area of disturbed sediment is marked with dotted line.

Sorting describes variance in the grain size distribution and higher sorting means that sediment sizes are mixed together and do not form distinct layers composed of similar grain sizes as expected during changes in sedimentation. Also remaining parameters show that sediment inside the pockmark is homogeneous and well mixed. Resistivity shows no primary trends and has an average value of 0.57 Ωm and variance of ca. 5%. Similarly average density is 1.73 g/cm^3 with a variance of only 1%. P-wave velocity also shows no change in the entire unit

(average 1480 m/s, variance 0.6%). There is a slight decrease in the density value around 3.3 m matched with change in P-wave velocity however these signals do not seem to be related to any change in the lithology. It appears that in the first unit grain size changes randomly and is not matched by changes in other parameters, indicating greater sediment mixing than in the surrounding seabed. The physical properties of the bottom 2.3 m of this core on the other hand are more cohesive and typical for a homogenous unit. The mean grain size shows a linear trend and oscillates around 17 μm with little variability. This decrease in mean grain size is related to an increase in clay content in this unit with average 16% and very low sand content of 2.8% average. The silt content drops slightly (81%) but has much less variability than the top unit (2% variability). Resistivity shows a gradual increase from 0.6 Ωm to 0.79 Ωm with local maxima around 4.9 m of 1.0 Ωm. The spike in resistivity is matched by a small drop in density/porosity (1.67 g/cm^3; 0.6, respectively) however the data scatter in this area and the gap from the core break makes this signal troublesome to interpret. Notably however there is a small increase in sand content correlated with resistivity increase and it is possible these signals show the presence of a thin sand enriched layer that was not picked up by particle size analysis due to lower sampling resolution. P-wave velocity increases gradually to around 1500 m/s until 4.6m and then drops below meaningful values due to loss of acoustic coupling caused by air gaps between sediment and liner. Element profiles in the VC045 core show very little variability (Figure 46) which indicates well mixed homogenous sediment as documented by the physical property data. Small peaks in the Zr/Rb profile might show areas with higher clay content but it is difficult to verify due to insufficient resolution in the particle size data. The Rb profile shows some correlation with the clay content particularly at the 5m mark where clay increases from 14 to 18%. There are individual peaks in the Mn/Ti and S/Cl ratios that correspond to characteristic dark streaks on the sediment surface, visible in the optical image. Such local inhomogeneities could originate from decomposition of dead fauna or another carbon source that locally accelerates redox process. There is no increase in the magnetic susceptibility at the bottom of the core and no signals in element profiles that could be associated with pyrite formation as seen in the reference core. Overall physical properties of the VC_045 core show evidence of sediment mixing in the upper 4 m of the core. Element profiles for this core were not very informative with no major trends and only second order signals. They agree however with the conclusions derived from physical properties and show well mixed sediment with no distinguishable stratification.

With the active fluid system involved it is quite possible that this disturbance is caused by venting event that created the u1 of pockmark P1. The combined evidence from sub bottom data and physical properties of the sediment cores provides sufficient basis to construct a conceptual model of gas flow in the sediments underneath pockmark P1 (Figure 47).

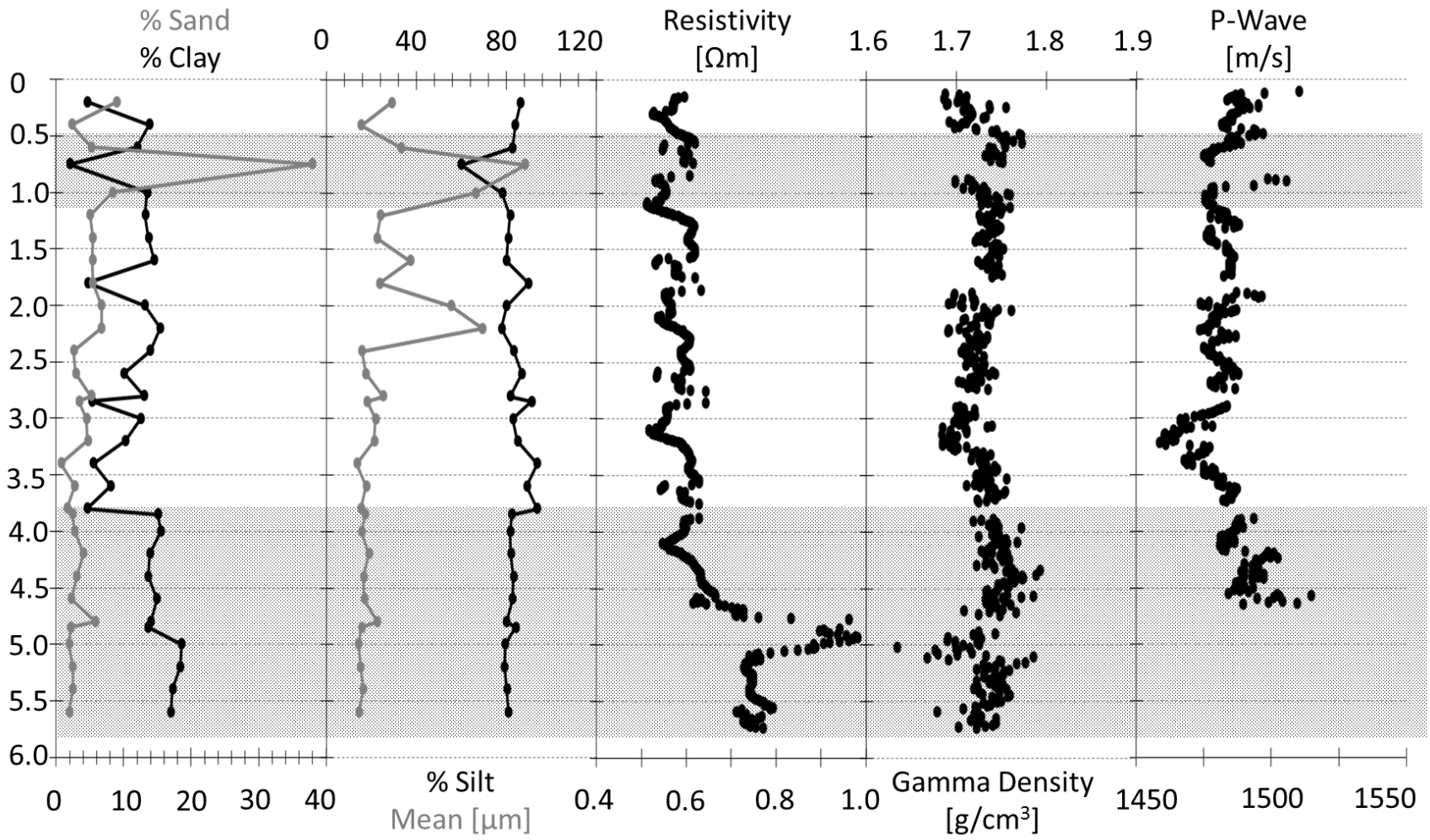

Figure 45. Physical properties of the VC045 core. Shaded areas shows sand rich band and a cohesive undisturbed unit 2.

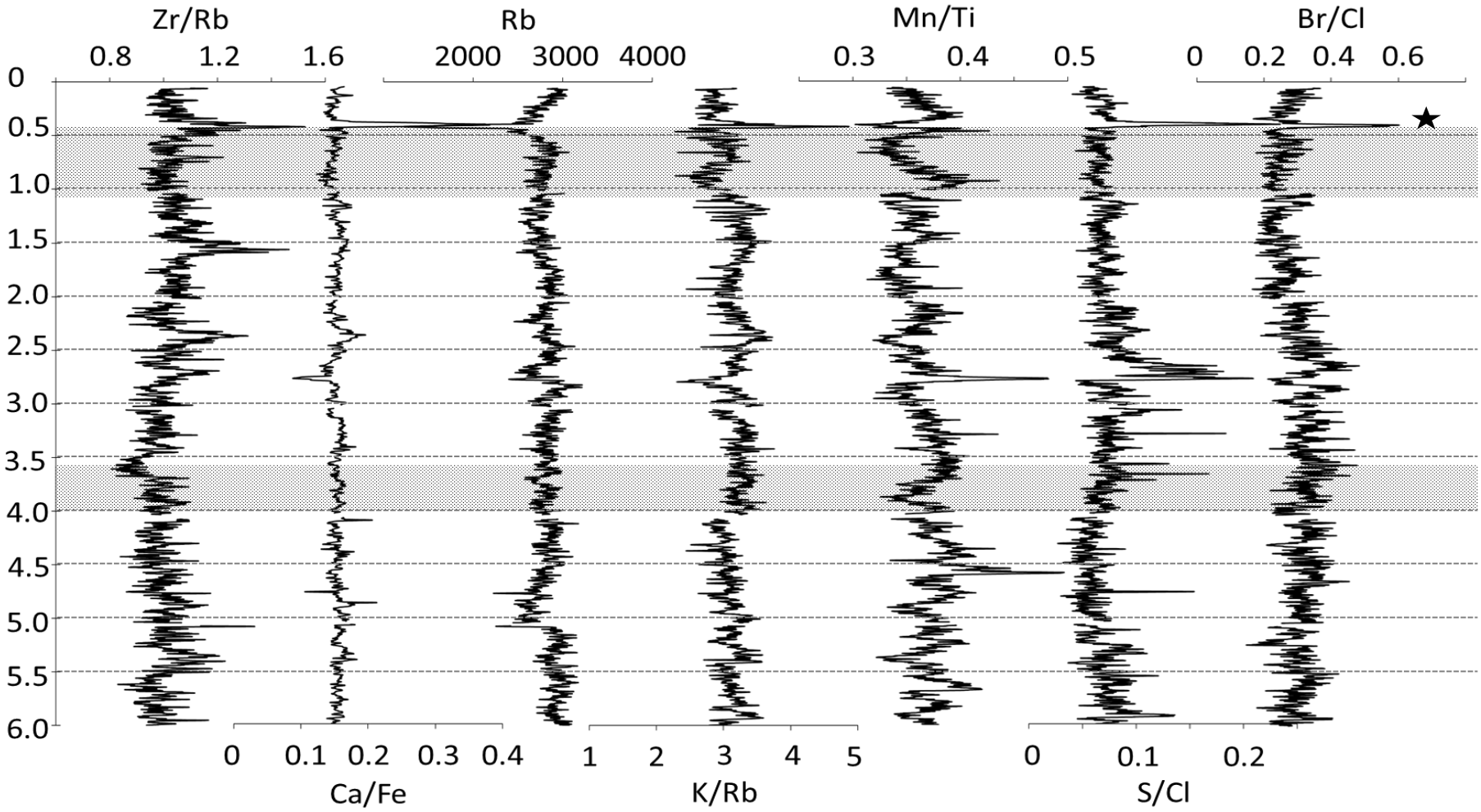

Figure 46. XRF profiles of selected elements and element ratios in the VC044 core. Peaks marked with star are artifacts related to water pocket.

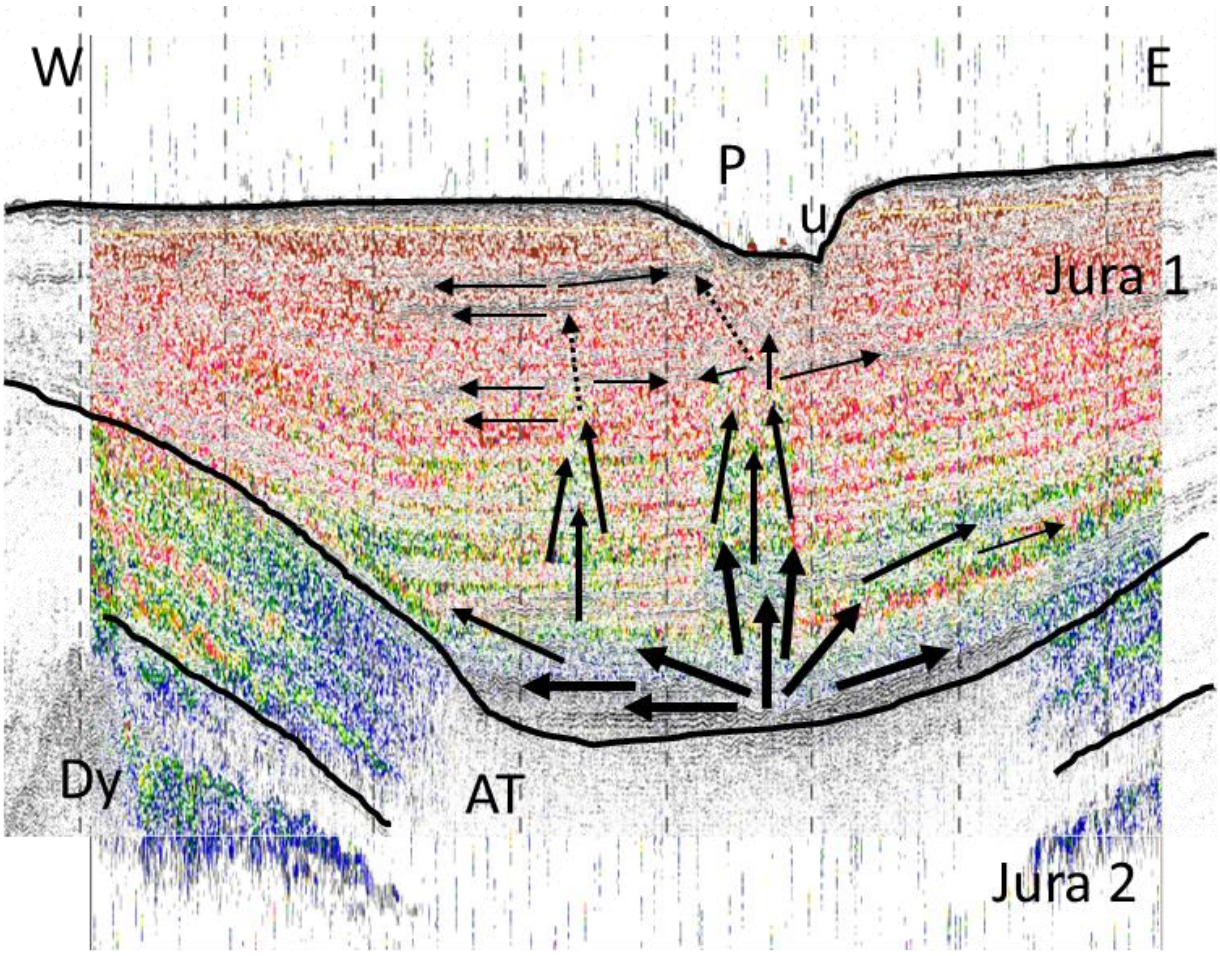

Figure 47. Conceptual model of fluid flow in the subsurface underneath the composite pockmark P1 shown over sub bottom profile merged with single beam profile for better gas front visualization.

In this model we assume that all gas enhanced reflectors observed in the subsurface correspond to small accumulations of gas in more permeable bodies just like the ones shown in core VC_044. The relatively young Jura-1 formation composed of predominantly fine grained sediments form a seal over coarser, more permeable sediments of the Jura-2 formation which trap the gas and form a reservoir. Main migration pathways are vertical with the main gas chimney like structure formed directly underneath the pockmark and a second less profound vertical migration front west from the main one. There are several lateral gas accumulations, the most profound being visible directly above the gas pocket and close to subsurface; there are also several minor ones in between. It is possible that in deeper parts of the sediment (>6m) where anoxic conditions prevail migration pathways are altered by cementation of sediment during microbially mediated formation of MDACs as well as or instead of migration through more permeable bodies. Nevertheless there was no evidence of MDACs formation in the top 6 m of the seabed as well as no evidence of active venting from acoustic and water column surveys (Xavier Monteys, GSI, personal communication). Absence of other gas expulsion features around the pockmark P1 indicates that migration pathways are confined to the parent pockmark area despite the fact that the gas pocket is considerably larger than the feature itself. This also

suggests that migrating gas utilizes the same migration pathways. Examples from other well studied pockmarks (e.g. Hovland, et al. 2005; Judd and Hovland, 2007) support this conclusion. As there are only three unit pockmarks we conclude that the rising gas column is dispersed by lateral migration and rarely reaches the critical pressure and height to form a new unit pockmark. The considerable size of these features suggests large scale and quite violent event capable of disturbing up to 4m of seabed.

2.4 Conclusions

The pockmark scarred Malin Shelf contains an active fluid system in the subsurface. The origin and the nature remains enigmatic however indirect evidence from sulphate profiles, conductivity measurements, acoustic data and geological constrains convinces us that this fluid is most likely methane, possibly of thermogenic origin. The sediments across this entire area have physical and geochemical characteristic, typical for marine environments. No anthropogenic input was observed in element profiles and radioactive nuclide concentrations suggesting pristine conditions for benthos and other meio- and macro-fauna. The sediments of the central part of the Malin Shelf, the Malin Deep are fine grained sandy muds which are ideal for pockmark formation. This is correlated to pockmark density confirming the observations from other settings that pockmarks are more frequent in this type of seabed. The first meters of sediment are Holocene with moderate sedimentation rates up to 0.12 m/ky. However radiocarbon dating is not entirely conclusive due to very low foraminifer counts. The dominant species was found to be *N.pachyderma* indicating temperate waters with no record of glacial conditions. Organic carbon in the surface sediments was lower than expected and averaged around 0.35%. This is possibly related to impoverishment of the water column in nutrients, limiting primary productivity and thus marine carbon deposition. Detailed investigations of large composite pockmark P1 show gas related acoustic signatures in the sub-bottom and single beam profiles. They have revealed a relatively large gas pocket approximately 20 meters underneath the pockmark feature, subtle fluid flow vertical signatures and indicators of lateral gas accumulation in the near-seabed subsurface. Despite an abundance of these subsurface gas related signals there was no evidence of seepage to the water column during data acquisition. However, an active fluid system is present and fluid is migrating within the sedimentary body. The proposed fluid flow model suggests lateral migration through minor reservoirs resulting in pressure drop in the main gas column. This result explains the limited number of unit pockmarks in vicinity of this active system. The model agrees with previously proposed models and is supported by conductivity profiles and acoustic data. Moreover sulphate profiles from both sediment cores indicate a recent upward movement of gas. They also show that methane flux is higher underneath the pockmark than in the reference site, suggesting that the main migration pathway is partially active and connected to the main gas accumulation reservoir

underneath. The subsurface directly beneath the pockmark (up to 4 m below seafloor) remains structureless, without the layering exhibited in the surroundings, suggesting that sediment has been mixed, possibly during pockmark formation. This finding was supported by detailed profiling of the 6 m vibracores for both physical properties and element profiles. The surrounding sediments on the other hand, including those around the reference core show narrowly spaced parallel layering and no obvious structural signs of fluid flow disruption.

CHAPTER 3 – SOURCES AND MOLECULAR COMPOSITION OF THE ORGANIC MATTER ON THE MALIN SHELF

3.1 Introduction

3.1.1 Sources and fate of organic matter in marine sediments

Organic matter deposited in marine sediments is a mix of autochthonous and allochthonous derived material. Autochthonous sources are almost exclusively related to primary productivity in the water column. Majority of plankton derived organic matter travels from the photic zone through the water column forming so-called '*marine snow*' and ultimately reaching the seabed in form of detrital deposits. Small part of it is dissolved and delivered to the seabed as dissolved organic carbon (DOC) and part is transported by downwelling processes. Occasionally carcasses of larger animals sink to the bottom and provide a food source for a variety of scavengers and opportunistic organisms. The impact of such events on sedimentary organic matter is spatially very limited and in the global context much less significant than the input from detrital biomass of microorganisms. Similarly fecal pellets, aggregates, epibenthic and infaunal biomass contribute on a small scale to the organic carbon pool of marine sediments (Schulz and Zabel, 2005). In settings such as the Black Sea, where high productivity and stagnant bottom waters favour anoxic conditions chemosynthetic organisms can be significant contributors to organic matter (Tissot and Welte, 1984). The majority of allochthonous sources are related to landmasses with the exception of in-situ sediment redisposition. Large volumes of sediment and its organic content can be moved due to erosion of the seabed and slope instability. Such deposits can range from small scale turbidities to large scale earthquake induced submarine landslides. Strong bottom currents can also carry suspended sedimentary matter over long distances. Violent pockmark formation can result with mobilization and suspension of large volumes of fine grained sediment which has a low settling velocity and can be carried away easily from the blow out site by strong currents (Judd and Hovland, 2007). Landmass derived organic matter can be both fresh and fossilized as it is derived from both the erosion of rocks of different maturity and terrigenous biomass. A major source of allochthonous organic carbon is fluvial input of dissolved and particulate matter discharged to the shelf waters (e.g. Galy et al. 2007). Aeolian input (wind carried dust and aerosols) of grains, spores and pollens can deliver terrigenous organic matter far into the open ocean (Rommerskirchen et al.

2003). Finally past glacial activity is another important source of terrigenous organic matter (e.g. Meckler et al. 2008).

Despite large fluxes of organic carbon towards the seabed only a fraction of that material is buried in sediments (Schulz and Zabel, 2005). The majority of organic matter derived from primary productivity and terrigenous organic matter is mineralized in the water column in the processes of respiration and heterotrophic activity, and then further reworked in the reactive, young sediments (Emerson and Hedges, 1988). The availability of oxygen in the water column (Pedersen and Calvert, 1990), changes in primary productivity (Demaison, 1990; Demaison and Moore, 1980), protection of organic matter by absorption onto minerals such as clays (Keil et al. 1994) and sedimentation rates (Ibach, 1982) are the proposed main controlling factors of accumulation rates of organic matter in sediment. Moreover Hedges et al. 1999 suggested that "*oxic degradation is more appropriately viewed as a set of as yet unknown processes that characteristically prevail under sedimentary conditions where O_2 is present, as opposed to a specific mechanism that directly involves molecular oxygen*". Therefore the exact mechanisms of 'oxic' transformations are still questionable. It is generally known though that anoxic conditions favour preservation of organic matter as anaerobic microorganisms are less potent in the consumption of sinking organic particles. However Kristensen et al. 1995 has shown in an incubation experiment that rates of anaerobic and aerobic degradation depend on the age and molecular composition of organic matter and both processes can be equally efficient in the case of substrates composed of simple and low molecular weight dissolved organic molecules. Similarly Hulthe et al. 1998 has shown that "old" organic matter is degraded faster (up to 3.6 times) in the presence of oxygen than without it while "fresh" organic carbon is consumed at similar rates regardless of oxygen presence or absence. Such labile organic matter is likely to be decomposed before it reaches the seabed in most settings though therefore these mechanisms will be applicable to shallow areas characterized by a very high input of fresh material. Nevertheless multiple studies from various settings demonstrated that regardless of whether anoxia is a result of changes in primary productivity or the opposite, the organic content of such sediments is better preserved than from oxygenated sites. Anoxic conditions are also considered one of the important conditions in the formation of organic matter source rocks that on a geological scale have developed or will develop into petroleum and gas bearing facies. Gelinas et al. 2001 have shown that low oxygen exposure favours the preservation of molecules considered petroleum precursors such as '*algaenans'* (a natural biopolymer produced by certain species of algae composed of esterified very long aliphatic chains), and that in general there is an inverse relationship between oxygen exposure and organic carbon content thus supporting the above hypothesis. A present day model of such a setting is the Black Sea where about 4% of total organic carbon input is buried in the sediments (Tissot and Welte, 1984). However in a '*normal*' oceanic setting natural water exchange provides sufficient concentrations of dissolved oxygen for gradual but efficient degradation of organic matter traveling through the water

column. Sedimentation rate also have a profound effect on organic carbon burial. Generally there is a positive relationship between organic carbon content and sedimentation rates (Ibach, 1982). Muller and Suess, 1979 concluded that for every tenfold increase in sedimentation rates organic carbon content in marine sediments doubles (Schulz and Zabel, 2005). Stein, 1986; 1990 and 1991 on the other hand has shown that high sedimentation rates can also result in dilution of organic matter and have the opposite effect. Furthermore there are examples of organic rich deposits such as the North Atlantic black shales formed during a large anoxic event 90 million years ago where sedimentation rates were quite low. Tissot and Welte, 1984 also point out: "*Up to a certain point, a high sedimentation rate can also help to preserve organic material. The importance of these two factors* (anoxia and sedimentation rate) *in the preservation of organic matter is hard to quantify, and certainly varies in different environments and localities*". One of the reasons why high sedimentation rates generally favour preservation of organic matter is the protective sorption of organic matter particularly labile components such as sugars and amino acids (Henrichs, 1992) on to mineral surfaces thus making it inaccessible to hydrolytic enzymes (Meyer, 1994). It has been shown that this protective mechanism can slow down mineralization rates by five orders of magnitude (Keil et al. 1994). In later work Meyer et al. 2004 reported that only a small fraction of organic matter is entrapped in mesopores of minerals and yet degradation of organic matter was still limited and that the organic matter was found to be preferentially associated with aluminous clay edges rather than siliceous clay faces that make up the large surface area of the clays. They concluded that: "*Enzyme exclusion may still be a protective mechanism for the bulk of organic matter, but only via more complicated microfabric arrangement*".

3.1.2 Molecular composition and diagenesis of marine organic matter

Natural organic matter (NOM) is one of the most complex mixtures of organic molecules known to man. Despite years of research and advances in analytical tools and techniques the molecular composition of NOM remains largely unknown. Hedges and Oades, 1997 estimated that over two thirds of organic matter in coastal marine sediments remains uncharacterised. Attempts to unravel the mystery of the uncharacterized part of the organic matter continue with use of both classical and novel, destructive and non-destructive approaches such as pyrolysis, selective degradation approaches targeting specific bonds, advanced Nuclear Magnetic Resonance, hyphenated techniques, multidimensional chromatography and many others.

The chemical composition of marine organic matter has been found to be similar and consistent with that of its main contributor: marine phytoplankton. In the early 1930s Alfred C. Redfield proposed that the molecular ratio of nitrogen and phosphorus of plankton (N:P is 16:1) is linked with the similar ratios of dissolved nitrate and phosphate in the ocean (Redfield, 1934).

In his further work carbon and oxygen were introduced in to the equation giving the birth of so called '*Redfield ratio*' or '*Redfield stoichiometry*' which defines the chemical composition of both "*living and dead*" organic matter to be C:N:P = 106:16:1 (Redfield, 1958; Redfield et al. 1963). This relationship is often further expanded to a general equation describing photosynthesis of marine phytoplankton, and after a summary yields a generic formula describing OM:

$$106\,CO_2 + 106\,H_2O + 16\,NH_3 + H_3PO_4 \rightarrow (CH_2O)_{106}(NH_3)_{16}H_3PO_4 + 106\,O_2$$

$$OM = C_{106}H_{264}N_{16}O_{110}P$$

Equation 25: Relationship describing formation of OM by marine phytoplankton during the process of photosynthesis including Redfield stoichiometry.

Over the years scientists have debated the empirical Redfield ratio and its meaningfulness for the description of organic matter. A number of examples were shown where this ratio is not preserved though the fundamental concept was acknowledged to be valid (e.g. Falkowski and Davis, 2004; Falkowski et al. 2004; Hedin, 2004). Several modifications were proposed to include local variables such as other nutrients i.e. silicic acid: C:Si:N:P = 106:15:16:1 (Brzezinski, 1985), isopycnal water layers: C:N:P = 140:16:1 (Takahashi et al. 1985), specificity of individual oceanic basins C:N:P = 117:16:1 (Anderson and Sermiento, 1994) or water depth: N:P = 15:1 (Falkowski, 1997). Despite the fact that the Redfield ratio is intended to describe both "*living and dead*" organic matter it is commonly accepted that diagenetic processes greatly change the composition of organic matter which is depleted in oxygen, phosphorus and nitrogen and simultaneously enriched in carbon, hydrogen and sulphur (Schulz and Zabel, 2005). On a molecular level organic matter was found to be composed of several chemical classes of organic molecules that vary greatly in terms of chemical properties, molecule sizes and their origin. In coastal settings Hedges and Oades, 1997 summarized that typical organic matter is composed of four major classes of compounds: amino acids (10-15%), carbohydrates (5-10%), lignin (3-5%) and lipids (<5%) with the remaining organic matter being uncharacterized.

Amino acids in marine sediments are a product of the degradation of proteinaceous material released from decaying organisms. Proteins are considered a labile component of organic matter and are quickly chemically or enzymatically degraded into amino acids and simple peptides. Most of the phytoplankton derived proteinaceous matter never reaches the seabed as it is readily degraded in the water column by heterotrophic organisms (Hollibaugh and Azam, 1983). In a recent study Nguyen and Harvey, 1998 showed that >92% of the initial protein load was lost during a flow-through incubation experiment mimicking natural conditions. However, they also found that a fraction of proteinaceous matter can survive early

diagenesis as an "*extensively modified and cross-linked, acid species*". The residence time of amino acids and peptides in marine sediments is generally short and their concentration decreases rapidly with depth as they are preferentially consumed by bacteria (Hamilton and Greenfield, 1957). Moreover amino acids begin to be reworked by organisms before they even reach the sediment thus source identification based on their isotopic signature might be troublesome (Keil and Fogel, 2001). Despite the vulnerability of amino acids and proteins recent research has demonstrated that both can survive in marine sediments even on geological time scales. Grutters et al. 2002 argue that amino acids in superficial sediments consist of a mixture of amino acids derived from refractory microbial cell walls and these are transported from the water column detritus. Furthermore they suggest that in situ production of bacterial cell walls from available amino acids is the first step in the preservation of these protein building blocks in the sediments. Other proposed preservation mechanisms are: aggregation through hydrophobic or other noncovalent associations (Nguyen and Harvey, 2001), encapsulation (Zang et al. 2001) and sorption on to mineral surfaces (Keil et al. 1994). Nucleic acids are also among the most labile components of organic matter (Schulz and Zabel, 2005). They are readily degraded and are found in marine sediments in very low amounts (Danovaro et al. 2005). However they are extremely potent trace molecules as they are organism specific and with the use of molecular tools, DNA/RNA can be used to reconstruct the sedimentary microbial population in situ (Venter et al. 2004), track down changes in phytoplankton composition (Boere et al. 2011) and even study viral population changes over a geological timescale (Coolen, 2011).

Carbohydrates are the second most abundant chemical class in marine sediments. They make up a significant proportion of live biomass particularly in the plant kingdom (Schulz and Zabel, 2005). Carbohydrates enter the marine environment mainly in the form of highly organized biopolymers which are easily degraded to dimers and monomers (e.g. pentoses, hexoses) by exoenzymes of various groups of organisms. Most naturally occurring carbohydrates are also considered labile components of organic matter and evidence has shown that they are effectively broken down in the early stages of diagenesis. However some abundant polysaccharides are more recalcitrant than others and resist degradation. Cellulose, xylans, galactans, chitin, dextran, xanthan and other heteropolysaccharides (Arnosti, 1993) are considered more resilient to degradation than starch or glycogen for example. Moreover the diagenetic products of carbohydrate breakdown are effectively buried and survive on geological timescales. Jensen et al. 2005 demonstrated that glucose polymers are selectively degraded in the water column and that initial degradation yields inert end products that escape mineralization and become permanently buried. Burdige et al. 2000 have shown that carbohydrates can be preserved in both estuarine and marine sediments. Moreover carbohydrates have been found in ancient sediments. For example Moers et al. 1994 reported carbohydrate presence in sediments as old as the Jurassic and Swain et al. 1970 reported

carbohydrates in Precambrian shales. The preservation of even the most labile carbohydrates can be enhanced by association with more resilient structures. Cellulose and hemicellulose can survive diagenesis through protection within recalcitrant lignified layers (Killops and Killops, 2005) and other mechanisms have been reviewed by Hattaka, 2001. Carbohydrates can be used to interpret paleoenvironmental fluctuations, such as redox potential changes discerned from the degree of metal-carbohydrate binding, estimation of the input of terrigenous organic matter reflected in relative proportions of certain monosugars (Mopper, 1973) and as indicators of the trophic state (Pusceddu et al. 2003).

Next to cellulose lignin is the second most abundant monosaccharide derived biopolymer. Lignin is a high molecular weight, polyphenolic compound synthesized by higher plants and some algae (Martone et al. 2009). In conjunction with hemicellulose it increases the mechanical strength of plant tissue (Killops and Killops, 2005). Lignin is composed of three basic propenyl phenolic monomers: sinapyl, coniferyl and coumaryl alcohols:

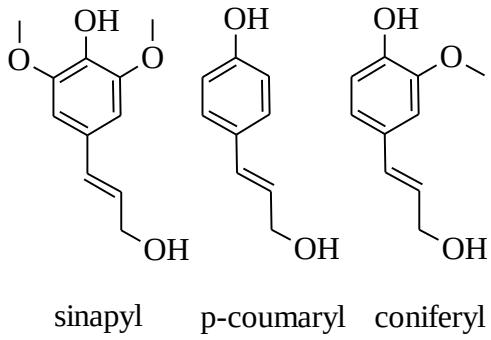

Figure 48. Lignin phenolic alcohol precursors

The subunits undergo enzymatic condensation primarily through β-O-4 linkage, however various secondary reactions and cross-links give lignin its unique structure (Killops and Killops, 2005). Contrary to other macromolecules such as polycarbohydrates, proteins and nucleic acids the structure of lignin is considered less organized, however Hatcher and Clifford, 1997 have shown based on studies of lignin derived coals that it is far from as random as previously thought. The abundance of lignin monomers is variable in different plant tissues (woody and non-woody), different in lower and higher vascular plants and dependent on the ontological development of the parent organism (Manskaya and Drozdova, 1968). This variability is successfully used by geochemists to elucidate sources of organic matter in the marine and terrestrial environment (e.g. Hedges and Ertel, 1982). Lignin is considered a recalcitrant biopolymer and it has been shown that it survives transportation and sedimentation mostly unchanged hence its utility for geochemists as a terrigenous organic matter biomarker (e.g. Hernes and Benner, 2006). In the marine environment diagenetic degradation of lignin is almost exclusively performed by bacteria and fungi (Hatakka, 2001). Lignin degrading bacteria and fungi utilize mechanisms such as tunnelling, erosion and cavitation to digest lignin (Li et al.,

2009). However despite these elaborate efforts solubilization and mineralization of lignin is very slow and occurs only superficially (Singh and Butcher, 1991). The most effective lignin degraders are these with the capacity to produce extracellular enzymes such as fungi from phylum *Ascomycota* (Bucher et al. 2004), *Basidiomycota* (Sarma and Vittal, 2001) and bacteria from the phylum *Actinobacteria*, such as *Streptomyces* spp. (Moran et al. 1995). Microorganisms incapable of secretion of lytic enzymes rely on intracellular digestion thus are able to digest only small lignin molecules and cannot degrade polymeric lignin (Hatakka, 2001). The most efficient bacteria from this group are *Pseudomonas* spp. which usually mineralizes less than 10% of lignin (Vicuna et al. 1993).

Lipids are a very diverse group of hydrophobic and amphiphilic organic molecules soluble in organic solvents such as acetone, chloroform, hydrocarbons, ethers and esters but not soluble in water. They have great structural diversity (Figure 49) but usually do not exceed 5% of the total organic carbon in marine sediments (Hedges and Oades, 1997). Several hundred individual lipids can be identified in typical organic solvent extracts. The main biological functions of lipids are energy storage, cell wall building, signalling molecules and pigments. The majority of cellular lipids exist in complex forms, usually as conjugates. The complex lipid can contain polar moieties such as sugars, amino sugars, and complex phosphate based head groups or apolar moieties such as esters of steroids, alkanes and others or contain both types of species in the form of glyceryl esters or ethers.

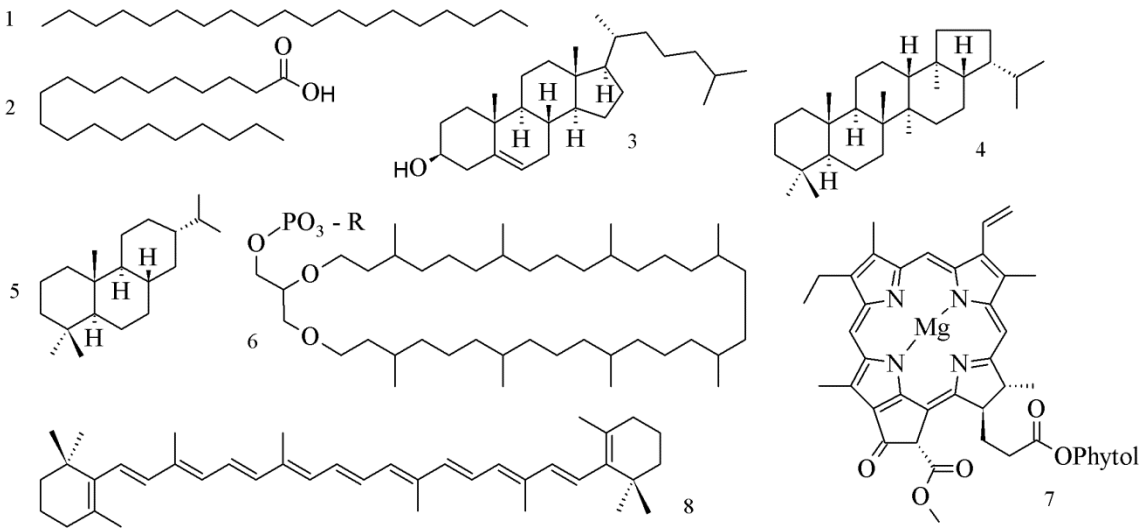

Figure 49. Example structures of different lipid classes. Structures depict: n-alkane (1), n-alkanoic acid (2), steroid (3), hopane (4), diterpenoid (5), cyclic biphytanyl diether (6), chlorophyll (7), carotenoid (8).

Structural complexity is reflected in the drastically different potential to survive early diagenesis and be incorporated into the sedimentary organic matter. Bacterial ester bound phospholipids are considered the most labile of all lipids. The polar head group is readily cleaved by enzymes released from dying cells in a manner of hours (White and Tucker, 1969). Harvey et al. 1986

have shown that 69% of phospholipids are degraded within 96 hours after the death of *Pseudomonadaceae* cultures. This fragility of phospholipids has been exploited to determine the content of live bacterial biomass in the sedimentary environment (White et al. 1979). Harvey et al. 1986 have also shown that glycosidic ether groups specific to *Archaea* have higher stability than bacterial phospholipids, as only 4% was degraded in the same time. Their findings were later confirmed by other researchers showing greater stability of ether versus ester links (e.g. Logemann et al. 2011). With both bacterial and archaeal intact polar lipids (IPLs) as prokaryotic biomass markers Lipp et al. 2008 have shown that while bacterial biomass dominates the surface of marine sediments, *Archaea* reign in the depths. Further studies by Schouten et al., 2010 have shown that fossilized intact polar lipids (IPLs) can be identified even at great sediment depths however they are difficult to distinguish from *in situ* produced IPLs. Lipp and Hinrichs, 2009 reported that fossilized *Archaeal* core lipids are structurally distinct from those of the live biomass IPL core lipids. The identification of polar groups further enhanced the chemotaxonomic potential of these types of lipids as both bacterial and *Archaeal* biomarkers (Suzumura, 2005; Sturt et al. 2004; Koga et al. 1993). It has been demonstrated they can be specific up to genus-level (e.g. Koga and Nakano 2008). Despite the evident loss of information with the initial degradation of polar head groups the hydrocarbon backbone, often referred to as the '*lipid core*', resists diagenesis and remains preserved even in very old rocks (e.g. Brocks and Banfield, 2009). The core lipids retain their biomarker potential and are widely used by geochemists to determine the source of organic matter. Many of these lipids are specific to parental organisms or group of organisms. The majority of simple lipids such alkanes, alkanoic acids, alkanols and common steroids are less informative but still provide valuable information from their distribution i.e. discrimination between terrigenous and marine sources (e.g. Yunker et al. 2005) or tracing anthropogenic inputs (e.g. Takada et al. 1997) and others (comprehensive biomarker review Jain, 2010). Furthermore routes of lipid diagenesis are structure specific and depend on the reactiveness of individual markers and sedimentary conditions (aerobic or anaerobic i.e.) which results in certain lipids being better preserved than others (Hedges and Prahl, 1993). In general however lipids become defunctionalized or modified in reactions such as dehydroxylation (e.g. elimination of hydroxyl groups in sterols and alkanols; Hollerbach and Dehmer, 1994), decarboxylation (e.g. elimination of carboxyl moiety; Johns and Shimoya, 1972) or cleavage of polyfunctionalyzed side chains (e.g. bacteriohopanepolyol side chain cleavage; Sinninghe Damste et al. 1995), hydrogenation of double bonds (e.g. alkanes and hydrocarbons; Johnson and Calder, 1973) and incorporation of sulphur species (e.g. formation of organic polysulphides and thiolanes; Aizenshtat et al. 1994). With increasing temperature aromatization via dehydrogenation (e.g. formation of aromatic steranes and terpenes (Peters et al. 2005), mineral catalysed structural rearrangements and ring opening reactions (e.g. montmorillonite catalyzed pentacyclic triterpene alteration Johns, 1979; Hayatsu et al. 1987) become the major alteration pathways.

3.1.3 Objectives

The objective of the work presented in this chapter was to provide molecular description of the organic matter in the Malin Shelf and elucidate its sources. This is achieved by combined lipid biomarker and NMR approach. Analysis of various lipid biomarkers is used to assess the contribution and discriminate between allochthonous and autochthonous organic matter. Free and bound lipid biomarkers are analysed separately to investigate diagenesis of organic matter and to aid discrimination between fresh and ancient input. Lipids are also subjected to chemolytic oxidation with CuO to help evaluating the contribution of woody and non-woody plant derived organic matter on the Malin Shelf. This part of the work is presented in paragraph 3.3.1. The NMR experiments are used to characterize whole organic matter including macromolecular and non-extractable components. This approach is also used to investigate differences between organic matter inside and outside of the large composite pockmark P1. This part of the results is presented in paragraph 3.3.2.

3.2 Materials and Methods

3.2.1 Sediment samples

Sediment samples were collected with use of grab samplers (Day and Shipek grabs), gravity corer (1 m and 3 m barrel) and a vibracorer (6 m barrel). Upon retrieval grab samples were processed and sub-sampled on deck, gravity cores were caped and sealed with wax. All samples and sub-samples were stored in the ships cold room at 2 ^{o}C for the duration of the cruise. After the expedition grab and gravity core samples were transferred to the laboratory, freeze dried and stored in -20 ^{o}C until analysis. Vibracores were kept sealed until they were logged on the Multi Sensor Core Logger (MSLC, Geotek) and scanned on the Itrax XRF scanner (Cox Analytical Systems) in the British Ocean Sediment Core Research Facility (BOSCORF). Cores were than split open and sub-sampled. All sub-samples were freeze dried and stored at -80 ^{o}C until analysis.

3.2.2 Analysis of the organic matter and lipid biomarkers

3.2.2.1 Lipid biomarkers extraction and partitioning

Method development for lipid extraction

Two different methods were tested for lipid extraction: pressured solvent extraction (ASE) and ultrasonic extraction (UAE). The ASE method utilizes a commercially available, automated system developed by Dionex (ASE 200, Dionex, USA). In this system pressurized

solvent passes through the sediment sample placed in a thermostated extraction cell. In conditions of elevated temperature and pressure the solubility and diffusion rates of the analytes increase significantly. Moreover the interactions between analytes and matrix (e.g. van der Waals forces, hydrogen bonds) are weakened or disrupted. The reduced solvent viscosity and surface tension allows for more efficient mass transfer as the solvent penetrates the pores more easily and more efficiently (Giergielewicz-Mozajska et al. 2007). The automated system uses less solvent and offers shorter extraction times than the classic Soxhlet extraction (Richter et al. 1996; Bull et al. 2000). The technique was validated against other commonly used separation techniques such as UAE, solid phase extraction and shown to be effective for marine matrices (Heemken et al. 1997). Although initially the ASE technique was applied to extraction of organic pollutants such as PAHs, PCBs and petroleum hydrocarbons (e.g. Richter et al. 1996) it was found to be efficient also in extracting natural lipids from environmental samples (e.g. Lichtfouse et al. 1994). Wiesenber et al. 2004 and Jansen et al. 2006 demonstrated that ASE can be successfully applied in lipid studies and that the technique offers reproducible and often improved extraction recoveries without affecting the overall lipid distribution patterns and yields with lipid material of good purity. Although this method offers high sample throughput and short extraction times, the instrument, consumables and carrier gas costs are quite high making this method an expensive alternative.

Wiesenberg et al. 2004 proposed a 93:7 (v/v) mixture of methylene chloride (DCM, CH_2Cl_2) and methanol (MeOH, CH_3OH) as a suitable extractant for lipids with the ASE technique. Two extraction cycles at 75^{o}C and 140^{o}C aimed to sequentially remove more labile material in milder conditions followed by elevated temperature to complete the extraction of less soluble lipids. Although this step is logical and finds confirmation in other studies where temperature effects were investigated (e.g. Richter et al. 1996), Wiesenberg et al. 2004 did not report the extraction yields for the second extraction cycle and focused on combined extracts. Jensen et al. 2006 reported that a single extraction cycle was as efficient as the standard Soxhlet extraction. To determine the optimal conditions for extraction, the sediment sample was extracted according to both methodologies and additionally an alternative 1:1 (v/v) mixture of hexane (Hx, C_6H_{14}) and acetone (Ac, C_3H_6O) mobile phase was introduced into the second cycle. The hexane acetone phase was successfully used to extract lipid material from solid matrices such as seeds (Jacks et al. 1970; Kuk et al. 2005) however it was not tested on sediment or soil matrices where 2-propanol was suggested (Jeannotte et al. 2008). Recoveries were tested on blanks (chromatographically clean sea sand, furnaced at 450^{o}C for 24 hours) spiked with a mixture of reference material (perdeuterated tetracosane, n-$C_{24}D_{50}$; perdeuterated octadecanoic acid, $C_{18}D_{35}O_2H$; and perduterated phenantrene, $C_{14}D_{10}$) as well as on combined lipid fractions from real sediment. ASE extraction conditions are given in Table 15.

Table 15. Lipid extraction methods tested. All methods are based on protocols published by Wiesenberg et al. 2004 and Jensen et al. 2006. Pressure conditions were selected to be in the mid-range to these proposed by Jensen et al. 2006: $5.6x10^6$ and $17x10^6$ Pa.

	Method A		Method B		Method C	
Parameter	Cycle 1	Cycle 2	Cycle 1	Cycle 2	Cycle 1	Cycle 2
Preheat [min]	5	5	5	5	5	-
Heat [min]	5	5	5	5	5	-
Static extraction [min]	20	20	20	20	20	-
Cycles	1	3	1	3	3	-
Pressure [Pa]	$12x10^6$	$12x10^6$	$12x10^6$	$10x10^6$	$12x10^6$	-
Temperature [°C]	75	140	75	110	75	-
Solvent	DCM/MeOH 93:7 (v/v)	DCM/MeOH 93:7 (v/v)	DCM/MeOH 93:7 (v/v)	Hx/Ac 1:1 (v/v)	DCM/MeOH 93:7 (v/v)	

Equal aliquots of sediment samples were extracted in triplicate and concentrated in pre-weighed vials in a stream of nitrogen. The recoveries of standards were evaluated by GC-MS after BSTFA (N,O-bis(trimethylsilyl) trifluoroacetamide)) derivatization. Recoveries are given in Table 16.

Table 16. Recoveries for total lipid extracts (TLE) and individual standards for all tested methods. Reference materials recovery was assessed relative to peak area in the TIC after and prior to extraction.

Analytes	Method A	Method B	Method C
Total lipid extract [mg]	7.2±0.2	6.8±0.1	6.8±0.4
n-$C_{24}D_{50}$ [%]	97±2	97±2	96±2
$C_{18}D_{35}O_2H$ as TMS ether [%]	85±4	86±5	82±6
$C_{14}D_{10}$ [%]	96±3	97±2	96±4

All methods yielded similar amounts of total lipid material; however methods with a second cycle (A and B) had lower variability in recoveries (lower SD). Aromatic and aliphatic standards show excellent recovery which is in with agreement with an evaluation published by Jensen et al. 2006 and Richter et al. 1996. Fatty acid standards had a slightly lower recovery which was also observed by Jensen et al. 2006. They suggested a decrease in polarity of the extractant in elevated pressure and temperature conditions as a possible cause for this sub-optimal extraction efficiency. Although the extraction efficiencies of all tested methods were very similar, method A was selected as is offered best efficiency with comparable recoveries at a cost of an additional 40 min per sample.

The application of different extraction methodologies was forced by ASE breakdown. Ultrasound assisted extraction (UAE) is considered a cost and time efficient alternative to Soxhlet and pressurized solvent extraction (Heemken et al. 1997). This extraction technique utilizes ultrasonic radiation which, through mechanical effects of acoustic cavitation, enhances mass transfer and solvent penetration (Metherel et al. 2009). Ultrasonic energy can break up mineral and organic matter aggregates resulting in better sample homogenization and improved exposure of the analytes to the extractant (Sperazza, et al. 2004). The UAE is often performed at

ambient temperature which eliminates the risk of decomposition of thermally labile analytes. However prolonged exposure to ultrasonic energy results in a spontaneous increase in temperature since part of the energy involved in formation and collapse of micro bubbles is released in the form of heat, next to pressure and mechanical shear (Chemat et al. 2004). This extraction methodology has been successfully used with a variety of matrices and evaluated in various comparison studies (e.g. Shen and Shao, 2005; Heemken et al. 1997) including marine matrices (e.g. Moreda-Pineiro et al. 2004, Bossio et al. 2008). The protocol for UAE was adopted from Otto et al. 2005 with modification introducing filtration through glass fibre filter instead of decantation. The recovery of TLE for this method (the same sample used for ASE in the same quantity) was slightly lower and reached 6.2±0.4 mg of lipid material. This finding is partially in agreement with other studies where extraction in ambient temperature conditions might result with slightly lower extraction efficiency particularly when ultrasonic energy is applied for a short time (e.g. Shen and Shao, 2005; Alupului et al. 2009). However Pernet and Tremblay, 2003 and others demonstrated that ultrasonication enhances cell disruption and allows for better recovery of lipid material associated with living biomass. Moreover it has been shown that short timed application of ultrasonic energy increases the overall extraction efficiency when compared to extractions in the same conditions without sonication (Salisova et al. 1997).

Lipid extraction methods overview

The general lipid material isolation procedure is presented in Figure 50. Sediment samples were sequentially extracted in a pressured solvent extractor (ASE 200, Dionex) according to a protocol modified after Wiesenberg et al. 2004. Dry, pulverized and sieved through 850µm sieve sediment samples were extracted twice at 70^{o}C and 140^{o}C at 12 x 10^{6} Pa with a methylene chloride/methanol (93/7; v/v). Preheat and heat time was set to 5 min while the static extraction time was 20 min and each sample was extracted in three cycles. In cases where there was insufficient amounts of available sediment to fill the entire extraction cell, organic free (furnaced at 450^{o}C) sea sand was added to avoid dead volumes which significantly increase solvent consumption.

Samples were sequentially extracted according to the UAE protocol adopted Otto et al. 2005 as follows. An aliquot of sediment was placed in a Teflon centrifuge tube and ultrasonicated twice for 15min with 30ml Nanopure grade deionized water at an ambient temperature (~20^{o}C). Tubes were centrifuged (2500-6000 rmp for 30min), decanted and freeze-dried. Subsequently water extracted sediment was ultrasonicated for 15min with 30ml of methanol followed by 30ml of methylene chloride/methanol (1:1; v/v) and 30ml of methylene chloride.

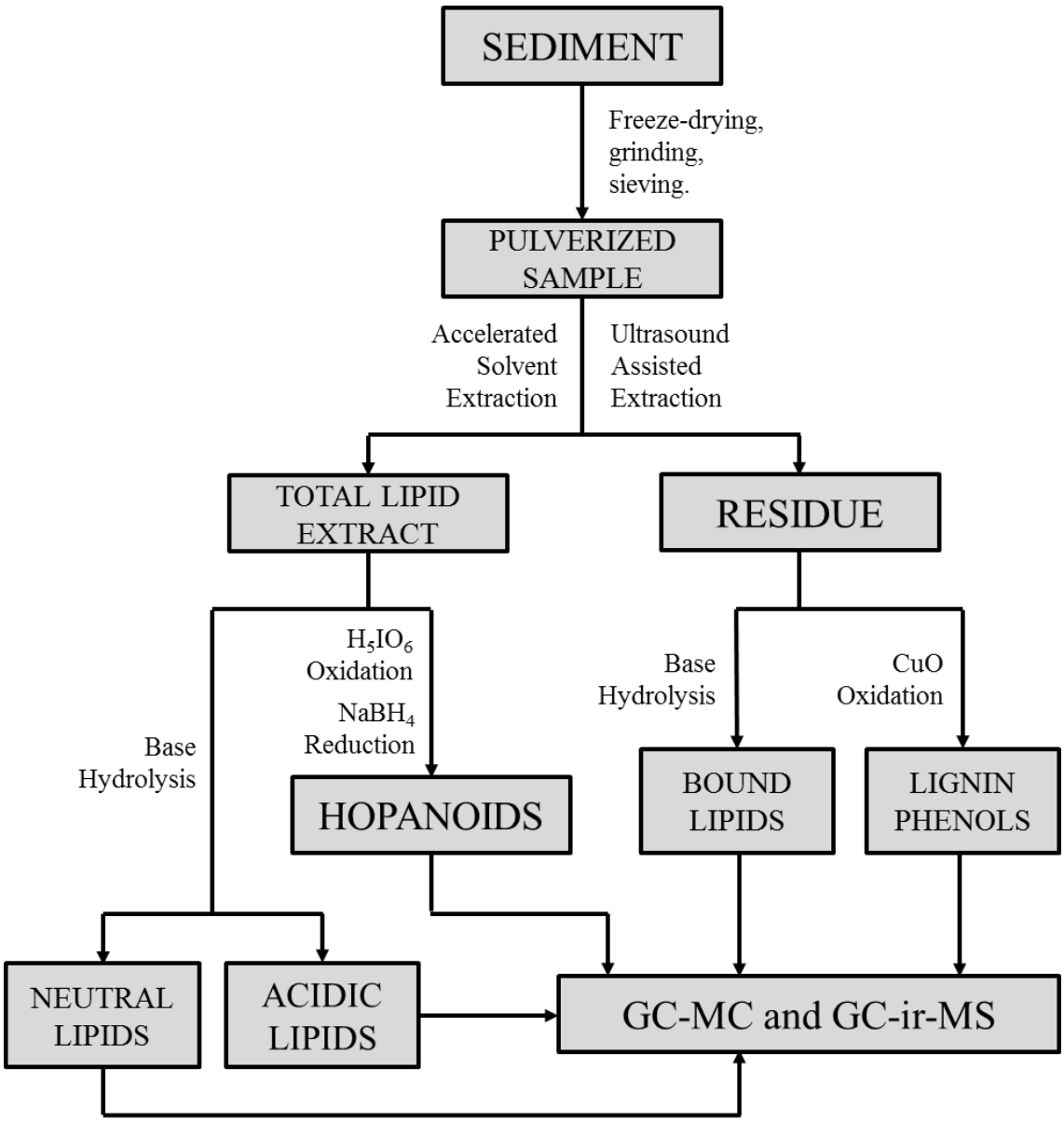

Figure 50. General lipid isolation and partitioning scheme.

All solvent extracts were combined and filtered through glass fibre filters (pre-extracted with methylene chloride and furnaced at 450^{o}C, Whatman GF/A). If immediate sample processing was not possible the TLE were stored frozen (-80^{o}C) under nitrogen to minimize oxidation and microbial contamination. Otherwise solvents were removed by rotary evaporation (bath <37^{o}C). Residual sediment was air dried and kept frozen (-80^{o}C) for bound lipid and lignin phenol analysis. All components of the extraction cells and Teflon centrifuge tubes that come in contact with the sediment were washed with detergent, thoroughly rinsed with deionized water followed by sonication with methanol and a methylene chloride rinse. Sample blanks were run routinely at the beginning of each batch of samples.

Method development for lipid partitioning

TLE was partitioned into three fractions according to modified protocols proposed by Otto et al. 2005, Belicka et al. 2002 and Innes et al. 1997. The method was largely adopted from Belicka et al. 2002 however the base hydrolysis conditions were slightly modified by introducing sonication during the hydrolysis. An aliquot of TLE was processed according to the methodology proposed by Innes et al. 1997 to screen for bacteriohopanoids and geohopanoids. In the original work authors proposed four protocols for the TLE processing to cover all of the possible hopanoid groups: methylation and acetylation of the TLE, thin layer chromatographic separation of the methylated fraction to screen for hopanoidal aldehydes and ketones and conversion of bacteriohopanpolyols to terminal alcohols with periodic acid (H_5IO_6) and sodium borohydride ($NaBH_4$). In this work only the latter methodology was applied as end products are amenable to GC-MS analysis. This treatment however comes with a loss of information coming from the cleavage of the polyol side-chain and inability to resolve its functionalities (Innes et al. 1997). Solvent extracted sediment was hydrolysed to release ester bound lipids according to methodology proposed by Otto et al. 2005. Small aliquots of solvent extracted sediment were oxidized with CuO to release lignin phenols according to the protocol of Otto et al. 2005 and Hedges and Ertel, 1982.

Lipid partitioning method overview

Neutral lipids and fatty acids

After solvents were rotary evaporated the TLE was hydrolysed with 15ml of 0.5 N methanolic KOH solution for 30min in an ultrasonic bath at 50^{o}C. Hydrolyzate was diluted with 30ml of Nanopure grade deionized water, transferred to a separation funnel fitted with a Teflon valve and extracted three times for 5min with 30ml of hexane/diethyl ether (9:1; v/v). The organic layer was collected in a separate flask and dried overnight over anhydrous sodium sulphate (Na_2SO_4). Dried organic layers were stirred for 3 hours with acid activated copper powder under a nitrogen atmosphere to remove elemental sulphur. The aqueous layer was acidified (pH <2) with a 6N HCl solution extracted in a similar manner. The acidified aqueous fraction was discarded. Organic fractions were filtered through glass fibre filters (pre-extracted with methylene chloride and furnaced at 450^{o}C, Whatman GF/A) and concentrated by rotary evaporation (bath temp. <37^{o}C). Extracts were transferred to 2ml vials, dried in a stream of nitrogen and stored frozen (-80^{o}C) for GC-MS and GC-ir-MS analysis.

Bound lipids

An aliquot of dried solvent extracted sediment was placed in a round bottom flask with a magnetic stirrer and amended with 50 ml of 1N methanolic KOH solution. The sediment was hydrolysed for 3 hours under reflux. The cooled suspension was acidified (pH <2) by careful addition of a 6N HCl solution to avoid excessive effervescence and filtered through a glass fibre

filter (pre-extracted with methylene chloride and furnaced at 450^{o}C, Whatman GF/A). The aqueous phase was stored at 4^{o}C for further processing. Hydrolysed sediment residue was washed with Nanopure deionized water and freeze-dried. Dried sediment residue was then extracted in an ultrasonic bath, twice for 15 min with methylene chloride/methanol (1:1; v/v). Organic extracts filtered through glass fibre filters (pre-extracted with methylene chloride and furnaced at 450^{o}C, Whatman GF/A) and the supernatant was combined with acidified aqueous hydrolyzate. Solvents were removed by rotary evaporation (bath temp. <37^{o}C) and the residue was redissolved in 50 ml of Nanopure grade deionized water. The redissolved extract was transferred into a separation funnel fitted with a Teflon valve and extracted twice for 5 min with 10 ml of diethyl ether. Combined ether layers were collected in separate flasks and dried overnight over anhydrous sodium sulphate (Na_2SO_4). The extracts were concentrated by rotary evaporation, transferred to 2 ml vials, dried in a stream of nitrogen and stored frozen (-80^{o}C) for GC-MS and GC-ir-MS analysis.

Oxidation with cupric oxide

Teflon lined digestion vessel (Parr Instruments, p/n 4744) was loaded with ca. 2 g of solvent extracted sediment, 1 g of CuO, 100 mg of ferrous ammonium sulphate hexahydrate [Mohr's Salt; $(NH_4)_2Fe(SO_4)_2x6H_2O$] and 15 ml of aqueous solution of 2M NaOH. Mohr's Salt and CuO were pre-extracted with methylene chloride and air dried while NaOH solution was sparged with nitrogen prior the reaction. The suspension was mixed and sparged with nitrogen for 15 min. The digestion vessel was sealed after the headspace was additionally purged with nitrogen and incubated in an oven at 170^{o}C for 2.5 hours. During incubation the vessel was occasionally shaken. The vessel was then cooled under running water and the content was resuspended by mixing and filtered through glass fibre filters (pre-extracted with methylene chloride and furnaced at 450^{o}C, Whatman GF/A). The solid residue was washed with a small quantity of Nanopure grade deionized water. Residual CuO particles in the filtrate were removed by centrifugation of the filtrate in Teflon tubes (2500-6000 rpm for 30 min). Decanted supernatant was acidified (pH=1) with 6N HCl and stored under nitrogen in the dark for 1 hour to prevent cinnamic acid reactions that are prone to light induced polymerization and dimerization (Otto et al. 2005; Koch et al. 1986). The supernatant was centrifuged (2500-6000 rpm for 30 min) and the aqueous supernatant decanted into a separation funnel fitted with a Teflon valve and extracted twice for 5 min with 50 ml of diethyl ether. Combined organic layers were transferred to separate flasks and dried overnight over anhydrous sodium sulphate (Na_2SO_4). The extracts were concentrated by rotary evaporation, transferred to 2 ml vials, dried in a stream of nitrogen and stored frozen (-80^{o}C) for GC-MS analysis.

Bacteriohopanoids

An aliquot of TLE was transferred to a tall 40 ml vial fitted with a Teflon lined cap and micro magnetic stirrer. The TLE was stirred for 1 h at room temperature with 300mg of periodic acid (H_5IO_6) in 3 ml of tetrahydrofuran (THF)/water (8:1, v/v). Subsequently the mixture was diluted with 10 ml of Nanopure grade deionized water and extracted three times for 3 min (vortex) with 15 ml of petroleum ether (40-60^oC). Organic layers were combined and the solvent removed by rotary evaporation. Residual water was removed by addition of acetone and evaporation of water/acetone (Lucia et al. 2008). The oxidized TLE was transferred to a new vial and stirred for 1 hour at room temperature with 100 mg of sodium borohydride ($NaBH_4$) in 3 ml of anhydrous ethanol (prepared by distillation over CaO). The reaction was quenched with careful addition of 15 ml of 100 mM aqueous solution of monopotassium phosphate (KH_2PO_4). The solution was extracted in a similar manner with petroleum ether (40-60^oC), concentrated, dried, transferred to 10 ml vials dried in a stream of nitrogen and stored frozen (-80^oC) for GC-MS analysis.

3.2.2.2 GC-MS and GC-ir-MS analysis

The operating conditions for GC-MS of free, bound lipids and CuO oxidation products analysis were adopted from Otto et al. 2005 with minor changes. Free lipids were shaken with acid activated copper powder for 1 hour prior to the analysis to remove elemental sulphur. Samples were redissolved in a 4:1 (v/v) mixture of hexane and diethyl ether and injected in splitless mode. The same temperature programme was used for all these fractions. The temperature programme for the analysis of bacteriohopanoids and geohopanoids was adopted from Saito and Suzuki, 2007 since in the original protocol by Innes et al. 1997 the column used had a greater maximum operating temperature to that used in this study.

GC-MS method summary

Derivatization

Neutral lipids and CuO oxidation products were treated with a 100µl of N,O-bis(trimethylsilyl)trifluoroacetamide (BSTFA) and pyridine mixture (9:1; v/v) to convert hydroxyl groups to more GC amenable trimethylsilyl ether (TMS) derivatives. Samples were incubated for 3 hours at 70^oC to ensure complete conversion. Fatty acids and bound lipids were methylated with boron trifluoride (BF_3) in methanol for 30 min at 70^oC and subsequently silylated in the same fashion. The derivatized extracts were spiked with internal standards and gently dried in a stream of nitrogen and redissolved. The hopanoid fraction was acetylated with 4:1 (v/v) mixture of acetic anhydride and pyridine for 1 hour at 50^oC, gently dried in a stream of nitrogen and subsequently silylated as described above.

Quantitation

Quantitation was based on the external standards methodology. Standards were chosen based on structural similarity with target compounds, namely: sterols (cholesterol), alkanols (1-hexadecanol, 1-ocatadecanol, 1-eicosanol), alkanes (squalane), phenols (vanillic acid), fatty acids (tricosanoic acid). Hopanoids were identified in full scan mode and quantitation was based on restricted scan mode as proposed by Innes et al. 1997 with squalane as internal standard.

GC-MS operating parameters

All samples were analysed using an Agilent HP 6890 gas chromatograph (GC) coupled with Agilent 5973N quadrupole mass selective detector (MSD) and IsoPrime isotope ratio mass selective detector (ir-MSD). Helium was used as the carrier gas and the GC was fitted with an Agilent HP-5MS capillary column (30 m x 0.25 mm x 0.25 μm). Samples were injected in splitless mode; injector temperature was set to 280^{o}C. The temperature programme for all fractions except hopanoids was as follows: initial temperature was 65^{o}C held for 2 min, ramp at a rate of 6^{o}C/min to 300^{o}C, isothermal hold at 300 ^{o}C for 20 min, transfer lines 320^{o}C (Otto et al. 2005; Belicka et al. 2002). The temperature programme for the hopanoid lipids analysis was as follows: initial temperature 65^{o}C held for 2 min, ramp at rate of 10^{o}C/min to 250^{o}C, ramp at a rate of 3^{o}C/min to 320^{o}C, isothermal hold at 320^{o}C for 20min, transfer lines 320^{o}C (Saito and Suzuki, 2007). The MSD operated in electron impact (EI) mode at 70 eV, data were collected in 50-650 Da scan mode for all fractions except hopanoids where an extended scan 50-900 Da and restricted scan mode (m/z 180-210; 1 cycle per second) were used.

Quality control

Method blanks were carried out during method development to ensure the lowest possible background and reduce contamination. Each protocol was tested with a chromatographically clean sea sand sample additionally combusted in a muffle furnace at 450^{o}C for 24 hours as an artificial matrix. Initial tests showed some persistent contaminant mainly from n-alkane series, C_{16} and C_{18} fatty acids, mid chain n-alkanols and phthalates (Table 17). Sources of these contaminants were traced to glassware, solvent bottle caps, filtration units and sampling bags. To remedy this all glassware that comes in contact with sample or solvents were accorded a rigorous protocol. New and used glassware including solvent and reagent bottles was washed thoroughly with detergent and rinsed with tap water and deionized water. Glassware was then dried in the oven and after cooling washed with methanol and methylene chloride. Dried glassware was wrapped in aluminium foil and combusted in 450^{o}C for 24 hours. Solvents and reagents were stored in furnaced bottles fitted with heavy duty Teflon lined caps or furnaced ground joint stoppers. Parafilm was only used with humid or moisture sensitive solids and Keck clamps were used only when necessary (shaking during liquid-liquid extractions).

Table 17. Major impurities in method blanks. Relative abundance is given according to: '-' indicates trace levels, '+'to '+++' indicates background level, '++++' and above indicates impurity.

Compound	Abundance	Compound	Abundance
Neutral lipids		**Bound lipids**	
Dodecyl acrylate	+	Dodecanoic acid	+
Cyclododecane	+	Hexadecanoic acid	+
Octadecan-1-ol	+++	Butyl phtalate	++
Hepatdec-1-ene	+	Ocetdecandienoic acid	++
Tetracosane	-	Octadecanenoic acid	++
Bis(2-ethylhexyl) phthalate (DEHP)	-	Ocetdecanoic acid	++
Monohexadecanoyl- glycerol	+	Octadecan-1-ol	+
Squalane	+	Eicosanoic acid	+
Monooctadecanoyl-glycerol	-	Bis(2-ethylhexyl) phthalate	++
Tris(2,4-di-tert-butylphenyl)phosphate (Irgafos 168 oxidation product)	++	Dioctyl phthalate (DOP), the 'phatalate band' m/z 149, 293	++
Bis(2-ethylhexyl) sebacate (DEHS)	++		
		CuO oxidation	
Fatty acids		Nonanoic acid	-
Pentadecanoic acid	-	3,4-dihydroxybutanoic acid	-
Hexadecanoic acid	+++++	Decanoic acid	+
Heptadecanoic acid	-	2,6-di-tert-butylquinone	-
Ocetdecandienoic acid	++	2-methyl-1,3-butandiol	+
Octadecanenoic acid	+++	Unknown m/z 73, 263, 278	++
Ocetdecanoic acid	+++++	Dodecanoic acid	++
Eicosanoic acid	+	3-deoxy-2-hydroxymethyl-erytro-pentono-1,4-lactone	++
Docsoanoic acid	-	2,4,6-tribromo phenol	++
Tetracosanoic acid	-	Tetradecanoic acid	++
Tris(2,4-di-tert-butylphenyl)phosphate	+	7,8-di-tert-butyl-1-oxaspiro[4,5]-deca-6,9-diene-2,8-dione	+
Cyclododecance	+	Hexadecanoic acid	+
Tetradecan-1-ol	-	Octadecanoic acid	-
Terephtalic acid (TPA)	++	Octadecan-1-ol	+
Isobutyl phtalate	-	Bis(2-ethylhexyl) phthalate	++
Hexadecen-1-ol	-	Unknown m/z 235, 531, 546	+
Octadecen-1-ol	++++		
$C_{20} - C_{26}$ n-alkane series	-		
Dodecan-1-ol	-		

This approach resulted in a reduction of the majority of contaminants to negligible levels. However Grosjean and Logan, 2007 have shown some contaminants including C_{16} and C_{18} fatty acids can leach to geological samples from sampling bags, liners and utensils even when frozen. Since polypropylene bags were used during storage and freeze-drying it is likely that these most abundant contaminants originated from this process and it is impossible to eliminate them completely. Because the storage times and the amount of sediment in the bag varied the contribution of these compounds to the real samples will vary as well and is impossible to assess. Some of the plastic additives typical for polypropylene (PP) reported by Grosjean and Logan, 2007 were also observed in blank runs. CuO oxidation blanks have shown the Teflon digestion vessel retains some of the oxidation products which are then carried over to the next sample. This is possibly due to micropores created in the vessel's surface during conditions of

elevated pressure. Various solvent washes, acid washes and sonication were unsuccessful in removing this background. The background was only removed through digestion with chromic acid at 100^{o}C. Table 3 shows identified impurities.

Data processing

The GC-MS signal output was processed with Agilent Chemstation, ACD/Labs MS Processor and AMDIS software packages. Analytes were identified primarily through mass spectra interpretation, comparison and literature and NIST, Wiley spectral library data and AOCS (American Oil Chemists' Society) Lipid Library online database (http://www.lipidlibrary.aocs.org).

Method development for the GC-ir-MS analysis

The GC-ir-MS used in this study is a custom built system that allows simultaneous analysis of the sample in MS and ir-MS/FID detectors utilizing only one GC unit (Figure 51). Effluent carrying separated volatilized sample components is split in a dead volume union type splitter (S1) and a portion of the effluent flows into the primary MS detector while the other portion is directed into the ir-MS/FID interface. The accurate and reproducible split is achieved through in-line pressure calibration however efficacy of this solution cannot be monitored on line. Another union splitter (S2) separates the effluent into a flame ionization detector (FID) and combustion interface. The heart split valve (HSV) controls the flow to the FID. When the valve is closed all effluent is directed to the combustion interface, when the valve is open a portion of the effluent controlled by pressure gradient reaches the FID.

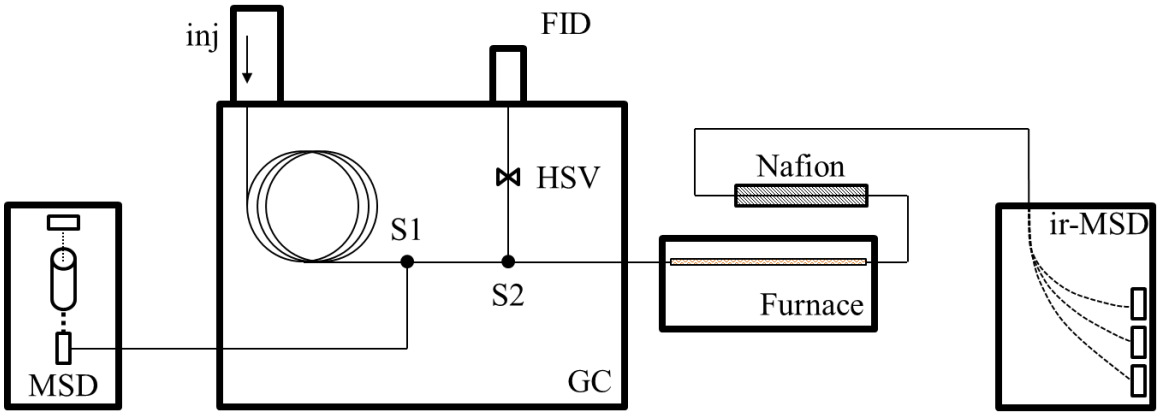

Figure 51. Schematic configuration of GC-MS and GC-ir-MS/FID system.

This solution allows the solvent peak to be vented off in the FID. Otherwise a large volume of solvent would enter the combustion interface and consume a large portion of the catalyst shortening the life span of the catalytic tube. The furnace contains the combustion interface fitted with a quartz tube housing the Pt catalyst and an oxygen source (CuO). The combustion

interface operates at 850°C allowing complete conversion of organic carbon into CO_2. Water produced during the conversion is removed via Nafion tube with a He counter flow which selectively and rapidly absorbs H_2O to ambient levels. Water can protonate CO_2 in the ir-MS ion source elevating the m/z 45 trace. The combusted effluent reaches the ir-MS detector where CO_2 is ionized and separated in the magnetic field into three mass traces corresponding to CO_2 isotopomers: m/z = 44 ($^{12}C^{16}O_2$), m/z = 45 ($^{13}C^{16}O_2$ and $^{13}C^{16}O^{17}O$) and m/z = 46 ($^{12}C^{16}O^{18}O$) which are collected in Faraday cup detectors. The performance of the ir-MS system was tested daily with a series of standard CO_2 pulses in a stability test and CO_2 pulses of variable pressure in a linearity test. The dynamic range of that system varies between 2 and 12 nmol of carbon therefore a sample of known concentration must be used in the analysis. The data was processed with MassLynx software (rev 4.0i). For natural samples that contain hundreds of components it is important to ensure baseline separation to avoid bias towards ^{13}C or ^{12}C. This is particularly important for smaller peaks where the ratio of total surface area to overlap area can be the highest. More importantly though, the differences in the isotopic substitution will result with minimal chromatographic separation of isotopomers and in effect cause isotopic peak inhomogeneity (Sessions, 2006). The errors arising from co-elution can significantly alter the results (Ricci et al. 1994). Although use of reference gas pulses are considered standard practise in GC-ir-MS studies they only validate the ir-MS detector response since they do not pass through the entire chromatographic system. To ensure proper performance samples are calibrated against an external standard that is injected prior and after to the analysis of a sample set. This standard consists of fifteen n-alkanes (C_{16} to C_{30}) of fivefold range of concentrations arranged in pentads with rising concentrations. To test the linearity and reproducibility of the system this standard was analysed periodically multiple times (Figure 52).The variance between individual runs ranged from 0.04 to 2.2% and was the highest for the smallest peaks (C_{16}, C_{21} and C_{26}). A possible cause for this discrepancy is the loss of effluent in the S1 split resulting in smaller quantities of the sample constituencies being converted to CO_2. In a typical setup >95% of the effluent is sent to the combustion interface with the remainder being sent to the FID or MSD (Sessions, 2006). However with the dual MSD/FID interface installed an additional portion of the effluent is sent to the additional detector. The effective loss of concentration can be remedied by increasing the sample concentration to the limit of the chromatographic column capacity however this solution shortens the life of the column, forces frequent inlet maintenance and increases the risk of overloading and tailing of the most abundant components. Without the perfect solution in this study only the major $\delta^{13}C$ peaks are reported to ensure the high quality of data.

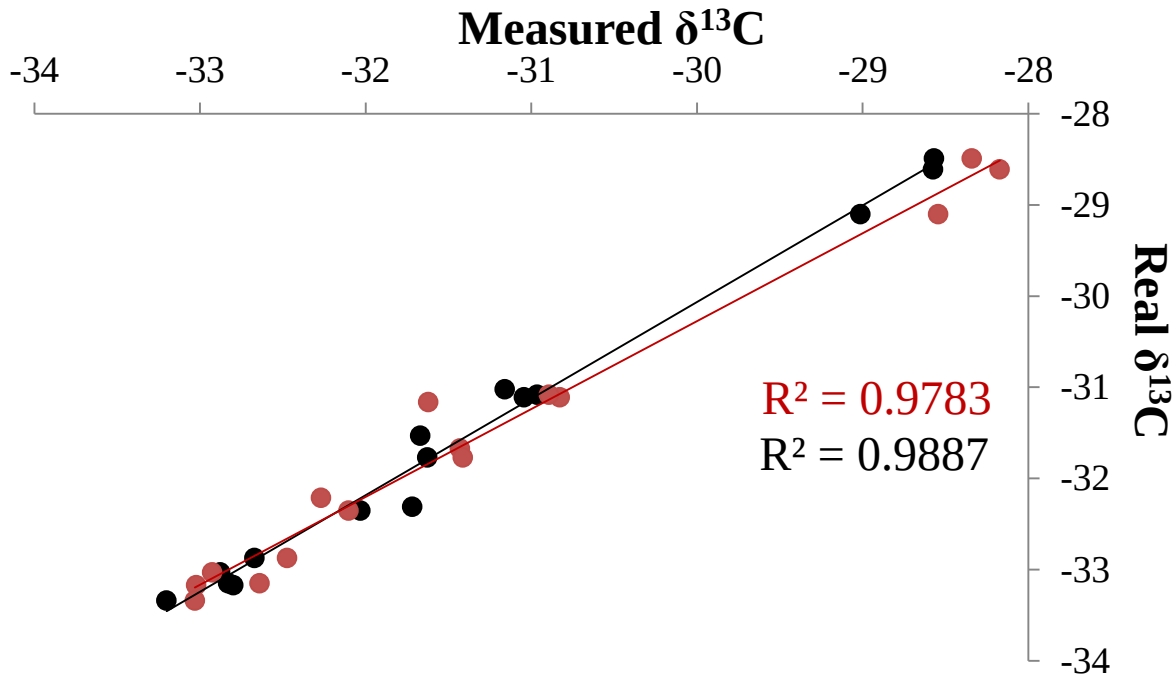

Figure 52. Calibration curves for the external n-alkane standard mix, measured in n=4 (red curve) and n=6 (black curve) replicates.

3.2.2.3 OM extraction for the NMR experiments

Method development for OM extraction

The developments in methodology for OM extraction were discussed in previous paragraphs. Liquid ^{1}H NMR experiments do not require the removal of paramagnetic species however liquid ^{13}C NMR does, although interfering ions are removed via a cation exchange process rather than harsh HF treatment (Cook, 2004). Moreover HF acid pretreatment of samples containing very little OC has been shown to be crucial in obtaining high quality NMR spectra in a reasonable timeframe (Goncalves et al. 2003). This is particularly important for the time demanding 2D NMR experiments. Comprehensive protocols that include recovery of solubilized OC for CP MAS ^{13}C NMR experiments (e.g. Gelinas et al. 2001; Durand and Nicaise, 1980) are very laborious and more importantly difficult to scale up. For samples with very low OC content (<1%) larger aliquots are required to effectively balance sample concentration and OC loss. Moreover because of imperfect extraction methodologies relatively large volumes of sediment are required to obtain sufficient quantities of OM suitable for solution 1D and 2D NMR experiments where the concentration of OC per ml of solvent must be high. The classic approach for combined liquid and solid state NMR experiments involves parallel analysis of OM extracted from non-HF-treated samples for liquid NMR experiments and analysis of HF-treated residue samples by solid-state experiments. The residual non-extractable carbon that remains in the solid matrix after the exhaustive extraction is troublesome to analyse and is generally not practised. The sample is depleted in OC and would have to be

treated to remove the matrix interferences however as mentioned above scaling up the HF treatment is challenging.

In this study we introduced maceration with deionized H_2O to at least partially capture the OC that will be lost during the deashing procedure. All of the water soluble OM particularly DOM and non-mineral bound labile OM is preserved and amenable for NMR analysis. We have found that usually only the first and in case of the superficial layers second maceration resulted in coloured supernatant indicating effective OM extraction. Although the acid soluble and mineral-bound OM will be lost in the treatment it has been shown that this loss is indistinguishable with the NMR approach (Goncalves et al. 2003). Interfering paramagnetic species are not extracted in the conditions of neutral pH therefore an ion exchange step is not necessary however removal of natural inorganic salts simplifies the process of thorough water removal which is crucial for ^1H NMR experiments. Natural salts complicate slightly sample preparation for NMR analysis however they do not affect the results. De-ashing of water extracted sediment with HF acid is the only step where loss of OM occurs. This loss is troublesome to quantify without DOC measurements in concentrated supernatants containing HF acid. It is possible to precipitate the excess of fluoride ions with calcium carbonate ($CaCO_3$) to form insoluble fluorite (CaF_2) as proposed by (Gelinas et al. 2001) or dialysis however for safety reasons in this study HF waste was discarded. The remaining part of the protocol does not deviate from the standard approach. Aliquots of de-ashed sediment were retained for potential solid-stated NMR experiments while the rest is extracted exhaustively with diluted NaOH solutions. The extract after clean-up was then analysed by solution-state NMR. Because solid-state NMR experiments are very laborious in this study they were not carried out routinely, but only if the findings of the liquid NMR justify it.

OM extraction method summary

OM extraction method is presented on Figure 53. Sediment samples were placed in acid washed amber glass jars and amended with Nanopure grade deionized water in a 1:2 (wg/v) sediment to water ratio. Slurries were shaken for 12-24 hours and left to settle. Supernatant was decanted and frozen (-80^{o}C). The process was repeated two more times and all supernatants were combined and kept frozen (-80^{o}C). Residual sediment was centrifuged and freeze-dried and the supernatant was pooled with previously collected aqueous extracts. The water extracts were pressure filtered through 0.22 μm polyvinylidene fluoride (PVDF) membranes, and the extract volume reduced through rotary evaporation (water bath <37^{o}C). The majority of residual water was then removed by freeze-drying, however high concentration of salts caused liquefaction of the samples. Liquefied samples were transferred to glass vials and dried in a

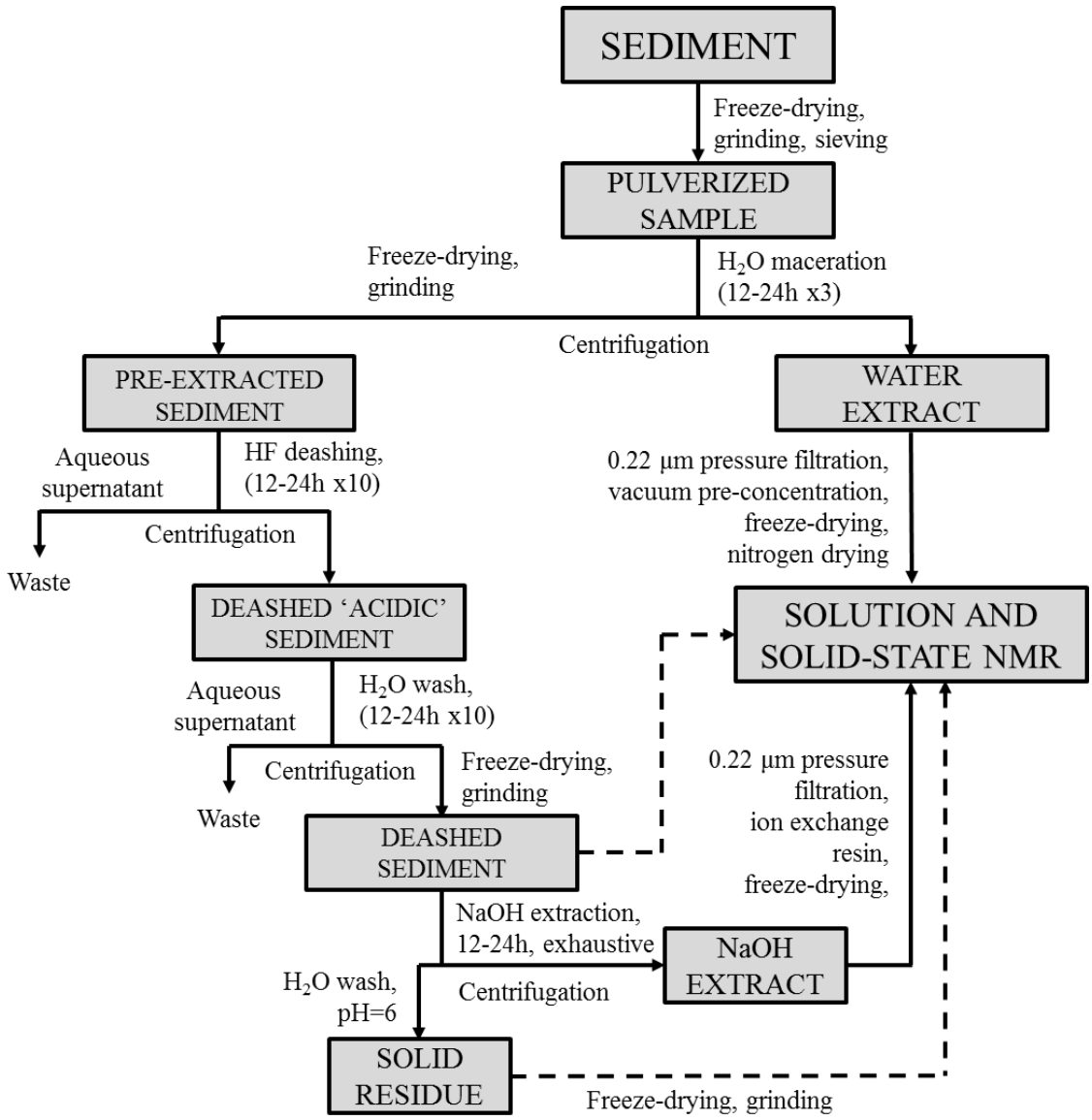

Figure 53. Exhaustive organic matter extraction scheme for the NMR experiments .

stream of nitrogen. Samples were kept frozen (-80^{o}C) until sent for analysis. Water extracted sediment was placed in 250 ml Teflon centrifuge tubes and shaken for 12-24 hours with 10% HF acid solution, and centrifuged (4500-9000 rpm for 30 min). The treatment was repeated at least ten times and after the last cycle 10% HF was exchanged for Nanopure water. Water wash cycles were repeated until supernatant pH = 6 (usually 10-12 washes sufficed). An aliquot of de-ashed sediment was kept for solid state NMR experiments while the remainder was exhaustively extracted with a nitrogen sparged 0.1N NaOH aqueous solution (1:4; wg/v sediment to extractant ratio). Samples were shaken for 12-24 hours and centrifuged (4500-9000 rpm for 30 min). Supernatants were pooled and kept frozen (-80^{o}C) until extraction was complete (no colour in the supernatant). The thawed extract was pressure filtered through 0.22 µm polyvinylidene fluoride (PVDF) membranes and the filtrate was passed through activated Amberlite 1200+ cation exchange resin. Pooled filtrate was freeze-dried and stored frozen (-80^{o}C) until sent for the analysis. The cation exchange resin was activated with consecutive

washes of column volumes of 10% HCl and 0.1M NaOH repeated at least ten times. The resin was regenerated after every 2 litres of filtrate with 4 column volumes of 10% HCl followed with 100 column volumes of Nanopure grade deionized water.

3.2.2.4 NMR methodology

Each sample (~40 mg) was re-suspended in 1 mL of deuterium oxide (D_2O) and titrated to pH 13 using NaOD (40% by weight) to ensure complete solubility. Samples were analysed using a Bruker Avance 500 MHz NMR spectrometer equipped with a ^{1}H-^{19}F-^{13}C-^{15}N 5 mm, quadruple resonance inverse probe (QXI) fitted with an actively shielded Z gradient. 1-D solution state ^{1}H NMR experiments were performed at a temperature of 298 K with 128 scans, a recycle delay of 3 s, 16384 time domain points, and an acquisition time of 0.8 s. Solvent suppression was achieved by presaturation utilizing relaxation gradients and echoes (Simpson and Brown, 2005). Spectra were apodized through multiplication with an exponential decay corresponding to 1 Hz line broadening, and a zero filling factor of 2. Diffusion-edited (DE) experiments were performed using a bipolar pulse longitudinal encode-decode sequence (Wu et al. 1995). Scans (1024) were collected using a 1.25 ms, 52.5 gauss/cm, sine-shaped gradient pulse, a diffusion time of 100 ms, 16384 time domain points and 819 ms acquisition time. Spectra were apodized through multiplication with an exponential decay corresponding to 10 Hz line broadening and zero filling factor of 2.

Heteronuclear Multiple Quantum Coherence (HMQC) spectra were obtained in phase sensitive mode using Echo/Antiecho gradient selection. The HMQC experiments were carried out using 256 scans with 128 time domain points in the F1 dimension and 1024 time domain points in the F2 dimension. A relaxation delay of 1 s and ^{1}J ^{1}H-^{13}C of 145 Hz were used. F2 dimenions in HMQC experiements were processed using an exponential function corresponding to a 15 Hz line broadening. The F1 dimension was processed using a sine-squared function with a $\pi/2$ phase shift and a zero-filling factor of 2.

3.3 Results and discussion

3.3.1 Distribution and sources of lipid biomarkers on the Malin Shelf

Sediment grab and core samples analysed for lipid biomarker content are shown in Figure 54; a more detailed sampling area depiction and description are given in Chapter 1 and 2.

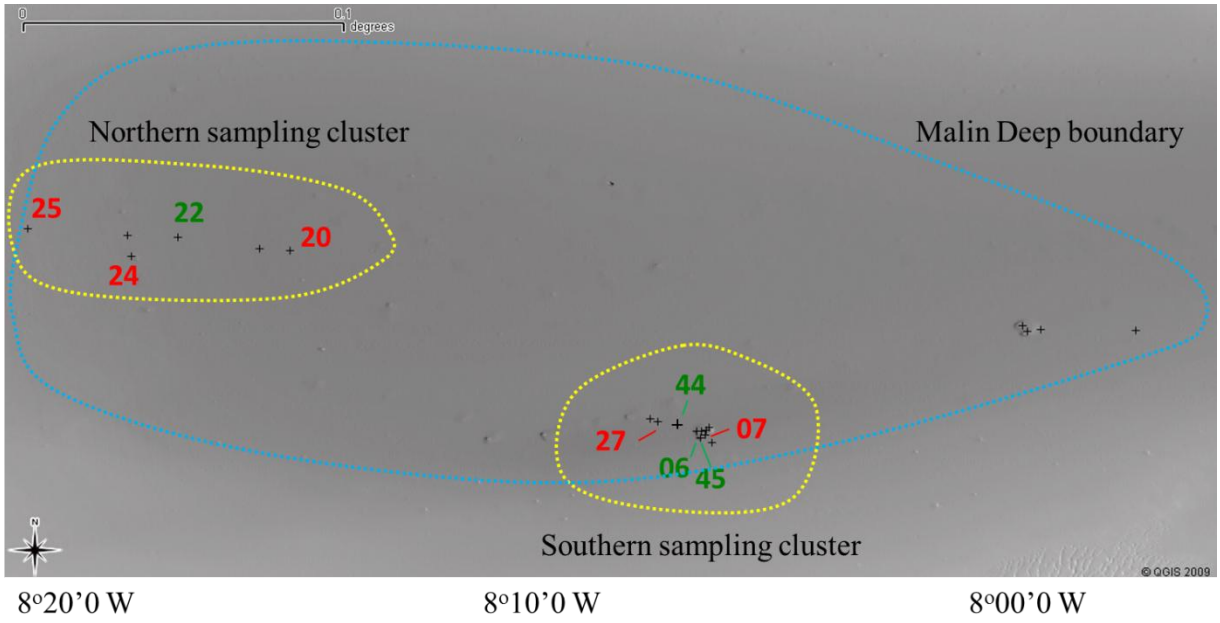

Figure 54. Shaded relief bathymetry of the Malin Deep with the locations of grab and core samples analysed for lipid content. Red symbols denote grabs while green represent cores, yellow dashed line denotes sampling clusters, blue dashed line denotes Malin Deep boundary.

3.3.1.1 Neutral lipids

The total neutral lipids in the surface sediments of the Malin Sea ranged from 18.22 µg/g (all concentrations are expressed as µg per g of dried weight of the sediment) to 35.55 µg/g. Representative chromatogram of neutral lipids fraction is given below (Figure 55). Samples from the western stations (25, 24, 20, 22) show slightly higher concentrations (31.93±3.16 µg/g; mean ±S.D.) than these from the southern stations (22.29±4.20 µg/g). On average the neutral lipid content in the surface sediment was 26.57±6.20 (Table 18). Neutral lipids were dominated by n-alkanols (11.00±3.62 µg/g) and n-alkanes (8.21±6.00 µg/g) with a large proportion of sterols and stanols (4.59±1.69 µg/g). Other detected neutral lipids included C28, C30 and C32 n-alkyl diols and n-alkyl keto alcohols, aliphatic ketones (heptacosan-2-one and nonacosane-2-one), phytol (3,7,11,15-tetramethyl-1-hydroxy-hexadec-2-ene) and its degradation products such as: 2,6,10,14-tetramethylopentadecan, 6,10,14-trimethylopentadeca-2-one, 3,7,11, 15-tetramethylhexadecan-1-ol and secondary n-alkanols, mono and

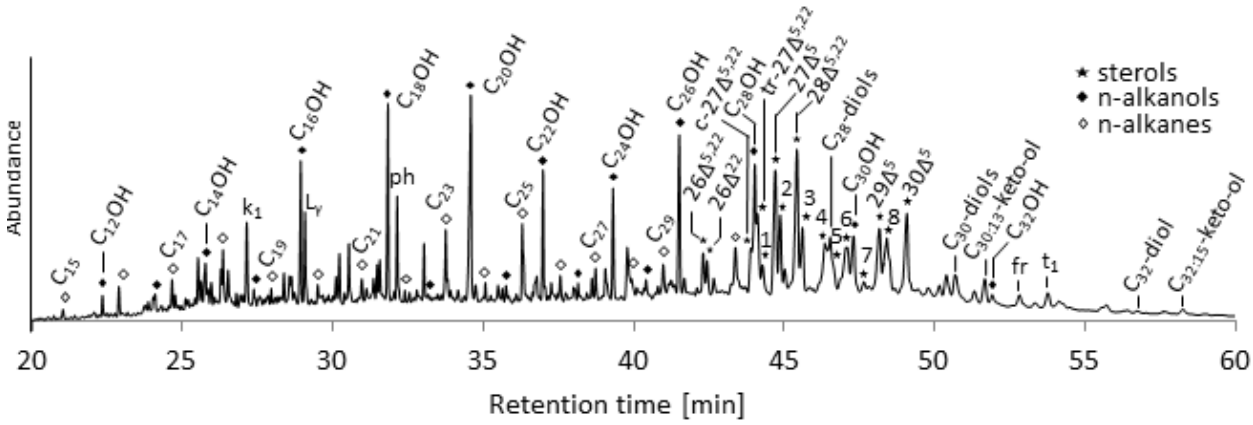

1 - 27Δ22, 2 - 27Δ0, 3 - 28Δ22, 4 - 28Δ5, 5 - 28Δ0, 6 - 29Δ5.22 , 7 - 28Δ5.24(24), 8 - 29Δ0, k_1 - 6,10,14-trimethylopentadeca-2-one, L_γ - γ lactone, ph - phytol, fr - fridelin, t_1 - unk terpenoid, d_1 and d_2 - deuterated standards

Figure 55. Representative TIC of neutral lipid fraction.

Table 18. Concentrations of neutral lipid biomarkers in the surface sediments of the Malin Shelf and selected molecular descriptors. Terrestrial Aquatic Ratio index was calculated according to $TAR_{HC} = \frac{C27+C29+C31}{C15+C17+C19}$ and $TAR_{AL} = \frac{C26+C28+C30}{C14+C16}$, (Fabbri et al. 2005); Carbon Preference Index was calculated according to $CPI_{HC} = \frac{1}{2} \times \left(\frac{C25+C27+C29+C31+C33}{C24+C26+C28+C30+C32} + \frac{C25+C27+C29+C31+C33}{C26+C28+C30+C32+C34}\right)$ and $CPI_{AL} = \frac{1}{2} \times \left(\frac{C24+C26+C28+C30+C32}{C23+C25+C27+C29+C31} + \frac{C24+C26+C28+C30+C32}{C25+C27+C29+C31+C33}\right)$, (Zhang et al. 2006); Average Chain Length index was calculated according to $ACL_{HC} = \frac{23\times C23+25\times C25+27\times C27+29\times C29+31\times C31+33\times C33}{C23+C25+C27+C29+C31+C33}$ and $ACL_{AL} = \frac{24\times C24+26\times C26+28\times C28+30\times C30+32\times C32}{C24+C26+C28+C30+C32}$, (Zhang et al. 2006); Higher Plant Alkanes index (also referred to as the alkanol preservation index) was calculated according to $HPA = \frac{(C24OH+C26OH+C28OH)}{(C24OH+C26OH+C28OH)+(C27+C29+C31)}$, (Westerhausen et al. 1993).

	Stations									
	25	**24**	**22**	**20**	**27**	**44**	**6**	**45**	**7**	**Mean ± S.D.**
Lipid class										
n-alkanes										
C16-C22	1.53	6.38	2.12	5.97	0.91	0.86	1.78	0.27	1.82	2.40±2.21
C23-C33	7.14	10.12	11.75	10.82	3.26	2.79	2.51	0.96	2.91	5.81±4.17
Σ_{HC}	8.67	16.50	13.86	16.79	4.18	3.65	4.29	1.23	4.73	8.21±6.00
n-alkanols										
C12-C20	1.56	2.45	1.20	1.15	2.71	1.85	2.36	1.81	2.00	1.90±0.54
C21-C31	13.58	11.90	9.68	10.59	13.45	6.71	3.33	6.57	6.15	9.11±3.60
phytol	1.00	1.05	0.76	0.94	0.21	0.19	0.25	0.75	0.82	0.66±0.35
Σ_{AL}	15.14	14.35	10.89	11.74	16.16	8.55	5.70	8.38	8.14	11.00±3.62
Sterols	3.06	2.76	2.97	3.46	5.75	6.04	7.37	6.14	4.96	4.72±1.70
$\Sigma_{NEUTRAL}$	28.77	35.55	29.87	33.53	29.39	21.03	21.05	18.22	21.74	26.57±6.20
Indices										
TAR_{HC}	12.1	2.7	13.0	3.8	6.5	5.7	3.3	9.6	2.5	6.6±4.1
TAR_{AL}	18.3	9.3	16.4	28.4	25.7	12.3	2.2	12.3	8.1	14.8±8.4
CPI_{HC}	3.2	3.0	3.6	4.7	4.8	4.2	5.3	4.5	4.1	4.2±0.8
CPI_{AL}	5.6	5.7	5.5	5.5	13.8	6.9	6.7	6.9	6.3	7.0±2.62
HPA	0.7	0.6	0.5	0.5	0.8	0.7	0.6	0.9	0.7	0.7±0.14
ACL_{HC}	27.7	27.8	28.0	28.1	27.4	27.4	26.5	28.0	27.6	27.6±0.5
ACL_{AL}	26.7	26.8	26.8	26.8	26.5	26.6	26.6	26.6	26.6	26.7±0.1

diacylglycerols and one terpenoid (friedelan-3-one; friedelin). The concentration of these components ranged from 1.55 µg/g to 3.91 µg/g.

n-alkanes

The normal long chain hydrocarbons (C23-C33) exhibited odd-over-even predominance in all samples with C27, C29 and C31 (ACL_{HC} = 27.6±0.5) being the most abundant. Hydrocarbons >C32 were present in very small amounts in most samples often co-eluting with other sample components. Long chain n-alkanes were visibly more abundant in the northern stations (from 7.14 µg/g to 11.75 µg/g) than in the southern ones (from 0.96 µg/g to 3.26 µg/g). This might indicate a source related relationship; however it more likely reflects changes in grain size patterns as n-alkanes are known to be more associated with coarse material than with fines (Gonzalez et al. 2008). Bound lipids on the other hand are less susceptible to grain size related fractionation at least in some settings (Jeng and Chen, 1995). The Carbon Preference Index (CPI_{HC}) calculated over C24-C34 range varied from 3.6 to 4.6 in the northern and southern stations respectively. More molecular indices are given in Table 18. The observed distribution indicates a predominantly terrigenous origin of the long chained alkanes. Low CPI_{HC} values and strong odd-over-even predominance is indicative of material derived from the leaf waxes of higher plants (Eglinton and Hamilton, 1967) and aeolian dust (Simoneit et al. 1977). This conclusion is supported by isotopic signatures of the major n-alkanes (C25-C31) which ranged from -29.3‰ to -32.1‰, values typical for terrestrial lipids (Peterson and Fry, 1987). Anthropogenic and petroleum derived hydrocarbons show little or no predominance (Volkman, 2006). Short chain alkanes (C16-C22) show no predominance with C17, C18 and C20 being the most abundant. Odd, short chained alkanes particularly C15, C17 and C19 and n-alkenes have been reported in microalgae with the latter being formed by decarboxylation of short chained n-alkanols (Volkman et al. 1998). Other named sources include marine phytoplankton in general (Blumer et al. 1971), benthic algae (Youngblood et al. 1971) and pelagic macroalgae (Burns and Teal, 1973). The total concentration of the n-alkanes in the southern stations was considerably lower than in the northern ones (Table 18). Short chained species on average comprised 28.3% of all alkanes, however, deviation between all stations was considerable (10.2%). The down core (stations 22, 6, 44 and 45) alkane distributions show little variation with depth (Figure 56). The contribution of short chain alkanes however, increased slightly with depth in the southern 6, 044 and 045 stations (from 1.78 µg/g to 4.27 µg/g; from 0.86 µg/g to 1.93 µg/g and from 0.27 µg/g to 1.33 µg/g respectively) while it remained fairly constant in the northern 22 station (1.63±0.73 µg/g). Although lack of predominance particularly in short chained alkanes is not uncommon, Grosjean and Logan, 2007 pointed out that plastic bags (used in this study to temporarily store frozen grab samples and core subsamples) can be a potent source of hydrocarbons and other contaminants in natural samples. Such unwanted ‘contribution’ can go unnoticed since standard quality protocols do not

encompass routinely used consumables. We therefore cannot exclude contribution from plastic bags to the n-alkane pool.

n-alkanols

Long chain n-alkanols exhibited even-over-odd predominance across their entire distribution with C24, C26 a C28 (ACL_{AL}=26.69±0.11) being most abundant and comprising from 58.5% to 90.2% of all n-alkanols, respectively (Table 18). These compounds when accompanied by odd-chain n-alkanes are a strong indication of plant wax input (Volkman, 2006). Isotopic signatures for C22-C28 ranged from -24.1‰ to -28.1‰ which falls within values typical for terrigenous material (Peterson and Fry, 1987). Other sources of at least some of the n-alkanols include cyanobacteria, such as *Anabaena cylindrica* which was reported to produce a C22-C28 series (Abreu-Grobois et al. 1977), diatoms from the genus *Navicula* (Volkman et al. 1993) and *Skeletonema* (Berge et al. 1995) which have been reported to contain substantial amounts of C34 and C18:1 respectively. In general however microorganisms are considered a rather minor source of these fatty alcohols. Short chain alcohols on the other hand, in marine sediments are in general associated with marine sources. Boon and de Leeuw, 1979 suggested that they might be formed by hydrolysis from esterified precursors present in a variety of organisms. Zooplankton have been proposed as a major source of these compounds (Volkman et al. 1999) however phytoplankton and bacteria can also contribute to this lipid class pool (Mudge and Norris, 1997). Short chain alkanols were more abundant in the southern stations and ranged from 16.8% to 41.5% of total alkanols (mean 25.2%; n=5) than in the northern ones where this proportion ranged from 11.1% to 17.1% (mean 12.1%; n=4). The distribution of short chain alkanols was dominated by C16, C18 and C20 which comprised 15.0% and 31.0% (mean 20.4%; n=5) and 8.0% to 10.3% (mean 8.6%; n=4) of total alkanols in the northern and southern stations, respectively. The short/long alkanol ratio as described by Treignier et al. 2006 indicated more a terrigenous signature (R<0.6; n=4) in northern stations with a more balanced distribution in the southern stations (R=1.0; n=5). This is even more emphasized by the Terrestrial Aquatic Index (TAR_{AL}, Table 18) where northern stations have shown on average 33% higher values than the southern ones (TAR_{AL} = 18.1 and 12.1 respectively). Particularly station 6 has shown an anomalously high content of C16 and C18 which accounted for up to 26.6% of total alkanols resulting in an unusually low TAR_{AL} of 2.22 while surrounding stations have shown significantly higher values. Such differences in the abundance of terrigenous biomarkers between these sampling clusters beside could also be explained by greater aeolian contribution. The down core distribution of n-alkanols was similar to that of the surface samples. In station 22 the short/long alkanol ratio had an average of 0.53±0.13 with no major changes in concentration except for horizon 0.65 where 50% lower concentrations were observed. Interestingly an increase in n-alkane concentration was also observed which might suggest intensified diagenetic dehydroxylation. The remaining cores

show higher short/long alkanols ratios ranging from 0.76±0.15 to 1.01±0.44 (stations 45 and 6 respectively). Moreover in the first meter of the sediment the total concentration of alkanols in these cores increased slightly (from 3.47 µg/g to 11.30 µg/g) followed by an inversed trend in the deep 44 and 45 cores paired with an increase in the concentration of n-alkanes (Figure 56).

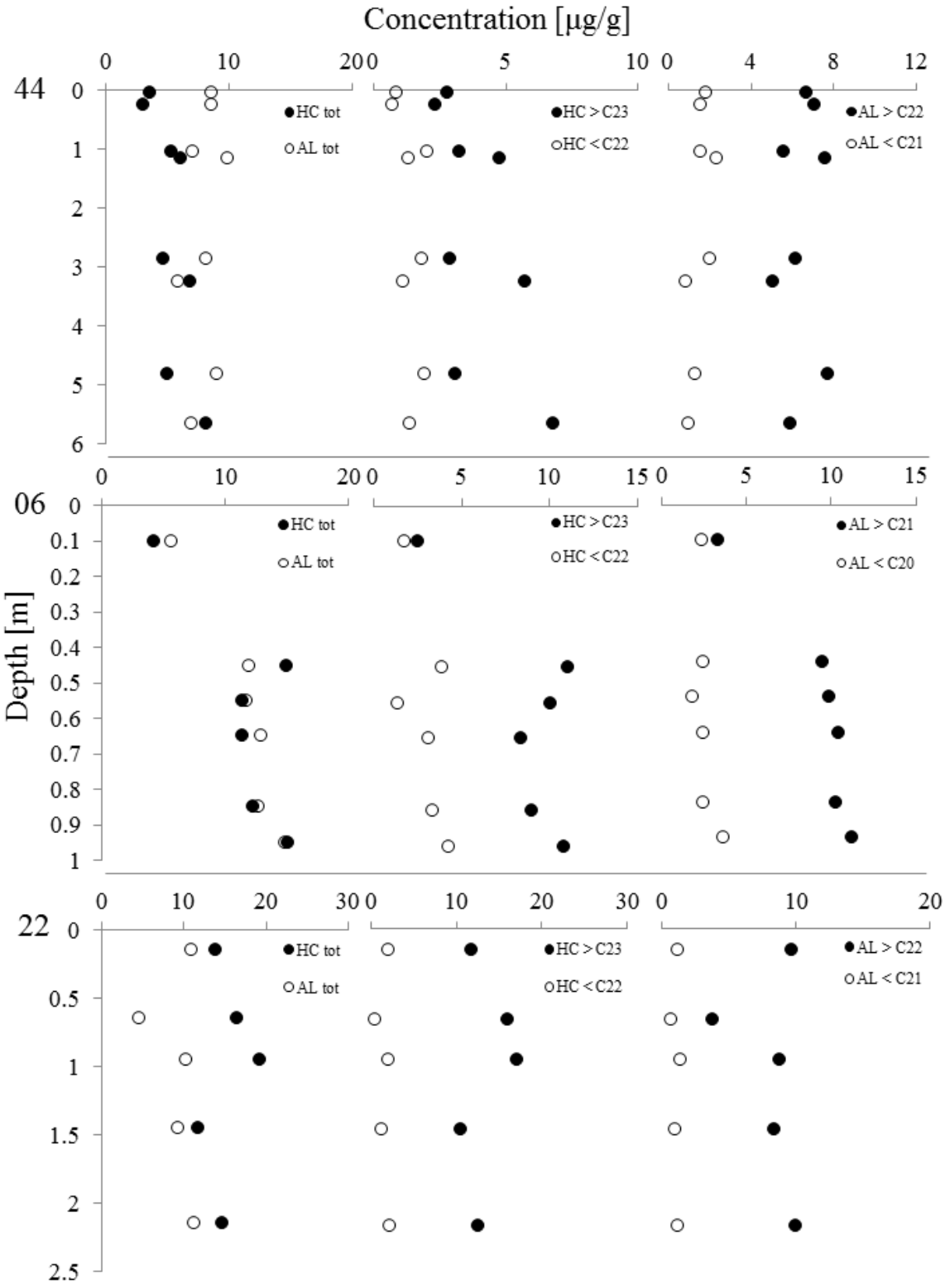

Figure 56. Down core profiles of n-alkanes and n-alkanols from stations 44 (top panel), 06 (middle panel) and 22 (bottom panel).

The above can possibly be explained by microbial mediated dehydroxylation as n-alkanols are considered relatively labile and less stable than other major lipids such as n-alakanes, alkenones, sterols or n-alkanoic acids (Cranwell, 1981).

Sterols

Sterol concentrations ranged from 2.76 μg/g to 7.37 μg/g with 5α-cholesta-5-en-3β-ol (cholesterol), 5α-cholesten-3β-ol (cholestanol), 24-methylcholesta-5,22-dien-3β-ol (brassicasterol), 4α,23,24-trimethyl-5α-cholesta-22-en-3β-ol (dinosterol) and (24-ethylcholesta-5-ene-3β-ol) β-sitosterol being the most abundant species. These major steroids comprised 34.9% to 50.4% of all sterols (mean 40.6%; n=9). Other abundant sterols included, cholesta-5,22-dien-3β-ol, 5β-cholesta-22-en-3β-ol, 24R-methylcholesta-5-en-3β-ol (campesterol) and 22E,24-ethylcholesta-5,22-dien-3β-ol (sito/stigmasterol). On average steroid compounds were more abundant in the southern stations (mean 6.05 μg/g; n=5) than in the northern ones (mean 3.06 μg/g; n=4) however the relative abundance of individual compounds varied only narrowly between stations indicating similar sources (Table 19). The stanol/sterol ratios varied from 0.2 to 1.2 with an average of 0.6. Sterol distributions in the Malin Shelf sediments represent mixed allochthonous and autochthonous sources. The average concentration of C27Δ5 ranged from 0.37 μg/g (n=4) in the north to 0.78 μg/g (n=5) in the south. In core 22 the concentration of this sterol decreased only slightly with depth (0.27 μg/g; n=4) while in the southern cores a more significant decrease was observed (0.44 μg/g; n=17) particularly in the deep horizons (0.25 μg/g; n=2). C27Δ5 (for all abbreviations see Table 19) is a major animal sterol, however it has also been reported in higher plants (Noda et al. 1998) and fungi (Weete, 1976) therefore accurate source ascription is challenging. In the marine environment C27Δ5 is usually attributed to zooplankton detritus (Belicka et al. 2002) however Volkman, 2003 points out that: "*(...) cholesterol is usually considered to be an animal sterol and yet it is surprisingly common in microalgae, and there are many examples where it is the major sterol present.*". For example marine eustigmatophytes produce C27Δ5 as their main sterol (Volkman et al. 1998) as well as many red algae such us those of the Rhodophyta genus (Beastall et al. 1971). Also certain species of diatoms are known to produce large amounts of C27Δ5 as shown by Barret et al. 1995 who studied 14 species or diatoms (Bacillariophyta) and found that one species produces C27Δ5 as a major sterol. Moreover Rampen et al. 2010 characterized 106 nonaxenic diatom species and found C27Δ5 as a major sterol in the radial centrics phylogenic group and certain species of raphid pennate diatoms. The C28Δ5.22 is very abundant in haptophytes, cryptophytes and other algae (Volkman, 2006). It is also considered a diatom biomarker being the major sterol in raphid and araphid pennates despite the fact that it is almost absent in the radial centrics and bi(multi) polar centrics (Rampen et al. 2010). C28Δ5.22 is also present in marine invertebrates, cyanobacteria and some higher plants (Goad and Akihisa, 1997) however the latter are not a likely source of this sterol in a marine setting. More algal input was observed in

the southern stations where C28Δ5.22 averaged 0.72 µg/g (n=5) in comparison to 0.27 µg/g (n=4) in the northern stations. A significant decrease in concentration was observed in all core samples. Core 22 averaged 0.14 µg/g (n=4) while in the southern core an average of 0.33 µg/g (n=16) was observed with some distinctive maxima in cores 44 and 45. C29Δ5 along with C28Δ5 and C29Δ5.22 are major sterols in many higher plants (Volkman, 1986). In estuarine and near-shore settings these sterols are indeed usually attributed to terrigenous sources; however as show by Butler et al. 2000 the importance of these sources decreases with increasing distance from landmass. This positive correlation suggests that in a shelf environment with limited fluvial input, such as the Malin Shelf, these major sterols might not be purely terrigenous in origin. Nevertheless the concentrations of these phytosterols decreased with increasing distance from the land mass which suggests that terrigenous matter is a significant source of these compounds on the Malin Shelf. On average all three species and their corresponding stanols (C28Δ0 and C29Δ0) ranged from 0.34 µg/g to 0.64 µg/g in the northern stations and from 0.71 µg/g to 1.11 µg/g in the southern ones. In all stations β-sitosterol (C29Δ5) was the dominant component and accounted for 46.6% to 69.2% in the northern stations and for 59.0% to 77.0% of all phytosterols. All of these compounds were fairly well preserved in the deeper horizons and have shown slight decreasing trends with local maxima particularly in the southern stations. C29Δ5 and C29Δ5.22 are abundant sterols found in many species of unicellular algae (Barrett et al. 1995). *Asterionella glacialis*, *Haslea ostrearia*, *Amphiprora hyaline* diatoms and *Olisthodiscus lutes* radiophyte are often cited examples (Volkman, 1986; Barrett et al. 1995; Patterson and Van Valkenburg, 1990). C29Δ5 is also a major sterol of many cyanobacteria (Paoletti et al. 1976). Algae, e.g. Chlorophyceae and Prasinophyceae as well as some marine invertebrates (Goad and Akihisa, 1997) contain significant quantities of C28Δ5 and possibly contribute to the sterol pool with terrigenous sources. C30Δ5 on the other hand is exclusively of marine origin and attributed to dinoflagellates (Volkmam, 1986) although there are a few species who produce other 4-methyl sterols instead (e.g. Kokke et al. 1981). Dinoflagellates were the main planktonic organism observed in the Malin Shelf waters by Gowen et al. 1998 thus high concentrations of C30Δ5 were expected. The northern surface sediments contained an average of 0.29 µg/g while in the southern sediments 0.66 µg/g was observed. However Gowen et al. 1998 reported that dominant species distribution had a clear geographic delineation with oceanographic parameters as controlling factors. Therefore changes in environmental conditions in last 15 years have most likely affected the phytoplankton composition and its distribution on the Malin Shelf. C26 sterols are more common in organisms higher in the food chain and are likely of dietary origin in organisms feeding on microalgae (Volkman, 2003). C27 sterols are believed to be the precursors, which are transformed possibly by demethylation of the side chain into the C26 species. Echinoderms (Asteroidea, Holothuroidea, Ophiuroidea and Echinoidea) were one example of the C26Δ5.22 sterol source (Goad et al. 1972) which was also identified in scallop *Placopecten magellanicus* (Idler et al. 1970).

			Stations								
Abbreviation	**Full name**	**Trivial name**	**25**	**24**	**22**	**20**	**27**	**44**	**6**	**45**	**7**
C26Δ5.22	22-*E*-5-nor-5α-cholest-5,22-dien-3β-ol	-	0.09	0.05	0.11	0.15	0.10	0.26	0.10	0.28	0.12
C26Δ22	5α-norcholesta-22-en-3β-ol	-	0.11	0.16	0.14	0.15	0.13	0.36	0.16	0.21	0.16
C27Δ5.22c	cholesta-5,22Z-dien-3β-ol	22-*cis*-dehydrocholesterol	0.10	0.11	0.12	0.17	0.22	0.18	0.22	0.43	0.15
C27Δ5.22t	cholesta-5,22E-dien-3β-ol	22-*trans*-dehydrocholesterol	0.18	0.17	0.30	0.21	0.30	0.43	0.48	0.17	0.16
C27Δ22	5α-cholesta-22-3β-ol	-	0.09	0.06	0.10	0.13	0.15	0.18	0.22	0.88	0.10
C27Δ5	cholest-5-en-3β-ol	cholesterol	0.39	0.30	0.39	0.40	0.73	0.71	0.94	0.71	0.66
C27Δ0	cholestan-3β-ol	cholestanol	0.23	0.12	0.11	0.27	0.52	0.51	0.50	0.60	0.57
C28Δ5.22	24-methyl-cholesta-5,22-dien-3β-ol	brassicasterol	0.29	0.20	0.45	0.16	0.81	0.69	1.13	0.32	0.35
C28Δ22	24-methyl-cholesta-22-en-3β-ol	-	0.14	0.14	0.19	0.15	0.29	0.26	0.36	0.35	0.20
C28Δ5.24(24^1)	24-methyl-cholesta-5,24(24^1)-dien-3β-ol	24-methylenecholesterol	0.23	0.17	0.07	0.31	0.32	0.34	0.41	0.30	0.27
C28Δ5*	24-methyl-cholest-5-en-3β-ol	campesterol	0.18	0.11	0.09	0.20	0.22	0.19	0.27	0.06	0.17
C28Δ0	24-methylcholestan-3β-ol	campestanol	0.11	0.12	0.00	0.12	0.13	0.16	0.18	0.17	0.09
C29Δ5.22	22-*E*-ethyl-cholesta-5,22-dien-3β-ol	stigmasterol	0.08	0.20	0.10	0.25	0.26	0.13	0.31	0.70	0.16
C29Δ5	24-ethyl-cholesta-5-en-3β-ol	β-sitosterol	0.32	0.37	0.23	0.30	0.51	0.55	0.62	0.40	0.60
C29Δ0	24-ethyl-cholestan-3β-ol	sito/stigmastanol	0.13	0.17	0.19	0.20	0.41	0.19	0.55	0.55	0.47
C30Δ5	4α-23,24-trimethyl-5α-cholesta-22-en-3β-ol	dinosterol	0.33	0.28	0.30	0.26	0.60	0.72	0.77	0.00	0.67
	fridelan-3-one	friedelin	0.09	0.05	0.11	0.15	0.10	0.26	0.10	0.28	0.12
C27 Δ0/Δ5	C27 stanol/sterol ratio		0.59	0.41	0.29	0.67	0.72	0.71	0.53	0.84	0.87
C28 Δ0/Δ5	C28 stanol/sterol ratio		0.40	0.45	0.84	0.68	0.79	0.35	0.89	1.37	0.78

Table 19. Concentrations of sterols and terpenoids in the neutral lipids fraction from the surface sediments on the Malin Shelf (μg/g). Notet that C28 Δ5 (*) coelutes with one of the alkyl diols and the data given are an estimation. Traces of four additional steroidal ketones were observed in all samples these were tentatively identified as: cholest-5-ene-24-one-3β-ol, cholesta-5,7-dien-7-one, 19-norcholesta-1,3,5(10)-trien-6-one and hydroxycholesta-5-ene-3β-ol. Moreover a total of six unidentified sterols were also observed: C26 diunsaturated (m/z: 111, 255, 285, 314, 351, 383, 398, 442), C26 monounsaturated (m/z: 253, 255, 269, 315, 339, 354, 366, 444), two C28 diunsaturated (m/z: 174, 255, 269, 296, 343, 380, 470 and 129, 133, 253, 283, 343, 365, 380, 470), C28 monounsaturated (m/z: 129, 255, 283, 331, 343, 370, 472), C29 monounsaturated (m/z: 257, 345, 374, 486) and three unidentified terpenoids (m/z: 189, 191, 203, 393, 410, 483, 496 and 189, 191, 205, 313, 342, 500 and 189, 203, 385, 424, 514).

The concentration of this sterol was the highest in the Ophiuroidea class which is divided into commonly known basket stars and brittle stars. The latter are very abundant benthic species in the north-western Atlantic, and are most likely the specific source of this sterol in the studied sediments. In the same study C26*Δ*22 was detected in a sterol mixture obtained from *Henricia sanguinolenta* species which is a large starfish also encountered in the study area. Interestingly this sterol was not observed in other studied Echinoderm classes. The C26*Δ*5.22 and C26*Δ*22 were also observed in a mixture of phytoplankton dominated by diatoms (mainly *Chaetoceros* sp.) and marine invertebrates (Boutry et al. 1971 and Bohlin et al. 1982 respectively). Bohlin et al. 1982 also suggested that C26*Δ*5.22 and C26*Δ*22 are suitable markers for marine, oxic conditions in the sediment. The concentration of these two sterols was similar in all stations and averaged 0.32 μg/g. Slightly higher values were observed in two vibrocores where both sterols were present in 0.61 μg/g and 0.53 μg/g (44 and 45 respectively). C27Δ5.22c and C27Δ5.22t were observed in all samples with the latter being slightly more abundant in most stations; both species are likely to be of marine origin, although they can originate from diverse marine biota sources. Both sterols together are rarely reported with only individual stereoisomers being commonly encountered in marine sediments. Kawashima et al. 2007 (and references within) reported both in tissues of marine bivalve *Megangulus zyonoensis* and among others scallops (e.g. *P. magellanicus*), clam (e.g. *Ruditapes decussatus*), mussels (e.g. *Mytilus edulis*) and oyster (e.g. *Ostrea edulis*). Volkman, 1986 reports that C27*Δ*5.22t is major sterol in some diatoms, notably commonly encountered *Biddulphia sinensis* where it can account for up to 82% of all sterols. Diatoms from the order Bacillariales such as *Cylindrotheca closterium* are known to produce C27*Δ*5.22 as major sterols (Barrett et al. 1995). Dinoflagellates also contain small amounts of the *trans* stereoisomer, notably *Gymnodinium wilczeki* (35% of total sterols). *Gymnodinium* spp. is commonly encountered in the Malin Shelf waters (Gowen et al. 1998). According to Gagosian et al. 1983 a sediment inventory of C27*Δ*5.22t could be derived from zooplankton faeces and moults. According to Hudson et al. 2001 the occurrence of C27*Δ*5.22 together with C28*Δ*5.24(24^1) is a good indicator of marine algal input in sediments. Mohammady, 2004 reported both of these sterols with the C28*Δ*5.24(24^1) being more abundant in commercially significant microalgal species. The C28*Δ*5.24(24^1) is a major sterol in many species of diatoms and was proposed by Rampen et al. 2010 and Volkman, 2006 as an alternative biomarker for this group of algae rather than the commonly cited C28*Δ*5.22. Notably, bi(multi) polar centrics, araphid pennates and radial centrics are known to produce C28*Δ*5.24(24^1) as the major sterol. Volkman, 2003 also gives the example of *Thalassiosira* and *Skeletonema* species as potential sources. C28*Δ*5.24(24^1) is also present in many pollens of many flowering plants, as well as in tissues of *Solanaceae* and in Chlorophyta green algae such as *Chaetomorpha aurea* (Goad and Akihisa, 1997). The source of the C27*Δ*22 and C28*Δ*22 is uncertain. The compounds have been reported in sediments and seawater (Volkman, 1986)

however the origin is not discussed in detail. Rampen et al. 2010 reported both sterols as a minor component of diatoms and Ingallas et al. 2004 mentioned them as components of muddy carbonate deposits. In this study the origin of these sterols is tentatively ascribed to phytoplankton sources, possibly diatoms as reported by Rampen et al. 2010 and Volkman, 1986. This conclusion is supported by the quantitative data as the concentrations of C28*Δ*22 follows the general trend of phytosterols, while C27*Δ*22 remains more constant across the entire study area, possibly representing a minor but widespread source. Other steroid compounds detected in the Malin Shelf sediments tentatively identified by the mass spectral library match are three steroidal ketones (cholest-5-ene-24-one-3β-ol, cholesta-5,7-dien-7-one, 19-norcholesta-1,3,5(10)-trien-6-one) and one steroidal diol (hydroxycholesta-5-ene-3β-ol). Steroidal ketones can be formed in a process of oxidation of the hydroxyl moiety in the molecule; however some native keto steroids, such 3-oxo steroids i.e., are minor constituent of various phytoplankton species (Volkman, 2006). Similarly steroidal diols have been reported as rare and unusual components of closely related Haptophta (genus *Pavlova*), however the hydroxyl group in the compound in question appears to be located in the side chain rather than at C3 as reported by Volkman et al. 1990. Schupfer et al. 2007 suggested that *Δ*5.7 sterols are the possible source of the 19-norcholesta-1,3,5(10)-trienes via catalytic backbone rearrangement. They also point out that photo/autoxidation of *Δ*5 sterols can lead to steratrienes. Based on these reports in this study these compounds are ascribed to diagenetic products of unidentified steroidal precursors. Similarly 5(α) stanols are thought to be the products of microbial reduction of corresponding *Δ*5 stenols (Wakeham, 1989 and Nishimura, 1982), however, they can also originate directly from dinoflagellates and some haptophytes (Volkman et al., 1998). Microbial reduction of *Δ*5 stenols is primarily an anaerobic process and in oxic conditions this transformation is not observed (Wakeham, 1989 and references within). Fresh organic matter with low inputs from natural stanol producers is characterized by low *Δ*0/*Δ*5 ratios. In the surface sediments of the Malin Shelf the average *Δ*0/*Δ*5 ratio was 0.61 (n=9) which suggests fresh, unaltered material and an oxygenated sediment surface (the opposite can occur in areas with unusually high organic matter load and in areas of active gas seepage, Schulz and Zabel, 2006). On the Malin shelf anoxic conditions are to be expected only in the longest (44 and 45) cores as the SMTZ is around 4 mbsf. In all cases *Δ*0/*Δ*5 gradually increased indicating microbial generation of stanols (Figure 57). This change is also visible in the 22 core; however it is not as profound as in the long cores. In this station the *Δ*0/*Δ*5 ratios at 2.4 mbsf were around unity (0.95 and 1.22 for C27 and C29 respectively), however the trend is clearly visible. Notably the overall increase in *Δ*0/*Δ*5 ratios in the two long cores indicates different dynamics in C27*Δ*0 formation. Although source sterols are present in similar concentrations throughout the core, C27 *Δ*0/*Δ*5 shows that in core 44 the C27*Δ*0 species is formed in smaller amounts than in core 45. The 45 core which is located directly on top of the large pockmark shows a gradual increase in all cases while the reference core only matches the trend for C29*Δ*5.

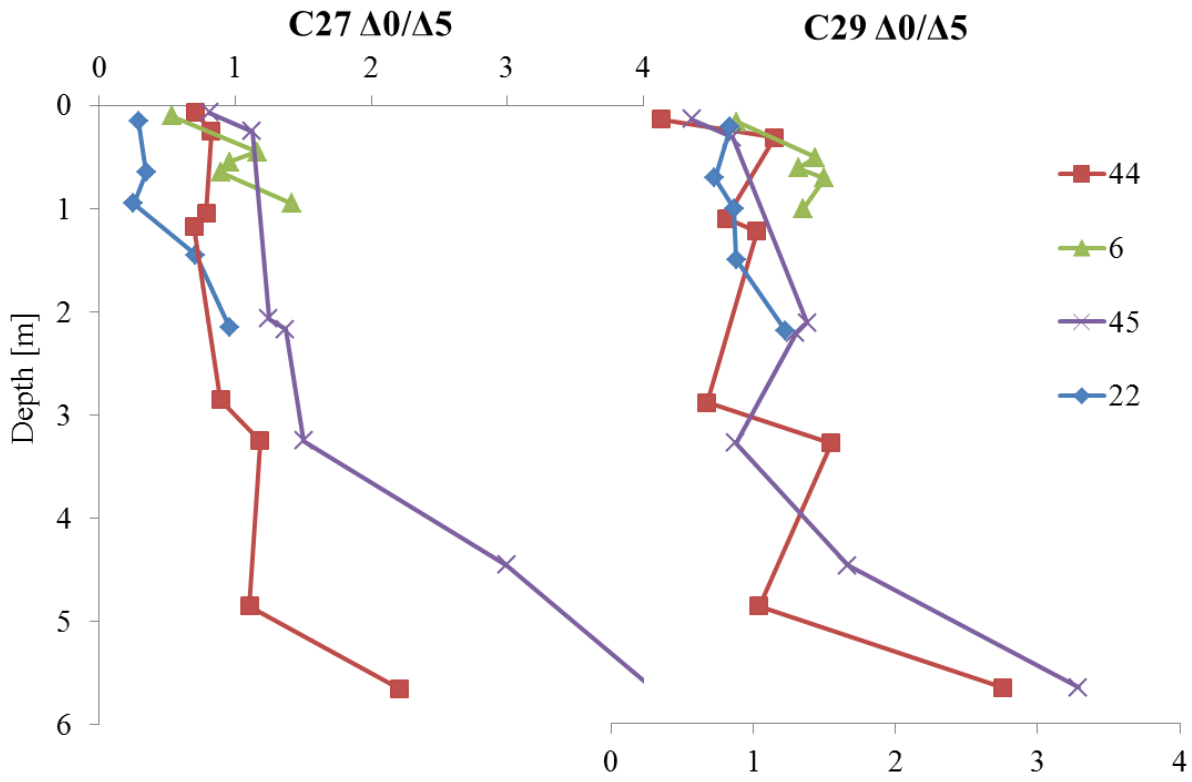

Figure 57. C27 and C29 stanol/stenol ratios for the sediment cores from the Malin Shelf.

The *Δ*0/*Δ*5 ratios for C28 show a similar trend in core 45 but surprisingly remain constant in core 44. Moreover in core 44 we observe a significant increase in C28 *Δ*0/*Δ*5 at 2.85 mbsf to a value of 3.7. This can be caused by changes in microbial populations in these two cores. O'Reilly et al. 2011 demonstrated that microbial populations can be very different in seepage or gas charged sites. Moreover the peak in C28 stanol at 2.85 mbsf coincides with a gas charged layer of sediment. This hypothesis is further supported by the NMR data which indicates significantly higher levels of microbial peptidoglycan observed in the reference core (see Chapter 3, section 3.3.2). It is not clear though why only C28 species demonstrated this anomalous behaviour. Overall the steroid pool represents a mixed input with predominance of marine sources. The comparison of the proportion of phytosterols (C28*Δ*5 C29*Δ*5.22 and C29*Δ*5) derived from higher plants to these derived from marine sources cannot be made without a higher sampling density and examination of the phytosterols relationship with TOC (Butler et al. 2000). Given these limitations in this study we assumed that the C29*Δ*5.22 and C29*Δ*5 represent mixed terrigenous (higher plants) and marine (phytoplankton) sources, while C28*Δ*5 is predominantly of terrigenous origin. Assuming a ratio of 1:1 (marine vs. terrigenous) for C29*Δ*5.22 and C29*Δ*5 terrigenous sterols accounted for 11.9% to 19.7% of total sterols in the northern stations (mean 16.7%, n=4) and 12.1% to 17.0% in the southern stations (mean 14.9%, n=5). The down core profiles have shown a general decrease in sterol concentration with depth (i.e. from 7.24 μg/g to 3.88 μg/g) except for core 45 where a slight increase was observed. This

trend was matched with an increase in the % of terrigenous sterols which agrees with the general notion of terrigenous organic matter being more recalcitrant than labile marine organic matter. The association of lipids with mineral and grain size phases and differences in the available bound lipids pool could also play a role in observed diagenetic pattern as shown by Jeng and Chen, 1995; Gonzalez et al. 1985 and others. The highest increase was observed in station 22 (from 11.9% to 27.4%) which also shows decrease in sterol count with many species being present in trace levels only. Southern stations exhibited a similar decrease (i.e. from 12.1% to 20.4% in 44 and from 14.8% to 19.8%).

Other biomarkers

Phytol was slightly more abundant in the northern stations (mean 0.94 μg/g; n=4) than in the southern ones (mean 0.44 μg/g; n=5). Various phytol degradation products were observed among which dehydrophytol (3,7,11,15-tetramethylhexadecan-1-ol) and C18 isoprenoid ketone (6,10,14-trimethylpentadecan-2-one) were the most abundant. Predominance of these products suggests that oxygen depletion is rapid in the Malin Shelf sediments as these compounds are a result of anaerobic microbial degradation (Sun et al. 1998). Phytol degradation products show an inverse relationship to the source alcohol, with more degradation products being observed in the southern stations (0.51 μg/g; n=5) than the northern ones (0.26 μg/g; n=4). This implies that in the southern stations phytoplankton might be slightly less abundant in the water column and that microbial activity in these sediments is higher than in the north of the Malin Shelf. This might be related to different physiochemical parameters of the water column. Differences in temperature, salinity, concentration of oxygen can influence plankton composition and its abundance. Moreover phytoplankton productivity varies seasonally (Gowen et al. 1998) which is reflected in lipid profiles (Carrie et al. 1998) thus more specific conclusions can only be drawn with time studies.

C28, C30 and C32 alkyl diols eluted as a mixture of isomers: 1,12-; 1,13-; 1,14- and 1,14-; 1,15-; 1,16- and 1,15- respectively, which is a common phenomenon under the chosen chromatographic conditions. Additionally C30 and C32 mid-chain keto-ols (1,15) were observed in most samples. Compounds were identified based on their fragmentation patterns and comparison with spectra published in the literature (Mejanelle et al. 2003; Versteegh et al. 1997; Versteegh et al. 2000 and Xu et al. 2007). These compounds are exclusively of marine origin and derive from marine algae from the class Eustigmatophyceae, genus *Nannochloropsis* (Volkman et al. 1992), from diatom genus *Proboscia* (Sinninghe Damste et al. 2003) and possibly other yet unidentified algal sources. Gelin, 1996 suggested that these compounds are intermediates or building blocks for highly aliphatic biopolymers produced by these organisms. Since their discovery various isomers were reported in different species of these algae and organisms feeding on them (Mejanelle et al. 2003). The 1,15-C30 isomer is usually the most

abundant in cultures, however Volkman et al. 1992 point out that distributions in source organisms differ significantly from those observed in sediments. Moreover the C28 isomers are usually not as abundant as C30. This is observed with the exception of station 6 where C28 isomers were slightly more concentrated than C30 (Table 20). Occurrences and concentration of these compounds varied significantly between northern and southern stations. Total alky-diols and keto-ols in the northern station ranged from 0.40 μg/g to 0.58 μg/g while in the southern stations they ranged from 1.32 μg/g to 1.87 μg/g. Moreover the concentration slightly decreased with depth in core 22 while it remained more constant in the remaining cores (6, 44 and 45) which suggest a more constant supply of phytoplankton.

Table 20. Concentrations of lipid classes in the neutral fraction from the surface sediment on the Malin Shelf. The lipid abbreviations are as follows: 6,10,14-trimethyl-pentadec-2-one (tri-Me-C15-2K), 6,10,14-trimethyl-pentadec-2-ol (tri-Me-C15-2OH), 4-hydroxyheptanoic acid gamma lacton (δ-C17-L), 3,7,11,15-tetramethyl-hexadecan-1-ol (tetra-Me-C16-1OH), heptacosan-2-one (C27-2K), nonocosan-2-one (C29-2K), mixture of C28 diols (C28 diols), mixture of C30 diols (C30 diols), triacontant-15-on-1-ol (C30-K15-1OH), dotriacontant-15-on-1-ol (C32-K15-1OH), dotriacontante-1,15-diol (C32-1,15-OH), monoacylglyceride and diacylglyceride with respective estrified fatty acid (MAG and DAG with Cx where x denotes fatty acid chain length).

	Stations								
Lipid	**25**	**24**	**22**	**20**	**27**	**44**	**6**	**45**	**7**
tri-Me-C_{15}-2K	0.17	0.22	0.14	0.01	0.42	0.33	0.41	0.33	0.26
tri-Me-C_{15}-2OH	0.02	0.02	0.02	0.02	tr.	nd.	nd.	nd.	tr.
δ-C17-L	0.05	0.06	0.04	0.03	0.17	0.16	0.36	0.15	0.19
tetra-Me-C_{16}-1OH	0.02	0.02	0.01	0.01	0.07	0.07	0.10	0.07	0.12
C_{27}-2K	0.22	0.21	0.18	0.19	n/a	n/a	n/a	n/a	n/a
C_{29}-2K	0.09	0.09	0.08	0.08	n/a	n/a	n/a	n/a	n/a
C_{28} diols	coel.	coel.	coel.	coel.	0.45	0.35	0.48	0.34	0.46
C_{30} diols	0.15	0.16	0.18	0.21	0.88	0.58	0.42	0.57	0.80
C_{30}-K15-1OH	0.25	0.22	0.15	0.26	0.26	0.22	0.29	0.22	0.28
C_{32}-K15-1OH	0.18	0.12	0.05	0.09	0.09	0.11	0.09	0.12	0.16
C_{32}-1,15-OH	tr.	tr.	0.02	tr.	0.14	0.13	0.04	0.13	0.17
MAG C16	tr.	0.17	0.16	0.17	0.17	0.12	0.27	0.12	0.16
MAG C17	0.08	0.08	0.07	0.07	tr.	nd.	0.14	nd.	tr.
MAG C18:1	tr.	tr.	tr.	tr.	tr.	nd.	0.04	nd.	tr.
MAG C18	0.03	0.03	0.02	0.03	0.03	0.28	0.08	0.26	0.03
DAG C16, C15	tr.	tr.	0.56	tr.	0.40	0.27	0.30	0.25	0.30

A series of odd chain n-alkane-2-ones spanning from C25 to C31 with the predominance of C27 and C29 was detected in the northern and southern stations. The concentration of the most abundant compounds ranged from 0.08 μg/g to 0.20 μg/g for C29 and C27 respectively. Unfortunately the quantitative data for the southern stations is not yet available, however, judging from the relative abundance they occur in similar quantities. The remaining n-alkan-2-ones were not quantified due to very low abundance and co-elution. The n-alken-2-ones are commonly reported in marine and lacustrine environments but were also observed in soils, glacier ice and paleosols, stalagmites, peats, aerosols and higher plants tissues

(e.g. Oyo-Ita et al. 2010; Zheng et al. 2011 and references within). The odd chain predominance with the maximum at C27 is typical for the *Sphagum* species which is widespread in Ireland and could potentially be transported onto the shelf with weathered terrigenous material (Zheng et al. 2001). Other likely terrigenous sources include weathered soils and plant debris (Zheng et al. 2011). Nevertheless the n-alkan-2-ones can also be of autochthonous origin. Hernandez et al. 2001 proposed these ketones as a marker for seagrass input, however C25 appears to be the dominant species in these organisms. Alternatively, due to similarities in the distribution of terrigenous n-alkanes and n-alkanoic acids, microbial oxidation of n-alkanes and/or β-oxidation of n-alkanoic acids followed by decarboxylation have been proposed as the in situ source of these compounds (Allen et al. 1971; Jaffe et al. 1993). Due to the relatively low abundance of these compounds such a comparison of distributions cannot be made and therefore a microbial source remains a possibility. Finally Qu et al. 1999 have shown that n-alkan-2-ones can originate from lacustrine cyanobacteria and microalgae; this finding is yet to be confirmed in marine microorganisms.

Mono and diacylglycerides are transformation products of triacyloglycerides which are major constituents of plant oils and animal fats (Harwood and Russel, 1984). The detected species were esterified with fatty acids ranging from C15 to C18 and overall were more abundant in the southern stations (Table 20).

3.3.1.2 Fatty acids

A diverse array of fatty acids (also referred to as n-alkanoic acids) was detected in three of the cores from the Malin Shelf. The fatty acid distribution included normal, unsaturated, methyl branched as well as isoprenoid species, α- and β-hydroxy, ω-hydroxy, (ω-1)-hydroxy. Two cholanic acids were also observed. Typical fatty acid distribution is given in Figure 58.

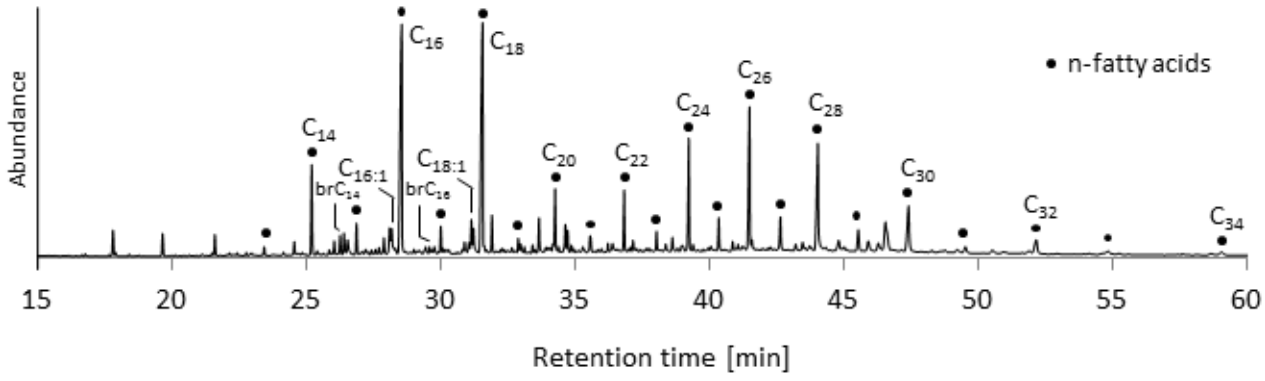

Figure 58. Representative EIC (m/z 74) of fatty acid fraction.

In general concentrations of most fatty acid classes were visibly higher in the southern stations; however more specific conclusions can only be made when a full data set is available. The total fatty content ranged from 8.43 μg/g in station 22 to 21.19 μg/g in the station 44 (Table 21).

Normal saturated fatty acids ranged from C12 to C34 and exhibited strong even-over-odd predominance in all cases. CPI_{FA} calculated over the range C21-C31 was slightly lower in the northern station than in the south (7.7 and 9.1 respectively). The distributions were bimodal with the first maximum at C16 and C18 and second at C26. Short chain fatty acid (SCFA, < C20) distributions were dominated by C16 and C18, however these compounds were observed in some of the process blanks therefore their contribution, particularly C18 might be overestimated. Fatty acids of diatoms and some microalgae (e.g. Chlorophyta) are known to contain a high content of C16 (Mayzaud et al. 1989) while most dinoflagellates contain significant quantities of C18 (Colombo et al. 1996).

Table 21. Concentrations of acidic lipid biomarkers in the surface sediments of the Malin Shelf and selected molecular descriptors. Samples marked with n/a were analysed but not integrated thus quantitative data is not available. Carbon Preference Index was calculated according to: $CPI_{FA} = \frac{1}{2} \times \left(\frac{C22+C24+C26+C28+C30}{C21+C23+C25+C27+C29}\right) + \frac{C22+C24+C26+C28+C30}{C23+C25+C27+C29+C31}$, (Eglinton and Hamilton, 1967); Average Chain Length index was calculated according to $ACL_{HC} = \frac{23\times C23+25\times C25+27\times C27+29\times C29+31\times C31+33\times C33}{C23+C25+C27+C29+C31+C33}$ and $ACL_{AL} = \frac{24\times C24+25\times C25+27\times C27+28\times C28+29\times C29+30\times C30+31\times C31+32\times C32+33\times C33+34\times C34}{C24+C25+C26+C27+C28+C29+C30+C31+C32+C33+C34}$, (Eglinton and Hamilton, 1967).

	Stations									
	25	**24**	**22**	**20**	**27**	**44**	**6**	**45**	**7**	**Mean ± S.D.**
Lipid class										
n-fatty acids										
C12-C20	n/a	n/a	3.45	n/a	n/a	5.89	6.16	n/a	n/a	5.17±1.49
C21-C34	n/a	n/a	3.04	n/a	n/a	8.21	3.19	n/a	n/a	4.81±2.94
$\Sigma_{n\text{-FA}}$	n/a	n/a	6.49	n/a	n/a	14.10	9.35	n/a	n/a	9.98±3.84
iso-FA	n/a	n/a	0.24	n/a	n/a	0.62	0.53	n/a	n/a	0.46±0.20
anteiso-FA	n/a	n/a	0.16	n/a	n/a	0.39	0.39	n/a	n/a	0.31±0.13
isoprenoid-FA	n/a	n/a	0.20	n/a	n/a	0.42	0.36	n/a	n/a	0.33±0.12
$\boldsymbol{\Sigma_{branched\text{-}FA}}$	n/a	n/a	0.64	n/a	n/a	1.53	1.39	n/a	n/a	1.19±0.48
MUFA	n/a	n/a	0.59	n/a	n/a	2.79	2.60	n/a	n/a	1.99±1.22
α,β FA	n/a	n/a	0.14	n/a	n/a	1.01	0.36	n/a	n/a	0.51±0.45
(ω-1) FA	n/a	n/a	0.13	n/a	n/a	0.20	0.12	n/a	n/a	0.15±0.04
ω FA	n/a	n/a	0.38	n/a	n/a	1.10	0.59	n/a	n/a	0.69±0.37
$\Sigma_{OH\text{-}FA}$	n/a	n/a	0.71	n/a	n/a	2.78	1.50	n/a	n/a	1.66±1.04
Σ_{FA}	n/a	n/a	8.43	n/a	n/a	21.19	14.84	n/a	n/a	14.82±6.38
Indices										
CPI_{FA}	n/a	n/a	7.7	n/a	n/a	9.2	9.0	n/a	n/a	8.65±0.80
ACL_{FA}	n/a	n/a	27.0	n/a	n/a	28.4	26.6	n/a	n/a	27.31±0.94

Overall however, SCFA are ubiquitous in both terrigenous and marine environments, in a marine setting though they are usually attributed to unspecified autochthonous sources (Cranwell, 1982). The SCFA accounted for 41.7% to 65.9% of total fatty acids. The concentration of SCFA remained constant with minor minima and maxima observed in all cores (Figure). Their overall contribution to the fatty acid pool decreased in cores 22 and 6 to 40.3% and 39.4% respectively. In core 44 a slightly opposite trend was observed with an increase to 48.5%. The long chain fatty acids (LCFA, >C21) ranged from 3.04 μg/g to 14.10 μg/g and on

average were abundant in the southern stations. The LCFA with even-over-odd predominance are typical markers for the presence of organic matter derived from epicuticular plant waxes (Eglinton and Hamilton, 1967), however a minor contribution from microalgae and bacteria is possible (Volkman et al. 1989; Eglinton and Hamilton, 1967). Typically odd chain SCFA are known to be abundant in bacteria (Gillan and Hogg, 1984). The isotopic signature of the major LCFA ranged from -27.7‰ to -28.1‰ (from C20 to C28 respectively), which is typical for predominantly terrigenous sources (Peterson and Fry, 1987). Concentrations of LCFA generally increased with depth in stations 22 and 6 (8.36 μg/g; n=4 and 7.60 μg/g; n=4 respectively) and slightly decreased in station 44 (6.35 μg/g; n=4). Profiles are given in Figure 59. Several monounsaturated fatty acids (MUFA) were observed in all stations and one diunsaturated fatty acid (C18:2) was detected in the deeper horizons of core 6. The concentration of MUFA ranged from 0.59 μg/g to 2.79 μg/g in the southern cores (Table 21). MUFAs were not a major component of the fatty acid pool and comprised 7.0% and from 12.6% to 18.8% in the northern and southern stations, respectively (22, 6 and 44, respectively).The concentration of MUFAs show no significant changed with depth and in station 22 core vary from 0.59 μg/g to 1.14 μg/g (n=4) and a decrease in the southern stations from 2.60 μg/g to 2.13 μg/g (n=4) and from 2.78 μg/g to 0.47 μg/g (n=4; 6 and 44 respectively). Profiles of down core trends are shown in Figure 59. In general these compounds act as cell membrane components in many organisms including plants, phytoplankton and bacteria therefore accurate source determination is challenging and most likely a mixed input is observed (Cranwell, 1982). Carrie et al. 1998 discussed the sources of fatty acids in the surface sediment of the Hebridean Shelf break approximately 90 km north from the study area. They attributed MUFA as mainly of microbial, phyto and zooplankton sources. Interestingly though they did not observe any LCFA >C24 and concluded that terrigenous input is limited.

Branched fatty acids ranged from 0.64 μg/g to 1.46 μg/g; n=2 in the northern and southern station respectively. All branched fatty acids were more abundant in the southern stations (Table 7). Down core profiles of total branched fatty acids are shown in Figure. Methyl branched fatty acids were dominated by *iso* and *anteiso* types with the first being more abundant in all stations (0.24 μg/g in the 22 and 0.57 μg/g; n=2 in the 44 and 6). Specifically *i*-C12, *ai*-C12, *i*-C13, *i*-C14, *ai*-C14, *i*-C15, *i*-C16, *ai*-C16 were detected among which *i*-C14 and *ai*-C14 were most abundant in all stations (from 0.18 μg/g, n=2 in 22 to 0.52 μg/g, n=4 in 44 and 6). Additionally two other methyl branched fatty acids were observed, however the location of the Me group was not determined due to very low abundance and poor spectrum quality. These two fatty acids eluted before the *iso* and *anteiso* isomers therefore mid chain branching is likely (Christie, 1989). Terminally methyl branched fatty acids (both *iso* and *anteiso*) are known to be present in elevated concentrations in bacterial biomass however they are not taxa specific (Perry et al. 1979). Other organisms rarely produce terminal branched fatty acids however in the

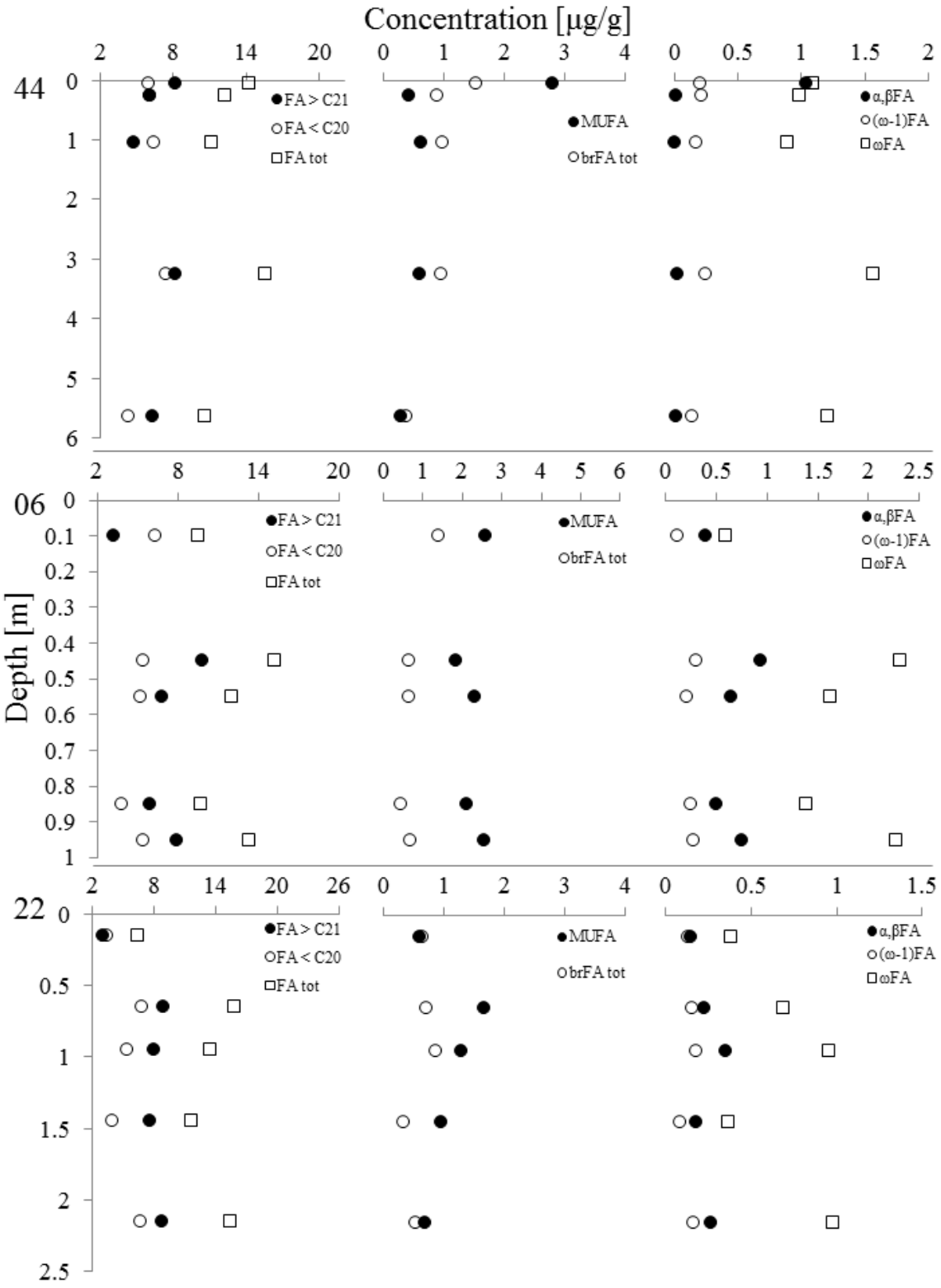

Figure 59. Down core profiles of normal saturated, unsaturated, branched and hydroxylated fatty acids from stations 44 (top panel), 06 (middle panel) and 22 (bottom panel).

marine environment they are often a dietary component of benthic biota (Christie, 1989). Four isoprenoid fatty acids were detected namely 3,7,15-trimethyldodecanoic acid (tri-Me-C12), 4,8,12-trimethyltridecanoic acid (tri-Me-C13), 5,9,13-trimethyltetradecanoic acid (tri-Me-C14), 3,17,11,15-tetramethyltetradecanoic acid (tetra-Me-C14 or phytanic acid) and traces of 6.10.14-

trimethylpentadecan-2-one. These compounds are products of microbial degradation of phytol, the chlorophyll *a* side chain alcohol (Rontani et al. 1999). The concentration of these isoprenoid fatty acids varied from 0.15 μg/g in station 22 to 0.20 μg/g in southern stations. This trend is in agreement with the previously discussed hydroxy- degradation products of phytol. Down core phytol degradation products show little variability and on average were observed in similar concentrations (i.e. 0.18 μg/g, 0.12 μg/g and 0.11 μg/g in the 22, 6 and 44 respectively). This suggests constant degradation of free, available phytol by microorganisms and abiotic mechanisms such as hydrolysis of phytol photoxidation products (Rontani and Grossi, 1995). Additionally 4,8,12,16-tetramethylheptadecan-4-olide and 4,8,12,16-tetramethyl-4-methoxyheptadecanoic acid were detected. The origin of the latter compound is uncertain as it has not so far been reported in the literature, however Rontani et al. 2007 suggested that the 4,8,12,16-tetramethylheptadecan-4-olide can potentially be an autoxidation (via radical pathways) product of α-tocopherol (vitamin E). Similarity in structure of the 4,8,12,16-tetramethyl-4-methoxyheptadecanoic acid with the γ-lactone derived from tocopherol suggests that this compound might be derived from the same source but not necessarily in a similar process. Concentrations of these compounds ranged from 0.07 μg/g in station 22 (slight increase in concentration down core – 0.09 μg/g; n=4) to 0.20 μg/g and 0.24 μg/g (slight depletion down core 0.06 μg/g; n=4 and 0.14 μg/g; n=4, 06 and 44, respectively).

Hydroxy fatty acids observed in the Malin Shelf cores can be divided into four groups: the α-hydroxy fatty acids, β-hydroxy fatty acids (α,β-FA), ω-hydroxy fatty acids (ω-FA) and (ω-1)-hydroxy fatty acids [(ω-1)-FA]. Additionally six methyl branched β-FAs *iso* and *anteiso* C12 (M+-15; m/z 301), C14 (M+-15; m/z 329) and C16 (M+-15; m/z 357) were observed. Interestingly these fatty acids appear to be identified as C13, C15, C17 in the literature (e.g. Skerratt et al. 1992) which is sometimes a problem encountered when reporting methyl branched fatty acids with some authors reporting chain length and other carbon number (Christie, 1989). The spectrum of methyl branched β-FA is indistinguishable to that of normal β-FAs and these compounds were identified based on their retention times as described by Boon et al. 1977a. Further analysis of actual standards (which were not available at the time of analysis) should be performed to confirm the identity of these two groups of compounds. α,β-FA quantities are given cumulatively as they are known to coelute even in an high resolution chromatographic columns (Volkman, et al. 1999). The relative proportion of the α-FAs and β-FAs are estimated based on their characteristic signals of the mass spectra (m/z 175 for β-FAs and M^+-15 for α-FAs) as described by Volkman, et al. 1999. In all stations ω-FAs were the dominant species and accounted for 50.1% and 39.1% and 39.5% (22, 6 and 44 respectively) followed by α,β-FAs accounting for 20.3% and 24.2% and 36.5% (22, 6 and 44 respectively) and (ω-1)-FAs accounting for 18.8% and 7.8% and 7.2% (22, 6 and 44 respectively) of all monohydroxy fatty acids (Table 21). The ω-FAs ranged from C14 to C30 and had a visible

even-over-odd predominance. The short chain (C14 to C20) ω-FAs had a higher content of the odd chain species while in the long chain series the odd chain species were observed only in trace amounts or were not detected at all. The concentration of these compounds increased with depth in all cores from 0.38 μg/g to 0.75 μg/g in station 22, from 0.59 μg/g to 1.90 μg/g and from 1.1 μg/g to 1.4 μg/g in stations 6 and 44 respectively (Figure 59). ω-FAs can be of both allochthonous and autochthonous sources. Kolattukudy, 1980 has shown that ω-FAs particularly C16-18 are an abundant constituent of plant cutin, while C16-C22 are abundant in suberin. ω-FAs can also partially be generated *in situ* by terminal microbially, and/or chemically, mediated oxidation processes (Boon et al. 1977a). Other potential sources for the long chain ω-FA is the detritus of the seagrass *Zostera* (Volkman et al. 1980). This is a widespread species of seagrass in the northwestern Atlantic, however it was not observed during video tows. Nevertheless organic detritus can potentially be transported on to the shelf by bottom currents. The α,β-FA distributions were dominated by β-FAs in the range C10 to C20 and α-FAs were the dominant components in the range C22 to C26. The α,β-FA also exhibited even-over-odd predominance with the odd chain species present in trace amounts only identifiable in the extracted ion chromatograms (m/z 175). The concentrations of normal α,β-FAs in surface samples are given in Table 7. The amounts of α,β-FAs increased down core from 0.14 μg/g to 0.25 μg/g and 0.36 μg/g to 0.69 μg/g in stations 22 and 6 respectively (Figure 59). In core 44 surprisingly only the surface samples contained appreciable amounts of the normal α,β-FAs. The *iso* and *anteiso* β-FA co-eluted with the other components and because of low concentrations quantification was not possible. Nevertheless down core profiles of these fatty acids have shown a significant increase in abundance. The α- and β-FAs are commonly encountered in marine, lacustrine and estuarine sediments (Fukushima et al. 1992a; Fukushima et al. 1992b). They are known metabolic and biosynthetic intermediates in α- and β-oxidation of normal saturated fatty acids by various organisms including plants, animals and bacteria (Volkman et al. 1999). However Boon et al. 1977a pointed out that in such enzymatically catalysed processes intermediates are short lived and therefore such processes are unlikely to be a significant source of the α,β-FAs. They also suggested that organisms living in the oxic water column are a potential source of short chain (<C20) α-FAs while the higher homologs with distribution maxima at C24 and C26 can be derived from plant material. The short chain α-FAs along with ω-FAs have been observed in *Zostera* seagrass (Volkman et al. 1980). Both α-FAs and β-FAs were observed in eustigmatophytes and yeast (Volkman et al. 1999; Fulco, 1967) but in general these fatty acids are rarely reported in microalgae except in Chlorophytes which produce cell walls with α-FAs as major components (Volkman, 2006). The short chain (C10-C18) β-FAs are unique structural components of the liposaccharide endotoxin, lipid A, characteristic of Gram-negative bacteria cell walls (de Leeuw et al. 1995) such as *Rhodobacter* spp. (Kaltashov et al. 1997) as well as *Thiobacillus* spp. (Kerger et al. 1987) and *Bacillus* spp. (Findlay and White, 1983). The methyl branched β-FAs ranging from C15 to C18 were observed in a marine bacterium *Desulfovibrio*

desulfuricans which is a common sulphate reducing bacterium (Boon et al. 1977b; Edlund et al. 1985). The C15 and C17 were the predominant β-FAs observed in this species, and thus detected β-FAs might originate from this or similar organisms. Interestingly *Desulfovibrio* spp. is an obligatory anaerobe thus abundance increase with depth as observed in the sediment cores is expected. Also (ω-1)-FAs have been observed in bacteria and cyanobacteria, however the exact source of these compounds in marine and lacustrine sediments is unclear. Abreu-Grobois et al. 1977 observed C26 species in *Anabaena cylindrical* and de Leeuw et al. 1992 detected the same compound in *Aphanizomenon flos-aquae*. Interestingly Skerrat et al. 1992 demonstrated C24, C26 and C30 (ω-1)-FAs in type I and II methanotrophic bacteria, although type II appeared to produce higher amounts of (ω-1)-FAs. Detected (ω-1)-FAs ranged from C16 to C30 with maxima at C24, C26 and C30 with only even chain species observed. The concentration of these fatty acids ranged from 0.13 μg/g to 0.12 μg/g and 0.20 μg/g. Down core profiles of (ω-1)-FAs show little variability and no significant increase in abundance of C26, C28 and C30 (ω-1)-Fas, potentially associated with methanotrophic bacteria, was observed. Overall the concentration of these fatty acids increased with depth in the pockmark region (from 0.12 μg/g to 0.26 μg/g and from 0.20 μg/g to 0.25 μg/g stations 6 and 44) and remained constant in station 22 (0.14 μg/g; n=4). A general increasing trend is expected as *in situ* methane generation occurs only past the sulphate depletion zone and in anaerobic microcosms above that zone. Assuming that (ω-1)-FAs are indeed associated with methanotrophic bacteria it is at first surprising that no increase in (ω-1)-FAs concentration is observed in gas charged sediment. Although aerobic and anaerobic methanotrophic bacteria have been cultured it is known that these types of organisms, particularly the anaerobic ones, grow slowly especially in conditions of nutrient deprivation which are common in natural environments (Hanson and Hanson, 1996). The timing of gas migration is unknown just as the exact conditions that occur in the sediment when pore fluid is displaced by moving gas fronts. Such conditions might not be appropriate for methanotrophic bacteria to thrive despite a surplus of their primary carbon source. Moreover the gas residence might have been too short to have an effect on slow growing communities or the methanotrophic bacteria were not present above in sufficient numbers.

Three cholic acids were also observed: 3α-hydroxycholan-24-oic acid, 5β-hydroxycholan-3-one-24-oic acid and 25-methyl-3α-hydroxy-5β-cholan-24-oic acid. The 3-keto cholic acid was the most abundant in all stations and ranged from 0.15 μg/g to 0.11 μg/g and 0.13 μg/g (22, 6 and 44 respectively). The 25 methyl cholic acid was only observed in small quantities in the deeper sections of core 44 (0.06 μg/g; n=4). The concentration of the 3α cholic acid decreased with depth in core 22 (0.03 μg/g; n=4) and this compound was only observed in trace amounts in core 6. Microbial oxidation of sterols was proposed as a possible source of these compounds in sediments (Smith, 1981 and references within).

3.3.1.3 Ester bound lipids

The bound lipid inventory represents input from mineral bound and to a lesser extent macromolecular species. Ester bound phospholipids and glycolipids partially contribute to this group, however lipids bound by amide and ether bonds are not released in the alkaline saponification procedure. These bonds are readily hydrolysed in acidic conditions. Biological and geological polymers and macromolecules such as lipopolysaccharides or humic and fulvic acids or kerogen will contribute to this group only with ester linked lipids. Microorganisms in marine environments are not motile and dwell on the surface of minerals as well as in the cavities of clays. They can form lipid films bound to mineral surfaces or in between clay layers (e.g. Hao et al. 2006 and Lu et al. 2010). Alkaline hydrolysis permits the release of such ester linked lipid components (Leenheer et al. 1984). Thus bound lipids can also represent input from lipids incorporated in geopolymers, and to a limited extent microbial material protected by clays. Mineral adsorption and protection can limit the possibility of microbial mineralization thus bound lipids tend to be better preserved in oxic conditions than free (or solvent extractable) lipids (Didyk et al. 1977).

Fatty acids

The bound lipid fractions consisted of several classes of compounds. The average bound lipid content on the Malin Shelf was 42.56 µg/g, which is comparable to the solvent extractable lipids 43.35 µg/g. Total bound lipids ranged from 35.83 µg/g in the northern 22 core to an average of 44.81 µg/g (n=3) in the southern stations. The bound lipids content was visibly higher in stations 44 and 45 (Table 22). Normal fatty acids and sterols were the dominant classes and accounted from 41.1% to 67.0% in the northern and southern stations respectively (mean 50.7%; n=3). The normal fatty acids exhibited bimodal distribution with strong even-over-odd predominance and ranged from C12 to C34 with maxima at C16, C18 and C24 similar to the free fatty acids (Figure 60). The FAs above C28 co-eluted with abundant sterols thus this end of the distribution was not always preserved in the surface samples where sterols were the dominant lipid class.

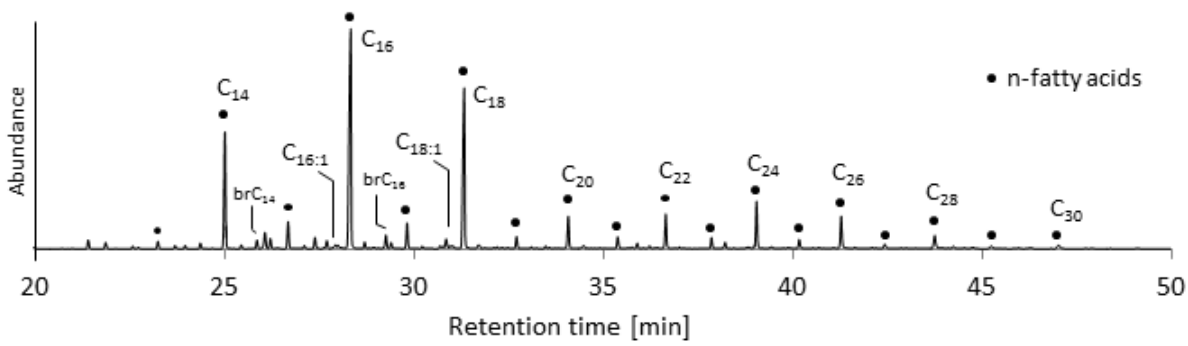

Figure 60. Representative gas chromatogram (EIC; m/z 74) of bound lipids acids.

Free fatty acids have shown balanced distributions with similar contributions from SCFA and LCFA. This type of distribution was also observed in the bound fatty acid fractions in stations 44 and 45 while remaining stations have shown clear domination of SCFA over the LCFA. Interestingly in all stations SCFA dominated with C16 and C18 and contributed from 56.5 to 85.3% and from 24.4 to 69.7% of all SCFA and all n-FA respectively.

Table 22. Concentrations of bound lipid classes from the surface sediment on the Malin Shelf. Samples marked with n/a were analysed but not integrated thus quantitative data is not available.

	Stations									
Lipid class	**25**	**24**	**22**	**20**	**27**	**44**	**6**	**45**	**7**	**Mean ± S.D.**
Fatty acids										
C12-C20	n/a	n/a	8.60	n/a	n/a	9.26	9.18	7.20	n/a	8.56±0.95
C21-C34	n/a	n/a	2.88	n/a	n/a	9.47	1.19	7.42	n/a	5.24±3.86
MUFA	n/a	n/a	1.69	n/a	n/a	2.74	0.86	2.85	n/a	2.04±0.94
$\Sigma_{n\text{-}FA}$	n/a	n/a	11.47	n/a	n/a	18.73	10.37	14.62	n/a	13.80±3.74
α,β OH	n/a	n/a	2.67	n/a	n/a	5.92	1.11	4.95	n/a	4.16±2.96
ω OH	n/a	n/a	2.72	n/a	n/a	6.23	0.66	4.23	n/a	3.46±2.35
(ω-1) OH	n/a	n/a	0.33	n/a	n/a	1.10	0.09	0.72	n/a	0.56±0.44
$\Sigma_{OH\text{-}FA}$	n/a	n/a	5.72	n/a	n/a	15.25	1.86	9.89	n/a	8.18±5.74
$\Sigma_{iso\text{-}FA}$	n/a	n/a	0.75	n/a	n/a	0.33	0.22	0.31	n/a	0.40±0.24
$\Sigma_{anteiso\text{-}FA}$	n/a	n/a	0.12	n/a	n/a	0.42	0.23	0.22	n/a	0.25±0.13
$\Sigma_{isoprenoid\text{-}FA}$	n/a	n/a	0.91	n/a	n/a	0.70	1.59	0.46	n/a	0.91±0.48
$\Sigma_{branched\text{-}FA}$	n/a	n/a	1.78	n/a	n/a	1.46	2.04	0.99	n/a	1.57±0.45
α,ω FA	n/a	n/a	1.57	n/a	n/a	1.09	0.14	0.87	n/a	0.92±0.59
n-alkanols										
$\Sigma_{n\text{-}OH}$	n/a	n/a	3.05	n/a	n/a	8.84	4.33	7.49	n/a	5.92±2.69
Phenols										
$\Sigma_{Phenols}$	n/a	n/a	0.57	n/a	n/a	0.55	0.00	0.64	n/a	0.44±0.29
Sterols										
$\Sigma_{sterols}$	n/a	n/a	3.26	n/a	n/a	8.28	8.73	8.50	n/a	7.19±2.63
$\Sigma_{bound\ lipids}$	n/a	n/a	35.83	n/a	n/a	58.56	28.49	47.37	n/a	42.56±13.19

The relative contribution of these two groups to the free and bound lipids pool did not change significantly with depth. This suggests that at least in some stations terrigenous fatty acids are possibly not associated with macromolecules, enter the shelf sediments degraded and remain in free form rather than being incorporated into geopolymers. This is expected in a shelf setting where terrigenous lipid sources are limited and autochthonous input is significant. Stations 44 and 45 show significantly different proportion of terrigenous fatty acid incorporated to the bound lipid pool, this might be source related but also reflect the dynamic of diagenetic processes. Bound MUFA and *iso* and *anteiso* FAs that are associated with microbial sources have shown similar contributions to their free counterparts. Bound MUFA ranged from 0.86 μg/g to 2.74 μg/g in the surface sediment (22 and 44 respectively) and shown little variation down core with average concentration values ranging from 0.98± 0.31 μg/g to 1.08±0.23 μg/g. Methyl branched FAs ranged from 045 μg/g to 0.87 μg/g (6 and 22 respectively) and also shown little variability down core. The hydroxy fatty acids were detected in significantly higher

concentrations in the bound lipid pool. Notably the α,β-FAs were as abundant as the ω-FAs which were the dominant hydroxy fatty acid in the free lipids pool (Table 22). In surface samples concentrations of α,β-FAs ranged from 1.11 μg/g in the northern stations to 2.67 μg/g and 5.92 μg/g in the southern ones (22 and 44 respectively). This is in contrast to the barely detectable free α,β-FAs. Interestingly down core initial decrease in concentration in the first 0.7 m of the sediment (to 0.57 μg/g in station 22 and 1.20 μg/g; n=2, in 44 and 6) is matched, however not quantitatively, in the increase of free α,β-FAs. In the lower sections of the cores the bound α,β-FAs increased in abundance (to 1.97 μg/g, 1.72 μg/g and 4.95 μg/g; 22,6 and 44 respectively). A possible explanation is that α,β-FAs in the Malin Shelf sediment represents mixed inputs. Those deposited on surface sediments originate predominantly from the water column with lesser terrigenous input, and are deposited in a conjugated, bound form. Such detritus is a perfect energy source for the benthic food web which gradually release α,β-FAs to the free lipids inventory. Obviously a large portion of organic matter from detritus is completely mineralized through a series of trophic levels thus a non-quantitative relationship is expected. The increase in concentration in deeper sections of the cores can be explained by the contribution from microbial sources, past records of increased productivity of the water column or burial of terrigenous matter. The increase in productivity resulting in increased flux of detritus to the seabed would possibly be also recorded in other planktonic biomarkers such as sterols but is not observed. However to fully discount such an eventuality higher resolution biomarker analysis should be performed. Moreover the sediment is a Holocene record and no significant paleooceanographic changes are known to occur in that period of time. The last explanation appears to be plausible only for station 22 where a shift in distribution from short chain β-FAs toward α-FAs with prominent maxima in C24 and C26 (0.39 μg/g and 0.29 μg/g respectively) is observed. In core 22 the contribution of short chain β-FAs decreases from an initial 60.2% to 39.8% at 1.4 mbsf and 41.6% at 2.4 mbsf, while in the southern stations it increases gradually with depth from 67% to 73% and from 38.7% to 61.7% (6 and 44, respectively). Thus microbial contribution in the absence of significant paleoceanographic signals and past seems the most plausible explanation for the increased β-FAs content. The ω-FAs observed in the bound fraction ranged from C8 to C30 and similarly as with the free ω-FAs the short chain species have shown little or no predominance toward even chain length, while the long chain ω-FAs were almost exclusively even chain ones. The concentration ranged from 0.66 μg/g to 6.23 μg/g in the southern (6 and 44 respectively) stations and 2.72 μg/g in the north (station 22) and were higher than in the free lipids (Table 18). Higher concentrations of these fatty acids are expected in bound fractions as the source macromolecules (i.e. cutin and suberin) are cross-linked biopolymers that are known to be resistant to oxidation and microbial enzymatic attack (Killops and Killops, 2009). The ω-Fas appear to be partially liberated from the bound fraction, particularly in the superficial sediments where a slight decrease in concentration is observed (0.78 μg/g and 1.27 μg/g in 22 and 44, respectively) matched with

increase in free fraction (0.96 μg/g and 0.89 μg/g in 22 and 44, respectively) and followed by an increase in deeper layers (1.52 μg/g and 4.23 μg/g in 6 and 44, respectively). Interestingly in core 6, the majority of ω-FAs is present in the free form contrary to what is observed in core 44. The exchange between the bound and free lipid pool of these compounds can represent both humification processes as well as diagenesis of parent material which, due to its recalcitrant nature, could have reached the shelf relatively unaltered. The origin of C8-C14 ω-FAs remains uncertain, terminal hydroxy fatty acids with such short chains have not been reported in the literature. Microbial oxidation followed by another degradation process or complete microbial oxidative cleavage of the mid chain unsaturated fatty acids are potential sources of these fatty acids (Hou, 1995). Other major constituents of suberin and cutin are dicarboxylic acids or α,ω-FAs. Cutin contains a high proportion of C16 and C18 while in suberin an even chain C16-C22 series is abundant (Volkman, 2006). In the Malin shelf α,ω-FAs ranged from C7 to C14 with a maximum at C9 and no predominance thus they are not derived from these biopolymers. The concentrations of α,ω-FAs ranged from 0.14 μg/g to 1.09 μg/g in the southern locations (6 and 44 respectively) and 1.57 μg/g in the north (station 22), and have shown no visible trend with depth. Such a distribution suggests that these fatty acids are either derived from one or more sources that constantly supply them to the sediment or they are generated *in situ* in a relatively slow process. Although short chain α,ω-FAs do exist in some plants, more importantly they are also a product of oxidative scission of unsaturated fatty acids (Volkman, 2006). Such oxidation can be mediated by certain metals in mineral phases and microbial liposomes alike (e.g. Waters, 1971). The concentrations of MUFA and α,ω-FAs are moderately positively correlated (R^2 ranging from 0.53 to 0.79; 44 and 6 respectively), thus such mechanism of *in situ* α,ω-FAs generation is possible as a partial source of these compounds. The bound (ω-1)-FAs observed ranged from C24 to C30 with small amounts of C14 and C16 detected only in the southern stations. The bound (ω-1)-FAs similarly to free (ω-1)-FAs were detected in very small concentrations which ranged from 0.09 μg/g to 1.10 μg/g (6 and 44 respectively). The down core profiles show slight decrease in concentrations with no visible trend (average of 0.18 μg/g; n=4, 0.20 μg/g; n=4 and 0.31 μg/g; n=3 in 6, 22 and 44 respectively). All isoprenoid fatty acids observed were phytol degradation products described before in the free fatty acids fraction. Interestingly bound phytol was only detected in station 44 in the deeper sections and ranged from 1.65 μg/g to 0.17 μg/g (from 1 to 5.6 mbsf respectively). The isoprenoid fatty acid concentrations ranged from 0.46 μg/g to 1.59 μg/g in (stations 45 and 6 respectively) and show little variability with depth.

Sterols

Sterols were the second major constituent of the bound lipid fraction. Representative gas chromatogram depicting sterol content is shown below (Figure 61). Concentrations of sterols were significantly higher in the surface sediments and ranged from 3.26 μg/g in the

northern stations (22) to an average of 8.50 µg/g (n=3) in the southern stations (Table 23). Bound sterols represented a similar contribution to the free species although a slight predominance of the bound fraction was observed in all cases. The bound sterol input ranged from 53.0 to 59.8% (mean 55.7%; n=4).

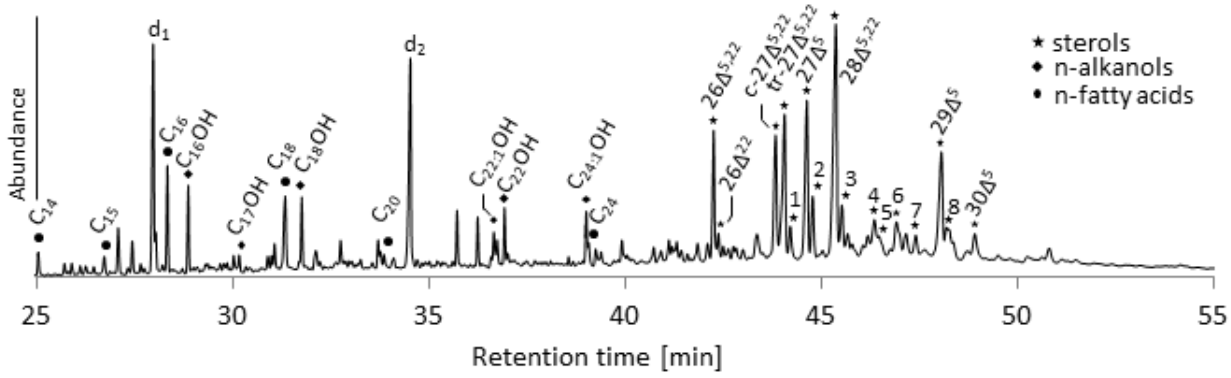

Figure 61. Representative gas chromatogram (TIC) of bound lipids with predominant sterol region between 40-50 min.

The concentration of sterols decreased significantly with depth indicating that the conjugate form is only abundant in surface sediments and diagenetic incorporation of sterols into bound form is not rapid in the Malin Shelf sediments. Lajat et al. 1989 observed an opposite trend in Santa Barbara Basin organic rich sediment and concluded that gradual accumulation of sterols in the bound fraction with depth results from a diagenetic accumulation of sterols and reflects productivity fluctuation induced by El Nino events. However in their study anoxic conditions at the sediment water interface favour preservation of free species rather than bound sterols as shown by Lee et al. 1977. Didyk et al., 1978 have demonstrated that under oxic conditions the trend is reversed and bound lipids are better preserved. There are no records of anoxic events in the water column in the Malin Shelf area and an observed free and bound sterol relationship is not unexpected. This further suggests that bound sterols on the Malin Shelf are predominantly recent deposits rather than diagenetic products. The source of bound sterols is most likely of marine phyto and zooplankton as discussed in the neutral lipids paragraph. The water depth of this shelf setting is another important factor indirectly affecting the potential for survival of the sinking detritus. In moderately shallow settings the time for detritus to reach the seabed will be undoubtedly shorter and thus less chance for opportunistic organisms to feed on it before it is deposited. Settling velocities for various types of plankton detrital particles vary greatly. The algal particles which contain little mineral ballast can have very long residence time in the water column. Fecal pellets and calcareous or siliceous biogenic detritus on the other hand have higher densities and can reach the seabed much faster and deliver the organic matter in a less degraded state (Schulz and Zabel, 2006). Such situations can be observed in shallow lacustrine settings

Table 23. Concentrations of sterols in the bound lipids fraction from the surface sediments on the Malin Shelf (μg/g). The full names of sterols are given in the Table 19.

	22						**6**					**44**				**45**			
Sterol	**0.15**	**0.25**	**0.65**	**0.95**	**1.45**	**2.15**	**0.15**	**0.45**	**0.55**	**0.85**	**0.95**	**0.05**	**1.05**	**2.80**	**5.65**	**0.05**	**0.25**	**2.20**	**5.65**
C26Δ5.22	0.15	0.02	0.07	0.02		0.04	0.53	0.15	0.15	0.05	0.13	0.63	0.24	0.26		0.78	0.19	0.16	0.10
C26Δ22	0.04	0.02	0.02			0.01	0.10	0.03	0.03	0.01	0.03	0.17	0.07	0.07		0.12	0.03	0.03	0.02
C27Δ5.22c	0.26	0.06	0.24				0.73					0.39				0.51	0.09	0.08	
C27Δ5.22t	0.26	0.08	0.13	0.08		0.06	0.74	0.13	0.12	0.03	0.08	0.22	0.39	0.47	0.03	0.54	0.17	0.13	0.09
C27Δ22	0.09	0.03	0.04				0.17	0.04	0.04	0.02		0.25	0.17	0.18		0.20	0.03	0.03	0.02
C27Δ5	0.41	0.14	0.29	0.30	0.08	0.16	0.92	0.23	0.19	0.06	0.17	1.45	0.65	0.68	0.10	1.26	0.34	0.25	0.16
C27Δ0	0.29	0.08	0.22				0.31	0.11	0.10	0.05	0.07	0.42	0.27	0.23	0.02	0.33	0.13	0.10	0.08
C28Δ5.22	0.58	0.15	0.29	0.24			1.73	0.18	0.16	0.05	0.16	1.58	0.75	0.79		1.59	0.25	0.18	0.12
C28Δ22	0.15	0.06	0.06				0.32	0.06	0.06	0.02	0.05	0.47	0.19	0.20		0.42	0.06	0.06	0.03
C28Δ5							0.32	0.09	0.08	0.04	0.08	0.34	0.13	0.09		0.33	0.17	0.11	0.07
C28Δ0	0.03	0.01					0.08	0.03	0.02			0.09	0.03	0.02		0.07	0.02	0.02	0.01
C29Δ5.22	0.11	0.06	0.11	0.17	0.03	0.05	0.24	0.03	0.02	0.01	0.09	0.25	0.12	0.12	0.09	0.18	0.38	0.18	0.12
C29Δ5	0.55	0.30	0.51	1.11	0.21	0.27	0.83	0.15	0.16	0.05	0.04	1.17	0.39	0.41	0.53	1.18	2.08	1.15	0.72
C29Δ0	0.21	0.05	0.07	0.03	0.03	0.03	0.32	0.14	0.12	0.07	0.01	0.37	0.22	0.22	0.03	0.19	0.14	0.11	0.07
C30Δ5	0.15	0.06	0.08	0.09			0.22	0.06	0.05	0.04	0.05	0.36	0.18	0.19		0.26	0.11	0.07	0.04
$\Sigma_{unknown}$	-	-	-	-	-	-	0.59	0.11	0.11	0.05	-	0.55	0.12	0.15	0.04	0.54	0.29	0.24	0.17
$\Sigma_{sterols}$	3.26	1.12	2.14	2.04	0.35	0.62	8.28	1.55	1.44	0.55	0.96	8.73	3.91	4.08	0.85	8.50	4.77	2.88	1.81

(Cranwell, 1981) and estuaries (Shi et al. 2001). That in mind it is interesting to observe that bound sterol concentrations decrease significantly in the first 0.5-1.0 mbsf and reach values similar to that of free sterols (Figure 62, Table 23).

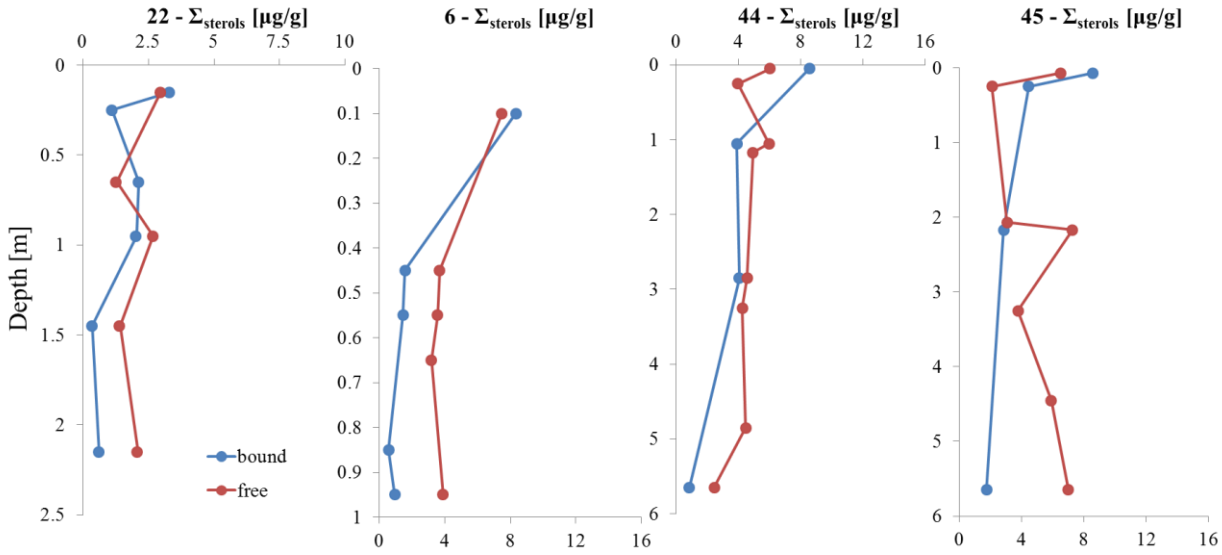

Figure 62. Concentration versus depth plots of total free and bound sterols in the Malin Shelf sediment cores.

That implies that bound sterols are in fact in majority associated with the detritus rather than adsorbed on to mineral phases and geopolymers. The contribution of individual sterols to free and bound lipids has shown some interesting patterns (Figure 63). The C26Δ5.22 which possibly represents input from marine benthic animals shows considerably more contribution to the bound lipids in the southern stations where it ranged from 6.9% to 9.8% than in the north (3.8% and 4.5% free and bound respectively). The northern stations have a much higher sand content and thus the habitat is more challenging for burrowing animals. Because many of the larger animals prefer to adhere to hard substrates which are almost absent in the Malin Shelf (except for few scattered rock outcrops) this sterol contribution might be predominantly associated with smaller biota such as detritus feeders and other active diggers such as little brittle stars and worms (i.e Polychaete). This to some extent can explain the lower input of these sterols in the northern station however habitat is only one of many factors influencing macrobenthos density in the seabed. The bound C26Δ5.22 appears to have a constant contribution while the free species in stations 22 and 6 shows depletion with 1.0 m depth of the seabed, perhaps related to lower biota density. Interestingly C26Δ5.22 shows a significant increase in the free fraction in the shallow subsurface in stations 6 and 45 (to 7.8% at 0.45 m and to 10.2% at 0.25 m respectively) which could potentially be explained by increased presence and activity of burrowing animals and other active diggers. Overall the contribution of this sterol shows little diagenetic change. The C27Δ5.22, both *cis* and *trans* are associated with

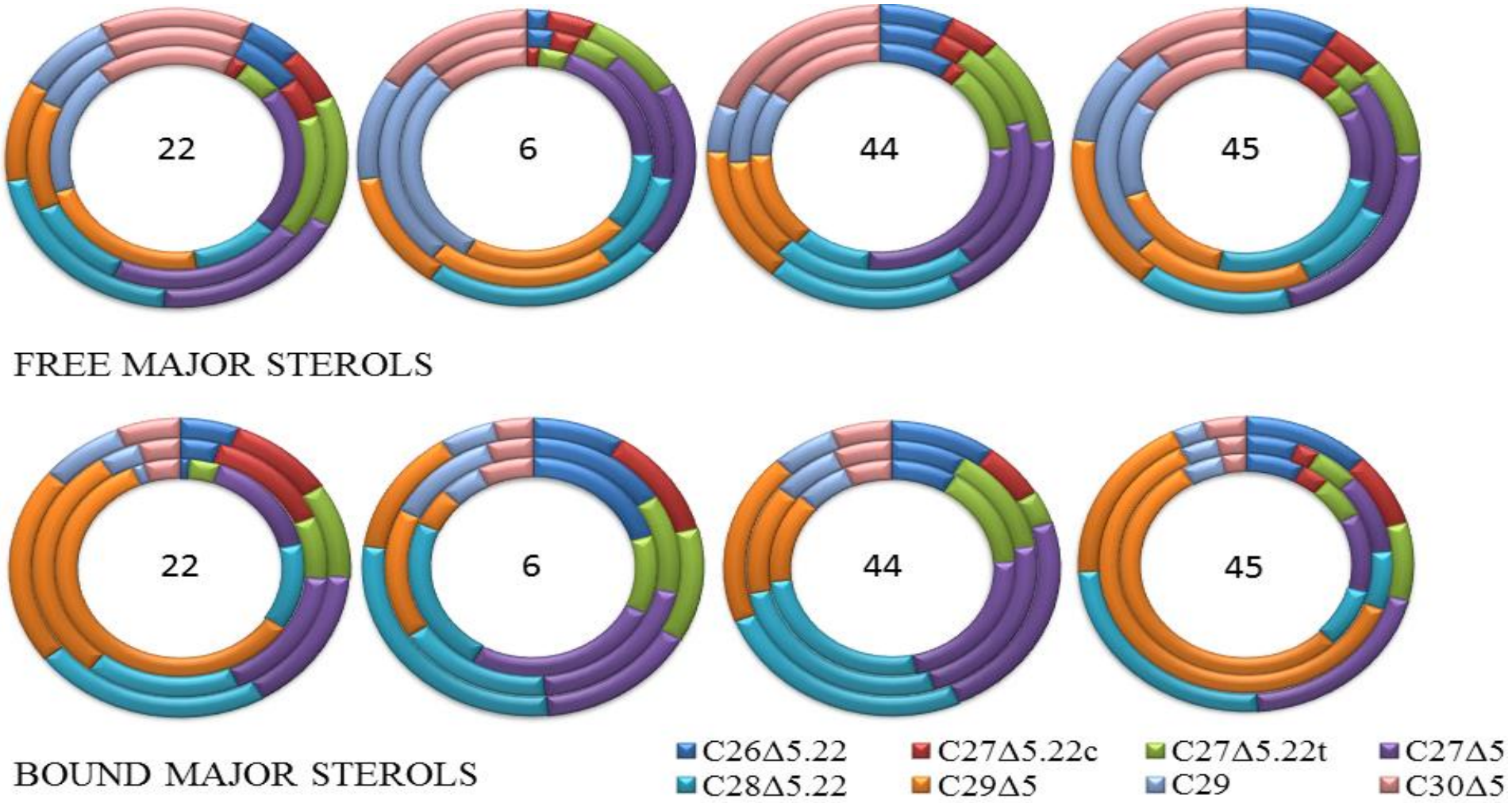

Figure 63. Contribution of free and bound major sterols to the sediment in the Malin Shelf sediment. The contributions as expressed as percentage of total sterol pool in both fractions. The outer rings represent the surface samples while the inner rings show change with depth. For the station 22 depth intervals are 0.1, 0.65 and 0.95 mbsf; for stations 6 depth intervals are 0.1, 0.55 and 0.95 mbsf; for station 44 depth intervals are 0.05, 1.05 and 2.85 mbsf, for station 45 depth intervals are 0.05, 1.05 and 3.2 mbsf.

diatom and zooplankton input and show significant contribution to free and bound pools in all stations (average surface sediment contribution 11.1% and 14.0%; n=4 free and bound respectively). Frustule dissolution and direct deposition of detrital matter are the most common sources of these sterols (Lee et al. 1980). However, in all stations bound species contribution is higher than the free ones. The *cis* isomer was particularly abundant in stations 22 and 6 and the *trans* isomer was dominant in the remaining ones. Both C27*Δ*5.22 isomers show a decreasing trend with depth in the free form. Bound isomers show more variability and so in stations 45 and 6 the *cis* species was absent in deeper horizons; station 22 has an initial increase in abundance from 7.9% to 11.1% followed by complete depletion and station 45 has a similar trend to that observed for the free sterols. These changes are not correlated with phytol content which is also associated with phytoplankton input. This fact suggests input from other sources and different diagenetic potential of deposited organic matter. The C27*Δ*5 appears to be equally distributed among both free and bond sterols with an average contribution of 13.1% to the surface free sterol inventory and 14.5% (maximum at 44 with 17.7%) to the surface bond sterols pool. This sterol show gradual decrease in concentration in all stations reaching an average of 11.9% and 13.8% in the deeper horizons (free and bound respectively). C28*Δ*5.22 was next to C27*Δ*5 the most abundant sterol in the bound group. The C28*Δ*5.22 contribution to the free pool decreased with depth in all stations from a surface average to 13.0% (maximum of 15.6% and 15.4% in stations 22 and 6 respectively) to an average of 8.6%. The contribution to the bound pool in the surface sediments was also significant, on average 20.0% and shows only a slight decrease with depth. The above suggests constant input of this sterol from one or more dominant sources possibly different algal species. The C29*Δ*5 shows a constant contribution to the free lipids pool which ranged from 7.9% to 10.9% and a gradual increase with depth to an average of 11.8% in the deeper horizons. The bound lipid pool contribution of C29*Δ*5 was similar to that of free sterols in stations 6 and 44. The remaining two stations show an opposite trend with contributions reaching 43.6% and 54.3% of all sterols (45 and 22 respectively) in the deepest sections. As C29*Δ*5 is a major phytosterol predominantly associated with terrigenous sources such variability might suggest that land derived matter could have reached the Shelf in greater quantities in the past. However there are no lithological indications of that process in the core records. In the case of station 22 a coarser, terrigenous material is predominant in the top section of the core rather than the bottom ones and core 45 shows little stratification. Alternatively microalgal blooms could be responsible for the increased content of the bound C29*Δ*5. The free C29*Δ*0 attributed to microbial reduction of stenols shows an expected increase with depth in all stations. The bound C29*Δ*0 on the other hand remains constant or decreases with depth (station 22). This is expected as conjugated sterols are not easily degradable by bacteria as shown by Eyssen et al. 1973. The C30*Δ*5 contribution is significant to both free and bound sterol pools. This is also expected as dinoflagellates are a major component of the

phytoplankton in the Malin Shelf waters (Gowen et al. 1998) and are well preserved in anoxic conditions (Lee et al. 1980). In the surface sediments C30Δ5 average contribution was 10.4% and 3.8% to the free and bound sterols, respectively. Down core free C30Δ5 show a slightly decreasing trend in the southern stations while the opposite was observed for station 22 with maximum of 12.5%. Bound C30Δ5 species show little variability and similar abundance in all stations (mean 4.2±1.5%, n=16).

Other bound biomarkers

Among the remaining bound lipids (Table 22) even chain fatty alcohols were the most abundant class (Figure 60). They ranged from C12 to C30 with a maximum at C18 comprising 20.9 to 43.0% of all fatty alcohols (stations 6 and 45 respectively). On average southern stations show a slightly higher abundance of fatty alcohols which is opposite to the situation observed in the free pool however in general conjugated alcohol input was comparable. Phenolic species shown a greater diversity of structures in the northern station where a total of four compounds were identified: 4-methoxybenzoic acid (*p*-anisic acid), 3-hydroxybenzoic acid, 4-hydroxybenzoic acid, 4-methoxy-3-hydroxybenzoic acid (isovanillic acid). The 4-hydroxybenzoic acid was the most abundant (0.46 μg/g) while the remaining phenols were present in very small amounts (average of 0.06 μg/g; n=3). Interestingly in the southern stations only benzenepropenoic acid (cinnamic acid) and 4-hydroxybenzoic acid were detected in significant quantities (from 0.12 μg/g to 0.32 μg/g). This suggests a diversification of the terrigenous input and/or different deposition mechanisms. Alternatively, phenolic compounds can originate from *in situ* microbial activity where methoxylated substrates can be demethylated and yield other phenolic derivatives (Crawford et al. 1973). Conjugated branched fatty acids detected in bound lipids were structurally identical to these observed in free lipid extracts and comprised microbial and phytol derived species as discussed above. They were most abundant in the surface sediments where they ranged from 0.99 μg/g to 2.04 μg/g (45 and 6 respectively). In general they show decrease in concentration with depth, however in station 44 an increase was observed from 1.46 μg/g to 2.94 μg/g (1.05 mbsf) and 2.65 μg/g (2.8 mbsf) which was attributed to a higher abundance of phytol derivatives rather than microbial sources. Small quantities of dihydroactinidiolide (DHAO) were observed in station 22. This terpene occurs naturally in the environment i.e. in plants and as a signalling pheromone in insects however in marine sediments it is most likely derived from degradation processes of algal carotenoids via photo-oxidation of (Klok et al. 1984). Small amounts of fatty aldehydes identified as acetals (m/z: 75) are also present, which are derived from so called '*plasmalogens*', a specific phospholipid observed in invertebrates and anaerobic bacteria (Goldfine, 2010). Due to the very low abundance of the molecular ion the chain length was not determined for these compounds.

3.3.1.4 CuO oxidation products

The total yield from the Malin Shelf sediment alkaline oxidation products ranged from 38.68 μg/g to 247.46 μg/g (station 24 and 20 respectively) and averaged 145.49±86.50 μg/g in the surface sediments (Table 24). Northern stations on average show lower yields (111.54 μg/g; n=3) than the southern stations (151.62 μg/g; n=5), however a higher sample density would be required to confirm a genuine spatial relationship. Ester bound lipids were the dominant components in all stations and ranged from 19.8% to 51.7% of all oxidation products (average 35.1±12.4%; n=8) while total lipid derived products (including ether bound compounds) ranged from 23.3% to 58.5% (average 44.1±13.3%, n=8). Aromatic products ranged from 8.80 to 81.89 μg/g (average 43.90±28.09 μg/g; n=8) and on average accounted for 29.3% of all oxidation products. Aliphatic components were predominant in all stations and ranged from 29.88 to 165.57 μg/g. The average contribution of these compounds was 70.7±5.4% of all products (with eLIP contributing from 30.2 to 67.7% of that figure). Lignin derived products were detected in very small concentrations which ranged from 0.33 to 5.84 μg/g and were limited to vanillic acid, *p*-coumaric acid, ferulic acid and *p*-hydroxybenzoic acid. The *p*-hydroxybenzoic acid was the most abundant compound (average of 11.80±8.20 μg/g; n=8) however since it can be derived from other than lignin sources it is not considered a diagnostic molecule. Nevertheless total lignin products with one exception have shown a very good correlation (R^2=0.96) with *p*-hydroxybenzoic acid (Figure 64) and thus it is likely that this compound is also lignin derived.

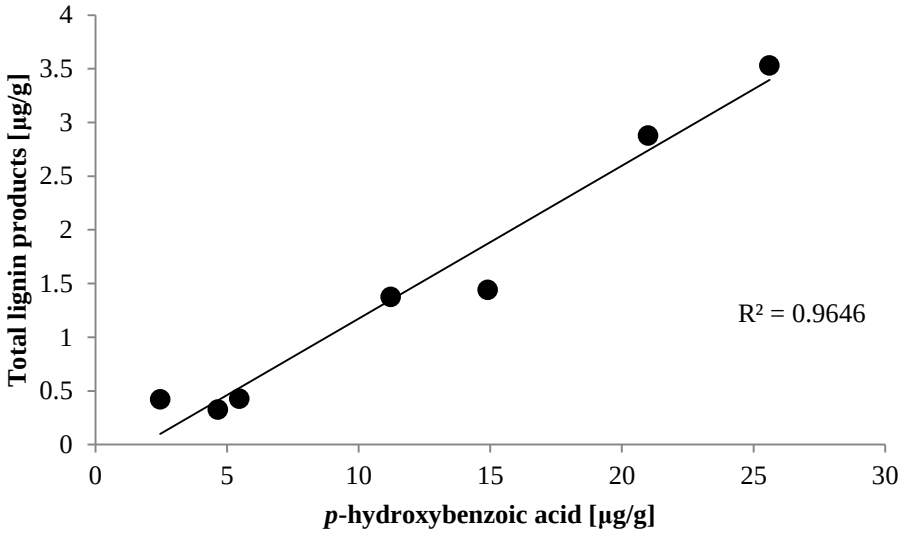

Figure 64. Correlation of total lignin derived products with p-hydroxybenzoic acid.

In station 45 a higher concentration of vanillic acid is observed and the above mentioned relationship is not preserved. Ferulic acid co-eluted with an unidentified polyaromatic compound thus regrettably quantitative data for this compound is unavailable. Remaining components of the vanillyl series (vanilin and acetovanillone) and *p*-hydroxyphenyl series (*p*-

hydroxyacetophenone and *p*-hydroxybenzaldehyde) were not detected. Observed concentrations of lignin derived phenols were very low, approximately an order of magnitude lower than expected from a setting with lignin derived organic matter as a contributing source (Hedges and Ertel, 1982). Moreover phenolic aldehydes were not observed and since high acid to aldehyde ratios are a common indicator of lignin 'freshness' (Goni et al. 1993) this suggest that small amounts of lignin matter present in these sediment is in a degraded state rather than fresh (Bourbonniere and Meyers, 1983). The observed *p*-hydroxyphenyl and vanillyl series structural units are also more resistant to degradation than syringyl units in hardwood polymers (Hedges et al. 1985) thus they are expected to survive intact longer i.e during transportation where they are exposed to microbial and environmental degradation. Moreover since most efficient lignin degraders are predominantly terrigenous organisms (e.g. white rot fungi) degradation of lignin had most likely pre-depositional character. The syringyl series compounds were not detected which suggests that woody and non-woody angiosperm derived terrigenous matter does not contribute to the scarce lignin pool observed in the Malin Shelf sediments. The cinnamyl series products (ferulic acid and *p*-coumaric acid) represent input from non-woody plant tissues (Hedges and Mann, 1979). Since angiosperms are not a major source of lignin in this setting the gymnosperms alone are likely to be responsible for this contribution. Interestingly Hedges and Ertel, 1982 reported 'superoxidation' as an experimental artefact that can result in preferential removal of syringyl phenols, overall low phenol yields and oxidation of aldehydes to acids and is more likely to occur in samples with little organic matter. They suggest that such an artefact is caused by incomplete oxygen removal, introduction of oxygen during charging of the bomb or from elevated temperature. Although all of the above mentioned symptoms of 'superoxidation' were observed in the analysed samples a lack of lignin derived phenolic methoxyl signatures in the NMR data have shown that lignin is indeed a minor component of the sedimentary organic matter in the Malin Shelf.

Other aromatic products included protein, tannin and more generally humic-like substance derived compounds. Although the structure and composition of these parent substances is still debated (humic and tannin like substances) or very variable (proteinaceous matter) Goni and Hedges, 1995 have shown that monomeric oxidation products retain structural information that permits them to be linked with the parent macromolecule or the macromolecule's known structural components. Among these products compounds derived from phenylalanine (Phe) were the most abundant and had highest yields. Similar concentrations were observed for *p*-hydroxybenzoic acid which can be produced from tyrosine (Tyr), however as was discussed before this compound is likely to be derived from lignin rather than protein. Goni and Hedges, 1995 observed a higher content of Phe derived products in pure samples of zoo- and phytoplankton followed by green macroalgae and bacteria as minor sources. Benzoic acid was by far the most abundant product and was observed in notably higher

Table 24. Concentrations of CuO oxidation products of surface sediment samples on the Malin Shelf. The precursors and possible sources of these are given after Goni and Hedges, 1995; Hedges and Mann, 1979; Goni and Hedges, 1990; Schnitzer and Ortiz de Serra, 1973; Bourbonniere and Meyers, 1983; Goni et al. 1998; Hedges and Ertel, 1982. Low molecular organic acid and diacids were identified based on spectrum similarity with Wiley Spectral Library data, samples marked with a '*' are identified tenatively. Precursors and sources abbreviations: ALG – alginic acid, HS – humic substances, nwLIG – non woody lignin, pLIG – p-hydroxyl group lignin vLIG – vanillyl group lignin, eLIP – ester bound lipids, oLIP – ether bound lipids, MIC – microbial, PR – proteinaceous matter, Asp – aspartic acid, Glu – glutamic acid, Phe – phenylalanine, Pro – proline, Thr – threonine, Trp – tryptophan, Tyr – tyrosine, TAN – tannin.

Compound	Abbreviation	Precursor/Source	25	24	20	27	44	6	45	7
Benzoic Acid	Bz	PR (Phe, Trp)	0.12	0.24	4.43	7.42	6.99	35.50	15.15	2.80
Phenylacetic acid	PhAc	PR (Phe)		0.09	1.53	1.39	0.85	2.56	1.73	0.95
Pyrrole-2-carboxylic acid	Py-2-COOH	PR (Pro)	0.28	1.29	15.33	2.96		6.70	9.74	11.57
2-hydroxybenzoic acid	2-OH-Bz	TAN, HS	1.05	1.56	7.41	5.92		8.87	3.95	5.26
4-methoxybenzoic acid	4-MeO-Bz	HS	0.42	0.32	2.84	1.48				1.74
3-hydroxybenzoic acid	3-OH-Bz	TAN	1.28	0.80	11.02	4.15	2.18	3.33	2.23	6.50
4-hydroxybenzoic acid	4-OH-Bz	PR (Tyr), pLIG	4.65	2.46	25.61	14.91	5.46	11.22	9.10	20.99
4-hydroxyphenylacetic acid	4-OH-PhAc	PR (Phe)	0.33	0.15	1.31	0.98	0.53	1.63	0.42	1.26
3-hydroxy-4-methoxybenzoic acid (isovanillic acid)	iVan	MIC, HS	0.27	0.16	2.42	1.08				2.35
4-hydroxy-3-methoxybenzoic acid (vanillic acid)	Van	vLIG	0.33	0.26	2.49	1.12		1.38	5.20	2.00
2,5-dihydroxybenzoic acid	2,5-OH-Bz	HS	4.63	0.27	1.19	0.55				0.44
3,5-dihydroxybenzoic acid	3,5-OH-Bz	TAN	0.43	0.57	4.17	1.20	0.38	2.09	0.69	3.52
3,4-dihydroxybenzoic acid	3,4-OH-Bz	HS	0.78	0.46	1.10	0.37	0.34	1.21		1.31
4-hydroxycynnamic acid (p-coumaric acid)	pCa	nwLIG		0.16	1.04	0.32	0.42		0.64	0.88
4-hydroxy-3-methoxycynnamic acid (ferulic acid)	Fa	nwLIG	coel	coel	coel	coel	coel	coel	coel	coel
Ethanedioic acid (oxalic acid)	C2 DA	HS. PS					0.53	5.67		0.40
3-hydroxypropanoic acid (hydracrylic acid)*	C3 MA 3-OH		0.06	0.10	0.84	1.63		2.48	0.94	0.38
Butanedioic acid (succinic acid)	C4 DA	PR (Glu), PS	1.31	3.39	18.89	15.00	0.21	21.98	11.12	18.45
2-hydroxybutanoic acid	C4 MA 2-OH	HS, PS	0.02	0.23	2.90	0.75	0.88	5.76	3.67	0.91
3-hydroxybutanoic acid*	C4 MA 3-OH		0.03	0.11	0.58	1.52		8.63	1.22	0.34
3,4-dihydroxybutanoic acid	C4 MA 3,4-OH	HS, PS					2.02	2.56	1.12	
2-methoxy-2-hydroxybutanoic acid*	C4 MA 2-OH,Me			0.26	1.33	1.61				0.85
Butenedioic acid (fumaric acid)	C4:1 DA	PR (Asp), PS	0.89	1.67	10.05	2.38	0.49	9.78	0.84	12.80

2-methyl-2-butenedioic acid (methyl maleic acid)	C4:1 DA 2-Me	HS	1.14	1.15	9.57	4.21	1.44	8.30	2.69	10.20
2,3-dihydroxy-2-butenedioic acid*	C4:1 DA 2,3-OH						1.18	3.09	1.60	
2-methylbutanedioic acid*	C4 DA 2-Me		0.59	1.35	11.90	6.87	0.74	15.49	3.59	9.37
2-hydroxybutanedioic acid (malic acid)	C4 DA 2-OH	PR (Thr), PEC, ALG						3.21	5.35	
pentadioic acid (glutaric)	C5 DA	HS, PS	0.87	0.88	6.43	4.21	0.98	5.50	4.70	6.13
4-ketopentanoic acid*	C5 MA 4-K		0.20	0.11	0.36	0.64				0.28
2-hydroxypentadioic acid	C5 DA 2-OH	HS	0.45	0.38	1.44	0.96		2.18	0.22	1.54
3-ketopentadioic acic	C5 DA 3-K	HS						1.38		
hexanedioic acid (adipic)	C6 DA	oLIP	1.89	1.53	11.44	6.98	0.68	3.61	3.23	9.46
2-hydroxy hexanedioic acid	C6 DA 2-OH	HS	0.34	0.31	1.58	0.64	0.47	1.64	0.32	1.26
1-Propene-1,2,3-tricarboxylic acid (aconitic acid)	C6:1 TA						0.73	3.09	4.56	
2-hydroxyheptanoic acid	C7 MA 2-OH			0.77	3.76	2.12				3.20
heptanedioic acid (pimelic)	C7 DA	oLIP	0.86	0.54	4.81	3.00	1.44		2.15	4.31
octanedioic acid (suberic)	C8 DA	oLIP	1.18	0.65	5.56	4.12	0.31	3.16	1.20	5.62
decanedioic acid (sebacic)	C10 DA	oLIP	0.75	0.46	3.82	1.79	0.34		1.31	2.63
undecanedioic acid	C11 DA	oLIP	0.35	0.40	2.39	1.51	0.71		1.33	2.91
dodecanediocic acid	C12 DA	oLIP	0.17	0.17	0.43	0.37	0.43		0.63	0.86
tridecanediocic acid	C13 DA	oLIP	0.05	0.04	0.22	0.40	0.29		0.67	0.20
tetradecanedioic acid	C14 DA	oLIP					0.20		0.38	
Aliphatic fatty acids	C8-C18 MA	eLIP	22.77	15.36	67.26	85.59	33.50	46.55	25.15	65.34
Σ CuO products			48.49	38.68	247.46	190.15	64.74	228.56	126.86	219.00
Σ lignin derived products			5.24	3.04	31.56	17.42	5.89	12.59	14.94	26.22

concentrations in the southern stations although its concentration varied significantly (2.80 – 35.50 μg/g; stations 7 and 6 respectively). This relationship is also true for all aromatic products which cumulatively varied from 8.80 to 14.56 μg/g (mean 11.68±4.08 μg/g; n=2) and from 17.17 to 81.89 μg/g (mean 54.64±23.40 μg/g; n=6) in northern and southern stations respectively. Station 20, although located in the northern cluster had a compositional signature typical of the southern stations. This further confirms that the parent molecules are most likely particle bound as station 20 has similar grain size distribution to all southern stations (mean 66.1 μm) unlike stations 25 and 24 (mean 134.9 and 95.0 μm respectively). Although Phe is a primary source of benzoic acid, tryptophan (Trp) can significantly contribute to the whole benzoic acid pool. Proline (Pro) derived pyrrole-2-carboxylic acid was also an abundant product and reached a maximum of 11.57 μg/g and 15.33 μg/g in stations 7 and 20 respectively. In marine organisms this oxidation product is abundant particularly in bacteria as well as zooplankton, secondary sources include red algae and phytoplankton (Goni and Hedges, 1995). Tannin and humic-like aromatic oxidation products ranged from 2.57 to 29.12 μg/g (stations 44 and 20, respectively) with 3-hydroxybenzoic acid being the most abundant in this group.

Aliphatic oxidation products ranged from 29.88 to 165.57 μg/g (stations 24 and 20 respectively; average 101.60±59.95 μg/g; n=8) and in general have followed the trend observed for the aromatic products where northern stations (excluding station 20) have shown lower yields (31.90±2.85 μg/g) than the southern ones (124.83±49.40 μg/g). Succinic (C4 DA), fumaric (C4:1 DA) and 2-methylbutanedioic acids were on average the most abundant products (cumulative average 22.39 μg/g) and accounted for 22.0% of all aliphatic products. The first two compounds can originate from various polysaccharides as well as proteinaceous matter, glutamic and aspartic acids specifically. A tentatively identified 2-methylbutanedioic acid was not previously reported in CuO oxidation studies. In Gulf of Mexico sediments C4 DA and C4:1 DA were also dominant and Goni et al. 1998 attributed that fact to site specificity, diagenetic processes and/or specific organic input. Nevertheless Goni and Hedges, 1995 have observed a particularly high content of fumaric acid in the oxidation products of pectin, alginic acid and aspartic acid. On an organism level fumaric acid is particularly abundant in brown algae, zoo- and phytoplankton and green algae, secondary sources include bacteria and red algae. Succinic acid on the other hand can be derived from more than one amino acid, notably tryptophan, phenylalanine, aspartic acid and proline, however Goni and Hedges, 1995 reported the highest yields from glutamic acid. Succinic acid in small quantities can also be derived from polysaccharides (excluding cellulose) but is more so a general proteinaceous matter marker. Oxalic acid, 2-hydroxybutanoic and 3,4-dihydroxybutanoic acid have been reported by Bourbonniere and Meyers, 1983 in humic acid oxidation products and are most likely linked to the polysaccharide component of these substances as they were previously reported in saccharide derived beverages and alkaline degradation of wood (e.g. Lowendahl et al. 1976 and

Lowendahl et al. 1975). Malic acid (C4 DA 2-OH) can originate from protein, specifically threonine (Thr), but is also observed in small amounts in the oxidation products of proline. It is a common oxidation product particularly abundant in brown and red algae as well as phytoplankton. The highest content of this compound was observed in alginic acids and protein thus an algal source is probable. Goni and Hedges, 1995 observed malic acid in oxidation products of various biopolymers thus more specific source correlation is troublesome. Methyl maleic acid was previously reported in soils (e.g. Otto et al. 2005) and is possibly related to an unidentified structural component of humic substances. Similarly to aconitic acid, methyl maleic acid can be derived from microbial metabolites or otherwise catalytically converted from citric acid. Citric acid is abundant in the environment as it plays a key role in the Krebs cycle which is used by all aerobic organisms to gain energy from oxidation of acetate to carbon dioxide (Krebs, 1987). Aconitic acid though can be formed spontaneously from citric acid upon heating, which was the early synthetic method to obtain this compound (Pawolleck, 1875) thus it is possible that it was generated during the oxidation procedure. The ester bound fatty acids represent a non-extracted remnant lipid material and their sources were discussed in detail in previous paragraphs. Ether bound lipids (oLIP) are not released during basic hydrolysis procedures and thus represent a new pool of lipids. These compounds, along with ester bound counterparts are a common component of cell membranes in a variety of organisms and are generally termed '*plasmalogens*'. Some cartilaginous fish are known to have a high content of plasmalogens (Magnusson and Haraldsson, 2011) however in marine sediments they are derived from various microorganism rather than higher organisms. Ether bound species are represented by corresponding diacids that are formed during oxidation. They range from C6 to C14 and are a major component in the Malin Shelf sediments. Shorter diacids were more abundant with C6 reaching 11.44 µg/g. Overall this class of compounds ranged from 3.79 to 28.68 µg/g (station 24 and 20) and comprised of 3.0 to 11.87% (average 9.0±3.0%; n=8) of all oxidation products.

3.3.1.5 Bacteriohopanoids

Pentacyclic triterpenoids of the hopane family are a widespread group of compounds and according to Ourisson and Albrecht, 1992 are potentially the most abundant natural products on Earth. Hopanoids are found in all types of organic matter and in various types of sedimentary environment and in most cases are linked to bacterial input (Rohmer et al. 1984). Hopanoids derived from plants are rare and in the case of higher plants can be distinguished from bacterial and lower eukaryotes species by a characteristic oxygen function at C3. This is a direct consequence of the biosynthetic precursor used, the oxidosqualane. Lower eukaryotes (lichens, mosses and ferns in particular) and bacteria synthesise hopanoids via direct cyclisation of squalane (Rohmer, 2008). Hopanoids are thought to be surrogates for sterols in bacterial cell membranes and thus play a role in adjustment of membrane fluidity (Christie and Han, 2010; Ourisson and Rohmer, 1992) and permeability (Poralla et al. 2006) which are important

environmental stress adaptation mechanisms in microbes. Hopanoids are usually divided into biohopanoid and geohopanoid groups. The relationship between the two is that of precursor and diagenetic alteration product respectively. Bacterially derived biohopanoids are often termed bacteriohopanoids. These molecules have amphiphilic character (hydrocarbon skeleton with highly polarity side chain) and low solubility in organic solvents thus extraction of these compounds can be troublesome. The geohopanoids are readily analysed by standard GC-MS approaches, however most of the biohopanoids due to their polyfunctional side chains are not amenable to standard analysis with this technique. However, with high temperature GC-MS operating parameters and high temperature resistant capillary columns, analysis of up to tetrafunctionalized bacteriohopanetetrol and aminobacteriohopanetriol as acetates is possible (e.g. Blumenberg et al. 2006) though atmospheric pressure chemical ionization LC-MS (APCI-LC-MS) is generally the technique of choice for analysis of the bacteriohopanoids (Talbot et al. 2003). When only the GC-MS approach is available, as was in this study, side chain cleavage is necessary to reduce the molecular mass of the bacteriohopanoids before GC-MS analysis (Figure 65). This procedure compensates for additional mass introduced in the derivatization step and keeps the molecular mass below 600 Da (in GC-MS applications 1000 Da is rarely exceeded with 500 Da being the limit for standard analysis). This procedure obviously results in a loss of information similarly to that incurred in phospholipid head cleavage in fatty acid analysis; however the method still permits the identification of a number of functionalities of the parent molecule and in the case of pentafunctionalized bacteriohopanoids the determination of the location of the first hydroxyl moiety (Figure 10). In the analysed samples only one degradation product was abundant enough to permit identification. The isolated compound was C32 ββ-bishomohopanol and thus it was derived from tetrafunctionalized biohopanoid. Possible sources include bacteriohopanetetrol, aminobacteriohopanetriol or composite bacteriohopanoids with sugars and amino acids moieties in position X (Figure 65). Additional signals were observed in the areas of the chromatogram where based on literature one would expect other degradation products, however the abundance of these peaks was very low and did not allow identification. Samples were analysed in reduced scan mode as described by Innes et al. 1997 but the concentration of target compounds was again too low and quantitation was not possible. Given the above, larger aliquots of sediment samples should be considered in further experiments. The observed bishomohopanol is an abundant and often dominant or even the only product in many hopanoid producing prokaryotes (Rohmer et al. 1984) including cyanobacteria (some strains of *Calothrix*, *Oscillatoria*, *Scytonema*, *Synechocystis*), purple non-sulphur bacteria (some strains of *Rhodomicrobium*, *Rhodopseudomonas*, *Rhodospirillum*), Gram negative chemoautotrophs (some strains of *Nitrosomonas*), Gram negative chemoheterotrophs (some strains of *Methylobacterium*, *Hyphomicrobium*), Gram positive bacteria (some strains of *Bacillus*, *Streptomyces*) and was the major hopanol observed in other studies (Innes et al. 1997 and the references within).

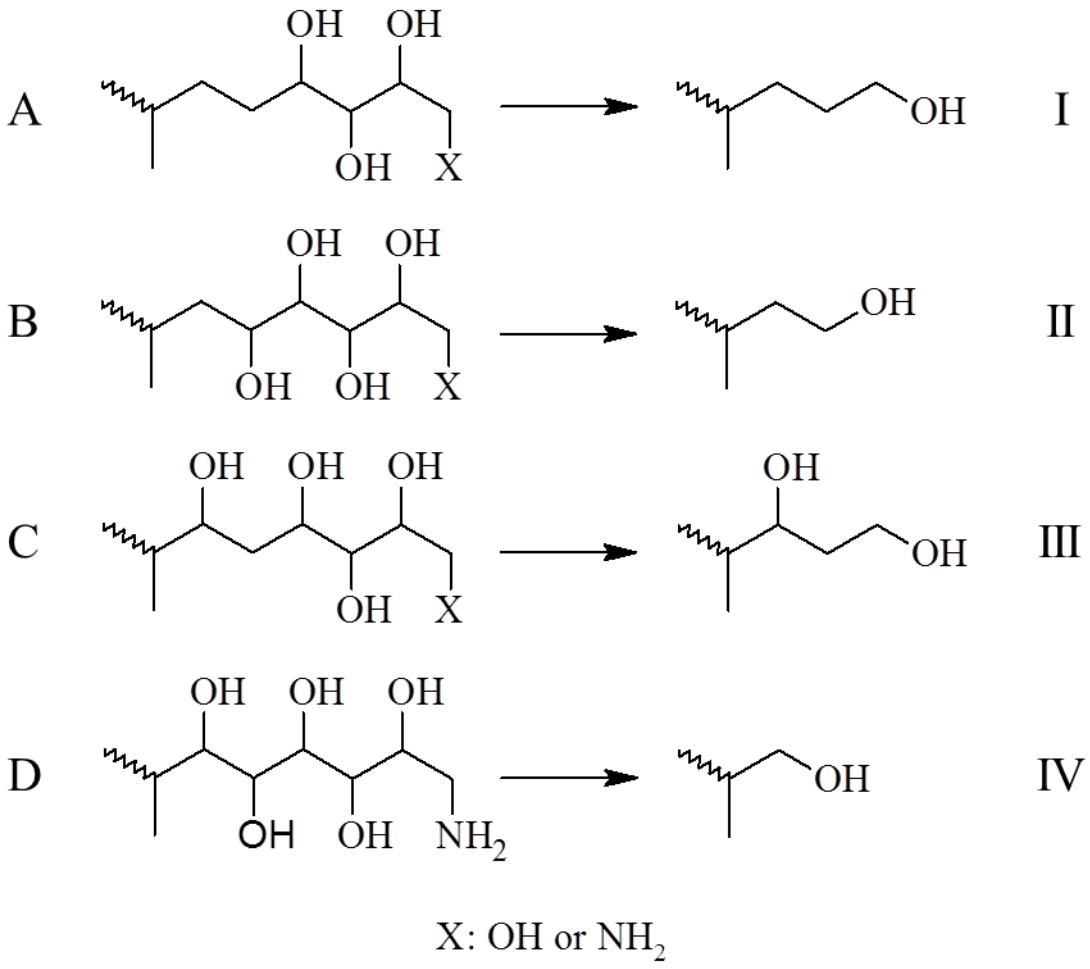

Figure 65. Structural degradation of a typical side chain of the bacteriohopanetetrol, chain in the periodic acid/sodium borohydride treatment. Structures on the left represent source hopanoid: tetrafunctionalized bacteriohopanetetrol or aminobacteriohopanetriol (A), pentafunctionalized bacteriohopanepentol or aminobacteriohopanetetrol (B,C) and hexafunctionalized aminobacteriohopanepentol (D). Structures on the right represent degradation products: ββ-bishomohopanol (I), ββ-homohopanol (II), ββ-bishomohopandiol (III) and ββ-hopanol (IV). Adopted from Rohmer et al. 1984 and Innes et al. 1997.

Although initially hopanoids were considered biomarkers related to aerobic organisms, discovery of hopanoid biosynthesis genes and hopanoid in pure cultures of anaerobic organisms such as *Geobacter* and *Magnetospirillum* (Fischer et al. 2005) or *Desulfovibrio* (Blumenberg et al. 2006) demonstrated that anaerobes also produce hopanoids. Lower concentrations of the bishomohopanol were observed in type I and type X methanotrophs where ββ-hopanol was the main product and also in certain *Azotobacter* (Gram negative) and *Nostoc* sp. strains (cyanobacteria).

Unexpectedly the periodic acid/sodium borohydride treatment allowed more insight into the hopane series in the Malin Shelf sediments. Some of these compounds could be observed in the m/z 191 trace of neutral fraction however most of them co-eluted with more abundant

components. A possible explanation for this finding is that compounds previously coeluting with hopanes containing various functionalities underwent side reactions during the bacteriohopanoids derivatization procedure that resulted in products showing shorter retention times and thus permitting the observation of a full hopane series. The observed compounds ranged from C27 to C35 (Figure 66) and were identified as αβ configuration. Traces of demethylated hopanes (m/z 177) were also observed. This finding was somewhat surprising since αβ-hopanes are typical of mature sediments and oils (Killops and Killops, 2009) and are rarely reported in recent, immature sediments. Hopanes with αβ and βα configuration are isomerization products of biological configuration ββ (Seifert et al. 1986) and in recent sediments are usually attributed to ancient sediment and natural or anthropogenic oil or oil based material input. The most common signature of such input is observed here as a C27 to C35 series (Volkman, 2006).

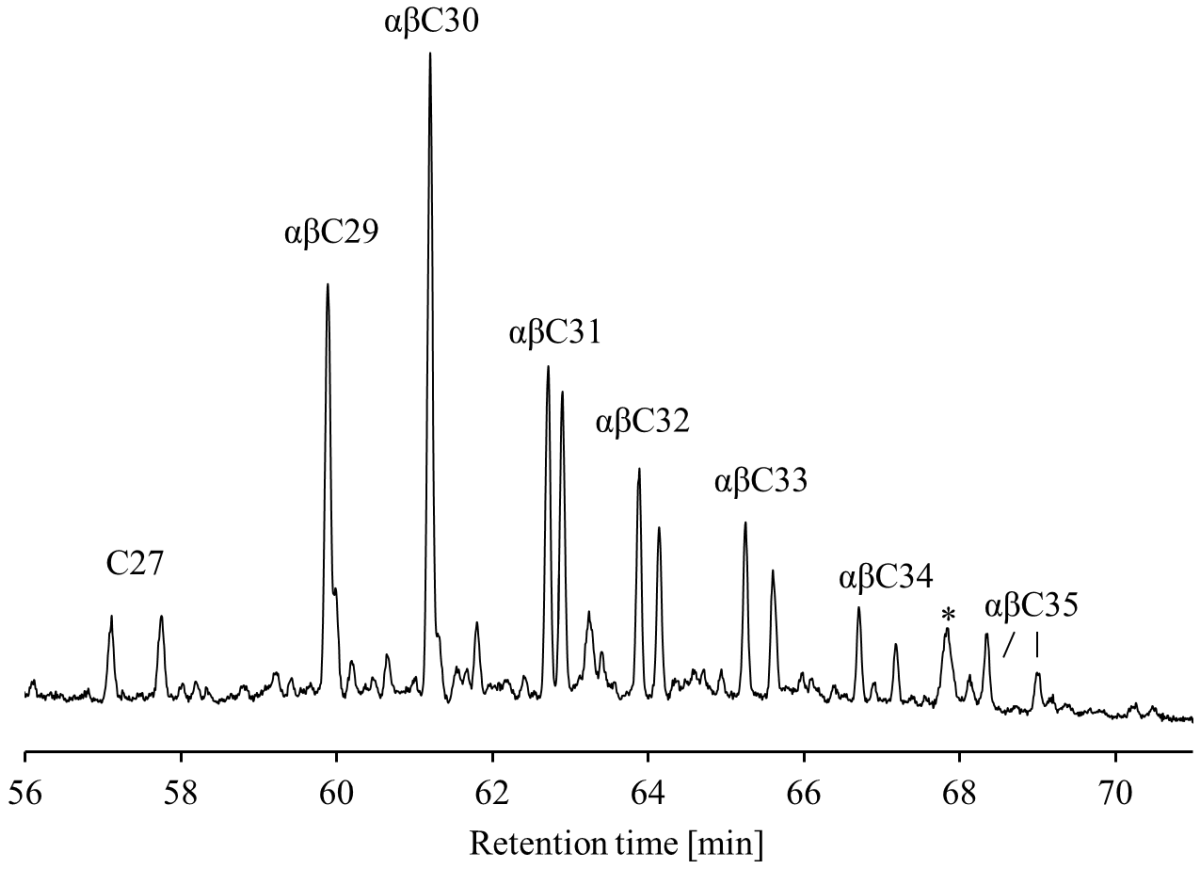

Figure 67. The EIC, m/z 191 trace showing hopane series in the Malin Shelf sediments. The number denotes number of carbon atoms in the molecule, while the greek letters denote stereo configuration at C17 and C21, * - Irgafos 168 related contaminant.

However the natural configuration of hopanes in these samples might not be preserved due to their capacity for acid catalysed isomerization (e.g. Tritz et al. 1999; Hauke et al. 1993) considering that the αβ configuration is the most stable thermodynamically. In natural

environments this process is very slow and requires thermal stress provided after the deposited sediment reaches appropriate burial depth for the particular setting. It is at least theoretically possible that in the presence of periodic acid such isomerization took place and thus in future studies hopane isolation by means of solid phase extraction or column chromatography could be used to separate these compounds from co-eluting components and permit accurate determination of their stereo configuration.

3.3.1.6 Transport of OM

The discussion of the spatial distribution of lipid biomarkers on the Malin Shelf is hampered by clustering and the small coverage of the area by the sampling stations. The distributions of lipid biomarkers although similar in general suggest that northern and southern stations experience slightly different inputs from both terrigenous and marine sources. This is also reflected in particle size distribution in these two sampling clusters (see Chapter 2 paragraph 3.3.1). Notably the northern stations show a higher content of terrigenous markers such as long chain n-alkanes, n-alkanols. There is an opposite trend however observed for the long chain normal fatty acids. This suggests diversification of the terrigenous organic matter inputs. The differences are also visible in both terrigenous and marine sterols which are more abundant in the southern cluster. The oceanographic conditions of the Malin Shelf limit the routes of entry for the terrigenous OM (Figure 68). The area is an open shelf setting with limited water exchange from neighbouring seas that experience higher terrigenous load from river discharges (Bowden, 1980). Direct fluvial contribution from the northern coast of Ireland includes particulate and suspended matter carried by the river Bann and numerous small creeks and streams (McDowell et al. 2005). Potential terrigenous input from the Irish Sea is limited since the salinity gradient and wind driven water outflow from the North Channel has been found to be almost parallel to the coast with a slow diffusive transverse and tidal transport mechanisms being dominant in the western direction (Bowden and Hughes, 1961; Bowden, 1980). Davis and Xing, 2002 reported that tidal activity is not sufficient to effectively suspend sediment therefore wind forcing and other physical mechanisms are required for efficient transport. The strong shelf edge current (velocities up to 50 cm/s) front passes ca. 150 km west from the Malin Shelf and thus matter delivered to this area would have to be further transported by tidal and diffusive action on to the Malin Shelf and therefore its importance as a potential source is limited (Lynch et al. 2004). Nevertheless seasonal recruitment is observed possibly caused by narrowing shelf topography resulting in focusing and intensification of the flow. This current passes directly through the Malin Shelf and can reach velocities of up to 20 cm/s in the top 30m. The Irish Coastal Current, according to findings by Fernand et al. 2006 is another viable mechanism for delivery and deposition of terrigenous matter discharged from the western coast of Ireland and possibly is the dominant source of the fresh terrigenous input in this area particularly to the southern stations cluster.

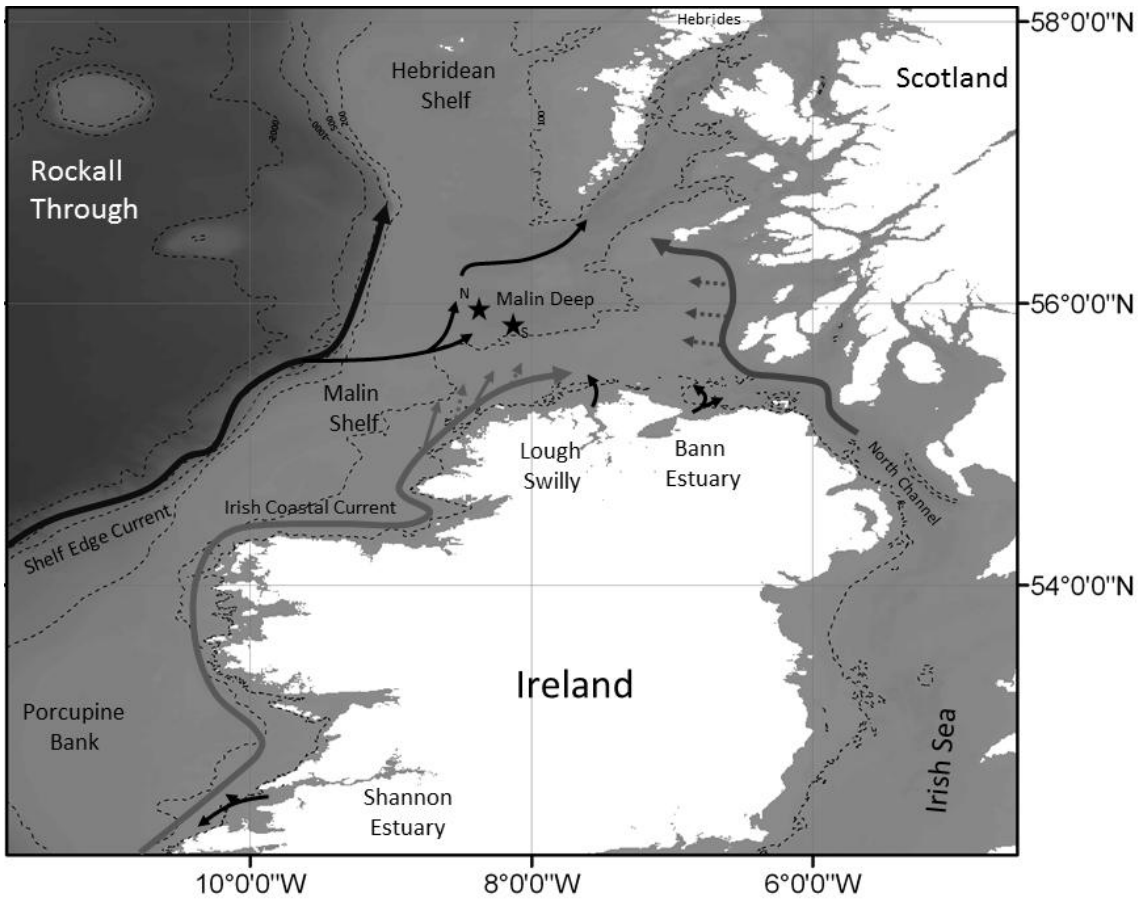

Figure 68. Potential present time routes of entry for the OM on the Malin Shelf. Black stars depicts northern and southern sampling clusters Malin Deep area, solid lines depict main hydrodynamic transport pathways of suspended and particulate matter: the Shelf Edge Current, the Irish Coastal Current, water exchange through the North Channel and contribution from main estuaries, dashed arrows symbolize diffusive and tidal transport. See text for references.

The relative importance of the contributions of the above mentioned sources of organic matter to the Malin Shelf is difficult to assess mainly due to lack of studies characterizing the OM in the surrounding area but also lack of such studies around Ireland in general. To our knowledge this is the first study of the organic matter and lipid biomarkers in this part of the European Shelf apart of work by Carrie et al. 1998 who reported the composition of fatty acids at the Hebridean shelf edge approximately 100 km N-W from the Malin Shelf.

3.3.2 Composition of whole organic matter

3.3.2.1 Composition of sedimentary OM in the P1 composite pockmark cluster

The NMR spectra were acquired for alkaline organic extracts and water macerates from six depths from both the inside and outside of the P1 pockmark (stations 45 and 44 respectively). The spectra for depths of 3 and 5 mbsf within the pockmark (not shown) were very broad even after repeated analysis. This may be due to a high concentration of magnetic

species present in these fractions within the pockmark as this problem was not encountered outside (Pake and Estle, 1973; Simpson et al. 2006). We therefore only compare samples taken

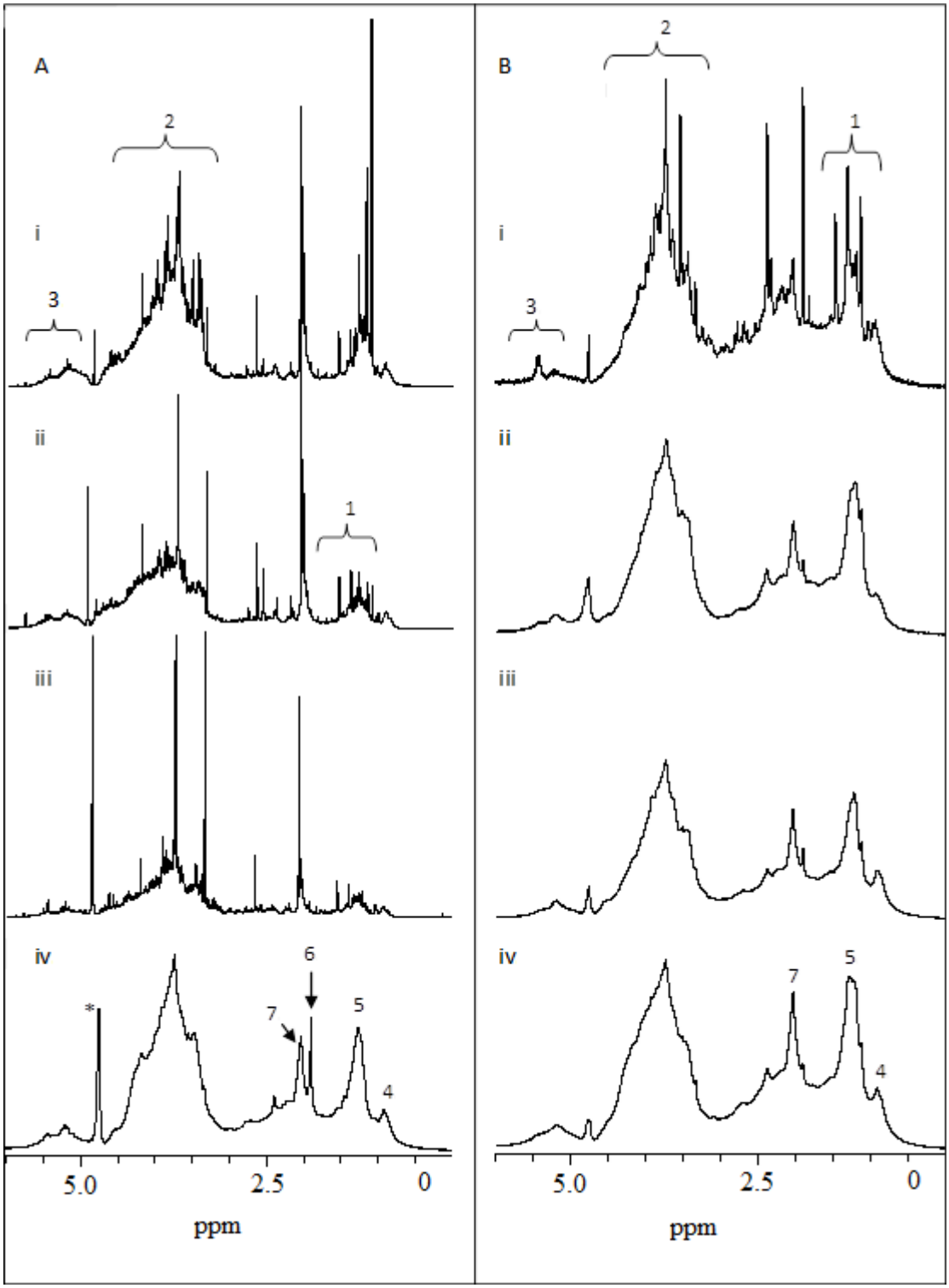

Figure 69. 1D ^{1}H NMR spectra (0-6 ppm) of sediment profiles from outside (A) and inside (B) of the P1 pockmark. (i) Surface, (ii) 2 mbsf, (iii) 4 mbsf and (iv) 6 mbsf. Designations 1-3 indicate general spectral regions: 1) aliphatics; 2) carbohydrates and amino acids (O-alkyl) and 3) anomeric carbon. Designations 4-7 indicate specific assignments: 4) aliphatic CH3; 5) aliphatic methylene (CH2)n; 6) acetic acid; 7) peptidoglycan. *Residual water.

from depths of 0, 2, 4 and 5.7 mbsf. Figure 69 displays the ^{1}H NMR spectra from different core depths inside and outside the pockmark. The ^{1}H NMR spectra are sub-divided into two separate regions (0-6 ppm in Figure 69 and 6- 9 ppm in Figure 72) so as to better highlight compositional differences. Microbial cells appear to be in abundance as indicated by the very intense signal from peptidoglycan at 2.03 ppm (N-acetyl functional group) which is a major component in bacterial cell walls (Simpson et al. 2007b). However, this peak cannot be assigned with certainty from the 1H NMR spectra alone. Alternatively, HMQC NMR spectroscopy provides ^{1}H-^{13}C bond correlations which help resolve overlapping signals from ^{1}H NMR data (Simpson, 2001). Figure 70 shows the HMQC NMR spectrum of an alkaline extract from inside the pockmark at 6 mbsf. The N-acetyl functional group from peptidoglycan is prominent in this and all HMQC NMR spectra from all depths inside and outside the pockmark. Peptidoglycan is a polymer that consists of sugars and amino acids that forms a layer outside the plasma membrane of bacteria.

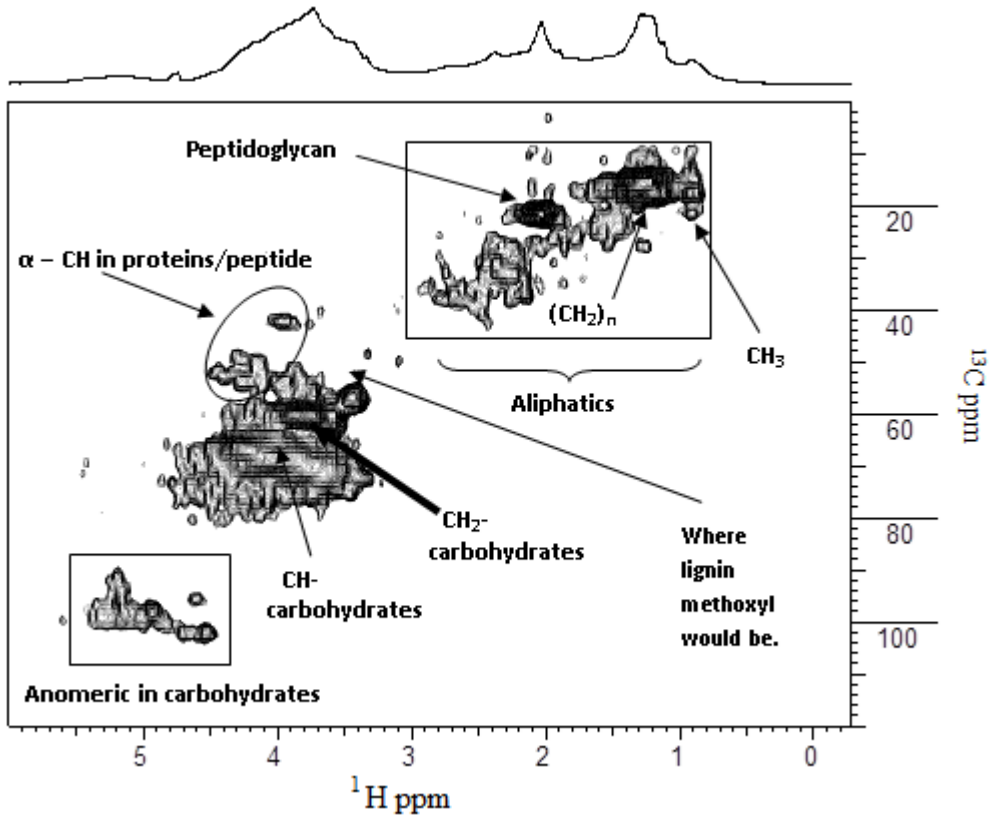

Figure 70. Zoom region of ^{1}H-^{13}C HMQC for sediment extract from inside the P1 pockmark (6 mbsf). The lack of a strong resonance in the methoxyl region indicates that lignin is not a major component of the samples studied here.

It has been used to estimate bacterial concentrations (Benner and Kaiser, 2003; Simpson et al. 2007b) and can be protected from microbial degradation after cell death by copolymerization reactions and transformation, substantially adding to the refractory nitrogen pool (Benner and Kaiser, 2003; Loll and Bollag, 1983). Muramic acid is only found in peptidoglycan, where it is

linked to both a glycan strand and peptide side chain. Gram-positive cells contain 5- to 10-fold greater yields of muramic acid than Gram-negative cells (Moriarty, 1977; Benner and Kaiser, 2003). However, most bacteria in seawater and marine sediments are Gram-negative (Moriarty and Hayward 1982; Giovannoni, 2000) including methanotrophic bacteria. Archaea do not contain muramic acid in their cell walls (Brock et al. 1994) and as yet an NMR indicator or signal that allows us to differentiate between bacteria and Archaea has not been reported. Archaea comprise about half of the total direct count of cells in deep water (Karner et al. 2001) and therefore archael residue is likely to be present in the organic extracts. From the NMR data reported here, we can say that both living and non-living Gram-positive and negative cells are strongly contributing to the sedimentary organic matter. Additionally, the peptidoglycan signature is very significant at all depths outside the pockmark but is less dominant within.

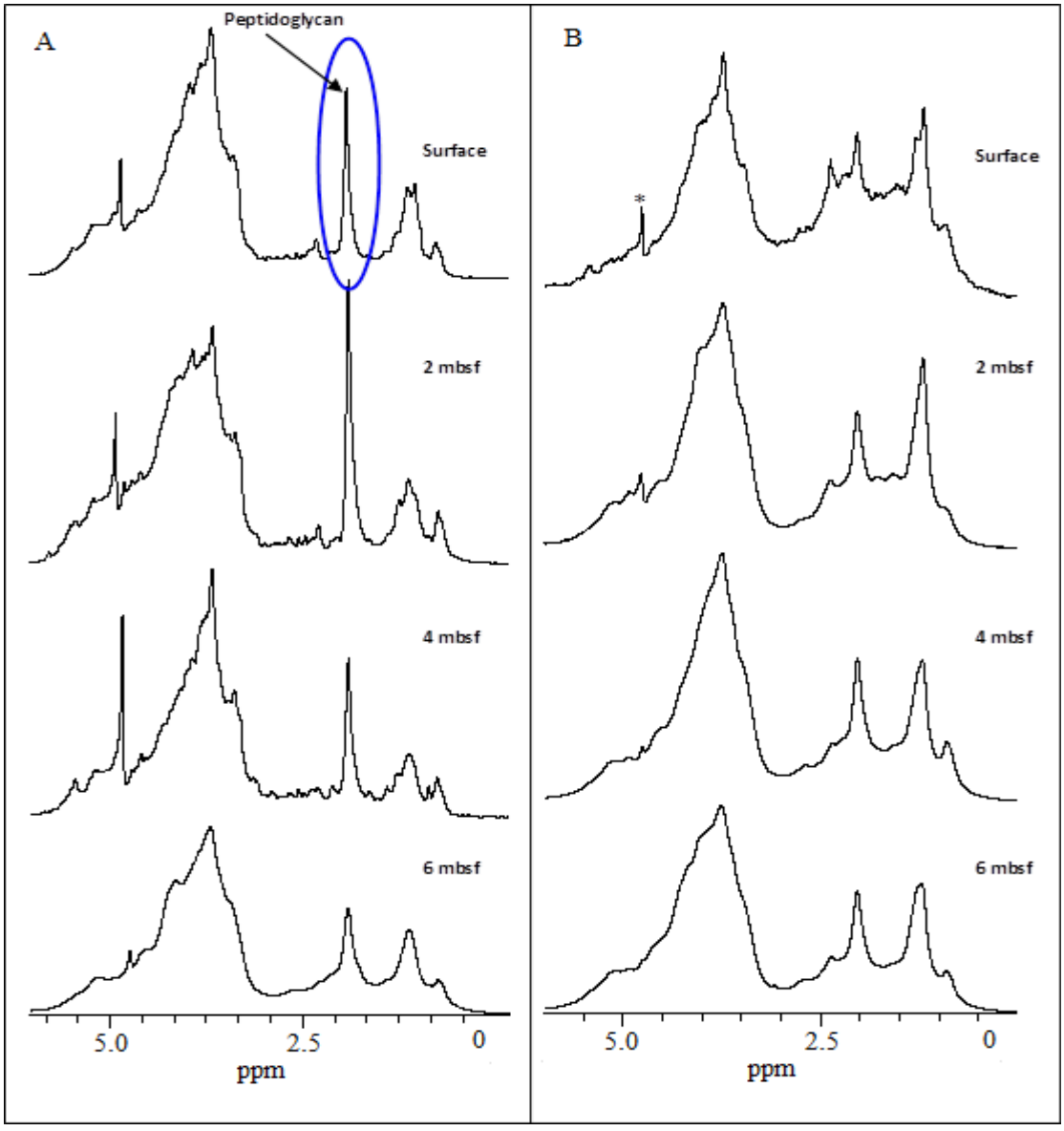

Figure 71. DE ^{1}H NMR of sediment cores from outside (A) and inside (B) of the P1 pockmark. Profound peptidoglycan signals are found in outside core indicating increased microbial presence.

To further emphasize the strong signature from microbial biomass, diffusion edited (DE) NMR was performed. In diffusion edited NMR experiments, small molecules are essentially gated from the final spectrum but signals from macromolecules and/or rigid domains (for example cellular structures) which display little translational diffusion are not gated and appear in the spectrum (Wu et al. 1995; Simpson et al. 2003). The diffusion edited spectra of the four depths from both cores are shown in Figure 71. The presence of aliphatic chains and carbohydrates suggests that they exist in rigid domains or are macromolecular in structure. Peptidoglycan is macromolecular and its resonance peak is extremely strong in all spectra but particularly so outside the pockmark.

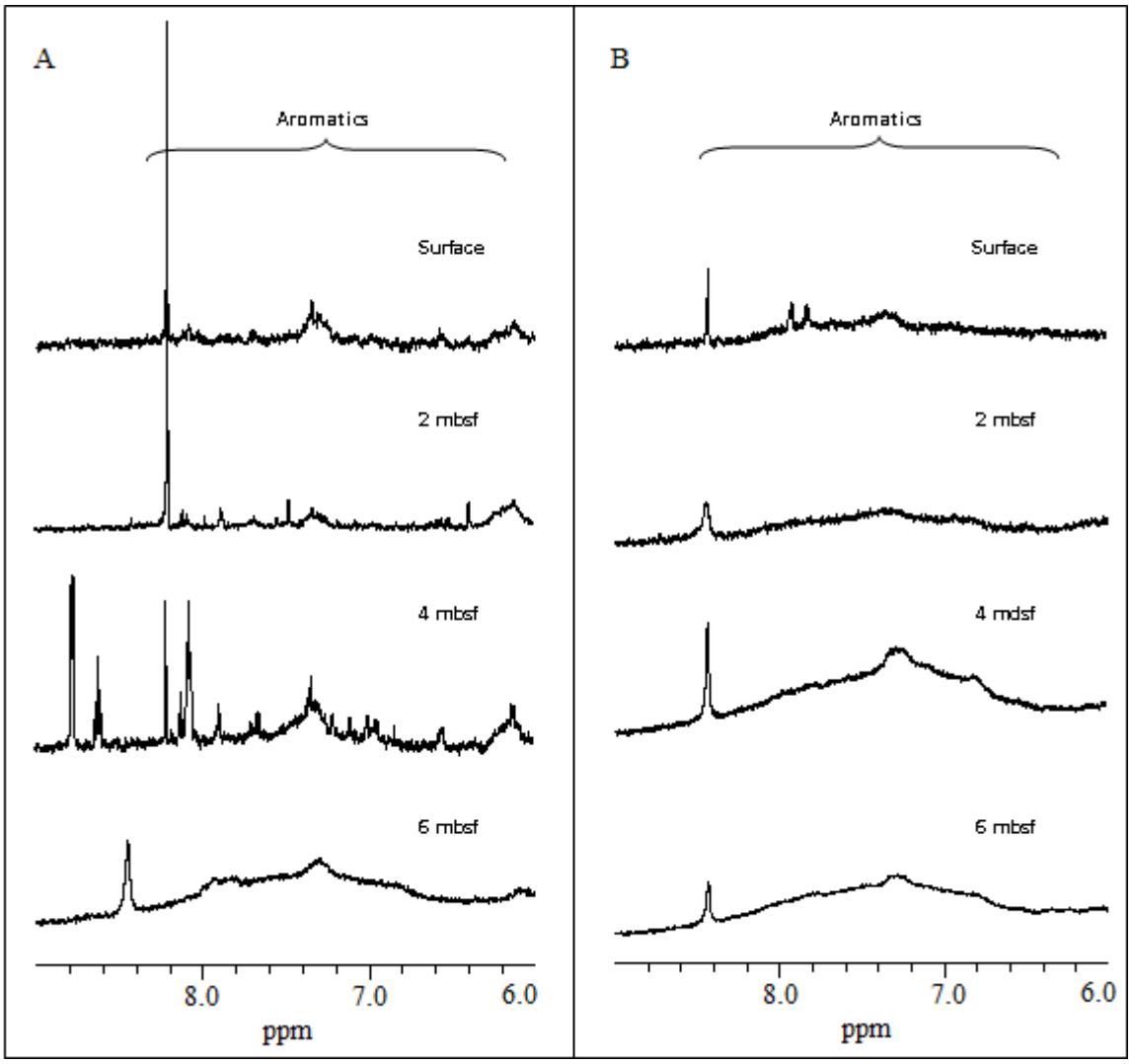

Figure 72. 1D ^{1}H NMR (6-9 ppm) spectra of sediment profiles from outside and inside the pockmark showing aromatic signal distribution in the sediment.

The organic matter outside the pockmark is dominated by microbial biomass and there is less organic matter obvious from other sources. This is particularly evident when comparing the relative intensities of the peptidoglycan peaks to those in the aliphatic region of the spectra. The microbial signature is not as strong relative to other carbon such as carbohydrates and lipids

in the first three depths from inside in the pockmark core. The organic matter from the outside core appears to be strongly associated with bacteria while much of the organic matter inside core may come from other sources. While there are clear differences in the top three depths between the cores, the DE spectra for the lowest depth (6 m) are again similar. Further evidence of the dominance of microbial biomass is provided by the clear contribution from α-CH units in Figure 70 that give a very characteristic group of resonances in H-C 2D NMR (Simpson et al. 2007a). α-CH groups are likely from microbial peptides/proteins and vertical elongation, along the ^{13}C axis, of the CH3 band indicates that side chains in proteinaceous matter also resonate here (Simpson et al. 2007a, Simpson et al. 2007b). Sharp resonances in Figures 69 and 72 are consistent with small molecules which can be related to microbial activity in environmental samples (Simpson et al. 2010). Metabolic activity of microbes is evident on the surface sediment of both cores and is consistent down the inside core profile apart from the lowest depth. However, signs of activity are only detectable on the surface of the inside core and not observed down core suggesting that the activity within the pockmark is considerably decreased. Signatures of microbial activity differ on the surface of both cores indicating that microbial communities may not be the same. Despite the lack of activity within the inside core, there are still strong peptidoglycan signals and an accumulation of aliphatic structures (e.g. lipids). In this case, the microbial signatures may be derived from the cell walls of non-living microbes that are degrading or dormant microbes that are less active than their counterparts from outside the pockmark. This trend is also evident in Figure 71 where there are sharp resonances indicative of biological activity present at all depths outside the pockmark apart from 6 mbsf and little sign of activity inside the pockmark. Also prominent in the 2D spectra (Figure 70) are CH and CH2 functionalities originating from carbohydrates. All spectra are dominated by carbohydrate resonances. Carbohydrate is presumed to be relatively reactive in the marine environment and its presence is likely due to a combination of newly synthesized structures and/or labile structure catabolism into the more stable alkyl fractions (Baldock et al. 1990). Degraded carbohydrate may become more recalcitrant through interactions with biopolymers such as lignin. Lignin presence would indicate a terrestrial influence but there are no clear indicators of the presence of lignin in abundance either in the 1 or 2D experiments (Figures 69 and 70) indicating that in this case, the high concentrations of carbohydrate do not rely on this mechanism for survival (Kelleher and Simpson, 2006; Simpson et al. 2003a; Simpson et al. 2003b). Again, a large portion of carbohydrates are likely derived from dead and living marine microbial cells (Simpson et al. 2007a). In addition, it has been reported that O-alkyl and acetal carbon (labile carbon) can serve as substrates for bacteria in sediment organic matter and increased microbial activity can result in the synthesis of new carbohydrates, initially increasing the labile SOM concentration (Sjögersten et al. 2003). Over time, the catabolism of O-alkyl carbon by microbes leads to a net alkyl carbon accumulation by the synthesis of new alkyl

carbon structures which may help explain some of the alkyl carbon observed at the lowest depth outside and at 2, 4 and 6 mbsf inside the pockmark (Baldock et al. 1990).

3.3.2.2 Composition of water soluble OM in the P1 composite pockmark cluster

The water soluble OM is in general structurally similar to the OM extracted by alkaline medium (Figure 73). The intensity of aliphatic, carbohydrate and amino acid as well as anomeric carbon signals represented by unresolved resonances is comparable; however water extracted matter lacks the sharp resonances typical of small molecules and resembles marine DOM in that respect (Hertkorn et al. 2006). Interestingly water soluble OM from the surface sediment outside of the pockmark shows a higher broad resonance in the peptidoglycan area (7) and a more abundant signal from the acetic acid (6). Moreover aliphatic methylene signals are also broadened and intensified in the water soluble OM. The most striking difference between the sediment from the inside (B) and outside (A) is that the quantity of the water soluble OM is considerably higher in the outside surface sediments. Although the data on quantity of DOM from the water column is not available given the close proximity of the stations it is safe to assume that the contribution from the water column is similar. Observed differences thus might indicate different rates of diagenetic remobilization of carbon in these two surface settings (Berry Lyons et al. 1979). These processes are related to benthic and microbial activity. The samples from 5.7 mbsf are less interesting and show great similarities between two fractions with barely noticeable differences (Figure 73). The diffusion edited spectra (Figure 74) of water and alkali extracted sediment are very similar and show distinct broad resonances typical of methyl groups bound to aliphatic carbon (1), peptidoglycan (*) and heteroatom substituted protons typically associated with carbohydrates and α-CH of peptides (3). Interestingly the carboxylic-rich alicyclic molecule region (CRAM) which consists of fused alicyclic molecules with carboxylic functionalities, thought to be derived from biomolecules bearing structural similarities to sterols and hopanoids, and the most abundant component of deep water DOM (Hertkorn et al. 2006) was not prominent in any of the spectra. This suggests that organic matter in the Malin Shelf has a signature typical for heteropolysaccaride dominated OM with little CRAM component (Repeta et al. 2002; Hertkorn et al. 2006). Peptidoglycan signals show similar intensity in the outside core (A) in both fractions which implies that a significant portion of the microbial biomass is not permanently bound to the solid phase. The DE spectrum of the surface sample from inside the pockmark (B), shows that peptidoglycan is a significant component in the water soluble OM fraction despite overall low yield.

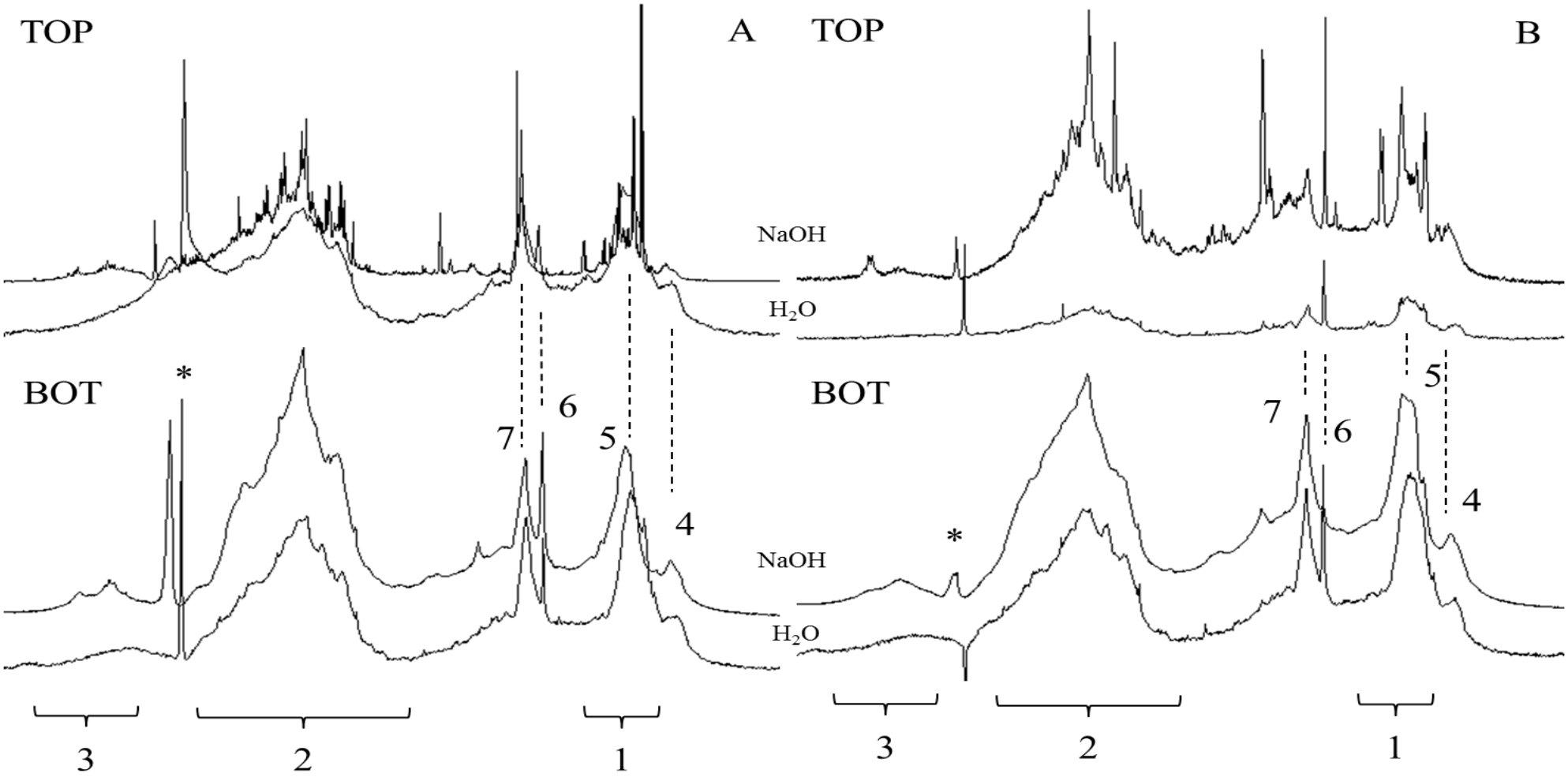

Figure 73. 1D ^{1}H NMR (0-6 ppm) spectra showing quantitative comparison of the alkaline and water extracted OM from the top (surface) and bottom (5.7 mbsf), outside (A) and inside (B) of the P1 pockmark pockmark. Designations 1-3 indicate general spectral regions: 1) aliphatics; 2) carbohydrates and amino acids (O-alkyl) and 3) anomeric carbon. Designations 4-7 indicate specific assignments: 4) aliphatic CH3; 5) aliphatic methylene (CH2)n; 6) acetic acid; 7) peptidoglycan. *Residual water.

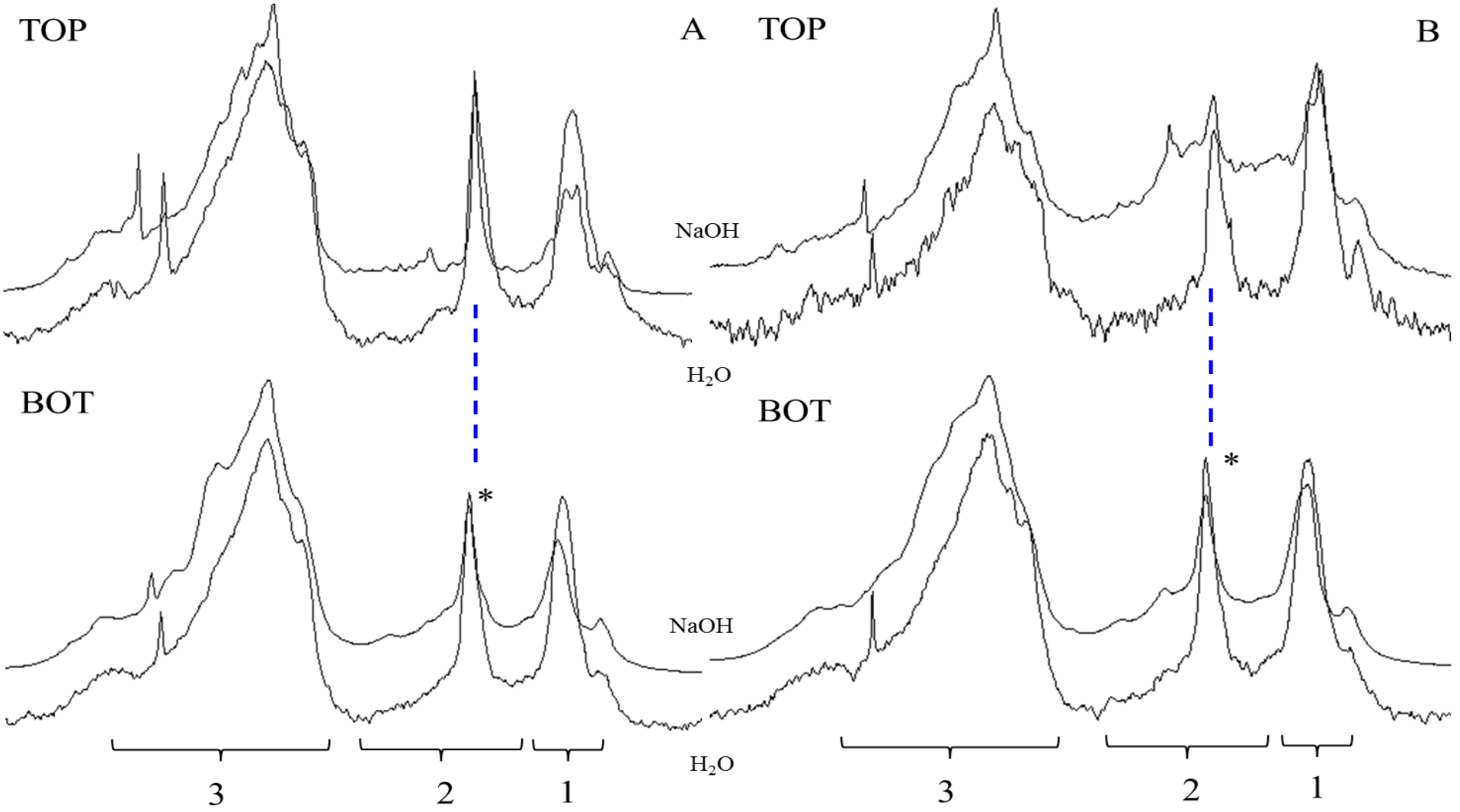

Figure 74. DE ^{1}H NMR spectra showing quantitative comparison of the alkaline and water extracted OM from the top (surface) and bottom (5.7 mbsf), outside (A) and inside (B) of the P1 pockmark pockmark. Designations 1-3 indicate general spectral regions: 1) aliphatics; 2) CRAM region 3) carbohydrates and amino acids (O-alkyl). Dashed blue line and * marks the peptidoglycan signal.

3.4 Conclusions

The examination of lipid biomarkers reveals that OM on the Malin Shelf is derived from terrigenous and marine sources. The main sources of the observed lipid biomarkers are given in Table 25. Dominant terrigenous biomarkers include long chain (>C20) n-alkanes, n-alkanols and n-fatty acids. The distribution of these species suggest that epicuticular leaf waxes derived from higher plants represent the major source of the terrigenous OM. This finding is further supported by the isotopic composition of the main aliphatic lipids and their molecular indices such as CPI, ACL and TAR. More evidence is provided by the significant abundance of phytosterols present in the sterol inventory such as C28Δ5, C29Δ5 and C29Δ5.22. Hydroxy fatty acids, particularly long chain (>C20) α,β-OH, ω-OH and (ω-1)-OH species can also be traced back to cutin, suberin and higher plants in general. Lignin is quite possibly not a major component of the terrigenous OM on the Malin Shelf. The distribution of lignin oxidation products suggests that non woody gymnosperms are the major source of this biopolymer with a minimal input from woody gymnosperms. However the total low yields of lignin oxidation products and the absence of phenolic aldehydes raises the question as to whether the results are not distorted by 'superoxidation' or other experimental errors.

Autochthonous sources of the OM on the Malin Shelf include phyto- and zooplankton, bacteria and benthic animals. The planktonic sources include algae, diatoms and dinoflagellate. These are a prominent sources of marine OM and in general are represented by short chain (<C20) n-alkanols, n-alkanes, α,β-OH and n-fatty acids. More specifically the presence of Eustigmatophytes is evident from C28-C30 alkyl diols and C30 keto-ols and short chain β-OH fatty acids. Dinoflagellate contribution is reflected in high amounts of C30Δ5 and possibly C27Δ5.22t, however the later can also be derived from zooplankton faeces, moults and benthic animals. Other algae are represented by C28Δ5, C28Δ5.22 and C28Δ5.24(24^1) which is particularly abundant in diatoms. The C26Δ5.22 and C26Δ22 are indicative of an input from marine invertebrates such as echinoderms and brittle stars. The contribution from other animals such as mussels, clams and scallops is at least partially represented by high amounts of *cis* and *trans* isomers of C27Δ5.22 sterols which are particularly abundant in their tissues. However both isomers can be derived from planktonic sources as well. Marine bacteria are represented by the terminal methyl branched (*iso* and *anteiso*) fatty acids, normal short chain β-OH fatty acids, *iso* and *anteiso* branched β-OH FA (Desulfovibrio), ββ-C32-bishomohopanol as well as C27Δ0, C28Δ0 and C29Δ0 stanols.

The distribution of lipid biomarkers between bound and free fractions revealed that lipid biomarkers are not selectively incorporated into the bound pool in diagenetic processes.

Table 25. Lipid biomarkers groups and major biomarker sources.

Biomarker group	Compounds	Major sources
n-alkanes	< C22, odd	Microorganisms, algae (Volkman et al. 1998)
	> C22, odd predominance	Epicuticular waxes of higher plants (Eglinton and Hamilton, 1967)
n-alkanols	< C20	Microorganisms, microalgae, zooplankton (Volkman et al. 1998)
	> C20, even predominance	Epicuticular waxes of higher plants (Eglinton and Hamilton, 1967)
	phytol, dehydrophytol, C18-isoprenoid ketone, isoprenoid fatty acids	Degradation of Chlorophyll-*a* (Rontani et al. 1999; Sun et al. 1998)
Sterols	C26Δ5.22, C26Δ22	Marine invertebrate, diatoms (Idler et al. 1970; Boutry et al. 1971)
	C27Δ5.22 *cis*, C27Δ5.22 *trans*, C27Δ22, C27Δ5, C28Δ5	Phytoplankton, diatoms, zooplankton, dinoflagellate (Barret et al. 1995; Rampen et al. 2010; Volkman, 1986)
	C30Δ5	Dinoflagellate (Volkman, 1986)
	C28Δ5.22, C28Δ5.24(24^1)	Alagae, diatoms (Volkman, 2006; Rampen et al. 2010)
	C28Δ5, C29Δ5.22, C29Δ5	Higher plants (Volkman, 1986)
	C270, C280, C290	Microbial reduction of Δ5 stenols (Wakeham, 1989; Nishimura, 1982)
Alkyl-diols	C28 (1,12;1,13;1,14), C29 (1,14;1,15;1,16), C30 (1,15)	Eustigmatophytes (Volkman, 1992; 1999b)
Keto-ols	C30 (1,15), C32 (1,15)	
n-fatty acids	< C20	Unspecified autochthonous (Cranwell, 1982)
	> C20, even predominance	Epicuticular waxes of higher plants (Eglinton and Hamilton, 1967), minor sources include microalgae and bacteria (Volkman et al. 1989)
	MUFA	Phytoplankton, zooplankton, bacteria (Carrie et al. 1998)
iso and *anteiso* branched	*i*,*ai*-C12; *i*-C13; *i*,*ai*-C14; *i*-C15; *i*-C16	Bacteria (Christie, 1989; Perry et al. 1979)
Hydroxy fatty acids	< C20 α,β-OH	Autochthonous, eustigmatophytes, bacteria (Boon and de Leeuw, 1979)
	i,*ai*-β-OH-C13; *i*,*ai*-β-OH-C15, *i*,*ai*-β-OH-C17*	Desulfovibrio (Boon et al. 1977b)
	ω-OH	Higher plants, minor sources include microbial oxidation and seagrass (Boon et al. 1977a; Volkman et al. 1980)
	(ω-1)-OH	Methanotrophs, cyanobacteria, higher plant waxes (Abreu-Grobois et al. 1977; de Leeuw et al. 1992; Skerrat et al. 1992)
Hopanoids	C27-C35 α,β-series	Petroleum, ancient rock weathering (Volkman, 2006)
	ββ-C32-bishomohopanol	Degradation of bacteriohopanetetrol and/or aminobacteriohopanetriol (Innes et al. 1997; Rohmer et al. 1984)
Lignin, humic substances	Vanillic acid, p-coumaric acid, ferulic acid, p-hydroxybenzoic acid	Higher plant, woody and non-woody gymnosperms (Hedges and Ertel, 1982; Goni and Hedges, 1995)
	< C6 hydroxy acids and diacids	Humic substances, polysaccharides, protein (Goni and Hedges, 1995; Schnitzer and Ortiz de Serra, 1973)

However a significant portion of marine and to a lesser extent terrigenous lipids particularly sterols and fatty acids are deposited in a conjugate form. The depth profiles of both free and bound lipids suggest that there is a qualitatively uniform input of the organic matter over the period of time preserved in the extracted sedimentary record. Moreover the profiles suggest that sources of the OM in the Malin Shelf did not change significantly in at least the last 5000 years.

The oceanographic conditions of the Malin Shelf limit the routes of entry for the terrigenous OM (Figure 68). Possible routes of entry for the terrigenous matter include transportation via Irish Coastal Current and seasonally shelf edge current. Other although possibly less important mechanisms involve direct fluvial contribution from the northern coast of Ireland notably river Bann and tidal and diffusive transport of suspended particulate matter. Marine OM was dominated by matter derived from phyto- and zooplankton with a strong contribution from algae and dinoflagellates and a relevant but not as significant contribution from benthic invertebrates and bacteria. Sterols, alkyl diols and short chain fatty acids were the most abundant groups of marine lipids. The depth profiles of both bound and free lipid biomarkers suggest a qualitatively uniform input of the organic matter in at least the last 5000 years.

Investigations into the whole OM have revealed prominent signals from carbohydrate, protein and aliphatic protons as its main components in the sediments of the composite pockmark P1. Additionally unusually high levels of peptidoglycan coinciding with a lateral gas body and increased conductivity of the sediment were observed in one of the cores (station 44). This relationship may be attributed to increased bacterial presence or presence of bacterial necromass. The NMR experiments revealed that peptidoglycan is macromolecular and appears to be the dominant component of the OM in the reference core along with carbohydrate and aliphatic domains. Organic matter inside of the pockmark feature on the other hand appears to have more lipid-like composition with significant, but not as high as in the outside core, peptidoglycan presence. The abundance of small molecules evident from sharp resonances in the NMR spectra in the reference core and paucity in the pockmark core suggest differences in microbial activity and/or community structure. This suggests that OM inside the pockmark feature can be more related to dormant or dead microorganism and other sources. General bacterial biomarkers did not reflect the microbially dominated organic matter as suggested by the NMR. However the methodology of the lipid extraction did not involve acid hydrolysis and thus did not permit a quantitative evaluation of the β-hydroxy fatty acids in the sediment. The question of whether Gram-negative bacteria indeed contribute significantly to the whole OM as suggested by high peptidoglycan signatures discovered in the NMR datasets remains unanswered. In future work biomarkers such as Gram-negative specific short chain (C12-C18) β-hydroxy fatty acids should be examined, preferably using the PLFA approach and microbial

ecology tools to assess the microbial biomass contribution to the OM in this setting. The composition of water soluble OM was similar to the alkali extracted OM and had a heteropolysaccharide signature.

CHAPTER 4 – SURVEY OF THE DUNMANUS BAY POCKMARK FIELD

4.1 Introduction

4.1.1 Geology, oceanography and biology of the Dunmanus Bay

Dunmanus Bay is located in the west of Ireland in the County Cork, south of the larger and better known Bantry Bay. The bay is 7 km wide from Sheep's Head to Three Castle Head and 25 km long from its mouth to Four Mile Water head (INFOMAR website, www.infomar.ie). It is a fjord-like setting with only one small river, Durrus, and several streams draining into the bay. Water depth in bay does not exceed 20 m and reaches over 70 m at its mouth (Figure 75). Dunmanus Bay received little attention from the scientific community and hydrological and biological data is scarce with the exception of data from one reference station reported by Cross and Southgate, 1983 in their ecological monitoring study hydrographic and plankton survey by Raine et al. 1990. However in the latter study authors focus mainly on Bantry Bay and Roaringwater Bay. In general this area experiences strong influences from coastal upwelling but tidal activity is low as Dunmanus Bay is out of the main tidal flow. Salinities reported in this study are typical for the marine environment from 34.7 to 35.2 (PSS), with little water freshening ranging. Since the study area is only approximately 2 km long, little variability of the hydrological parameters is expected. However, overall favourable thermal fronts and adequate nutrient concentrations support high levels of phytoplankton production in these waters (Raine et al. 1990). Notably, blooms of *Gyrodinium aureolum* (dinoflagellate responsible for the so called '*red tides*') are frequent in these waters affecting the aquaculture of the region (Jenkinson and Connors, 1980; Roden et al. 1980, 1981). Raine et al. 1990 reported phytoplankton populations dominated by diatoms with seasonal spikes of dinoflagellates with *N. seriata*, *L. minimus*, *C. debile*, *R., delicatula*, and *Chaetoceros* spp. being particularly abundant. Chlorphyll *a* concentration measured in the same study varied from 0.5 to 7.2 mg/m^{-3} between 1985 and 1987, more recent data is not available. In the waters close to shore and rocky outcrops there are frequent report of sightings of sea lettuce (*Ulva lactuca*), snails (*Nucella lapillus*), barnacles (*Balanus balanoides*, *Chthamalus montagui*), mussles (*Mytilus* spp.), limpets (*Patella vulgate*, *Patella aspera*) however the benthic fauna of the Dunmanus Bay remains largely unstudied (Cross and Southgate, 1983). Similarly the bedrock geology of Dunmanus Bay was not studied *per se* but inferred from the geology of

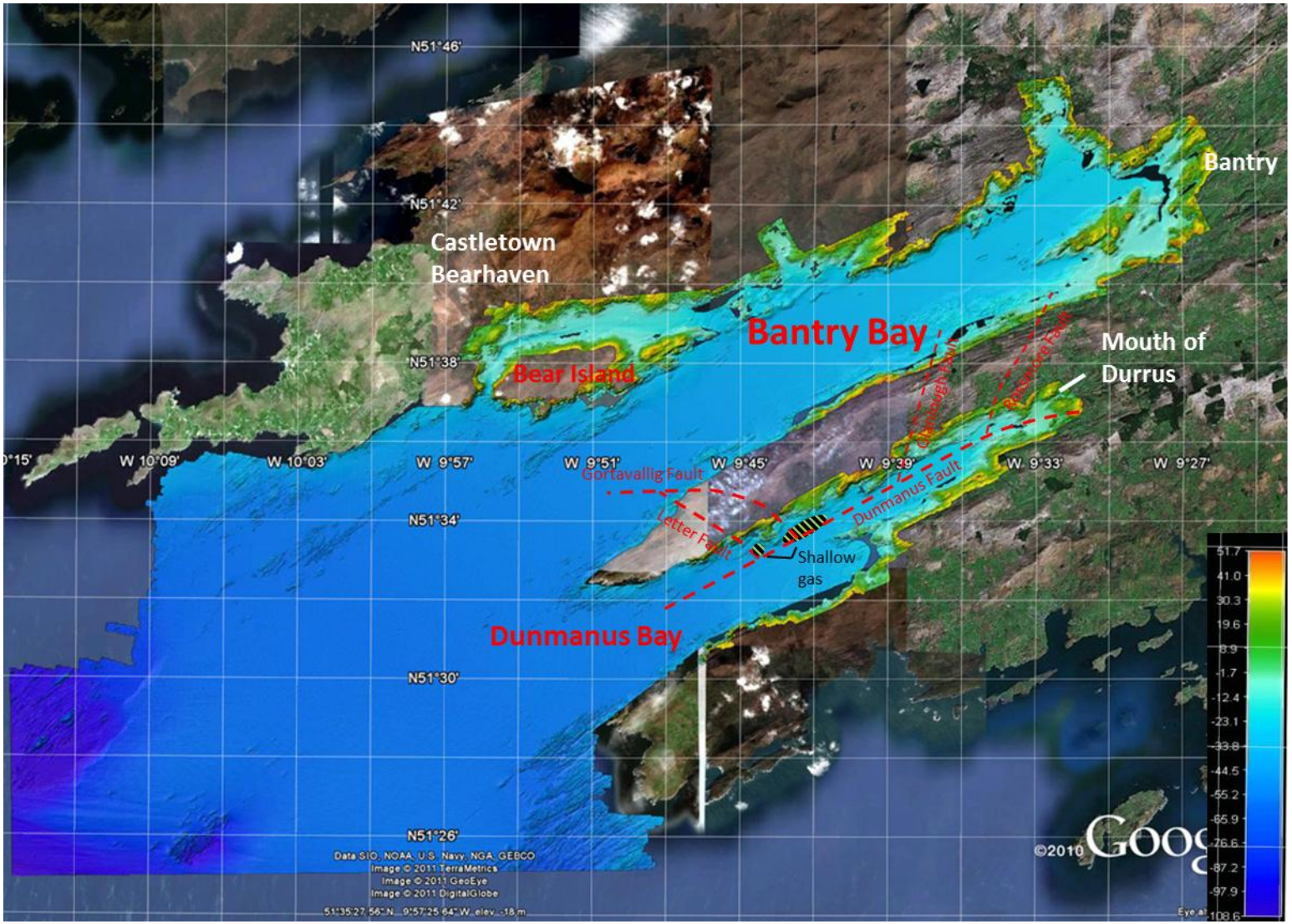

Figure 75. Shaded relief MBES bathymetry of Bantry and Dunmanus Bays. Bathymetric data INFOMAR, Ireland. Red dashed lines depict major faults in the area. Image created with Google Earth.

bordering landmasses in the 1850s by Jukes, 1864 and Jukes et al. 1861 and more recently by Naylor, 1975, Naylor and Sevastopulo, 1993 and MacCarthy, 2007. Both Bantry and Dunmanus Bays lie in the South Munster Basin separated by the Sheeps Head anticline. The formation of the South Munster Basin began in the Late Devonian with development of the Killarney-Mallow Fault which separated the original Munster Basin into the North Munster Shelf and the South Munster Basin. The stratigraphy of the South Munster Basin is dominated by the Upper and Lower Carboniferous and Upper Devonian formations consisting of deep and shallow marine shelf siliciclastic, non-marine coastal plain siliciclastic and non-marine fluvial siliciclastic rocks (MacCarthy, 2007). These formations rest on Caledonian granite and older pre Caledonian basement formations. Detailed descriptions of these strata are provided by Naylor, 1975 and Naylor and Sevastopulo, 1993. Vermeulen et al. 2000 conducted a thorough seismic survey of the Munster Basin and discussed several faults present in this area. This study was further reviewed and expanded by Quin, 2008. The major, sedimentation controlling fault in this area is the Dunmanus Fault (DF) crossing the entire bay parallel to the landmass (Figure 75). Two major branchings of this fault occur in the vicinity of the pockmark field area: the Gortavallig Fault (GVF) and the Letter Fault (LF). Moreover there are several minor faults in the northern part of the Dunmanus syncline separate from the DF, notably the Rossmore Fault (RF) and the Glanlough Fault (GF). Faults are often associated with fluid migration (e.g. Kutas et al. 2004) provided that source rocks are present and thermal conditions favour hydrocarbon generation. Early Carboniferous formations abundant in the area contain in places organic-rich shales, so called '*marine bands*' (Naylor, 1975) and according to Parnell et al. 1996 the bitumen maturity increases through Ireland in a south-western manner with both the North Munster Shelf and South Munster Basin formations being the most mature. There is therefore potential for a thermogenic hydrocarbon source in Dunmanus Bay. However Jukes, 1864 and Hunt, 1859 reported that among the above mentioned lithofacies, "*Alluvium, Peat-bog*" is present in the Dunmanus and Bantry area. Unfortunately they do not provide any information on the distribution of these facies. Furthermore, in landmasses surrounding Dunmanus Bay blanket bogs occur frequently (Irish Peatland Conservation Council website, www.ipcc.ie). These facies can contain up to 97% of organic carbon (Bord na Bona website, www.bnm.ie) and due to high rainfall in this area (> 2800 mm/annum) will drain into the bay. Similarly large woodland located in the catchment of the Durrus river lies on peat podsols and blanket bog. As this river is the main drainage for this region substantial organic load is expected to enter the bay at Durrus (O'Tuama and O'Rourke, 2010). However it is unlikely that these recent organic rich facies could enter to the marine environment and become ultimately a source of methane. The ancient *"Peat-bog*" facies reported by Jukes, 1864 and Hunt, 1859 on the other hand were formed before the Dunmanus syncline was in-filled with sediment and therefore can be a potential source of microbial methane. Monteys et al. 2010 employed acoustic methods to characterize the Quaternary sediments of Dunmanus Bay. The distribution of echo-facies was further

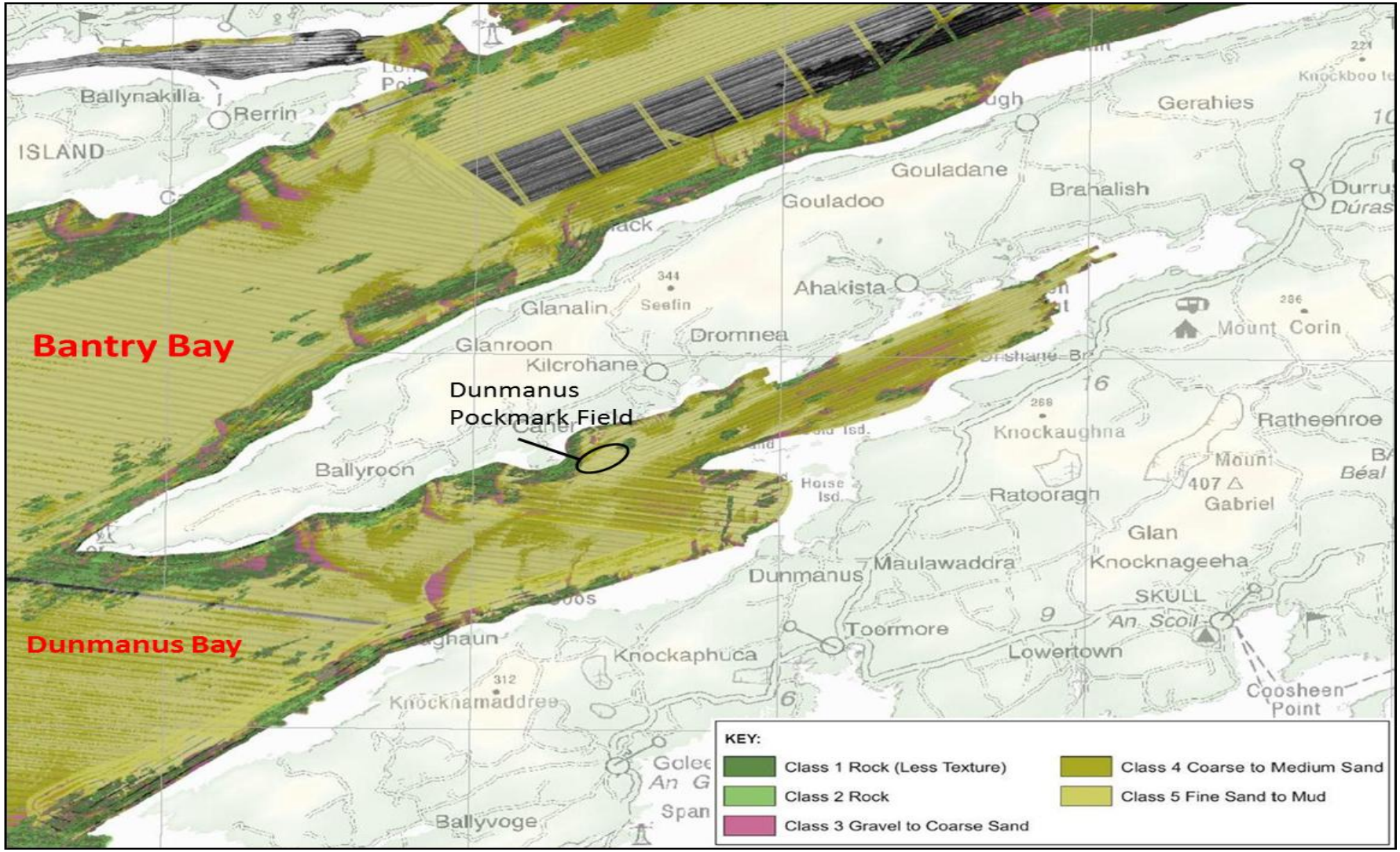

Figure 76. Acoustic seabed classification of Bantry and Dunmanus Bay, Monteys et al., 2010. Image: INOMAR, Ireland. Reprinted with permission.

confirmed by ground-truthing activities. The thickness of recent glacio-marine and terrigenous sediment cover has been evaluated with a 3.5 kHz SBP during the INFOMAR mapping survey and generally do not exceed 25 m particularly in the vicinity of the shallow gas accumulations. Sediment classification by Monteys et al. 2010 revealed a diverse seabed structure in Dunmanus Bay (Figure 76). The northern part of the bay is dominated by sand patches with a high mud component and bedrock outcrops, gravel and coarse sand is infrequent and mainly localized in the centre of syncline and close to the landmass. Moving towards the mouth of the bay mud becomes the major sediment facies with coarser sediment not uniformly distributed and occurring in patches. The studied area is localized approximately 650 m east of the Dooneen Point and ca. 2.4 km west of the Carbery Island. It comprises 225000 m^2 of seabed. Surface sediments are dominated by mud and fine sands with two major rock outcrops southeast and northwest of the pockmark field (Figure 76&77).

4.1.2 Distribution of pockmarks in Dunmanus Bay

Dunmanus Bay field contains 60+ pockmarks that reach up to 20 m in diameter and range from 0.3 to 0.8 m in depth. Pockmarks occur in clusters of 5-9 larger features with small, random satellite pockmarks (1-2 m wide) in the vicinity of these clusters (Figure 77).

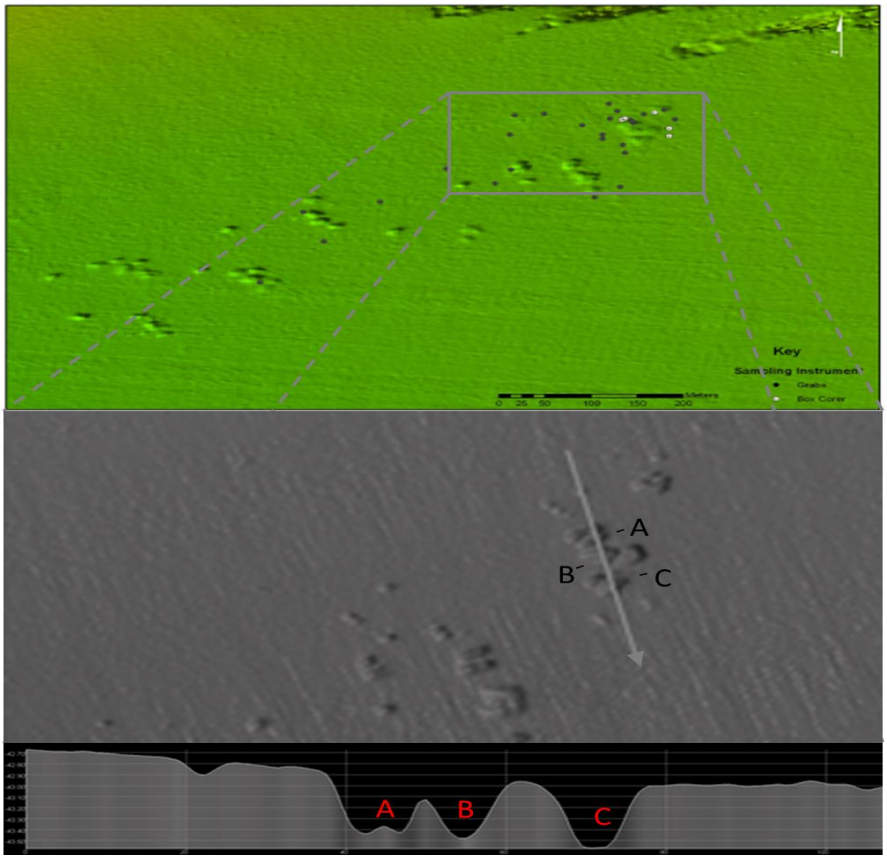

Figure 77. Shaded relief bathymetry of Dunmanus Bay pockmark field (top panel), and a magnification of the northern pockmark cluster with cross section profile (bottom panel).

The clusters appear to be parallel to each other however the entire field shows clear NE-SW orientation limited by two rock outcrops.

4.1.3 Objectives

First objective of the Dunmanus Bay survey is the characterization of the small pockmark field detected during the INFOMAR mapping programme; investigation of the nature of the fluids involved in formation of these features and understanding of the fluid dynamics in this area. This is achieved by analysis of physical and geochemical properties of the seabed and the water column. The results are presented in paragraphs 4.3.1 and 4.3.2. Second objective is to investigate the relationship between benthic communities, pockmarks and fluids involved in their formation. The results are reported in paragraph 4.3.3.

4.2 Materials and Methods

4.2.1 Geophysical characterization of the seabed and the subsurface

4.2.1.1 Bathymetry

Pockmarks in Dunmanus Bay were identified in 2007 during a multibeam survey carried out by the RV Celtic Voyager as a part of the INFOMAR program. Bathymetric data of Dunmanus Bay was acquired in 2006 during a Tenix Lidar survey (shallow water) and on board the RV Celtic Explorer (mouth and outer part of the bay). Although data acquired during these surveys permitted identification of the pockmark field, low resolution of the data limited insight into the morphology of these features. In April 2009 the RV Celtic Voyager acquired very high resolution data that permitted further insight into morphology and distribution of the Dunmanus Bay pockmarks (Szpak et al. 2009). For details on instruments used and data acquisition parameters see Chapter 2, paragraph 2.2.2.

4.2.1.2 Sub bottom profiler

Sub-bottom profiler data was acquired during 2007 RV Celtic Voyager seabed mapping survey. During the CV09_23 research cruise carried out in April 2009 additional sub-bottom data was acquired. However since the quality of these data sets were comparable the data acquired in 2009 were not processed and the data from 2007 is now the primary data set. For details on instruments used and data acquisition parameters see Chapter 2, paragraph 2.2.2.

4.2.2 Physical and chemical properties of the water column

4.2.2.1 CTD measurements and water sampling

Conductivity, temperature and density (CTD) profiles were recorded with an SBE 911 CTD (Sea-Bird Electronics Inc., USA). Additionally, turbidity of the water column was monitored with a CST-1098DR transmissometer. Profiles were acquired during descent of the carousel. Water column samples were collected with 5 l Niskin type bottles mounted on a SBE 32 Carousel Water sampler (Sea-Bird Electronics Inc., USA). The collected CTD measurements permitted sample depth selection in a more informative manner. Upon retrieval, water samples were transferred immediately to 125 ml serum bottles and crimp sealed with gas-tight thick butyl rubber septa. All water samples were poisoned with a saturated mercuric chloride ($HgCl_2$) solution to inhibit microbial activity and stored at 2-4^{o}C until analysis.

4.2.2.2 Chlorophyll *a*

Chlorophyll *a* concentrations were derived from fluorescence measurements acquired during the CTD casts with an ECO AFL/AF fluorometer (Wet Labs, USA). The instrument was calibrated on-land against chlorophyll *a* standards prior to the cruise. The range of calibration was from 0.04 to 200 µg/l.

4.2.2.3 Dissolved methane analysis

METS

A dissolved methane sensor METS (Franatech GmbH, Germany) was mounted on the Sea-Bird 911 CTD (Sea-Bird Electronics Inc., USA) unit. The CTD's water pump feeding tubes were modified to ensure that both sensors analyse the same representative water sample. The sensor was calibrated by the manufacturer for methane concentrations ranging from 2 to 200 nmol/l in a temperature range from 2 to 20^{o}C. The METS type sensors has a relatively slow response time, therefore an equilibration test was performed to assess the minimal time necessary to reach baseline signal after saturation. Lag time varied between 200 and 300 s depending on saturation conditions. The sensor was deployed with the CTD and held 5 m above the seabed until the signal stabilized. Between deployments the sensor was kept powered on and immersed in running surface water to minimize humidity and temperature variability.

Direct analysis by gas chromatography

Samples were analysed according to a modified head-space method with salting out as described by Gal'chenko et al. 2004. Briefly samples were boiled in a water bath for 1 h on the day of analysis to ensure full desorption of methane. Due to the breakdown of a portable gas chromatograph (Model 312, PID Analyzers) the methane content from head-space was

determined on shore after the cruise on a Carlo Erba gas chromatograph equipped with HP-PLOT Q capillary column (30 m × 0.32 mm i.d., 20 µm film thickness) and flame ionization detector (GC-FID). The detector temperature was set to 225°C and H_2 was used as carrier gas. Samples were quantified based on the methane gas standard response as described in Gal'chenko et al. 2004. Method robustness was tested with methane standards across a range of concentrations and yielded with a precision of ± 0.5 nM, n=4 for concentrations <25 nM.

4.2.3 Physical properties of the sediment

Sediment samples for physical and geochemical analysis were collected with use of box and gravity corers (2 m barrel). Samples for biological screening were collected with a Day Grab sampler. Instrument performance was excellent with the box corer and Day Grab yielding from 80 to 100% recovery. The gravity corer on the other hand performed below expectations and yielded recoveries from 50 to 60%.

4.2.3.1 Particle size analysis

Samples were analysed according to the dry sieving methodology. Approximately 100 g of oven dried sediment was carefully pulverized with mortar and pestle and sieved through a series of Wentworth sieves (McMahon et al. 1996) and a calculation made of the contributions of fractions (Table 26).

Table 26. Sediment particle size ranges using during dry sieving. After Szpak et al. 2009.

Range of Particle Size	Classification	Phi Unit
<63 µm	Silt/Clay	>4 Ø
63-125 µm	Very Fine Sand	4 Ø, 3.5 Ø
125-250 µm	Fine Sand	3 Ø, 2.5 Ø
250-500 µm	Medium Sand	2 Ø, 1.5 Ø
500-1000 µm	Coarse Sand	1 Ø, 0.5 Ø
1000-2000 µm	Very Coarse Sand	0 Ø, -0.5 Ø
>2000 µm	Gravel	-1 Ø, -1.5 Ø, -2 Ø, -3 Ø, -4 Ø

4.2.4 Geochemical properties of the sediment

4.2.4.1 Pore water methane analysis

The sediment core liner was cut with a reciprocating saw and the core was split with the help of cheese wire. Immediately after opening the core small sediment cores were sampled with cut-off syringes (10 cm^3) and transferred to prepared head-space vials filled with an NaCl water solution poisoned with a saturated mercuric chloride ($HgCl_2$) solution as described by Gal'chenko et al. 2004 and processed similarly to the water samples. The concentration of interstitial methane was determined in a similar manner as the water column samples.

4.2.4.2 Oxidation reduction potential (E_h)

Upon retrieval samples were transferred to an Argon purged inflatable glove box and after interstitial methane sampling was performed redox potential (E_h) measurements were taken with the use of a temperature compensated push-in Pt electrode with an Ag/AgCl reference junction (SCHOTT). The electrode was routinely checked for sulphide poisoning and tested for reproducibility between measurement series with saturated quinhydrone (Sigma-Aldrich) pH buffer solutions (pH = 4.0 and 7.0, with expected $\Delta Eh = 172 \pm 4$ mV).

4.2.4.3 Pore water sulphate and chloride screening

Whole sediment subsamples for dissolved sulphate and chloride analysis were collected using plastic spatula and transferred to centrifuge tubes. Samples were stored at 4°C for the duration of the cruise. Pore fluid was extracted through centrifugation and analysed on shore by the standard ion chromatography approach (see Chapter 2, paragraph 2.2.4.4).

4.2.5 Benthos survey

4.2.5.1 Sediment sampling

Sediment samples for benthos survey were collected with a 0.1 m^2 Day Grab sampler in five replicates. Subsamples for meiofaunal analysis were collected directly from the Day Grab with 10 cm Perspex core (φ - 5 cm) across the entire depth of the recovered sediment, washed with freshwater and fixed with a 10% buffered formalin solution. The remaining sediment was intended for macrofaunal analysis. Sediment was transferred from the sampler onto a 1 mm mesh sieve and wet sieved. Retained macrofaunal assemblage was fixed with a 10% buffered formalin solution. Samples were stored at 4°C for the duration of the cruise and transferred to the laboratory immediately after conclusion of the expedition. In the laboratory meiofaunal samples were sieved through 1 mm sieve to separate macrofaunal species. All assemblages were sorted under a microscope into four groups: Polychaeta, Mollusca, Crustacea and others consisting mainly of echinoderms, nematodes, nemerteans, cnidarians and other lesser phyla.

4.2.5.2 Univariate and multivariate analysis

Univariate and multivariate statistical analyses were carried out on the combined replicate station-by-station faunal data. The following diversity indices were calculated: Margalef's species richness index (D), (Margalef, 1958), Pielou's Evenness index (J), (Pielou, 1977) and Shannon-Wiener diversity index (H'), (Pielou, 1977). The PRIMER ® programme (Clarke and Warwick, 2001) was used to carry out multivariate analyses. All species/abundance data were fourth root transformed and used to prepare a Bray-Curtis similarity matrix in PRIMER ®. The fourth root transformation was used in order to down-weigh the importance of the highly abundant species and to allow the mid-range and rarer species to play a part in the

similarity calculation. The Bray-Curtis similarity matrix was subjected to a non-metric multi-dimensional scaling (MDS) algorithm and cluster analysis (Kruskal and Wish, 1978).

4.2.5.3 Sediment Profile Imagery

Sediment profile images were taken in five replicates at the same locations as benthic samples with Sediment Profile Imagery camera (SPI; AQUAFACT International Services Ltd., Ireland). SPI cameras permit *in situ* images of the undisturbed sediment water interface to be obtained which is impossible to obtain *ex situ* mainly due to sediment disruption and compaction during sampling with use of conventional apparatus (Somerfieled and Clarke, 1997). SPI cameras mounted on a frame are slowly lowered on to the seabed to minimize sediment disruption and then hydraulic or gravity based system is triggered from the vessel to insert the prism into the seabed (Figure 78)

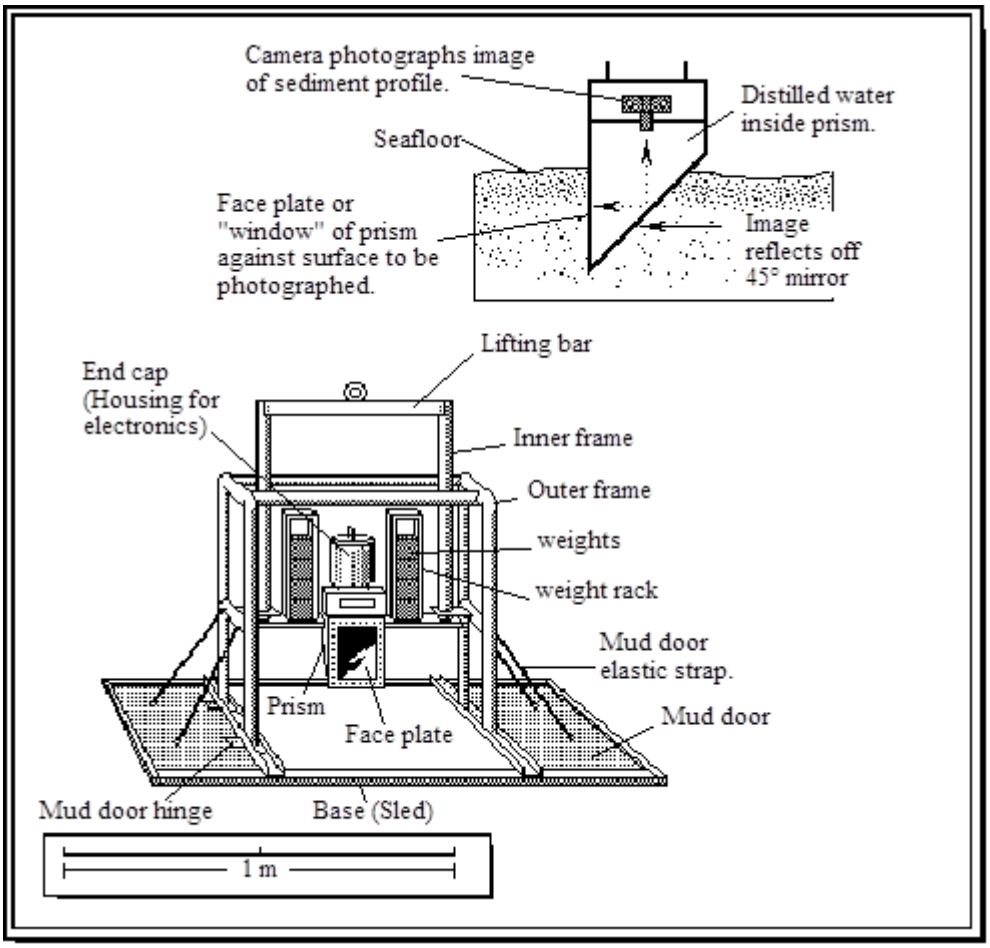

Figure 78. SPI system used to obtain images of sediment water interface (Szpak et al. 2009; AQUAFACT International Services Ltd.).

4.3 Results and discussion

4.3.1 Physical properties of the seabed and the water column

4.3.1.1 Particle size distribution

Particle size distributions show that the seabed has a uniform structure and in generally fits into the sediment type that is considered pockmark prone (Judd and Hovland, 2007). Overall sediment in all stations was similar across all size classes and comprised mainly sands with a small percentage of gravel and with significant but not dominant silt/clay component (Table 27). The percentage of gravel varied from 6.0 to 19.2% and more gravel was found in the stations located in the vicinity of rock outcroppings suggesting erosional origin rather than typical drop stones. The roundness of gravel varied and both angular and rounded clasts were present implying mixed origin. Sands were almost evenly distributed across their size classes and ranged from 49.0 to 70% (mean 56.5%, n=10) with the finer facies being slightly more abundant (from 24.1 to 50.1%). Silt and clay comprised of approximately a third (mean 32.8%, n=10) of the total volume of the sediment and ranged from 24.7 to 38.6%. With the sedimentary matrix being relatively uniform across all stations grain size changes should have a negligible effect on the benthos community structure (Clarke and Green, 1988).

Table 27. Particle size distribution of the surface sediments in Dunmanus Bay pockmark field.

	Grain size (µm)									
Site	>2000	>1000	>500	>250	>125	>63	<63	Gravel	Sand	Silt/Clay
17	14.9	13	10.4	8.9	8.9	11.2	32.7	14.9	52.4	32.7
18	7.4	9.9	9.7	8.1	9.2	17.1	38.6	7.4	54	38.6
41	19.2	10.2	10.2	9.4	9	15.6	26.4	19.2	54.4	26.4
19	6.3	12.3	14.1	11.7	10.8	12.5	32.3	6.3	61.4	32.3
20	12.3	9.8	8.7	7.9	6.9	15.7	36	12.3	49	36
21	15.1	10.9	9.1	7.6	9.3	14	33.8	15.1	50.9	33.8
22	6	12.1	12.4	11	10.8	13.6	34.1	6	59.9	34.1
39	5.3	6.9	39	5.1	6.9	12.1	24.7	5.3	70	24.7
16	2.2	5.5	5.8	4.7	14.3	31.1	36.4	2.2	61.4	36.4
40	15.4	12.8	9.7	8.4	9.3	11.6	32.8	15.4	51.8	32.8

4.3.1.2 Water column physio-chemical structure

Thermo and haloclines were well defined on an average depth of 11 m. The average surface water temperature was 10.6 ^{o}C and 10.2 ^{o}C below the thermocline and 9.6 ^{o}C at near bottom. The salinity reaches average open ocean values and generally follows the thermocline fronts with surface water reaching a salinity of 34.92 psu increasing to 35.05 psu below the pycnocline and 35.08 psu in near bottom waters. These values indicate that Dunmanus Bay is more marine than estuarine environment with little freshwater influence. The effects of weak coastal upwelling could be observed in the water column but generally tidal activity is low as

Dunmanus Bay is out of the main tidal flow (Cross and Southgate, 1983). Uniform water column structure was expected as the survey area is only 2 km long. This is an important finding since significant variability in the water column characteristics can affect benthic community structure (Clarke and Green, 1988).

4.3.1.3 Chlorophyll *a*

Chlorophyll *a* (Chl *a*) concentrations were similar in all stations and varied between 3.33 - 2.33 µg/l. Chl *a* maximum was present on an average depth of 17 m. The concentration of phytoplankton started to increase just after the pycnocline, with the lower boundary located around 30 m. A slight decline in concentrations (R^2=0.41, n=9) can be observed across the transect (Figure 79). These values are consistent with previously reported for sister Bantry Bay (Gribble et al. 2007) as there is no plankton data published on Dunmanus Bay.

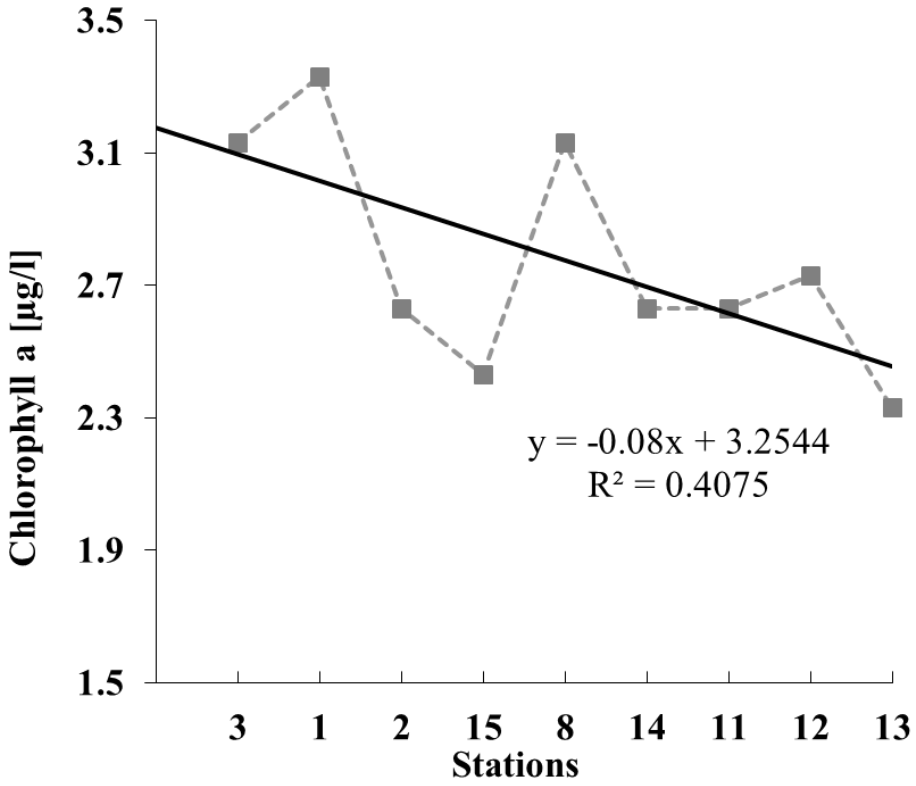

Figure 79. Chlorophyll a concentrations across the Dunmanus Bay pockmark field.

4.3.2 Formation of Dunmanus Bay pockmarks

Pockmarks are seabed features associated with fluid expulsion through the seabed (see Chapter 1). The fluid involved in the formation of most marine pockmarks, discovered in areas not adjacent to landmass and therefore devoid of a potential aquifer influence, is hydrocarbon gas (Judd and Hovland, 2007). Nevertheless exceptions to this generalisation have been reported. In areas of the Florida Escarpment which is a part of the Florida Platform freshwater

seeps occurs at depths exceeding 3000 m (Paull et al. 1984). Another example is Black Ridge located ca. 200 km offshore at 600 m depth (Judd and Hovland, 2007). However in general estuarine, lacustrine and coastal settings groundwater escape is a viable mechanism of pockmark formation. Pockmarks formed by this mechanisms have been widely reported (e.g. Christodoulou et al. 2003; Judd and Hovland, 2007). Since Dunmanus Bay pockmarks are located just 650 m away from the landmass freshwater expulsion is a potential and probable formation mechanism of these features. Moreover abundance differences of micro, meio- and macrofauna in areas where seepage has been reported in comparison to unaffected seabed suggests a genuine relationship between these features and benthic communities (Straugham, 1982). To unravel the question of pockmark formation and their impact if any on the habitat of Dunmanus Bay a comprehensive survey was performed that involved characterization of the water column, seabed, sub surface and benthic communities with use of both direct and remote techniques. Locations of sampling stations are given in Figure 80.

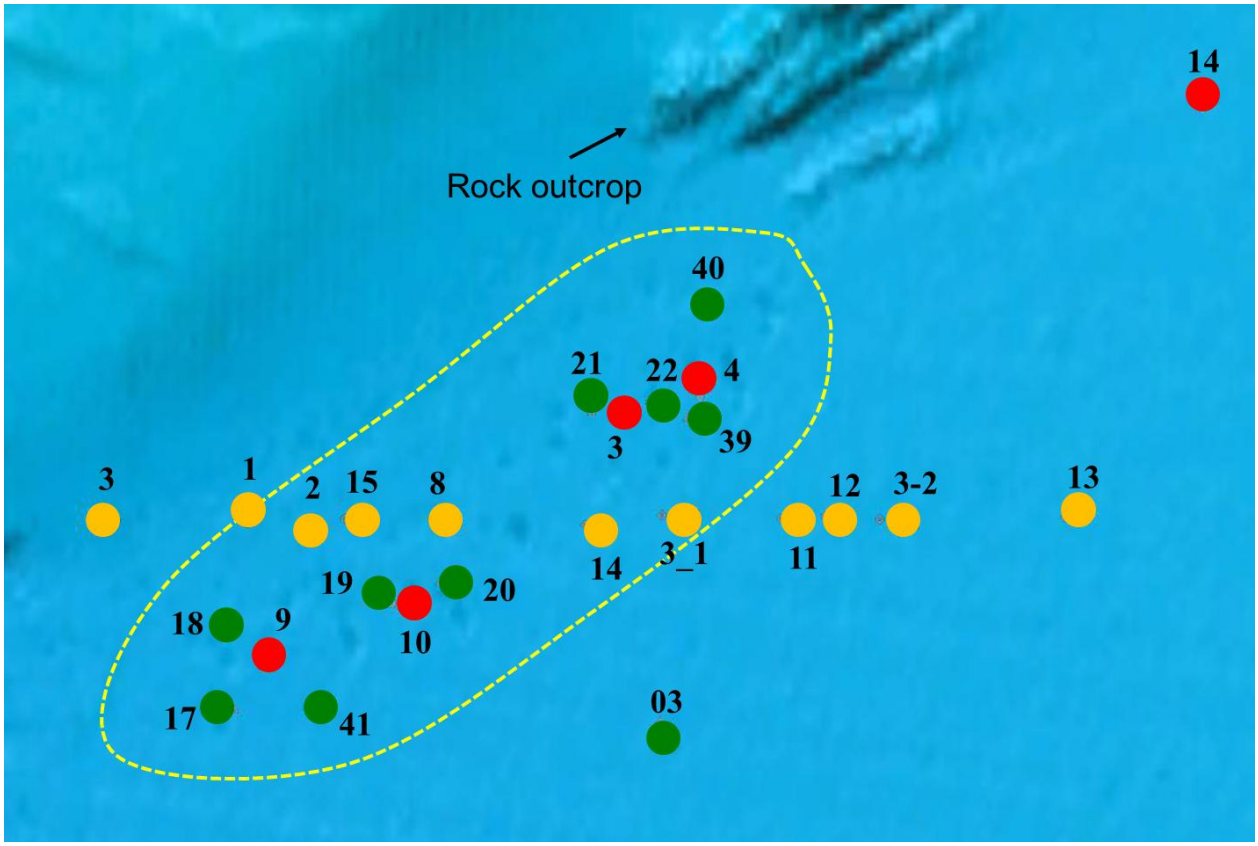

Figure 80. Sampling stations in the Dunmanus Bay pockmark field. Stations are colour coded for clarity. Green: benthos, particle size distribution; red: gravity cores; yellow: CTD casts. Yellow dashed line delineates pockmark field. Box cores locations are not shown for clarity.

There was no evidence of salinity changes similar to that reported by Christodoulou et al. 2003 and others that would imply active flow of freshwater into the water column. The salinity in the last 10 m of the water column shows a gentle increasing trend in all stations to reach an average value of 35.07 psu. Unfortunately the CTD carousel due to weather conditions

had to be kept approximately 5 m above the seabed to compensate for the swell induced rocking of the vessel and protect the instrument from contacting the seabed. Interestingly the salinity decrease reported by Christodoulou et al. 2003 was observed in the 3 m water layer above the seabed and the water column above was not affected. It is therefore possible that moderate freshwater flow was not recorded in the above mentioned experimental conditions. Detailed video surveying of these pockmarks with a fly-by camera during a 2011 CE11_017 research cruise did not reveal any visible freshwater flow (Xavier Monteys, personal communication). This finding however does not necessarily eliminate the possibility of freshwater expulsion which might occur periodically. The western coast of Ireland is known for high precipitation and the Dunmanus Bay area is one of the two locations in the entire country (the other being west of Connaught) where annual mean rainfall exceeds 2800 mm/year (Met Eireann, 1961-1990 annual mean, www.met.ie/climate/rainfall.asp). Moreover there is little vegetation that could assimilate at least a portion of the rainfall, and permeable rocks such as limestone and sandstone are the dominant rock type in the area (Naylor, 1975). According to Burnett et al. 2003 these are the main factors along with groundwater abstraction and topography that control the likelihood of a groundwater discharge in a coastal setting. Given the above it could be expected that periodically, particularly after heavy rainfall, the amount of freshwater in unconfined aquifers will increase. This can result in a pressure gradient that can potentially result in pore fluid displacement and/or freshwater expulsion (Judd and Hovland, 2007). This hypothesis is however not supported by the pore fluid data from the collected sediment core, although profiles show some interesting features (Figure 81). The concentration of chloride in the entire core appears to be lower than that typically expected for seawater (560 mM). Moreover the sulphate curve shows a decreasing linear gradient up to 1 mbsf, the concentration then stabilizes at around 16.5 mM and the last measuring point in both chloride and sulphate shows a slight increase. Low chloride content throughout the core in general might indicate dilution with freshwater from deeper sections of the sediment thus supporting the hypothesis of aquifer contribution to subsurface pore fluids. However an upward diffusion or advection and even more so an extrusion of freshwater would certainly have more significant impact on the shape of both chloride and sulphate curves. A sharp decrease would be expected in the case of intrusion and for a diffusive/advective scenario a linear or concave profile would be expected (Schulz and Zabel, 2005). Unfortunately a poor gravity core performance did not permit sampling for longer cores to verify these scenarios. Nevertheless assuming steady state conditions and extrapolating the sulphate profile, the depletion of sulphate could occur at around 2.3 mbsf. However results from the recent cruise (CE11_017) where 6 m long vibro cores were collected revealed that trends observed here are indeed correct (O'Reilly et al. 2011). The sulphate profiles show an initial decrease and then at around 1.5 mbsf the trend is reversed possibly by re-oxidation of sulphite.

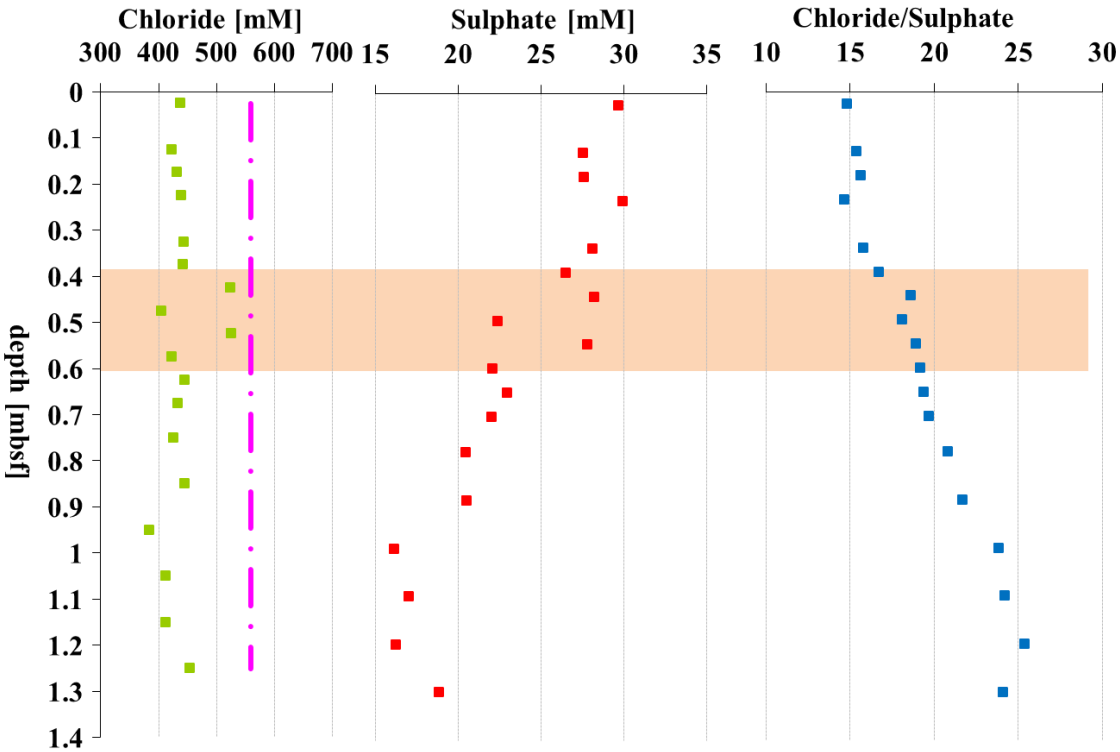

Figure 81. Pore fluid sulphate and chloride depth profiles in a sediment core from a pockmark location. Dashed line denotes typical for seawater chloride concentration (560 mM). Orange area denotes sandy layer.

Chloride on the other hand shows a linear profile throughout the entire core with a concentration of 580 mM. The mysterious low chloride concentration is most likely related to an accidental sample freezing that occurred during the cruise. For a short period of time part of the sediment designated for pore water analysis was placed in a freezer. When this was discovered samples were immediately transferred to a refrigerator, however they were partially frozen. It is a known phenomenon that inorganic seawater salts that precipitate during freezing do not redissolve completely upon thawing (Schulz and Zabel, 2005). Interestingly sulphate values were not affected. Given the above we find no evidence of pore water freshening of both water column and the sediment. Therefore despite favourable environmental and geological conditions we can conclude that freshwater expulsion is not a likely mechanism for the formation of Dunmanus Bay pockmarks.

Since freshwater is rather unlikely the fluid involved in the formation of these features alternatively hydrocarbon gas can be responsible. The sub bottom data contain multiple signals that are commonly interpreted as associated with shallow gas and gas venting into the water column (Figure 82). Numerous and extensive areas of acoustic turbidity (AT) as well as hyperbolic reflectors (HR) in the water column in the vicinity of the AT are visible (middle panel). As discussed in Chapter 1 (paragraph 1.1.4) and Chapter 2 (paragraph 2.3.2) AT is a

strong indicator of shallow gas accumulation, similarly as observed in the Malin Shelf. The AT appears to be extended over a relatively wide area and yet also confined to a particular sedimentary facies as there is clearly less turbidity above and below the main feature. Moreover acoustic blanking (AB) observed below the gas front in the composite pockmark P1 in the Malin Shelf is virtually absent in this setting. Only one visible amplitude decrease is observed below one of the pockmarks that could be ascribed to weak AB (Figure 82, bottom panel). Although it is not as apparent as in the Malin Shelf area however weakening and partial discontinuity of the bedrock reflector below this feature is clearly visible. In this area gas appears to be more dispersed and more evenly distributed in the sediment. Moreover the AT is less profound than in the area to the north-west which might be related to grain size distribution and compaction of the sediment, however the latter is of a less importance composed almost exclusively of young, non-consolidated sediments. These two parameters control the porosity of the sediment and indirectly size of the pore space available for the gas to occupy. As discussed previously the weaker AT signal might not necessarily mean that there is less gas in the sediment as signal attenuation is related to bubble diameter rather than concentration. Therefore it is impossible to infer gas concentrations from seismic data alone and ground-truthing is necessary (for explanation see Chapter 1, paragraph 1.1.4). An important feature of these seismic profiles is the lack of AB signals below the prominent AT area. This suggests that gas might be generated in this lateral facies rather than vented from faults in the bedrock, except for the location discussed above where a deeper source cannot be ruled out. Assuming that gas is continuously vented from a deeper source, namely bedrock fault, signals such as AB or AT connecting with the bedrock are to be expected. However this is only true for a continuous gas supply scenario. Periodic gas migration caused by successive cycles of seal failure-renewal could still be a viable scenario particularly given the vicinity of Gortavallig and Dunmanus Faults. Importantly the Gortavallig Fault crosses directly underneath the area where weak AB and discontinuity of bedrock reflector were observed. The acoustic signals in the water column (HR) can easily be mixed up with fish swim bladders. Shape and migration patterns are two means of distinguishing between the two (Judd and Hovland, 2007). Fish shoals according to Judd et al. 1997 are more diffuse and horizontally extended whereas seeping gas will have more columnar, vertically extended characteristics. The shape of hyperbolic reflectors observed in pinger data (Figure 82) is both horizontally and vertically extended and thus ambiguous and difficult to interpret. However MBES data also contains very narrow and exclusively vertical signals that are most likely caused by ascending bubbles. (Figure 83). These signals do not appear to be artefacts since they occur in multiple places (not all of such signatures detected are shown on Figure 83) in different areas and more importantly the same verticals signals are observed in different lines in the same seabed area (e.g. Figure 83, middle panel).

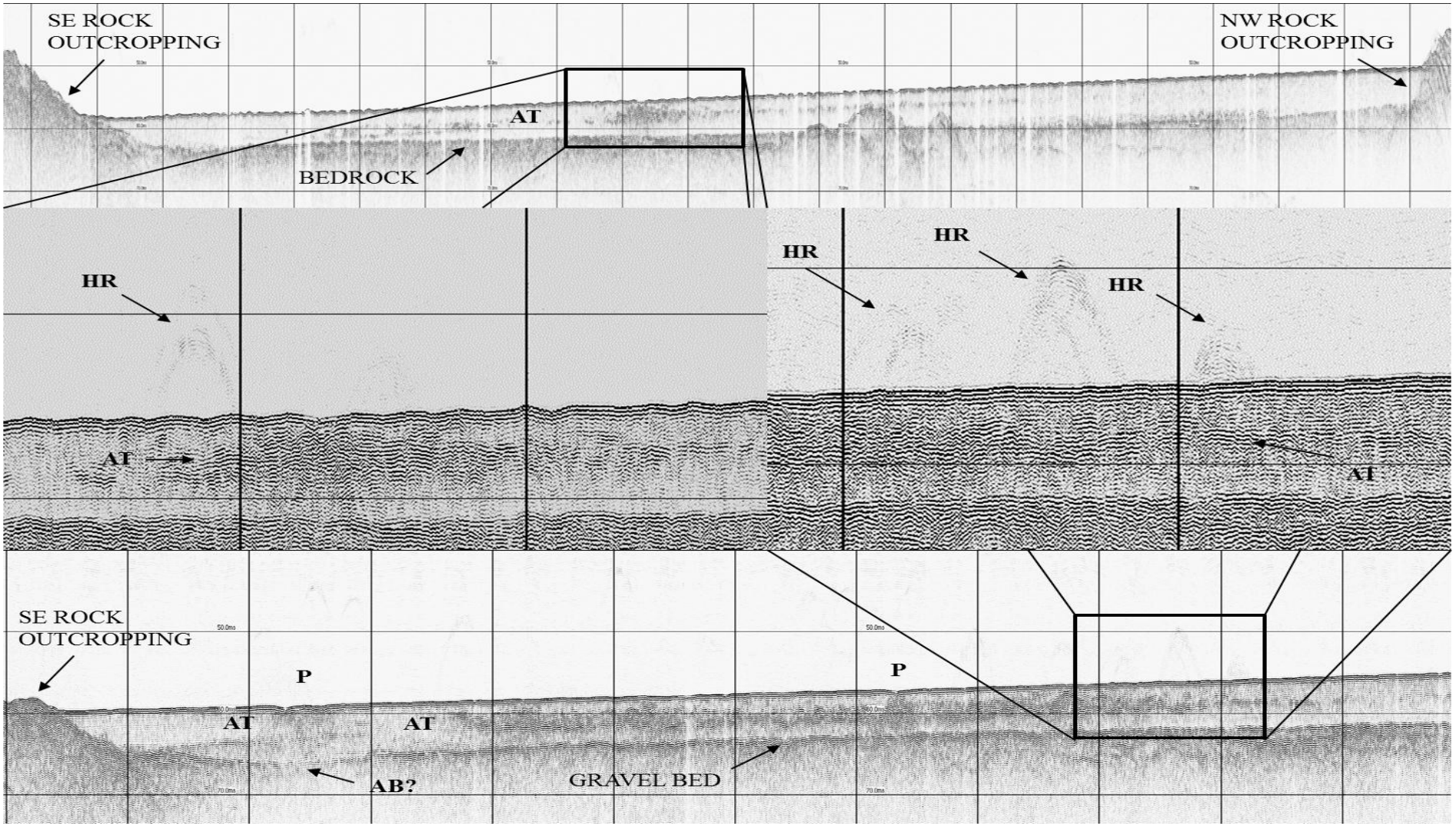

Figure 82. Sub-bottom 3.5 kHz profile (pinger) of the seabed across the pockmark field in Dunmanus Bay. Numerous and extensive areas of acoustic turbidity (AT) as well hyperbolic reflectors (HR) are visible. In areas where pockmark (P) features are visible the acoustic turbidity appears to be reaching the water sediment interface. Middle panel shows magnification of areas marked with a black rectangular, the image was corrected to highlight the hyperbolic reflectors in the water column.

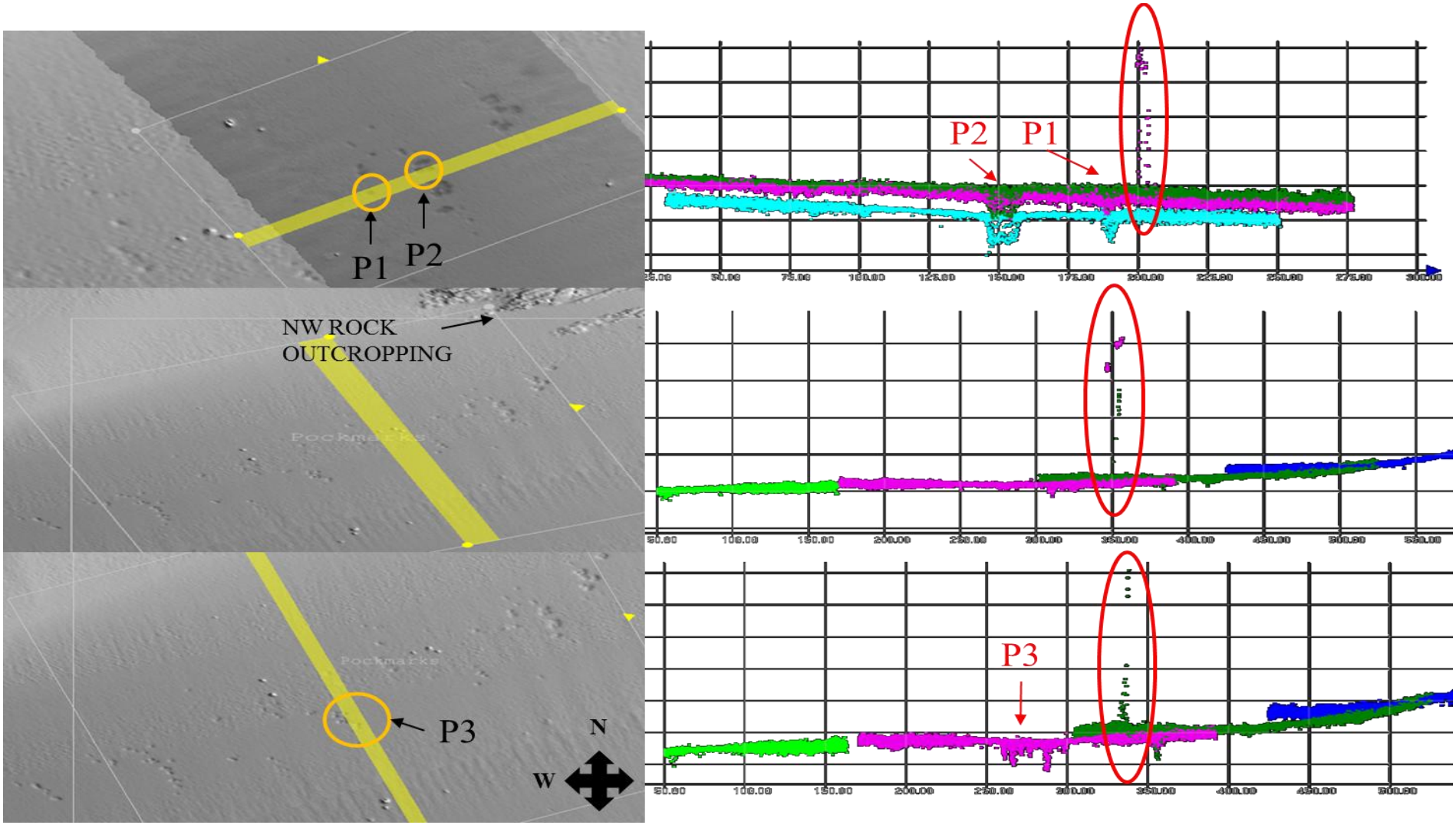

Figure. 83. MBES shaded relief bathymetry (left panel) and individual multibeam lines (right panel) data showing gas bubbles in the water column in the vicinity of the pockmark features.

Judging from the pockmark size and the acoustic signals in the subsurface, gas venting may be moderate in nature. The pockmarks are relatively small and they are accompanied by scattered small satellite features. Hovland et al. 2010 suggested that small satellite unit-pockmarks represent most recent and most active local seepage locations. Detection of active venting can be troublesome according to current pockmark formation models (e.g. Cathles et al. 2010) and field data (Judd and Hovland, 2007). Periodic gas expulsion, particularly after initial violent pockmark formation, is typical for most pockmarks and they are considered settings where moderate fluid migration is dominant. Nevertheless active venting has been reported. Newman et al. 2008 demonstrated methane concentrations reaching 100 nM in pockmarks along the US mid-Atlantic shelf break. Christodoulou et al. 2003 reported both freshwater and gas related active pockmarks systems in the Patras and Corinth gulfs, Greece. In both of these studies the METS sensor (Garcia and Masson, 2004) was used to measure methane concentrations in the water column above and in the vicinity of pockmarks. We have employed the same instrument in Dunmanus Bay. Methane concentrations were measured only at 5 m above the seabed since ROV was not available and the sensor had to be mounted on a CTD. The CTD was kept in the water until the sensor signal stabilized. METS response slopes are given in Figure 84.

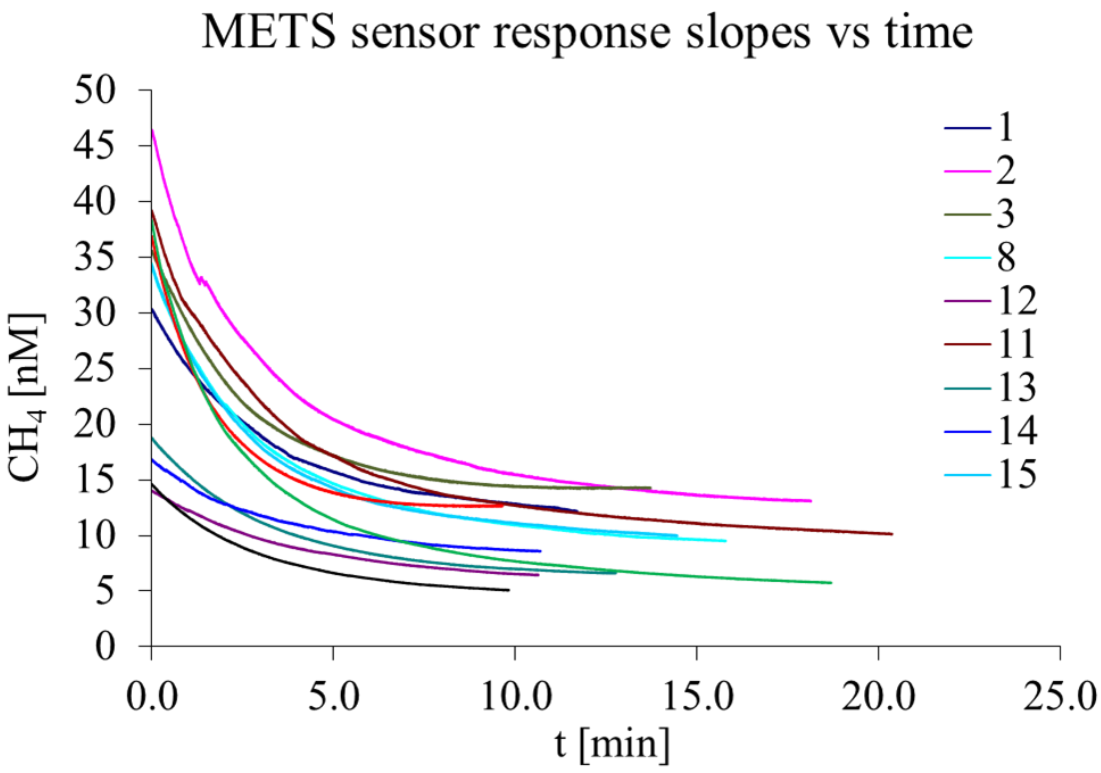

Figure 84. METS sensor response slopes vs time plot.

Methane concentrations recorded by the METS sensor along the SE to NW transect (Figure 80) ranged from 5.1 to 14.2 nM (Table 28). Slightly higher values were consistently

recorded in the western part of the pockmark field however overall variability of the data is low and the highest concentrations only slightly exceed typical marine water methane values (Holmes et al. 2000).

Table 28. Methane concentration in the bottom water measured by METS.

Cast	Lat	Long	CH_4 [nM]
CV0923_03	51.55817	-9.71867	14.2
CV0923_01	51.55700	-9.71667	12.1
CV0923_02	51.55767	-9.71567	13.1
CV0923_15	51.55967	-9.71517	10.2
CV0923_08	51.55933	-9.71383	9.5
CV0923_14	51.55633	-9.71150	8.6
CV0923_3_1	51.56183	-9.71033	5.7
CV0923_11	51.55983	-9.70850	10.2
CV0923_12	51.56133	-9.70783	6.5
CV0923_3_2	51.55950	-9.70700	5.1

The data shows no evidence of major gas plumes in the water column which is in concordance with acoustic data discussed above. It is important to mention that the water sampling campaign was performed 4 days after the bathymetric survey to meet other cruise objectives. The gas plumes recorded were most likely emitted to the atmosphere and the dissolved methane was dispersed in the water column. During the water sampling gas bubbles were not observed. The concentration of methane in the water column shows slightly lower values to those recorded by the METS sensor. Methane in the water column ranged from 1.3 to 7.7 nM (Figure 86). The methane concentrations were slightly higher in the photic zone than in bottom waters however in general it was uniformly distributed in the water body with no strong primary trends. Although it was disappointing to find such low methane concentrations despite acoustic evidence of seepage this is not uncommon even in areas where shallow gas accumulation and venting is more vigorous. Dando et al. 1991 reported methane concentrations from a large active pockmark in the North Sea and only in two of six stations these concentrations exceeded 25 nM, in half of them methane was below 15 nM. They found higher concentrations exceeding 50 nM only in areas where an echo sounder showed gas bubbles in the water column. The water column methane data indicates that we were unable to capture any of the plumes recorded previously. The data suggest discreet and periodic seepage that requires a more targeted approach with use of instruments that are not confined to location but can cover a larger area and are quick to deploy to the active area. The concentration of methane in the sediment cores (Figure 86) shows a general increasing trend with depth. The values range from < 1.0 µM to 6 µM in the deeper sections. Higher hydrocarbons C_{2+} (mostly C2) were present in trace amounts therefore the gas can be considered dry and lack of higher homologs implies microbial origin (Faber and Stahl, 1984; Floodgate and Judd, 1992).

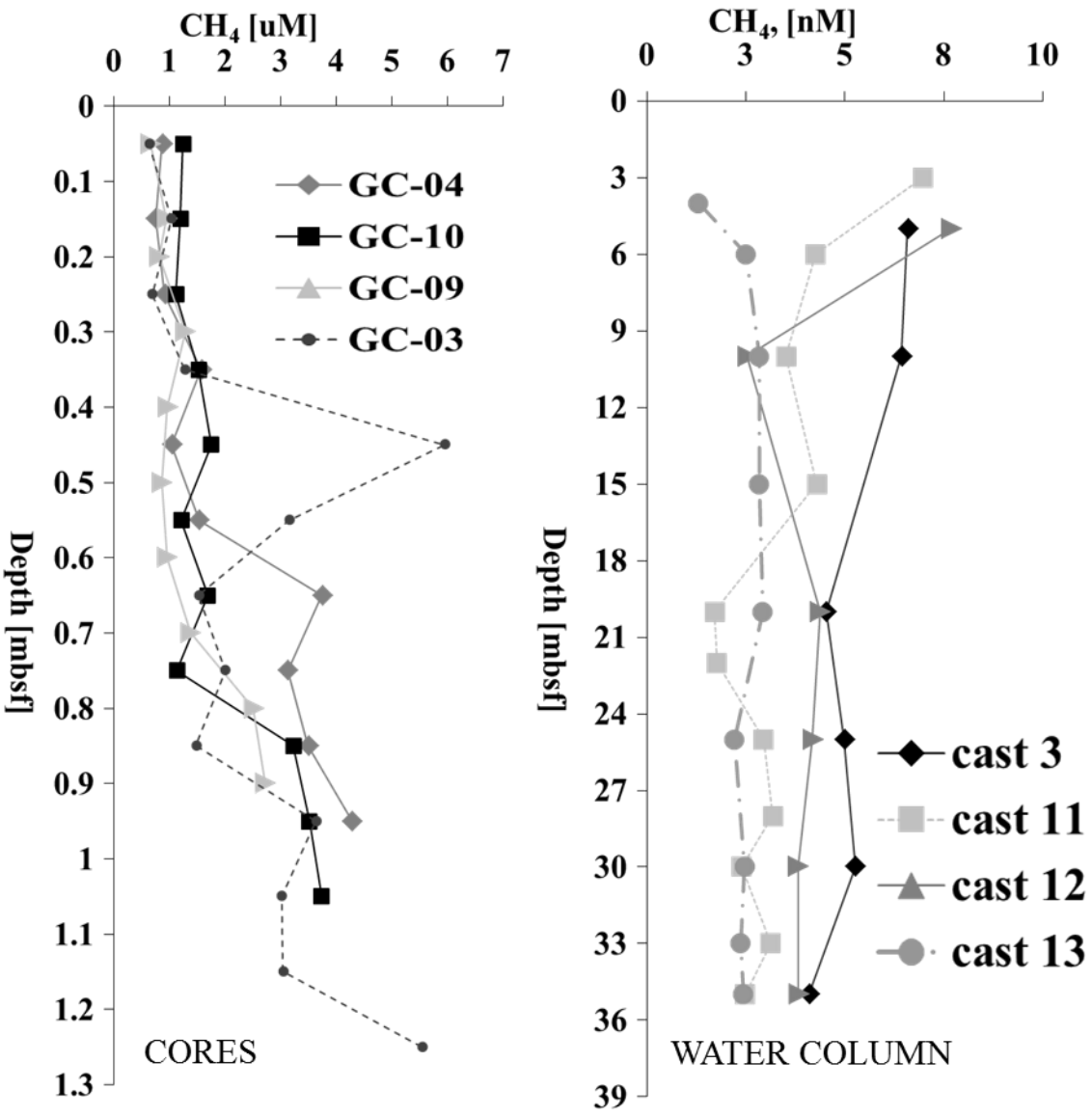

Figure 86. Methane concentrations in the sediment cores (left panel) and the water column (right panel) measured by head-space method.

In a normal setting where shallow gas is absent, methane generation is only possible after sulphate has been depleted and methane is not present in the sediment above the sulphate depletion depth (Schulz and Zabel., 2005). The sulphate is far from depleted yet methane presence was recorded in the sediment. This suggests that the methane is migrating upward from the AT area observed in the sub bottom profile. The in-situ generation of methane in the sediment analysed is not possible since the optimal conditions for microbial methanogenesis were not met. Moreover the conditions in the sediment must be anaerobic since all methanogens are strict anaerobes and contain typically more than 0.5% of organic carbon available to the microbes. The redox potential measurements suggest that conditions in the sediment are indeed anoxic (Figure 87) although sediment was not fully reduced (black).

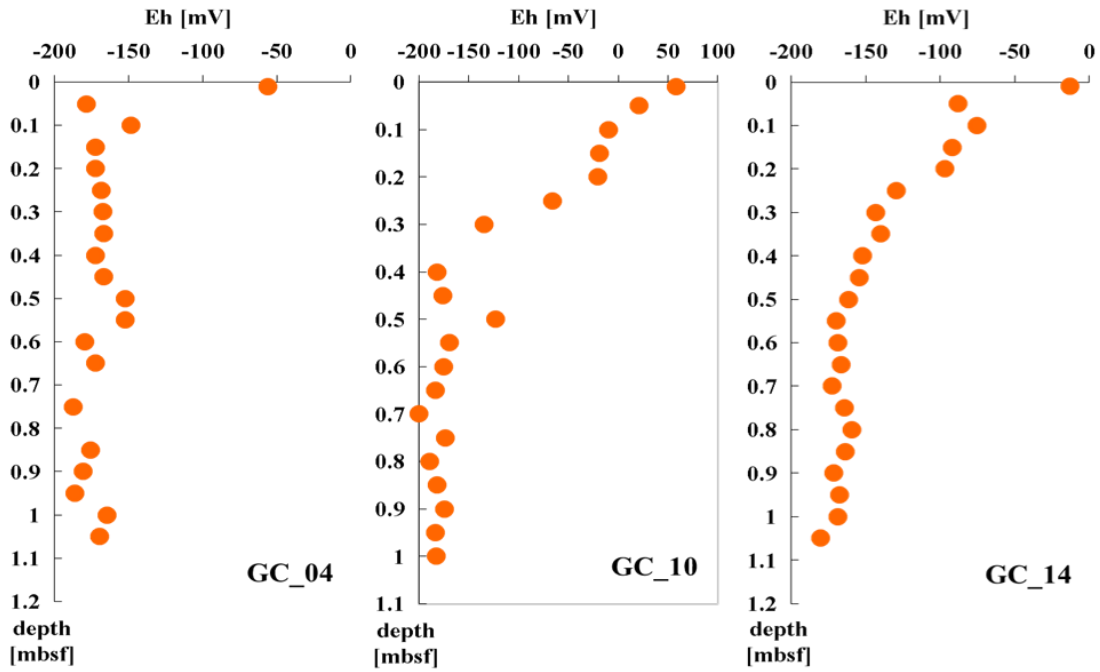

Figure 87. Redox potential (E_h) depth profiles in the sediment core from Dunmanus Bay.

This is an interesting finding given that low redox potential (< 150mV) marking the beginning of anoxic zone is usually, however not always, coupled with depletion of sulphate which we do not observe. Nevertheless given that sulphate is not depleted in the whole 6 m of the seabed (Shane O'Reilly, personal communication), the microbial generation of methane, if it occurs must be take place much deeper.

Dunmanus Bay pockmarks are clearly features created by gas expulsion. The acoustic data confirms presence of shallow, lateral gas accumulation and bubbles in the water column however the water column sampling did not provide solid evidence that these bubbles are methane gas. The pore water data do not provide clear indication as to origin of the gas involved in Dunmanus Bay pockmark formation. The isotopic composition of methane should be determined to answer that question.

4.2.5 Benthos survey

The variety and abundance of marine life associated with seepages can be astounding across all trophic levels. Dynamic, energetic venting systems are known to support unique ecosystems (Kiel, 2010). There is evidence that pockmarks on a smaller scale can support local communities however the debate on that matters continuous (see Chapter 1, paragraph 1.1.8). To examine if local communities from Dunmanus Bay are affected by these features a benthic survey was conducted over the pockmark area (Figure 80).

The benthic infauna taxonomic identification revealed a total of 122 species, comprising 8865 individuals, ascribed to 12 phyla present in the surface sediments. The most abundant organisms were ascribed to polychaetes (57 species), crustaceans (25 speices), molluscsc (13 species) and echinoderms (8 species). Eight phyla were grouped as others; this group consisted of cnidarians, plathyhelminthes, nemerteans, nematodes, priapulids, sipunculids, oligochaetes and phoronids. Species numbers ranged from 23 to 77 (station 21 and 16 respectively). Numbers of individuals ranged from 382 to 1878 (station 20 and 19 respectively). The 5 most abundant species were *Leptopentacta elongata* (Cucumariidae, Duben and Koren), *Amphiura filiformis* (Amphiuridae, Muller), *Tubificoides amplivasatus* (Annelida, Erséus), *Scalibregma inflatum* (Annelida, Rathke) and *Magelona alleni* (Annelida, Wilson) and accounted for over 80% of individuals. Highest species richness was found in the control site and ranged from 3.47 to 11.16 (station 21 and 16 respectively). Evenness index ranged from 0.35 to 0.61 (station 21 and 20 respectively). Diversity ranged from 1.6 to 3.66 (station 21 and 16 respectively). Detailed data are given in Table 29.

Table 29. Diversity indices for the Dunmanus Bay pockmark filed benthic communities.

Station	Species	Individuals	Richness	Evenness	Diversity
16	77	908	11.16	0.58	3.66
17	46	632	6.98	0.57	3.14
18	39	1462	5.21	0.37	1.96
19	43	1878	5.57	0.37	2.01
20	34	382	5.55	0.61	3.09
21	23	568	3.47	0.35	1.60
22	43	786	6.30	0.36	1.94
39	35	929	4.98	0.42	2.17
40	32	741	4.69	0.40	2.02
41	41	579	6.29	0.60	3.19

Classification and cluster analysis was performed to find "natural groupings' of samples, i.e. samples within a group that are more similar to each other, than they are similar to samples in different groups (Figure 88). A highest similarity of 73.9 % was observed between stations 18 and 19. In these stations 53 species were found with three species accounting for 90% of the whole assemblage: sea cucumber *Leptopentacta elongata* (52.7%), polychaete *Scalibregma inflatum* (31.9%) and polychaete *Diplocirrus glaucus* (5.4%). These species accounted for 28% similarity within this group. Because of the dominance of the three species these stations had low richness (5.21 – 5.57), evenness (0.37) and diversity (1.96 - 2.01). Stations 17 and 41 grouped at a similarity level of 71.2 %. These stations contained 57 species with four species accounting for 78.5% of total assemblage: brittlestar *Amphiura filiformis* (25.8%), sea cucumber *Leptopentacta elongata* (24%), polychaete *Diplocirrus glaucus* (14.7%) and polychaete *Scalibregma inflatum* (14%). These four species also accounted for 28% of similarity in this

group. The dominance of these species was not as significant as in other stations as shown by higher diversity indices (Table 29). All four of these stations grouped at a similarity level of

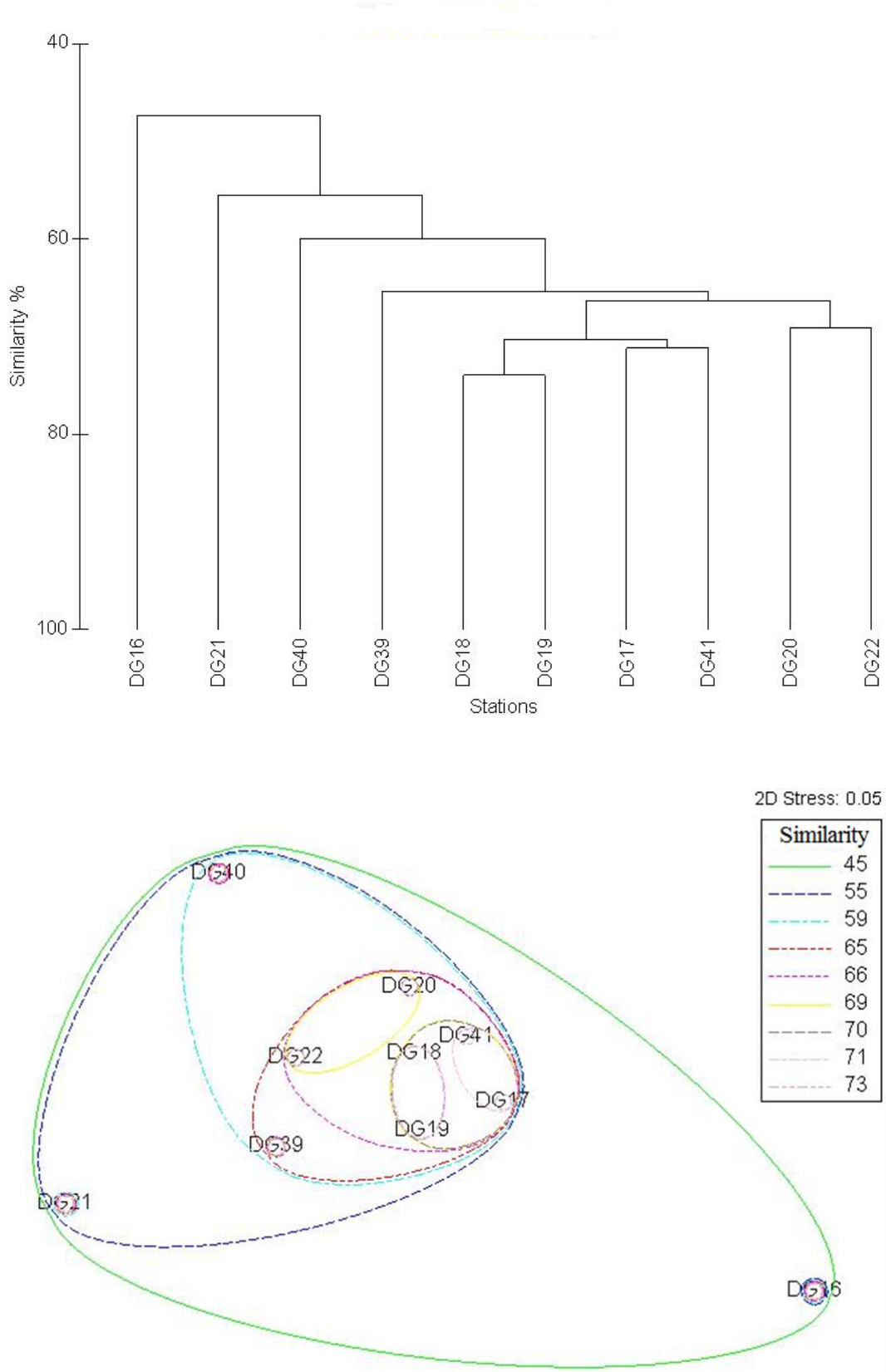

Figure 88. Dendrogram (top panel) and a MDS (bottom panel) plots presenting similarity between benthic communities in the pockmarked area of the Dunmanus Bay.

70.33%. The next most similar stations were 20 and 22 grouping at a similarity level of 69.1 %. A total of 51 species were found in these stations of which three accounted for 80.4% of the whole assemblage: sea cucumber *Leptopentacta elongata* (53.3%), polychaete *Scalibregma inflatum* (21.9%) and polychaete *Diplocirrus glaucus* (5.2%). Because of low numbers of individuals station 20 had the highest evenness and moderate richness and diversity. Station 22 on the other had moderate richness and low evenness and diversity. All six of these stations grouped at a similarity level of 66.4 %. Station 39 grouped with these stations at a similarity level of 65.4 %. In this station 35 species were observed with three accounting for 88.9% of the whole assemblage: sea cucumber *Leptopentacta elongata* (46.9%), polychaete *Scalibregma inflatum* (34.6%) and polychaete *Diplocirrus glaucus* (7.4%). Dominance of three species was reflected in low diversity indices. Next station 40 joined the previously discussed stations with 59.9 % similarity. A total of 32 species with three species accounting for 87.6% of the whole assemblage: polychaete *Scalibregma inflatum* (58.7%), sea cucumber *Leptopentacta elongata* (25%), and polychaete *Diplocirrus glaucus* (3.9%). This station was characterized by low richness, evenness and diversity. Station 21 had a 55.5% similarity with previous stations. A total of 23 species were observed in this station and three species accounted for 89% of individuals: sea cucumber *Leptopentacta elongata* (74.5%), polychaete *Scalibregma inflatum* (11.4%) and oligochaete *Tubificoides amplivasatus* (3.2%). This station was characterized by low richness, evenness and diversity. Finally station 16 had a 47.4 % similarity with 77 species of which four accounted for 75% of all individuals: polychaete *Scalibregma inflatum* (27.9%), sea cucumber *Leptopentacta elongata* (16.2%), brittlestar *Amphiura filiformis* (25.8%) and polychaete *Diplocirrus glaucus* (15%). In this station the highest species number was observed which resulted with high richness and diversity. These delineations were also preserved in the MDS analysis (stress value <0.05). Control station 16 grouped separately from the other stations. Stations 18, 19, 17, 41, 20 and 22 formed a central group with stations 39, 40 and 21 at varying distances from the central group (Figure 88).

Benthic communities in the Dunmanus Bay pockmark field were dominated by four species: sea cucumber *Leptopentacta elongata* (43.6%), polychaete *Scalibregma inflatum* (28.9%), polychaete *Diplocirrus glaucus* (7.5%) the brittlestar *Amphiura filiformis* (6.1%). The *Leptopentacta elongate* is a burrowing sea cucumber often found in U-shaped burrows. It prefers muddy sands or mud and shallow waters. This species is widespread around Great Britain and Ireland. *Scalibregma inflatum* is a segmented worm, an active burrower, often found buried deep in sand or mud. It feeds on organic detritus and this species is widespread around Great Britain, but not that frequently encountered around Ireland. *Diplocirrus glaucus* is also a segmented worm, detritus feeder, often found in sandy and muddy bottoms. This species is widespread in the Northern Atlantic. *Amphiura filiformis* is a small brittle star with very long arms living buried in the sediment with arms extended into the water current to catch suspended

matter. This species is also widespread around Ireland and Great Britain. None of these species has been reported in abundance in active pockmarked areas. The dominant species in the observed benthic community structure are typical representatives of sublittoral benthos around Ireland. The lack of species that are known to be abundant in methane venting settings (e.g. Dando et al. 1991; Jensen et al. 1992; Kiel, 2010) suggests that benthic communities do not benefit nor rely on the occasionally released hydrocarbon gas. Benthic counts indicate a pristine and healthy habitat although with low diversity and low richness.

Images taken from the sediment water interface with the SPI camera show numerous burrows, mainly vertical but lateral are also present, and in places infauna can be spotted (Figure 90). The substrate on the images comprises mainly of very fine sand with a few patches of coarser sand. Progression of natural geochemical zonation is visible in most images in a form of colour change. However in most images the transition is not sharp (i.e image 19) and marked with abundant dark streaks. This might be indicative of bioturbation and/or bioirrigation given the high count of actively burrowing species. The images are in good agreement with the redox potential profiles taken on undisturbed box cores (Figure 89). The oxygenated sediment (with typical values > +200 mV) was found to be present only in the very top layer of the sediment. This layer comprised of photodetrital drift and loose sands therefore measurement of redox potential in such mobile and unconsolidated substrate was not possible in most cases.

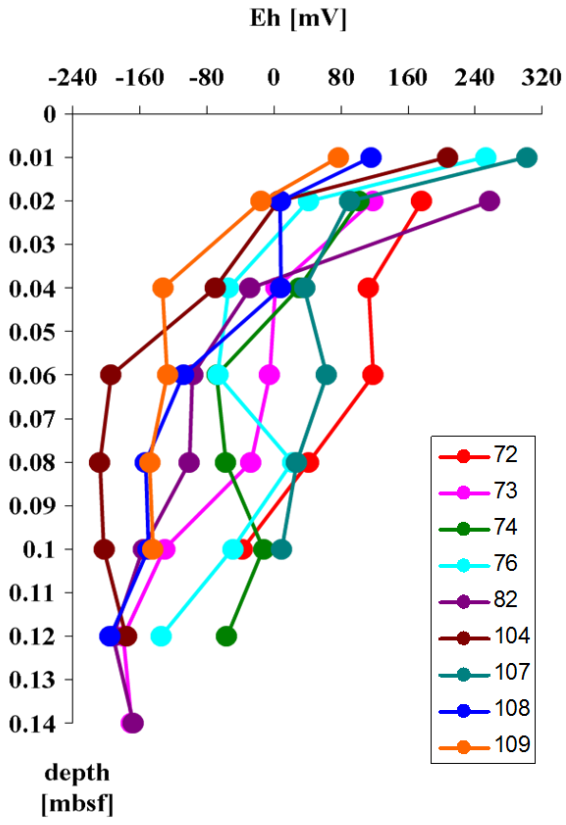

Figure 89. Redox potential (E_h) depth profiles of box cores takes in Dunmanus Bay.

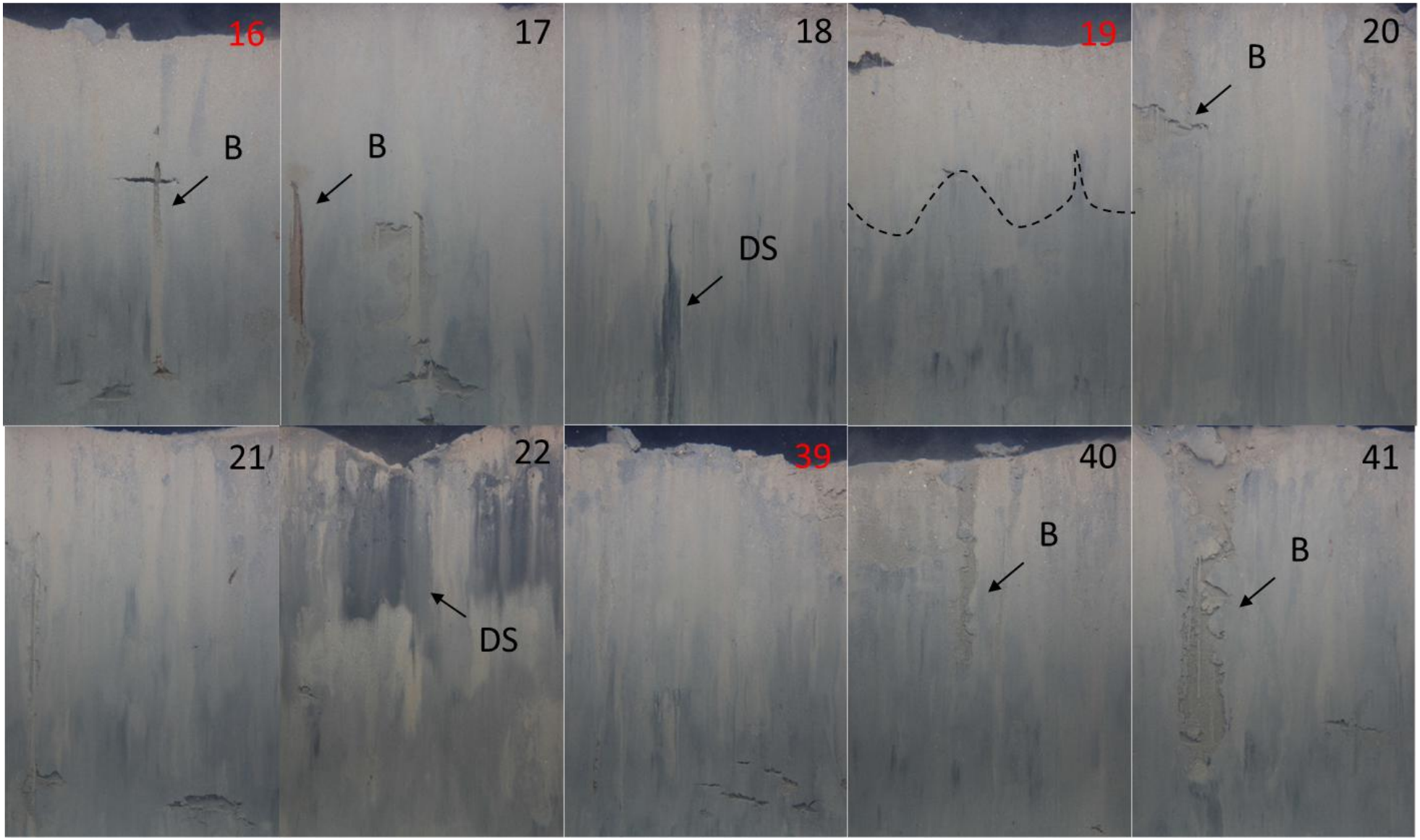

Figure 90. SPI images of the sediment water interface and the first 20 cm of the seabed. Numerous burrows (B), dark streaks (DS) are visible.

This is a natural finding as the penetration of oxygen in marine sediments usually does not exceed a few cm and in areas with high organic input from the water column (high productivity) it can be as low as a few mm or be absent (Schulz and Zabel, 2005). The post oxic zone (with typical values from -150 to +200 mV) depth ranged from a shallow 4 cm to more than 15 cm in most stations. Anoxic conditions (typically < -200 mV) were detected only in one station.

3.4 Conclusions

The survey of the Dunmanus Bay pockmarks revealed gas related features and that an active fluid system is present in the subsurface. The shallow gas accumulation was laterally extended and in most areas did not reach the bedrock. Although penetration of suspected gas accumulation was not achieved based on the methane analysis and pore water profiles we can assume that the gas below is likely to be mainly methane. The pockmarks appear to periodically vent accumulated gas however the scale of these events is small. Similarly as in the Malin Shelf the origin of the gas remains unknown. The sediment in Dunmanus Bay comprised mainly of sands mixed with gravel and finer fractions. The benthic communities were dominated by four common species and overall show structures typical for the sublittoral environment around Ireland. Organisms frequently encountered in areas with methane gas seepages were not observed and thus we conclude that benthic communities do not rely on methane as food source.

CHAPTER 5 – CONCLUDING REMARKS

Geophysical and geochemical characterization of the Malin Shelf, Ireland revealed active fluid system in the subsurface resulting in formation of pockmark features. The fluid involved in the formation of Malin Shelf pockmarks is most likely methane and judging from the geological constrains it can be of thermogenic origin but further studies are required to confirm this hypothesis. Active venting was not observed during this study however migration of fluids in the subsurface was evident from the acoustic data and pore water profiles. The physical properties of the sediment support this finding with the evidence of permeable lithofacies correlated to acoustic gas signatures. Malin Shelf is a setting with relatively high sedimentation rates, dominated with sandy mud in the central part and surrounded with muddy sand on the outskirts. This is in concordance with previous predictions from acoustic seabed classification model. Foraminifera and radiocarbon dating suggest temperate waters with no record of glacial conditions typical of young Quaternary sediments. Geochemical screening of these young sediments revealed typical marine characteristics with no evidence of anthropogenic influence. Future studies of this setting will focus on confirmation of the identity and origin of the gas responsible for formation of pockmarks. To further constrain the time frame of the formation events further radiocarbon studies are necessary. Moreover, acquired data set gives solid grounds for modelling of the fluid flow mechanisms which can be a basis for creating an expanded pockmark formation mechanism that includes lateral fluid migration. This study suggests that distribution of major and trace elements in the Malin Shelf is uniform. In future studies better coverage and sample density could help to validate this suggestion. Similarly low sample density impeded more thorough understanding of the sedimentological regime in this area. Future sedimentological investigations should consider higher sampling density to more accurately describe sources of Malin Shelf sediments and the sedimentation driving forces..

Organic matter on the Malin Shelf has strong heteropolysaccharide signature with abundant lipid component. Prominent peptidoglycan signals discovered in the gas bearing sediment core suggest significant contribution of microbial biomass to the organic carbon in this setting. This hypothesis was further coupled with abundance of sharp resonances indicative of microbial activity. In contrast in the sediment core devoid of gas the contribution of microbial biomass appears to be less significant. This suggests that the presence of gas within the sedimentary framework can stimulate the microbial communities. This hypothesis was to date not confirmed by the analysis of general lipid biomarker signatures typical of bacteria. However the biomarker approach was not targeting the bacterial lipids specifically and thus the question

of whether there is a genuine relationship between the gas presence in the sediment and the microbial activity and the community structure remains open. Future work should focus on validating the suggested relationship between lateral gas bodies and microbially derived organic matter. Studies of phospholipid fatty acid distribution and analysis of microbial populations with molecular tools such as analysis of DNA, or culturing techniques would greatly enhance the understanding of processes described in this work. Organic matter on the Malin Shelf is derived from both allochthonous and autochthonous sources. The allochthonous organic carbon is dominated by input from epicuticular waxes of higher plants possibly gymnosperms with minimal input from woody tissues. Autochthonous organic matter is predominantly derived from planktonic sources with significant contributions from benthic organisms and bacteria. The partitioning of lipids between bound and free forms suggest that a significant proportion of the lipids are deposited in a conjugate forms. Moreover, the evidence from lipid biomarker depth profiles suggests a qualitatively and quantitatively uniform input of the organic matter in at least the last 5000 years. Sources of organic matter on the Malin Shelf have been well defined in this study, however, due to limited coverage and lack of samples from areas closer to the landmass, river mouths etc. it was not possible to draw more definite conclusions on provenance of the organic matter.

The survey of Dunmanus Bay, Ireland revealed that previously discovered pockmarks in this area are gas features. There was no evidence of groundwater influence on both water column and sediment pore fluids despite favourable environmental and geological conditions. Acoustic data collected show evidence of gas bubbles in the water column indicating active seepage. However direct analysis of water samples collected four days after acoustic survey did not confirm elevated methane concentrations in the water column. This suggests that the magnitude of gas expulsion is low and periodic in nature. Pore water profile show evidence of sulphate reduction but sulphate-methane transition zone was not reached due to poor recovery. Despite sulphate presence methane accumulation was recorded in the sediment cores indicating upward migration of gas in this setting. The origin of the methane gas remains uncertain as there is indirect evidence supporting both thermogenic and biogenic sources. Further studies were undertaken during the CE11_017 research cruise to unravel the origin of this gas including isotopic studies of methane. Conducted biological survey revealed low diversity and low richness benthic communities dominated by four common species inhabiting predominantly muddy sands with moderate gravel component. The community structure suggests pristine conditions and more importantly that benthos does not contribute or rely on periodically vented hydrocarbon gas. It is clear that the magnitude of gas venting that takes place in the Dunmanus Bay is low. In such low energy settings chemosynthetic meio- and macrofauna is rarely observed. Future work could verify these finding by more sensitive techniques such as stable isotopes analysis of tissues. Although conditions might not be optimal for larger organisms to take advantage of the fluid flow, it is often observed that microorganisms are capable to exploit

such conditions. Future work could focus on characterization of microorganisms from Dunmanus Bay by means of isotopic and molecular techniques and investigate if they actively exploit, described here, active fluid system.

REFERENCES

Abdel Aal, G.Z., Atekwana, E.A., Atekwana, E.A., (2010a). Effects of bioclogging in porous media on complex conductivity signatures. Journal of Geophysical Research 115:G00G07

Abdel Aal, G.Z., Atekwana, E.A., Rossbach, S., *et al.*, (2010b). Sensitivity of geoelectrical measurements to the presence of bacteria in porous media. Journal of Geophysical Research 115:G03017

Abreu-Grobois, F.A., Billyard, T.C., Walton, T.J., (1977). Biosynthesis of heterocyst glycolipids of *Anabaena cylindrica*. Phytochemistry 16:351-354

Adams, R.S., Bustin, R.M., (2001). The effects of surface area, grain size and mineralogy on organic matter sedimentation and preservation across the modern Squamish Delta, British Columbia: the potential role of sediment surface are in the formation of petroleum source rocks. International Journal of Coal Geology 46:93-112

Agilent, (2007). Technical note: What are the major causes of GC capillary column performance degradation? Agilent Technologies, USA

Agrawal, Y.C., Pottsmith, H.C., (2000). Instruments for particle size and settling velocity observations in sediment transport. Marine Geology 186:89-114

Aharon, P., Gupta, B.K.S., (1994). Bathymetric reconstructions of the Miocene-age "calcari a Lucina" (Northern Apennines, Italy) from oxygen isotopes and benthic foraminifera. Geo-Marine Letters 14:219-230

Aizenshtat, Z., Krein, E.B., Vairavamurthy, M.A., *et al*., (1994). Role of Sulfur in the Transformations of Sedimentary Organic Matter: A Mechanistic Overview. In: Geochemical Transformations of Sedimentary Sulfur, 16-37, Vairavamurthy, M.A., Schoonen, M.A.A., (Eds). American Chemical Society Symposium Series 612, Washington, 467pp.

Al-Jaroudi, S.S., Ul-Hamid, A., Mohammed, A-R.I., *et al*., (2007). Use of X-ray powder diffraction for quantitative analysis of carbonate rock reservoir samples. Powder Technology 175:115-121

Allen, J.E., Forney, F.W., Markovetz, A.J., (1971). Microbial subterminal oxidation of alkanes and alken-1-enes. Lipids 6:448-452

Allen, J.P., Atekwana, E.A., Atekwana, J.W., et al., (2007). The microbial community structure in petroleum-contaminated sediments corresponds to geophysical signatures. Applied and Environmental Microbiology 73:2860-2870

Ali, I., Aboul-Enein, H.Y., (2002). Determination of metal ions in water, soil, and sediment by capillary electrophoresis. Analytical Letters 35:2053-2076

Alperin, M.J., Reeburgh, W.S., Whiticar, M.J., (1988). Carbon and hydrogen isotope fractionation resulting from anaerobic methane oxidation. Global Biochemical Cycles 2:279-288

Alt, J.C., (2003). Hydrothermal fluxes at mid-ocean ridges and on ridge flanks. Comptes Rendus Geoscience 353:853-864

Alupului, A., Calinescu, I., Lavric, V., (2009). Ultrasonic vs. microwave extraction intensification of active principles from medicinal plants. AIDIC Conference Series 9:1-8

Ambles, A., (2001). Methods to reveal the structure of humic substances. In: Biopolymers. Vol. 1. Lignin, Humic Substances and Coal, Hofrichter, M., Steinbuchel, A., (Eds). Weiley-Verlag, Weinheim, Germany, 2001, 523pp.

Anderson, L.A., Sarmiento, J.L., (1994). Refield ratios of remineralization determined by nutrient data analysis. Global Biogeochemical Cycles 8:65-80

Archer, D., Buffet, B., (2004). Temperature sensitivity and time dependence of the global ocean clathrate reservoir. American Geophysical Union, Fall Meeting 2004, abstract #GC51D-1069

Archie, G.E., (1942). The electrical resistivity log as an aid in determining some reservoir characteristics. Transactions of the American Institute of Mineralogical, Metallurgical and Petrological Engineering 146:54-62

Armstrong, R.A., Lee, C., Hedges, J.I., *et al.*, (2002). A new, mechanistic model for organic carbon fluxes in the ocean: Based on the quantitative association of POC with ballast minerals. Deep Sea Research Part II 49:219-236

Arnosti, C., (1993). Structural characterization and bacterial degradation of marine carbohydrates. PhD thesis, 239pp., Massachusetts Institute of Technology and Woods Hole Oceanographic Institution, USA

Asano, K., Ingle Jr., J.C., Takayanagi, Y., (1968). Origin and development of Globigerina quinqueloba Natland in the North Pacific. Science Reports of the Tohoku Univeristy, 2nd Series (Geology) 39:213-241

Atekwana, E.A., Werkema, D. D., Duris, Jr. J. W., *et al*., (2004). In-situ apparent conductivity measurements and microbial population distribution at a hydrocarbon-contaminated site. Geophysics. 69, 56–63

Avnimelech, Y., Ritvo, G., Meijer, L.E., *et al.*, (2001). Water content, organic carbon and dry bulk density in flooded sediments. Aquacultural Engineering 25:25-39

Aycik, G.A., Cetaku, D., Erten, H.N., *et al.*, (2004). Dating of Black Sea sediments from Romanian coast using natural ^{210}Pb and fallout ^{137}Cs. Journal of Radioanalytical and Nuclear Chemistry 259:177-180

Baldock., J.A., Oades, J.M., Vassallo, M.A., *et al*., (1990). Significance of microbial activity in soils as demonstrated by solid-state ^{13}CNMR. Environmental Science and Technology 24:527-530

Baldock, J.A., Oades, J.M., Waters, A.G., *et al*., (1992). Aspects of the chemical structure of soil organic material as revealed by solid-state ^{13}C NMR spectroscopy. Biogeochemistry 16:1-42

Ballester, J.M., Dopazo, C., (1996). Drop size measurements in heavy oil sprays from pressure-swirl nozzles. Atomization and Sprays 6:377-408

Bange, H.W., Bartell, U.H., Rapsonmanikis, S., *et al*., (1994). Methane in the Baltic and North seas and a reassessment of the marine emissions of methane. Global Biogeochemical Cycles 8:465-480

Barrett, S.M., Volkman, J.K., Dunstan, G.A., *et al*., (1995). Sterols of 14 species of marine diatoms (Bacillariophyta). Journal of Phycology 31:360-369

Barreto, W.J., Barreto, S.R.G., Nozaki, J., *et al*., (2004). Comparison of metal analysis in sediment using EDXRF and ICP-OES with the HCl and Tessie extraction methods. Talanta 64:345-354

Barry, J.M., Kochevar, R.E., (1998). A tale of two clams: differing chemosynthetic life styles among vesicomyids in Monerey bay cold seeps. Cahiers de Biologie Marine 39:329-331

Barton Jr., J.M., Cairncross, B., McLachlan, I., (2004). Rb-Sr isotopic and elemental studies of the origin of glauconite in the Permian northern Karoo Coal Fields, South Africa: evidence for a thermal Mid-Jurassic influence. South African Journal of Geology 107:499-504

Bauch, D., Darling, K., Simstich, J., *et al*., (2003). Palaeoceanographic implications of genetic variation in living North Atlantic *Neogloboquadrina pachyderma*. Nature 424:299-302

Beastall, G.H., Rees, H.H., Goodwin, T.W., (1971). Sterols in *Porphyridium cruentum*. Tetrahedron Letters 12:4935-4938

Behrenfeld, M.J., O'Malley, R.T., Siegel, D.A., *et al*., (2006). Climate-driven trends in contemporary ocean productivity. Nature 444:752-755

Belicka, L.L., Macdonald, R.W., Harvey, H.R., (2002). Sources and transport of organic carbon to shelf, slope and basin surface sediments of the Arctic Ocean. Deep-Sea Research I 49:1463-1483.

Benner, R., Kaiser, K., (2003). Abundance of amino sugars and peptidoglycan in marine particulate and dissolved organic matter. Limnology and Oceanography 45:118-128

Bentham, M.S., Kirk, K.L., Williams, J., *et al*., (Eds), (2008). Basin-by-basin analysis of CO_2 storage potential of all-island Ireland. Scientifc Report CR/08/036, British Geological Survey

Benton, M.J., Twitchett, R.J., (2003). How to kill (almost) all life: the end-Permian extinction event. TRENDS in Ecology and Evolution 18:358-365

Berge, J.P., Gouygou, J.P., Dubacq, J.P., *et al.*, (1995). Reassessment of lipid composition of the diatom *Skeletonema costatum*. Phytochemistry 39:1017-1021

Berger, W.H., Smetacek, V.S., Wefer, G., (1989). Ocean productivity and paleoproductivity – an overview. In: Productivity of the ocean: present and past. Life Sciences Research Reports 44:1-34, Berger, W.H., Smetacek, V.S., Wefer, G., (Eds), Wiley-Interscience, New York, 470pp.

Berner, R., Raiswell, R., (1983). Burial of organic carbon and pyrite sulphur in sediments over Phanaerozoic time: A new theory. Geochimica et Cosmochimica Acta 47:855-862

Bernhard, R.K., Chasek, M., (1955). Soil density determination by direct transmission gamma rays. Proceedings of the American Society for Testing Materials 55:1199-1223

Berkson, J.M., Clay, C.S., (1973). Possible syneresis marine seismic study of late Quaternary sedimentation origin of valleys on the floor of Lake Superior, Nature 245:89-91

Berry Lyons, W., Gaudette, H.E., Hewitt, A.D., (1979). Dissolved organic matter in pore water of carbonate sediments from Bermuda. Geochimica et Cosmochimica Acta 43:433-437

Beuselnick, L., Govers, G., Poesen, J., *et al*., (1998). Measurement of the sortable silt current speed proxy using Sedigraph 5100 and Coulter Multisizer IIe: precision and accuracy. Sedimentology 46:1001-1014

Bianchi, G.G., Hall, I.L., McCave, I.N., *et al*., (1999). Measurement of sortable silt current speed proxy using the Sedigraph 5100 and the Coulter Multisizer IIe: precision and accuracy. Sedimentology 46:1001-1014

Biersmith, A., Benner, R., (1998). Carbohydrates in phytoplankton and freshly produced dissolved organic matter. Marine Chemistry 63:131-144

Birch, G.F., (2000). Marine pollution in Australia, with special emphasis on central New South Wales estuaries and adjacent continental margin. International Journal of Environment and Pollution 13:573-607

Blott, S.J., Pye, K., (2001). GRADISTAT: a grain size distribution and statistics package for the analysis of unconsolidated sediments. Earth Surface Processes and Landforms 26:1237-1248

Blum, P., (1997). Physical properties Handbook: a guide to the shipboard measurement of physical properties of deep-sea cores. ODP Technical Note 26 [Online]. Available from http://www-odp.tamu.edu/publications/tnotes/tn26/INDEX.HTM.

Blumenberg, M., Kruger, M., Nauhaus, K., *et al*., (2006). Biosynthesis of hopanoids by sulfate-reducing bacteria (genus Desulfovibrio). Environmental Microbiology 8:1220-1227

Blumer, M., Guillard, R.R.L., Chase, T., (1971). Hydrocarbons of marine phytoplankton. Marine Biology 8:183-189

Boe, R., Rise, L., Ottesen, D., (1998). Elongate depressions on the southern slope of the Norwegian Trench (Skagerrak): morphology and evolution. Marine Geology 146:191-203

Boere, A.C., Rijpstra, W.I.C., de Lange, G.J., *et al*., (2011). Preservation potential of ancient plankton DNA in Pleistocene marine sediments. Geobiology 9:377-393

Boetius, A., Ravenschlag, K., Schubert, C.J., *et al*., (2000). A marine microbial consortium apparently mediating anaerobic oxidation of methane. Nature 407:623-626

Bohlin, L., Sjostrand U., Sodano, G., *et al*., (1982). Sterols in marine invertebrates. 33. Structures of five new 3β-(hydroxymethyl)-A-norsteranes: indirect evidence for transformation of dietary precursors in sponges. Journal of Organic Chemistry 47:5309-5314

Bond, G., Broecker, W., Lotti, R., *et al*., (1992). Abrupt colour changes in isotopic stage 5 in North Atlantic deep-sea cores: implications for rapid change of climate-driven events. In: Start of a Glacial, p.185-205, Kukla, J., Went, E. (Eds), Springer, Berlin

Bondarev, V.N., Rokos, S.I., Kostin, D.A., *et al*., (2002). Underpermafrost accumulation of gas in the upper part of the sedimentary cover of the Pechora Sea. Russian Geology and Geophysics 43:545-56

Bondevik, S., Svendsen, J.I., Johnsen, G., *et al*., (1997). The Storegga tsunami along the Norwegian coast, its age and runup. Boreas 26:29-53

Bondevik, S., Mangerud, J., Dawson, S., *et al*., (2003). Record-breaking heigh for 8000-year-old tsunami in the North Atlantic. EOS, Transactions, American Geophysical Union 84:289-300

Bondevik, S., Lovholt, F., Harbitz, C., *et al*., (2006). The Storegga Slide tsunami – Deposits, run-up heights and radiocarbon dating of the 8000-year-old tsunami in the North Atlantic. EOS, Transactions, American Geophysical Union, Abstract OS34C-01

Boon, J.J., de Lange, F., Schuyl, P.J.W., *et al*., (1977a). Organic geochemistry of Walvis Bay diatomaceous ooze. II. Occurrence and significance of the hydroxy fatty acids. In: Advances in organic geochemistry 1975, Campos, E. (Ed), Proceedings of the 7th International Meeting on Organic Geochemistry, Madrid, Spain

Boon, J.J., de Leeuw, J.W., Hoek, G.J., *et al*., (1977b). Significance and taxonomic value of iso and anteiso monoenoic fatty acids and branched beta-hydroxy acids in Desulfovibrio desulfuricans. Journal of Bacteriology 129:1183-1191

Boon, J.J., de Leeuw, J.W., (1979). The analysis of wax esters, very long mid-chained ketones and sterols ethers isolated from Walvis Bay diatomaceous ooze. Marine Chemistry 7:117-132

Borowski, W.S., Paull, C.K., Ussler, W., (1996). Marine pore-water sulfate profiles indicate in situ methane flux from underlying gas hydrate. Geology 24:655-658

Bossio, J.P., Harry, J., Kinney, C.A., (2008). Application of ultrasonic assisted extraction of chemically diverse organic compounds from soils and sediments. Chemosphere 70:858-864

Boudreau, B.P., (1997). Diagenetic models and their implementation: modeling transport and reactions in aquatic sediments. Springer, Berlin, Heidelberg

Boulton, G.S., Slot, T., Blessing, K. *et al.*, (1993). Deep circulation of groundwater in overpressured subglacial aquifiers and its geological consequences. Quaternary Science Reviews 12:739-745

Bourbonniere, R.A., Meyers, P.A., (1983). Characterization of sedimentary humic matter by alkaline hydrolysis. Organic Geochemistry 5:131-142

Bouriak, S., Vanneste, M., Saoutkine, A., (2000). Inferred gas hydrates, shallow gas accumulations and clay diapirs on the southern edge of the Voring Plateau, offshore Norway. Marine Geology 163:125-148

Boutry, J.L., Alcaide, A., Barbier, M., (1971). Sur la presence d'un sterolen C26 dans un plancton marin vegetal. Comptes Rendus de l'Académie des Sciences. Serie D 272:1022-1023

Bowden, K.F., Hughes, P., (1961). The flow of water through the Irish Sea and its relation to wind. Geophysical Journal of the Royal Astronomical Society 5:265-291

Bowden, K.F., (1980). Physical and dynamical oceanography of the Irish Sea. In: The North-West European shelf seas: the sea bed and the sea in motion II. Physical and chemical oceanography, and physical resources, Banner, F.T., Collins, M.B., Massie, K.S., (Eds). Elsevier, Amsterdam, Holland, 1980, 638pp.

Boyce, J.W., Hodges, K.V., Olszewski, *et al*., (2005). The importance of material characterization in (U-Th)/He thermochronometry: Diffusivity of He and heterogeneous distribution of U and Th in monazite. Geophysical Research Abstract 7, 09935

Boyle, E., (1988). Climate, ocean circulation, and the chemistry of benthic fossil shells. Applied Geochemistry 3:109

Boyle, J., (2004). A comparison of two methods for estimating the organic matter content of sediments. Journal of Paleolimnology 31:125-127

Brassell, S.C., Eglinton, G., Marlowe, I.T., *et al*., (1986). Molecular stratigraphy: A new tool for climatic assessment. Nature 320:129-133

Breitzke, M., Spieß, V., (1993). An automated full waveform logging system for high-resolution P-wave profiles in marine sediments. Marine Geophysical Researches 15:297-321

Breitzke, M., (2000a). Physical properties of marine sediments. In: Schulz, H.D., Zabel, M. (Eds) Marine Geochemistry, Springer-Verlag 2006

Breitzke, M., (2000b). Acoustic and elastic characterization of marine sediments by analysis, modeling, and inversion of ultrasonic P wave transmission seismograms. Journal of Geophysical Research 105:21411-21430

Breger, I.A., (1961). Kerogen. In: McGraw Hill Encyclopedia of Science and Technology. New York

Brock, T.D., Madigan, M.T., Martinko, J.M., *et al.*, (1994). Biology of microorganisms. 7th edition. Prentice Hall, 909pp.

Brocks, J.J., Banfield, J., (2009). Unraveling ancient microbial history with community proteogenomics and lipid geochemistry. Nature Reviews Microbiology 7:601-609

Broecker, W., Bond, G., Klas, M., *et al*., (1990). Origin of the northern Atlantic's Heinrich events. Climate Dynamics 6:265–273

Brown, J.E., Jones, S.R., Saxen, R., *et al*., (2004). Radiation doses to aquatic organisms from natural radionuclides. Journal of Radiological Protection 24:A63-A67

Brzezinski, M.A., (1985). The Si:C:N ratio of marine diatoms: interspecific variability and the effect of some environmental variables. Journal of Phycology 21:347-357

Bruchert, V., Currie, B., Peard, K., *et al*., (2004). Dynamics of methane and hydrogen sulphide in the water column and sediment of the Namibian shelf. Proceedings of the Goldschmidt Conference, Copenhagen, 5-11 June, abstract A340

Bucher, W., Hyde, K.D., Pointing, S.B., *et al*., (2003). Production of wood decay enzymes, loss of mass, and lignin solubilization in wood by marine ascomycetes and their anamorphs. Fungal Diversity 15:1-14

Bui, H., Dvorkin, J., Nur, A., (2007). Subsurface fluid flow and its implications for seabed pockmarks and mud volcanoes: An approach of distinct element method (DEM). SEG Expanded Abstracts 25:2055

Bull., I.D., van Bergen, P.F., Nott, C.J., *et al*., (2000). Organic geochemical studies of soils from the Rothamsted Classical Experiment – V. The fate of lipids in different long-term experiments. Organic Geochemistry 32:253-258

Burdige, D.J., Skoog, A., Gardner, K., (2000). Dissolved and particulate carbohydrates in contrasting marine sediments. Geochimica et Cosmochimica Acta 64:1029-1041

Burdige, D.J., (2006). Geochemistry of Marine Sediments. Princeton University Press

Burnett, W.C., Bokuniewicz, H., Huettle, M., et al., (2003). Groundwater and pore water inputs to the coastal zone. Biogeochemistry 66:3-33

Burns, K.A., Teal, J.M., (1973). Hydrocarbons in the pelagic *Sargassum* community. Deep-Sea Research 20:207-211

Burke, I.T., Kemp, A.E.S., (2002). Microfabric analysis of Mn-carbonate laminae deposition and Mn-sulfide formation in the Gotland Deep, Baltic Sea. Geochimica et Cosmochimica Acta 66:1589-1600

Butler, E.C.V., Parslow, J.S., Volkman, J.K., *et al*., (2000). Huon Estuary Study: environmental research for integrated catchment management and aquaculture 96/284. Hobart, Tasmania, CSIRO Division of Marine Research, FRDC project, 285pp.

Byers, S.C., Mills, E.L., Stewart, P.L., (1978). A comparison of methods of determining organic carbon in marine sediments, with suggestion for a standard method. Hydrobiologia 58:43-47

Cai, W.-J., Sayles, F.L., (1996). Oxygen penetration depths and fluxes in marine sediments. Marine Chemistry 52:123-131

Campbell, C., (1998). Late Holocene lake sedimentology and climate change in southern Alberta, Canada. Quaternary Research 49:96-101

Caplat, C., Texier, H., Barillier, D., *et al*., (2005). Heavy metals mobility in harbour contaminated sediments: The case of Port-en-Bessin. Marine Pollution Bulletin 50:504-511

Cardellicchio, N., Cavalli, S., Ragone, P., *et al*., (1999). New strategies for determination of transition metals by complexation ion-exchange chromatography and post column reaction. Journal of Chromatography A 847:251-259

Carman, P.C., (1956). Flow of gases through porous media. Butterworths Scientific Publications, London, 182 pp.

Carrie, R.H., Mitchell, L., Black, K.D., (1998). Fatty acids in surface sediments at the Hebridean shelf edge, west of Scotland. Organic Geochemistry 39:1583-1593

Casas, D., Ercilla, G., Baraza, J., (2003). Acoustic evidence of natural gas in the continental slope sediments of the Gulf of Cadiz (E Atlantic). Geo-Marine Letters 23:300-310

Cathles, L.M., Zheng, S., Chen, D., (2010). The physics of gas chimney and pockmark formation, with implications for assessment of seafloor hazards and gas sequestration. Marine and Petroleum Geology 27:82-91

Chappell, A., (1998). Dispersing sandy soil for the measurement of particle size distributions using optical laser diffraction. Catena 31: 271-281

Chebykin, E.P., Goldberg, E.L., Grachev, M.A., *et al*., (2005). Uranium isotopes in the sediments of Lake Baikal as geochronometers and proxy for Paleo-Humidity. Geophysical Research Abstracts 7, 00977

Cheesman, S.J., (1989). A short baseline transient electromagnetic method for use on the sea floor. Res. Appl. Geophys., Univ. Toronto, 46, 138 pp.

Chemat, F., Grondin, I., Costes, P., *et al*., (2004). High power ultrasound effects on lipid oxidation of refined sunflower oil. Ultrasonics Sonochemistry 11:281-285

Chen, J., Chen, Y., Liu, L., *et al*., (2006). Zr/Rb ratio in the Chinese sequences and its implications for changes in the East Asian winter monsoon strength. Geochimica et Cosmochimica Acta 70:1471-1482

Chen, M., Ma, L.Q., (2001). Comparison of three aqua regia digestion methods for twenty Florida soils. Soil Science Society of America Journal 65:491-499

Chevaldonne, P., (1997). The fauna at deep-sea hydrothermal vents, an introduction. Handbook of Deep-Sea Hydrothermal Vent Fauna, Plouzane, IFREMER, 7-20

Childress, J.J., Fisher, C.R., Brooks, J.M., *et al*., (1986). A methanotrophic marine molluscan (Bivalvia, Mytilidae) symbiosis: Mussels fuelled by gas. Science 233:1306-1308

Christie, W.W., (1989). Gas Chromatography and Lipids: a Practical Guide. The Oily Press, Ayr, 307pp.

Christie, W.W., Han, X., (2010). Lipid Analysis – Isolation, Separation, Identification and Lipidomic Analysis, 4th ed., The Oily Press, Bridgewater, 448pp.

Christodoulou, D., Papatheodorou, G., Ferentinos, G., *et al*., (2003). Active seepage in two contrasting pockmark fields in the Patras and Corinth gulfs, Greece. Geo-Marine Letters 23:194-199

Clarke, K.R., Green, R.H., (1988). Statistical design and analysis for a 'biological effects' study. Marine Ecology Progress Series 46:213-226

Clarke, K.R., Warwick, R.M., (2001). Change in marine communities: an approach to statistical analysis and interpretation, 2nd edition. PRIMER-E, Plymouth

Clauer, N., Huggett, J.M., Hillier, S., (2005). How reliable is the K-Ar glauconite chronometer? A case study of Eocene sediments from the Isle of Wight. Clay Minerals 40:167-176

Clayton, R.N., Grossman, L., Mayeda, T.K., (1973). A component of primitive nuclear composition in Carbonaceous meteorites. Science 182:485-488

Clement, R.E., Yang, P.W., Koester, C.J., (2001). Environmental Analysis. Analytical Chemistry 73:2761-2790

Clifton, J., Mcdonald, P., Plater, A., *et al*., (1999). An investigation into the efficiency of particle size separation using Stokes Law. Earth Surface Processes Landforms 24:725-730

Cole, D., Stewart, S.A., Cartwright, J.A., (2000). Giant irregular pockmark craters in the Palaeogene of the Outer Moray Firth Basin, UK North Sea. Marine Petroleum Geology 17:563-577

Colman, S.M., (2007). Conventional wisdom and climate history. Proceedings of the National Academy of Sciences of the United States of America 104:6500-6501

Colombo, J.C., Silverberg, N., Gearing, J.N., (1996). Lipid biogeochemistry in the Laurentian Trough 1. Fatty acids, sterols and aliphatic hydrocarbons in rapidly settling particles. Organic Geochemistry 25:211-225

Commeau, R.F., Paull, C.K., Comineau, J.A., *et al*., (1987). Chemistry and mineralogy of pyrite-enriched sediments at a passive margin sulfide brine seeps: abyssal of Gulf of Mexico. Earth & Planetary Science Letters 82:267-279

Cook, R.L., (2004). Coupling NMR to NOM. Analytical and Bioanalytical Chemistry 378:1484-1503

Coolen, M.J.L., (2011). 7000 Years of Emiliania huxleyi Viruses in the Black Sea. Science 333:451-452

Coquery, M., Carvalho, F.P., Azemard, S., *et al*., (1999). The IAEA worldwide intercomparison exercises (1990-1997): determination of trace elements in marine sediments and biological samples. The Science and Total Environment 237:501-508

Cornford, C., (1998). Source rocks and hydrocarbons of the North Sea. In: Petroleum Geology of the North Sea. Glennie, K.W., (Eds), Blackwell Science Ltd, Oxford, 641pp.

Cotrim de Cunha, L., Serve, L., Blaxzi, J.-L., (2002). Neutral sugars as biomarkers in the particulate organic matter of a French Mediterranean river. Organic Geochemistry 33:953-964

Cranwell, P.A., (1981). Diagenesis of free and bound lipids in terrestrial detritus deposited in a lacustrine sediment. Organic Geochemistry 3:79-89

Cranwell, P.A., (1982). Lipids of aquatic sediments and sedimenting particulates. Progress in Lipid Research 21:271-308

Crawford, R.L., McCoy, E., Harkin, J.M., *et al.*, (1973). Degradation of methoxylated benzoic acids by a Nocardia from a lignin-rich environment: significance to lignin degradation and effects of chloro substituents. Applied Microbiology 26:176-184

Crofield, R., (2003). Signatures of time. Chemistry in Britain 39:22-25

Croker, P.F., Kozachenko, M., Wheeler, A.J., (2005). Gas-related seabed structures in the western Irish Sea (IRL-SEA6). Technical report, Strategic Environmental Assessment SEA6

Cross, T.F., Southgate, T., (1983). An approach to ecological monitoring in the rocky intertidal: A survey of Bantry Bay and Dunmanus Bay, Ireland. Marine Environmental Research 8:149-163

Croudace, I.W., Rindby, A., Rothwell, R.G., (2006). ITRAX: description and evaluation of new multi-function X-ray core scanner. In: New Techniques in Sediment Core Analysis, Geological Society Special Publications 267:51-63, Rothwell, R.G. (Eds), London

Dadey, K.A., Janecek, T., Klaus, A., (1992). Dry-bulk density: its use and determination. In Taylor B and Fujioka K et al. (Ed), Proceedings of Ocean Drilling Program, Scientific Results, Vol. 126, 1992

D'Amore, J.J., Al-Abed, S.R., Scheckel, K.G., *et al*., (2005). Methods for speciation of metals in soils: A review. Journal of Environmental Quality 34:1707-1745

Dando, P.R., Austen, M.C., Burke Jr., R.A, *et al*., (1991). Ecology of a North Sea pockmark with and active methane seep. Marine Ecology Progress Series 70:49-63

Dando, P.R., (2001). A Review of Pockmarks in the UK Part of the North Sea, with Particular Reference to their Biology. Strategic Environmental Assessment – SEA2, Technical Report TR_001. London, Department of Trade and Industry

Dando, P., Clayton, C., Fannin, N., *et al*., (2007). Methane release from Pockmarks in the Witch Ground Basin, North Sea. Geophysical Research Abstracts, EGU2007-A-08870

Danovaro, R., Corinaldesi, C., Luna, G.M., *et al*., (2005). Molecular tools for the analysis of DNA in marine environments. In: Marin Organic Matter. Biomarkers, Isotopes and DNA, Volkman, J.K., (Ed), Springer-Verlag, Berlin, Heidelberg, 374pp.

Davies, A.M., Xing, J., (2002). Processes influencing suspended sediment movement on the Malin-Hebrides shelf. Continental Shelf Research 22:2081-2113

Davies, E.E., Goodfellow, W.D., Bornhold, B.D., *et al*., (1987). Massive sulfides in a sedimented rift valley, northern Juan de Fuca Ridge. Earth & Planetary Science Letters 82:49-61

Davies, T.A., Hay, W.W., Southam, J.R., *et al*., (1977). Estimates of Cenozoic Oceanic Sedimentation Rates. Science 197:53-55

Davis, E.E., Goodfellow, W.D., Bornhold, B.D., et al., (1987). Massive sulfides in a sedimented rift valley, northern Juan de Fuca Ridge. Earth and Planetary Science Letters 82:49-61

de Boer, G.B., de Weerd, C., Thoenes, D., *et al*., (1987). Laser diffraction spectrometry: Fraunhofer versus Mie scattering. Particle Characterization 4:14-19

de Leeuw, J.W., Irene, W., Rijpstra, C., *et al*., (1992). The absence of long-chain alkyl diols and keto-1-ols in cultures of the cyanobacterium Aphanizomenon flos-aquae. Organic Geochemistry 18:575-578

de Leeuw, J.W., Frewin, N.L., Van Bergen, P.F., et al., (1995). Organic carbon as a palaeoenvironmental indicator in the marine realm. In: Marine Palaeoenvironmental Analysis from Fossils, Bosence, D.W.J., Allison, P.A., (Eds). Geological Society Special Publications 83:43-71

Dean Jr., W.E., (1974). Determination of carbonate and organic matter in calcareous sediments and sedimentary rocks by loss on ignition: comparison with other methods. Journal of Sedimentary Petrology 44:242-248

DeLong, E.F., (2000). Resolving a methane mystery. Nature 407:577-579

Demaison, G.J., Moore, G.T., (1980). Anoxic environments and oil source bed genesis. Bulletin of the American Association of Petroleum Geologists 64:1179-1209

Demaison, G.J., (1991). Anoxia vs productivity: What controls the formation of organic-carbon-rich sediments and sedimentary rocks? Discussion and reply. Bulletin of the American Association of Petroleum Geologists 75:499-501

Demeny, A., Kele, S., Siklosy, Z., (2010). Empirical equations for the temperature dependence of calcite-water oxygen isotope fractionation from 10 to 70^{o}C. Rapid Communications in Mass Spectroscopy 24:3521-3526

Devaud, M., Hocquet, T., Bacri, J.-C., *et al*., (2008). The Minnaert bubble: an acoustic approach. European Journal of Physics 29:1263

Devol, A.H., Ahmed, S.I., (1981). Are high rates of sulphate reduction associated with anaerobic oxidation of methane? Nature 291:407-408

Didyk, B.M., Simoneit, B.R.T., Brassell, S.C., *et al*., (1978). Organic geochemical indicators of paleoenvironmental conditions of sedimentation. Nature 272:216-222

Dobson, M.R., Evans, D., (1974). Geological structure of the Malin Sea. Journal of the Geological Society 130:475-478

Dobson, M.R., Whittington, R.J., (1992). Aspects of the geology of the Malin Sea area. In: Parnell, J., (Ed.) Basins on the Atlantic Seaboard: Petroleum Geology, Sedimentology and Basin Evolution. Geological Society Special Publications 62:291-311

Dorschel, B., Wheeler, A.J., Monteys, X., *et al*., (2010). Atlas of the deep-water Ireland. Springer, Science & Business Media B.V., 161 pp.

Dunlop, P., Shannon, R., McCabe, M., *et al*., (2010). Marine geophysical evidence for ice sheet extension and recession on the Malin Shelf: New evidence for the western limits of the British Irish Ice Sheet. Marine Geology 276: 86-99

Durand, B., Nicaise, G., (1980). Procedures for kerogen isolation. In: Kerogen: insoluble organic matter from sedimentary rocks, 35-53, Durand, B. (Ed). Technip, Paris, 525pp.

Edlund, A., Nichols, P.D., Roffey, R., *et al.*, (1985). Extractable and lipopolysaccharide fatty acids and hydroxy acid profiles from Desulfovibrio species. Journal of Lipid Research 26:982-988

Eganhouse, R.P., (1997). Molecular markers and environmental organic geochemistry: An overview. In: Molecular Markers in Environmental Chemistry, 1-20, Eganhouse, R.P. (Ed). American Chemical Symposium Series, Washington, 426pp.

Eglinton, G., Hamilton, R.J., (1967). Leaf epicuticular waxes. Science 156:1322-1335

Ehhalt, D.H., Schmidt, U., (1978). Sources and sinks of atmospheric methane. Pure and Applied Geophysics 116:452-464

Ehhalt, D.H., Prather, M., Dentener, F., *et al*., (2001). Atmospheric chemistry and greenhouse gases. In: Houghton, J.T., Ding. Y., Griggs, D.J., *et al*., Climate Change 2001: the Scientific Basis, 241-287

Ekpo, B.O., Oyo-Ita, O.E., Wehner, H., (2005). Even-n-alkane/alkene predominances in surface sediments from the Calabar River, SE Niger Delta, Nigeria. Naturwissenschaften 92:341-346

Elderfield, H., Schultz, A., (1996). Mid-ocean ridge hydrothermal fluxes and the chemical composition of the ocean. Annual Reviews of Earth and Planetary Science 24:191-224

Ellis, D.V., Singer, J.M., (2007). Well logging for Earth scientists. Springer, Amsterdam, 692pp.

Ellis, J.P., McGiunnes, W.T., (1986). Pockmarks of the northwestern Arabian Gulf. Advances in Underwater Technology, Ocean Science and Offshore Engineering, vol. 6, London, Graham and Trotman, 353-367

Ellis, M., Evans, R.L., Hutchinson, D., *et al*., 2008. Electromagnetic Surveying of Seafloor Mounds in the Gulf of Mexico. Marine and Petroleum Geology 25:960-968.

Emeis, K.-C., Robertson, A.H.F., Richter, C., *et al.*, (Eds) (1996). Proceedings of the Ocean Drilling Program, Initial Reports 160, ODP, College Station, Texas, 972 pp.

Emerson, H.S., Young, A.K., (1995). Method development for the extraction of naturally occurring radionuclides in marine sediments. The Science of the Total Environment 173/174:313-322

Emerson, S., Hedges, J.I., (1988). Process controlling the organic carbon content of open ocean sediments. Paleoceanography 3:621-634

Erk, M., Musani, L., Raspor, B., (1998). The interactions of ^{54}Mn with humic acids in freshwater systems. Water Research 32:1753-1758

Eshel, G., Levy, G.J., Mingelgrin, U., *et al*., (2004). Critical evaluation of the use of laser diffraction for particle-size distribution analysis. Soil Science Society of America Journal 68:736-743

Estrada-Vasquez, C., Macarie, H., Kato, M.T., *et al*., (2003). The effect of the supplementation with a primary carbon source on the resistance to oxygen exposure of mehanogenic sludge. Water Science and Technology 48:119-124

Evans, H.B., (1965). GRAPE – A device for continuous determination of density and porosity. Proceedings of the 6th Annual SPWLA Logging Symposium, Society of Professional Well Log Analysts, Dallas, USA, Vol 2:B1-B25

Evans, R.L., (2007). Using CSEM techniques to map the shallow section of seafloor; from the coastline to the edges of the continental slope. In: Marine controlled-source electromagnetic methods. Geophysics 72:WA105-WA116

Eyssen, H.J., Parmentier, G.G., Compernolle, F.C., et al., (1973). Biohydrogenation of sterols by Eubacterium ATCC 21. 408-Nova species. European Journal of Biochemistry 36:411-421

Faber, E., Stahl, W., (1984). Geochemical surface exploration for hydrocarbons in the North Sea. Bulletin of the American Association of Petroleum Geologists 68:363-386

Fabbri, D., Sangiorgi, F., Vassura, I., (2005). Pyrolysis-GC-MS to trace terrigenous organic matter in marine sediments: a comparison between pyrolytic and lipid markers in the Adriatic Sea. Analytica Chimica Acta 530:253-261

Fader, G.B.J., (1991). Gas-related sedimentary features from the eastern Canadian continental shelf. Continental Shelf Research 11:1123-1153

Falkowski, P.G., (1997). Evolution of the nitrogen cycle and its influence on the biological sequestration of CO_2 in the ocean. Nature 387:272-275

Falkowski, P.G., Davis, C.S., (2004). Concept Natural proportions. Nature 431:131

Falkowski, P.G., Katz, M.E., Knoll, A.H., *et al*., (2004). The Evolution of Modern Eukaryotic Phytoplankton. Science 305:354-360

Farrow, G.E., (1978). Recent sediments and sedimentation in the Inner Hebrides. Proceedings of the Royal Society of Edinburgh 83B:91-105

Ferdelman, T.G., Fossing, H., Neumann, K., *et al.,* (1999). Sulphate reduction in surface sediments of the Southeast Atlantic continental margin between 15°38'S and 27°57'S (Angola and Namibia), Limnology and Oceanography 44:650-661,

Fernand, L., Nolan, G.D., Raine, R., *et al*., (2006). The Irish coastal current: A seasonal jet-like circulation. Continental Shelf Research 26:1775-1793

Findlay, R.H., White, D.C., (1983). Polymeric Beta-hydroxyalkanoates from environmental samples and Bacillus megaterium. Applied and Environmental Microbiology 45:71-78

Fisher, A.T., Fisher, K., Lavoie, D., *et al.*, (1994). Geotechnical and hydrogeological properties of sediments from Middle Valle, northern Juan de Fuca Ride. Proceedings of the Ocean Drilling Program, Mottle, M.J., et al., (eds), Scientific Results 139:627-647, College Station, Texas

Fischer, W.W., Summons, R.E., Pearson, A., (2005). Targeted genomic detection of biosynthetic pathways: anaerobic production of hopanoid biomarkers by a common sedimentary microbe. Geobiology 3:33-40

Flood, R.D., (1981). Pockmarks in the deep sea. EOS- Transactions of the American Geophysical Union, 62:304

Floodgate, G.D, Judd, A.G., (1992). The origins of shallow gas. Continental Shelf Research 12:1145-1156

Folk, R.L., (1954). The distinction between grain size and mineral composition in sedimentary-rock nomenclature. Journal of Geology 62:344-359

Folk, R.L., Ward, W.C., (1957) Brazos River bar: a study in the significance of grain size parameters. Journal of Sedimentary Petrology 27:3-26

Fossing, H., Ferdelman, T.G., Berg, P., (2000). Sulphate reduction and methane oxidation in continental margin sediments influenced by irrigation (South-East Atlantic off Namibia), Geochimica et Cosmochimica Acta 64:897-910

Francis, G.W., (1981). Alkythiolation for the determination of double-bond position in unsaturated fatty acids esters. Chemistry and Physics of Lipids 29:59-65

Fukushima, K., Kondo, H., Sakata, S., (1992a). Geochemistry of hydroxy acids in sediments – I. Some freshwater and brackish water lakes in Japan. Organic Geochemistry 18:913-922

Fukushima, K., Uzaki, M., Sakata, S., (1992b). Geochemistry of hydroxy acids in sediments – II. Estuarine and coastal marine environments. Organic Geochemistry 18:923-932

Fulco, A.J., (1967). Chain elongation, 2-hydroxylation, and decarboxylation of long chain fatty acids by yeast. The Journal of Biological Chemistry 242:3608-3613

Furukawa, Y., Barnes, H.L., (1995). Reactions forming pyrite from precipitated amorphous ferrous sulfide. In: Geochemical Transformations of Sedimentary Sulfur, Vairavamurthy, M.A. and Schoonen, M.A.A. (Eds), ACS Symposium Series 612:168-193

Fyfe, W.S., (1994). The water inventory of the Earth: fluids and tectonics. In:Geofluids: Origin, Migration and Evolution of Fluids in Sedimentary Basins, Parnell, J., (Ed), Geological Society of London, Special Publication 78:1-7

Gagosian, R.B., Volkman, J.K., Nigrelli, G.E., (1983). The use of sediment traps to determine sterol sources in coastal sediments off Peru, 369-379. In: Advances in Organic Geochemistry, 1981. Bjoroy, M. et al., (Eds). Wiley, Chichester, 800pp.

Gal'chenko, V.F., Lein, A.Yu., Ivanov, M.V., (2004). Methane content in the bottom sediments and water column of the Black Sea. Microbiology 73:211-223

Galy, V., France-Lanord, C., Beyssac, O., *et al*., (2007). Efficient organic carbon burial in the Bengal fan sustained by the Himalayan erosional system. Nature 450:407-410

Games, K.P., (2001). Evidence of shallow gas above the Connemara oil accumulation, Block 26/28, Porcupine Basin. Shannon, P.M., Hughton, P.D.W., Corcoran, D.V., (Eds) The Petroleum Exploration of Ireland's Offshore Basins, Geological Society Special Publications 188:361-373, London.

Garcia, M.L., Masson, M., (2004). Environmental and geologic application of solid-state methane sensors. Environmental geology 46:1059-1063

Garcia, X., Monteys, X., Evans, R., *et al*., (2007). Geohazard identification and early reconnaissance for hydrocarbon potential using marine electromagnetic and high frequency acoustic methods. Geophysical Research Abstracts, Vol. 9, 09524.

Gasparics, T., Csato, I., Zaray, Gy., (1997). Analysis of Antarctic Marine Sediment by Inductively Coupled Plasma Atomic Emission and Total Reflection X-Ray Fluorescence Spectrometry. Microchemical Journal 55:56-63

Gelin, F., (1996). Isolation and chemical characterization of resistant macromolecular constituents in microalgae and marine sediment. PhD Thesis, Utrecht University, Utrecht, 147pp., Geologica Ultraiectina 139.

Gelinas, Y., Baldock, J.A., Hedges, J.I., (2001a). Organic carbon composition of marine sediments: effect of oxygen exposure on oil generation potential. Science 294:145-148

Gelinas, Y., Baldock, J.A., Hedges, J.I., (2001b). Demineralization of marine and freshwater sediments for CP/MAS ^{13}C NMR analysis. Organic Geochemistry 32:677-693

General Statement of 14C Procedures, National Ocean Sciences Accelarated Mass Spectrometry Facility, Woods Hole Oceanographic Institution, Available on line: http://www.whoi.edu/nosams/page.do?pid=40144

Gerland, S., Villinger, H., (1995). Nondestructive density determination on marine sediment cores from gamma-ray attenuation measurements. Geo-Marine Letters 15:111-118

Giancoli Barreto, S.R., Nozaki, J., De Oliviera, E., *et al*., (2004). Comparison of metal analysis in sediments usisng EDXRF and ICP-OES with the HCl and Tessie extraction methods. Talanta 64:345-354

Giergielewicz-Mozajska, H., Dabrowski, L., Namiesnik, J., (2007). Accelerated solvent extraction (ASE) in the analysis of environmental solid samples – some aspects of theory and practise. Critical Reviews in Analytical Chemistry 31:149-165

Gillan, F.T., Hogg, R.W., (1984). A method for estimation of bacterial biomass and community structure in mangrove-associated sediments. Journal of Microbiological Methods 2:275-293

Giovannoni, S., Rappe, M., (2000). Evolution, diversity, and molecular ecology of marine prokaryotes, p. 47-84. In: Microbial ecology of the oceans, Krichman, D.L., (Ed). Wiley, 620pp.

Goad, L.J., Rubinstein, I., Smithm A.G., (1972). A discussion of biosynthesis of sterols and related compounds. Proceedings of the Royal Society of London, Series B, Biological Sciences 180:223-246

Goad, L.J., Akihisa, T., (1997). Analysis of sterols. Blackie Academic & Professional, an imprint of Chapman & Hall, London, UK, 437pp.

Goncalves, C. N., Dalmolin, R. S. D., Dick, D. P., Knicker, H., *et al*., (2003). The effect of 10% HF treatment on the resolution of CP MAS ^{13}C NMR spectra and on the quality of organic matter in Ferralsols. Geoderma 116:373– 392.

Goni, M.A., Hedges, J.I., (1990). Cutin-derived CuO reaction products from purified cuticules and tree leaves. Geochimica et Cosmochimica Acta 54:3065-3072

Goni, M.A., Nelson, B., Blanchette, R.A., *et al*., (1993). Fungal degradation of wood lignins: geochemical perspectives from CuO-derived phenolic dimers and monomers. Geochimica et Cosmochimica Acta 57:3985-4002

Goni, M.A., Hedges, J.I., (1995). Sources of reactivities of marine-derived organic matter in coastal sediments as determined by alkaline CuO oxidation. Geochimica et Cosmochimica Acta 59:2965-2981

Goni, M.A., Ruttenberg, K.C., Eglinton, T.I., (1998). A reassessment of the sources and importance of land-derived organic matter in surface sediments from the Gulf of Mexico. Geochimica et Cosmochimica Acta 62:3055-3075

Gontharet, S., Pierre, C., Blanc-Valleron, M.-M., *et al.*, (2007). Nature and origin of diagenetic carbonate crusts and concretions from mud volcanoes and pockmarks of the Nile deep-sea fan (eastern Mediterranean Sea). Deep-Sea Research II 54:1292-1311

Gonzales, C., Saliot, A., Pillon, P., (1985). N-alkanes in an equatorial sedimentary environment: their distribution as a function of particle size. International Journal of Environmental Analytical Chemistry 22:47-59

Gonzalez, I., Jordan, M.M., Sanfeliu, T., *et al*., (2007). Mineralogy and heavy metal content in sediments from Rio Gato, Carelmapu and Cucao, Southern Chile. Environmental Geology 52:1243-1251

Gold, T., (1992). The deep, hot biosphere. Proceedings of National Academy of Science USA 89:6045-6049

Gold, T., (1999). The Deep Hot Biosphere. New York, Copernicus Books, 243pp.

Goldfine, H., (2010). The appearance, disappearance and reappearance of plasmalogens in evolution. Progress in Lipid Research 49:493-498

Goodfriend, G.A., Stanley, D.J., (1996). Reworking and discontinuities in Holocene sedimentation in the Nile Delta: documentation from amino acid racemization and stable isotopes in mollusk shells. Marine Geology 129:271-283

Gowen, R.J., Raine, R., Dickey-Collas, M., *et al*., (1998). Plankton distribution in relation to physical oceanographic features on the southern Malin Shelf, August 1996. ICES Journal of Marine Science 55:1095-1111

Gribble, K.E., Nolan, G., Anderson, D.M., (2007). Biodiversity, biogeography and potential trophic impact of Protoperidinium spp. (Dinophyceae) off the southwestern coast of Ireland. Journal of Plankton Research 29:931-947

Grosjean, E., Logan, G.A., (2007). Incorporation of organic contaminants into geochemical samples and an assessment of potential sources: Examples from Geoscience Australia marine survey S282. Organic Geochemistry 38:853-869

Grutters, M., van Raaphorst, W., Epping, E., *et al*., (2002). Preservation of amino acids from in situ-produced bacterial cell wall peptidoglycans in northeastern Atlantic continental margin sediments. Limnology and Oceanography 47:1521-1524

Guggenheim, S., Martin, R.T., (1995). Definition of clay and clay mineral: Joint report of the AIPEA nomenclature and CMS nomenclature committees. Clays and Clay Minerals 43:255-256

Gungor, H., Elik, A., (2007). Comparison of ultrasound-assisted leaching with conventional and acid bomb digestion for determination of metals in sediment samples. Microchemical Journal 86:65-70

Halevy, I., Johnston, D.T., Schrag, D.P., (2010). Explaining the structure of Archean mass-independent sulphur isotope record. Science 329:204-207

Hallock, P., Lidz, B.H., Cockney-Burkhard, E.M., *et al*., (2003). Foraminifera as bioindicators in the coral reef assessment and monitoring: the foram index. Environmental Monitoring and Assessment 81:221-238

Hamilton, E.L., (1957). Planktonic foraminifera from an Equatorial Pacific core. Micropaleontology 3:9-73

Hamilton, E.L., (1976). Variations of density and porosity with depth in deep-sea sediments. Journal of Sedimentary Research 46:273-279

Hamilton, R.D., Greenfield, L.J., (1967). The utilization of free amino acids by marine sediment microbiota. Zeitschrift fur allgemeine Mikrobiologie/Journal of Basic Microbiology 7:335-342

Hampton, L.D., Anderson, A.L., (1974). Acoustics and gas in sediments. In: Natural gases in marine sediments, Kamplan, I.R., (Eds), Plenum Press, New York, 324pp.

Hampton, M.A., Lee, H.J., Locat, J., (1996). Submarine landslides. Reviews of Geophysics 34: 33-59

Hanson, R.S., Hanson, T.E., (1996). Methanotrophic bacteria. Microbiology and Molecular Biology Reviews 60:439-471

Hao, J., Cleveland, C., Lim, E., *et al*., (2006). The effect of adsorbed lipid on pyrite oxidation under biotic conditions. Geochemical Transactions 7:1-9

Harada, N., Handa, N., Oba, T., *et al*., (1997). Age determination of marine sediments in the Western North Pacific by aspartic acid chronology. Journal of Oceanography 53:1-7

Harwood, J.L., and Russell, N.J. (1984). Lipids in Plants and Microbes. George Allen and Unwin, London, pp 7-9, 35-54.

Harvey, H.R., Fallon, R.D., Patton, J.S., (1986). The effect of organic matter and oxygen on the degradation of bacterial membrane lipids in marine sediments. Geochimica et Cosmochimica Acta 50:795-804

Haschke, M., (2006). The Eagle III BKA system, a novel sediment core X-ray fluorescence analyser with very high spatial resolution. In: New Techniques in Sediment Core Analysis, Geological Society Special Publications 267:32-37, Rothwell, R.G. (Eds), London

Hatakka, A., (2001). Biodegradation of lignin, 129-180. In: Biopolymers. Vol. 1 Lignin, Humic Substances and Coal. Steinbuchel, A. (Ed), Wiley-Vch, Weinheim, Germany, 523pp.

Hatcher, P.G., Clifford, D.J., (1997). The organic geochemistry of coal: from plant materials to coal. Organic Geochemistry 27:251-274

Hauke, V., Graff, R., Wehrung, P., *et al*., (1993). Rearranged des-E-hopanoid hydrocarbons in sediment and petroleum. Organic Geochemistry 20:415-423

Hayes, J.M., Freeman, K.H., Popp, B.N., *et al*., (1990). Compound-specific isotope analyses, a novel tool for reconstruction of ancient biogeochemical processes. Organic Geochemistry 16:1115-1128

Hayes, J.M., (1993). Factors controlling ^{13}C contents of sedimentary organic compounds: Principles and evidence. Marine Geology 113:111-125

Hayes, M.H.B., (1985). Extraction of humic substances from soil. In: Humic Substances in Soil, Sediment, and Water; Geochemistry, Isolation and Characterization, Aikem, G.R., McKnight, D.M., Wershaw, R.L., et al., (Eds.). John Wiley & Sons, New York, 692pp.

Hayatsu, R., Botto, R.E., Scott, R.G., *et al*., (1987). Thermal catalytic transformation of pentacyclic triterpenoids: alteration of geochemical fossils during coalification. Organic Geochemistry 11:245-250

Hedberg, H.D., (1980). Methane generation and petroleum migration. Problems of Petroleum Migration, American Association of Petroleum Geologists, Studies in Geology 10:179-206

Hedges, J.I., Mann, D.C., (1979). The characterization of plant tissues by their lignin oxidation products. Geochimica et Cosmochimica Acta 43:803-1807

Hedges, J.I., Ertel, J.R., (1982). Characterization of lignin by gas capillary chromatography of cupric oxide oxidation products. Analytical Chemistry 54:174-178

Hedges, J.I., Cowie, G.L., Ertel, J.R., *et al*., (1985). Degradation of carbohydrates and lignins in buried woods. Geochimica et Cosmochimica Acta 49:701-711

Hedges, J.I., Prahl, F.G., (1993). Early diagenesis: Consequences for applications of molecular biomarkers. In: Organic Geochemistry. Principles and Applications, 237-254, Engel, M.H., Macko, S.A., (Eds). Plenum Press, New York, 884pp.

Hedges, J.I., Keil, R.G., (1995). Sedimentary organic matter preservation: an assessment and speculative synthesis. Marine Chemistry 49:81-115

Hedges, J.I., Oades, J.M., (1997). Comparative geochemistries of soils and marine sediments. Organic Geochemistry 27:319-361

Hedges, J.I., Hu, S.F., Devol, A.H., *et al*., (1999). Sedimentary organic matter preservation: A test for selective degradation under oxic conditions. American Journal of Science 299:529-555

Hedin, L., (2004). Global organization of terrestrial plant-nutrient interactions. Proceedings of National Academy of Science USA 30:10849-10850

Heemken, O.P., Theobald, N., Wenclawiak, B.W., (1997). Comparison of ASE and SFE with Soxhlet, sonication, and methanolic saponification extractions for the determination of organic micropollutants in marine particulate matter. Analytical Chemistry 69:2171-2180

Heider, F., Zitelsberger, A., Fabian, K., (1996). Magnetic susceptibility and remanent coercive force in grown magnetic crystals from 0.1 μm to 6 mm. Physics of Earth and Planetary Interiors 93:239-256

Henrichs, S.M., Reeburgh, W.S., (1987). Anaerobic mineralization of marine sediment organic matter: Rates and role of anaerobic processes in the oceanic carbon economy. Journal of Geomicrobiology 5:191-237

Henrichs, S.M., (1992). Early diagenesis of organic matter in marine sediments: progress and perplexity. Marine Chemistry 39:119-149

Hensen, C., Zabel, M., Pfeifer, K., *et al.*, (2003). Control of sulfate pore-water profiles by sedimentary events and the significance of anaerobic oxidation of methane for the burial of sulphur in marine sediments. Geochimica et Cosmochimica Acta 67:2631-2647

Hernandez, M.E., Mead, R., Peralba, M.C., *et al*., (2001). Origin and transport of n-alkane-2-ones in a subtropical estuary: potential biomarkers for seagrass-derived organic matter. Organic Geochemistry 32:21-32

Hernes, P.J., Benner, R., (2006). Terrigenous organic matter sources and reactivity in the North Atlantic Ocean and a comparison to the Arctic and Pacific oceans. Marine Chemistry 100:66-79

Hertkorn, N., Benner, R., Frommberger, M., *et al*., (2006). Characterization of major refractory component of marine dissolved organic matter. Geochimica et Cosmochimica Acta 70:2990-3010

Hibrecht, H., (1996). Extant planktic foraminifera and the physical environment in the Atlantic and Indian Oceans. Mitteilungen aus dem Geologischen Institut der Eidgen. Technischen Hochschule und der Universitat Zurich, Neue Folge. No. 300, 99 pp.; Zurich. On line edition: http://www.fuhrmann-hilbrecht.de/Heinz/geology/HH1996/aa_start.html

Highwood, E.J., Shine, K.P., Hurley, M.D., *et al*., (1999). Estimation of direct radiative forcing due to non-methane hydrocarbons. Atmospheric Environment 33:759-767

Hilton, J., Lishman, J.P., Millington, A., (1986). A comparison of some rapid techniques for the measurement of density in soft sediments. Sedimentology 33:777-781

Hinrichs, J., Schnetger, B., (1999). A fast method for the simultaneous determination of ^{230}Th, ^{234}U and ^{235}U with isotope dilution sector field ICP-MS. The Analyst 124:927-932

Hitchen, K., Stoker, M.S., (1993). Mosozoic rocks from the Hebrides Shelf and implications for hydrocarbon prospectivity in the northern Rockall Trough. Marine and Petroleum Geology 10:246-254

Hochella Jr., M.F., Lower, S., Maurice, P.A., *et al*., (2008). Nanominerals, mineral nanoparticles, and Earth Systems. Science 319:1631-1635

Hoehler, T.M., Alperin, M.J., Albert, D.B., *et al*., (1994). Field and laboratory studies of methane oxidation in an anoxic marine sediment: Evidence for a methanogenic-sufate reducer consortium. Global Biogeochemical Cycles 8:451-463

Hollerbach, A., Dehmer, J., (1994). Diagenesis of organic matter. In: Diageneis, IV. Developments in Sedimentology 51:390-354, Wolf, K.H., Chilingarian, G.V., (Eds). Elsevier Science, Amsterdam, 546pp.

Hollibaugh, J.T., Azam, F., (1983). Microbial degradation of dissolved proteins in seawater. Limnology and Oceanography 28:1104-1116

Holmes, M.E., Sansone, F.J., Rust, T.M., *et al*., (2000). Methane production, consumption, and air-sea exchange in the open ocean: An evaluation based on carbon isotopic ratios. Global Biogeochemical Cycles 14:1-10

Homma, H., Kuroyagi, T., Izumi, K., *et al*., (2000). Evaluation of surface degradation of silicone rubber using gas chromatography/mass spectrometry. IEEE Transactions on Power Delivery 15:796-803

Hosgörmez, H., (2006). Origin of the natural gas seep of Çirali (Chimera), Turkey: Site of the first Olympic fire. Journal of Asian Earth Sciences, 30:131-141

Houghton, J.T., Ding, Y., Griggs, D.J., *et al*., (Eds.), (2001). Climate Change 2001: The Scientific Basis. Cambridge University Press for Intergovernmental Panel on Climate Change

Hou, C.T., (1995). Microbial oxidation of unsaturated fatty acids. Advances in Applied Microbiology 41:1-23

Hovland, M., (1981b). Characteristics of pockmarks in the Norwegian Trench. Marine Geology 39:103-117

Hovland, M., (1981a). A classification of pockmark related features in the Norwegian Trench. Continental Shelf Institute

Hovland, M., (1982). Pockmarks and the recent geology of the central section of the Norwegian Trench. Marine Geology 47:283-301

Hovland, M., Judd, A.G., King, L.H., (1984). Characteristic features of pockmarks on the Morth Sea Floor and Scotian Shelf. Sedimentology 31:471-480

Hovland, M., Sommerville, J.H., (1985). Characteristics of two natural gas seepages in the North Sea. Marine and Petroleum Geology 20:319-326

Hovland, M., Judd, A.G., (1988). Seabed pockmarks and seepages. Impact on geology, biology and marine environment. Graham and Trotman, London

Hovland, M., Mortensen, P.B., (1999). Norwegian coral reefs and seabed processes. Bergen, John Grieg Forlag, English summary

Hovland, M., Gallagher, J.W., Clennell, M.B., *et al*., (1997). Gas hydrate and free gas volumes in marine sediments: example from the Niger Delta front. Marine and Petroleum Geology 14:245-255

Hovland, M., (2003). Geomorphological, geophysical, and geochemical evidence of fluid flow through the seabed. Journal of Geochemical Exploration 78-79:287-291

Hovland, M., Svensen, H., Forsberg, C.F., *et al*., (2005). Complex pockmarks with carbonate-ridges off mid-Norway: Products of sediment degassing. Marine Geology 218:191-206

Hovland, M., Heggland, R., De Vries, M.H., *et al*., (2010). Unit-pockmarks and their potential significance for predicting fluid flow. Marine and Petroleum Geology 27:1190-1199

Hudson, E.D., Parrish, C.C., Helleur, R.J., (2001). Biogeochemistry of sterols in plankton, settling particles and recent sediments in a cold ocean ecosystem (Trinity Bay, Newfoudland). Marine Chemistry 76:253-270

Hulthe, G., Hulth, S., Hall., P.O.J., (1998). Effect of oxygen on degradation rate of refractory and labile organic matter in continental margin sediments. Geochimica et Cosmochimica Acta 62:1319-1328

Hunt, R., (1858). Memoirs of the Geological Survey of Britain, and of the Museum of Practical Geology. Geological Survey of Great Britain, London, 867pp.

Hydes, D.J., Gowen, R.J., Holliday, N.P., *et al*., (2004). External and internal control of winter concentrations of nutrients (N, P and Si) in north-west European shelf areas. Estuarine, Coastal and Shelf Science 59:151-161

IAEA (1988) Assessing the impact of deep sea disposal of low-level radioactive waste on living marine resources. Technical Report Series No. 288, International Atomic Energy Agency, Vienna

Ibach, L.E., (1982). Relationship between sedimentation rate and total organic carbon content in ancient marine sediments. Bulletin of the American Association of Petroleum Geologists 66:170-188

Idler, D.R., Wiseman, P.M., Safe, L.M., (1970). A new marine sterol, 22-trans-24-norcholesta-5,22-dien-3β-ol. Steroids 16:451-461

Ingalls, A.E., Aller, R.C., Lee, C., *et al*., (2004). Organic matter diagenesis in shallow water carbonate sediments. Geochimica et Cosmochimica Acta 68:4363-4379

Innes, H.E., Bishop, A.N., Head, I.M., *et al.*, (1997). Preservation and diagenesis of hopanoids in recent lacustrine sediments of Priest Pot, England. Organic Geochemistry 26:565-576

International Standard ISO-13320-1:1999, Particle size analysis – laser diffraction methods – Part 1: General principles. International Organization for Standardization

Iversen, N., Jorgensen, B.B., (1985). Anaerobic methane oxidation rates at the sulphate-methane transition in marine sediments from Kattegat and Skagerrak (Denmark). Limnology and Oceanography 30:944-955

Jacks, T.J., Yatsu, L.Y., Hensarling, T.P., (1970). Extraction of lipids from cottonseed tissue: I. Comparison of hexane-acetone-water, its nonaqueous components and chloroform-methanol. Journal of the American Oil Chemists' Society 47:222-223

Jackson, D.R., Williams, K.L., Wever, T.F., *et al.*, (1998). Sonar evidence for methane ebullition in Eckernförde Bay. Continental Shelf Research 18:1893-1915

Jackson, P.D., Lovell, M.A., Roberts, J.A., *et al*., (2006). Rapid non-contacting resistivity logging of core. In: New Techniques in Sediment Core Analysis, Geological Society Special Publications 267:209-217, Rothwell, R.G. (Eds), London

Jaffe, R., Cabrera, A., Hausmann, K., *et al*., (1993). On the origin and fate of n-alkan-2-ones in freshwater environments, 356-359. In: Organic Geochemistry: Applications in Energy and the Natural Environment, Manning, D. (Ed). Manchester University Press, Manchester, UK, 480pp.

Jahnke, R.A., Jahnke, D.B., (2004). Calcium carbonate dissolution in deep sea sediments: reconciling microelectrode, pore water and benthic flux chamber results. Geochimica et Cosmochimica Acta 68:47-59

Jain, K.K., (2010) The Handbook of Biomarkers. Springer, New York, 492pp.

Jansen, B., Nierop, K.G.J., Kotte, M.C., *et al*., (2006). The applicability of accelerated solvent extraction (ASE) to extract lipid biomarkers from soils. Applied Geochemistry 21:1006-1015

Jansen, J.H.F., Van der Gaast, S.J., Koster, B., *et al.*, (1998). CORTEX, a shipboard XRF-scanner for element analyses in split sediment cores. Marine Geology 151:143-153

Jamtveit, B., Svensen, H., Podladchikov, Y., et al., (2004). Hydrothermal vent complexes associated with sill intrusions in sedimentary basins. In: Physical Geology of High-Level Magmatic Systems, Breitkreutz, C., and Petford, N., (Eds), Geological Society of London, Special Publications 234:233-241

Jayaraju, N., Sundara Raja Reddy, B.C., Reddy, K.R., (2008). The response of benthic foraminifera to various pollution sources: A study from Nellore Coast, East Coast of India. Environmental Monitoring and Assessment 142:319-323

Jeannotte, R., Hamel., C., Jabaji, S., *et al*., (2008). Comparison of solvent mixtures for pressurized solvent extraction of soil fatty acid biomarkers. Talanta 77:195-199

Jeng, W-L., Chen, M-P., (1995). Grain size effect on bound lipids in sediments off northwestern Taiwan. Organic Geochemistry 23:301-310

Jenkinson, I.R., Connors, P.P. (1980). The occurrence of the red tide causing organism, *Gyrodinium aureolum*, Hulbert (Dinophyceae), round the south and west of Ireland in August and September, 1979. Journal of Sherkin Island 1:127-146

Jensen, P., Aagaard, I.,Burke Jr, R.A., *et al*., (1992). 'Bubbling reefs' in the Kattegat: submarine landscapes of carbonate-cemented rocks support a diverse ecosystem at methane seeps. Marine Ecology Progress Series 83:103-112

Jensen, M.M., Holmer, M., Thamdrup, B., (2004). Composition and diagenesis of neutral carbohydrates in sediments of the Baltic-North Sea transition. Geochimica et Cosmochimica Acta 69:4085-4099

Johns, W.D., Shimoya, A., (1972). Clay minerals and petroleum-forming reactions during burial and diagenesis. American Association of Petroleum Geologists Bulletin 56:2160-2167

Johns, W.D., (1979). Clay mineral catalysis and petroleum generation. Annual Review of Earth and Planetary Sciences 7:183-198

Johnson, R.W., Calder, J.A., (1973). Early diagenesis of fatty acids and hydrocarbons in salt marsh environment. Geochimica et Cosmochimica Acta 37:1943-1955

Jonasz, M., (1987). Nonsphericity of suspended marine particles and its influence on light scattering. Limnology and Oceanography 32:1059-1065

Jonasz, M., (1991). Size, shape, composition and structure of microparticles from light scattering. In: Principles, methods, and application of particle size analysis, Syvitske, J.P.M., (Ed.), Cambridge University Press, 368pp.

Jones, R.W., (1993). Preliminary observations on benthonic foraminifera associated with biogenic gas seeps in the North Sea. In: Jenkins, D.G., and Graham, D., *Applied Micropaleontology*, Dordrecht, Kluwer, Academics Publishers, 69-91

Josenhans, H.W., King, L.H., Fader, G.B.J., (1978). A side scan sonar mosaic of pockmarks on the Scotian Shelf. Canadian Journal of Earth Science 15:831-841

Judd, A.G., (1981). Evaluating the hazard potential of pockmarks. Oceans 13:694-698

Judd, A.G., Hovland, M., (1989). The role of chemosynthesis in supporting fish stocks in the North Sea. Journal of Fish Biology 35:329-330

Judd, A.G., Hovland, M. (1992). The evidence of shallow gas in marine sediments. Continental Shelf Research 12:1081-1095

Judd, A.G., Davies, G., Wilson, J., *et al.*, (1997). Contributions to atmospheric methane by natural seepages on the UK continental shelf. Marine Geology 140:427-455

Judd, A.G., Sim, R., Kingston, P., McNally, J., (2002). Gas seepage on an intertidal site: Torry Bay, Firth of Forth, Scotland. Continental Shelf Research 22:2317-2331

Judd, A.G., (2003). The global importance and context of methane escape from the seabed. Geo-Marine Letters 23:147-154

Judd, A.G., (2004). Natural seabed gas seeps as sources of atmospheric methane. Environmental Geology 46:988-996

Judd, A.G., Hovland, M., (2007). Seabed fluid flow. The impact on geology, biology, and the marine environment. Cambridge University Press, 475pp.

Judd, A.G., Croker, P.F., Tizzard, L., *et al.*, (2007). Extensive methane-derived authigenic carbonates in the Irish Sea. Geo-Marine Letters 27:259-267

Jukes, J.B., Kinahan, G.H., Du Noyer, G.V., *et al.*, (1861). Explanations to accompany Sheets 200, 203, 204 and 205, and part of 199. Memoirs of the Geological Survey of Ireland

Jukes, J.B., (1864). Explanation to accompany Sheet 192 and part of Sheet 199. Memoirs of the Geological Survey of Ireland

Kaltashov, I.A., Doroshenko, V., Cotter, R.J., *et al.*, (1997). Confirmantion of the structure of Lipid A derived from the Lipopolysaccharide of Rhodobacter sphaeroides by a Combination of MALDI, LSIMI, and tandem Mass Spectrometry. Analytical Chemistry 69:2317-2322

Karner, M.B., Delong, E.F., Karl, D.M., (2001). Archaeal dominance in the mesopelagic zone of the Pacific Ocean. Nature 409:507-510

Kasten, S., Freudenthal, T., Gingele, F.X., *et al*., (1998). Simultaneous formation of iron-rich layersat different redox boundaries in sediments of the Amazon Deep-Sea Fan. Geochimica et Cosmochimica Acta 62:2253-2264

Kato, M.T., Field, J.A., Lettinga, G., (1993). High tolerance of methanogens in granular sludge to oxygen. Biotechnology and Bioengineering 42:1360-1366

Kawashima, H., Ohnishi, M., Negishi, Y., *et al*., (2007). Sterol composition in muscle and viscera of the marine bivalve Megangulus zyonoensis from coastal waters of Hokkaido, Northern Japan. Journal of Oleo Science 56:231-235

Kenyon, N.H., Akhmetzhanov, A.M., Wheeler, A.J., *et al*., (2003). Giant carbonate mud mounds in the southern Rockall Trough. Marine Geology 195:5-30

Keeling, R.F., (2007). Deglaciation Mysteries. Science (Washington DC, US) 316:1440-1441

Keil, R.G., Montlucon, D.B., Prahl, F.G., *et al*., (1994). Sorptive preservation of labile organic matter in marine sediments. Nature 370:549-552

Keil, R.G., Fogel, M.L., (2001). Reworking of amino acids in marine sediments: Stable carbon isotopic composition of amino acids in sediments along the Washington coast. Limnology and Oceanography 46:14-23

Kelleher, B.P., Simpson, M.J., Simpson, A.,J., (2006). Assessing the fate and transformation of plant residues in the terrestrial environment using HR-MAS NMR spectroscopy. Geochimica et Cosmochimica Acta 70:4080-4094

Kelleher, B.P., Simpson, A.J., Rogers, R.E., *et al*., (2007). Effects of natural organic matter from sediments on the growth of marine gas hydrates. Marine Chemistry 103:237-249

Kelley, C., (2003). Methane oxidation potential in the water column of two diverse coastal marine sites. Biogeochemistry 65:105-120

Kelley, J.T., Dickson, S.M., Belknap, D.F., *et al*., (1994). Giant seabed pockmarks: Evidence for gas escape from Belfast Bay, Marine Geology 22:59-62

Keogh, S.M., Aldahan, A., Possnert, G., *et al*., (2007). Trends in the spatial and temporal distribution of ^{129}I and ^{99}Tc in coastal waters surrounding Ireland using *Fucus vesiculosus* as a bio-indicator. Journal of Environmental Radioactivity 95:23-38

Kerger, B.D., Nichols, P.D., Sand, W., *et al*., (1987). Association of acid-producing thiobacilli with degradation of concrete: analysis by 'signature' fatty acids from the polar lipids and lipopolysaccharide. Journal of Industrial Microbiology 2:63-69

Khilyuk, L.F., Robertson Jr., J.O., Endres, B., et al., (2000). Gas migration: events preceding earthquakes. Gulf Professional Publishing, 400pp.

Kiel, S., (Ed) (2010). The Vent and Seep Biota, Topics in Geobiology 33, Landman, N.H., Harries, P., (series Eds), Springer, Germany, 487pp.

Kim, D.C., Lee, G.S, Lee, G.H., *et al*., (2008). Sediment echo types and acoustic characteristics of gas-related acoustic anomalies in Jinhae Bay, southern Korea. Geosciences Journal 12:47-61

Kim, J.-H., Schouten, S., Hopmans, E.C., *et al*., (2008) Global sediment core-top calibration of the TEX_{86} paleothermometer in the ocean. Geochimica et Cosmochimica Acta 72:1154-1173

King, L.H., MacLean, B., (1970). Pockmarks of the Scotian Shelf. Geological Society of America Bulletin 81:3141-3148

Killops, S., Killops, V., (2005). Introduction to Organic Geochemistry – 2^{nd} ed. Blackwell Publishing, UK, 393pp.

Kippax, P., Morton, D., (2008). Aerolization analysis: unlocking the secrets of dry powder inhaler plume. Drug Delivery Technology 8:53-58

Klok, J., Baas, M., Cox, H.C., *et al*., (1984). Loliolides and dihydroactinidiolide in a recent marine sediment probably indicate a major transformation pathway of carotenoids. Tetrahedron Letters 25:5577-5580

Koch, H., Laschewsky, A., Ringsdorf, H., *et al*., (1986). Photodimerization and photopolymerization of amphiphilic cinnamic acid derivatives in oriented monolayers, vesicles and solution. Die Makromolekulare Chemie 187:1843-1853

Koga, Y., Nishihara, M., Morii, H., *et al*., (1993). Ether polar lipids of methanogenic bacteria: structure, comparative aspects, and biosyntheses. Microbiological Reviews 57:164-182

Koga, Y., Nakano, M., (2008). A dendrogram of archaea based on lipid component parts composition and its relationship to rRNA phylogeny. Systematic and Applied Microbiology 31:169-182

Kolattukudy, P.E., (1980). Biopolymer membranes of plants cutin and suberin. Science 208:990-1000

Kokke, W.C.M.C., Fenical, W., Djerassi, C., (1981). Sterols with unusual nuclear unsaturation from three cultured marine dinoflagellates. Phytochemistry 20:127-134

Komatsu, G., Kargel, V.R., Baker, R.G., *et al*., (2000). A chaotic terrain formation hyphotesis: explosive outgas and outflow by dissociation of clathrate on Mars. Lunar and Planetary Science XXXI Conference Materials, Poster 1434

Konert, M., Vandenberghe, J., (1997). Comparison of laser grain size analysis with pipette and sieve analysis: a solution for the underestimation of the clay fraction. Sedimentology 44:523-535

Kowalska, J., Kransodębska-Ostręga, B., Golimowski, J., (2002). Electroanalytical methods determination of the metal content and acetic-acid-available metal fractions in soils. Anaytical and Bioanalytical Chemistry 373:116-118

Krebs, H.A., Weitzman, P.D.J., (1987). Krebs' citric acid cycle: half a century and still turning. Biochemical Society, London, 198pp.

Kristensen, E., Ahmed, S.I., Devol, A.H., (1995). Aerobic and anaerobic decomposition of organic matter in marine sediments: Which is fastest? Limnology and Oceanography 40:1430-1437

Krumbein, W.C., (1938). Size frequency distribution of sediments and the normal phi curve. Journal of Sedimentary Petrology 8:84-90

Kruskal, J. B. and Wish, M. (1978). Multidimensional Scaling. Sage University Paper series on Quantitative Applications in the Social Sciences, number 07-011. Sage Publications, Newbury Park, CA

Kuffner, I.B., Andersson, A.J., Jokiel, P.L., *et al*., (2008). Decreased abundance of crustose coralline algae due to ocean acidification. Nature Geoscience 1:114-117

Kuk, M.S., Tetlow, R., Dowd, M.K., (2005). Cottonseed extraction with mixtures of acetone and hexane. . Journal of the American Oil Chemists' Society 82:609-612

Kutas, R.I., Paliy, S.I., Rusakov, O.M., (2004). Deep faults, heat flow and gas leakage in the northern Black Sea. Geo-Marine Letters 24:163-168

Kvenvoldem, K.A., (1983). Marine gas hydrates – I: geochemical evidence. Natural Gas Hydrates: Properties, Occurrence and Recovery. Boston, Butterworth, 63-72

Kvenvolden, K.A., Lilley, M.D., Lorenson, T.D., *et al.*, (1993). The Beaufort Sea continental shelf as a seasonal source of atmospheric methane. Geophysical Research Letters 20:2459-2462

Kvenvolden, K.A., (1999). Potential effects of gas hydrate on human welfare. Proceedings of the National Academy of Sciences, USA, 96:3420-3426

Kvenvolden, K.A., Lorenson, T.D., Reeburgh, W.S., (2001). Attention turns to naturally occurring methane seepages. EOS 82:457

Kvenvolden, K.A., Cooper, C.K., (2003). Natural seepage of crude oil into the marine environment. Geo-Marine Letters 23:140-146

Lajat, M., Saliot, A., Schimmelmann, A., (1989). Free and bound lipids in recent (1835-1987) sediments from Santa Barbara Basin. Advances in Organic Geochemistry 16:793-803

Lambert, G., Schmidt, S., (1993). Reevaluation of the oceanic flux of methane: uncertainties and long term variations. Chemosphere 26:579-589

Lamble, K.J., Hill, S.J., (1998). Microwave digestion procedures for environmental matrices – a critical review. The Analyst 123:103R-133R

Lee, C., Gagosian, R.B., Farrington, J.W., (1977). Sterol diagenesis in recent sediments from Buzzard's Bay, Massachusetts. Geochimica et Cosmochimica Acta 41:985-992

Lee, C., Gagosian, R.B., Farrington, J.W., (1980). Geochemistry of sterols in sediments from the Black Sea and the Southwest African shelf and slope. Organic Geochemistry 2:103-113

Lechner, P., Fiorini, C., et al., (2001). Silicon drift detectors for high count rate X-ray spectroscopy at room temperature. Nuclear Instruments and Methods 458A:281-287

Leenheer, M.J., Flessland, K.D., Meyers, P.A., (1984). Comparison of lipid character of sediments from Great Lakes and the Northwestern Atlantic. Organic Geochemistry 7:141-150

Lehninger, A.L., (1975). Biochemistry. The Molecular Basis of Cell Structure and Funcion. 2nd Ed., Worth Publishing, New York, 1104pp.

Leong, L.S., Tanner, P.A., (1999). Comparison of methods for determination of organic carbon in marine sediment. Marine Pollution Bulletin 38:875-879

Leroueil, S., Locat, J., Levesque, C., *et al*., (2003). Towards an approach for the assessment of risk associated with submarine mass movement. Submarine Mass Movements and Their Consequences. Dordrecht, Kluwer Academic Publishers, 59-68

Levin, L.A., James, D.W., Martin, C.M., *et al.,* (2000). Do methane seeps support distinct macrofaunal assemblages? Observations on community structure and nutrition from the northern Californian slope and shelf. Marine Ecology Progress Series 208:21-39

Levy, E.M., Lee, K., (1988). Potential contribution of natural hydrocarbon seepage to benthic productivity and the fisheries of Atlantic Canada. Canadian Journal of Fisheries and Aquatic Sciences, 45:349-352

Li, J., Yuan, H., Yang, J., (2009). Bacteria and lignin degeneration. Frontiers of biology in China 4:29-38

Lichtfouse, E., Elbisser, B., Balesdent, J., *et al*., (1994). Isotope and molecular evidence for direct input of maize leaf wax n-alkanes into crop soil. Organic Geochemistry 22:349-351

Liebezeit, G., Wiesner, M.G., (1990). Pyrolysis of recent marine sediments - I. Biopolymers. Organic Geochemistry 16:1179-1185

Ligero, R.A., Ramos-Lerate, I., Barrera, M., *et al*., (2000). Relationship between sea-bed radionuclide activities and some sedimentological variables. Journal of Environmental Radioactivity 57:7-19

Lipp, J.S., Morono, Y., Inagaki, F., *et al*., (2008). Significant contribution of Archaea to extant biomass in marine subsurface sediments. Nature 454:991-994

Lipp, J.S., Hinrichs, K-.U., (2009). Structural diversity and fate of intact polar lipids in marine sediments. Geochimica et Cosmochimica Acta 73:6816-6833

Lipps, J.H., (1973). Test structure in Foraminifera. Annual Review of Microbiology 27:471-488

Lo, J.M., Sakamoto, H., (2005). Comparison of the acid combinations in microwave-assisted digestion of marine sediments for heavy metal analyses. Analytical Sciences 21:1181-1184

Locat, J., (2001). Instabilities along ocean margins: a geomorphological and geotechnical perspective. Marine and Petroleum Geology 18:503-512

Logemann, J., Graue, J., Koster, J., *et al*., (2011). A laboratory experiment of intact polar lipid degradation in sandy sediments. Biogeosciences Discussions 8:3289-3321

Loll, M.J., Bollag, J.M., (1983). Protein transformation in soil. Advances in Agronomy 36:351-382

Lorenson, T.D., Kvenvolden, K.A., Hostettler, F.D., et al., (2002). Hydrocarbon geochemistry of cold seeps in the Monterey Bay National Marine Sanctuary. Marine Geology 18:285-304

Lovell, M.A., (1985).Thermal conductivity and permeability assessment by electrical resistivity measurements in marine sediments. Marine Geotechnology 6:205-240

Lowendahl, L., Petersson, G., Samuelson, O., (1975). Oxygen-alkali treatment of cellobiose. Acta Chemica Scandinavica B 29:975-980

Lowendahl, L., Petersson, G., Samuelson, O., (1976). Formation of carboxylic acids by degradation of carbohydrates during craft cooking of pine. Tappi 50:118-121

Lucey, J.A., Vintro, L.L., Boust, D., *et al*., (2007). A novel approach to the sequential extraction of plutonium from oxic and anoxic sediment using sodium citrate to inhibit post-extraction resorption. Journal of Environmental Radioactivity 93:63-73

Lu, D., Song, Q., Wang, X., (2010). Decomposition of algal lipids in clay-enriched marine sediment under oxic and anoxic conditions. Chinese Journal of Oceanology and Limnology 28:131-143

Lucia, A., Amale, A., Taylor, R., (2008). Distillation pinch points and more. Computers and Chemical Engineering 32:1342-1364

Lukac, P., Patzeltova, N., Foldesova, M., (1999). Uptake of plutonium from nuclear waste water by natural and chemically modified sorbents. Journal of Radioanalytical and Nuclear Chemistry 242:231-233

Lund, D.C., Lynch-Stieglitz, J., Curry, W.B., (2006). Gulf Stream density structure and transport during the past millennium. Nature 444:601-604

Lynch, D.R., Smith, K.W., Cahill, B., (2004). Seasonal mean circulation on the Irish shelf – a model-generated climatology. Continental Shelf Research 24:2215-2244

MacCarthy, I.A.J., (2007). The South Munster Basin of southwest Ireland. Journal of Maps 2007:149-172

Macias-Zamora, J.V., Villaescusa-Celaya, J.A., Munoz-Barbosa, A., *et al*., (1999). Trace metals in sediment cores from the Campeche shelf, Gulf of Mexico. Environmental Pollution 104:69-77

Mackenzie, F.T., Lerman, A., Ver, L.M., (1998). Role of the continental margin in the global carbon balance during the past three centuries. Geology 26:423-426

Magnusson, C.D., Haraldsson, G.G., (2011). Ether lipids. Review. Chemistry and Physics of Lipids. 164:315-340

Manskaya, S.M., Drozdova, T.V., (1968). Organic substances in geochemistry, 16-22. In: Geochemistry of organic substances, Manskaya, S.M., Drozdova, T.V., (Eds). Pergamon Press, Oxford, 347pp.

MARDOS (1995). Sources of radioactivity in the marine environment and their relative contribution to overall dose assessment from marine radioactivity. IAEA, Technical report, IAEA-TECDOC-838, Vienna

Margalef, R. (1958). Temporal succession and spatial heterogeneity in natural phytoplankton. Perspectives in Marine Biology, University of California Press, 323-349 pp.

Martens, C.S., Berner, R.A., (1977). Interstitial water chemistry of Long Island Sound sediments. I, Dissolved gases. Limnology and Oceanography 22:10-25

Martone, P.T., Estevez, J.M., Lu, F., *et al*., (2009). Discovery of lignin is seaweed reveals convergent evolution of cell-wall architecture. Current biology 19:169-175

Masiello, C.A., (2007). Quick burial at sea. Nature 450:360-361

Masson, D.G., Bett, B.J., Billett, D.S.M., *et al*., (2003) The origin of Deep-water, coral-topped mounds in the northern Rockall Trough, Northeast Atlantic. Marine Geology 194:159-180

Mayzaud, P., Chanut, J.P., Ackman, R.G., (1989). Seasonal changes of the biochemical composition of marine particulate matter with special reference to fatty acids and sterols. Marine Ecology Progress Series 56:189-204

Max, M.D., (2000). Hydrate resource, methane fuel, and a gas-based economy? Natural Gas Hydrates in Oceanic and Permafrost Environments, Dordrecht, Kluwer Academic Publishers, 361-370

McCave, I.N., Manighetti, B., Beveridge, N.A.S., (1995). Circulation in the glacial North Atlantic inferred from grain-size measurements. Nature 374:149-152

McCubbin, D., Leonard, K.S., Young, A.K., *et al*., (2004). Application of a magnetic extraction technique to assess radionuclide-mineral association in Cumbrian shoreline sediments. Journal of Environmental Radioactivity 77:111-131

McDowell, J.L., Knight, J., Quinn, R., (2005). High-resolution geophysical investigations seaward of the Bann Estuary, Northern Ireland coast. In: High resolution morphodynamics and sedimentary evolution of Estuaries, FitzGerald, D.M., Knight, J., (Eds). Springer, Dordrecht, The Netherlands, 370pp.

MacDonald, I.R., Guinasso Jr., N.L., Sassen. R., *et al*, (1994). Gas hydrate that breaches the sea floor on continental slope of the Gulf of Mexico. Geology, 22:699-702

MacDonald, I.R., Reilly II, J.F., Guinasso, N.L., *et al*., (1990). Chemosynthetic mussels at a brine-filled pockmark in the northern Gulf of Mexico. Science 248:1096-1099

McGonigle, C., Brown, C.J., Quinn, R., (2010). Operational Parameters, Data Density and Benthic Ecology: Considerations for Image-Based Classification of Multibeam Backscatter. Marine Geology 33:16-38

McIver, R.D., (1982). Role of naturally occurring gas hydrates in sediment transport. American Association of Petroleum Geologists, Bulletin 66:789-792

McKenna, P., Longworth, R.D., (1997). Residual Chernobyl fallout and Sellafield pollutants found on the Isle of Man. The Science of the Total Environment 173/174:7-14

McMahon, T.E., Zale, A.V., Orth, D.J., (1996). Aquatic habitat measurements. In Murphy, B.R., Willis, D.W. (Eds), Fisheries Techniques, 2nd edn. American Fisheries Society, Bethseda, USA, 732pp.

McQuillin, R., Fannin, N.G.T., (1979). Explaining the North Sea's lunar floor. New Scientist 83:90-92

Meckler, A.N., Schubert, C.J., Hochuli, P.A., *et al*., (2008). Glacial to Holocene terrigenous organic matter input to sediments from Orca Basin, Gulf of Mexico – A combined optical and biomarker approach. Earth and Planetary Science Letters 272:251-263

Mejanelle, L., Sanchez-Gargallo, A., Bentaleb, I., *et al*., (2003). Long chain n-alkyl diols, hydroxyl ketones and sterols in a marine eustigmatophyte, Nannochloropsis gaditana, and in Brachionus plicatilis feeding on the algae. Organic Geochemistry 34:527-538

Merrill, R.B., Beck, J.W., (1995). The ODP color digital imaging system: Color logs of Quaternary sediments from Santa Barbara Basin, Site 893. Proceedings of Ocean Drilling

Program, Scientific Results, 146:45-60, Kennett, J.P., Baldauf, J.G., Lyle, M. (Eds), Ocean Drilling Program, Texas

Metherel, A.H., Taha, A.Y., Izadi, H., *et al*., (2009). The application of ultrasound energy to increase lipid extraction throughput of solid matrix samples (flaxseed). Prostaglandins, Leukotrienes and Essential Fatty Acids 81:417-423

Meyer, L.M., (1994). Surface area control of organic carbon accumulation in continental shelf sediments. Geochimica et Cosmochimica Acta 58:1271-1284

Meyer, L.M., Schick, L.L., Hardy, K.R., *et al*., (2004). Organic matter in small mesopores in sediments and soils. Geochimica et Cosmochimica Acta 68:3863-3872

Meyers, P.A., (1997). Organic geochemical proxies of paleoceanographic, paleolimnologic, and paleoclimatic processes. Organic Geochemistry 27:213-250

Michel, H., Levent, D., Barci, V., *et al*., (2008). Soil and sediment sample analysis for the sequential determination of natural and anthropogenic radionuclides. Talanta 74:1527-1533

Middelburg, J.J., Meysman, F.J.R., (2007). Burial at Sea. Science 316:1294-1295

Mihai, S.A., Hurtgen, Ch., Georgescu II, (1999). Radioactive accumulation in alga samples from Romanian Black Sea coast. Journal of Radioanalytical and Nuclear Chemistry 242:419-422

Milligan, T.G., Kranck, K., (1991). Electroresistance particle size. In: Principles, methods, and application of particle size analysis. Syvitski, J.P.M (Ed.), Cambridge University Press, 368pp.

Mil-Homens, M., Stevens, R., Abrantes, F., *et al*., (2003). Nornalization to aluminium for the assessment of heavy metal contamination in Portuguese Shelf surface sediments. Geophysical Research Abstracts 5:122241

Millard, A.R., (2006). Bayesian analysis of Pleistocene chronometric methods. Archaeometry 48:359-375

Mobius, S., Ramamonjisoa, T.-L., Jongisook, W., *et al*., (1995). Ion chromatography and liquid scintillation counting coupled to determine α- and β- emitters. The Science of the Total Environment 173/174:231-235

Moers, M.E.C., de Leeuw, J.W., Baas, M., (1994). Origin and diagenesis of carbohydrates in ancient sediments. Organic Geochemistry 21:1093-1106

Mohammady, N.G., (2004). Total, free and conjugated sterolic forms in three microalgae used in mariculture. Verlag der Zeitschrift für Naturforschung 59c:619-624

Monteys, X., Hardy, D., Doyle, E., *et al*., (2008a). Distribution, morphology and acoustic characterisation of a gas pockmark field on the Malin Shelf, NW Ireland. Symposium OSP-01, 33rd International Geological Congress, Oslo.

Monteys, X., Garcia, X., Szpak, M., *et al*., (2008b). Multidisciplinary approach to the study and environmental implications of two large pockmarks on the Malin Shelf, Ireland. "9th International Conference on Gas in Marine Sediments", Bremen, Germany, ICSG 2008 Abstract Volume pp. 42-43

Monteys, X., Garcia, X., Evans, R., *et al*., (2009). Geohazard Seabed Mapping in the Malin Shelf, NW Ireland. Scientific Report, GSI/PIP – IS05/16. Geological Survey of Ireland 2009

Monteys, X., Bloomer, S., Chapman, R., (2010). Multi-frequency acoustic seabed characterization in shallow gas bearing sediments in Dunmanus Bay, SW Ireland. Geophysical Research Abstracts 12, EGU2010-10707-2, European Geophysical Union General Assembly, Vienna

Moon, D.-S., Hong, G.-H., Kim, Y.I., *et al*., (2003). Accumulation of anthropogenic and natural radionuclides in bottom sediments of the Northwest Pacific Ocean. Deep-Sea Research II 50:2649-2673

Moore, T.S., Murray, R.W., Kurtz, A.C., *et al*., (2004). Anaerobic methane oxidation and the formation of dolomite. Earth and Planetary Science Letters 229:141-154

Mopper, K., (1973). Aspects of the biogeochemistry of carbohydrates in aquatic environments. PhD thesis, 221pp., Massachusetts Institute of Technology and Woods Hole Oceanographic Institution, USA

Moran, M.A., Rutherford, L.T., Hodson, R.E., (1995). Evidence for indigenous Streptomyces populations in a marine environment determined with a 16S rRNA probe. Applied and Environmental Microbiology 61:3695-3700

Moreda-Pineiro, A., Bermejo-Barrera, A., Bermejo, Barrera, P., (2004). New trends involving the use of ultrasonic energy for the extraction of humic substances from marine sediment. Analytical Chimica Acta 524:97-107

Moriarty, D.J.W., (1977). Improved method using muramic acid to estimate biomass of bacteria in sediments. Oecoologia 26:317-323

Moriarty, D., Hayward, A.C., (1982). Ultrastructure of bacteria and the proportion of Gram-negative bacteria in marine sediments. Microbial Ecology 8:1-14

Morse, J.W., (1999). Sulfides in sandy sediments: new insights on the reactions responsible for sedimentary pyrite formation. Aquatic Geochemistry 5:75-85

Morse, J.W., Mackenzie, F.T., (1990). Geochemistry of Sedimentary Carbonates, Elsevier.

Morvan, J., le Cadre, V., Jorissen, F., *et al*., (2004). Foraminifera as potential bio-indicators of the "Erika" oil spill in the Bay of Bourgneuf: field and experimental studies. Aquatic Living Resources 17:317-322

Mudge, S.M., Norris, C.E., (1997). Lipid biomarkers in the Conwy Estuary (North Wales, UK): a comparison between fatty alcohols and sterols. Marine Chemistry 57:61-84

Muller, P.J., Suess, E., (1979). Productivity, sedimentation rate and sedimentary organic matter in the oceans – organic carbon preservation. Deep-Sea Research 27A:1347-1362

Munoz, O., Volten, H., Hovenier, J.W., *et al*., (2006). Experimental and computational study of light scattering by irregular particles with extreme refractive indices: hematite and rutile. Astronomy & Astrophysics 446:525-535

Murphy, R.C., Fiedler, J., Hevko, J., (2001). Analysis of nonvolatile lipids by mass spectrometry. Chemical Review 101:479-526

Murray, J.W., (2006). Ecology and Applications of Benthic Foraminifera. Cambridge University Press, New York, 426pp.

Murray, J., Rohling, E.J., - Sampling planktonic foraminifera – not published protocol; www.noc.soton.ac.uk/soes/teaching/courses/oa432_624/basics.pdf

Myasoedov, B.F., Pavlotskaya, F.I., (1989). Measurement of radioactive nuclides in the environment. Analyst 114:225-263

NAS (1971). Radioactivity in the Environment. National Academy of Science, Washington DC

Naylor, D., (1975). Upper Devonian-Lower Carboniferous stratigraphy along the south coast of Dunmanus Bay, Co. Cork. Proceedings of the Royal Irish Academy 75:317-337

Naylor, D., Sevastopulo, G.D., (1993). The Reenydonagan Formation (Dinantian) of the Bantry and Dunmanus Synclines, County Cork. Irish Journal of Earth Sciences 12:191-203

Nederbragt, A.J., Dunbar, R.B., Osborn, A.T., *et al*., (2006). Digital sediment colour analysis as a method to obtain high resolution climate proxy records. In: Image Analysis, Sediments, Paleoenvironments. Developments in Paleoenvironmental Research 7:105-124, Francus, P., (Ed), Kluwer, Dordrecht

Nelson, H., Thor, D.R., Sandstrom, M.W., *et al*., (1979). Modern biogenic gas-generated craters (sea-floor "pockmarks") on the Bering Shelf, Alaska. Geological Society of America Bulletin 90:1144-1152

Newman, K.R., Cormier, M.-H., Weissel, J.K., *et al*., (2008). Active methane venting observed at giant pockmarks along the U.S. mid-Atlantic shelf break. Earth and Planetary Science Letters 267:341-352

Nguyen, R.T., Harvey, H.R., (1998). Protein preservation during early diagenesis in marine waters and sediments. In: Nitrogen-Containing Macromolecules in the Bio- and Geosphere, 88-112, Stankiewicz, B., van Bergen, P.F., (Eds). American Chemical Society Symposium Series, Vol. 707

Nguyen, R.T., Harvey, H.R., (2001). Preservation of protein in marine systems: Hydrophobic and other associations as major stabilizing forces. Geochimica et Cosmochimica Acta 65:1467-1480

Nichols, R.J., Sparks, R.S.J., Wilson, C.J.N., (1994). Experimental studies of the fluidization of layered sediments and the formation of fluid escape structures. Sedimentology 41:233-253

Niewohner, C., Hensen, C., Kasten, S., *et al.*, (1998). Deep sulfate reduction completely mediated by anaerobic methane oxidation in sediments of the upwelling area off Namibia. Geochimica et Cosmochimica Acta 64:455-464

NIRAS (2007). L070424 analytical report. AMEC NNC Limited, Cheshire, UK

Nishimura, M., (1982). 5β-isomers of stanols and stanones as potential markers of sedimentary organic quality and depositional paleoenvironments. Geochimica et Cosmochimica Acta 46:423-432

Nip, M., Tagelaar, E.W., de Leeuw, J.W., *et al*., (1986). A new non-saponifiable highly aliphatic and resistant biopolymer in plant cuticules: evidence from pyrolysis and ^{13}C NMR analysis of present day and fossil plants. Naturwissenschaften 73:579-585

Noureddine, A., Baggoura, B., Hocini, N., *et al*., (1998). Uptake of radioactivity by marine surface sediments collected in Ghazaouet, west coast of Algeria. Applied Radiation and Isotopes 49:1745-1748

Nowack, B., Gunter Kari, F., Hilger, S.U., *et al*., (1996). Determination of Dissolved and Adsorbed EDTA Species in Water and Sediments by HPLC. Analytical Chemistry 68:561-566

Noda, M., Tanaka, M., Seto, Y., *et al*., (1998). Occurrence of cholesterol as a major sterol component in leaf surface lipids. Lipids 23:439-444

Oades, J.M., Vasallo, A.M., Waters, A.G., et al., (1987). Characterization of organic matter in particle size and density fractions from a red-brown earth by a solid-state ^{13}C NMR. Australian Journal of Soil Research 25:81-82

O'Connor, B., Szpak, M.T., Kelleher, B., *et al*., (2009) Pockmark ground-truthing survey in Dunmanus Bay, Co. Cork. Scientific Report, INFOMAR, MI, Ireland

Olley, J.M., De Deckker, P., Roberts, R.G., *et al*., (2004). Optical dating of deep-sea sediments using single grains of quartz: a comparison with radiocarbon. Sedimentary Geology 169:175-189

Olsson, I.U., (1970). The use of Oxalic acid as a Standard. In Olsson IU ed. Radiocarbon Variations and Absolute Chronology, Nobel Symposium, 12th Proceeding, John Wiley & Sons, New York

Orange, D.L., Yun, J., Maher, N., *et al.*, (1999). Widespread fluid expulsion on a translational continental margin: mud volcanoes, fault zones, headless canyons, and organic-rich substrate in Monterey Bay, California. Bulletin, Geological Society of America: 111:992-1009

Orange, D.L., Yun, J., Maher, N., *et al*., (2002). Tracking California seafloor seeps with bathymetry, backscatter and ROVs. Continental Shelf Research 22:2273-2290

O'Reilly, S., Szpak, M., Monteys, X., *et al*., (2011). Characterising microbial diversity and organic matter cycling in marine seabed gas seepage structures by coupling molecular biological techniques with hyphenated chemical techniques. Oral presentation, CASi – 6th Conference on Analytical Sciences in Ireland. February 21-22, Dublin, Ireland

OSPAR (2000). Quality Status Report. OSPAR Commission, London, UK

OSPAR III (2000). Quality Status Report. Region III - Celtic Seas. OSPAR Commission, London, UK

OSPAR (2011). Discharges of radioactive substances from non-nuclear sectors in 2009. OSPAR Commission Report, London UK

Orr, J.C., Fabry, V.J., Aumont, O., *et al.*, (2005). Anthropogenic ocean acidification over the twenty-first century and its impact on calcifying organisms. Nature 437: 681-686

Otto, A., Shunthirasingham, C., Simpson, M.J., (2005). A comparison of plant and microbial biomarkers in grassland soils from the Prairie Ecozone of Canada. Organic Geochemistry 36:425-448.

O'Tuama, P., O'Rourke, P., (2010). Ballydehob Forest (CK21) Forest Management Plan, Coillte, Cork.

Ourisson, G., Albrecht, P., (1992). Hopanoids. 1. Geohopanoids: the most abundant natural products on earth? Accounts of Chemical Research 25:398-402

Ourisson, G., Rohmer, M., (1992). Hopanoids. 2. Biohopanoids: A novel class of bacterial lipids. Accounts of Chemical Research 25:403-408

Owens, N.J.P., Law, C.S., Mantoura, R.F.C., *et al*., (1991). Methane flux to the atmosphere from the Arabian Sea. Nature 353:293-296

Oyo-Ita, O., Ekpo, B.O., Oros, D.R., *et al*., (2010). Distributions and sources of aliphatic hydrocarbons and ketones in surface sediments from the Cross river estuary, SE Niger delta, Nigeria. Journal of Applied Sciences in Environmental Sanitation 5:1-11

Pake, G.E., Estle, T.L., (1973). The Physical Principles of Electron Paramagnetic Resonance, 2nd edition, Chapter 2, Benjamin, W.A., (Ed), Reading, MA, 306pp.

Parkes, R.J., (1999). Oiling the wheels of controversy. A review of *The Deep Hot Biosphere*, by Thomas Gold. Nature 401:644

Parnell, J., (1992). Burial histories and hydrocarbon source rocks on the North West Seaboard, In: Parnell, J., (Ed), Geochemistry and source rock potential of the west of Shetlands, Geological Society Special Publications 62, 3-16

Parnell, J., Monson, B., Geng, A., (1996). Maturity and petrography of bitumens in the Carboniferous of Ireland. International Journal of Coal Geology 29:23-38

Parnell, J., Bowden, S., Andrews, J.T., *et al*., (2007). Biomarker determination as a provenance tool for detrital carbonate events (Heinrich events?): Fingerprinting Quaternary glacial sources into Baffin Bay. Earth and Planetary Science Letters 257:71-82

Paoletti, C., Pushparaj, B., Florenzano, G., *et al*., (1976). Unsaponifiable matter of green and blue-green algal lipids as a factor of biochemical differentiation of their biomasses. II. Terpenic alcohol and sterol fractions. Lipids 11:266–271

Parrish, R.R., Noble, S.R., (2003). Zircon U-Th-Pb geochronology by Isotope Dilution - Thermal Ionization Mass Spectrometry (ID-TIMS). Reviews in Mineralogy and Geochemistry 53:183-213

Patterson, G.W., Van Valkenburg, S.D., (1990). Sterols of Dictyocha fibula (Chryzophyceae) abd Olisthodiscus luteus (Raphidophyceae). Journal of Phycology 26:484-489

Paull, C.K., Hecker, B., Commeau, R., *et al*., (1984). Biological communities at Florida Escarpment resemble hydrothermal vent taxa. Science 226:965-967

Paull, C., Ussler, W., III, Maher, N., *et al*., (2002). Pockmarks of Big Sur, California. Marine Geology 181:323-335

Pawolleck, B., (1875). Substitutionsproducte der Citronensäure und ein Versuch zur Synthese der letzteren. Justus Liebig's Annalen der Chemie 178:150-170

Pedersen, T.F., Calvert, S.E., (1990). Anoxia vs productivity: What controls the formation of organic-carbon-rich sediments and sedimentary rocks? Bulletin of the American Association of Petroleum Geologists 74:454-466

Peeters, F., Ivanova, E., Conan, S., *et al*., (1999). A size analysis of planktic foraminifera from the Arabian Sea. Marine Micropaleontology 36:31-63

Pernet, F., Tremblay, R., (2003). Effect of ultrasonication and grinding on the determination of lipid class content of microalgae harvested on filters. Lipids 38:1191-1195

Perry, G.J., Volkman, J.K., Johns, R.B., (1979). Fatty acids of bacterial origin in contemporary marine sediments. Geochimica et Cosmochimica Acta 43:1715-1725

Peters, K.E., Walters, C.C., Moldowan, J.M., (2005). The Biomarker Guide. Volume 1: Biomarkers and Isotopes in the Environment and Human History, 2nd Edition. Cambridge University Press, United Kingdom, 490pp.

Peters, V., Conrad, R., (1995). Methanogenic and other strictly anaerobic bacteria in desert soil and other oxic soils. Applied and Environmental Microbiology 61:1673-1676

Peterson, B.J., Fry, B., (1987). Stable Isotopes in Ecosystem Studies. Annual Review of Ecology and Systematics 18:293-320

Peterson, B.J., Howarth, R.W., (1987). Sulfur, carbon, and nitrogen isotopes used to trace organic matter flow in the salt-marsh estuaries of Sapelo Island, Georgia. Limnology and Oceanography 32:1195-1213

Philip, R.P., Calvin, M., (1976). Possible origin for insoluble organic (kerogen) debris in sediments from insoluble cell-wall materials of algae and bacteria. Nature 262:134-136

Pielou, E.C. (1977). Mathematical ecology. Wiley, New York, 385pp.

Pierre, C., Fouquet, Y., (2007). Authigenic carbonates from methane seeps of the Congo deep-sea fan. Geo-Marine Letters 27:249-257

Pilcher, R., Argent, J., (2007). Mega-pockmarks and linear pockmark trains on the West African continental margin. Marine Geology 244:15-32

Pimenov, N.V., Ul'yanova, M.O., Kanapatskii, T.A., *et al*., (2008). Microbiological and biogeochemical processes in a pockmark of the Gdansk depression, Baltic Sea. Microbiology 77:579-586

Plastino, W., Kaihola, L., Bartolomei, P., Bella, F., (2001). Cosmic background reduction in the radiocarbon measurement by scintillation spectrometry at the underground laboratory of Gran Sasso. Radiocarbon 43:157-161

Pointecorvo, B., (1941). Neutron well-logging. Oil and gas Journal 40:32-33

Ponce-Velez, G., Botello, A.V., Diaz-Gonzalez, G., (2006). Organic and inorganic pollutants in marine sediments from northern and southern continental shelf of the Gulf of Mexico. International Journal of Environment and Pollution 26:295-311

Poralla, K., Mutha, G., Hartnera, T., (2006). Hopanoids are formed during transition from substrate to aerial hyphene in Streptomyces coelicolor A3(2). FEMS Microbiology Letters 189:93-95

Premadas, A., Srivastava, P.K., (1999). Rapid laser fluorometric method for the determination of uranium in soil, ultrabasic rock, plant ash, coal fly and red mud samples. Journal of Radioanalytical and Nuclear Chemistry 242:23-27

Prescott, J.R., Robertson, G.B., (1997). Sediment dating by luminescence: A review. Radiation Measurements 27:893-922

Prince, P.K., (1990). Current drilling practice and the occurrence of shallow gas. Safety in Offshore Drilling: the Role of Shallow Gas Surveys. Dordrecht, Kluwer Academic Publishers, 3-25

Prior, D.B., Hooper, J.R., (1999). Sea floor engineering geomorphology: recent achievements and future directions. Geomorphology 31:411-439

Prohic, E., Miko, S., Peh, Z., (1995). Normalization and trace element contamination of soils in a Karstic Polje - an example from the Sinjsko Polje, Croatia. Geologia Croatica 48:67-86

Pryor, T.A., (1995). New described super-nodule resource. Sea Technology, September, 15-18

Pusceddu, A., Dell'Anno, A., Danovaro, R., *et al*., (2003). Enzymatically hydrolysable protein and carbohydrate sedimentary pools as indicators of the trophic state of detritus sink systems: A case study in the Mediterranean coastal lagoon. Estuaries 26:641-650

Pye, K., Blott, S.J., (2004). Particle size analysis of sediments, soils and related particulate materials for forensic purposes using laser granulometry. Forensic Science International 144:19-27

Pye, K., Blott, S.J., Croft, D.J., *et al*., (2005). Forensic comparison of soil samples: Assessment of small-scale spatial variability in elemental composition, carbon and nitrogen isotope ratios, colour, and particle size distribution. Forensic Science International 163:59-80

Pye, K., Blott, S.J., Croft, D.J., *et al*., (2006). Discrimination between sediment and soil samples for forensic purposes using elemental data: An investigation of particle size effects. Forensic Science International 167:30-42

Quenea, K., Derenne, S., Largeau, C., *et al*., (2004). Variation in lipid relative abundance and composition among different particle size fractions of a forest soil. Organic Geochemistry 35:1355-1370

Querellou, J., (2003). Biotechnology of marine extremophiles. Book of Abstracts, International Conference on the sustainable development of the Mediterranean and Black Sea environment. Thessaloniki, Greece, 28 May – 1 June, extended abstract

Quin, J.G., (2008). The evolution of thick shallow marine succession, the South Munster Basin, Ireland. Sedimentology 55:1053-1082

Qu, W., Dickman, M., Wang, S., *et al*., (1999). Evidence for an aquatic plant origin of ketones found in Taihu Lake sediments. Hydrobiologia 397:149-154

Raine, R., O'Mahony, J., McMahon, T., *et al*., (1990). Hydrography and phytoplankton of waters off south-west Ireland. Estuarine, Coastal and Shelf Science 30:579-592

Rampen, S.W., Abbas, B.A., Schouten, S., *et al*., (2010). A comprehensive study of sterols in marine diatoms (Bacillariophyta): Implications for their use as tracers for diatom productivity. Limnology Oceanography 55:91-105

Rausa, R., Mascolo, G., Bassetti, A., (1999). Thermal treatment of sediments as a function of temperature and reacting atmosphere. Journal of Analytical and Applied Pyrolysis 52:115-135

Raven, J.A., Falkowski, P.G., (1999). Oceanic sinks for atmospheric CO_2 Plant, Cell and Environment 22:741-755

Rawle, A., (1996). Particle sizing in the paint industry. European Coatings Journal 4:195-198

Raz, S., Testeniere, O., Hecker, A., *et al*., (2002). Stable amorphous calcium carbonate is the main component of the calcium storage structures of the Crustacean *Orchestia cavimana* Biology Bulletin 203:269-274

Redfield, A.C., (1934). On the proportions of organic derivations in sea water and their relation to the composition of plankton. In: James Johnstone Memorial Volume, 177-192, Daniel, R.J., (Ed), University of Liverpool

Redfield, A.C., (1958). The biological control of chemical factors in the environment. American Scientist

Redfield, A.C., Ketchum, B.H., Richards, F.W., (1963). The influence of organisms on the composition of sea water. In: The sea, 2, 26-77, Hill, M.N., (Ed), Wiley Interscience, New York

Reinhart, D., (2007). Long-term treatment and disposal of landfill leachate. Report 0532022-07, Florida Center for Solid and Hazardous Waste Management, USA

Rein, van H., Brown, C.J., Quinn, R., *et al*., (2011). An evaluation of acoustic seabed classification techniques for marine biotope monitoring over a broad-scales (>1 km^2) and meso-scales (10 m^2-1 km^2). Estuarine, Coastal and Shelf Science 93:336-349

Repeta, D.J., Quan, T.M., Aluwihare, L.I., *et al.*, (2002). Chemical characterization of high molecular weight dissolved organic matter in fresh and marine waters. Geochimica et Cosmochimica Acta 66:955-962

Ricci, M.P., Merritt, D.A., Freeman, K.H., *et al*., (1994). Acquisition and processing of data for isotope-ratio-monitoring mass-spectroscopy. Organic Geochemistry 21:561-571

Richter, B.E., Jones, B.A., Ezzell, J.L., *et al*., (1996). Accelerated solvent extraction: A technique for sample preparation. Analytical Chemistry 68:1033-1039

Richter, T.O., Van der Gaast, S., Koster, B., *et al*., (2006). The Avaatech XRF Core Scanner: technical description and application to NE Atlantic sediments. In: New Techniques in

Sediment Core Analysis, Geological Society Special Publications 267:40-50, Rothwell, R.G. (Eds), London

Robinson, S.G., (1993). Lithostratigraphic applications for magnetic susceptibility logging of deep-sea sediment cores: examples from ODP Leg 115. In: High Resolution Stratigraphy, Hailwood, E.A., Kidd, R.B., (Eds), Geological Society Special Publications 70:65-98, London

Robl, T.L., Davis, B.H., (1993). Comparison of HF-HCl and HF-BF_3 maceration techniques and the chemistry of a resultant organic concentrates. Organic Geochemistry 20:249-255

Roden, C.M., Ryan, T., Lennon, H.J., (1980). Observations of the 1978 red tide in Roaringwater Bay, Co. Cork. Journal of Sherkin Island 1:105-118

Roden, C.M., Lennon, H.J. Mooney, E., *et al*., (1981). Red tides, water stratification and species succession around Sherkin Islands, S.W. Ireland. Journal of Sherkin Island 1:50-68

Roden, J., (2008). Cross-dating of tree ring $\delta^{18}O$ and $\delta^{13}C$ time series. Chemical Geology 252:72-79

Rogerson, M. Weaver, P.P.E., Rohling, E.J., *et al*., (2006). Colour logging as a tool in high-resolution palaeoceanography. In: New Techniques in Sediment Core Analysis, Geological Society Special Publications 267:99-112, Rothwell, R.G. (Eds), London

Rohmer, M., Bouvier-Nave, P., Ourisson, G., (1984). Distribution of hopanoid triterprenes in Prokaryotes. Journal of General Microbiology 130:1137-1150

Rohmer, M., (2008). From molecular fossil of bacterial hopanoids to the formation of isoprene units: discovery and elucidation of the methylerythritol phosphate pathway. Lipids 43:1095-1107

Rommerskirchen, F., Eglinton, G., Dupont, L., *et al*., (2004). A north to south transect of Holocene Southeast Atlantic continental margin sediments: Relationship between aerosol transport and compound-specific $\delta^{13}C$ land plant biomarker and pollen records. Geochemistry Geophysics Geosystems 4:1101-1130

Rontani, J-F., Grossi, V., (1995). Abiotic degradation of the intact and photooxidized chlorophyll phytyl chain under simulated geological conditions. Organic Geochemistry 23:355-366

Rontani, J-F., Bonin, P.C., Volkman, J.K., (1999). Biodegradation of free phytol by bacterial communities isolated from marine sediments under aerobic and anaerobic and denitrifying conditions. Applied and Environmental Microbiology 65:5485-5492

Rontani, J-F., Nassiry, M., Mouzdahir, A., (2007). Free radical oxidation (autoxidation) of α-tocopherol (vitamin E): A potential source of 4,8,12,16-tetramethylheptadecan-2-olide in the environment. Organic Geochemistry 38:37-47

Rothwell, R.G., Rack, F.R. (2006). New technique in sediment core analysis: an introduction. In: New Techniques in Sediment Core Analysis, Geological Society Special Publications 267:1-29, Rothwell, R.G. (Eds), London

Rothwell, R.G., Hoogakker, B., Thomson, J., *et al*., (2006). Turbidite emplacement on the southern Balearic Abyssal Plain (western Mediterranean Sea) during Marine Isotope Stages 1-3: an application of ITRAX XRF scanning of sediment cores to lithostratigraphic analysis. In: Rothwell, R.G., (Ed). New Techniques in Sediment Core Analysis. Geological Society of London Special Publications 267:79-98

Różański, K., Stichler, W., Gonfiantini, R., *et al*., (1992). The IAEA ^{14}C intercomparison exercise 1990. Radiocarbon 34:506-519

Rudneva, I., (2003). Impact of the metallurgical industry on the coastal ecosystems of Black Sea countries. NATO Science Series, IV: Earth and Environmental Sciences 20:27-33

Rullkotter, J., Michaelis, W., (1990). The structure of kerogen and related materials. A review of recent progress and future trends. Organic Geochemistry 16:829-852

Rumpel, C., Kogel-Knabner, I., Bruhn, F., (2002). Vertical distribution, age, and chemical composition of organic carbon in two forest soils of different pedogenesis. Organic Geochemistry 33:1131-1142

Rumpel, C., Rabia, N., Derenne, S., *et al*., (2006). Alteration of soil organic matter following treatment with hydrofluoric acid (HF). Organic Geochemistry 37:1437-1451

Ruttenberg, K.C., Berner, R.A., (1993). Authigenic apatite formation and burial in sediments from non-upwelling, continental margin environments. Geochimica et Cosmochimica Acta 57:991-1007

Ryskin, G., (2003). Methane-driven oceanic eruptions and mass extinctions. Geology 31:741-744

Saito, H., Suzuki, N., (2007). Distributions and sources of hopanes, hopanoic acids and hopanols in Miocene to recent sediments from ODP Leg 190, Nankai Trough. Organic Geochemistry 38:1715-1728

Salisova, M., Toma, S., Mason, T.J., (1997). Comparison of conventional and ultrasonically assisted extractions of pharmaceutically active compounds from *Salvia officinalis*. Ultrasonics Sonochemistry 4:131-134

Sandler, A., Harlavan, Y., Steinitz, G., (2004). Early formation of K-feldspar in shallow-marine sediments at near-surface temperatures (southern Israel): evidence from K-Ar dating. Sedimentology 51:323-338

Sannigrahi, P., (2005). Composition and cycling of natural organic matter: insights from NMR spectroscopy. PhD thesis, 135pp. School of Earth and Atmospheric Sciences, Georgia Institute of Technology.

Sansone, F.J., Holmes, M.E., Popp, B.N., (1999). Methane stable isotopic ratios and concentrations as indicators of methane dynamics in estuaries. Global Biogeochemical Cycles 13:463-474

Sarma, V.V., Vittal, B.P.R., (2001). Biodiversity of manglicolous fungi on selected plants in the Godavari and Krishna deltas, east coast of India. Fungal Diversity 6:115-130

Sasaki, T., Waren, A., Kano, Y., *et al*., (2010). Gastropods from recent hot vents and cold seeps: systematics, diversity and life strategies. In: The Vent and Seep Biota, Kiel, S., (Ed), Topics in Geobiology 33

Saxby, J.D., (1970). Isolation of kerogen in sediments by chemical methods. Chemical Geology 6:173-184

Scancar, J., Milacic, R., Horvat, M,. (2000). Comparison of variuos digestion and extraction procedures in analysis of heavy metals in sediments. Water, Air and Soil Pollution 118:87-99

Schiebel, R., Bijma, J., Hemleben, C., (1997). Population dynamics of the planktic foraminifer Globigerina bulloides from the eastern North Atlantic. Deep-Sea Research I 40:1701-1713

Schmidt, F., Hinrichs, K.-U., Elvert, M., (2010). Sources, transport, and partitioning of organic matter at a highly dynamic continental margin. Marine Chemistry 118:37-55

Schnitzer, M., Ortiz de Serra, M.I., (1973). The chemical degradation of humic acid. Canadian Journal of Chemistry 51:1554-1566

Schoell, M., (1980). The hydrocarbon and carbon isotope composition of methane from natural gases of various origins. Geochimica et Cosmochimica Acta 44:649-662

Schonhofer, F., (1995). Liquid scintillation spectrometry in environmental measurements. The Science of the Total Environment 173/174:29-40

Schroot, B.M., (2003). Surface and subsurface expressions of shallow gas accumulations in the southern North Sea. Search and Discovery, article 40090

Schouten, S., Hopmans, E.C., Schefuß, E., *et al*., (2002). Distributional variations in marine crenarchaeotal lipids: A new tool for reconstructing ancient sea water temperatures? Earth and Planetary Science Letters 204:265-274

Schouten, S., Middelburg, J.J., Hopmans, E.C., *et al*., (2010). Fossilization and degradation of intact polar lipids in deep subsurface sediments: A theoretical approach. Geochimica et Cosmochimica Acta 74:3806-3814

Schubel, J.R., (1974). Gas bubbles and the acoustically impermeable or turbid character of some estuarine sediments. In: Natural gases in marine sediments, Kaplan, I.R., (Eds), Plenum Press, New York, 324pp.

Schulten, H.R., Gleixner, G., (1999). Analytical pyrolysis of humic substances and dissolved organic matter in aquatic systems: structure and origin. Water Research 33:2489-2498

Schultheiss, P.J., McPhail, S.D., (1989). An automated P-Wave logger for recording of fine-scale compressional wave velocity structures in sediments. In: Proceedings of the Ocean Drilling Program, Scientific Results, 108:407-413, Ruddiman, W., Sarnthein, M., et al., (Eds), Ocean Drilling Program, Texas

Schultheiss, P.J., Francis, T.J.G., Holland, M., *et al.*, (2006). Pressure coring, logging and subsampling with the HYACINTH system. In: New Techniques in Sediment Core Analysis, Geological Society Special Publications 267:152-163, Rothwell, R.G. (Eds), London

Schulz, H.D., Dahmke, A., Schinzel, U., *et al*., (1994). Early diagenetic processes, fluxes, and reaction rates in sediments of the South Atlantic, Geochimica et Cosmochimca Acta 58:2041-2060

Schulz, H.D., Zabel, M., 2006. Marine Geochemistry. 2nd edition. Springer, Berlin, Heidelberg, 574pp.

Schumm, S.A., (1970). Experimental studies on the formation of lunar surface features by fluidization. Geological Society of America (Bulletin) 81:2539-2552

Schupfer, P., Finck, Y., Houot, F., *et al*., (2007). Acid catalysed backbone rearrangement of cholesta-2,4,6-triene: On the origin of ring A and ring B aromatic steroids in recent sediments. Organic Geochemistry 38:671-681

Schwarzschild, B., (2001). Isotopic analysis of Pristine microshells resolves a troubling paradox of paleoclimatology. Physics Today 54:16-18

Seifert, W.K., Moldowan, J.M., Gallegos, E.J., (1986). Application of mass spectrometry to petroleum exploration, p121-139. In: Mass spectrometric characterization of shale oils, Aczel, t., (Ed), ASTM Special Technical Publications 902, Philadelphia, USA, 153pp.

Selley, R.C., (1992). Petroleum seepages and impregnations in Great Britain. Marine and Petroleum Geology 9:226-244

Senesi, N., Loffredo, E., (2005). Soil Humic Substances. Biopolymers Online

Sessions, A.L., Burgoyne, T.W., Schimmelmann, A., *et al*., (1999). Fractionation of hydrogen isotopes in lipid biosynthesis. Organic Geochemistry 30:1193-1200

Sessions, A.L., (2006). Isotope-ratio detection for gas chromatography. Journal of Separation Science 29:1946-1961

Shaw, M.J., Hill, S.J., Jones, P., *et al*., (2000). Determination of uranium in environmental matrices by chelation ion chromatography using a high performance substrate dynamically modified with 2,6-pyridinedicarboxylic acid. Chromatographia 51:695-700

Shen, J., Shao, X., (2005). A comparison of accelerated solvent extraction, Soxhlet extraction, and ultrasonic-assisted extraction for analysis of terpenoids and sterols in tobacco. Analytical and Bioanalytical Chemistry 383:1003-1008

Shi, W., Sun, M-Y., Molina, M., *et al*., (2001). Variability in the distribution of lipid biomarkers and their molecular isotopic composition in Altamaha estuarine sediments: implications for the relative contribution of organic matter from various sources. Organic Geochemistry 32:453-467

Showstack, R., (2000). Harnessing methane. EOS – Transactions of the American Geophysical Union 81:222

Sillanpaa, M., Ramo, J., (2001). Adsorption of metal-ethylenediaminetetraacetic acid chelates onto lake sediment. Chemosphere 45:881-885

Simoneit, B.R.T., Chester, R., and Eglinton, G., (1977). Biogenic lipids in particulates from the lower atmosphere over the eastern Atlantic. Nature 267:682–685.

Simoneit, B.R.T., Elias, V.O., Cardoso, J.N., (1997). Even n-alkane predominances on the Amazon Shelf and a Northern Pacific hydrothermal system. Naturwissenschaften 84:415-420

Simoneit, B.R.T., (2004). A review of current applications of mass spectrometry for biomarker/molecular tracer elucidations. Mass Spectrometry Reviews 24:719-765

Simpson, A.J., (2001). Multidimensional solution state NMR of humic substances: A practical guide and review. Soil Science 166:795-809

Simpson, A.J., Kingery, W.L., Hatcher, P.G., (2003a). The identification of plant derived structures in humic materials using three dimensional NMR spectroscopy. Environmental Science and Technology 37:337

Simpson, A.J., Kingery, W.L., Williams, A., *et al*., (2003b). Identifying residues of Natural Organic Matter through spectral prediction and pattern matching of 2-D NMR datasets. Magnetic Research in Chemistry 42:14-22

Simpson, A.J., Brown, S. A., (2005). PURGE NMR : Effective and easy solvent suppression. Journal of Magnetic Resonance 175:340–346.

Simpson, A.J., Simpson, M.J., Kingery, W.L., *et al*., (2006). The application of ^{1}H High-Resolution Magic-Angle Spinning NMR for the study of Clay-Organic associations in natural and synthetic complexes. Langmuir 22:4498-4503

Simpson, A.J., Simpson, M.J., Smith, E., *et al*., (2007a). Microbially derived inputs to soil organic matter: Are current estimates too low. Environmental Science and Technology 41:8070-8076

Simpson, A.J., Song, G.X., Smith, E., et al., (2007b). Unravelling the structural components of soil humin by use of solution-state nuclear magnetic resonance spectroscopy. Environmental Science and Technology 41:876-883

Simpson, A.J., McNally, D., Simpson, M.J., (2010). NMR Spectroscopy in Environmental Science: From molecular-level interactions to global processes. Invited by Progress in Nuclear Magnetic Resonance Spectroscopy, published online 24th Sept 2010 - Doi:10.1016/j.pnmrs.2010.09.001

Singh, A.P., Butcher, J.A., (1991). Bacterial degradation of wood cell walls: a review of degradation patterns. Journal of the Institute of Wood Science 12:143-157

Sinninghe Damste, J.S., Van Duin, A.C.T., Hollander, D., *et al*., (1995). Early diagenesis of bacteriohopanepolyoln derivatives: Formation of fossil homohopanoids. Geochimica et Cosmochimica Acta 59:5141-5157

Sinninghe Damste, J.S., Rampen, S., Rijpstra, W.I.C., *et al*., (2003). A diatomaceous origin for long-chain diols and mid-chain hydroxy methyl alkanoates widely occurring in quaternary marine sediments: indicators for high-nutrient conditions. Geochimica et Cosmochimica Acta 67:1339-1348

Sjogersten, S., Turner, B.L., Mahieu, N., (2003). Soil organic matter biochemistry and potential susceptibility to climate change across the forest-tundra ecotone in the Fennoscandian mountains. Global Change Biology 9:759-772

Skerrat, J.H., Nichols, P.D., Bowman, J.P., et al., (1992). Occurrence and significance of long-chain (ω-1)-hydroxy fatty acids in methane-utilizing bacteria. Organic Geochemistry 18:189-194

Skjemstad, J.O., Clarke, P., Taylor, J.A., *et al*., (1994). The removal of magnetic materials from surface soils. A solid state ^{13}C CP/MAS NMR study. Australian Journal of Soil Research 32:1215-1229

Sloan, E.D., (1998). Clathrate Hydrates of Natural Gas, 2nd edition. New York, NY, Marcel Dekker

Smith, L.L., (1981). Cholesterol autoxidation. Plenum Press, New York, 681pp.

Smith, J.N., (2001). Why should we believe ^{210}Pb sediment geochronologies? Journal of Environmental Radioactivity 55:121-123

Snoecks, H., Rea, D.K., (1994). Late Quaternary $CaCO_3$ stratigraphy of the eastern equatorial Pacific. Paleoceanography 9:341-353

Somayajulu, B.L.K., Radhakrishnamurty, C., Walsh, T.J., (1978). Susceptibility as a tool for studying magnetic stratigraphy of marine sediments. Journal of Earth System Science 87:201-213

Somerfield, P. J., Clarke, K. R., (1997). A comparison of some methods commonly used for the collection of sublittoral sediments and their associated fauna. Marine Environmental Research 43:145-156

Solheim, A., Elverhoi, A., (1993). Gas-related sea floor craters in the Barents Sea. Geo-Marine Letters 13:235-243

Soloviev, V.A., (2001). Gas-hydrate-prone areas of the ocean and gas hydrate accumulations. Journal of Conference Abstracts, 6, abstract/poster 158

Soloviev, V.A., (2002). Global estimation of gas content in submarine gas hydrate accumulations. Russian Geology and Geophysics 43:648-661

Southward, A.J., Southward, E.C., Dando, P.R., *et al*., (1981). Bacterial symbionts and low 13C/12C ratios in tissues of Pogonophora indicate unusual nutrition and metabolism. Nature 293:616-619

Sperazza, M., Moore, J.N., Hendrix, M.S., (2004). High-resolution particle size analysis of naturally occurring very fine-grained sediment through laser diffractometry. Journal of Sedimentary Research 74:736-743

Stankiewicz, B.A., Briggs, D.E.G., Evershed, R.P., (1997). Chemical composition of Paleozoic and Mesozoic fossil invertebrate cuticles as revealed by Pyrolysis-Gas Chromatography / Mass Spectrometry. Energy & Fuels 11:515-521

Stankiewicz, B.A., Briggs, D.E.G., Michels, R., *et al*., (2000). Alternative origin of aliphatic polymer in kerogen. Geology 28:559-562

Stein, R., (1986). Organic carbon and sedimentation rate – further evidence for anoxic deep-water conditions in the Cenomanian/Turonian Atlantic Ocean. Marine Geology 72:199-209

Stein, R., (1990). Organic carbon content/sedimentation rate relationship and its paleoenvironmental significance for marine sediments. Geo-Marine Letters 10:37-40

Stein, R., (1991). Accumulation of organic carbon in marine sediments. Lecture Notes in Earth Sciences 34:1-217

Stevens, N., Shrimpton, J., Palmer, M., *et al*., (2007). Accuracy assessments for laser diffraction measurements of pharmaceutical lactose. Measurement Science and Technology 18:3697-3706

Stevenson, F.J., (1994). Humus Chemistry. Genesis, Composition, Reactions. 2nd edition. John Wiley and Sons, New York, 512pp.

Stoker, M.S., (1981). Pockmark morphology: a preliminary description. Evidence for slumping and doming. Institute of Geological Sciences, Marine Geophysics Unit, Report 81/10

Straughan, D., (1982). Observations on the effects of natural oil seeps in the Coal Oil Point area. Philosophical Transactions of the Royal Society of London, B, 297:269-283

Sturt, H.F., Summons, R.E., Smith, K., *et al*., (2004). Intact polar membrane lipids in prokaryotes and sediments deciphered by high-performance liquid chromatography/electrospray ionization multistage mass spectroscopy – new biomarkers for biogeochemistry and microbial ecology. Rapid Communications in Mass Spectroscopy 18:617-628

Suess, E., Massoth, G.J., (1984). Evidence for venting of pore waters from subducted sediments of t he Oregon continental margin. EOS - Transactions of the American Geophysical Union, Abstract 65: 1089

Sun, M-Y., Wakeham, S.G., Aller, R.C., *et al.*, (1998). Impact of seasonal hypoxia on diagenesis of phytol and its derivatives in Long Island Sound. Marine Chemistry 62:157-173

Suzumura, M., (2005). Phospholipids in marine environments: a review. Talanta 66:422-434

Swain, F.M., Bratt, J.M., Kirkwood, S., (1970). Carbohydrates from Precambrian and Cambrian rocks and fossils. Geollogical Society of America Bulletin 81:499-504

Szpak, M., O'Connor, B., Kelleher, B., et al., (2009). Pockmarks ground-truthing survey in Dunmanus Bay, Co. Cork. INFOMAR Technical Report, project CV09_23, Marine Institute, Ireland, 139pp.

Szpak, M., Monteys, X., O'Reilly, *et al*., (2011). Geophysical and geochemical survey of a large marine pockmark on the Malin Shelf, Ireland. Geochemistry, Geophysics, Geosystems (in press), doi:10.1029/2011GC003787

Tagelaar, E.W., Hollman, G., van der Vegt, P., *et al*., (1995). Chemical characterization of the periderm tissue of some angiosperm species: recognition of an insoluble, non-hydrolyzable aliphatic biomacromolecule (Suberan). Organic Geochemistry 23:239-251

Tagelaar, E.M., de Leeuw, J.W., Derenne, S., *et al.*, (1989). A reappraisal of kerogen formation. Geochmica et Cosmochimica Acta 53:3103-3106

Takada, H., Satoh, F., Bothner, M.H., *et al*., (1997). Anthropogenic molecular markers: Tools to identify the sources and transport pathways of pollutants. In: Molecular Markers in Environmental Geochemistry, 178-195, Eganhouse, R.P., (Ed). American Chemical Society Symposium Series 671, Washington, 426pp.

Takahashi, T., Broecker, W.S., Langer, S., (1985). Redfield ratio based on chemical data from isopycnal surfaces. Journal of Geophysical Research 90:6907-6924

Talbot, H.M., Squier, A.H., Keely, B.J., et al., (2003). Atmospheric pressure chemical ionization reverse-phase liquid chromatography/ion trap mass spectrometry of intact bacteriohopanepolyols. Rapid Communications in Mass Spectrometry 17:728-737

Taniguchi, M., Burnett, W.C., Cable, J.E., *et al*., (2002). Investigation of submarine groundwater discharge. Hydrological Processes 16:2115-2129

Tappin, D.R., Watts, P., McMurtry, G.M., *et al*., (2001). The Sissano, Papua New Guinea tsunami of July 1998 – offshore evidence on the source mechanism. Marine Geology 175:1-23

Tauhata, L., Vianna, M.E.C.M., de Oliveira, A.E., *et al*., (2006). The Brazilian National Intercomparison Program (PNI/IRD/CNEN): evaluation of 15 yeras of data. Technical note. Journal of Environmental Radioactivity 86:384-390

Taylor, D.I., (1992). Nearshore shallow gas around the UK coast. Continental Shelf Research 12:1135-1144

Taylor, J.D., Glover, E.A., (2010). Chemosynthetic bivalves. In: The Vent and Seep Biota, Kiel, S., (Ed), Topics in Geobiology 33

Tegelaar, E.W., Derenne, S., Largeau, C., *et al*., (1989). A reappraisal of kerogen formation. Geochimica et Cosmochimica Acta 53:2001-2024

Teichert, B.M.A., Bohrmann, G., Suess, E., (2005). Chemoherms on Hydrate Ridge – Unique microbially-mediated carbonate build-ups growing into the water column. Palaeogeography, Palaeoclimatology, Palaeoecology 227:67-85

Ternois, Y., Kawamura, K., Keigwin, L., *et al*., (2001). A biomarker approach for assessing marine and terrigenous inputs to the sediments of Sea of Okhotsk for the last 27,000 years. Geochimica et Cosmochimica Acta 65:791-802

Thomson, J., Croudace, I.W., Rothwell, R.G., (2006). A geochemical application of the ITRAX scanner to a sediment core containing eastern Mediterranean sapropel units. In:. Rothwell, R.G., (Ed.). New Techniques in Sediment Core Analysis, Geological Society of London Special Publications 267:65-77

Tissot, B.P., Welte, D.H., (1984). Petroleum Formation and Occurrence. Springer-Verlag, Heidelberg, 699pp.

Torres, M.E., Linke, P., Trehu, A., *et al*., (1999). Gas hydrate dynamics at Hydrate Ridge, Cascadia. EOS – Transaction of the American Geophysical Union. 80, Abstract F527

Treibs, A., (1936). Chlorophyll- und Häminderivate in organischen Mineralstoffen. Angewandte Chemie 49:682-686

Treignier, C., Derenne, S., Saliot, A., (2006). Terrestrial and marine n-alcohol inputs and degradation processes relating to a sudden turbidity current in the Zaire canyon. Organic Geochemistry 37:1170-1184

Tribble, J., Mackenzie, F., Urmos, J., *et al*., (1992). American Association of Petroleum Geologists (AAPG) Bulletin 76:792-804

Trimm, D.L., Beiro, H.H., Parker, S.J., (1998). Comparison of digestion techniques in analyses for total metals in marine sediments. Bulletin of Environmental Contamination and Toxicology 60:425-432

Tritz, J.-P., Herrmann, D., Bisseret, P., *et al*., (1999). Abiotic and biological hopanoid transformation: towards the formation of molecular fossils of the hopane series. Organic Geochemistry 30:499-514

Tung, J.W.T., (2004). Determination of metal components in marine sediments using energy-dispersive X-ray fluorescence (ED-XRF) spectrometry. Annali di Chimica 94:837-846

UNSCEAR (2000). Scientific Annex J: Exposures and effects of the Chernobyl accident. In UNSCEAR 2000 Report, Sources and Effects of Ionizing Radiation, Vol. II Effects, United Nations Scientific Committee on the Effects of Atomic Radiation Report to the General Assembly

UNSCEAR (2000). Scientific Annex G: Biological effects at low radiation doses. In UNSCEAR 2000 Report, Sources and Effects of Ionizing Radiation, Vol. II Effects, United Nations Scientific Committee on the Effects of Atomic Radiation Report to the General Assembly

Uosif, M.A.M., (2007). Gamma-ray spectroscopic analysis of selected samples from Nile river sediments in upper Egypt. Radiation Protection Dosimetry 123:215-220

Upstill-Goddrad, R.C., Barnes, J., Frost, T., *et al.*, (2000). Methane in the southern North Sea: Low-salinity inputs, estuarine removal, and atmospheric flux. Global Biogeochemical Cycles 14:1205-1217

Urey, H.C., (1947). The thermodynamic properties of isotopic substances. Journal of Chemical Society 562:581

Urey, H.C., (1952) .The Planets, Their Origin and Development. Yale University Press, New Haven, CT

US EPA method 3050B (1996). Acid digestion of sediments, sludges, and soils. US Environmental Protection Agency

Vacelet, J.N., Boury-Esnault, N., Fiala-Medioni, A., *et al*., (1995). A methanotrophic carnivorous sponge. Nature 377:296

Vacelet, J.N., Fiala-Medioni, A., Fisher, C.R., *et al*., (1996). Symbiosis between methane-oxidizing bacteria and a deep-sea carnivorous cladorhizid sponge. MarineEcology Progress Series 145:77-85

Vandecasteele, B., De Vos, B., Tack, F.M.G., (2002). Identification of dredged sediment-derived soils in the alluvial plains of the Leie and the Upper and Sea Scheldt rivers (Belgium) based on physico-chemical soil properties. Journal of Environmental Monitoring 4:306-312

Van Dover, C.L., (2000). The Ecology of Deep-Sea Hydrothermal Vents. Princeton, NJ, University Press

Van Iperen, J., Helder, W., (1984). A method for determination of organic carbon in calcareous marine sediments. Marine Geology 64:179-187

Venter, C.J., Remington, K., Heidelberg, J.F., *et al.*, (2004). Environmental Genome Shotgun Sequencing of the Sargasso Sea. Science 304:66-74

Ver, L.M.B., Mackenzie, F.T., Lerman, A., (1999). Carbon cycle in the coastal zone: effects of global perturbations and change in the past three centuries. Chemical Geology 159:283-304

Vermeulen, N.J., Shannon, P.M., Masson, F., *et al*., (2000). Wide-angle seismic control on the development of the Munster Basin, SW Ireland. In: New Perspectives on the Old Red Sandstone, Friend, P.F. and William, B.P.J., (Eds), Geological Society, London, Special Publications 180:223-237

Versteegh, G.J.M., Bosch, H-J., de Leeuw, J.W., (1997). Potential palaeoenvironmental information of C24 to C36 mid-chain diols, keto-ols and mid-chain hydroxy fatty acids; a critical review. Organic Geochemistry 27:1-13

Versteegh, G.J.M., Jansen, J.H.F., de Leeuw, J.W., *et al*., (2000). Mid-chain diols and keto-ols in SE Atlantic sediments: A new tool for tracing past sea surface water masses? Geochimica et Cosmochimica Acta 64:1879-1892

Veto, I., Hetenyi, M., Demeny, A., *et al*., (1994). Hydrogen index as reflecting intensity of sulphide diagenesis in nonbioturbated, shaly sediments. Organic Geochemistry 22:299-310

Vianna, M.E., Tauhata, L., Oliviera, J.P., *et al*., (1995). Quality of radionuclied analysis in environmental samples. The Science of the Total Environment 173/174:15-18

Vicuna, R., Gonzalez, B., Seelenfreund, D., *et al*., (1993). Ability of natural bacterial isolates to metabolize high and low molecular weight lignin-derived molecules. Journal of Biotechnology 30:9-13

Vilks, G., Rashid, M.A., (1975). Foraminifera and organic geochemistry of two sedimentary cores from pockmarked basin of the Scotian Shelf. Report of Activities, Part C; Geological Survey of Canada; Paper 75-1C:5-8

Vintro, L.L., Smith, K.J., Lucey, J.A., *et al*., (2009). The environmental impact of the Sellafield discharges. http://homepage.eircom.net/~radphys/scope.pdf

Volkman, J.K., (1980). Microbial lipids of and intertidal sediments – I. Fatty acids and hydrocarbons. Geochimica et Cosmochimica Acta 44:1133-1143

Volkman, J.K., (1986). A review of sterol markers for marine and terrigenous organic matter. Organic Geochemistry 9:83-99

Volkman, J.K., Jeffrey, S.W., Nichols, P.D., *et al*., (1989). Fatty acids and lipid composition of 10 species of microalgae used in mariculture. Journal of Experimental Marine Biology and Ecology 128:219-240

Volkman, J.K., Barrett, S.M., Dunstan, G.A., *et al*., (1992). C30-C32 alkyl diols and unsaturated alcohols in microalgae of the class Eustigmatophyceae. Organic Geochemistry 18:131-138

Volkman, J.K., Barrett, S.M., Dunstan, G.A., *et al*., (1994). Geochemical significance of the occurrence of dinosterol and other 4-methyl sterols in a marine diatom. Organic Geochemistry 21:7-15

Volkman, J.K., Barrett, S.M., Blackburn, S.I., *et al*., (1998). Microalgal biomarkers: A review of recent research developments. Organic Geochemistry 29:1163-1179

Volkman, J.K., Barrett, S.M., Blackburn, S.I., (1999a). Fatty acids and hydroxy fatty acids in three species of freshwater Eustigmatophytes. Journal of Phycology 35:1005-1012

Volkman, J.K., Barrett, S.M., Blackburn, S.I., (1999b). Eustigmatophyte microalgae are potential sources of C29 sterols, C22-C28 n-alcohols and C28-C32 n-alkyl diols in freshwater environments. Organic Geochemistry 37:1170-1184

Volkman, J.K., (2003). Sterols in microoganisms. Applied Microbiology and Biotechnology 60:495-506

Volkman, J.K., (2006). Lipid markers for marine organic matter. In: Handbook of Environmental Chemistry Vol.2, Part N. Marine organic matter: biomarkers, isotopes and DNA, 27-70, Volkman, J.K. (Ed). Springer-Verlag, Berlin, Heidelberg, 379pp.

Vrieling, E.G., Hazelaar, S., Gieskes, W.W.C., *et al*., (2003). Silicon biomineralization: towards mimicking biogenic silica formation in diatoms. Progress in Molecular and Subcellular Biology 33:301-334

Waddams, P., Cordingley, T., (1999). The regional geology and exploration potential of the NE Rockall Basin. In: Petroleum Geology of Northern Europe. Fleet, A.J., Boldy, S.A.R., (Eds), The Geological Society, Bath, 724pp.

Wang, Q., Morse, J.W., (1995). Laboratory simulation of pyrite formation in anoxic sediments. In: Geochemical Transformations of Sedimentary Sulfur, Vairavamurthy, M.A. and Schoonen, M.A.A. (Eds), ACS Symposium Series 612:206-223

Wakeham, S.G., (1989). Reduction of stenols to stanols in particulate matter at oxic-anoxic boundaries in sea water. Nature 342:787-790

Walter, D.J., Lambert, D.N., Young, D.C., *et al*., (1997). Mapping sediment acoustic impedance using remote sensing acoustic techniques in a shallo-water carbonate environment. Geo-Marine Letters 17:260-267

Waters, W.A., (1971). The kinetics and mechanism of metal-catalyzed autoxidation. Journal of the American Oil Chemists' Society 48:427-433

Weaver, P.P.E., Schultheiss, P.J., (1990). Current methods for obtaining, logging and splitting marine sediment cores, p.85-101. In: Marine Geological Surveying and Sampling, Hailwood, E.A., Kidd, R.B. (Eds), Kluwer, Dordrecht

Weber, M.E., Niessen, F., Kuhn, G., *et al*., (1997). Calibration and application of marine sedimentary physical properties using a multi-sensor core logger. Marine Geology 136:151-172

Weber, M.E., Wiedicke-Hombach, M., Kudrass, H.R., *et al*., (2003). Bengal Fan sediment transport activity and response to climate forcing inferred from sediment physical properties. Sedimentary Geology 155:361-381

Weeks, S.J., Currie, B., Bakun, A., *et al*., (2004). Hydrogen sulphide eruptions in the Atlantic Ocean off southern Africa: implications of a new view based on SeaWiFS satellite imagery. Deep-Sea Research I 51:153-172

Weete, J.D., (1976). Algal and Fungal Waxes. In: Chemistry and Biochemistry of Natural Waxes, P.E. Kolattukudy (Ed). Elsevier, Amsterdam, pp 383-391.

Wellsbury, P., Goodman, K., Cragg, B.A., *et al*., (2000). The geomicrobiology of deep marine sediments from Blake Ridge containing methane hydrates (Sites 994, 995 and 997) Proceedings of the Ocean Drilling Program, Scientific Results 164:379-391

Westerhausen, L., Poynter, J., Eglinton, G., *et al*., (1993). Marine and terrigenous origin of organic-matter in modern sediments of the equatorial east Atlantic – the $\delta^{13}C$ and molecular record. Deep-Sea Research I, Oceanographic Results Papers 40:1087-1121

Wharton, D.A., (2002). Life at the Limits. Organisms in extreme environments. Cambridge University Press, UK, 307pp.

Wheeler, A.J., Beyer, A., Freiwald, A., *et al*., (2007) Morphology and Environment of Cold-water Coral Carbonate Mounds on the NW European Margin , International Journal of Earth Science 96:37-56

White, D.C., Tucker, A.N., (1969). Phospholipid metabolism during bacterial growth. Journal of Lipid Research 10:220-223

White, D.C., Davis, W.M., Nickels, J.S., *et al*., (1979). Determination of the sedimentary microbial biomass by extractable lipid phosphate. Oecologia 40:51-62

Whiticar, M.J., (1999). Carbon and hydrogen isotope systematics of bacterial formation and oxidation of methane. Chemical Geology 161:291-314

Whitman, W.B., Coleman, D.C., Wiebe, W.J., (1998). Prokaryotes: The unseen majority. Proceedings of National Academy of Science USA 95:6578-6583

Whitmarsh, R.B., (1971). Precise sediment density determination by gamma-ray attenuation alone. Journal of Sedimentary Petrology 41:882-883

Wiesenberg, G.L.B., Schwark, L., Schmidt, M.W.I., (2004). Improved automated extraction and separation procedure for soil lipid analysis. European Journal of Soil Science 55:349-356

Wilmut, M., Bloomer, S., Preston, J.M., (2009). Discriminant Analysis in Image-Based Seabed Classification. Proceedings of Underwater Acoustic Measurements: Technologies & Results, Napfilton, Greece

Wilhelmy, S.A.S., Flegal, A.R., (1991). Trace element distribution in coastal waters along the US-Mexican boundary: relative contributions of natural processes vs. anthropogenic inputs. Marine Chemistry 33:371-392

Williams, R., Conway, D.V.P., Hunt, H.G., (1994). The role of copepods in the planktonic ecosystems of mixed and stratified waters of the European shelf seas. Hydrobiologia 292/293:521-530

Willoughby, E.C., Mir, R., Scholl, C., *et al*., (2008). Netune-Canada based geophysical imaging of gas hydrate in the bullseye vent. Proceedings of the 6th International Conference on Gas Hydrates (ICGH 2008), Vancouver, British Columbia, Canada, July 6-10, 2008

Wilkens, R.H., Richardson, M.D., (1998). The influence of gas bubbles on sediment acoustic properties: in situ, laboratory, and theoretical results from Eckernförde Bay. Baltic sea. Continental Shelf Research 18:1859-1892

Wilson, P.S., Reed, A.H., Wood, W.T., *et al*., (2008). The low-frequency sound speed of fluid-like gas-bearing sediments. Journal of Acoustical Society of America 123:EL99-EL104

WOMARS (2005) Worldwide marine radioactivity studies. Radionuclide levels in oceans and seas. IAEA Technical report, IAEA-TECODC-1429, Vienna

Woolsey, T.S., McCallum, M.E., Schumm, S.A., (1975). Modelling of diaterme emplacement by fluidization. Physics and Chemistry of the Earth 9:29-42

Wu, D., Chen, A., Johnson, C. S. Jr., (1995). An improved diffusion ordered spectroscopy experiment incorporating bipolar-gradient pulses. Journal of Magnetic Resonance A 115: 260.

Youngblood, W.W., Blumer, M., Guillard, R., *et al*., (1971). Saturated and unsaturated hydrocarbons in marine benthic algae. Marine Biology 8:190-201

Yuan, F., Bennell, J.D., Davis, A.M., (1992). Acoustic and physical characteristics of gassy sediments in the western Irish Sea. Continental Shelf Research 12:1121-1134

Yunker, M.B., Belicka, L.L., Harvey, H.R., *et al*., (2005). Tracing inputs and fate of marine and terrigenous organic matter in Arctic Ocean sediments: A multivariate analysis of lipid biomarkers. Deep Sea Research Part II: Topical Studies in Oceanography 52:3478-3508

Xu, Y., Simoneit, B.R.T., Jaffe, R., (2007). Occurrence of long-chain n-alkenols, diols, keto-ols and sec-alkanols in a sediment core from hypereutrophic, freshwater lake. Organic Geochemistry 38:870-883

Zabel, M., Schulz, H.D., (2001). Importance of submarine landslides for non-steady state conditions in pore-water systems – Lower Zaire (Congo) deep-sea fan, Marine Geology 176: 87-99

Zachos, J., Pagani, M., Sloan, L., *et al*., (2001). Trends, Rhythms, and Aberrations in Global Climate 65 Ma to present. Science (Washington DC, United Satetes) 292:686-693

Zang, X., Nguyen, R.T., Harvey, H.R., *et al*., (2001). Preservation of proteinaceous material during the degradation of the green alga Botryococcus braunii: A solid-state 2D ^{15}N ^{13}C NMR spectroscopy study. Geochmica et Cosmochimica Acta 65:3299-3305

Zhao, M., Mercer, J.L., Eglinton, G., *et al*., (2006). Comparative molecular biomarker assessment of phytoplankton paleoproductivity for the last 160 kyr off Cap Blanc, NW Africa. Organic Geochemistry 37:72-97

Zhang, Z., Zhao, M., Eglinton, G., *et al*., (2006). Leaf wax lipids as paleovegetational and paleoenvironmental proxies for the Chinese Loess Plateau over the last 170 kyr. Quaternary Science Reviews 25:575-594

Zhou, Y., Goldfinger, C., Johnson, J.E., *et al*., (1999). Distribution and morphology of venting-related carbonates near Hydrate Ridge, Oregon Margin, based on sidescan sonar and multibeam imagery. EOS – Transactions of the American Geophysical Union 80, Abstract F510

Zheng, Y., Zhou, W., Liu, X., *et al*., (2011). n-Alkan-2-one distribution in a northeastern China peat core spanning the last 16kyr. Organic Geochemistry 42:25-30

Zhuikov, B.L., (2005). Gas chemical methods for the separation of elements in radioisotope production and activation analysis. Journal of Radioanalytical and Nuclear Chemistry 263:65-70

Zimmer, C., (2001). “Inconvincible” bugs eat methane on the ocean floor. Science 293:418-419

Zuhlsdorff, C., Wien, K., Stuut, J.-B.W., *et al*., (2007). Late Quaternary sedimentation within a submarine channel-levee system offshore Cap Timiris, Mauretania. Marine Geology 240:217-234